Biomass Densification for Minimal Drying Energy and Optimised Pellet Quality

by

Johnson Ho Kwong Lau MEng (Oxon.) AMIChemE

Thesis submitted to the University of Nottingham for the Degree of Engineering Doctorate

May 2024

Abstract

Biomass power generation has been gaining increasing importance globally in recent years to provide renewable energy and combat climate change. However, several constraints have limited the expansion of biomass power generation, and in particular, the use of alternative biomass feedstocks to wood. The major challenges of the industry include the high drying energy of biomass, the need for biomass densification and the variability in the properties of biomass. This thesis addresses several of the major challenges of the industry through the study of the properties of alternative biomass feedstocks, the development of a new novel low-energy biomass drying process, the in-depth investigation of biomass pelleting and pellet milling behaviour, and the use of Life Cycle Analysis (LCA) to study the environmental benefits of biomass power generation from a system perspective.

The results presented have provided new insights and addressed multiple gaps in knowledge in the existing literature. In addition, the new knowledge presented is valuable for the industry to improve the understanding of unconventional biomass feedstocks and industrial processes, and the new tools and methods developed can be used by industry to deliver substantial environmental and economic benefits.

The characterisation of several conventional and alternative biomass feedstocks was conducted. The characteristics of cardboard materials, including char morphology, burnout performance and particle shape change during combustion, were studied in detail and a new method of using thermogravimetric analysis to measure calcium carbonate content in cardboard was developed. In general, cardboard chars are more porous and thin-walled than eucalyptus chars, indicating a better char burnout performance. The challenges of using cardboard for power generation applications would include potential handling difficulties, a low calorific value and high ash content.

The feasibility of a new novel combined pasteurisation and natural drying process was established using a set of experiments with miscanthus and spent grains, which can dramatically decrease the drying energy of biomass. Biomass briquettes were

pasteurised and monitored over a storge period of up to nine weeks. Substantial decrease of moisture content was achieved by natural drying, while optimised pasteurisation strategies can provide effective fungal growth suppression during the storage period. It was also found that microwave pasteurisation can achieve similar or better levels of fungal growth suppression with shorter processing times compared to conventional oven pasteurisation.

The pelleting and pellet milling behaviour of sugarcane straws was investigated and new parameters were developed to quantify the pelleting process. The influence of various factors on pelleting and pellet milling was investigated, including moisture content, particle size and harvest season. It was found that pelleting failure was more likely to occur at low moisture contents, at fine particle sizes, and with the dry season sample.

Lastly, an LCA study of a biomass power generation system using bagasse from the United States to generate power in the United Kingdom was conducted. It was found that for the system studied, the overall carbon footprint of the electricity generated is 81.6 g CO_2/kWh. The main opportunities of reducing carbon emissions are the electricity use at the pellet plant and shipping between the origin port and the destination port. It was also concluded that substantial benefits in terms of global warming potential could be achieved by the system studied, particularly if carbon capture and storage is also integrated.

Acknowledgements

I would like to thank my academic supervisors, Dr Orla Williams, Prof. Edward Lester and Prof. Jon McKechnie, for their invaluable support and advice throughout the course of this doctorate. My journey through the doctorate would not have been possible without this support.

I would like to thank my industrial supervisors, Mr Richard Hanby and Dr Frances Flower, for providing advice from the industrial perspective. I would also like to thank Net Zero Research, EPSRC and the University of Nottingham for providing the funding and necessary resources for this project.

Finally, I would like to thank my family and my partner for supporting and encouraging me throughout this journey.

Table of Contents

List of Figures

List of Tables

List of Abbreviations

Notation	Description
$Al_2Si_2O_5(OH)_4$	Kaolin
BECCS	Bioenergy carbon capture and storage
C	Carbon
$CaCO_3$	Calcium carbonate
CaO	Calcium oxide
CBK	Carbon Burnout Kinetic Model
CCC	Calcium carbonate content
CCS	Carbon capture and storage
CFD	Computational fluid dynamics
CO	Carbon monoxide
CO_2	Carbon dioxide
dafb	dry-ash-free basis
DTF	Drop-tube furnace
EngD	Engineering Doctorate
Euc	Eucalyptus
f.u.	Functional unit
HHV	Higher heating value
HTST	High-temperature short-time
LCA	Life cycle analysis
LCI	Life cycle inventory analysis
LCIA	Life cycle impact assessment
LHV	Lower heating value
LTLT	Low-temperature long-time
M1-8	*Miscanthus briquettes number 1-8*
M1b	Sample taken from the bottom of the M1 briquette (illustrative example)
M1m	Sample taken from the middle of the M1 briquette (illustrative example)
M1t	Sample taken from the top of the M1 briquette (illustrative example)
MF	Muffle furnace
$Mg_3(Si_2O_5)_2(OH)_2$	Talc
MLA	Mineral liberation analysis
MSW	Municipal solid waste
PCB	Printed cardboard
pchip	Piecewise cubic hermite interpolating polynomial function
PDF®	Powder diffraction file
PF	Pulverised fuel
PPB	Printed paperboard
PPC	Post-pasteurisation contamination

PSD	Particle size distribution
RH	Rice husks
SG1-8	*Spent grains briquettes number 1-8*
SRMV	SERC Mississippi Valley subregion
SSDS	Sugarcane straws (dry season)
SSDS (fine, 20%)	Dry season sugarcane straw sample with fine particle size at 20% pelleting feed moisture content (illustrative example)
SSWS	Sugarcane straws (wet season)
tC	Thin-walled cellular
TC	Thick-walled cellular
TCH	Thick-walled cellular high aspect ratio
tCH	Thin-walled cellular high aspect ratio
TCL	Thick-walled cellular low aspect ratio
tCL	Thin-walled cellular low aspect ratio
TGA	Thermogravimetric analysis
TiO_2	Titanium dioxide
tP	Thin-walled porous
TP	Thick-walled porous
TPH	Thick-walled porous high aspect ratio
tPH	Thin-walled porous high aspect ratio
TPL	Thick-walled porous low aspect ratio
tPL	Thin-walled porous low aspect ratio
UCB	Unprinted cardboard
UHT	Ultra-high-temperature
UPB	Unprinted paperboard
XRD	X-ray diffraction

List of Mathematical Expressions

Notation	Description
B	*Characteristic system dimension (m)*
$1/x_2 - 1/x_1$	*von Rittenger parameter*
a	*Maximum intercept through the particle (equivalent to the diameter of the circumscribing sphere)*
A	*Projection area of the particle*
A_{char}	*Ash content of char (%)*
AR	*Particle aspect ratio*
$AR_{average}$	*Average aspect ratio*
A_{raw}	*Ash content of raw biomass (%)*
AR_{pellet}	*Pellet aspect ratio*
BD	*Bulk density (kg/m3)*
C	*Particle circularity*
C_c	*Curvature coeeficient (dimensionless)*
C_u	*Uniformity coeeficient (dimensionless)*
d	*Particle size (µm)*
D	*Pellet durability (%)*
d'	*Characteristic particle size (µm)*
d_{10}	*10^{th} percentile of the cumulative particle size distribution*
d_{16}	*16^{th} percentile of the cumulative particle size distribution*
d_{25}	*25^{th} percentile of the cumulative particle size distribution*
d_{30}	*30^{th} percentile of the cumulative particle size distribution*
d_5	*5^{th} percentile of the cumulative particle size distribution*
d_{50}	*50^{th} percentile of the cumulative particle size distribution*
d_{60}	*60^{th} percentile of the cumulative particle size distribution*
d_{75}	*75^{th} percentile of the cumulative particle size distribution*
d_{80}	*80^{th} percentile of the cumulative particle size distribution*
d_{84}	*84^{th} percentile of the cumulative particle size distribution*
d_{90}	*90^{th} percentile of the cumulative particle size distribution*
d_{95}	*95^{th} percentile of the cumulative particle size distribution*
d_A	*Diameter of a circle with area A*
d_c	*Maximum chord (local)*
$d_{c,min}$	*Minimum chord*
d_{Fe}	*Feret diameter (local)*
$d_{Fe,max}$	*Feret diameter*
d_n	*Nominal diameter (defined as the diameter of a sphere with the same volume as the particle)*

d_P	*Particle size (m)*
d_{Pe}	*Diameter of a circle with perimeter length P*
$E_{combustion}$	*Combustion efficiency (%)*
E_e	*Specific effective milling energy (kWh/ton)*
eff	*Electricity generation efficiency (HHV basis) (%)*
E_{total}	*Total specific pelleting or milling energy (kWh/ton)*
GE	*Grinding energy of the pellets (MJ/kg)*
GS_i	*Inclusive graphic skewness (dimensionless)*
H_d	*Hydrogen content (dry basis) (%)*
HHV_d	*Higher heating value (dry basis)*
HHV_w	*Higher heating value (wet basis)*
hs	*Geometric standard deviation of the high region*
IQR	*Interquartile range*
K_g	*Graphic kurtosis (dimensionless)*
k_v	Stokes shape factor
K_{VR}	*von Rittinger constant (kWh·mm/ton)*
LHV_d	*Lower heating value (dry basis)*
ls	*Geometric standard deviation of the low region*
m	*Output mass (ton)*
M	*Initial mass of pellets before the tumbling procedure*
m_1	*Mass of the empty drying container*
m_2	*Mass of the drying container and the sample before drying*
m_3	*Mass of the drying container and the sample after drying*
MC	*Moisture content (%)*
M_{Din}	*Moisture content of the material at the dryer inlet (%)*
M_{Dout}	*Moisture content of the material at the dryer outlet (%)*
M_{Dout}	*Moisture content of the material at the dryer outlet (%)*
M_{HMin}	*Moisture content of the material at the hammermill inlet (%)*
M_{HMout}	*Moisture content of the material at the hammermill outlet (%)*
m_i	*Mass of material retained on the 3.15 mm round hole sieve after the tumbling procedure*
M_{Pin}	*Moisture content of the material at the pelletiser inlet (%)*
M_{Pout}	*Moisture content of the pellets at the pelletiser outlet (%)*
MRS	*Mass relative span*
m_{TP}	*Mass of the test portion (kg)*
n	*Rosin–Rammler size distribution parameter*
N_d	*Nitrogen content (dry basis) (%)*
O_d	*Oxygen content (dry basis) (%)*
P	*Perimeter length of the particle*
$P_{average}$	*Total average power (kW)*

PE	*Pelleting efficiency (%)*
P_i	*Instantaneous power (kW)*
P_{idle}	*Idle power (kW)*
$P_{idle,average}$	*Average idle power (kW)*
$PP_{average}$	*Average pelleting power (kW)*
Q_1	*Lower quartile*
Q_3	*Upper quartile*
R(d)	*Cumulative undersize mass (%)*
s	Geometric standard deviation of the total region
Stk	*Stokes number (dimensionless)*
Symm	*Particle symmetry*
t	*Time (hr or s)*
t_1	*Start time of the pelleting or milling region (s)*
t_2	*End time of the pelleting or milling region (s)*
u_0	*Velocity of the particle far away from an obstacle (m/s)*
UL_{21}	*Unrecoverable losses represented by stream 21 in the process flow diagram (%)*
UL_{HM}	*Unrecoverable losses from the hammermill (%)*
UL_P	*Unrecoverable losses from the pelletiser (%)*
UL_{PC}	*Unrecoverable losses from the pellet cooler (%)*
UL_{PG}	*Unrecoverable losses from the pellet grinder (%)*
UL_{PPS}	*Unrecoverable losses from the pellet plant storage (%)*
UL_{PSS}	*Unrecoverable losses from the power station storage (%)*
UL_T	*Unrecoverable losses from transport to the UK (%)*
V	*Volume of the test portion (m3)*
W_{ash2}	*Amount of ash to be disposed from the boiler per f.u. (kg)*
W_{Bin}	*Weight of the pellets per f.u. at the pellet grinder inlet (kg)*
W_{Din}	*Weight of the material per f.u. at the dryer inlet (kg)*
W_{Dout}	*Weight of the material per f.u. at the dryer outlet (kg)*
W_{feed}	*Weight of the material per f.u. at the pellet plant feed (kg)*
W_{HMin}	*Weight of the material per f.u. at the hammermill inlet (kg)*
W_{HMout}	*Weight of the material per f.u. at the hammermill outlet (kg)*
W_{in}	*Theoretical amount of raw biomass input*
W_{out}	*Theoretical amount of char produced*
W_{PCin}	*Weight of the pellets per f.u. at the pellet cooler inlet (kg)*
W_{PCout}	*Weight of the pellets per f.u. at the pellet cooler outlet (kg)*
W_{PGin}	*Weight of ground pellets per f.u. at the boiler inlet (kg)*
W_{Pin}	*Weight of the material per f.u. at the pelletiser inlet (kg)*
W_{Pout}	*Weight of the pellets per f.u. at the pelletiser outlet (kg)*

X_F	*Fraction of the dryer outlet diverted to fuel the furnace (dimensionless)*
Y	*Yield of the char production process (%)*
θ_{en}	*Burning enhancement factor*
ρ_P	*Particle density (kg/m^3)*
ϕ	*Particle sphericity or operational sphericity*
$\varphi_{average}$	*Average sphericity*

List of Proposed Publications and Conference Presentations

Proposed Journal Publications:

Williams, O., Lau, J., Martinez, K., Guerrero, J., Barraza, J., Gil, N., Saltaren, J., Güleç, F., Lester, E. (2024). *The Potential for Colombian Sugarcane Straw Utilisation in Domestic and Global Bioenergy Markets.* Submitted to *Renewable and Sustainable Energy Reviews.*

Lau, J., Lester, E., McKechnie, J., Williams, O. *The properties of cardboard for power generation.*

Lau, J., Lester, E., McKechnie, J., Williams, O. *A novel low-energy biomass drying strategy with combined pasteurisation and natural drying.*

Lau, J., Lester, E., McKechnie, J., Williams, O. *An investigation of the pelleting and pellet milling behaviour of Colombian sugarcane straws.*

Lau, J., Lester, E., McKechnie, J., Williams, O. *Life cycle analysis study of a biomass power generation system using sugarcane bagasse from the US to generate electricity in the UK.*

Conference Presentations:

Lau, J., Lester, E., McKechnie, J., Robinson, J., Williams, O. (2019) *Non-conventional drying strategies for biomass densification.* (Poster presentation) In: 17th ICCS&T (The International Conference on Coal Science & Technology)

Lau, J., Lester, E., McKechnie, J., Robinson, J., Williams, O. (2021) *Biomass characterisation and densification for evaluating suitability of non-conventional biomass sources for power generation.* (Oral presentation) In: 1st FERIA (The European Conference on Fuel and Energy Research and its Applications)

Lau, J., Lester, E., McKechnie, J., Robinson, J., Williams, O. (2021) *Optimising the integration of torrefaction and novel drying strategies in biomass pelleting plants by life cycle analysis.* (Oral presentation) In: 1st FERIA (The European Conference on Fuel and Energy Research and its Applications)

Lau, J., Lester, E., McKechnie, J., Robinson, J., Williams, O. (2021) *Comminution and densification behaviour of cashew shells, spent coffee grounds, bagasse trash and refuse-derived fuel through a repeated pelleting and milling experimental procedure.* (Poster presentation) In: 1st FERIA (The European Conference on Fuel and Energy Research and its Applications)

Williams, O., Martinez, K., Nichols, D., Lau, H., Barraza, J., Guerrero, J., Forero, C., Saltaren, S., Lester, E. (2021) *Combustion potential of bagasse and sugarcane straw for bioenergy applications.* (Oral presentation) In: 1st FERIA (The European Conference on Fuel and Energy Research and its Applications)

Lau, J., Lester, E., McKechnie, J., Robinson, J., Williams, O. (2022) *Life cycle analysis of sugarcane bagasse for power generation: environmental benefits and economic viability.* (Oral presentation) In: Total Food 2022

Lau, J., Lester, E., McKechnie, J., Robinson, J., Williams, O. (2022) *Benefits and challenges of cardboard materials as solid biofuel for power generation.* (Poster presentation) In: 30th EUBCE (The European Biomass Conference and Exhibition)

Lau, J., Lester, E., McKechnie, J., Robinson, J., Williams, O. (2023) *Pelleting and pellet milling of bagasse trash: the influence of harvest season, moisture content and particle size.* (Oral presentation) In: 2nd FERIA (The European Conference on Fuel and Energy Research and its Applications)

Lau, J., Lester, E., McKechnie, J., Robinson, J., Williams, O. (2023) *A novel biomass drying strategy with combined pasteurisation and natural drying.* (Oral presentation) In: 2nd FERIA (The European Conference on Fuel and Energy Research and its Applications)

Chapter 1 - Introduction

1.1 Project Rationale and Context

Biomass power generation has been gaining increasing importance globally in recent years as an option to provide renewable energy and combat climate change. In the UK, biomass power generation is an integral part of the country's electricity mix as the government has committed to phasing out coal power generation by October 2024 (Department for Business, Energy & Industrial Strategy, 2021) and renewable energy sources will continue to increase in importance. Currently, biomass power generation provides around 6-9% of the UK's electricity needs (Voegele, 2023) and Drax Power Station, which provides 11% of the UK's renewable power (Drax Power, n.d.), is the largest biomass power generation plant in the UK and a major consumer of biomass pellets. Although the policy of phasing out coal has remained in place (Espiner, 2022), the Russian invasion of Ukraine in February 2022 has resulted in an energy crisis and highlighted energy security concerns and one of the measures taken by the UK government to mitigate this was to delay the planned closure of some coal-fired power stations (Espiner, 2022; Taylor, 2023). Despite previous expectations that current subsidies for Drax would end in 2027 and would only be provided if the plants are fitted with carbon capture and storage technology (Thomas, 2019), the UK government has recently set out proposals to extend subsidies beyond 2027, which are designed as an interim measure to support the plant as carbon capture and storage technology is being installed (Millard, 2024; Voegele, 2024). Apart from the UK, continental Europe and Japan are among the markets where the biomass-to-power industry is expected to continue to grow (The International Centre for Sustainable Carbon, 2024).

Biomass power generation has several unique advantages compared to other types of renewable energy. In principle, it can generate a baseline electricity load and help balance out the fluctuations in other types of renewables like solar and wind power (Thrän et al., 2015), playing a role previously filled by fossil fuel power generation. The increased use of bioenergy can also provide benefits in energy security (Kumar et al., 2022), as most countries would have some available biomass resource. In cases

where imports are required, biomass can potentially be sourced from a large selection of countries rather than solely from countries with fossil fuel resources. It is also widely recognised that the reduction of greenhouse gas emissions to the atmosphere alone may not be sufficient to mitigate climate change and negative emissions technologies may be needed to compensate for emissions from hard-to-decarbonise sectors (Cabral et al., 2019; Pires, 2019). In this capacity, bioenergy is unique as a renewable energy option which can be integrated with carbon capture and storage (CCS) as bioenergy with carbon capture and storage (BECCS) systems.

In spite of its potential benefits, large-scale biomass power generation can be a controversial topic and has been criticised by environmental groups for reasons such as inefficient land use and air pollution, with some groups claiming that it is no better for the climate compared to burning fossil fuels (Biofuelwatch, 2018). The use of woody fuels has also drawn particularly serious criticism due to concerns with sourcing and reports of primary forests being harvested for bioenergy purposes (Biofuelwatch, 2024). The recent proposal for extending subsidies for Drax beyond 2027 has also been criticised by climate groups and MPs (Ambrose, 2024). Another limitation of biomass power generation is its cost. With a reported cost of £75-80/MWh, Drax is endeavouring to reduce this to £50/MWh, which would allow the company to compete to provide power at peak times (Thomas, 2019).

In this context, there has been increasing interest in using alternative biomass sources to wood to improve the environmental sustainability, economic viability and supply security of biomass power generation (De Laporte et al., 2016; de Wit & Faaij, 2010; Dungani et al., 2014). However, several technological constraints have limited the expansion of biomass power generation, and in particular, the use of alternative biomass feedstocks.

Biomass feedstocks can have a high degree of variability and pose a challenge for power generators due to a number of factors, including species variabilities, production conditions, harvesting time and methods, and collection and storage practices (Kenney et al., 2013). Therefore, it is desirable to continue to develop a deeper understanding of the characteristics of a large variety of biomass feedstocks. The high moisture content of raw biomass materials is also a major limitation as

drying is an energy-intensive process (Thek & Obernberger, 2012). Densification (with pelleting being one of the most common densification methods) is necessary for the transport of biomass materials over large distances in an economical manner due to their low energy density, and continuous improvement of pelleting processes would be highly valuable to industry. Lastly, to ensure that the desired environmental benefits are realised, biomass power generation should be studied from a system perspective, using techniques such as life cycle analysis (LCA). This study is designed to address these known challenges of biomass power generation and contribute to reducing energy use and improving the economics and environmental performance of the industry.

1.2 Aims and Objectives

The aim of this thesis is to address the current challenges faced by the biomass power generation industry through improving the understanding of the properties of various biomass feedstocks and the pelleting process, reduction of biomass drying energy and quantification of the environmental benefits of biomass power generation systems. The research objectives of the thesis are:

1. Review the major current challenges and potential solutions of the biomass power generation industry
2. Characterise the properties of several conventional and alternative biomass feedstocks and evaluate the implications for their use for power generation implications, using both conventional and novel techniques
3. Develop and evaluate a new novel low-energy biomass drying solution to provide energy and cost savings
4. Provide a detailed study of the pelleting and pellet milling processes through laboratory-scale experiments
5. Conduct a life cycle analysis (LCA) study of a power generation system involving the pelleting, international transport and combustion of biomass

1.3 The Engineering Doctorate Scheme (EngD)

This thesis forms part of the assessment for the Engineering Doctorate (EngD) degree at the University of Nottingham. The EngD also includes a formal training programme consisting of a number of compulsory and optional modules. The EngD research

project is co-funded by the EPSRC Centre for Doctoral Training in Resilient Decarbonised Fuel Energy Systems and Net Zero Research. Net Zero Research is a membership organisation consisting of multiple members, including British Sugar, Doosan Power Systems, Drax Group plc, EDF Energy plc, the Electric Power Research Institute (EPRI) and Lynemouth Power. Industrial supervision for this project was provided by Drax Power, with Dr Frances Flower and Mr Richard Hanby as the industrial supervisors.

1.4 Additional Funding

Additional funding with a total amount of £4,436 was provided by the University of Nottingham Interdisciplinary Centre for Analytical Science (UNICAS) through the UNICAS at the Researcher Academy scheme. This grant was used to conduct the fungal growth testing work presented in Chapter 6. The author was the principal investigator for this grant, and the other applicants were Dr Stephen Lawrence, Dr John Robinson, Dr Orla Williams and Prof Edward Lester.

1.5 COVID-19 Impact

This research project was impacted by COVID-19 in multiple ways, although efforts have been made to reschedule and adjust research activities to mitigate these impacts and allow the completion of the project with valuable results for academia and industry. The original plan of the project, as agreed with the industrial sponsor, would involve international visits to pelleting plants, and life cycle analysis (LCA) of the industrial sponsor's operations would be conducted based on these visits. Due to Covid-related travel restrictions and company policy on visitors, these visits could not be undertaken and the LCA was refocused from a site-based study to a desk-based study with some data provided by the industrial sponsor.

Starting from the initial lockdown in March 2020 until August 2020, there was no access to all university facilities, including laboratories essential for the project. Access to offices and laboratories was gradually restored from August 2020, although a rota system limiting access to 2.5 days per week remained in place for some facilities until late 2021.

1.6 Thesis Structure and Overview

There are eight further Chapters in this thesis, organised into three main parts. Part I (Chapters 2 and 3) reviews the existing literature relevant to the research project and details the methodologies used in the thesis. Part II (Chapters 4-8) presents the results, analysis and discussion of the experimental and desk-based studies. Part III (Chapter 9) presents the overall conclusions of the research project and recommendations for future work. A summary of the Chapters is provided here:

Chapter 2 provides a literature review of the topics relevant to the research project, including the challenges and current understanding of various processes in the biomass power generation industry, the applicability of char morphology and burnout prediction techniques for biomass, the industrial significance of particle shape, the background of pasteurisation as a possible technique of biomass treatment and existing studies on biomass power generation systems. Knowledge gaps in the current literature, where further study would be beneficial to academia and industry, were identified.

Chapter 3 provides detailed descriptions of the experimental and desk-based research and analysis methodologies used, which are referenced in the subsequent Chapters.

Chapter 4 presents the characterisation of several biomass feedstocks, including eucalyptus, rice husks and sugarcane straw, using a range of experimental techniques.

Chapter 5 presents an in-depth study of the properties of cardboard materials, and the potential opportunities and challenges of using cardboard materials for power generation applications were identified and discussed. New techniques for the characterisation of cardboard materials were developed and the change in particle size and shape during combustion was investigated.

Chapter 6 details the development of a new novel combined pasteurisation and natural drying process, which can substantially reduce the drying energy required for biomass drying. Experiments using miscanthus and spent grains were conducted and

different pasteurisation conditions were used to investigate the optimal configurations for such a process.

Chapter 7 focuses on the pelleting and pellet milling behaviour of sugarcane straws. Pelleting and pellet milling experiments were conducted with a lab-scale pellet machine and a lab-scale ring-roller mill. The influence of moisture content, harvest season and particle size was investigated and new parameters for characterising the pelleting process were proposed. The change in particle size and shape during the complete journey of pelleting and pellet milling was also quantified and discussed.

Chapter 8 presents a detailed life cycle analysis (LCA) study of a biomass power generation system which uses sugarcane bagasse from the United States for large-scale power generation in the UK. A bespoke model was developed, which includes the collection of bagasse from sugar mills, processing and pelleting of the raw material, transport to the power station, and combustion. The overall carbon footprint was calculated and the results were discussed.

Chapter 9 draws on the work presented in Chapters 4-8 to provide a summary of the findings and conclusions of the research project. Recommendations for future work are also provided, based on the findings of the project.

Chapter 2 - Literature Review

2.1 Biomass Feedstocks for Power Generation

Various types of biomass feedstocks are currently in use, or can potentially be used for the purpose of large-scale power generation. A brief review of the current use of several biomass feedstocks relevant to this thesis is provided in this Section, including woody biomass, cardboard materials, sugarcane bagasse and sugarcane straw.

2.1.1 Woody Biomass

Woody biomass refers to biomass materials originating from trees, bushes and shrubs (The British Standards Institution, 2022a). As previously discussed in Section 1.1, there has also been increasing interest in using alternative biomass sources to wood. Despite this, woody biomass has remained the predominant fuel used for bioenergy applications, including electricity generation (Lucadamo et al., 2019). In the UK, the consumption of wood pellets in power stations was estimated to be 8.3 million tonnes in 2018, which is equivalent to 21% of the global wood pellet production (Brack et al., 2021). Among the types of wood used for bioenergy applications, eucalyptus is one of the widely used species (Andritz, 2022; Voegele, 2018).

2.1.2 Cardboard Materials

2.1.2.1 Raw materials and the cardboard manufacturing process

Cardboard can be manufactured from various types of wood and recycled paper products. Either wood or recycled paper products are generally used to produce pulp for cardboard manufacturing (Lorang et al., 2023), although other types of non-woody biomass such as rice husks, bagasse, wheat straws, and other agricultural wastes have also been used (Barbash & Yashchenko, 2020; Jeetah et al., 2015; Kissinger et al., 2007). Among the types of virgin wood, eucalyptus is one of the common sources for pulp production (Magaton et al., 2009).

The production of cardboard starts with the milling and pulping of the raw material. Pulp consists of discrete fibres dispersed in water, and pulping may be conducted by chemical or mechanical means, or a combination of the two (Biermann, 1996).

Among these methods, the Kraft process is the predominant process used (Biermann, 1996; Fearon et al., 2020). It uses a mixture of sodium hydroxide and sodium sulphide at high temperatures to dissolve and remove most of the lignin and hemicellulose, resulting in a cellulose-rich pulp, which is then dried to produce paper and cardboard (Biermann, 1996). In the case of corrugated cardboard, starch glue is also typically used as an adhesive to join the layers of sheets together to produce the final product (Pereira et al., 2020).

Alongside wood, recycled paper products and alternative biomass sources, fillers are also known to be an important raw material in cardboard manufacturing. Fillers can be defined as pigment powders that are usually produced from natural minerals and typically have a particle size of 2-10 μm (Grönfors, 2010).

There are several reasons for the use of fillers, including their low cost compared to biomass-derived raw materials (Grönfors, 2010), improvement of surface properties and printability, and improvement of optical properties such as opacity and brightness (Biermann, 1996). The most common filler used in paper and cardboard manufacturing is calcium carbonate, closely followed by kaolin, with talc and titanium (TiO_2) used in smaller quantities for special applications (Grönfors, 2010). The amount of filler used varies between the types of product, but could be as high as 30% by weight (Grönfors, 2010).

2.1.2.2 Recycling and combustion of waste cardboard

It has been estimated that 5.4 million tons of paper and cardboard packaging wastes were generated in the UK in 2021, with a recycling rate of roughly 71% (Statista, 2023). The recycling process typically consists of shredding, followed by pulping (where the shredded cardboard is mixed with water), drying and rolling (QCR Recycling Equipment, 2022). This is similar to the manufacturing process of cardboard from raw biomass materials, although chemical or mechanical processes to separate the cellulose fibres are usually not required.

Despite the widespread recycling of cardboard, there is also a practical limit on the number of times that cardboard can be recycled (usually between five and seven times) due to the shortening of fibre length, resulting in the decrease in quality as the

material is recycled (QCR Recycling Equipment, 2022). Thus, not all cardboard wastes can be recycled and there is potential to use cardboard wastes for energy applications, particularly in the context where there is increasing interest from industry in using alternative biomass sources to wood (see Section 1.1). In addition, waste cardboard would represent a domestic source of biomass, which would provide additional benefits as most of the biomass used in the UK is imported, with the majority being wood pellets from the USA and Canada (Office for National Statistics, 2019).

The combustion of cardboard for energy applications has been investigated previously, although the number and breadth of studies are not as substantial as many other types of more commonly used biomass. Municipal solid waste (MSW) often contains a significant proportion of paper and cardboard products, although the exact proportion would vary between regions (De Feo et al., 2021; Montejo et al., 2011). As incineration with energy recovery is a common waste management strategy, the combustion of cardboard as part of MSW is also commonly carried out in industry. The co-firing of cardboard-containing wastes with coal or other types of biomass for power generation has also been fairly widely studied (Glushkov et al., 2019; Ryu et al., 2007; Vainikka et al., 2013), and the high ash content and low calorific value of cardboard have been cited as the main drawbacks (Zhuikov et al., 2022). There are comparatively few studies which treat cardboard as a distinct category or focus on the dedicated combustion of cardboard. Glushkov, Kuznetsov and Paushkina (2020) studied the combustion characteristics of co-firing coal with each of the components of MSW, including cardboard. Leyssens et al. (2014) also studied the co-firing of cardboard and sawdust in a domestic boiler.

In addition, none of the studies on the combustion of cardboard have investigated the differences between the types of cardboard and the potential impact of fillers. There are no studies on the char morphology of cardboard, despite the significance of the topic on combustion behaviour and burnout. Thus, further investigation of the properties of cardboard materials would be highly valuable for academia and industry, filling a knowledge gap in the existing literature, particularly in these aforementioned areas.

2.1.3 Sugarcane Straw and Bagasse

Large quantities of process and agricultural residues are produced during the cultivation, harvesting and processing of sugarcane. This represents a significant opportunity for the use of these residues for bioenergy applications (Ungureanu et al., 2022). Sugarcane straw refers to the green leaves, dried leaves, and buds, which are commonly left in the fields after sugarcane harvesting, while sugarcane bagasse refers to the fibrous residue left after extracting juice from sugar cane in the sugar production process (Martinez-Mendoza et al., 2023). The potential feedstocks of particular interest for the present study are bagasse from the US state of Louisiana and sugarcane straws from the Valle de Cauca region of Colombia.

Sugarcane bagasse is commonly used to provide the electrical and thermal energy requirements of sugar mills (Kim & Day, 2011). However, there is also usually an energy surplus (Ungureanu et al., 2022) and excess bagasse would be available for other applications. In the US state of Louisiana, which houses the largest commercial sugarcane industry in the US, it is estimated that 0.32-0.59 million tons of excess bagasse is available annually (Kim & Day, 2011).

Traditionally, sugarcane straw is an agricultural residue with limited applications and is often burned in the fields (Flórez-Pardo et al., 2018; Santiago-De La Rosa et al., 2018). The Valle de Cauca region of Colombia, a prominent area for sugarcane cultivation, produces approximately 1.82 million tons of sugarcane straws annually (Martinez-Mendoza et al., 2023).

2.2 Biomass Handling Challenges

Agglomeration is a commonly observed phenomenon in various industries, where particles demonstrate a tendency to adhere to each other (Palzer, 2011), potentially introducing handling difficulties. Some biomass materials, in particular shredded paper, are known to possess extreme particle shapes, which causes severe handling challenges (Owonikoko et al., 2010). Static electricity can also cause the formation of agglomeration, although this is mostly observed for very fine particles at micron or sub-micron sizes (Deng et al., 2023; Šupuk et al., 2012). Shredded paper is also known to easily form clumps (Elliston et al., 2013; Windsor & Bate, 2019), and associated

handling issues, such as trapped clumps in reaction vessels, have been described (Elliston et al., 2013). Particle size and shape are important factors affecting handleability (Ilic et al., 2018), and it has been cited that traditional sieve analysis is insufficient for stringy and fibrous materials, and techniques such as image analysis and 3-D scanning are needed to study particle shape (Lam & Sokhansanj, 2014; Ramírez-Gómez, 2016).

2.3 Slagging/Fouling Issues

Potassium is known to be the most problematic element in terms of causing ash-related issues during combustion (Steenari et al., 2009). The use of additives is a fairly common measure to mitigate slagging issues. Calcium carbonate (Llorente et al., 2008; Steenari et al., 2009) and kaolin (Llorente et al., 2008; Morris et al., 2022; Roberts et al., 2019; Steenari & Lindqvist, 1998) are among the additives that have been widely studied and used to reduce slagging. Steenari et al. (2009) studied the use of both calcium carbonate and kaolin as an additive up to 30% of fuel weight, with the caveat that high percentages of additives are unlikely to be used in practice due to economic reasons. With potassium being a particularly problematic element, one of the primary mechanisms to mitigate slagging issues by these additives is by reacting with low-temperature-melting potassium-containing compounds (mainly potassium chloride) into less problematic species with higher melting points (L. Wang et al., 2014).

As discussed in Section 2.1.2, both calcium carbonate and kaolin are used as fillers in the cardboard manufacturing process, and it follows that cardboard materials could potentially be used as both a fuel and an additive for tackling ash-related issues, which could have a synergistic impact of using a waste to improve economics and combustion performance. However, the use of cardboard as a fuel and additive for combustion has not been investigated in literature before, representing a significant knowledge gap.

2.4 Char Morphology and Burnout Prediction

2.4.1 Background

The study of the structure of char, an intermediate combustion product, has been widely used in academia and industry to predict combustion behaviour. Lester et al. (2018) found that thick-walled chars tended to be a problem particularly as their combustion rates were much slower than those of thin-walled chars. Regardless of fuel type, the transformation of particles during combustion generally consists of three stages (Avila et al., 2011):

1. Pyrolysis or devolatilisation, where the particle may soften and swell and eject gaseous products consisting mostly of moisture and hydrocarbons, resulting in a carbon-rich char.
2. Char conversion, where the char particles undergo combustion in the presence of an oxidant gas.
3. Deposition of ash.

There are a large number of studies on coal char and how their morphology can be used to predict combustion behaviour (Lester et al., 2010). Although slight differences in classification systems exist, the following discriminating features have been commonly used to classify coal char structures (Lester et al., 2010):

1. **Wall thickness**

   Chars can be seen as either thin-walled or thick-walled, where thin-walled chars are derived from more reactive materials and would burn out more quickly (Lester et al., 2018).
2. **Char voidage and porosity**

   The char voidage and porosity are indicators of how fast a char may burn out. Chars can be classified as either spheres (single-pore structures) or networks (multi-pore structures).
3. **Fused and unfused structures**

   During pyrolysis or combustion, some coal particles would form new, potentially anisotropic structures (known as unfused), while some

'unreactive' particles would remain a relatively isotropic solid material with little sign of deformation (known as fused).

Using these discriminating features, coal chars are generally classified into six main morphologies, as shown in Figure 2-1 (Lester et al., 2010; Perkins et al., 2020).

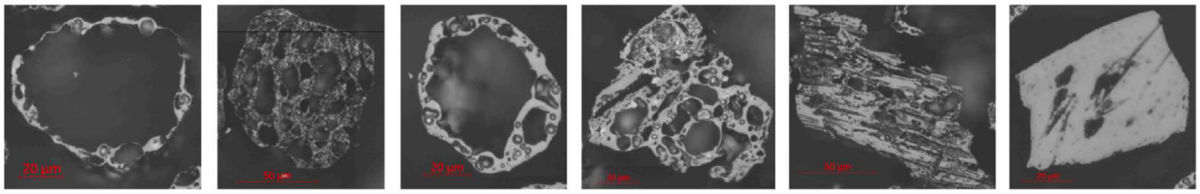

Figure 2-1 The six main morphologies of coal chars (Lester et al., 2010; Perkins et al., 2020)

While char morphology is a well-established technique for coal that has been used for decades, the study of biomass char, particularly for the purpose of combustion characterisation (Valentim, 2020), is a relatively new subject. A reasonable number of studies on biomass char morphology have been published in recent years, indicating a growing interest in the subject from academia and industry (Avila et al., 2011; Guizani et al., 2017; Güleç et al., 2022; Lester et al., 2018; Pang et al., 2018).

In addition, a formal biomass char classification system has been developed by Lester *et al.* (2018). It was concluded that for biomass chars:

1. Wall thickness is an applicable variable for biomass chars as well as coal chars.
2. The concept of char voidage and porosity can be adapted for biomass chars. Biomass chars demonstrate two types of porosity: a) retained cellular structure based on the initial cell wall (W.-H. Chen et al., 2014) or b) a structure consisting of open rounded pores similar to 'spheres' in traditional coal char classification. Cellular structures are indicative of controlled devolatilisation, while porous structures indicate a less controllable and more chaotic devolatilisation process.
3. The concept of fused and unfused structures is not useful for distinguishing biomass chars, as virtually all biomass particles consist of anisotropic structures (Guo et al., 2012).

4. Aspect ratio (defined as length divided by width) should be introduced as a new classification parameter for biomass chars. Biomass particles typically have much higher aspect ratios compared to coal (Guo et al., 2012). It is also known that high-aspect-ratio particles burn faster than low-aspect-ratio particles (Momeni et al., 2013) and also have superior aerodynamic properties (Lester et al., 2018). Therefore, aspect ratio was introduced as a new distinguishing feature for biomass char, with particles with aspect ratio <3 classed as low aspect ratio and particles with aspect ratio >3 classed as high aspect ratio.

Past studies on char morphology have used several methods to produce chars for subsequent analysis by microscopy. Most research on coal char morphology has been conducted under pulverised fuel (PF) conditions, and there are considerably fewer studies on char from fluidised bed or other combustion systems (Valentim, 2020), although methods to simulate both PF and fluidised bed combustion have been described.

A drop-tube furnace (DTF) is a commonly used tool to simulate PF combustion where combustion is in the milli-second range at temperatures up to 300 °C. The temperature, residence time and oxygen level can also be controlled (Bridge, 2018; Cloke et al., 2002; Tao Wu et al., 2006). One method to simulate a fluidised bed or stoker furnace is by using a muffle furnace to rapidly heat a biomass/coal sample in a ceramic crucible at 900-1000°C, which would allow pyrolysis to occur but also minimise combustion by limiting air ingression (Avila et al., 2011; Lester et al., 2018).

While the char morphology of coal is a proven and mature technique, the application of this technique to biomass is a relatively new development. Therefore, there is value in studying the char morphology of additional types of biomass materials. In particular, the char morphology of cardboard materials has not been studied before.

2.4.2 Burnout Prediction

Char morphology is a highly important topic for the power generation industry, as it is well-documented that the relative abundance of char structures has clear effects on fuel burnout (Tao Wu et al., 2006). The accurate prediction of burnout is valuable

as poor burnout can lead to several undesired effects, including reduced efficiency (Wells & Smoot, 1991), increased particulate emissions and wastes (Perkins, 2020), and increased NO_x emissions (Lv et al., 2023). Therefore, an efficient and accurate burnout prediction method would allow the assessment of the performance of fuels prior to purchase and contribute to the commercial decisions of which purchase option to pursue.

Several widely accepted burnout models have been developed using a combination of kinetic models and char morphology (Cloke et al., 2003; Hurt et al., 1998; Hurt & Calo, 2001). The Carbon Burnout Kinetic Model (CBK) developed by Hurt et al. (R. Hurt et al., 1998) is the most commonly used kinetic model for this purpose. However, the accuracy of these models is known to be highly sensitive to the input distributions of particle size and density (Maloney et al., 2005). To accurately represent char combustion, a wide array of transport and kinetic parameters also need to be determined (Hurt et al., 1998; Ma & Mitchell, 2009), and the resulting models are usually highly complex.

To simplify these complexities, a novel burnout model was developed by Perkins (2020) to simulate char burnout. This model uses char images to simulate burnout by iteratively eroding individual char particles, thus avoiding complex kinetics calculations. It was also shown that the results of this model have a good correlation between experimentally obtained and simulated burnout results following the refinement of the model with experimental data. In addition, this method has been successfully applied to biomass by Williams et al. (2024). By analysing char particles of coal, burnout profiles of the various char morphology classes were developed, which could be used in combination with the morphology data of any particular char sample to predict burnout behaviour. However, this burnout model has not been applied to cardboard materials to date.

2.5 Significance of Particle Shape in Particle Flow and Combustion

Particle shape can influence the physical properties of biomass materials, including in contexts relevant to large-scale power generation from biomass, such as pneumatic conveying, mill classification and combustion processes.

When considering the particle flow of spherical particles in the Stokes regime (where the Reynolds number is low), the Stokes number, which is a measure of the ability of particles to follow the surrounding fluid flow, can be represented by equation (2.1) (Toneva et al., 2011). A low Stokes number indicates that the particle is able to follow the flow of the fluid closely, whereas a high Stokes number indicates that the movement of the particle is dominated by inertia and that the particle would be unable to follow the flow of the fluid.

$$Stk = \frac{\rho_P d_P^2 u_0}{18\eta B} \quad \textbf{(2.1)}$$

Where Stk is the Stokes number (dimensionless); ρ_P is the particle density (kg/m^3); d_P is the particle size (m); u_0 is the velocity of the particle far away from an obstacle (m/s); η is the fluid dynamic viscosity (Pa s); and B is a characteristic system dimension (m).

However, equation (2.1) assumes that the particle is a perfect sphere. For non-spherical particles, a shape factor may be used to correct for the effects of particle shape (Leith, 1987). It has been shown by Xie & Zhang (2001) that the Stokes shape factor (k_v) can be correlated with sphericity for a wide range of particle shapes, as shown in equation (2.2). Equation (2.2) also demonstrates that compared to perfectly spherical particles with the same volume, particles with a lower sphericity would have a lower drag force and thus superior aerodynamic performance. This is also consistent with the findings by Mandø et al. (2010), who stated that large biomass particles with low sphericities can have aerodynamic properties similar to those of much smaller coal particles, which typically have higher values of sphericity.

$$k_v = \phi^{0.83} \quad \textbf{(2.2)}$$

Where k_v is the Stokes shape factor; and ϕ is the particle sphericity.

Particle shape is known to be an important factor in combustion modelling. It has been noted by multiple authors (Bharadwaj et al., 2004; Lu et al., 2008; Mandø et al., 2010; Riaza et al., 2020) that for the modelling of biomass combustion, it is

unsatisfactory to assume that all particles are spherical and particle shape must be taken into account.

Many authors have developed comprehensive combustion models for biomass. Lu et al. (2008) used a single-particle reactor to develop a combustion model of biomass particles with idealised shapes and also postulated that by using particle shape statistics such as aspect ratio, volume and surface area, the model could be extended to cover particles of any shape. Gubba et al. (2011) developed a Computational Fluid Dynamics (CFD) model that considered the influence of particle shape and internal thermal gradients of biomass particles. Yin et al. (2004) developed a numerical combustion model which includes a widely used burning enhancement factor to represent the increase in surface reaction rate of a non-spherical particle compared to a spherical particle of equivalent volume, as shown in equation (2.3). Li and Zhang (2016) further refined this empirical expression between the burning enhancement factor and particle sphericity for specific types of shapes.

$$\theta_{en} = \frac{0.3\phi + 0.7}{\phi} \qquad \textbf{(2.3)}$$

Where θ_{en} *is the burning enhacement factor.*

As discussed in Section 2.4.2, burnout models such as the Carbon Burnout Kinetic Model (CBK) (R. Hurt et al., 1998) require a wide array of transport and kinetic parameters to be determined (Ma & Mitchell, 2009), which are dependent on particle shape. In addition, char morphology, which is traditionally also used for coal to predict carbon burnout and combustion behaviour, has been extended by Lester et al. (2018) to include aspect ratio as a discriminating feature to classify biomass chars. The topic of char morphology was previously discussed in Section 2.4.

Despite the importance of particle shape in particle flow and combustion, the availability of biomass shape data is limited as it is difficult to obtain for large sample sizes, and most of the available data on biomass shape are obtained using microscopy (Bharadwaj et al., 2004; Guo et al., 2012) or other 2D imaging techniques (Gil et al., 2014). These techniques are usually limited by a small sample size and the inability to accurately measure 3D shape factors such as sphericity. Thus, there is substantial

value in studying the particle shape of additional types of biomass and using techniques that can measure 3D shape factors, such as the Camsizer, particularly for new fuels such as cardboard.

Many existing combustion models assume that particle shape remains constant during combustion (J. Li & Zhang, 2016; Lu et al., 2008), which may not be a valid assumption in all situations as particle breakage and change in shape can occur. If this assumption is found to be invalid in some situations, then the applicability of these models should be studied in greater detail, as changes in particle shape would affect the trajectories and residence time of particles, with factors such as shape, size and density being known as important variables for fluid dynamics modelling (Zahirović et al., 2010).

Several authors have attempted to study the change in particle shape experimentally (Lu et al., 2008; Momeni et al., 2013; Riaza et al., 2020). It was concluded by Riaza et al. (2020) that during devolatilisation, particle size and shape appear to change only slightly and swelling was rarely observed, while during char combustion, changes are more pronounced and particles become more rounded in most cases. In addition, these experiments, which focus on using imaging techniques to study the combustion of single particles, are limited by a small sample size, and it is not always clear how and whether the results from single particle studies are applicable at larger scales. For example, it was noted by Toneva, Wirth and Peukert (2011) that in order to generalise the findings of idealised single-particle experiments, multiphase interactions need to be taken into account. Single-particle studies are also only feasible with relatively large particle sizes. For example, the minimum particle sizes used in several such studies are 300 µm (Riaza et al., 2020), 1.31 mm (Momeni et al., 2013) and 3 mm (Lu et al., 2008). Therefore, there is value in studying the change in particle shape statistics during combustion at larger scales and for a wider particle size range than what is possible in single-particle studies.

2.6 Biomass Drying

Biomass drying is an essential process in biomass power generation, as it delivers multiple crucial benefits, including increased calorific value of the fuel, more complete combustion, reduced carbon monoxide (CO) emissions and fly ash

(Shirinbakhsh & Amidpour, 2017). The development of energy-efficient drying systems is critical for biomass power generation, as up to 93% of the total specific energy consumption of pellet production is associated with the thermal energy used for drying (Thek & Obernberger, 2012). It has also been claimed that due to the energy-intensive nature of drying operations, drying accounts for approximately 25% of the total cost in wood pelleting plants (Frodeson et al., 2013), showing that the economic performance of pelleting operations can be significantly improved if more energy-efficient drying systems are developed.

2.6.1 Theory and Modelling of Biomass Drying

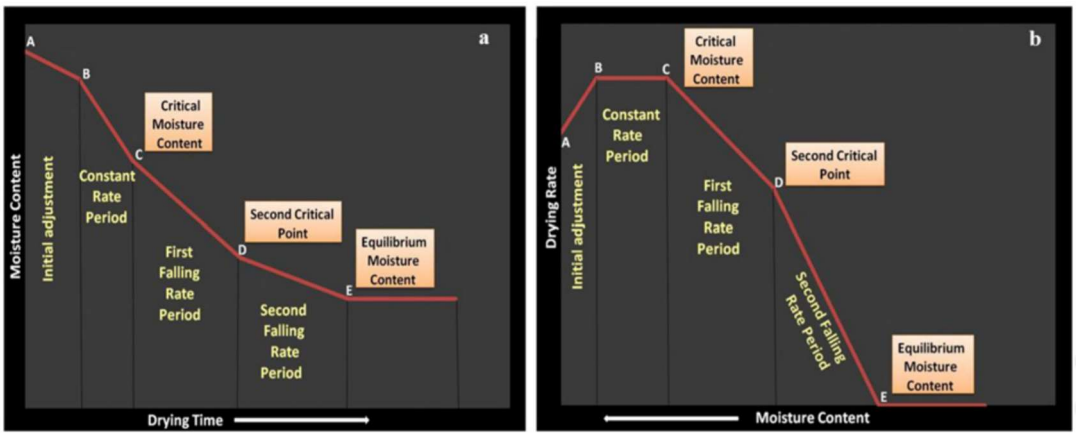

Figure 2-2 Drying model illustrated by plots of (a) moisture content against drying time and (b) drying rate against moisture content (Lachman et al., 1986)

It is well-established in the literature that drying consists of a preheating period, a constant drying-rate period, and one or more falling drying-rate periods as shown in Figure 2-2. During the constant drying-rate period, evaporation of unbound water at the particle surface occurs while during the falling drying-rate period, the evaporation of bound water within the particle occurs, and the falling drying rate is caused by the increased mass and heat transfer resistances (Schlünder, 2004). This type of model is found to be accurate for biomass drying using a range of drying methods and has been used by multiple authors (Schlünder, 2004; Soysal, 2004; Tunde-Akintunde et al., 2005), although most of these studies focus on food processing applications rather than bioenergy applications. A study by Sahni & Chaudhuri (2012) reviewing existing modelling approaches in drying also illustrated

that other complex and detailed models based on the physical processes of drying and experimental findings have been developed by multiple authors.

2.6.2 Biomass Drying Technologies

The main types of available drying technologies for biomass are reviewed in this Section to provide the relevant context for the development of a new novel low-energy biomass drying solution.

2.6.2.1 Rotary Drum Dryer

As a common dryer type for biomass, there is an abundance of existing research on the rotary drum dryer, which has also been referred to as the rotary cascade dryer and drum dryer by different authors. A rotary drum dryer consists of a large, inclined rotating cylindrical drum (Yi et al., 2019), as shown in Figure 2-3. A series of flights on the inner surface of the cylinder is used to improve heat and mass transfer, and both direct and indirect heating can be used (Del Giudice et al., 2019). Hot flue gas or air can be used as the drying medium. Both concurrent and countercurrent types have been described in the literature. A key advantage of the rotary drum dryer is its low cost of maintenance and reasonably low specific energy consumption compared to other dryer types (Meza et al., 2008). It is well-established from multiple literature sources that the rotary drum dryer is one of the most commonly used dryer types for biomass drying (Fagernäs et al., 2010; Thek & Obernberger, 2012).

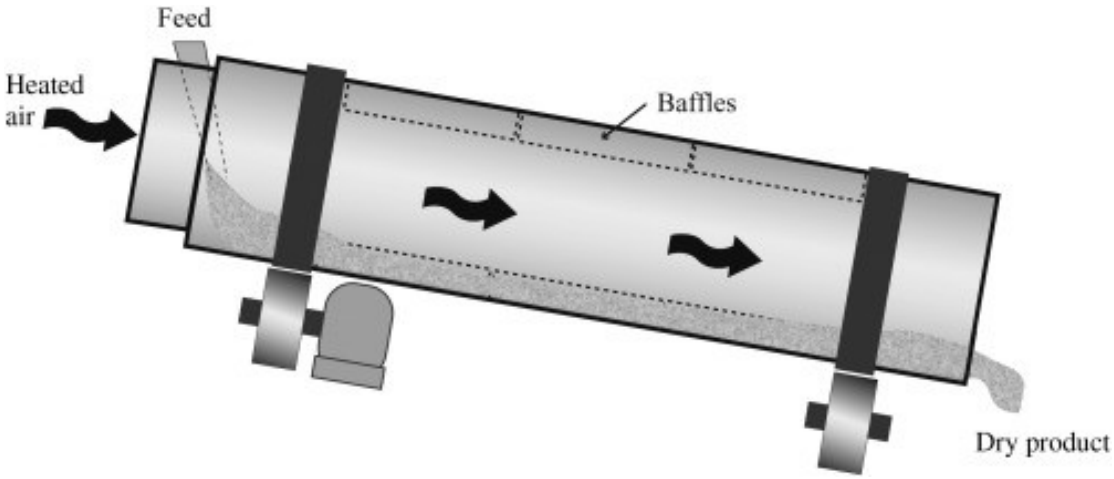

Figure 2-3 Illustration of a rotary drum dryer (Kerr, 2019)

2.6.2.2 Tube Bundle Dryer

The tube bundle dryer consists of an indirectly heated tube bundle. The heating medium flows through the tube bundle, while the material flows through the drum between the tubes, with good heat transfer characteristics obtained by the recurrent trickling of the material using transport blades (Thek & Obernberger, 2012). This type of dryer has low emissions and low energy consumption due to a small exhaust volume and a low level of fire hazard, although capital costs can be high due to the tubing requirements, rotating seals, and other components (Fagernäs et al., 2010). The energy benefits of the tube bundle dryer would be more pronounced in situations where a suitable source of steam is available.

2.6.2.3 Belt Dryer

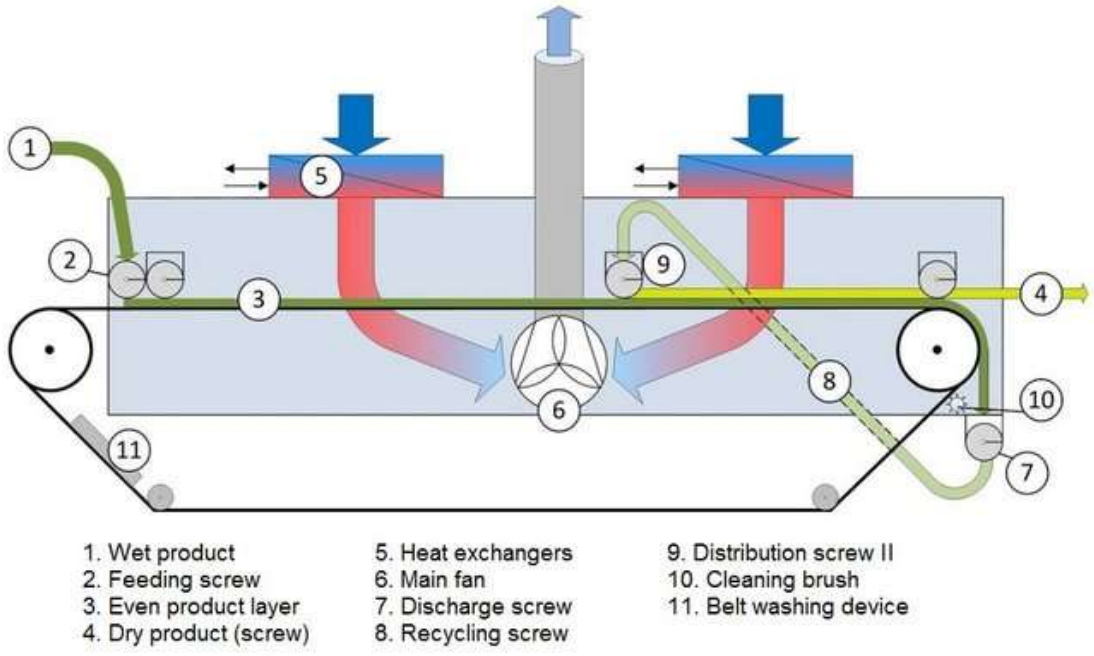

Figure 2-4 Illustration of a belt dryer (Turunen, 2017)

In a belt dryer (Figure 2-4), the biomass material is spread on a moving perforated conveyor and fans blow the drying medium through the belt and the biomass material (Li et al., 2012). It has also been referred to as the conveyor dryer, grate dryer, moving bed dryer and band conveyor dryer by different authors. Compared to other dryer types, the residence time, and moisture content and maximum temperature of the product can be easily controlled (Fagernäs et al., 2010). Belt

dryers are generally significantly larger and more expensive than tube bundle and rotary drum dryers of the same capacity, but these drawbacks could potentially be compensated by the lower drying temperature (Thek & Obernberger, 2012). Thus, belt dryers are better suited to take advantage of low-grade heat if they are available from other processes (Li et al., 2012).

2.6.2.4 Fluidised Bed Dryer

In fluidised bed dryers (Figure 2-5), the drying medium is blown upward through a bed of biomass particles so that all particles are suspended. Excellent heat and mass transfer characteristics can be achieved. Fluidised bed dryers have been used for drying a large range of agricultural products, including brown rice, corn, carrots, chilli, and others (Yahya et al., 2017). However, the use of the fluidised bed dryer for biomass energy remains limited (Fagernäs et al., 2010). The non-uniform shape and low density of biomass particles present a challenge for biomass drying in fluidised beds, as stable fluidisation is difficult to achieve (Y. Liu et al., 2014).

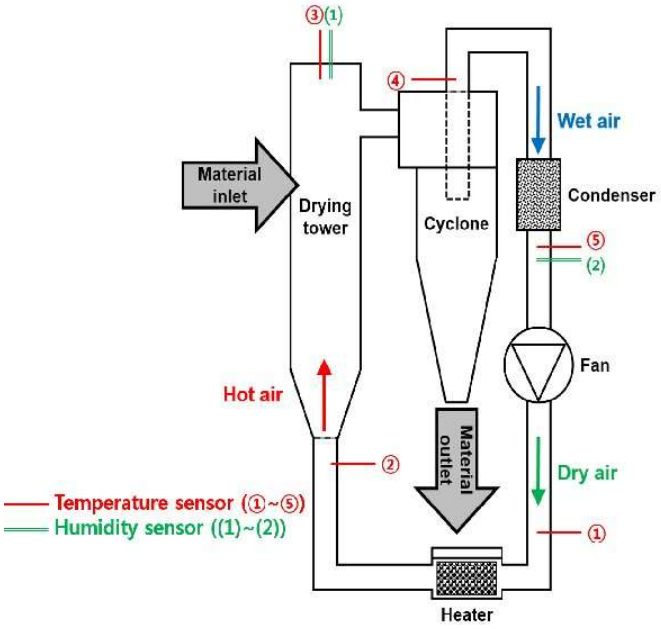

Figure 2-5 Illustration of a fluidised bed dryer for wood (Park et al., 2016)

2.6.2.5 Solar Drying

The advantages of using solar energy for drying include reducing or eliminating fuel consumption and improving the environmental performance of the plant, while the

disadvantages include a longer drying duration and dependence on weather conditions and time of day (Norkulova et al., 2016). These major disadvantages of solar drying could be mitigated by including thermal storage in the dryer design, although a backup heater may still be necessary, as shown in the study by Madhlopa & Ngwalo (2007).

The solar kiln is a common drying method using solar energy, where solar energy is directed into an insulated chamber via several possible methods, including a greenhouse system and solar collectors (Ugwu et al., 2015). A detailed mathematical model of a solar kiln was developed by Khouya & Draoui (2019). Aside from designing dedicated drying systems using solar energy, it is also possible to incorporate the use of solar energy into existing designs. There have been several studies on solar-assisted belt dryers (Shirinbakhsh & Amidpour, 2017) and solar-assisted fluidised bed dryers (Ceylan & Gürel, 2016; Yahya et al., 2017).

Few solar driers have been installed in large-scale bioenergy plants despite the considerable effort expended on the development of solar drying systems in the laboratory stage (Yi et al., 2019). This is primarily due to the high capital costs and the requirement of large areas of land to utilise solar power (Kabir et al., 2018).

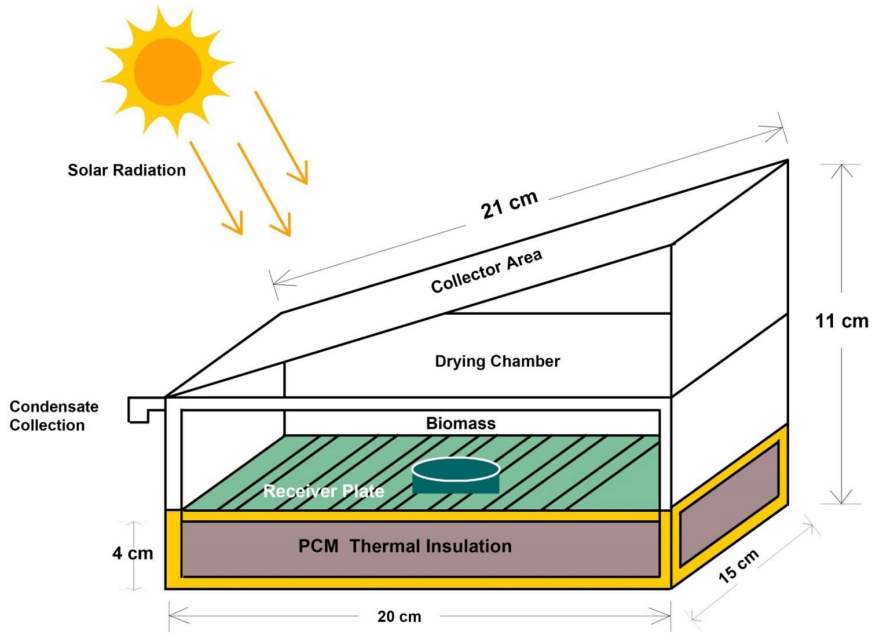

Figure 2-6 Illustration of a passive solar dryer (Kalaiselvan & Mathimani, 2022)

2.6.2.6 Natural Drying

Natural drying refers to the removal of water from biomass through evaporation by exposing it to the atmosphere, taking advantage of the environmental conditions without incurring an energy cost. It has been widely used as an initial processing step for raw wood and could reduce the moisture content to 30% or lower (Labbé et al., 2018), and it is a viable and effective method to improve the quality and energy efficiency of wood-based fuels (Röser et al., 2011). Although natural drying does not require any direct energy input, the duration needed for natural drying could be significant and it would incur a cost as immobilised capital (Labbé et al., 2018).

Despite being widely used to reduce the moisture content of woody biomass feedstocks, the use of natural drying for other biomass types, such as straws and industrial residues, has not been widely reported. Although baling and briquetting for the purpose of long-term storage are common operations in industry, these are primarily for the purpose of long-term storage and the material is usually already at low moisture contents before the baling or briquetting process (Darr & Shah, 2012; Kpalo et al., 2020). If high-moisture-content biomass is left exposed to the atmosphere for significant periods of time for the purpose of natural drying, it is likely that fungal and microbial growth would occur and could potentially become a health hazard (Kaaya & Kyamuhangire, 2010), representing a major limitation of natural drying.

2.7 Biomass Pasteurisation

2.7.1 Traditional Uses and Practices of Pasteurisation

Pasteurisation is a process named after Louis Pasteur, who discovered that heating wine to fairly low temperatures (such as 60°C) can extend its shelf life by destroying spoilage organisms (Holsinger et al., 1997). Unlike sterilisation, which aims to completely kill all microorganisms, pasteurisation aims to reduce their number to a sufficient extent so that they are unlikely to cause disease or other hazards (The National Advisory Committee on Microbiological Criteria for Foods, 2006; Watts, 2016). In addition to mitigating the microbial threat, pasteurisation also has the effect

of inactivating enzymes, some of which can have detrimental effects on product quality (Deeth, 2021).

Extending the shelf life of milk is one of the most well-known and common uses of pasteurisation and many studies are available on the topic of milk pasteurisation. Multiple strategies of milk pasteurisation in terms of temperature and duration exist, including thermisation, low-temperature long-time (LTLT), high-temperature short-time (HTST), and ultra-high-temperature (UHT) pasteurisation. The conditions used in these methods are summarised in Table 2-1.

Method	Conditions	Reference
Thermisation (milk used for cheese production and not direct consumption)	65°C for no less than 16 seconds	(Hudson et al., 2003)
Low-temperature long-time (LTLT)	63°C for 30 mins	(Holsinger et al., 1997; Sarkar, 2015)
High-temperature short-time (HTST)	71°C for at least 15 seconds	(Holsinger et al., 1997; Ranieri et al., 2009)
Ultra-high-temperature (UHT)	135 to 150°C for a few seconds	(Chavan et al., 2011)

Table 2-1 Common pasteurisation methods for milk

Although traditional heat treatment via direct or indirect heating is the most common form of pasteurisation, other methods are also in use with varying levels of maturity, including ultrasound, irradiation, microwave, ohmic heating and ultraviolet light (Barbosa-Cánovas & Bermúdez-Aguirre, 2010). The National Advisory Committee on Microbiological Criteria for Foods (2006) developed a set of principles for establishing the equivalence of alternative methods of pasteurisation. It was proposed that time-temperature parameters are critical for all heat treatment processes, which includes

both conventional oven and microwave pasteurisation, and the heat transfer properties of the material also needs to be considered.

2.7.2 Use of Pasteurisation for Non-food Applications

Since the traditional use of pasteurisation is for extending the shelf life of foodstuffs, the primary goal is traditionally the thermal inactivation of microbial pathogens such as *E. coli* (Hudson et al., 2003). However, the goal and hazards to be considered for non-food applications of pasteurisation could differ from those of traditional pasteurisation, for example, the severity of the pasteurisation required and the types of microorganisms of concern.

Pasteurisation of biomass has only been explored for a few applications. One of the main areas is as a pre-treatment before other processes. González-Bautista et al. (2020) explored the effect of pasteurisation conditions on dephenolisation in sugarcane bagasse for ethanol production and they observed that changing the specific pasteurisation conditions from 70 to 75 °C and from 5 to 10 h favoured dephenolisation of lignocellulose. Pasteurisation above 80 ℃ has been shown to effectively kill mesophilic microorganisms in wheat straw, improving the colonisation and selective degradation of *I. lacteus* and increasing sugar yield (Niu et al., 2023). Ferrero et al. (2009) observed that microorganism activity would decrease in wood chip piles when the temperature is above 80°C.

However, there are no studies to date which explore the potential of combining the pasteurisation of biomass with natural drying to extend storage potential and reduce drying energy by suppressing microbial and fungal growth.

2.7.3 Post-pasteurisation storage

The growth of microorganisms and spoilage can occur even after effective pasteurisation and effective post-pasteurisation storage strategies are needed. In general, lower temperatures would allow the pasteurised material to remain in a sufficiently sterile condition for longer (Lewis, 2010). Post-pasteurisation contamination (PPC) refers to the introduction of microorganisms after pasteurisation and is a known issue in the food industry (H. Deeth, 2010). Pasteurisation may also have the undesired effect of eliminating competition, as both

harmful and non-harmful microorganisms are inactivated, and harmful organisms (either retained or introduced due to PPC) may grow to high numbers as the competition from non-harmful organisms is removed by pasteurisation (The National Advisory Committee on Microbiological Criteria for Foods, 2006).

2.7.4 Microorganisms of Concern for Biomass

Although both fungi and bacteria are expected to be present on biomass, fungi are generally expected to be more important for the purpose of studying potential health hazards as they are superior to bacteria in metabolising the main compounds of most types of biomass (Graham, 2015; Noll & Jirjis, 2012). The most common fungi found in biomass include those of the genera *Aspergillus*, *Penicillum*, *Mucor*, *Trichoderma*, *Fusarium* and *Rhizopus* (Mirski et al., 2023). The main cause of potential health hazards originates from the release of spores, which may be inhaled or ingested by workers or deposited on their skin (Grisoli et al., 2009).

The main types of microorganisms of concern with regard to health risks are pathogenic fungi (e.g. *Candida*, *Aspergillus*, *Mucoraceae*, *Geotrichum*) and opportunistic yeast-like fungi (e.g. *Zygomycetes*, *Fusarium* and *Scedosporium*) (Noll & Jirjis, 2012). Among these, fungi species of the genus *Aspergillus* (especially *Aspergillus fumigatus*) have been identified as one of the greatest health risks of biomass storage (Lieskovský & Gejdoš, 2023; Mullerova, 2014).

2.7.5 Conventional Oven Pasteurisation

2.7.5.1 Principles and characteristics

Conventional oven pasteurisation uses hot air to provide heating to the material. The advantages of such a system include the simplicity of operation and a relatively low cost (Megías-Pérez et al., 2014). Slow heating rates and heat transfer limitations are a major problem when processing solids, which could result in the centre of the material failing to hit the target temperature for a sufficient period, as the process relies on thermal diffusivity from the surface of the material (Regier et al., 2009; Stanley & Petersen, 2017).

2.7.5.2 Effect of Heat Treatment on Microorganisms

Pasteurisation is usually insufficient to kill bacterial spores (dormant structures which are more resistant to heat and other stress treatments), while vegetative cells (actively growing cells which are less resistant to stress) are usually eliminated (de Vries, 2006).

More severe pasteurisation conditions do not always result in better suppression of microorganism growth. For example, Ranieri et al. (Ranieri et al., 2009) found that when conducting HTST pasteurisation of milk at conditions more severe than those typically used (see Table 2-1), a higher level of bacterial growth was observed during refrigerated storage. This indicates the need to choose appropriate pasteurisations specific to the type of material and the extent of microorganism elimination required.

2.7.6 Microwave Pasteurisation

2.7.6.1 Principles and Characteristics of Microwave Processing

Microwave processing can be defined as the use of electromagnetic waves at specific frequencies to generate heat in a material (The National Advisory Committee on Microbiological Criteria for Foods, 2006). As a pasteurisation method, it has been used for milk, juice, egg and other foodstuffs commercially (Barbosa-Cánovas & Bermúdez-Aguirre, 2010; The National Advisory Committee on Microbiological Criteria for Foods, 2006).

When a material is exposed to microwaves, microwaves are absorbed by polar molecules (primarily water in the case of biomass) and heat is generated (Barbosa-Cánovas & Bermúdez-Aguirre, 2010). A unique nature of microwaves is that heat is generated inside the material, enabling volumetric heating as microwaves can penetrate the body of the material, in contrast to conventional oven heating, where heat is transmitted from the outside of the material to the centre through convection and conduction (Gaukel et al., 2017).

A key advantage of microwave processing is a very fast heating rate and targeted heating ability compared to conventional heat treatment (Barbosa-Cánovas & Bermúdez-Aguirre, 2010; Stanley & Petersen, 2017). However, several limitations

have also been reported in the literature. A key issue is the unevenness in the microwave field inside the cavity, which can result in non-uniform heating and the presence of 'hot' and 'cold' spots (Birla & Pitchai, 2017; Gaukel et al., 2017; Wäppling Raaholt & Isaksson, 2017). The presence of hot spots also represents a significant fire hazard (Siddique et al., 2022; Yadav et al., 2021). Factors that contribute to uneven heating by microwaves include standing wave patterns within the material, edge and corner overheating due to scattering phenomena, and cavity design (Wäppling Raaholt & Isaksson, 2017). In addition, conventional thermocouples cannot be used to measure temperature distributions during heating, as microwaves would interfere with their operation, and other measurement options such as fibre optic probes, infrared thermography and microwave radiometry are needed (Knoerzer et al., 2017).

2.7.6.2 Effect of microwave treatment on microorganisms

Similar to heat treatment via convection and/or conduction, microwave treatment is also recognised to be effective in eliminating vegetative cells of bacteria, yeast and moulds, while the elimination of spores is more difficult (Raso & Barbosa-Cánovas, 2003). In general, microwave processing can be regarded as a type of heat treatment, and the thermal effects on microorganisms discussed in Section 2.7.5.2 also apply to microwave processing (The National Advisory Committee on Microbiological Criteria for Foods, 2006).

In addition to the effects of elevated temperatures caused by microwave irradiation, microwaves are known to have additional effects on microorganisms and may also cause other physical changes in the pasteurised material, potentially providing a significant enhancement or magnification of thermal effects (Chandrasekaran et al., 2013). In a study comparing the effects of UHT and microwave treatment on milk, Clare et al. (2005) found that when under equivalent heat processing conditions (heating rate and peak temperature), both regimes achieved near-complete elimination of microorganism growth, although microwave treatment resulted in less substantial changes in flavour.

2.8 Biomass Densification

Due to their low bulk density, biomass materials need to be densified to reduce transport costs and increase their energy density, with the most common form of densification being pelletisation. The aim of pelleting is to provide a medium which can bind biomass particles during transport while also being able to break down to the correct particle size for combustion during milling for pulverised fuel power generation (Williams et al., 2015, 2016). This Section of the literature review covers the current research and developments in pellet operations and production, including the effects of feedstock properties and densification process variables.

2.8.1 Background and Principles

Pellet mills designed for pelletising wood are commonly used by large-scale pellet producers for densifying biomass (Thek & Obernberger, 2012). The briquette press and screw extruder have also been described as fairly common methods for densifying biomass (Tumuluru et al., 2011).

The manufacturing and use of wood pellets is a fairly mature industry and there are multiple established international standards in pellet quality. BS EN ISO 17225-2:2021 (The British Standards Institution, 2021b) classifies wood pellets into grades and gives a detailed specification of the required properties. There is also a similar standard for non-woody pellets, namely BS EN ISO 17225-6:2021 (The British Standards Institution, 2021c). A standardised pellet durability testing method (The British Standards Institution, 2015d) has also been developed, which involves using a rotating tumble drum to expose the pellet sample to mechanical stress and measuring the percentage of pellets that survive the tumbling procedure.

Biomass particles undergo complex transformations when exposed to high pressures during densification. Tumuluru et al. (2011) gave a comprehensive summary of the deformation and bonding mechanisms of biomass particles under compression, as shown in Figure 2-7. The binding forces between individual particles in densified products are categorised into five groups: (i) solid bridges, (ii) attraction forces between particles, (iii) mechanical interlocking bonds, (iv) adhesion and cohesion forces, (v) interfacial forces and capillary pressure (Kaliyan & Morey, 2009b).

Scanning Electron Microscopy (SEM) images of densified biomass suggest that solid bridges are the dominant mode of bonding between particles (Kaliyan & Morey, 2010). The natural binders in biomass are water-soluble carbohydrates, lignin, protein, starch and fat, which are activated either under high pressures in the presence of water (water-soluble carbohydrates) or under high temperatures (lignin and others) (Kaliyan & Morey, 2010). Lignin is the most prevalent among these natural binders in most biomass types and plays a crucial role in biomass densification. Under good densification conditions, this lignin would partially melt and act as a binder for the densified product (Kaliyan & Morey, 2010). The role of lignin as a binder is illustrated by the findings of Serrano et al. (2011), who found that a moisture content of 19% was necessary to achieve good agglomeration when using barley straw, while a moisture content of 12% is sufficient for blends of barley straw and pine sawdust, due to the higher lignin content in pine.

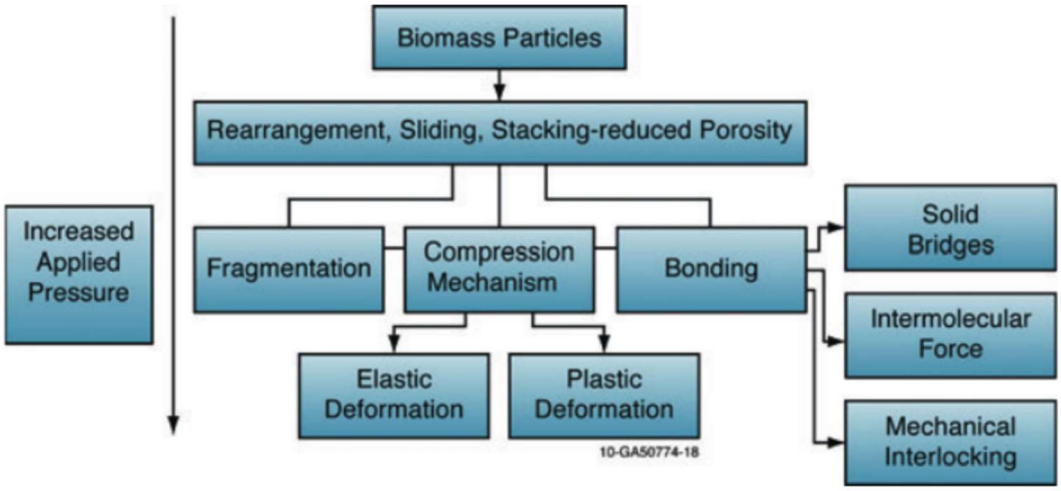

Figure 2-7 Deformation and bonding mechanisms of biomass particles under compression (Tumuluru et al., 2011)

2.8.2 Effects of Feedstock Properties on Pellet Quality

2.8.2.1 Effect of Feed Moisture Content

Water can act as a binder in the pelleting process (Narra et al., 2012). Multiple authors have reported that there is a minimum moisture content in order for pelleting to be successful. Larsson et al. (2008) found that a minimum raw material

moisture content of 13.8% is needed for the continuous production of pellets. Jackson et al. (2016) found that for some grasses, a minimum moisture content of 10% is necessary for pellet formation in a flat die pellet mill and for samples with moisture content <10%, no pellets could be formed.

It was reported by Kaliyan & Morey (2009b) that multiple studies showed that the strength and durability of densified biomass products increased with increasing moisture content up to a maximum value. Larsson et al. (2008) claimed that increasing the moisture content beyond an optimum limit does not improve production but instead leads to other problems, such as a decrease in pellet quality. These results are consistent with the findings by Lisowski et al. (2017), who found that for the densification of three biomass materials, the pellet strength increases when increasing the feedstock moisture content from 10% to 20% but decreases when further increasing the moisture content to 30%. The findings by Serrano et al. (2011) showed when pelletising straw with moisture content in the range of 8-23%, inlet moisture content only correlates weakly with the pellet moisture content, and increasing the inlet moisture content increases the pellet durability. In the study of corn stover densification by Kaliyan & Morey (2009a), it was found that the optimal moisture content is dependent on whether preheating is used. With no preheating, the optimal moisture content is 15-20%, whereas with preheating to 75°C, the optimal moisture content is 10-15%. Narra et al. (2012) conducted pelleting experiments with rye straw and wheat straw at moisture contents at 14-20% and found that the pellets with the highest durability were those at the middle of the range, and pellets with moisture contents at both ends of the range have lower durability. Larsson et al. (2008) found that pellet bulk density is negatively correlated to moisture content in the range of 13-16%.

In summary, the existing literature mostly agrees that while the exact effect of feed moisture content depends on the type of biomass, an optimal feed moisture content exists across different types of biomass, where the pellet durability would decrease if the feed moisture content is either below or above the optimal value.

2.8.2.2 Effect of Particle Size

It is known that particle size is important for binding mechanisms in the pelletisation process and can affect pellet quality (Narra et al., 2012). The density and durability of pellets should be inversely proportional to the particle size due to the larger surface area of small particles (Tumuluru et al., 2011). However, there is some inconsistency in the existing literature on the effect of material particle size on pellet quality. It is also claimed by Kaliyan & Morey (2009b) that finer particle sizes produce pellets with higher strength and durability. The experiments on barley straw by Serrano et al. (2011) showed that using mill screens of 4 and 7 mm (resulting in different particle sizes) had little effect on pellet density. Mani et al. (2006) found that finer particle sizes increase the pellet density for a range of grasses. In terms of the effect of particle size on pellet diameter, Shaw & Tabil (2007) found that particle size has little effect on the expansion of pellets after exiting the die, while pellet density can be increased by decreasing particle size.

2.8.3 Change in Particle Size and Shape during Pelleting

Rezaei et al. (2016) found that ground pellet particles are more circular than ground wood chip particles when milled to similar sizes, and pelletisation reduced the variability in size distribution and particle shape of ground particles. The differences between particle size and shape of milled biomass which has not been pelletised previously and milled pellets suggest that significant changes in particle size and shape are caused by the pelleting process.

In a separate recent study by Rezaei et al. (2024), it was found that pelletisation reduces the particle size, resulting in finer particles in the disintegrated pellets compared to the raw material. Masche et al. (2019) also found that for the pelletisation of pine and beech, particles become more circular and less elongated, mainly due to the breakage of particles across their longest dimension.

Although there are a number of studies on the change in particle size and shape during pelleting, these are mostly focused on wood pellets and it would be valuable to assess whether these results can be extended to other types of biomass.

2.8.4 Pelleting Process Characterisation

The characterisation of the pelleting process is also an important topic as these can determine the cost and capacity of industrial pelleting operations. In a review paper on biomass densification systems by Tumuluru et al. (2011), it was shown that specific pelleting energy has been quite widely studied. Pelletiser current was measured as a proxy for energy consumption by some authors (Holm et al., 2006; Larsson et al., 2008). In particular, Holm et al. (2006) found that pellet mill blockage would occur at high-load conditions, suggesting that the load of the pelletiser (current or power consumption rate) could be used as an indicator of how likely pellet mill blockage and pelleting failure would occur. The specific energy consumption for densifying biomass materials has been reported at 36.8 kWh/t for sawdust and 22-55 kWh/t for straws (Tumuluru et al., 2011).

While the minimisation of energy use is desired, specific pelleting energy does not fully describe the pelleting process and industrial processes would be limited by factors such as power requirements and achievable throughput, which can only be assessed by additional parameters. While there are a good number of studies on the effect of various factors on pellet quality (Carone et al., 2011; X. Cui et al., 2021; Gageanu et al., 2021; Nielsen et al., 2020), the study of pelleting process parameters, other than pelleting energy, represent an underexplored area in the available literature.

Many existing studies also use single pellet presses rather than lab-scale or industrial-scale equipment (Shaw & Tabil, 2007), and it is unclear how applicable the results from single pellet presses would be for industrial applications. The importance of conducting experiments at larger scales is also illustrated by Tumuluru et al. (2011), who presented data showing large differences between reported energy requirements for commercial operations and laboratory results. Some authors (Larsson et al., 2008; Puig-Arnavat et al., 2016) have conducted pelleting experiments at larger scales. However, the number of such studies is limited and it is desirable to obtain additional experimental data from pelleting processes at larger scales for a larger variety of biomass types and feed conditions.

The pelleting of a large range of biomass feedstocks has been studied, including various types of wood, straws, sugarcane bagasse and others (Younis et al., 2018). However, despite the potential of sugarcane straw as a bioenergy resource, there are no in-depth studies of sugarcane straw pelleting behaviour to date. Although some generalisations could be made between the pelleting behaviour of different biomass feedstocks, it is understood that pelleting behaviour is dependent on the exact material type (Holm et al., 2006; Ibitoye et al., 2021). Therefore, there is significant value in further research on the pelleting behaviour of sugarcane straw.

2.9 Pellet Milling

Biomass milling is known to be an energy-intensive process and the energy requirement depends on multiple factors, including the type of milling equipment, initial and final particle size, and the type of material (Tymoszuk et al., 2019). In addition, the milling of biomass pellets is an important topic as it is desirable to minimise energy consumption. Characteristics such as particle size and shape are determined by the milling process, which in turn affects the combustion and flow characteristics of the material.

2.9.1 Change in Particle Size and Shape during Pellet Milling

Biomass pellets need to be milled in power station before combustion, and apart from breaking down the pellets, the pellet constituent particles also typically undergo some level of final particle size reduction (Temmerman et al., 2013).

Williams et al. (2016) observed that for a range of biomass pellets, the milling process does not cause a significant change in particle shape, even for cases where there is a large change in particle size. Based on the comparison of particle size and shape, it was concluded by Rezaei et al. (2016) that the pulverisation of wood pellets typically primarily turns the pellets back into their constituent particles and very little further milling occurs.

Similar to the change in particle size and shape during pelleting (Section 2.8.4), although there are several studies on the change in particle size and shape during pellet milling, these are mostly focused on wood pellets and it would be valuable to assess whether these results can be extended to other types of biomass.

2.9.2 Milling Theory

The von Rittinger's first theory of comminution states that "the energy required for size reduction is proportional to the new surface area generated", and is expressed mathematically in equation (2.4) (von Rittinger, 1867).

$$E_e = K_{VR}\left(\frac{1}{x_2} - \frac{1}{x_1}\right) \quad \textbf{(2.4)}$$

Where E_e is the specific effective milling energy (kWh/ton), K_{VR} is the von Rittinger constant (kWh·mm/ton), x_1 is the 50th (d_{50}) or 80th (d_{80}) percentile of the cumulative particle size distribution before milling (mm), and x_2 is the 50th or 80th percentile of the cumulative particle size distribution after milling (mm). The term ($1/x_2 - 1/x_1$) is also referred to as the von Rittinger parameter.

The von Rittinger theory has been used for the milling of biomass and biomass pellets by multiple authors and was found to fit the experimental results well (Ghorbani et al., 2010; Temmerman et al., 2013; Williams, Lester, et al., 2017). While some authors (Temmerman et al., 2013) have used the d_{50} values for equation (2.4), Williams (2016) used the d_{80} values since it would be closer to the 1 mm size often cited as the maximum size needed for pulverised combustion (Tamura et al., 2014).

2.10 Life Cycle Analysis (LCA) of Biomass Power Generation

2.10.1 The Life Cycle Analysis Technique

Life cycle analysis (LCA) is a well-established technique to help understand the environmental impacts of a product by assessing the entire product life cycle (Guinée et al., 2011). BS EN ISO 14040:2006+A1:2020 (The British Standards Institution, 2020) sets out the principles and framework of LCA, which should consist of the following elements:

- Goal and scope definition

  This should include the system boundary, and the depth and breadth of LCA can differ considerably depending on the goal.
- Life cycle inventory analysis (LCI)

  This is an inventory of input/output data of the system being studied.
- Life cycle impact assessment (LCIA)

This assigns LCI results to impact categories and provides information on the environmental issues associated with the product system.

- Interpretation

  This is a summary and discussion of the results of LCI and LCIA.

Additional detailed requirements and guidelines for LCA are provided in BS EN ISO 14044:2006+A1:2020 (The British Standards Institution, 2021a). Illustrative examples of studies conducted in accordance with the standards are also provided in PD ISO/TR 14047:2012 (The British Standards Institution, 2012).

Various proprietary softwares are available for conducting LCA, including SimaPro, GaBi and Umberto (Hayes et al., 2023). These options, however, require a high cost of investment (Silva et al., 2017). Free open-source softwares such as CCalC and Open LCA are also available, although limitations such as a lack of freely available datasets and poorly documented datasets have been cited (Silva et al., 2017). The choice of LCA tool can affect the results of the study, and it has been reported that while the results from the common softwares are similar in most cases, substantial differences have been occasionally observed (Herrmann & Moltesen, 2015; Lopes Silva et al., 2019).

2.10.2 Existing LCA studies on biomass power generation systems

There are a number of examples from existing literature using LCA to evaluate the environmental impact of biomass power generation systems. It was found that most existing studies are focused on woody fuels, with a limited number of studies on olive husk, corn stover, and other less conventional feedstocks. A comprehensive LCA study was provided by Kabir & Kumar (2012), covering the raw material sourcing, transport, pellet plant and combustion stages of multiple biomass/coal co-firing pathways. Some limitations of the study can be identified though, namely the lack of detailed considerations of the individual processes within the pellet plant, as the pellet plant stages were treated as a “black box” using typical values for their overall energy use from other literature sources, whereas the LCA conducted in Chapter 8 of this thesis considered the unit operations within the pellet plant.

Several LCA studies of sugarcane bagasse electricity generation by direct combustion are available in the existing literature. For example, Silva et al. (2014) employed LCA to study the environmental impact of electricity generation from sugarcane bagasse and supplying surplus electricity to the grid in Brazil. Mohammadi et al. (2020) conducted a similar study for the sugarcane industry in Iran. In addition, several studies encompass the international transport and use of biomass for power generation (Beagle & Belmont, 2019; Turconi et al., 2014). However, no studies focusing specifically on the densification and international transport and use of bagasse could be found, despite the reported interest from industry (Thomas, 2019). Thus, this is an underexplored area in the existing literature which needs to be addressed.

2.11 Conclusions

This Chapter has provided an in-depth literature review of multiple topics relevant to the research topic of the present study. The main gaps of knowledge in the existing literature were identified, which are addressed in the subsequent Chapters. These represent areas where further study would provide substantial benefits to academia and industry.

Cardboard is a potential biomass feedstock which has good availability and the advantage of being a domestic source of biomass. However, the combustion of cardboard is an underexplored area. Further investigation of the properties of cardboard materials would be highly valuable, particularly in the areas of char morphology, potential impacts of fillers, and the differences between the types of cardboard. Particle shape data (especially 3D shape factors) are important in particle flow and combustion, and it is desirable to study the particle shape of additional types of biomass.

Natural drying is an attractive option to reduce the drying energy of biomass, as it has the unique advantage of not requiring any direct energy input. However, its major limitation would be fungal and microbial growth, which may become a health hazard. Pasteurisation is a common process in the food industry to suppress microbial activity, but its use for alternative applications is limited. In addition, there are no

studies to date which explore the option of a combined pasteurisation and natural drying process.

While the pelleting process is a well-studied topic, most studies focus on the production of wood pellets and there is value in improving the understanding of the pelleting process for other types of biomass, including the change in particle size and shape during pelleting and pellet milling. The study of pelleting process parameters other than pelleting energy is also an underexplored area in the existing literature. Studying the pelleting process at a larger scale rather than with single pellet presses is also highly desirable.

There are multiple examples of using LCA to study biomass power generation systems in the existing literature. However, there are no studies to date focusing specifically on the densification and international transport and use of bagasse. This represents an area that should be addressed in the present study. In addition, detailed considerations of the individual processes within the pellet plant would need to be included.

Chapter 3 - Methodologies

This Chapter details the experimental and analysis methods used in this thesis. The Sections of this Chapter are roughly organised in the order that the methods are used in the subsequent Chapters, although some methods are used in multiple Chapters.

3.1 Thermal Characterisation of Samples

3.1.1 Thermogravimetric Analysis (TGA)

Thermogravimetric analysis (TGA) was used for biomass characterisation tests in this thesis. Most of the samples used in this thesis were obtained from commercial suppliers or industrial partners, and many were supplied on a commercially sensitive basis. Therefore, the information available on the source and properties of the samples was often limited and TGA was used to provide basic characterisation data for the samples. TGA tests were conducted on a TA Instruments Q500 autosampler Thermogravimetric analyser (New Castle, DE, USA). For each test, 10-15 mg of sample was used, and both proximate analysis (slow pyrolysis) and intrinsic reactivity tests were used.

The reliability of TGA results can be affected by factors such as heating rate and particle size (Lester et al., 2007). As different heating rates are required for proximate analysis and intrinsic reactivity tests, this is discussed in their respective sections (3.1.1.1 and 3.1.1.2). For particle size, a fine particle size should be used for TGA tests, as it is beneficial for achieving effective heat transfer and the effective release of gaseous reaction products. Therefore, all samples for the TGA tests were milled to <300 µm as described in Section 3.5.2.

3.1.1.1 Proximate Analysis (slow pyrolysis)

Proximate analysis was conducted using the slow pyrolysis method developed by Lester et al. (2007), who suggested that a heating rate of 5°C/min as a standard condition for a reasonable compromise between peak definition and experimental run time. The sample was loaded onto a platinum pan, which was then heated at 5°C/min in nitrogen (100 ml/min flowrate) from ambient temperature to 900°C. This temperature was held for five minutes, after which the gas was switched to air (100

ml/min flowrate) and the sample was held at 900°C again for 20 minutes before ramping down to ambient temperature. The weight of the sample was continuously monitored throughout the process. The results were analysed in Matlab R2021a and graphs of weight vs time and derivative weight vs time were plotted. The moisture, volatile, fixed carbon and ash contents were calculated and analysed according to BS EN ISO 16993:2016 (The British Standards Institution, 2016a).

Each measurement was conducted in duplicate and the mean values were presented. This is the suggested procedure for hard coal and coke according to BS ISO 562:2024 (The British Standards Institution, 2024). The standards BS EN ISO 18123:2023 (The British Standards Institution, 2023) and BS EN ISO 18122:2022 (The British Standards Institution, 2022b) also provides additional information on the expected repeatability limits of the measurements for biofuels. For volatiles content, the repeatability limit was stated to be 1.0% of the mean result. For ash content, the repeatability limit was stated to be dependent on the sample and was reported to be in the range of 0.05-0.51% (absolute) for several biomass types.

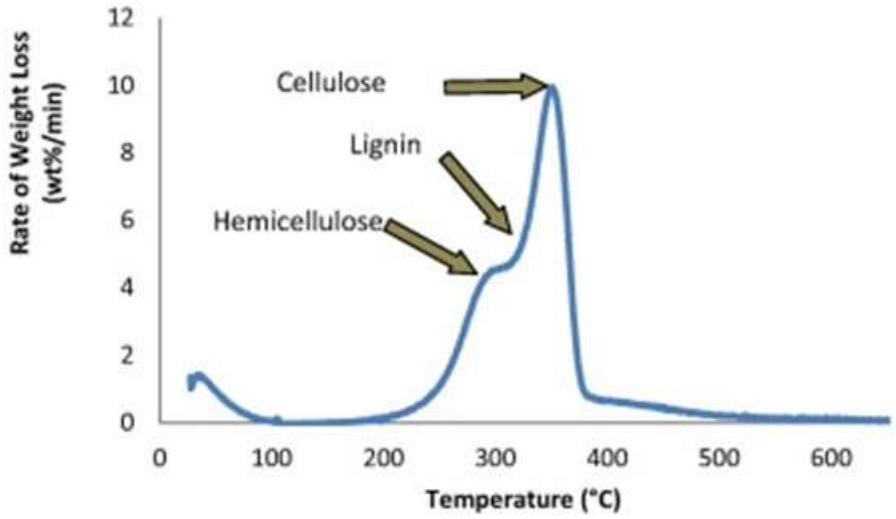

Figure 3-1 The 'contributions' of lignin, cellulose and hemicellulose to biomass devolatilisation profile during slow pyrolysis (Pang et al., 2014)

Slow pyrolysis tests were also used to identify the presence/absence of the biomass components of lignin, cellulose and hemicellulose, using a method based on the work of Pang et al. (2014). The three biomass components can be seen to contribute to the

devolatisation profile at specific temperature ranges, resulting in a characteristic shape in the derivative weight vs time graph, which consists of a hemicellulose 'shoulder' and a cellulose peak, with the lignin peak being obscured by the other two components, as seen in Figure 3-1. By inspecting the shape of the curve, the presence/absence of lignin, cellulose and hemicellulose were determined.

3.1.1.2 Intrinsic Reactivity

The intrinsic reactivity of samples was studied using a non-isothermal method based on the work of Unsworth et al. (1991), which has also been used by multiple authors (Lester et al., 2006; Williams, 2016) to study coal and biomass. Intrinsic reactivity tests were conducted in duplicate and mean values were presented. The sample was heated at a constant rate of 10°C/min in air from ambient temperature to 900°C. The results were analysed in Matlab R2021a and graphs of derivative weight vs time were plotted. Three peaks are normally observed, corresponding to the moisture release, devolatilisation and combustion processes. The derivative weight vs time graphs were analysed to determine the following parameters:

1. Peak temperature (for each peak): the temperature at which the rate of change of weight is at its maximum
2. Peak rate (for each peak): the maximum rate of change of weight in %wt/min for the peak
3. Burnout temperature: the temperature where the rate of change of weight falls below 1%wt/min

These measurements give an indication of the reactivity of the samples, as in principle, a more reactive sample would have lower peak temperature and burnout temperature values.

3.1.2 Calorific Value Measurement

An IKA C5000 Bomb Calorimeter (Staufen, Germany) was used to measure the higher heating value (HHV) of samples in accordance with BS EN ISO 18125:2017 (The British Standards Institution, 2017a). Pellets of the biomass samples were made and fully combusted in oxygen in a pressurised chamber, and certified benzoic acid tablets

were used as a standard with a nominal HHV of 26691 J/g. The HHV (dry basis) was calculated from the measured HHV (wet basis) using equation (3.1).

$$HHV_d = \frac{HHV_w}{1 - MC} \quad \textbf{(3.1)}$$

Where HHV_d is the higher heating value (dry basis), HHV_w is the higher heating value (wet basis), and MC is the moisture content.

Lower heating value (LHV), or net calorific value, is often used in fuel quality specifications such as BS EN ISO 17225-2:2021 (The British Standards Institution, 2021b) and BS EN ISO 17225-6:2021 (The British Standards Institution, 2021c). The LHV was calculated in accordance with BS EN ISO 18125:2017 (The British Standards Institution, 2017a) using equation (3.2). The hydrogen, nitrogen and oxygen content used in equation (3.2) were measured using the method described in Section 3.2.3.

$$LHV_d = HHV_d - 212.5 \times H_d - 0.8 \times (O_d + N_d) \quad \textbf{(3.2)}$$

Where LHV_d is the lower heating value in J/g (dry basis), H_d is the hydrogen content in percentage (dry basis), O_d is the oxygen content in percentage (dry basis), and N_d is the nitrogen content in percentage (dry basis).

3.2 Chemical Characterisation of Samples

3.2.1 X-ray Diffraction (XRD)

Powder X-ray Diffraction (XRD) analysis was conducted for mineral identification using a Bruker D8 Advance with Da Vinci X-ray Diffractometer (D8 Adv DV), with a 2θ range of 5°–80°. The experimental data were analysed using the DIFFRAC.EVA V5.0 software. Peaks in the experimental data were matched with the powder diffraction file (PDF®) database to identify the species present in the samples.

3.2.2 Ashing

Several ash samples were prepared for XRD analysis. These were prepared using a high-temperature muffle furnace (Vecstar Furnaces & Ovens, Chesterfield). The samples were placed into porcelain crucibles and heated to 850°C for 24 hours, after which the ash was collected.

3.2.3 Ultimate Analysis

Ultimate analysis was carried out to determine the carbon, nitrogen and hydrogen content of samples using a LECO CNH628 elemental analyser. Analysis was conducted in accordance with BS EN ISO 16948:2015 (The British Standards Institution, 2015a).

3.3 Moisture Content Measurement

The moisture content of samples was measured using the oven dry method in accordance with BS EN ISO 18134-2:2017 (The British Standards Institution, 2017b). First, the mass of an empty heat-resistant drying container was recorded. A sample of 300 ± 10 g of sample was placed onto the drying container, and the mass of the container with the sample was recorded. It was then placed into a GallenKamp oven pre-heated to 105°C. After 24 hours, the sample was removed from the oven and the weight of the container with the dried sample was immediately recorded. The moisture content of the sample was calculated using Equation (**3.3**) (The British Standards Institution, 2017b).

$$MC = \frac{m_2 - m_3}{m_2 - m_1} \times 100 \qquad \textbf{(3.3)}$$

Where m_1 is the mass of the empty drying container; m_2 is the mass of the drying container and the sample before drying; m_3 is the mass of the drying container and the sample after drying.

3.4 Combustion Characterisation

The ultimate goal of large-scale biomass power generation systems is to generate electricity in an efficient manner through combustion, and the combustion characteristics of the final product must be considered when designing and optimising the upstream processes. Combustion characterisation was carried out for several eucalyptus and cardboard samples. This was done by producing char (as discussed in Section 2.4) from milled biomasses at various particle sizes with two different methods (drop-tube furnace and muffle furnace) and analysing the morphology of the char produced. Comparisons were then drawn from the different biomasses, particle sizes and char production methods.

3.4.1 Drop Tube Furnace

Two particle sizes were used for producing char with the drop tube furnace (DTF): 600-850 µm and 106-300 µm. These were obtained by milling the raw biomass with a knife mill using a 4 mm screen as in Section 3.5.1, followed by sieving as in Section 3.6.1. The DTF system simulates pulverised fuel (PF) combustion (Bridge, 2018; Cloke et al., 2002; Tao Wu et al., 2006) and the particle sizes were chosen to be in the range of typical biomass PF combustion systems (Tamura et al., 2014). The DTF used (shown in Figure 3-2) was manufactured by Severn Thermal Furnaces, which has been used for reliable and repeatable char production (Bridge, 2018). A residence time of 200 ms, a combustion temperature of 1300°C and an oxygen level of 1% were used. For each sample, approximately 5 g of material was fed through the drop tube furnace.

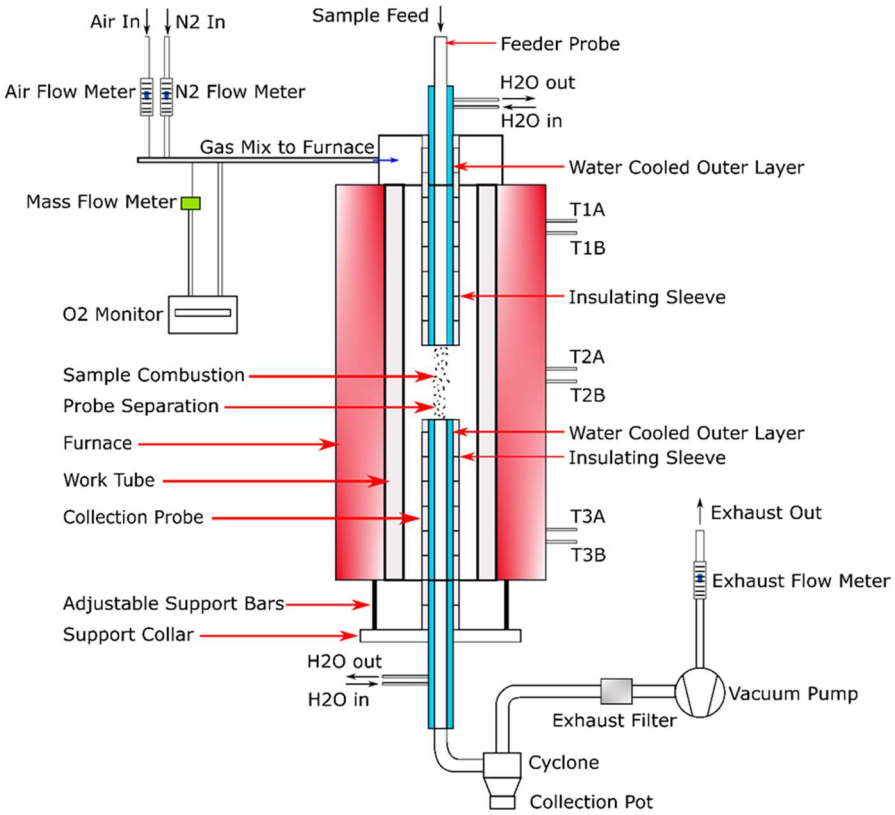

Figure 3-2 Schematic of the drop tube furnace

3.4.2 Muffle Furnace

It has been previously described in the literature that muffle furnaces can be used to simulate fluidised bed combustion (Avila et al., 2011; Lester et al., 2018). Two particle

sizes of the milled biomass were used for producing char with a high-temperature muffle furnace (Vecstar Furnaces & Ovens, Chesterfield): 1180-2360 µm and 600-850 µm. These were obtained by milling the raw biomass with a knife mill using a 4 mm screen as in Section 3.5.1, followed by sieving as in Section 3.6.1.

Larger particle sizes were used for the muffle oven method compared to the drop tube furnace, as larger sizes are usually used in fluidised bed combustion (Afilaka, 2016). The 600-850 µm samples were used in both the drop tube furnace and muffle furnace methods to draw comparison between the two char production techniques.

For each sample, approximately 5 g of material was placed into a heat-resistant porcelain crucible and covered with a lid. The crucible was then placed into the muffle furnace and rapidly heated to 900°C. This temperature was maintained for three minutes, after which the oven was allowed to cool down rapidly to room temperature.

3.4.3 Yield and Combustion Efficiency Calculations

Proximate analysis of the chars was conducted as described in Section 3.1.1.1 and the data was used for yield and combustion efficiency calculations. Assuming that ash is 'indestructible' during the char production process and slow pyrolysis test, the yield of the char production process can be calculated using Equation (3.4).

$$W_{in} \times A_{raw} = W_{out} \times A_{char}$$

$$Y = \frac{W_{out}}{W_{in}} = \frac{A_{raw}}{A_{char}} \tag{3.4}$$

Where W_{in} is the theoretical amount of raw biomass input, W_{out} is the theoretical amount of char produced, A_{raw} is the ash content of the raw biomass as measured by proximate analysis, A_{char} is the ash content of the char as measured by proximate analysis, and Y is the yield of the char production process.

The combustion efficiency is defined as the proportion of combustible materials removed during the char production process, which can be calculated using Equation (3.5).

$$E_{combustion} = 1 - \frac{W_{in} \times Y \times (1 - A_{char})}{W_{in} \times (1 - A_{raw})} = 1 - \frac{Y \times (1 - A_{char})}{(1 - A_{raw})} \quad (3.5)$$

Where $E_{combustion}$ is the combustion efficiency (%)

3.4.4 Char Morphology using Microscopy

3.4.4.1 Sample preparation

Char blocks were prepared using a liquid resin and hardener (EPOFIX, Struers Ltd.). After placing the sample and the resin-hardener mixture in cylindrical moulds, the blocks were left to cure for at least 24 hours. Before microscopy, the blocks were ground with silicon carbide paper (800/1200/2400 grit, in this order) and then polished using a colloidal silica solution (Struers, OP-S, 0.04 µm) on a Struers Rotopol Automated Polishing System using 20N pressure throughout to create scratch-free surfaces for microscopy.

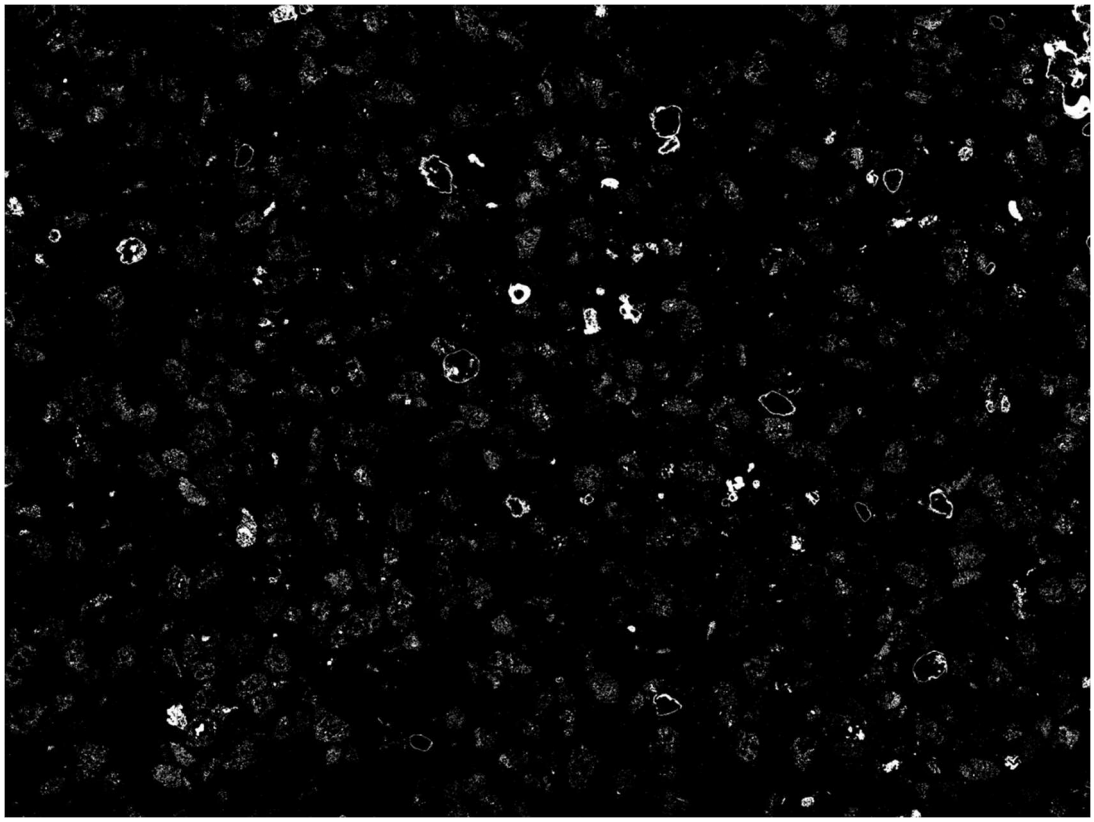

Figure 3-3 Example of mosaic image with 20x20 char images stitched together

3.4.4.2 Microscopy

Manual char morphology analysis was conducted with a Zeiss Leitz Ortholux II POL-BK microscope. For each sample, 500 points were collected by classifying the chars using the scheme described in Section 3.4.4.3. Additional images were collected using a Zeiss Imager M1 microscope. Mosaics of each sample (20 x 20 images) representing a total area of 4.75 x 3.6 mm with a resolution of 0.1288 µm per pixel were generated. An example of a mosaic image is shown in Figure 3-3.

3.4.4.3 Char classification scheme

According to Lester et al. (2018), biomass chars can be classified based on three morphological characteristics:

1. Aspect ratio

   If the aspect ratio is 3 or higher, the particle is considered to have a high aspect ratio. Particles with a high aspect ratio are known to burn faster than particles with a low aspect ratio.

2. Wall thickness

   This is a qualitative assessment of the thickness of the char, where thin-walled chars are expected to burn out more quickly than thick-walled chars. A wall thickness of <3 µm is considered thin and a wall thickness of >3 µm is considered thick. Whilst this, like wall thickness, is an arbitrary threshold, there is based on the allowable resolution of oil immersion microscopes.

3. Porosity

   Biomass chars can be classified as either cellular or porous. Cellular chars retain a visible cell structure, whereas porous chars contain substantial voids and the cell structure of biomass is no longer visible.

Based on this identification scheme, biomass chars can be classified into 8 types (Lester et al., 2018):

1. Thick-walled porous low aspect ratio (TPL)
2. Thin-walled porous low aspect ratio (tPL)
3. Thick-walled cellular low aspect ratio (TCL)
4. Thin-walled cellular low aspect ratio (tCL)

5. Thick-walled porous high aspect ratio (TPH)
6. Thin-walled porous high aspect ratio (tPH)
7. Thick-walled cellular high aspect ratio (TCH)
8. Thin-walled cellular high aspect ratio (tCH)

When comparing biomass chars with coal chars (which does not use aspect ratio as a discriminating property for classification, see Figure 2-1), this classification scheme can be collapsed into:

1. Thin-walled porous (tP)

   Analogous to tenuisphere in traditional coal char classification, include tPL and tPH
2. Thin-walled cellular (tC)

   Analogous to tenuinetwork in traditional coal char classification, include tCL and tCH
3. Thick-walled porous (TP)

   Analogous to crassisphere in traditional coal char classification, include TPL and TPH
4. Thick-walled cellular (TC)

   Analogous to crassinetwork in traditional coal char classification, include TCL and TCH

3.4.5 Burnout Prediction

Burnout was simulated using the burnout model developed by Perkins (2020) (see Section 2.4.2). A brief overview of the method is provided in this Section.

This model uses char images to simulate burnout by iteratively eroding individual char particles, thus avoiding complex kinetics calculations. By analysing char particles from different coals, burnout profiles of the various char morphology classes were developed. The burnout prediction for each sample was then computed by calculating the weighted average of these profiles according to the relative abundance of the types of char morphologies identified by manual char analysis. The burnout performances of the samples were then compared and analysed.

The burnout profiles for each char morphology (thin-walled porous/tenuisphere, thin-walled cellular/tenuinetwork, thick-walled porous/crassisphere, thick-walled cellular/crassinetwork) are shown in Figure 3-4, with the x-axis representing burnout simulation iterations. Whilst the x-axis is based on iterations, it could be (arbitrarily) swapped out for time, e.g. each iteration chosen to represent 20 ms of combustion time and each bite remained as 3 pixels in size (0.386 µm), thus creating a time profile of several hundred milliseconds.

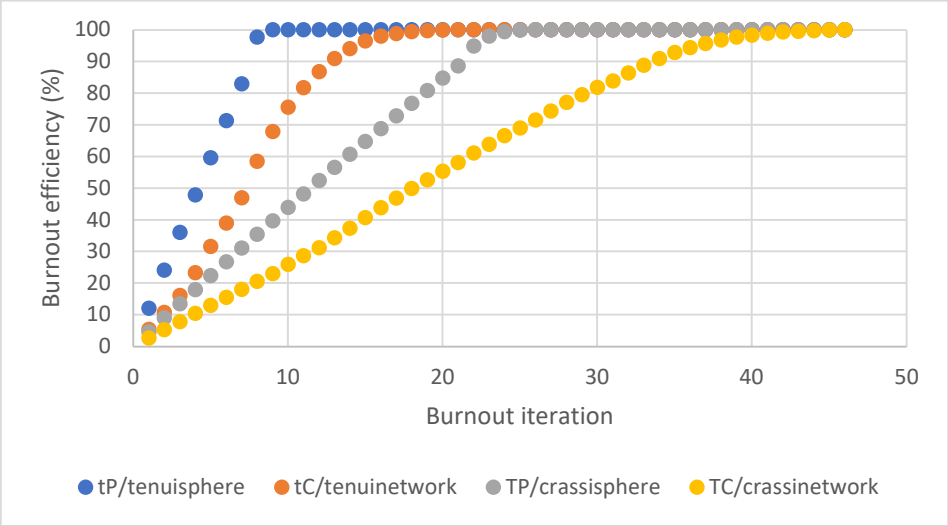

Figure 3-4 Burnout profiles for various char morphology classes

3.5 Biomass Milling

Several methods of milling have been used, including knife mill, ball mill and ring-roller mill. The knife mill was used for the initial size reduction for subsequent experiments and tests. The ball mill was used to produce fine powder samples for XRD and TGA analysis. The ring-roller mill, which is a type of mill used in coal and biomass power station, was used for pellet milling experiments.

3.5.1 Knife Mill

A Retsch SM300 cutting mill with a 3 kW drive was used for the initial reduction of particle size of samples for subsequent experiments and analysis. Several screen sizes were used, including 6 mm and 4 mm square hole screens. The screen(s) used were specified in the corresponding Chapters.

3.5.2 Ball Mill

Ball milling was conducted using a Retsch PM100 planetary ball mill, which has a 500 ml stainless steel grinding jar and 8 x 30 mm stainless steel grinding balls. The samples were milled for 5 mins at 380 rpm. After milling, the samples were sieved as described in Section 3.6.1 to check if all particles are below 300 µm. Any oversized particles were returned for further milling until all particles are below 300 µm.

3.5.3 Ring-Roller Mill

Figure 3-5 Lopulco LM 1.6 Ring-Roller Mill

The Lopulco LM 1.6 laboratory-scale ring-roller mill (shown in Figure 3-5) used for pellet milling in this thesis is similar to ring-roller mills used in coal and biomass-fired power stations. The mill is over 40 years old (Pang, 2012) and has recently been fully restored by Williams (2016). The sample is placed into a hopper and fed into the milling chamber with a rotating table and two rollers. Air is circulated in the mill by a fan, which feeds air to the underside of the mill. The airflow carries particles into the cyclone, where the milled material is dropped into a bucket for collection. Dense, oversized material may overflow from the rim of the milling table to a separate bucket.

3.6 Particle Size and Shape Analysis

Particle size and shape analysis is a vital part of biomass characterisation and milling performance, as these properties can affect downstream processes (such as pelleting) and combustion (see Section 2.5). Experimentally, sieving was conducted to collect data on particle size distributions, and the Camsizer was used to collect data on both particle size and shape distributions. These data were analysed to calculate multiple distribution parameters, which can be used to characterise and compare the samples. To represent the particle size distributions, semi-logarithmic charts of cumulative distribution against particle size were plotted (The British Standards Institution., 1998).

3.6.1 Sieves and Sieve Shakers

Sieving was conducted in accordance with BS EN ISO 17827-2:2016 (The British Standards Institution, 2016b) and various sieve stacks were used to measure the particle size distributions. The sieve aperture sizes used (in µm) include 4750, 3350, 2360, 2000, 1180, 850, 600, 300, 212, 106, 53. These were used in various combinations for the experiments in this thesis, with the exact combinations stated in the relevant Sections in the subsequent Chapters. Both tapping and vibratory sieve shakers were used. The models used are the Inclyno 1 sieve shaker manufactured by CAPCO (with a tapping mechanism) and the Retsch AS200 Control (Hann, Germany) vibratory sieve shaker.

3.6.2 Rosin-Rammler Analysis

The Rosin-Rammler distribution equation, which was originally developed to describe the distribution of coal fines from coal mills (Rosin, 1933), was used for particle size characterisation. It has also been shown that the Rosin-Rammler distribution equation is a good fit for biomass comminution (Bitra et al., 2009; Gil et al., 2012). The Rosin-Rammler equation is shown as follows:

$$R(d) = 100\left(1 - exp(-(d/d')\text{^}n)\right) \tag{3.6}$$

Where R(d) is cumulative undersize mass in percentage, d is particle size in µm, d' is the characteristic particle size (µm), and n is the Rosin–Rammler size distribution parameter.

The cumulative particle size distributions were plotted on semi-logarithmic plots. The Rosin–Rammler parameters were calculated using the Matlab GUI Tool developed by Brezáni and Zelenak (Brezáni & Zeleňák, 2010), which uses a non-linear curve fitting technique. The characteristic particle size (*d'*) is equivalent to the 63.2th percentile of the cumulative distribution. The value of the Rosin-Rammler sizer distribution parameter (*n*) represents the slope of the semi-logarithmic Rosin-Rammler plot, and a lower value of n indicates a lower slope, which in turn, indicates a higher diversity of particle sizes.

3.6.3 Size Distribution Analysis

3.6.3.1 Interpolated size parameters

The experimental data from sieving experiments were used to calculate the cumulative percentage mass undersize at various sieve sizes, which were then plotted on a semi-logarithmic scale. The size distribution was analysed by calculating multiple parameters, with each parameter providing insights into the dispersion and/or shape of the size distribution. The particle sizes at various percentiles of the distribution are important parameters that are also used to calculate other parameters. The piecewise cubic hermite interpolating polynomial function (pchip) in MATLAB (MathWorks, n.d.) was found to give a good fit for the size distribution of biomass and was used to interpolate between the data points to obtain the percentiles.

3.6.3.2 Dispersion parameters

The parameters described in this Section are grouped together and referred to as dispersion parameters, as they describe the nature of the spread or dispersion of the particle size distribution.

The geometric standard deviation of the total region (*s*) was calculated using Equation (3.6), and this measurement was also further divided into the geometric standard deviation of the high region (*hs*) and the geometric standard deviation of the low region (*ls*) (as shown in Equations (3.8) and (3.9) (Bitra et al., 2009).

$$s = \sqrt{d_{84}/d_{16}} \quad (3.7)$$

$$hs = d_{84}/d_{50} \quad (3.8)$$

$$ls = d_{50}/d_{16} \quad (3.9)$$

Where d_{16}, d_{50} and d_{84} are the particle sizes in µm at the 16th, 50th (also equal to the median) and 84th percentile of the cumulative particle size distribution respectively.

The mass relative span (*MRS*) was calculated using Equation (3.10), and a value greater than 1.0 describes a wide size distribution (Bitra, Womac, Yang, et al., 2009). A high *MRS* value indicates a high level of heterogeneity in particle sizes and a low *MRS* value indicates a low level of heterogeneity.

$$MRS = (d_{90} - d_{10})/d_{50} \quad (3.10)$$

Where d_{10} and d_{90} are the particle sizes in µm at the 10th and 90th percentile of the cumulative distribution respectively.

Some particle size distribution parameters used in the identification and classification of soil are also applicable for biomass. The uniformity coefficient (C_u) and the curvature coefficient (C_c) are defined in Equations (3.11) and (3.12) and are used in combination to give a quantitative description of the shape of the particle size distribution curve (The British Standards Institution, 2018).

$$C_u = d_{60}/d_{10} \quad (3.11)$$

$$C_c = \frac{(d_{30})^2}{d_{60} \cdot d_{10}} \quad (3.12)$$

Where d_{30} and d_{60} are the particle sizes in µm at the 30th and 60th percentile of the cumulative distribution respectively.

The particle size distribution curves can be categorised as ‘well graded’, ‘poorly graded’ or ‘gap graded’, with these terms defined in Table 3-1. When interpreting the C_u and C_c values for biomass, a uniformity coefficient of < 4.0 is indicative of a sample containing particles of roughly uniform size and a curvature coefficient between 1 and 3 is indicative of a well-graded size distribution (Bitra et al., 2009).

Category	Description
Well graded	There are no excess particles in any size ranges and no intermediate sizes are lacking, showing a gradual rising trend in the cumulative curve.
Poorly graded	The sizes of a high proportion of particles are within narrow limits.
Gap graded	Both large and small particles are present but the distribution has a relatively small amount of particles of intermediate sizes.

Table 3-1 Description of the graduation levels of particle size distributions, adapted from (Bitra et al., 2009)

3.6.3.3 Distribution shape parameters

The parameters described in this Section are grouped together and referred to as distribution shape parameters, as they describe the shape of the particle size distributions.

Skewness is a measurement of the level of asymmetry in a distribution. The inclusive graphic skewness (GS_i) is defined in Equation (3.13) (Folk, 1980). A perfectly symmetrical curve would have a GS_i value of 0, a distribution with a larger proportion of finer particles would have a positive GS_i value, and a distribution with a larger proportion of coarser particles would have a negative GS_i value.

$$GS_i = \frac{d_{16} + d_{84} - 2d_{50}}{2(d_{84} - d_{16})} + \frac{d_5 + d_{95} - 2d_{50}}{2(d_{95} - d_5)} \quad (3.13)$$

Where d_5 and d_{95} are the particle sizes in μm at the 5th and 95th percentile of the cumulative distribution respectively.

The parameter of graphic kurtosis (K_g) measures the level of departure of the distribution curve from a normal Gaussian distribution (which would have a K_g value of 1) and is defined in Equation (8) (Folk, 1980). If a curve is better sorted (closer to a normal Gaussian distribution) in the central portion compared to the tails, it has a K_g value of greater than 1 and is said to be leptokurtic; if a curve is better sorted in the

tails compared to the central portion, it has a K_g value of less than 1 and is said to be platykurtic.

$$K_g = \frac{d_{95} - d_5}{2.44(d_{75} - d_{25})} \tag{3.14}$$

Where d_{25} and d_{75} are the particle sizes in µm at the 25th and 75th percentile of the cumulative distribution respectively.

3.6.4 Size and Shape Analysis using a Camsizer

3.6.4.1 Experimental process

A Retsch Camsizer P4 was used for particle size and shape analysis for selected samples. The samples to be tested were placed onto a vibratory feeder. When the particles reach the end of the vibratory feeder, they drop through a test chamber between a light source and two high-speed cameras and then onto a collection tray. The particles are individually detected by the cameras and the images are digitally processed, with each particle scanned in up to 64 directions. The two cameras are referred to as 'basic' and 'zoom', which detect large and small particles respectively. The theoretical measurement range of the Camsizer is between 15 µm to 90 mm. Following image processing, particle size data is saved in up to 300 customisable size classes. These were conducted in duplicates, with close agreement observed between runs. Each run would measure in excess of a million particles, thus a high degree of accuracy is expected from the Camsizer results.

3.6.4.2 Camsizer particle size and shape parameters

The Camsizer software measures multiple particle size and shape parameters, and the parameters that were used in this thesis are described in this Section.

The minimum chord ($d_{c,min}$) and maximum Feret diameter ($d_{Fe,max}$) are the size characteristics used for the analysis of particle size and shape. For each of the 64 scanning directions, the Camsizer software determines the maximum chord (d_c) locally, which is the maximum distance between two boundary points perpendicular to the scanning direction, and the minimum chord diameter $d_{c,min}$ is defined as the minimum value of d_c in all scanning directions. The minimum chord diameter is thus

analogous to aperture sizes in sieve analysis (Microtrac Retsch GmbH, 2020). For each of the 64 scanning directions, the Camsizer software determines the Feret diameter (d_{Fe}) locally, defined as the maximum distance between two tangents parallel to the scanning direction. The maximum Feret diameter $d_{Fe,max}$ is defined as the maximum value of d_{Fe} in all scanning directions. The definitions of minimum chord ($d_{c,min}$) and maximum Feret diameter are illustrated in Figure 3-6, which uses the notations of x_c, $x_{c\,min}$, x_{Fe} and $x_{Fe\,max}$, corresponding respectively to the notations of d_c, $d_{c,min}$, d_{Fe} and $d_{Fe,max}$.

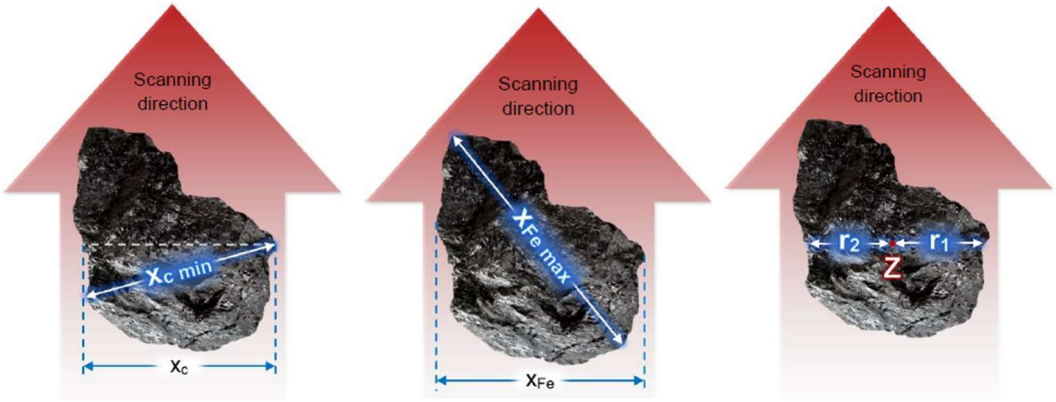

Figure 3-6 Illustrations of minimum chord (left), maximum Feret diameter (middle) and particle symmetry (right) (Microtrac Retsch GmbH, 2020)

The shape factors used in this thesis are sphericity, circularity, symmetry and aspect ratio. The operational sphericity (ϕ) was derived and defined by Krumbein and Sloss (1951) and shown in equation (3.15).

$$\phi = \frac{d_n}{a} \tag{3.15}$$

Where ϕ is the sphericity, d_n is the nominal diameter (defined as the diameter of a sphere with the same volume as the particle), and a is the maximum intercept through the particle (equivalent to the diameter of the circumscribing sphere).

Circularity (C), as defined in BS ISO 9276-6:2008 (The British Standards Institution, 2008) describes the degree of similarity between a particle or its projection and a perfect circle, with consideration of the smoothness of the perimeter of the particle. It is defined in equation (3.16).

However, the circularity values provided in the Camsizer software are represented as the square of the classically defined circularity, as shown in equation (3.17).

$$C = \sqrt{\frac{4\pi A}{P^2}} = \frac{d_A}{d_{Pe}} \quad \textbf{(3.16)}$$

$$C^2 = \frac{4\pi A}{P^2} = \left(\frac{d_A}{d_{Pe}}\right)^2 \quad \textbf{(3.17)}$$

Where C is the circularity, A is the projection area of the particle, P is the perimeter length of the particle, d_A is the diameter of a circle with area A, and d_{Pe} is the diameter of a circle with perimeter length P.

The symmetry (Symm) of a particle is defined in equation (3.18) and illustrated in Figure 3-6. The variables r_1 and r_2 are defined as the distances between the centre of area (point Z in Figure 3-6) and the particle boundary perpendicular to the scanning direction. The Camsizer software scans each particle in 64 directions and the minimum value of r_1/r_2 is used to calculate the symmetry of the particle (Microtrac Retsch GmbH, 2020).

$$Symm = \frac{1}{2}\left[1 + \min\left(\frac{r_1}{r_2}\right)\right] \quad \textbf{(3.18)}$$

The aspect ratio (AR) of a particle is defined as the ratio of the minimum chord to the maximum Feret diameter (Microtrac Retsch GmbH, 2020):

$$AR = \frac{d_{c,min}}{d_{Fe,max}} \quad \textbf{(3.19)}$$

3.7 Biomass Pasteurisation and Natural Drying

3.7.1 Overall Process

The basic process used for the biomass pasteurisation and natural drying experiments is shown in Figure 3-7. The samples were processed in the following order: milling, moisture addition, briquetting, pasteurisation and storage, with the moisture content and level of fungal growth measured at various points. Experiments were conducted for 16 briquettes in total (8 miscanthus briquettes and 8 spent grains briquettes). The availability of fungal growth tests (see Section 3.7.11) was limited,

which dictated the maximum number of briquettes that could be included in the experiments and duplicates could not be conducted. However, the principle goal of the biomass pasteurisation and natural drying experiments was to establish the feasibility of the novel process, and the validity of the conclusions drawn was not affected.

3.7.2 Milling

Milling was conducted using a knife mill (Restch SM300) with a 6 mm screen to reduce the particle size of the raw materials for briquetting (see Section 3.5.1). Only one particle size distribution (knife mill output) was considered to limit the complexity of the experiment design. Milling was only required for miscanthus as the spent grains were already at a suitable size for briquetting (as determined by preliminary experiments) as received after the brewing process.

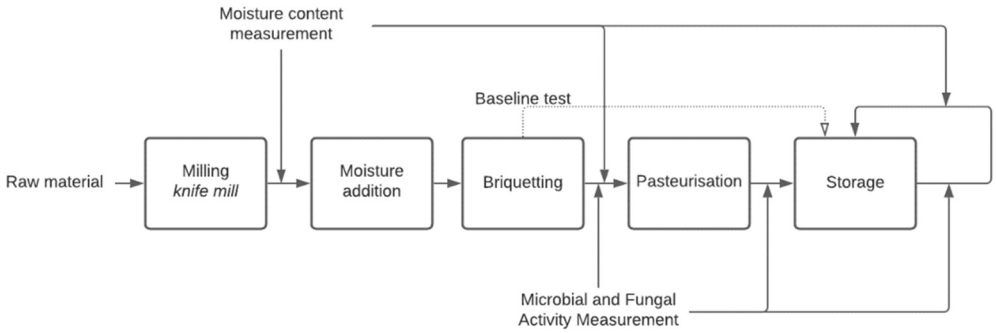

Figure 3-7 Flow diagram for the biomass pasteurisation and natural drying experimental process

3.7.3 Moisture Content Measurement and Conditioning

The initial moisture content of the samples was measured in accordance with BS EN ISO 18134-2:2017 (The British Standards Institution, 2017b) (Section 3.3). The spent grains samples were briquetted as received and no moisture conditioning was required as they were already at a high moisture content. The moisture content of each batch of spent grains samples was measured to be 62-67%. For the miscanthus samples, the moisture content was first measured, followed by the addition of the appropriate amount of water to achieve a moisture content of around 60%. The

samples were then mixed thoroughly and stored in airtight containers for 24 hours to ensure all moisture was absorbed. Following the moisture conditioning procedure, the exact moisture contents of the samples used for briquetting were measured and recorded.

3.7.4 Briquetting

The milled samples with added moisture were briquetted using a hand-operated briquette maker (Clarke CHT617 Briquette Maker). To make the briquettes, approximately 1100 g (for spent grains) or 410 g (for miscanthus) of samples were placed in the briquette maker. The material was then compressed in the briquette maker by manually pushing down the levers. After compression, the briquettes were removed and placed in storage as described in Section 3.7.8. The approximate dimensions of the briquette were 21 x 9 x 6 cm. Therefore, the approximate density of the briquettes was 0.97 g/cm^3 for spent grains and 0.36 g/cm^3 for miscanthus.

3.7.5 Baseline Briquette

The baseline levels of fungal growth of each material were established using the following process: milling, moisture addition, briquetting, and storage (as indicated by the baseline test arrow in Figure 3-7). The level of fungal growth was measured at regular intervals (see Section 3.7.11). These were then compared to the pasteurised samples to evaluate the effectiveness of the pasteurisation conditions.

3.7.6 Pasteurisation

Two methods of pasteurisation were used: conventional oven and microwave. Conventional oven pasteurisation was carried out using a Gallenkamp conventional oven. Microwave Pasteurisation was carried out using a Panasonic NE-1853 Microwave Oven (as shown in Figure 3-8). This microwave oven is capable of delivering various power levels from 340 W to 1800 W. For this thesis, ‘high power’ refers to the 1800 W setting and ‘low power’ refers to the 340 W setting. Both ‘high power, short duration’ and ‘low power, long duration’ configurations (both would consume the same amount of energy overall) were used. Contrary to domestic microwave ovens, which typically have a rotating disc, this microwave oven uses a combination of stationary (interior walls) and rotating antenna, which contribute to

a good distribution of microwaves within the cavity and a more even heating of the samples (Panasonic, n.d.).

Pasteurisation was conducted in two batches of four briquettes each for each material (i.e. 16 briquettes in total). The results from the first batch were studied before conducting the second batch of experiments, and the pasteurisation conditions used for the second batch were determined based on the results from the first batch. The first batch of miscanthus briquettes is referred to as M1-M4; the first batch of spent grains briquettes is referred to as SG1-SG4; the second batch of miscanthus briquettes is referred to as M5-M8; and the second batch of spent grains briquettes are referred to as SG5-SG8. The exact pasteurisation conditions of all briquettes are listed in Section 6.3.

Figure 3-8 Panasonic NE-1853 Microwave Oven

3.7.7 Briquette Heating Profiles

The effectiveness of pasteurisation in suppressing fungal growth would depend on the temperature experienced by the briquettes and the duration for which they are subjected to high temperatures. During pasteurisation, different areas of the briquettes could experience different temperatures for different durations, which would have an effect on the growth of fungi during storage. Therefore, experiments

were conducted to quantify the heating profiles of the briquettes at different locations.

A Pico USB TC-08 Thermocouple Data Logger and multiple RS Pro Type K Thermocouples (measurement range: -200°C to 1100°C) were used. The briquette heating profile experiments were not conducted for microwave pasteurisation as microwaves would interfere with traditional thermocouples (Section 2.7.6.1) and specialist equipment would be needed, which was not available for this research project.

3.7.8 Storage Configuration

Figure 3-9 Briquette storage configuration

The biomass briquettes were stored in stacked plastic boxes with holes for ventilation in an air-conditioned room set to 21°C for periods of either 4, 5, 8 or 9 weeks. The dimensions of each box were 35 x 25.2 x 19 cm. The storage configuration is shown in Figure 3-9. The first batch of briquettes (M1-M4 and SG1-SG4) was stored for eight or nine weeks, and the second batch (M5-8 and SG5-8) was stored for four or five

weeks. These storage periods were selected to accommodate for the availability of quantitative fungal growth tests and to allow for samples from the middle of the briquettes to be taken after different storage durations (Section 3.7.11), as taking samples from the middle would destroy the briquettes.

3.7.9 Temperature and Relative Humidity Monitoring

The temperature and relative humidity of the storage condition were continuously measured throughout the storage periods using several EL-WiFi-TH Temperature & Humidity Data loggers by Lascar Electronics. This is to ensure that the storage conditions have remained largely stable during the storage period.

3.7.10 Drying Rate Monitoring

The drying rate was monitored by periodically weighing the briquettes during the storage period. The weight loss was recorded and the drying rate was calculated.

3.7.11 Fungal Growth Quantification

Samples were periodically taken from the briquettes at the beginning of and during the storage period for fungal growth analysis. Samples from the top and bottom of the briquettes were taken every two weeks during the storage period. Samples for the middle of the briquettes were only taken at the end of the storage period, as taking samples from the middle would destroy the briquettes. These tests were conducted by Mr Wade Handley-Hartill and Dr Stephen Lawrence in the School of Biosciences at the University of Nottingham. Fungal growth analysis was carried out using the method used by Graham (2015) in their study on the degradation of biomass fuels during long-term storage:

“Two to three grammes of each sample was ground and 10ml of 0.1% (w/v) Tween 80 was added to 1g of the fine material and the mixture was then vortexed for 2 minutes. The liquid extract was serially diluted in 0.1% Tween 80 and 100-200µl samples were plated out onto Oxytetracycline (100ppm) malt extract agar (OMEA). Plates were incubated at 25ºC and inspected daily for 7 days.” (Graham, 2015)

After incubation, the number of colony forming units was counted and the amount of fungi on the samples was quantified as the number of colony forming units per

gram of sample (CFU/g), taking into account the dilutions and the original mass of sample used.

In addition to the quantitative analysis of fungal growth using the incubation method, photos of the briquettes were also taken periodically to demonstrate the change in appearance during the storage period.

3.8 Biomass Pelleting and Pellet Milling

3.8.1 Milling and Particle Size Selection for Pelleting

	Pellet Grade		
Particle size	**I1**	**I2**	**I3**
%wt below 3.15 mm	≥99%	≥98%	≥97%
%wt below 2.0 mm	≥95%	≥90%	≥85%
%wt below 1.0 mm	≥60%	≥50%	≥40%

Table 3-2 Disintegrated pellets particle size distribution specification for Grad I1, I2 and I3 pellets in BS EN ISO 17225-2:2021 (The British Standards Institution, 2021b)

Two particle sizes were used for the biomass pelleting experiments. These are referred to as 'coarse' and 'fine'. The 'coarse' size was created by milling the raw sample in a knife mill with a 6 mm screen (see Section 3.5.1), followed by removing the size fraction above 3.35 mm with a sieve and a sieve shaker (see Section 3.5.1). The 'fine' size was created by milling the raw sample in a knife mill with a 4 mm screen, followed by removing the size fraction above 2 mm with a sieve and a sieve shaker. The 'fine' and 'coarse' particle sizes are designed to approximately represent the particle size distribution requirements of disintegrated pellets for Grade I1 and I2 pellets respectively, as specified in BS EN ISO 17225-2:2021 (The British Standards Institution, 2021b), which is also shown in Table 3-2. For the 'coarse' size, the top size was selected to be 3.35 mm instead of 3.15 mm, as the 3.15 mm sieve was not available at this stage of the project when the pelleting experiments were conducted.

3.8.2 Moisture Conditioning

Three moisture contents were used in the pelleting experiments at 10, 15 and 20%. To create samples with these moisture contents, the material was first completely dried for 24 hours at 105°C, followed by the addition of the appropriate amount of water for each of the three moisture contents. The samples were then mixed thoroughly and stored in airtight containers for 24 hours to ensure all moisture was absorbed. This method is slightly different to the moisture conditioning method used for the pasteurisation and natural drying experiments (described in Section 3.7.3), as it involves completely drying the sample first before adding moisture.

3.8.3 Energy Data Logging

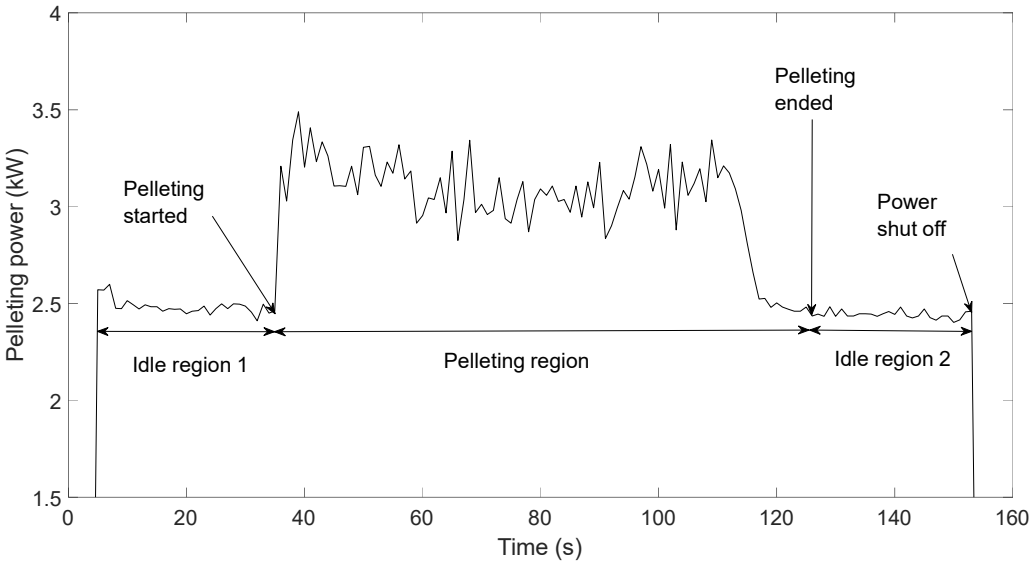

Figure 3-10 Example Pelleting Energy Measurement

Energy data were recorded using an Elcomponent SPCPro (Bishop's Stortford, UK) data logger for the pelleting (Section 3.8.4) and pellet milling (Section 3.8.6) experiments. The pellet machine and the ring-roller mill were connected through the data logger to the electricity supply and the current, voltage and phase angle were recorded at one-second intervals, and the data were processed with the Elcomponent Powerpack Pro software to calculate the power used by the pellet machine or the ring-roller mill.

The idle power is defined as the stable power measured before pelleting or milling was started and was determined by calculating the average value of the power measurement in the stable power region. An example of the pelleting energy measurement is shown in Figure 3-10. Zones with stable values of pelleting power can be observed at the beginning and end of the measurement. The point at which the material started being fed into the machine can also be easily identified. The same principles apply for the measurement of milling energy measurements, and the same basic shapes are observed for both the measurement of pelleting and milling energies.

The total specific pelleting or milling energy (E_{total}) was calculated from the Power-Time curve using equation (3.20) (Gravelsins & Trass, 2013).

$$E_{total} = \int_{t_1}^{t_2} \frac{P_i}{m}\, dt \qquad \textbf{(3.20)}$$

Where E_{total} is the total specific pelleting or milling energy (kWh/ton), t is time (s), t_1 is the start time of the pelleting or milling region (s), t_2 is the end time of the pelleting or milling region (s), P_i is the instantaneous power (kW), and m is the output mass (ton).

The specific effective energy was calculated as the difference between the total specific energy and the total idle energy, as shown in equation (3.21) (Bitra, Womac, Chevanan, et al., 2009).

$$E_e = \int_{t_1}^{t_2} \frac{P_i}{m}\, dt - \int_{t_1}^{t_2} \frac{P_{idle}}{m}\, dt \qquad \textbf{(3.21)}$$

Where P_{idle} is the idle power (constant) (kW)

3.8.4 Pelleting and Pelleting Behaviour Quantification

Pelleting was conducted using a Ceccato Olindo Wood Pellet Machine (single phase 230 V) (shown in Figure 3-11). The nominal pellet output rate is 20-35 kg/hr, the diameter of the die plate holes is 6 mm, and the typical pellet length is quoted to be 25-35 mm (Ceccato Olindo srl, n.d.). The specified feed properties are listed in Table

3-3. The pelleting experiments conducted for this thesis would often fall outside these manufacturer-specified feed conditions.

Figure 3-11 Ceccato Olindo Wood Pellet Machine

Property	Specification	Notes
Particle size	0.5-12 mm	N/A
Moisture content	10-14%	Dependent on the exact material, values are indicative
General description	Pure material	Free of contaminants especially metallic or any other kind that may damage the machine

Table 3-3 Manufacturer-specified feed conditions for the Ceccato Olindo Wood Pellet Machine (Ceccato Olindo srl, n.d.)

A batch process was used for the pelleting experiments, with the following steps:

1. A small amount of material is first fed into the machine until pellets production begins to ensure the die is completely filled. This initial step is necessary to ensure that the batch experiment is representative of a

continuous pellet production process, as this experimental design allows initial compaction of the material inside the die is completed first and the energy used to achieve this is not included in the pelleting energy calculations.

2. The pellet machine was turned on without feeding any material for approximately 30 s. This is to obtain the stable 'idle energy' of the machine, as exemplified in Figure 3-10.
3. 500±10 g of material is fed through the machine. The feed rate is kept roughly constant, taking care to ensure the rollers are not completely covered by the material (as advised by the manufacturer. to allow any steam produced to escape) (Ceccato Olindo srl, n.d.)
4. After feeding the material and pellet production is stopped, the pellet machine is kept running for at least 30 s. This is to confirm the 'idle energy' of the machine.
5. For each feed condition, the batch experiment was repeated three times to ensure consistency.

The pelleting experiments were conducted in triplicate for each condition and average values were calculated. The number of conditions and replicates was limited by the amount of samples available. In addition to the pelleting energy (defined in Section 3.8.3), the other process parameters measured during the pelleting experiments are the pelleting efficiency, average pelleting power and pellet production rate. The pelleting efficiency is defined as the percentage of material successfully transformed into pellets by the pellet machine, where pellets are defined as any material that is retained by a 3.15 mm round hole sieve. Average pelleting power is the difference between the average power delivered during pelleting and the idle power. Pellet production rate is the average rate at which pellets were produced in kg/hr. These parameters can be expressed as:

$$PE = \frac{Pellet\ output}{Total\ output} \times 100\% \quad \textbf{(3.22)}$$

Where PE is the pelleting efficiency (%)

$$PP_{average} = P_{total,average} - P_{idle,average} \quad \textbf{(3.23)}$$

Where $PP_{average}$ is the average pelleting power (kW), $P_{average}$ is the total average power (kW) and $P_{idle,average}$ is the average idle power (kW).

$$Pellet\ production\ rate = \frac{Pellet\ output}{Pelleting\ duration} \quad \textbf{(3.24)}$$

3.8.5 Pellet Characterisation

3.8.5.1 Pellet durability

Figure 3-12 Bioenergy TUMBLER 1000 R Pellet Durability Tester

Pellet durability tests were carried out in accordance with BS EN ISO 17831-1:2015 (The British Standards Institution, 2015d) with a Bioenergy TUMBLER 1000 R pellet durability tester (shown in Figure 3-12). A pellet sample of 500 ±10 g is placed into a tumbler box with an internal baffle. The tumbler box is then rotated at 50 rev/min for 500 rotations. After the tumbling procedure, the contents of the box were sieved with a 3.15 mm round hole sieve and the material retained on the sieve is weighed. The pellet durability was calculated using Equation (3.25) (The British Standards Institution, 2015d).

$$\mathrm{D} = \frac{m_i}{M} \times 100 \quad \textbf{(3.25)}$$

Where D is the pellet durability in %, M is the initial mass of pellets before the tumbling procedure, and m_i is the mass of material retained on the 3.15 mm round hole sieve after the tumbling procedure.

3.8.5.2 Pellet dimensions

Pellet length and diameter were measured for a random sample of 100 pellets for each pelleting condition using Vernier callipers (as shown in Figure 3-13) in accordance with BS EN ISO 17829:2015 (The British Standards Institution, 2015c). Statistical analysis was carried out to calculate the mean, median and standard deviation of both length and diameter. The pellet aspect ratio (AR_{pellet}) was also calculated using equation (3.26). The interquartile range (IQR) is defined in equation (3.27).

Figure 3-13 Measurement of pellet size - length (left) and diameter (right)

$$AR_{pellet} = \frac{length_{pellet}}{diameter_{pellet}} \quad \textbf{(3.26)}$$

$$IQR = Q_3 - Q_1 \quad \textbf{(3.27)}$$

Where IQR is the interquartile range, Q_3 is the upper quartile, and Q_1 is the lower quartile.

The data collected for length, diameter and aspect ratio were represented in box and whisker diagrams, which illustrates the mean, median, upper quartile, lower quartile, maximum value, minimum value, maximum value below (Q_3 + 1.5*IQR) and minimum value above (Q_1 – 1.5*IQR), as illustrated in Figure 3-14.

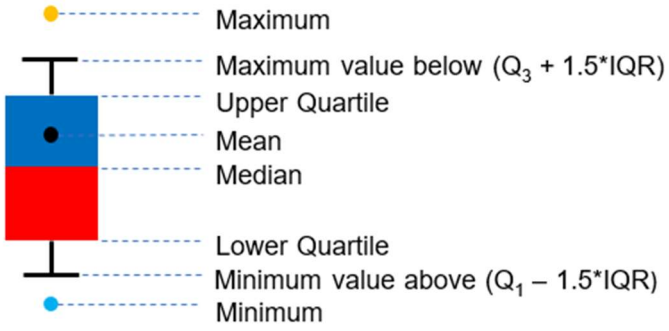

Figure 3-14 Box and whisker representation of pellet length, diameter and aspect ratio

3.8.5.3 Pellet bulk density

To measure the pellet bulk density, a 2-decimal-place balance was used to measure approximately 500 g of each pellet sample, which was then poured into a measuring jug with volume markings at 20 mL intervals. The volume was determined and bulk density was calculated using equation (3.28).

$$BD = \frac{m_{TP}}{V} \tag{3.28}$$

Where BD is the bulk density in kg/m^3, m_{TP} is the mass of the test portion in kg, and V is the volume of the test portion in m^3.

3.8.5.4 Pellet disintegration

Pellet disintegration tests were carried out in accordance with BS EN ISO 17830:2016 (The British Standards Institution, 2016c). Water just below the boiling point (the amount used was sufficient for the pellets to absorb their maximum capacity of water) was poured over the pellets. The resulting slurry was thoroughly stirred and then dried at 60°C until the moisture content was between 5 and 15%. Following pellet disintegration, the particle size distributions of the disintegrated pellets were analysed using the method specified in Section 3.6.

3.8.6 Pellet Milling and von Rittenger Analysis

Following the pelleting (Section 3.8.4) and pellet characterisation experiments (Section 3.8.5), the pellets were milled with a Lopulco LM 1.6 laboratory-scale ring-roller mill, Which is described in detail in Section 3.5.3. Von Rittinger analysis was

conducted based on the literature review presented in Section 2.9.2. The von Rittinger constant (K_{VR}) was calculated with equation (2.4) for each sample, and the milling performances of the samples were compared.

3.9 Life Cycle Analysis (LCA) of Biomass Power Generation

This Section outlines the methodology for the LCA presented in Chapter 8, which calculates the global warming potential (carbon footprint) for a biomass power generation system using sugarcane bagasse from the United States to generate electricity in the UK. BS EN ISO 14040:2006+A1:2020 (The British Standards Institution, 2020) sets out the principles and framework of LCA. Additional detailed requirements and guidelines for LCA are provided in BS EN ISO 14044:2006+A1:2020 [70]. These standards were used as the basis of the LCA methodology. The full development of the methodology is provided in Chapter 8, including the model structure, system boundary, functional unit, data and assumptions.

Although various softwares are available for carrying out LCA (Section 2.10.1), since only the climate change potential impact category was considered, it was not necessary to use specialist LCA softwares such as GaBi and SimaPro. As a relatively simple software that focuses on calculating carbon inventories for different supply chains (Azapagic, 2010), CCaLC was considered as a candidate for carrying out the study. However, CCaLC only allows for a linear production model with no feedback loops, whereas the system studied contains feedback loops (e.g. a portion the dried material from the dryer outlet should be used in a feedback loop as fuel for the dryer) and complexities that could not be readily modelled in CCaLC. Therefore, Microsoft Excel was chosen as the tool for conducting the LCA, which also allows for total control of the methodology. There are also examples of Excel-based tools being used for LCA in literature (Forth et al., 2019; Potrč Obrecht et al., 2020).

The data sources used for the LCA were obtained from a combination of industrial partners, literature sources and the GREET (Greenhouse gases, Regulated Emissions, and Energy use in Technologies) (M. Wang et al., 2023) and ecoinvent (ecoinvent, n.d.) databases. The list of data sources and the justification for their use are presented in Section 8.3. The LCA was also conducted in a way that allows for subsequent modifications, where data sources, type of biomass, pellet plant

configuration, and transport options can be changed to compare the bagasse power generation system with alternatives.

Chapter 4 - Biomass Characterisation

Biomass feedstocks can have a high degree of variability in their physical and chemical characteristics, which need to be studied and understood if they are to be used for power generation applications. Multiple types of biomass materials were used in this thesis. Many of these were supplied on a commercially sensitive basis by industrial partners, and full details about the source, origin and process history of these samples were not known. Using a range of experimental techniques, the characteristics of several biomass samples of various types were studied in this Chapter to provide a context of the properties of biomass and a basis for further study of some of these samples in Chapter 5 and Chapter 7.

4.1 Materials and Methods

Eucalyptus, rice husks, sugarcane straw and cardboard samples were used in this Chapter of the thesis, as they represent a variety of conventional and alternative fuels for bioenergy. Eucalyptus, rice husks and sugarcane straw samples were supplied by industrial partners and cardboard samples were collected by the author. Eucalyptus was also a useful comparison as it is a widely used wood-based fuels for bioenergy applications (Andritz, 2022; Voegele, 2018). Rice husks are an industrial residue from the processing of rice (Hossain et al., 2018). Sugarcane straws refer to the residues left in the field after sugarcane harvesting. The sugarcane straw samples used in this thesis were from the Valle del Cauca region of Colombia and were sub-divided into samples harvested in the wet and dry season as it is known that harvest season can affect the properties of sugarcane straw (Martinez-Mendoza et al., 2023). In this thesis, the abbreviations Euc, RH, SSDS and SSWS are used to refer to the eucalyptus, rice husks, sugarcane straw (dry season) and sugarcane straw (wet season) respectively. Cardboard is subdivided three types: 1. Unprinted cardboard (UCB); 2. Printed Cardboard (PCB); and 3. Printed paperboard (PPB). Due to the unique properties of cardboard materials found during the experiments, some results were presented separately alongside additional analysis in Chapter 5. The types of cardboard are also explained in further detail in Section 5.2. The appearance of the

eucalyptus and rice husks samples is shown in Figure 4-1 and photos of the cardboard and sugarcane straw samples are available in Chapter 5 and Chapter 7 respectively.

The methods used in this Chapter include milling and particle size analysis, elemental analysis, calorific value measurement, thermogravimetric analysis (proximate analysis and intrinsic reactivity) and X-ray diffraction. These methods were described in detail in Chapter 3.

Figure 4-1 Eucalyptus (milled) – left; and rice husks (as received) – right

4.2 Milling and Particle Size Analysis

The samples were milled in a knife mill with a 4 mm screen as specified in Section 3.5.1. The particle size distribution (PSD) was characterised with a sieve stack of 4750, 3350, 2360, 1180, 850, 600, 300, 212, 106, 53 µm. The cumulative particle size distributions of the milled eucalyptus, rice husks and sugarcane straw samples are shown in Figure 4-2. The Rosin-Rammler parameters, selected interpolated size parameters, dispersion parameters and distribution shape parameters (see Sections 3.6.2 and 3.6.3) are shown in Table 4-1 and Table 4-2. The particle size analysis of the milled cardboard samples is presented separately in Section 5.4.

It can be seen from Figure 4-2 that there are some differences between the PSDs of the different types of biomass, while the PSDs of the sugarcane straw samples (dry and wet season) are very similar. The Rosin-Rammler analysis gave a good fit for all four samples ($R^2 > 0.998$). The Rosin-Rammler size distribution parameter (*n)* is the

smallest for SSWS, followed by SSDS, eucalyptus and rice husks. This indicates that SSWS has the highest diversity of particle sizes while the distribution of the rice husks sample is the narrowest. This trend of the diversity of particle sizes is also indicated by the trend in the values of the geometric standard deviation of the total region (*s*), the mass relative span (*MRS*) and the coefficient of uniformity (C_u). Furthermore, for all four samples, the geometric standard deviation of the high region (*hs*) is significantly smaller than the geometric standard deviation of the low region (*ls*), indicating that the diversity of particle sizes is more concentrated in the lower region. The coefficients of curvature (C_c) of the four samples are in the range of 1.25-1.35, which is within the range of between 1 and 3 considered as a well-graded particle size distribution (Knappett & Craig, 2012).

The inclusive graphic skewness (GS_i) of all four samples are positive, indicating that all samples have a larger proportion of fine particles, with this effect being more pronounced for the sugarcane straw samples than the rice husks and eucalyptus samples. The values of graphic kurtosis (K_g) indicate that the PSD of both sugarcane straw samples are close to a Gaussian distribution (K_g values of 0.95-1.00), while the PSD of the eucalyptus (K_g = 1.10) and rice husks (K_g = 1.40) samples are leptokurtic, indicating that the curves are better sorted (closer to a normal Gaussian distribution) in the central portion compared to the tails.

Sample	**Rosin-Rammler**			**Size Parameters (µm) - Cubic interpolation**		
	d' (µm)	**n**	**R^2**	**d_{10}**	**d_{50}**	**d_{90}**
Euc	840	1.90	0.999	225	715	1285
RH	932	2.66	0.998	346	809	1390
SSDS	1012	1.71	0.999	265	815	1731
SSWS	1031	1.62	0.999	251	818	1776

Table 4-1 Rosin-Rammler and size parameters of milled eucalyptus, rice husks, SSDS and SSWS (knife mill with 4 mm screen)

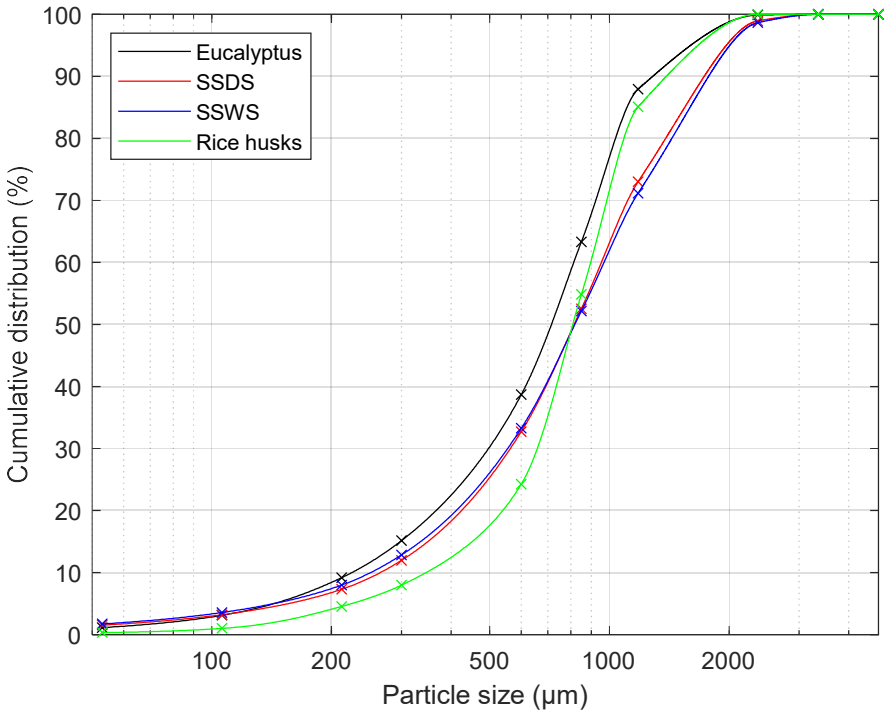

Figure 4-2 Cumulative particle size distribution of milled biomass (knife mill with 4 mm screen)

Sample	Dispersion Parameters						Distribution Shape Parameters	
	s	hs	ls	MRS	C_u	C_c	GS_i	K_g
Euc	1.87	1.53	2.29	1.48	3.61	1.34	0.09	1.10
RH	1.56	1.42	1.72	1.29	2.59	1.40	0.10	1.40
SSDS	2.04	1.86	2.23	1.80	3.60	1.25	0.24	1.00
SSWS	2.11	1.91	2.33	1.86	3.86	1.27	0.25	0.95

Table 4-2 Dispersion and Distribution Shape Parameters of milled eucalyptus, rice husks, SSDS and SSWS (knife mill with 4 mm screen)

4.3 Proximate Analysis

Proximate analysis was conducted using the method as described in Section 3.1.1, which also included a discussion of data quality and the repeatability of the experiments. The thermal composition of the eucalyptus, rice husks and sugarcane

straw samples are shown in Table 4-3. The values shown (except for moisture content) were calculated on both a dry basis and a dry-ash-free basis (dafb). The rice husks and sugarcane straw samples have much higher ash content (23.6-30.2%) compared to eucalyptus (0.6%). Rice husks are known to have a high ash content, mostly due to a high silica content (Hossain et al., 2018). Agricultural residues like sugarcane straws are known to have high ash content due to the presence of foreign matter, soil and mud (Martinez-Mendoza et al., 2023). The amount of soil and mud present is also expected to be higher in the wet season compared to the dry season, which is reflected in the higher ash content of the wet season sample. On a dry-ash-free basis, the volatiles to fixed carbon ratio is highest for SSWS, followed by SSDS, eucalyptus and rice husks. The high ash contents of rice husks and sugarcane straws could cause issues for power generators, as they exceed the requirements in commonly used biomass standards. For example, Grade B pellets in the non-woody biomass pellet standard BS EN ISO 17225-6:2021 (The British Standards Institution, 2021c) specify a maximum ash content of 10.0%.

		Dry basis			Dry-ash-free basis		
Sample	**Moisture %**	**Volatiles %**	**Fixed carbon %**	**Ash %**	**Volatiles %**	**Fixed Carbon %**	**Volatiles to Fixed carbon ratio**
Euc	8.3	84.8	14.6	0.6	85.3	14.7	5.79
RH	6.8	58.3	11.5	30.2	83.5	14.5	5.07
SSDS	7.8	66.3	10.1	23.6	86.8	13.2	6.55
SSWS	7.2	65.6	8.2	26.3	88.9	11.1	8.04

Table 4-3 Thermal composition of eucalyptus, rice husks and sugarcane straws samples

4.4 Intrinsic Reactivity

The intrinsic reactivity of the eucalyptus, rice husks and sugarcane straw samples were measured using a non-isothermal method as described in Section 3.1.1.2. The results of intrinsic reactivity analysis are shown in Table 4-4. For all three peaks, SSWS

was observed to have a significantly higher peak rate compared to all three other samples. The peak burnout temperature of the burnout peak is commonly used as an indicator of intrinsic reactivity (Pang et al., 2018). According to this metric, it can be concluded that the intrinsic reactivity of the samples follows the trend of SSDS>SSWS>rice husks>eucalyptus. Thus, the results suggest that the rice husks and sugarcane straw samples would have superior burnout performance compared to the eucalyptus sample.

	Moisture release		Volatiles release		Burnout		
Sample	**Temp (°C)**	**Rate (%/min)**	**Temp (°C)**	**Rate (%/min)**	**Temp (°C)**	**Rate (%/min)**	**Final burnout (°C)**
Euc	50	1.7	302	11.6	417	9.3	434
RH	48	2.1	296	9.5	401	4.2	434
SSDS	47	2.5	297	9.5	363	9.2	405
SSWS	39	4.9	275	18.3	375	12.9	417

Table 4-4 Intrinsic reactivity analysis of eucalyptus, rice husks and sugarcane straws

4.5 Ultimate Analysis and Calorific Value

The ultimate analysis and calorific value measurement of the eucalyptus, rice husks and sugarcane straws were carried out as described in Section 3.2.3 and 3.1.2. The lower heating value (LHV) was also determined from the higher heating value (HHV) using the ultimate analysis data, with the method and calculations specified in Section 3.1.2. The results of ultimate analysis and calorific value measurement are shown in Table 4-5, with all values calculated on a dry basis. Nitrogen content is an important characteristic as it reflects the NO_x emissions potential of a fuel (H. Chen et al., 2023; Zhan et al., 2018), and the nitrogen content of the rice husks and sugarcane straw samples (0.4-0.5%) is able to meet the requirements of the non-woody biomass pellet standard BS EN ISO 17225-6:2021 (≤1.5% for Grade A pellets and ≤2.0% for Grade B pellets) (The British Standards Institution, 2021c).

The LHV values of rice husks and sugarcane straws (14400-16000 J/g) are significantly lower than that of eucalyptus (19600 J/g). Although non-woody biomass is generally expected to have lower LHV values, as reflected in the lower LHV requirement for non-woody pellets compared to woody pellets (The British Standards Institution, 2021b, 2021c), the low calorific value of these alternative biomass feedstocks compared to wood could still be a concern for the power industry, as greater cost and environmental impact would be incurred through transport to produce the same amount of energy, provided that the transport distance and bulk density are similar. A lower pellet bulk density and lower HHV would result in significantly more biomass being required to provide the same thermal power output, with additional losses in efficiency due to increased transport and milling energy requirements due to increased throughput.

	Dry-ash-free basis				**Dry basis**	
Sample	**C %**	**H %**	**N %**	**O %***	**HHV (J/g)**	**LHV (J/g)**
Euc	46.7	6.3	0.2	46.8	21000	19600
RH	36.9	5.4	0.4	57.3	15600	14400
SSDS	39.9	5.9	0.4	53.8	16800	15500
SSWS	40.1	6.1	0.5	52.5	17200	16000

*calculated by difference

Table 4-5 Ultimate analysis and calorific value of eucalyptus, rice husks and sugarcane straws (dry basis)

4.6 X-ray Diffraction (XRD) Analysis

X-ray Diffraction (XRD) analysis was conducted using the method described in Section 3.2.1 for the eucalyptus, rice husks and sugarcane straw samples. The XRD analysis results of eucalyptus and rice husks are shown in Figure 4-3 and Figure 4-4. The XRD analysis graph of the sugarcane straws is provided in Appendix A and not shown here, as they are similarly shaped as the graphs for eucalyptus and rice husks. XRD is a powerful tool for identifying crystalline materials (Gräbner & Lester, 2016), and the

identification is achieved by matching any peaks observed with a database of the known XRD pattern of a large number of species. However, the XRD analysis graphs of the eucalyptus, rice husks and sugarcane straw samples do not contain any identifiable peaks, which is likely due to the lack of significant quantities of any crystalline species.

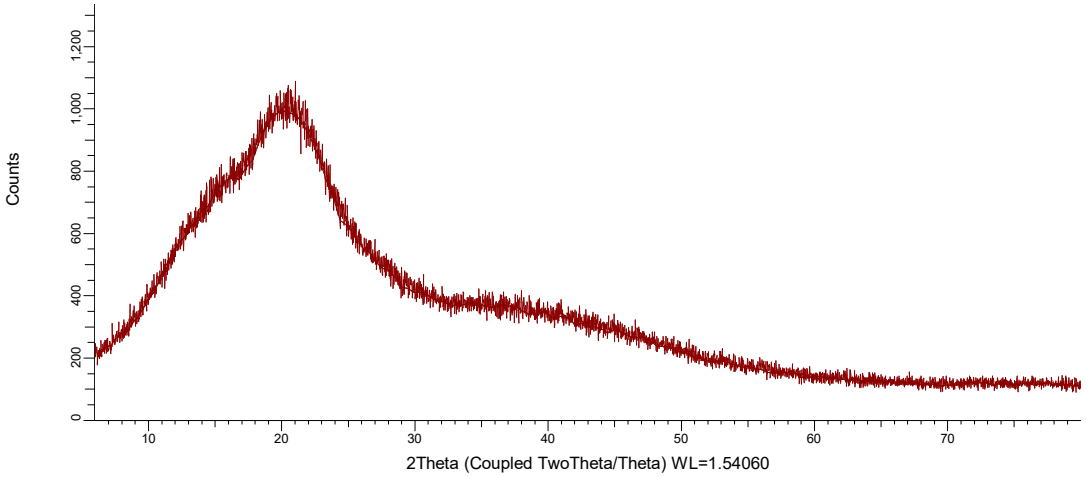

Figure 4-3 XRD analysis of eucalyptus

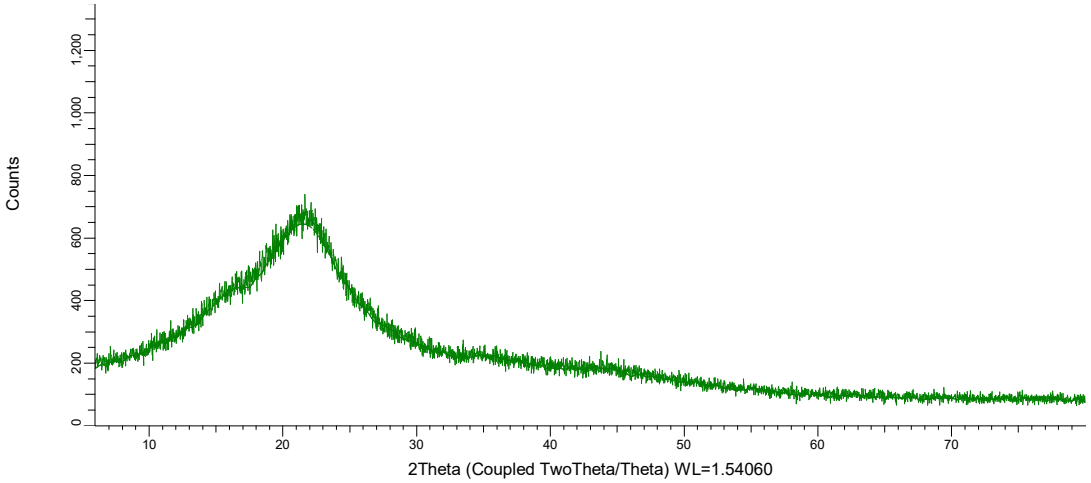

Figure 4-4 XRD analysis of rice husks

These results indicate that XRD analysis of raw biomass samples is not normally a useful technique for mineral identification and should not be conducted as a routine biomass characterisation method, except in cases where crystalline species may be present due to contamination or being intentionally added at some point during the process history of a material. It was found that cardboard materials represent such a case where XRD analysis can be a valuable technique, as further discussed in Chapter

5. The XRD analysis of biomass ash may also be a useful technique, as any non-combustible species present would be in higher concentrations in biomass ash compared to the raw samples.

4.7 Conclusions

Several biomass materials were characterised in this Chapter using a range of techniques. The tests conducted include milling and particle size analysis, proximate analysis, intrinsic reactivity analysis, ultimate analysis, calorific value measurement and X-ray diffraction (XRD) analysis. The characterisation of the eucalyptus, rice husks and sugarcane straw samples demonstrate the variability of biomass materials. Compared to commonly used woody fuels like eucalyptus, the use of some alternative biomass feedstocks such as rice husks and sugarcane straws for power generation may be challenging due to factors like their high ash content and low calorific value. In addition, it was found that XRD of raw biomass samples is not normally a useful technique for the characterisation of biomass, although it could be valuable in some special cases. As many of the samples used in this thesis were supplied by the industrial sponsor on a commercially sensitive basis, the characterisation data presented in this Chapter also provide a basis for further study of the cardboard materials in Chapter 5 and sugarcane straws in Chapter 7.

Chapter 5 - Cardboard Characterisation

5.1 Introduction

With an estimated 5.4 million tons of paper and cardboard packaging wastes generated in the UK in 2021 (Statista, 2023), this is a resource available in large quantities for various applications. There is also a practical limit on the number of times that cardboard can be recycled (usually between five and seven times) due to the shortening of fibre length and decrease of quality as the material is recycled (QCR Recycling Equipment, 2022). Thus, not all cardboard wastes can be recycled and there is potential to use cardboard wastes for energy applications, particularly in the context where there is increasing interest from industry in using alternative biomass sources to wood (see Section 1.1). In addition, with calcium carbonate and kaolin being commonly used fillers in cardboard manufacturing (Section 2.1.2.1) as well as common additives to mitigate slagging issues (Section 2.3), the use of cardboard materials as the main fuel or part of a blend of fuels for large-scale power generation could have unique implications. Cardboard is also a potential resource that is locally available in almost all geographies and it is an advantage over imported fuels, as transport requirements would be relatively low.

This Chapter studies the properties of cardboard as a potential biomass feedstock. The characterisation of cardboard materials was carried out using a range of techniques and potential opportunities and challenges of using cardboard materials for power generation applications were identified and discussed. Literature review (Section 2.1.2) has revealed that although there are a reasonable amount of existing studies on the combustion of cardboard, the number and breadth of studies is not as substantial as many other types of more commonly used biomass. Particular knowledge gaps include the differences in the different types of cardboard, the potential impact of fillers, the char morphology of cardboard materials and particle shape change during combustion. These knowledge gaps are among the areas studied in this Chapter.

5.2 Materials and Methods

Cardboard and eucalyptus are the biomass types used in this Chapter. Eucalyptus is a widely used wood-based fuel for bioenergy applications (Andritz, 2022; Voegele, 2018) and was used as a baseline comparison to evaluate the special properties of the cardboard materials. In addition, eucalyptus is one of the common raw materials used to manufacture cardboard (Magaton et al., 2009). Some of the experimental data of the eucalyptus sample previously discussed in Chapter 4 are also presented in this Chapter as it is necessary for clarity when comparing the cardboard materials with eucalyptus.

Figure 5-1 The structure of corrugated cardboard (Fruit Growers Supply, 2020)

Cardboard is subdivided into corrugated cardboard (which consists of 2 flat outer layers and a ruffled inner layer, as shown in Figure 5-1), and non-corrugated cardboard (or paperboard, which consists of one flat layer only), and corrugated carboard is further subdivided into unprinted and printed versions. This results in three types of cardboard samples: 1. Unprinted cardboard (UCB); 2. Printed Cardboard (PCB); and 3. Printed paperboard – PPB). In this thesis, UCB refers to corrugated cardboard with no or minimal printing, PCB refers to corrugated carboard with printing over the majority of the surface, and PPB refers to non-corrugated cardboard with printing over the majority of the surface. It should also be noted that PCB typically have a lower thickness than UCB. Theoretically, unprinted paperboard (UPB) can also exist and may have unique properties. However, UPB is not studied in

this thesis as it is seldom manufactured and used and therefore has limited industrial significance. The three cardboard samples (UCB, PCB and PPB) (shown in Figure 5-2) were analysed separately to evaluate potential differences between the types of cardboard caused by the presence of ink and glue, manufacturing methods and other factors.

The methods used in this Chapter are described in Chapter 3, including thermogravimetric analysis (Section 3.1.1), X-ray diffraction (Section 3.2.1), combustion characterisation (Section 3.4), and particle size and shape analysis (Section 3.6).

Figure 5-2 Three types of cardboard samples - Unprinted Cardboard (UCB), Printed Cardboard (PCB), Printed Paperboard (PPB) (from left to right)

5.3 Handling properties of Cardboard Materials

The three cardboard materials were milled in a knife mill (see Section 3.5.1) to assess their milling behaviour and to produce milled samples for subsequent analyses. It was observed that when cardboard materials are milled with a knife mill, the particles have a strong tendency to form large mats or clumps (see Figure 5-3). These are referred to as 'fluffy agglomerations'. These fluffy agglomerations typically consist of a wide range of particle sizes and have very low bulk densities (the agglomerations are easily compressible by hand and a large proportion of the volume consists of air). This phenomenon will likely cause severe handling issues if cardboard is used as a fuel for power generation, with quality degradation, longer processing time and

potential fire hazards (Papadakis & Bahu, 1992) being among the known issues with such materials. The tendency of shredded paper to form clumps is also known (Elliston et al., 2013; Windsor & Bate, 2019) and associated handling issues, such as trapped clumps in reaction vessels, have been described (Elliston et al., 2013).

In addition to handling issues, this tendency to form large agglomerations is also particularly problematic when conducting particle analysis with a traditional tapping sieve shaker (see Section 3.6.1), where particles of wide ranges of particle sizes would adhere to each other to form large clumps (Figure 5-3). Thus, no meaningful particle size analysis of the milled cardboard could be conducted using the tapping sieve shaker. However, it was found that this issue can be largely resolved by using a vibratory sieve shaker (see Section 3.6.1), as the continuous vibrations can temporarily revert the fluffy agglomerations to individual particles and prevent new agglomerations from forming (even though new agglomerations would form almost immediately after vibration is stopped).

Although many biomass materials are known to have different shapes compared to coal, which would cause handling issues (Owonikoko et al., 2010), the seriousness of the issue for milled cardboard was much more substantial than what is observed for other types of biomass. Electrostatic charges were also observed to be a contributing factor to the formation of agglomerations in milled cardboard, a phenomenon that is also sometimes observed for other types of biomass (Cui & Grace, 2006; Miller et al., 2002), although this is mostly observed for very fine particles at micron or sub-micron sizes (Deng et al., 2023; Šupuk et al., 2012), which is not the case for the milled cardboard. The presence of static electricity in shredded paper is also known (Sumner, n.d.), while there are no available studies in the existing literature on the impact of static electricity on handling issues and the formation of agglomerations for cardboard materials.

Therefore, the phenomenon of severe agglomeration in milled cardboard is an important but currently underexplored topic for industry. It is also possible that this phenomenon would depend on the type of mill and fracture mechanisms. Further studies on this topic would be valuable for industry, particularly focusing on the possible causes of the observed phenomenon and the impact of static electricity.

Figure 5-3 A 'fluffy agglomeration' of milled cardboard on a sieve

5.4 Particle size analysis

The eucalyptus and cardboard samples were milled in a knife mill with a 4 mm screen for subsequent tests and analysis (see Section 3.5.1). Using a vibratory sieve shaker (see Sections 3.6.1 and 5.3), the mass retained on each sieve was recorded and the data was used for particle size analysis in this Section. The cumulative particle size distributions of the milled eucalyptus and cardboard samples are shown in Figure 5-4. Tables 5-1 and Table 5-2 show the Rosin-Rammler parameters, selected interpolated size parameters, dispersion parameters and distribution shape parameters (see Sections 3.6.2 and 3.6.3).

The particle size distribution (PSD) of milled biomass is an important consideration for combustion. It can be observed from Figure 5-4 that the PSD of all three milled cardboard materials are similar to each other but are drastically different from that of milled eucalyptus. The Rosin-Rammler analysis also gave a good fit for all four samples ($R^2 > 0.997$).

Although the dispersion parameters display a degree of variance between the three milled cardboard samples, a clear trend is observed – the dispersion parameters of milled cardboard are comparable to each other while they deviate significantly from those of milled eucalyptus. The geometric standard deviation parameters (*s, hs and ls*) are all higher for milled eucalyptus than milled cardboard, indicating a narrower

distribution for milled cardboard. For all four materials, *ls* is significantly larger than *hs*, indicating that the lower regions of the distributions have a higher level of variance than the higher regions. The *MRS* values of all four materials are above one. This indicates a wide distribution, with milled eucalyptus having a wider distribution than milled cardboard, which is also indicated by the low *n* values from the Rosin-Rammler analysis.

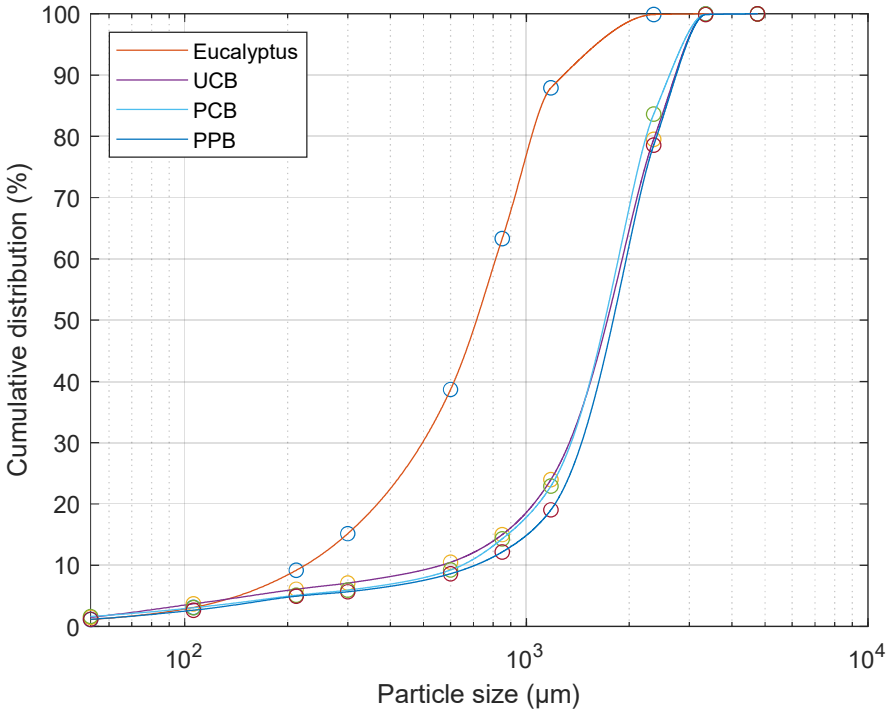

Figure 5-4 Cumulative particle size distributions of the milled eucalyptus and cardboard samples

Similar to the dispersion parameters, when considering the distribution shape parameters, the values for the milled cardboard materials are comparable to each other but are significantly different from those of milled eucalyptus. The milled eucalyptus has a positive GS_i and all three milled cardboards have a negative GS_i, indicating that the milled eucalyptus has a comparatively large proportion of fine particles, while the cardboards have a comparatively large proportion of coarse particles. The PSD of all four samples are leptokurtic, indicating that the curves are better sorted in the central parts than in the tails, with the milled eucalyptus being more leptokurtic than the milled cardboards.

The particle size analysis carried out in this Section indicates that there are multiple differences between the PSD of milled eucalyptus and cardboard materials, illustrating that cardboard materials have unique milling properties compared to eucalyptus and warrant attention when being used for combustion. However, there are no apparent differences between the three cardboard types, indicating that factors such as the presence of ink and/or glue, and the thickness of cardboard have minimal effects on milling behaviour.

Sample	Rosin-Rammler			Size Parameters (µm) - Cubic interpolation		
	d' (µm)	n	R^2	d_{10}	d_{50}	d_{90}
Euc	840	1.90	0.999	225	715	1285
UCB	1935	2.28	0.997	564	1726	2728
PCB	1886	2.50	0.998	648	1699	2625
PPB	2003	2.58	0.998	709	1796	2745

Table 5-1 Rosin-Rammler and size parameters of milled eucalyptus and cardboard

Sample	Dispersion Parameters						Distribution Shape Parameters	
	s	hs	ls	MRS	C_u	C_c	GS_i	K_g
Euc	1.87	1.53	2.29	1.48	3.61	1.34	+0.09	1.10
UCB	1.68	1.46	1.93	1.25	3.38	1.66	-0.08	1.12
PCB	1.60	1.40	1.84	1.16	2.87	1.52	-0.10	1.23
PPB	1.55	1.41	1.70	1.13	2.77	1.51	-0.08	1.23

Table 5-2 Dispersion and distribution shape parameters of milled eucalyptus and cardboard

5.5 X-ray Diffraction (XRD) Analysis

X-ray diffraction (XRD) was conducted using the method described in Section 3.2.1 for the raw and ash samples for the eucalyptus and cardboard materials to investigate their mineral content, with the main goal of identifying fillers which may be present in the cardboard materials. It is known that various fillers are used in the cardboard manufacturing process, with the most common fillers being calcium carbonate ($CaCO_3$) and kaolin ($Al_2Si_2O_5(OH)_4$), with talc ($Mg_3(Si_2O_5)_2(OH)_2$) and titanium dioxide (TiO_2) being used for special applications (Grönfors, 2010) (see Section 2.1.2.1). XRD is a powerful tool for identifying crystalline materials, but it is not generally possible to quantify the amount (Gräbner & Lester, 2016). Therefore, XRD is used in this Section to establish the presence/absence of fillers and not to quantify the amount present.

5.5.1 XRD of Raw Samples

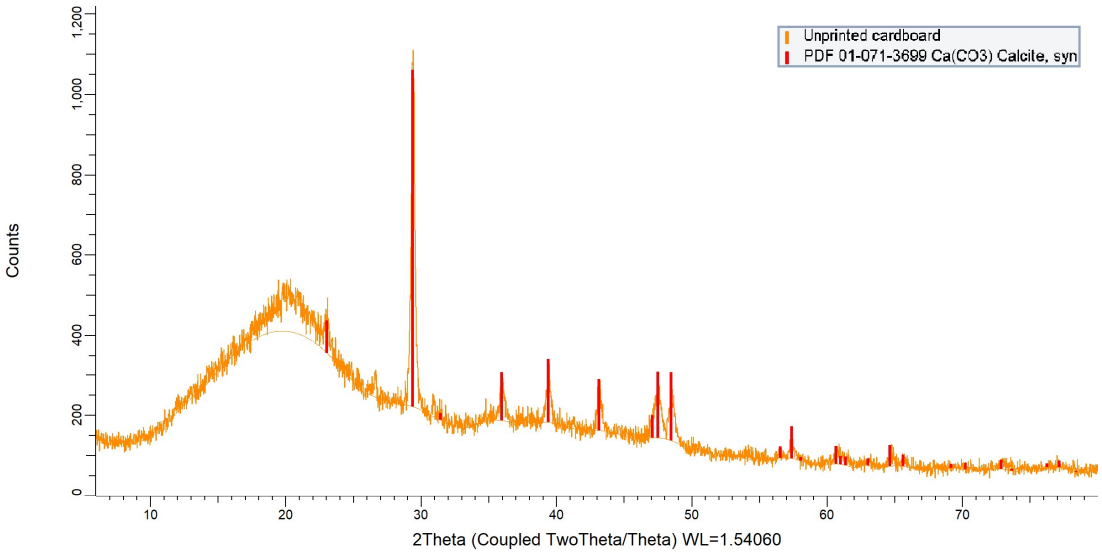

Figure 5-5 XRD analysis of unprinted cardboard

Results of the XRD analysis of three cardboard samples (milled to <300 µm as in Section 3.5.2) are shown in Figures 5-5, 5-6 and 5-7. The XRD analysis of the eucalyptus sample was previously shown in Figure 4-3, which did not have any identifiable peaks, likely due to the lack of significant quantities of any crystalline materials. In contrast, multiple peaks were detected for all of the cardboard materials. Using the Powder Diffraction File (PDF) database, calcium carbonate

($CaCO_3$) could be easily identified in all three cardboard samples. The XRD graph of PPB is more complex than the other 2 cardboard samples, with peaks suggesting the presence of kaolinite ($Al_2Si_2O_5(OH)_4$), although this is only a partial match and a conclusion on whether kaolinite is present in PPB cannot be drawn from the results of XRD analysis alone. Talc and titanium dioxide were also not detected in any of the samples. This confirms the presence of a significant amount of $CaCO_3$ in all three cardboard samples, while the presence/absence of other fillers could not be established through XRD analysis of the raw samples alone.

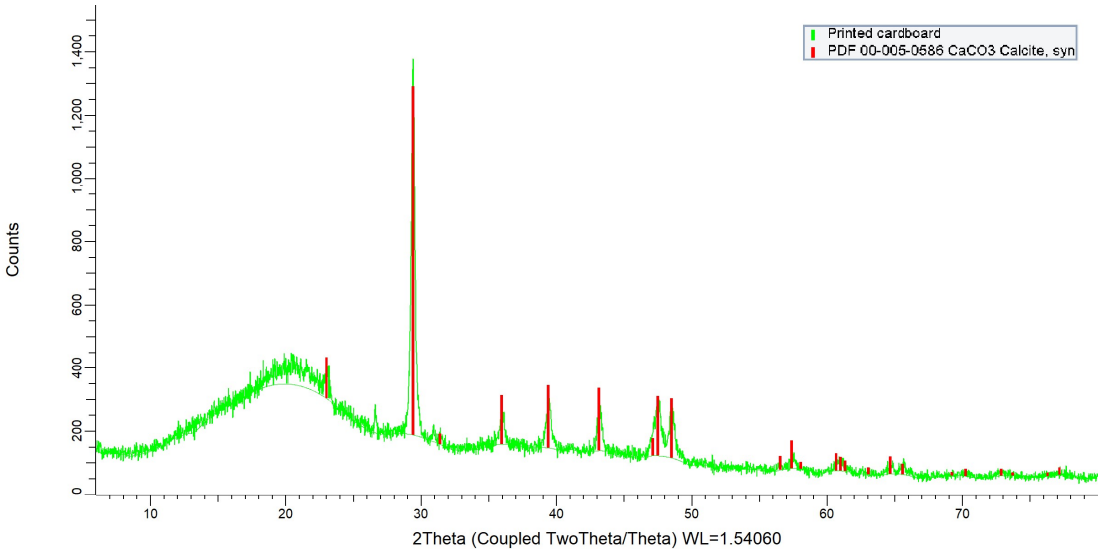

Figure 5-6 XRD analysis of printed cardboard

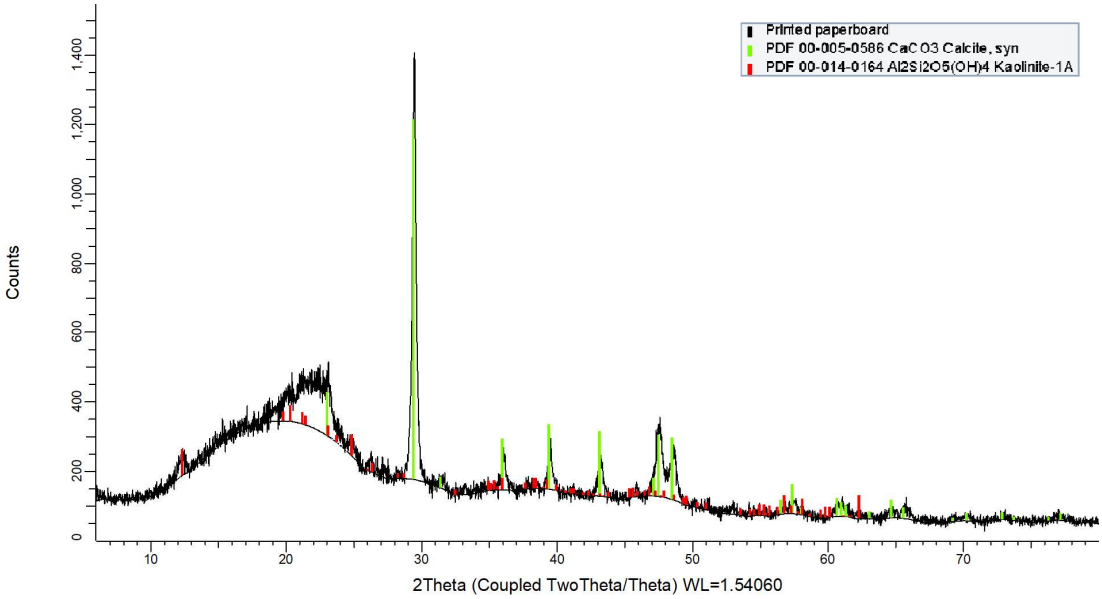

Figure 5-7 XRD analysis of printed paperboard

5.5.2 XRD of Cardboard Ashes

The ability of XRD analysis to identify a species is dependent on the concentration of the species present in the sample. Therefore, XRD analysis of the cardboard ash samples (produced as described in Section 3.2.2) was also carried out to further investigate the presence of fillers in the samples. If fillers are present in the raw sample, the ash samples should, in theory, contain the products of the fillers after being subjected to high temperatures. Results of the XRD analysis of the cardboard ashes are shown in Figure 5-8, Figure 5-9 and Figure 5-10. Calcium oxide (CaO) is identifiable in all three cardboard ash samples, confirming that $CaCO_3$ is present in the raw samples (see equation (5.1). Some silicon and aluminium-containing compounds were also identified, suggesting that kaolinite ($Al_2O_3 \cdot 2SiO_2 \cdot 2H_2O$) may be present in the raw samples. No magnesium and titanium-containing compounds could be identified, suggesting talc ($Mg_3(Si_2O_5)_2(OH)_2$) and titanium oxide (TiO_2) are not present in significant amounts.

Although the same compounds were identified in all three cardboard samples, the peaks of UCB are much lower than the other two samples, suggesting that fillers are used in much smaller amounts in UCB compared to PCB and PPB, likely due to differences in the manufacturing process for cardboard products not intended to be printed on.

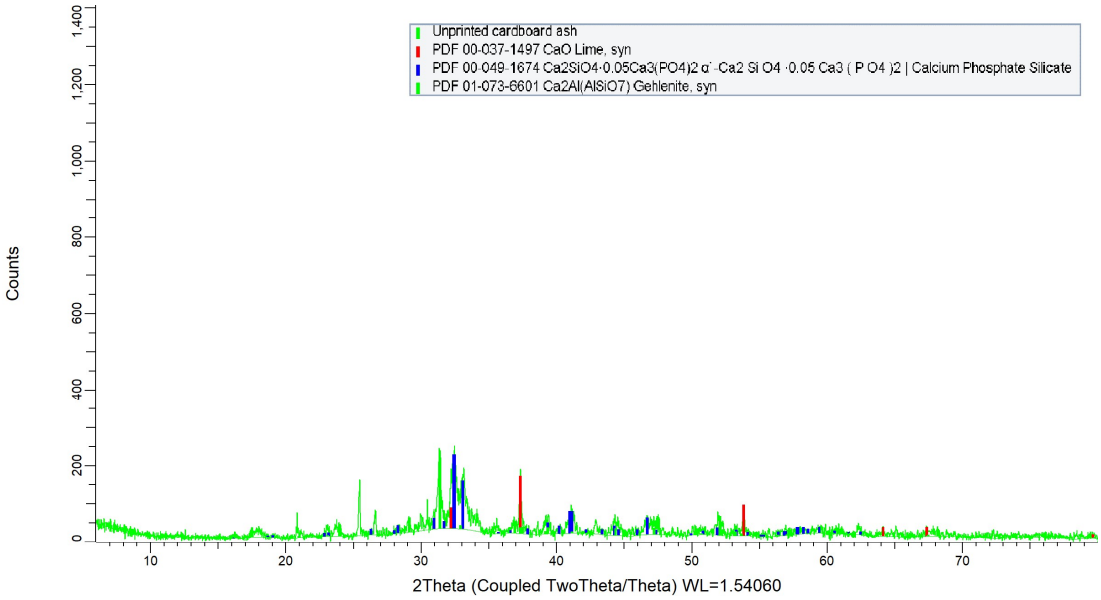

Figure 5-8 XRD analysis of unprinted cardboard ash

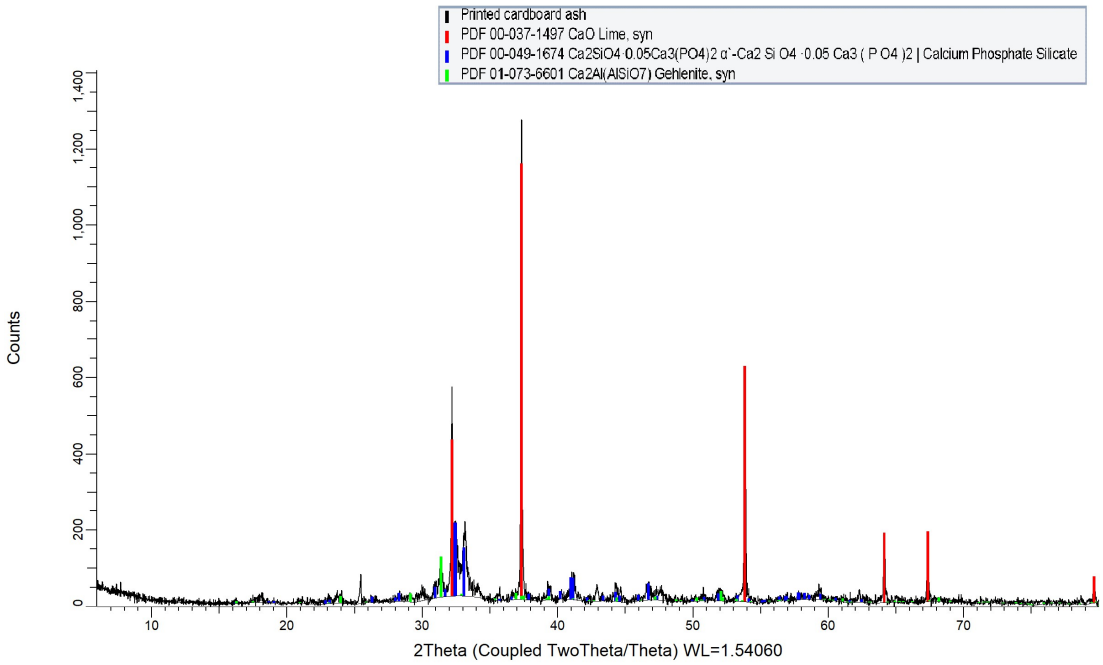

Figure 5-9 XRD analysis of printed cardboard ash

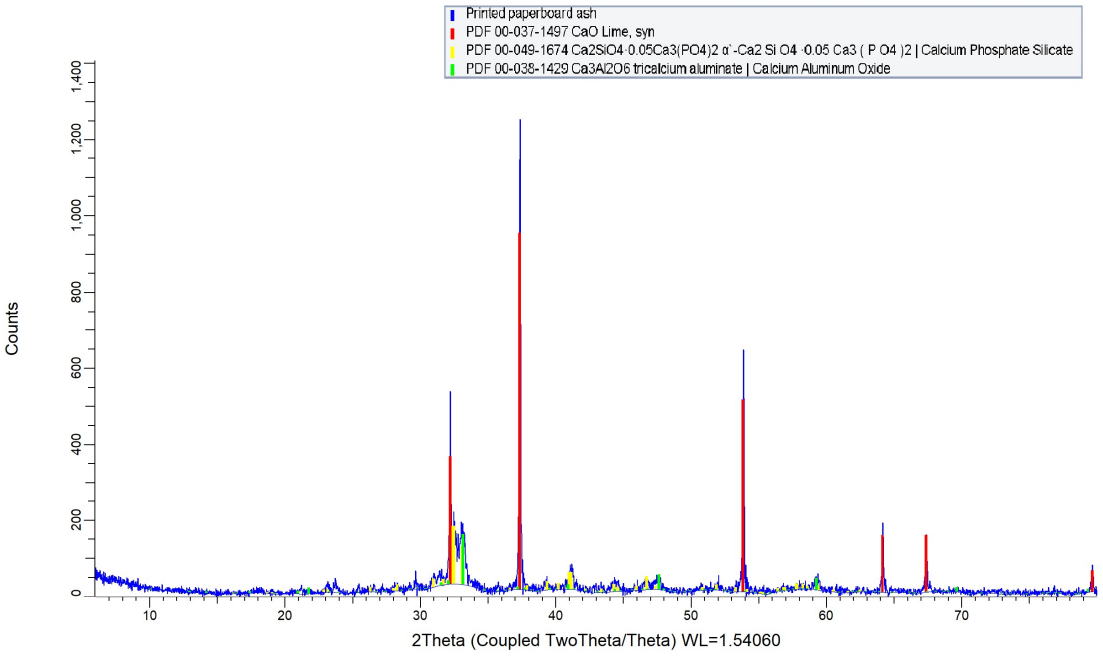

Figure 5-10 XRD analysis of printed paperboard ash

5.6 Proximate Analysis (raw samples)

Proximate analysis of eucalyptus and the cardboard materials was conducted using a thermogravimetric method as described in Section 3.1.1.1, which also included a

discussion of data quality and the repeatability of the experiments. The samples were first dried as in Section 3.3 and then milled with a ball mill to <300 µm as in Section 3.5.2 for TGA tests. The moisture content seen in TGA tests is due to the reabsorption of moisture from the atmosphere.

5.6.1 Thermal Composition and the Effect of Fillers

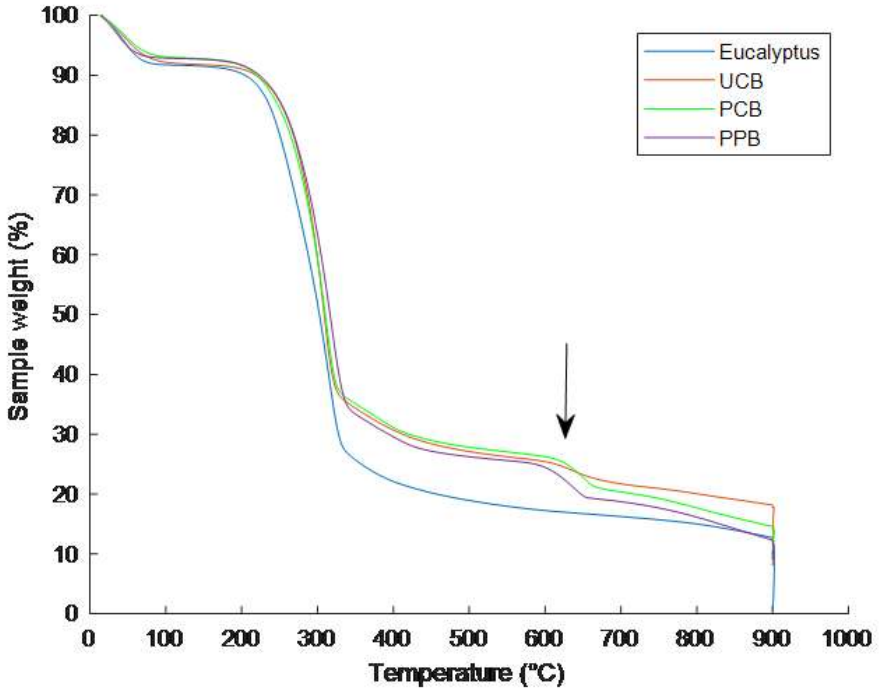

Figure 5-11 Slow pyrolysis test for eucalyptus and cardboard samples (weight vs temperature)

The change in sample weight during the slow pyrolysis test is shown in Figure 5-11. The rate of change (derivative) of weight is also shown in Figure 5-12. The black arrow in Figure 5-11 indicates an area where the curve for the cardboard materials follows an unusual shape, which is not normally expected for biomass, whereas the eucalyptus sample follows a typical shape for biomass. This area of unusual behaviour for the cardboard materials is also visible as additional peaks not normally seen in biomass in the derivative curves shown in Figure 5-12, indicated by the red arrow. The explanation for this unusual behaviour is the presence of calcium carbonate ($CaCO_3$), which is a common filler used in cardboard manufacturing (Grönfors, 2010). At high temperatures, calcium carbonate would decompose to form calcium oxide

(CaO) and carbon dioxide (CO_2), as shown in Equation (5.1). Using the molar mass of atoms, it is calculated that the complete decomposition of $CaCO_3$ should result in a mass loss of 43.97%.

$$CaCO_3 \rightarrow CaO + CO_2 \quad \textbf{(5.1)}$$

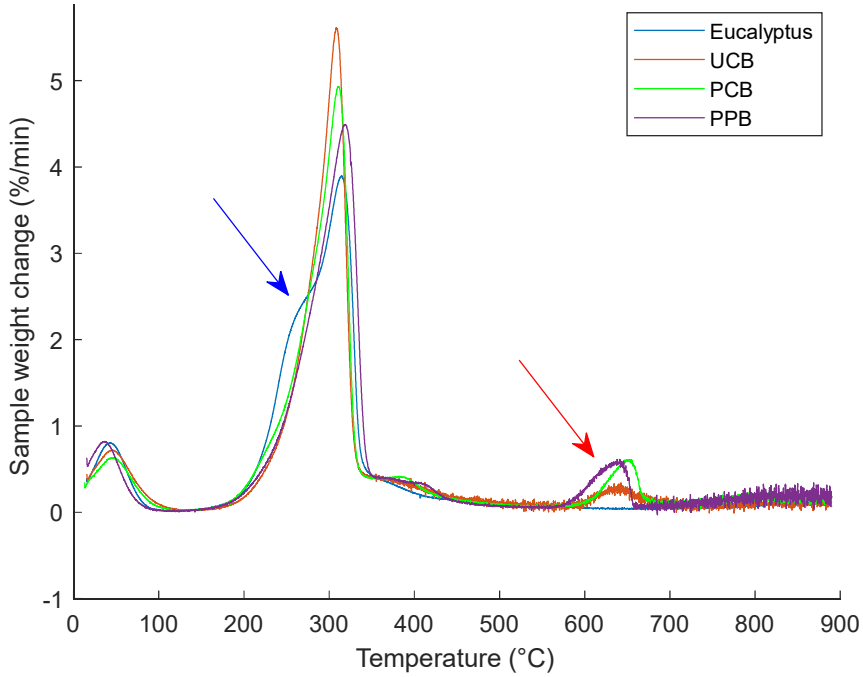

Figure 5-12 Slow pyrolysis test for eucalyptus and cardboard samples (derivative weight vs temperature)

Slow pyrolysis test was carried out with a commercially obtained calcium carbonate powder (purity >99.0%) to investigate the decomposition profile of $CaCO_3$ under slow pyrolysis conditions. The results are shown in Figure 5-13 and Figure 5-14. A mass loss of 44.02% was measured, which is very close to the theoretical value of 43.97%.

In addition to $CaCO_3$, kaolinite ($Al_2O_3 \cdot 2SiO_2 \cdot 2H_2O$) and talc ($Mg_3(Si_2O_5)_2(OH)_2$) are other common fillers used in cardboard manufacturing (Grönfors, 2010) (see Section 2.1.2.1. Kaolinite and talc undergo a dehydroxylation reaction and release water vapour at 450-700°C (Ptáček et al., 2010) and ~800°C (Liu et al., 2014) respectively. However, there are no observable peaks in the derivative weight vs time graphs of the slow pyrolysis tests for the cardboard samples in these temperature regions,

indicating that there is very little kaolinite and talc present in the sample. This is also consistent with the findings of XRD analysis presented in Section 5.5.

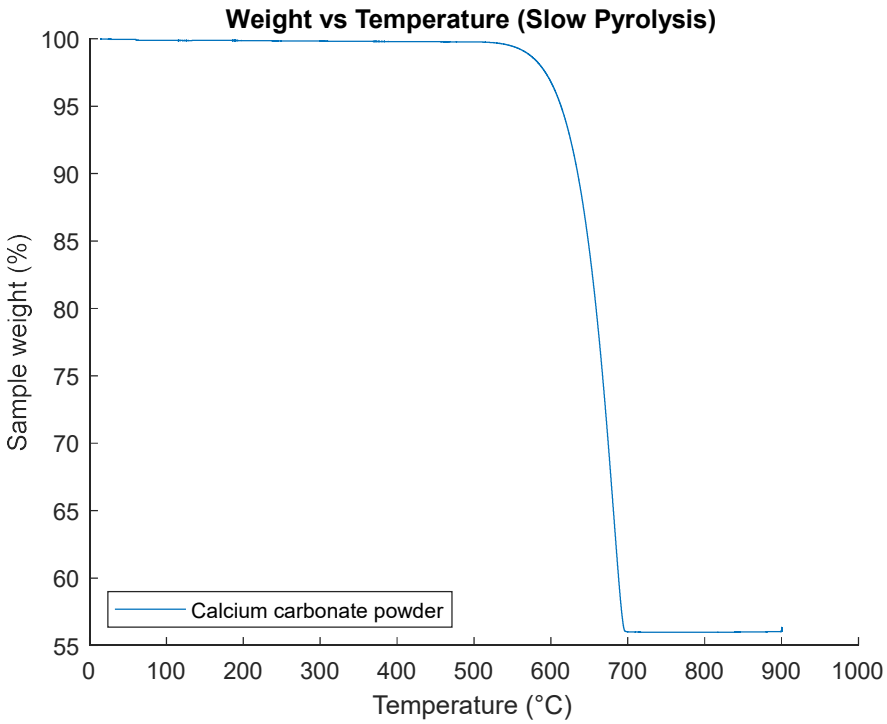

Figure 5-13 Slow pyrolysis test for calcium carbonate powder (weight vs temperature)

Since it is established that a significant amount of $CaCO_3$, which would decompose and release CO_2 gas during the slow pyrolysis test, is present in the cardboard samples, the proximate analysis method would need to be adapted to consider the effect of $CaCO_3$. A similar approach was used by Gräbner and Lester (2016) to correct the proximate analysis results of kaolinite-rich coals with regard to the effects of the dehydroxylation reaction of kaolinite.

The calcium carbonate content (CCC) of the three cardboard samples could be estimated from the slow pyrolysis data, where a clear peak in the region of $CaCO_3$ decomposition (560-700°C) is observed in Figure 5-12. Assuming that the peak is solely caused by the decomposition of $CaCO_3$, the amount of CO_2 released during the slow pyrolysis experiments was estimated by assuming a constant rate of weight loss from volatiles in the region of $CaCO_3$ decomposition and calculating the difference between the theoretical weight loss from volatiles only and the measured weight loss

at a point after the peak in the graph from $CaCO_3$ decomposition, as illustrated in Figure 5-15.

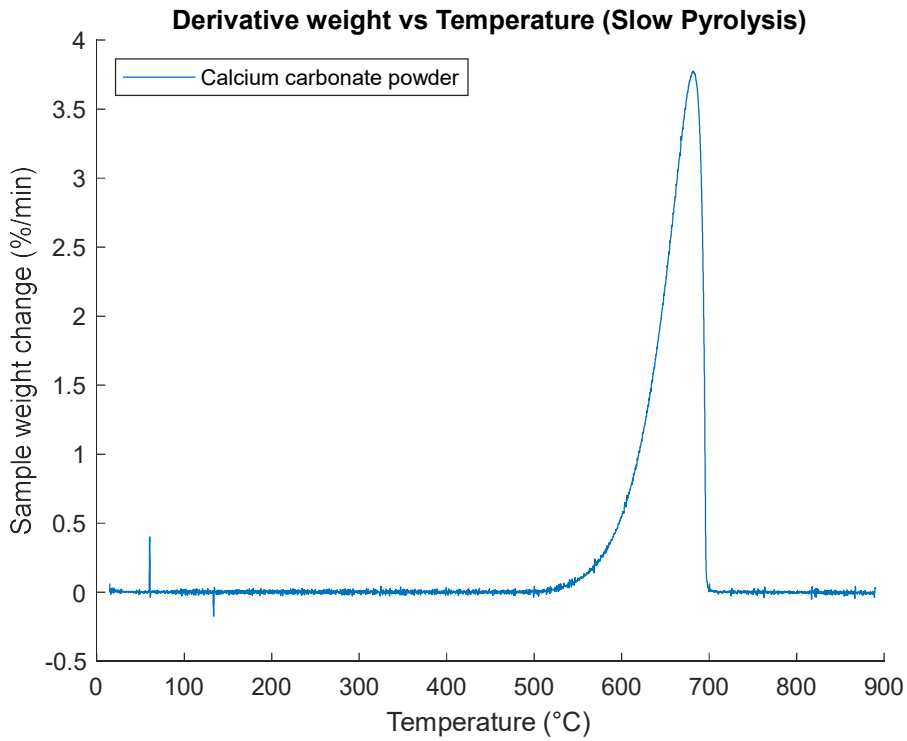

Figure 5-14 Slow pyrolysis test for calcium carbonate powder (derivative weight vs temperature)

This is a newly developed technique of estimating CCC from TGA data under slow pyrolysis conditions, which has not been described in literature before. Choi et al. (2017) also used TGA to measure the CCC of soil samples. However, apart from their method being used for soil rather than biomass, their calculations assumed that the decomposition of $CaCO_3$ is the only reaction that releases gaseous products occurring in the decomposition temperature range of $CaCO_3$, whereas this assumption was not made in the newly developed method. In addition, their experiments were conducted their test in air, whereas the newly developed method is conducted in a nitrogen atmosphere, which should result in a quicker and more complete decomposition reaction due to the effects of CO_2 partial pressure (Galan et al., 2013), thus providing a more accurate measurement.

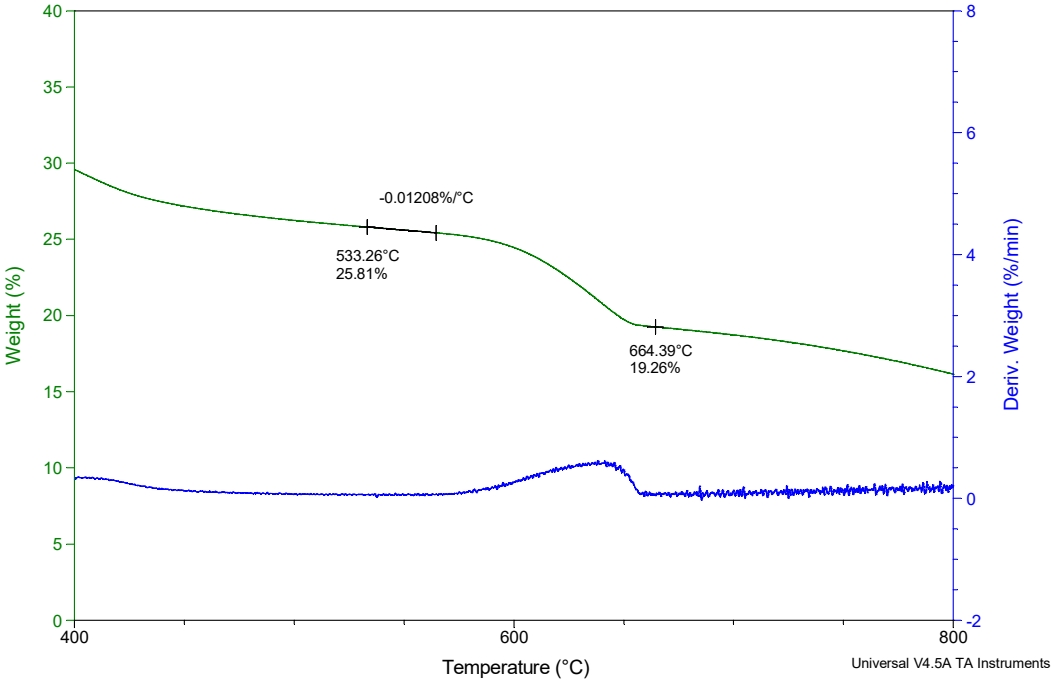

Figure 5-15 Printed paperboard $CaCO_3$ content calculation

		Dry basis					
Sample	Moisture %	Volatiles %[1]	Fixed carbon %	CO_2 released %	$CaCO_3$ %	Ash %[2]	% of CaO in ash
Euc	8.3	84.8	14.6	N/A	N/A	0.6	N/A
UCB	8.0	76.8	11.9	2.4	5.5	8.9	34.5
PCB	7.0	78.2	6.6	4.6	10.4	10.6	54.9
PPB	7.2	79.3	5.4	5.3	12.2	9.9	68.6

[1]excludes CO_2 released by $CaCO_3$ decomposition for cardboard samples

[2]includes CaO from decomposition of $CaCO_3$ for cardboard samples

Table 5-3 Proximate analysis for eucalyptus and cardboard samples (dry basis)

A commonly used method for measuring the carbonate content of soils is also described in ASTM D4373-21 (ASTM, 2021). This method uses hydrochloric acid, which reacts with carbonates in the sample in a sealed, fixed-volume container to release CO_2. The pressure inside the container after the completion of the reaction

was then measured, which was calibrated to measure the carbonate content of the sample in units of calcite equivalent %.

Although standards exist for measuring carbonate content in soils (ASTM, 2021), calcium content in raw biomass and calcium oxide content in biomass ash (The British Standards Institution, 2015b, 2015e), there is no current standard for measuring CCC in biomass. The newly developed technique to measure CCC in biomass represents a relatively simple method integrated into proximate analysis, which is already commonly conducted for biomass fuels. Further work should also be conducted to confirm the accuracy of this new method by comparing its results to other methods such as mineral liberation analysis (MLA) as conducted by Gräbner and Lester (2016).

	Dry ash-free basis			
Sample	Volatiles %[1]	CO_2 released %	Fixed carbon %	Volatiles to fixed carbon ratio
Eucalyptus	85.3	N/A	14.7	5.8
UCB	84.3	2.6	13.1	6.5
PCB	87.5	5.1	7.4	11.8
PPB	88.1	5.9	6.0	14.7

[1]excludes CO_2 released by $CaCO_3$ decomposition for cardboard samples

Table 5-4 Proximate analysis for eucalyptus and cardboard samples (dry ash-free basis)

This newly developed method was used to analyse the slow pyrolysis experimental data, and the results are shown in Table 5-3. The values shown (except for moisture content) were calculated on a dry basis. The volatiles content shown excludes the estimated amount of CO_2 released from the decomposition of $CaCO_3$. The printed samples (PCB and PPB) also have higher CCC (10.4-12.2%) compared to the unprinted samples (UCB, 5.5%). This is an expected result which is consistent with the results of XRD analysis (Section 5.5), as it is known that one of the main uses of fillers (predominantly $CaCO_3$) is to improve printability and it is therefore likely that more fillers would be added to manufacture cardboard materials that are intended to be

printed on (Biermann, 1996; Grönfors, 2010). All of the cardboard materials have fairly high ash contents (8.9-10.6%). PCB and PPB also have slightly higher ash contents than UCB, which could be explained by the presence of ink in the samples. In addition, a substantial percentage (34.5-68.6%) of the ash for the cardboard samples originates from the $CaCO_3$ present. The comparison of cardboard properties and commonly used biomass standards is provided in Section 5.12. The thermal compositions of the sample on a dry ash-free basis (dafb) are shown in Table 5-4. The volatiles to fixed carbon ratio of eucalyptus and UCB are similar (5.79 and 6.46 respectively), while it is much higher for PCB and PPB (11.78 and 14.70 respectively).

5.6.2 Lignin, Cellulose and Hemicellulose

Using the meth

od based on the work of Pang et al. (2014) and described in Section 3.1.1.1, the slow pyrolysis data could be used to give a qualitative assessment of the lignin, cellulose and hemicellulose content of the samples. The derivative weight vs time graph (Figure 5-12) of the eucalyptus sample shows a characteristic shape consisting of a hemicellulose 'shoulder' (indicated by the blue arrow in the figure) and a cellulose peak, with the lignin peak being obscured by the other two components (thus the presence/absence of lignin could not be confirmed using the slow pyrolysis results alone). However, the hemicellulose 'shoulder' is absent for the cardboard samples, indicating that the cardboard samples are hemicellulose-deficient.

It is known that the cardboard manufacturing process typically removes the majority of the lignin and hemicellulose in the raw material to produce a cellulose-rich pulp (Biermann, 1996; Fearon et al., 2020). Thus, the finding from the slow pyrolysis results that the cardboard samples are hemicellulose-deficient is consistent with the known practices in cardboard manufacturing. Although the deficiency in lignin could not be confirmed with the slow pyrolysis results as lignin peak would likely be obscured if it is present, the cardboard samples are also likely lignin-deficient as it is typically removed during the cardboard manufacturing process.

The deficiency in both hemicellulose and lignin could have an effect on the use of cardboard materials for power generation. Hemicellulose is the most reactive of the

three components, while lignin is less reactive. As cardboard is both hemicellulose- and lignin-deficient, the individual effects on the reactivity would cancel out to some extent and the overall effect is difficult to determine.

Pang et al. (2018) studied the link between lignocellulosic components and char morphology, finding that hemicellulose deficiency correlates with more thick-walled and less thin-walled porous chars while lignin deficiency correlates with less thick-walled chars. Considering the reactivity of the char types (see Section 2.4). It also follows that the individual effects of hemicellulose and lignin deficiency on reactivity would cancel out to some extent. The char morphology of eucalyptus and cardboard materials is studied in greater detail in Section 5.9.

5.7 Ultimate Analysis and Calorific Value

The ultimate analysis and calorific value measurement of the eucalyptus and cardboard samples were carried out as described in Sections 3.2.3 and 3.1.2. The lower heating value (LHV) was also determined from the higher heating value (HHV) using the ultimate analysis data and the method and calculations specified in Section 3.1.2.

Sample	C %	H %	N %	O %*	HHV (J/g)	LHV (J/g)
Eucalyptus	46.7	6.3	0.19	46.8	21000	19600
UCB	38.9	5.3	0.25	55.6	16400	15200
PCB	38.2	5.6	0.22	56.0	15900	14700
PPB	39.3	5.7	0.19	54.8	16500	15200

*calculated by difference

Table 5-5 Elemental analysis and calorific value data for eucalyptus and cardboard (dry basis)

For both the elemental composition and calorific value, the measured results of the three types of cardboard materials are comparable to the previously reported values in literature by Boumanchar et al. (2017) and Lela, Barišić and Nižetić (2016). The

results are shown in Table 5-5. All values were calculated on a dry basis. All three cardboard samples have lower carbon and hydrogen content and higher O content compared to the eucalyptus sample. The measured HHV values of all samples are within the typical range reported for biomass in literature (14000-21000 J/g (Demirbas, 2004)). Eucalyptus has a higher HHV than the cardboard samples, while all three cardboard samples have similar HHV (~15000 J/g). The low calorific value of cardboard materials compared to wood could be a concern for the power industry, as greater cost and environmental impact would be incurred through transport to produce the same amount of energy, provided that transport distances are similar.

5.8 Intrinsic Reactivity

The intrinsic reactivity of the eucalyptus and cardboard samples was measured using a non-isothermal method, as described in Section 3.1.1.2. In addition to the three normally observed peaks corresponding to the moisture release, devolatilisation and combustion processes, an additional peak associated with $CaCO_3$ decomposition was observed for the cardboard samples. The results of intrinsic reactivity analysis are shown in Table 5-6. For the cardboard materials, the $CaCO_3$ decomposition peak was not considered for the determination of burnout temperature, as the decomposition of $CaCO_3$ is not considered to be a combustion process.

	Moisture release		**Volatiles release**		**Burnout**			**$CaCO_3$ decomposition**	
Sample	Temp (°C)	Rate (%/min)	Temp (°C)	Rate (%/min)	Temp (°C)	Rate (%/min)	Final burnout (°C)	Temp (°C)	Rate (%/min)
Euc	50	1.7	302	11.6	417	9.3	434	N/A	N/A
UCB	51	1.9	300	13.4	370	7.1	412	621	0.5
PCB	51	1.9	296	14.6	346	6.6	392	623	0.8
PPB	43	2.7	308	20.3	372	3.7	414	636	1.5

Table 5-6 Intrinsic reactivity analysis of eucalyptus and cardboard samples

For the moisture release peak, eucalyptus, UCB and PCB have similar peak temperatures (50-51°C) and peak rates (1.7-1.9 %/min), while PPB has a significantly lower peak temperature (43°C) and higher peak rate (2.7 %/min). For the volatiles

release peak, all samples have a similar peak temperatures (296-308°C), and eucalyptus, UCB and PCB have similar peak rates (11.6-14.6 %/min), while PPB has a significantly higher peak rate of 20.3 %/min. The more rapid moisture and volatiles release of PPB could be due to PPB particles being generally of a smaller thickness. For the burnout peak, the peak burnout temperature is commonly used as an indicator of intrinsic reactivity (Pang et al., 2018), and it is concluded that the reactivity of the samples follows the trend of PCB>UCB>PPB>eucalyptus. The final burnout temperature also follows a similar trend. This indicates that cardboard materials generally have superior burnout performance compared to eucalyptus, which is also confirmed in the burnout simulation results in Section 5.9.2. For the $CaCO_3$ decomposition peak, all three cardboard samples have similar peak temperatures (621-636°C), while the peak rates roughly follow the trend of $CaCO_3$ content as determined in Section 5.6.1.

5.9 Combustion Characteristics and Char Morphology

The combustion behaviour of eucalyptus and cardboard materials was characterised by producing chars using a drop tube furnace and a muffle furnace, followed by an analysis of the morphology of the char produced. This Section presents, for the first time, a detailed study of the char morphology of cardboard materials.

5.9.1 Char Morphology

The methods used for char morphology analysis are described in Section 3.4. Chars were produced for four samples (eucalyptus, UCB, PCB, PPB) with two char production methods and for two particle sizes each, resulting in a total of 16 chars. The chars were examined under an oil immersion microscope and categorised using the method described by Lester et al. (2018) (Section 3.4.4), which categorised biomass char structures into eight types using three main distinguishing properties (wall thickness, porosity and aspect ratio). The char morphology of the eucalyptus and cardboard chars are summarised in Table 5-7 and also presented as a stacked bar chart in Figure 5-16. In addition, the relative abundance of char structures, grouped by the three distinguishing properties of biomass char, as well the ratios of chars identified as thin-walled vs thick-walled, porous vs cellular and high-aspect-ratio-vs low-aspect-ratio are presented in Table 5-8.

5.9.1.1 Influence of biomass type

All cardboard chars show higher thin-walled-to-thick-walled ratios and porous-to-cellular ratios compared to their eucalyptus counterparts with the corresponding char method and particle size. As thin-walled chars and porous chars are known to be more reactive and burn out more rapidly compared to thick-walled and cellular chars (Lester et al., 2018), these ratios show that cardboard chars would burn out more rapidly than eucalyptus chars if they have the same particle shape. The porous-to-cellular ratio also suggests that for the cardboard materials, either the cardboard manufacturing process has significantly disrupted the cellular structures (Section 2.1.2.1) or the cellular structures in cardboard are more easily disrupted by the char production process. As the char structures of cardboard materials are more porous and thin-walled than eucalyptus, cardboard materials are likely to burn quickly provided that the particles are 'discrete' (which may be affected by the tendency of milled cardboard to form large agglomerations as discussed in Section 5.3).

All char samples (eucalyptus and cardboard) have a large percentage of high-aspect-ratio particles (74.6-100%). This is an expected result as biomass particles are known to have higher aspect ratios compared to coal (Guo et al., 2012). The differences in char particle shape are further discussed in Section 5.11. Between the three types of cardboard materials studied, there are no apparent patterns between the material type and the relative abundance of the types of chars.

5.9.1.2 Influence of particle size

For the chars produced using the drop-tube furnace, which simulates PF conditions, the percentages of thin-walled and porous chars are higher for the smaller particle size (106-300 µm) compared to the larger particle size (600-850 µm). This suggests that the residence time (200 ms) used was not sufficient for the larger particle size sample to largely devolatilise, which is also confirmed with the proximate analysis of char samples (Section 5.10). The percentage of high-aspect-ratio particles is also consistently higher for the smaller particle size DTF chars compared to the larger particle size. The differences in char particle shape are further discussed in Section 0.

For the chars produced using the muffle furnace, which simulates a fluidised bed or stoker furnace system, particle size does not have an apparent relationship with the ratio of thin-walled to thick-walled chars or the ratio of porous to cellular chars. In contrast, all of the larger particle size sample (1180-2360 µm) were measured to have a larger percentage of high-aspect-ratio char particles compared to the smaller particle size sample (600-850 µm). This result is consistent with the observation in the literature that the average aspect ratio of biomass particles typically decreases with particle size (Guo et al., 2012).

5.9.1.3 Influence of combustion system

Samples with a particle size of 600-850 µm were processed with both the DTF and the muffle furnace (MF). Comparing the morphologies of the DTF and muffle furnace chars for the 600-850 µm particle size, both the ratio of thin-walled to thick-walled chars and the ratio of porous to cellular chars are higher for the muffle furnace chars compared to the DTF chars for all four types of biomass. This shows that although the muffle furnace used a much lower temperature (900°C) compared to the DTF (1300°C), the longer residence time used (3 minutes for the muffle furnace and 200 ms for DTF) resulted in a greater extent of devolatilisation for the muffle furnace method.

5.9.2 Burnout Prediction

The burnout performances of the eucalyptus and cardboard chars were predicted using the method developed by Perkins (Perkins, 2020) and described in Section 3.4.5. The burnout profiles of the various char morphology classes (Figure 3-4) were used in conjunction with the char morphology data (Table 5-7) to predict the burnout profiles of the eucalyptus and cardboard samples. The predicted profiles are shown in Figure 5-17 to Figure 5-20.

The burnout of cardboard materials is substantially quicker than that of eucalyptus for all particle sizes and both combustion systems. This is mainly due to the higher percentage of thin-walled and porous chars in the cardboard chars compared to their eucalyptus counterparts with the corresponding char method and particle size.

When comparing the four combinations of char method and particle size, it was found that the three cardboard MF 1180-2360 µm chars have almost identical burnout behaviour, while the DTF 106-300 µm, DTF 600-850 µm and MF 600-850 chars vary significantly in terms of burnout behaviour. However, no clear trends of how this is affected by the type of cardboard could be identified.

While the exact effect of ink in the printed samples and the glue in the corrugated samples on burnout is not easily identifiable, it is clear that the different types of cardboard demonstrated a degree of variability in burnout behaviour, which should be considered by industry when considering and implementing the use of cardboard materials for combustion applications.

5.10 Proximate Analysis (Char Samples)

Proximate analysis was carried out using the method described in Section 3.1.1.1 to investigate the change in thermal composition during the char production process. The thermal composition of the raw size fractions and chars of eucalyptus and cardboard samples are shown in Figure 5-23. The results show that in general, the larger size fraction (600-850 µm) used for the DTF method did not have a sufficient residence time (200 ms) to largely devolatilise, while all of the MF chars have mostly devolatilised. This also supports the earlier finding (Section 5.9.1.2) that for the DTF chars, the percentages of thin-walled and porous chars are higher for the smaller particle size (106-300 µm) compared to the larger particle size (600-850 µm).

The yield and combustion efficiency for each char were calculated using the method described in Section 3.4.3 and the results are shown in Table 5-9. This data was also used in Section 5.11.1 for subsequent analysis. The $CaCO_3$ content of the raw size fractions and chars of cardboard samples was determined using the method developed in Section 5.6.1. The results are shown in Table 5-10, Table 5-11 and Table 5-12. It was observed that for all of the raw cardboard samples, the $CaCO_3$ content is more concentrated in the larger size fractions (600-850 and 1180-2360 µm) compared to the smallest size fraction (106-300 µm).

	Relative abundance (%)															
Sample	**Eucalyptus**				**UCB**				**PCB**				**PPB**			
	DTF 106-300	DTF 600-850	MF 600-850	MF 1180-2360	DTF 106-300	DTF 600-850	MF 600-850	MF 1180-2360	DTF 106-300	DTF 600-850	MF 600-850	MF 1180-2360	DTF 106-300	DTF 600-850	MF 600-850	MF 1180-2360
tCH	14	2.4	30	32	14	19.6	17.2	8	11.4	18	6.4	7.4	25	48.8	4	8.2
TCH	61	93.6	57	56	8	58.8	3.8	7	19.2	54	2.6	6	8.8	24.8	2	8.2
tPH	15	0	4	7	72	13.6	40.2	59	36.4	12	77.6	60.8	63.2	18.8	68	60.4
TPH	10	0	2	2	6	0.2	13.4	23	29	4	7.8	25.8	1.4	3.8	14	21.6
tCL	0	0	0	1	0	0	1.8	0	4	0	0	0	1.6	0	0	0
TCL	0	0	2	0	0	0	0.8	0	0	0	0.4	0	0	0	0	0
tPL	0	1.6	0	2	0	7.8	11.4	3	0	12	4	0	0	3.8	8	0
TPL	0	2.4	5	0	0	0	11.4	0	0	0	1.2	0	0	0	4	1.6
Total	100	100	100	100	100	100	100	100	100	100	100	100	100	100	100	100

Table 5-7 Relative abundance of char structures (%)

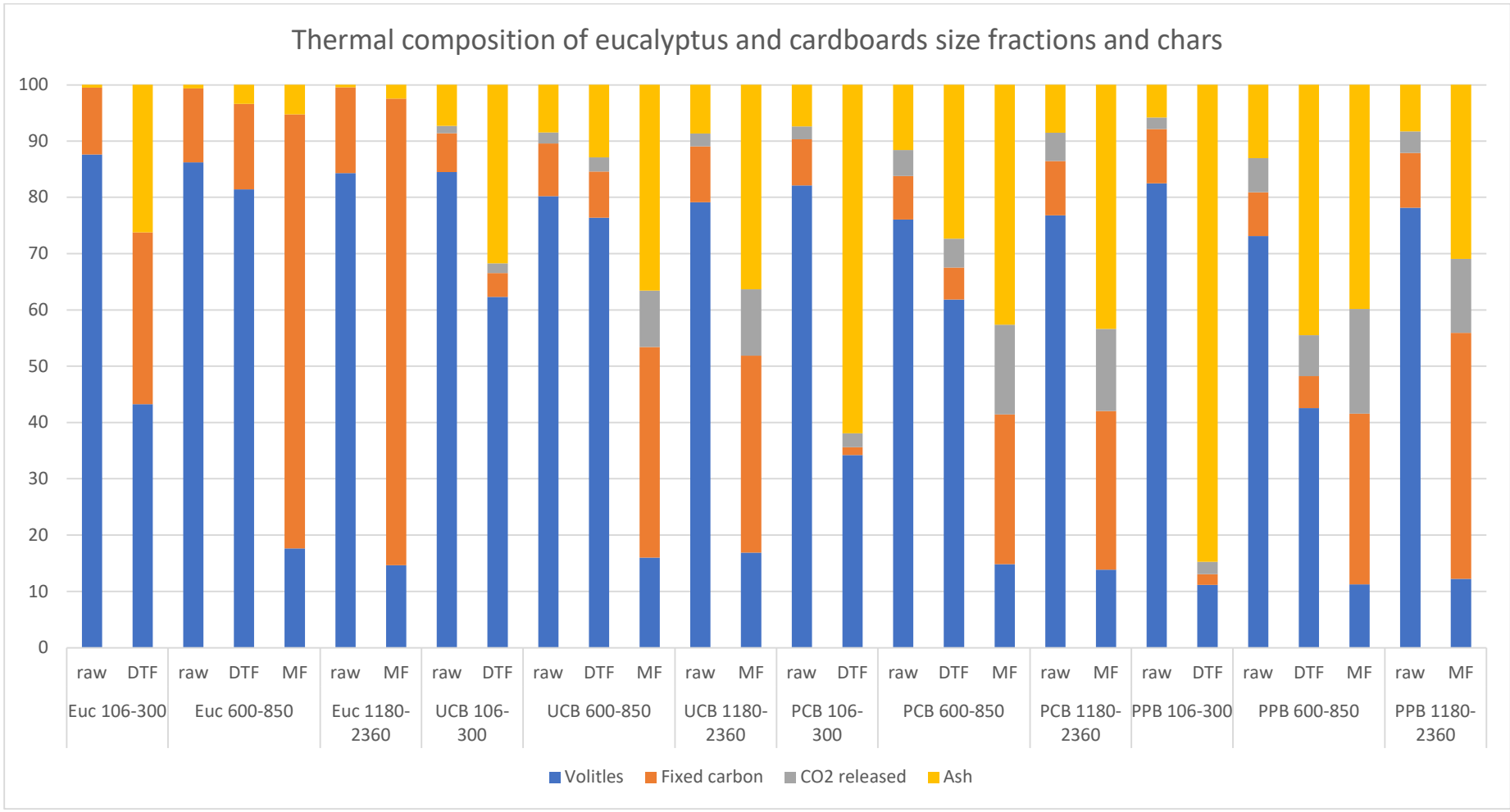

Figure 5-16 Relative abundance of char structures (%)

	Relative abundance (%)															
	Eucalyptus				UCB				PCB				PPB			
Sample	DTF 106-300	DTF 600-850	MF 600-850	MF 1180-2360	DTF 106-300	DTF 600-850	MF 600-850	MF 1180-2360	DTF 106-300	DTF 600-850	MF 600-850	MF 1180-2360	DTF 106-300	DTF 600-850	MF 600-850	MF 1180-2360
Thin-walled	29.0	4.0	34.0	42.0	86.0	41.0	70.6	70.0	51.8	42.0	88.0	68.2	89.8	71.4	80.0	68.6
Thick-walled	71.0	96.0	66.0	58.0	14.0	59.0	29.4	30.0	48.2	58.0	12.0	31.8	10.2	28.6	20.0	31.4
Thin-walled to thick-walled ratio	0.41	0.04	0.52	0.72	6.14	0.69	2.40	2.33	1.07	0.72	7.33	2.14	8.80	2.50	4.00	2.18
Cellular	75.0	96.0	89.0	89.0	22.0	78.4	23.6	15.0	34.6	72.0	9.4	13.4	35.4	73.6	6.0	16.4
Porous	25.0	4.0	11.0	11.0	78.0	21.6	76.4	85.0	65.4	28.0	90.6	86.6	64.6	26.4	94.0	83.6
Porous to cellular ratio	0.33	0.04	0.12	0.12	3.55	0.28	3.24	5.67	1.89	0.39	9.64	6.46	1.82	0.36	15.67	5.10
High aspect ratio	100	96	93	97	100	92.2	74.6	97	96	88	94.4	100	98.4	96.2	88	98.4
Low aspect ratio	0	4	7	3	0	7.8	25.4	3	4	12	5.6	0	1.6	3.8	12	1.6
Ratio of high-aspect-ratio to low-aspect-ratio	Inf	24.0	13.3	32.3	Inf	11.8	2.9	32.3	24.0	7.3	16.9	Inf	61.5	25.3	7.3	61.5

Table 5-8 Char properties and ratios

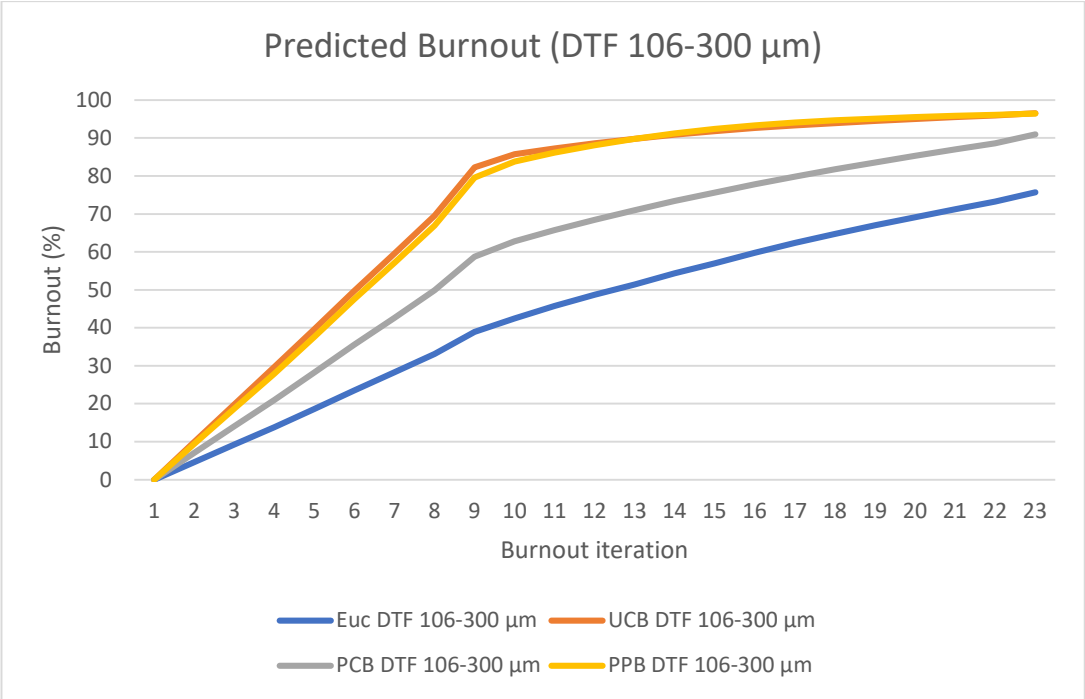

Figure 5-17 Predicted Burnout (DTF 106-300 µm)

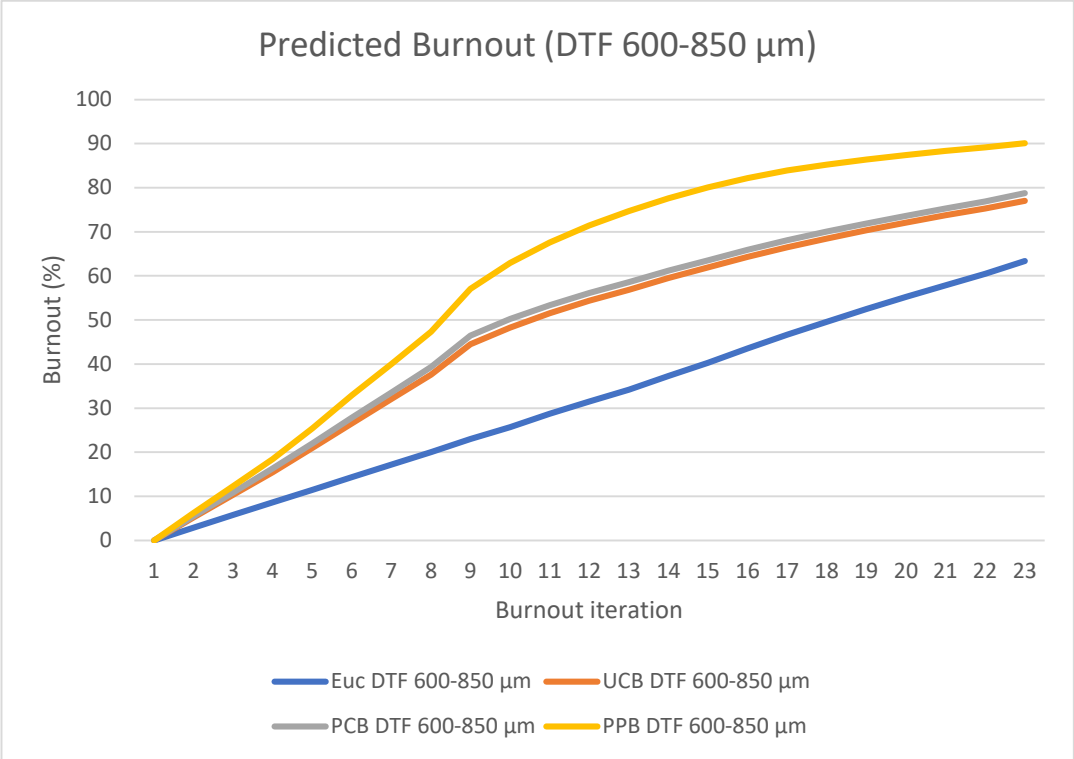

Figure 5-18 Predicted burnout (DTF 600-850 µm)

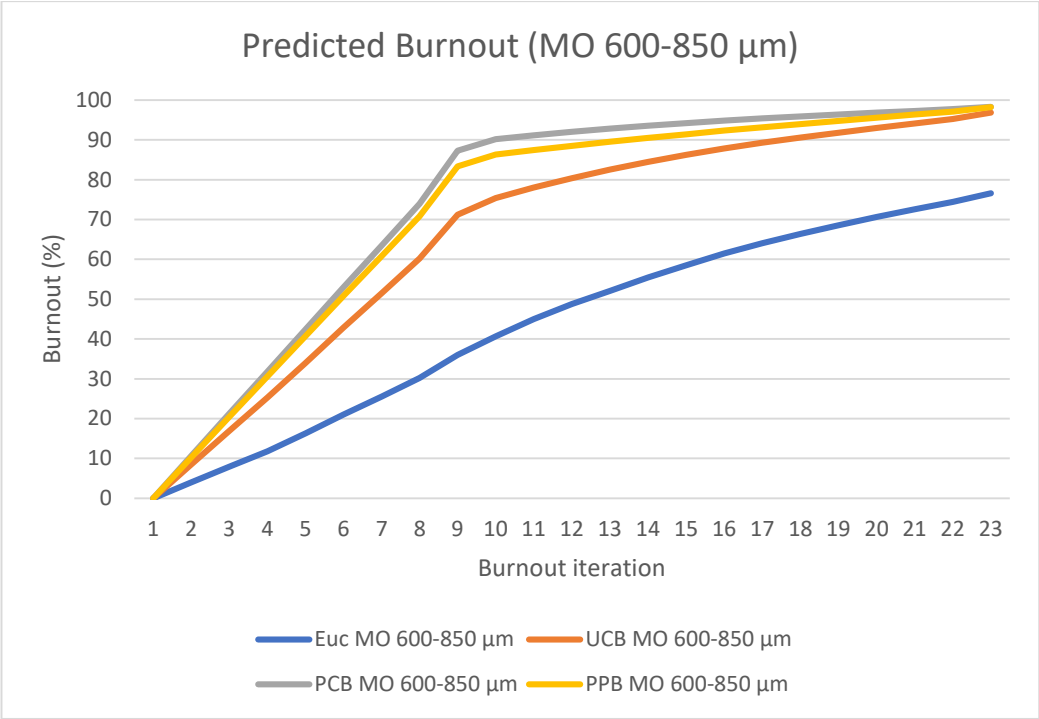

Figure 5-19 Predicted burnout (MO 600-850 µm)

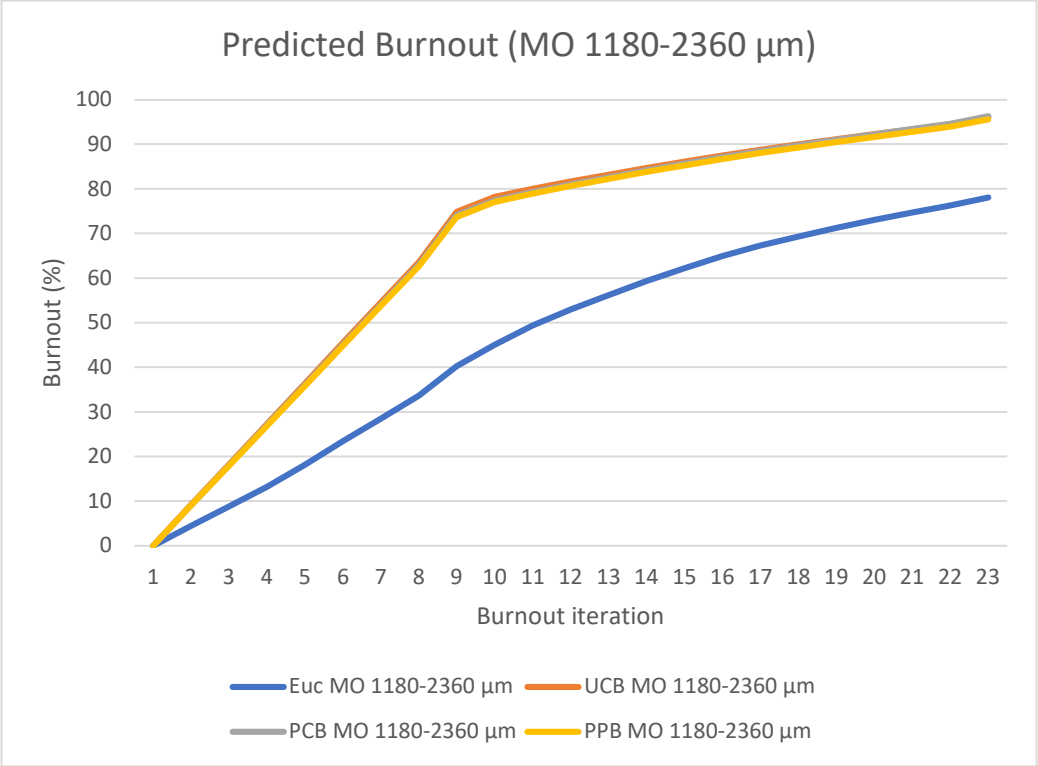

Figure 5-20 Predicted burnout (MO 1180-2360 µm)

Material	Size fraction (µm)	Char method	Yield (%)	Combustion efficiency (%)
Euc	**106-300**	**DTF**	1.9	98.6
Euc	**600-850**	**DTF**	19.1	81.4
Euc	**600-850**	**MF**	12.4	88.2
Euc	**1180-2360**	**MF**	17.8	82.6
UCB	**106-300**	**DTF**	23.1	83.0
UCB	**600-850**	**DTF**	65.7	37.5
UCB	**600-850**	**MF**	23.2	84.0
UCB	**1180-2360**	**MF**	23.8	83.5
PCB	**106-300**	**DTF**	12.0	95.1
PCB	**600-850**	**DTF**	42.4	65.2
PCB	**600-850**	**MF**	27.2	82.4
PCB	**1180-2360**	**MF**	19.7	87.8
PPB	**106-300**	**DTF**	6.8	98.9
PPB	**600-850**	**DTF**	29.4	81.3
PPB	**600-850**	**MF**	32.8	77.3
PPB	**1180-2360**	**MF**	26.8	79.8

Table 5-9 Yield and combustion efficiency for each char

Size fraction (µm)	106-300	106-300	600-850	600-850	600-850	1180-2360	1180-2360
Char method	Raw	DTF	Raw	DTF	MF	Raw	MF
$CaCO_3$ content (%)	2.96	4.00	4.51	5.71	22.78	5.26	26.76

Table 5-10 UCB size fractions and chars $CaCO_3$ content (dry basis)

Size fraction (µm)	106-300	106-300	600-850	600-850	600-850	1180-2360	1180-2360
Char method	Raw	DTF	Raw	DTF	MF	Raw	MF
$CaCO_3$ content (%)	5.19	5.58	10.46	11.61	36.21	11.46	33.17

Table 5-11 PCB size fractions and chars $CaCO_3$ content (dry basis)

Size fraction (µm)	106-300	106-300	600-850	600-850	600-850	1180-2360	1180-2360
Char method	Raw	DTF	Raw	DTF	MF	Raw	MF
$CaCO_3$ content (%)	4.70	4.93	13.70	16.61	42.33	8.73	29.85

Table 5-12 PPB size fractions and chars $CaCO_3$ content (dry basis)

5.11 Particle Size and Shape Comparison of Raw Biomass and Chars

This Section presents the analysis of the differences in particle size and shape of raw biomass and chars for the eucalyptus and cardboard samples. It was previously discussed in Section 2.5 that particle shape is an important factor in combustion modelling, and there is a need for additional biomass shape data, in particular 3D shape factors such as sphericity. The particle size and shape of the raw size fractions and chars were measured using a Camsizer P4 as described in Section 3.6.4. Sieving analysis was not conducted due to the insufficient amount of samples available. However, previous studies have shown that Camsizer and sieving results for biomass correlate well with each other (Trubetskaya et al., 2014; Williams, 2016).

5.11.1 Particle Size

The median particle sizes (d_{50}) of the raw biomass and chars are shown in Table 5-13, and the percentage changes in d_{50} were also calculated. A plot of percentage change in d_{50} vs combustion efficiency (defined in Section 3.4.3 and calculated in Section 5.10) is shown in Figure 5-21. Intuitively, it is expected that the change in d_{50} and combustion efficiency would be positively correlated, as combustion efficiency is a

measure of the extent of the transformation of the particles. However, it is observed in Figure 5-21 that there is no clear correlation between the parameters. Graphs of the PSD of raw biomass and chars were plotted to illustrate the decrease in particle size of the chars compared to the raw biomass. Selected graphs are shown in Figure 5-22 to Figure 5-27. The graphs for all samples are available in Appendix B. It is also concluded from the graphs that no observable swelling of particles had occurred.

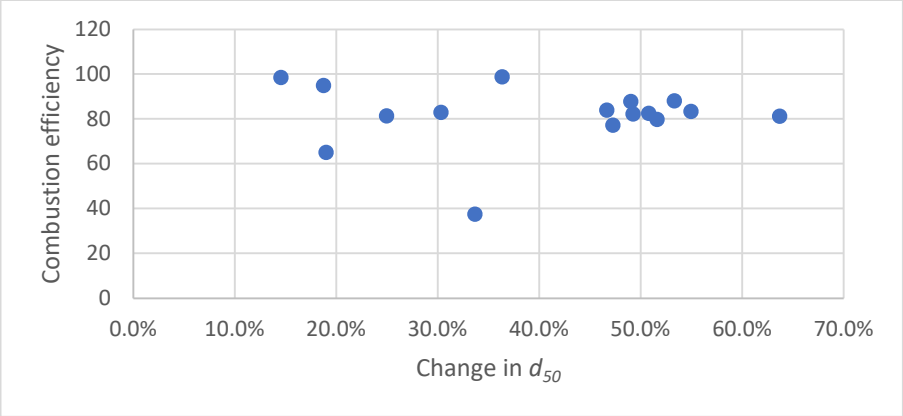

Figure 5-21 Change in d_{50} vs combustion efficiency for all chars

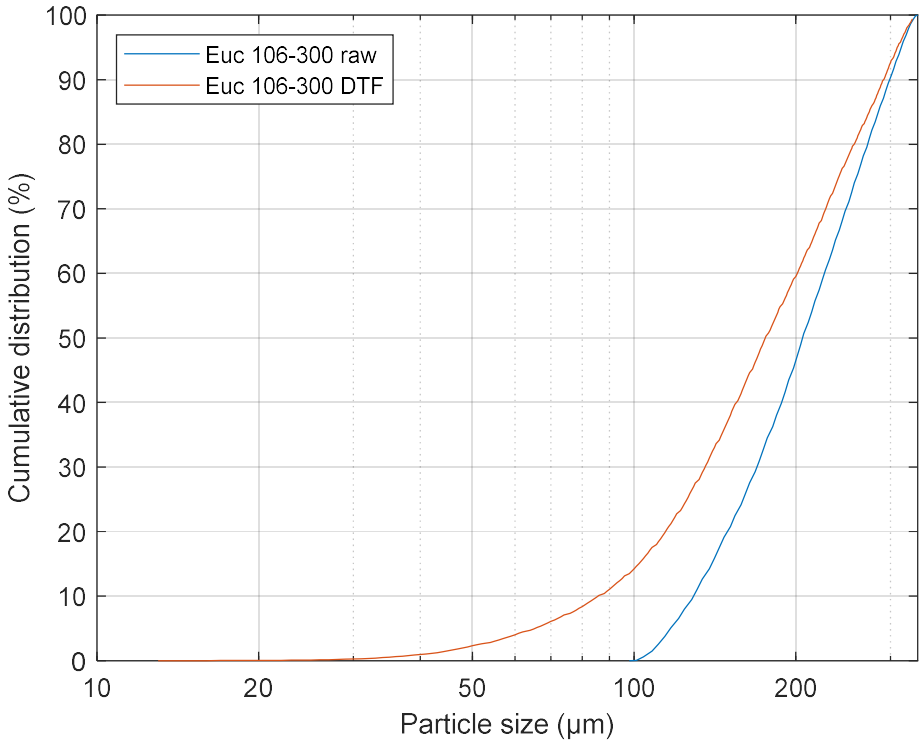

Figure 5-22 Particle size distribution of raw eucalyptus and DTF char (106-300 µm)

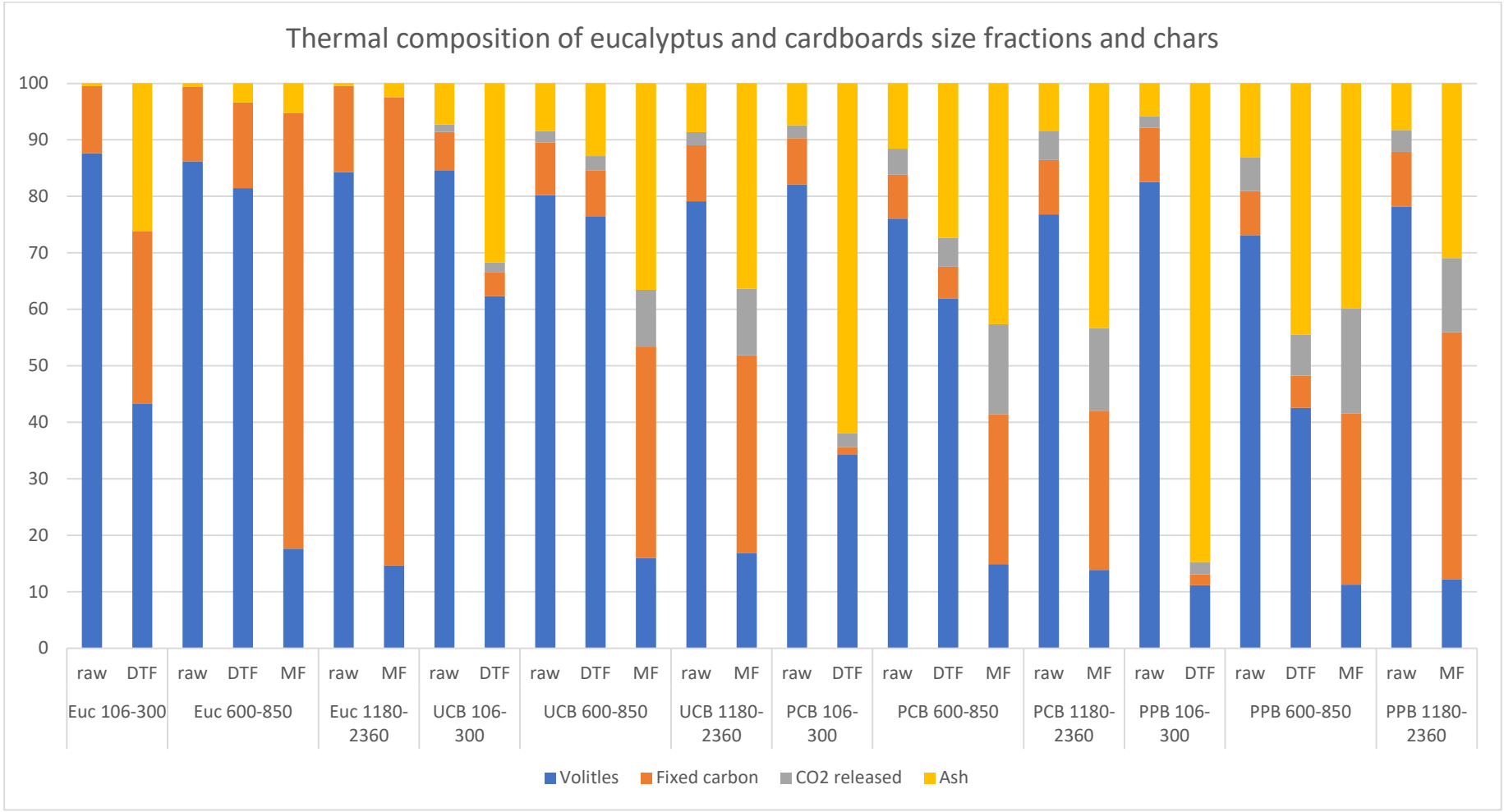

Figure 5-23 Thermal compositions of eucalyptus and cardboards size fractions and chars

Sample	Size fraction (µm)	Char method	Raw biomass d_{50} (µm)	Char d_{50} (µm)	Change in d_{50} (%)
Euc	106-300	DTF	206	176	14.6%
Euc	600-850	DTF	737	553	25.0%
Euc	600-850	MF	737	344	53.3%
Euc	1180-2360	MF	1520	748	50.8%
UCB	106-300	DTF	188	131	30.3%
UCB	600-850	DTF	722	479	33.7%
UCB	600-850	MF	722	385	46.7%
UCB	1180-2360	MF	1681	757	55.0%
PCB	106-300	DTF	192	156	18.8%
PCB	600-850	DTF	731	592	19.0%
PCB	600-850	MF	731	371	49.2%
PCB	1180-2360	MF	1770	902	49.0%
PPB	106-300	DTF	198	126	36.4%
PPB	600-850	DTF	730	265	63.7%
PPB	600-850	MF	730	385	47.3%
PPB	1180-2360	MF	1778	860	51.6%

Table 5-13 Median particle size (d_{50}) of raw biomass and chars for eucalyptus and cardboard samples

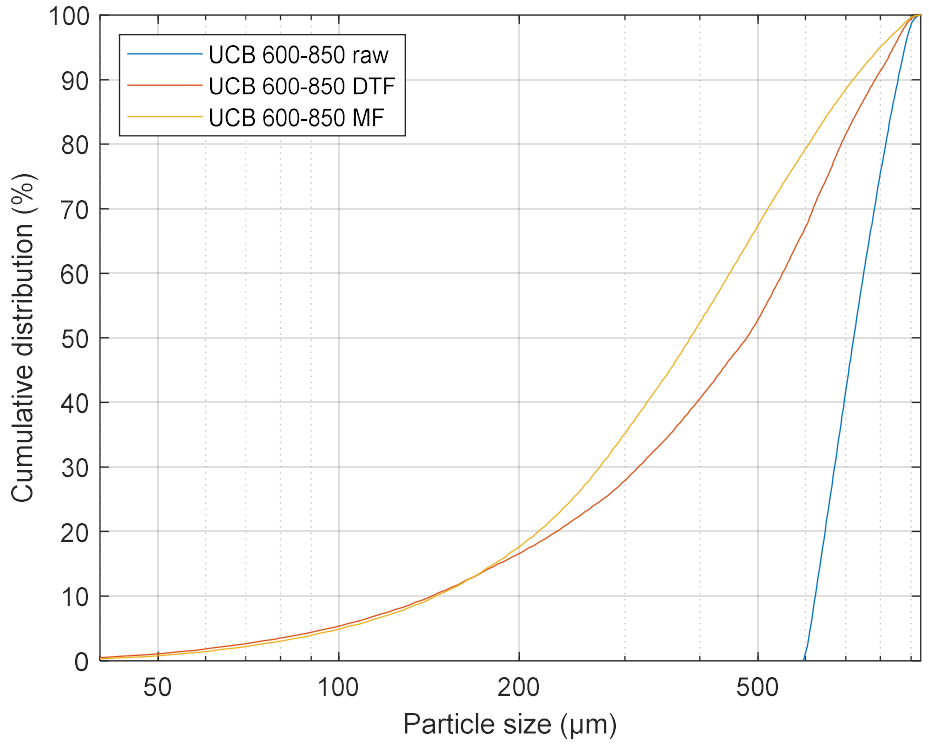

Figure 5-24 Particle size distribution of raw UCB and char (600-850 µm)

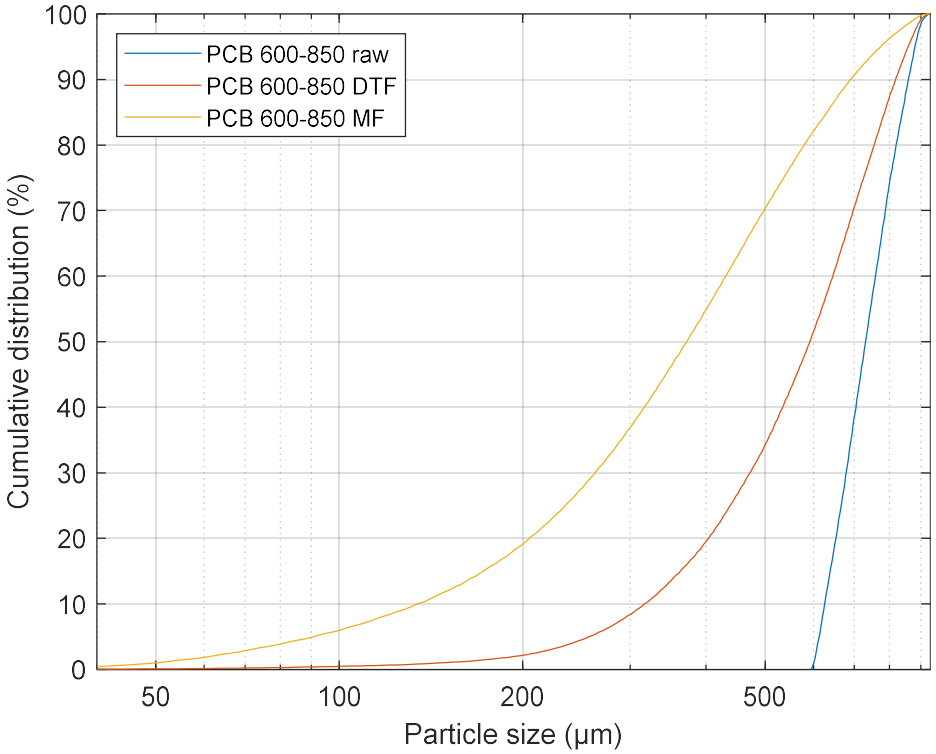

Figure 5-25 Particle size distribution of raw PCB and char (600-850 µm)

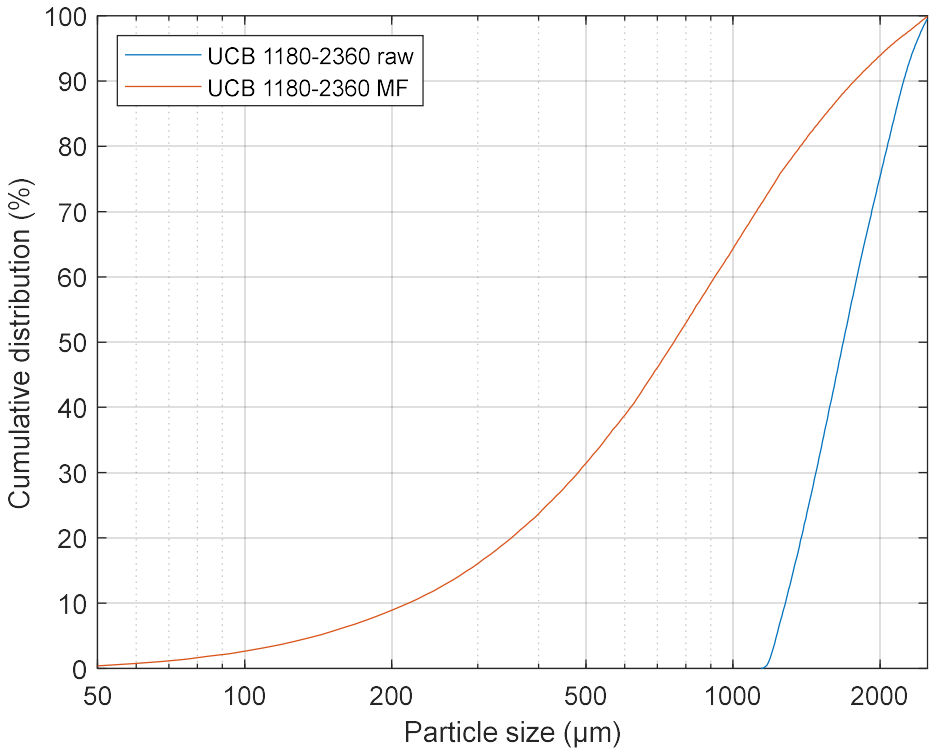

Figure 5-26 Particle size distribution of raw UCB and MF char (1180-2360 µm)

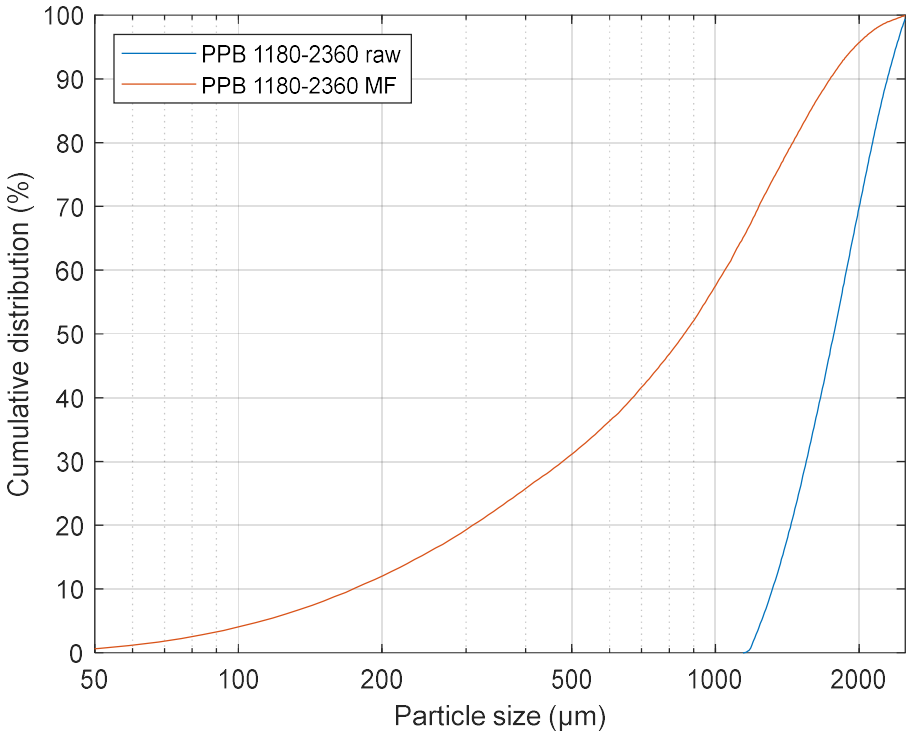

Figure 5-27 Particle size distribution of raw PPB and MF char (1180-2360 µm)

5.11.2 Particle Shape

The sphericity, circularity, symmetry and aspect ratio (defined in Section 3.6.4.2) of the raw biomass and char samples of the eucalyptus and cardboard samples were measured as described in Section 3.6.4.1.

5.11.2.1 Raw biomass particle shape distributions

The particle shape distributions of each raw biomass size fraction were plotted. Selected graphs are shown in Figure 5-28 to Figure 5-31 and all graphs can be found in Appendix C.

It was observed that in general, the shape distributions of the three cardboard materials are similar to each other while the shape distributions of eucalyptus is significantly different compared to that of the three cardboard materials. However, the circularity of the three cardboard materials shows a larger degree of variation compared to the other shape parameters. Eucalyptus also has a lower sphericity, higher circularity, higher symmetry and lower aspect ratio compared to the cardboard materials.

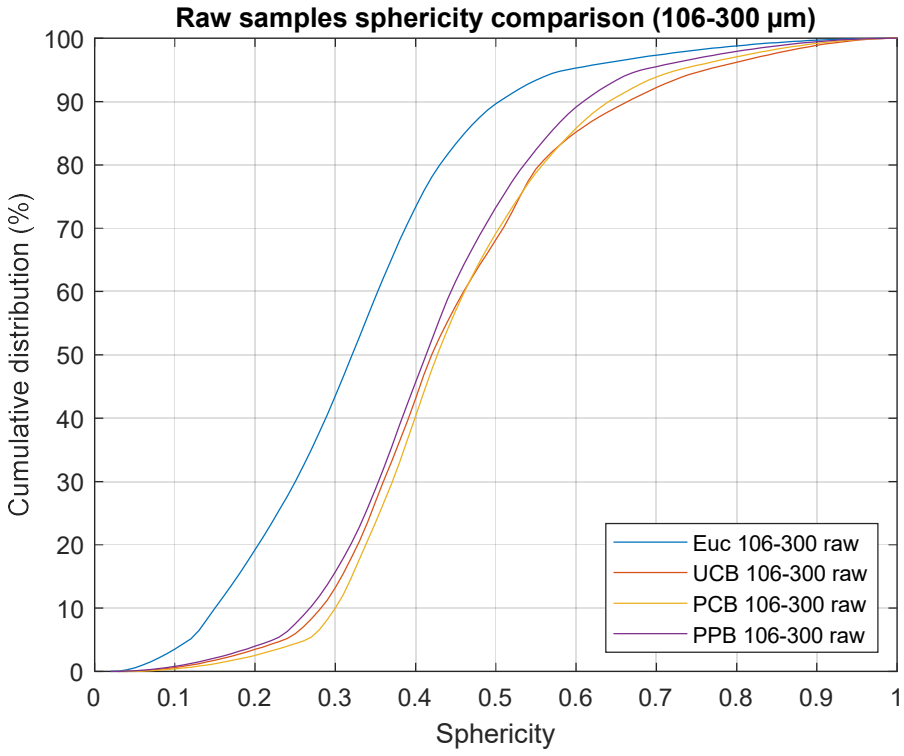

Figure 5-28 Raw samples sphericity comparison (106-300 µm)

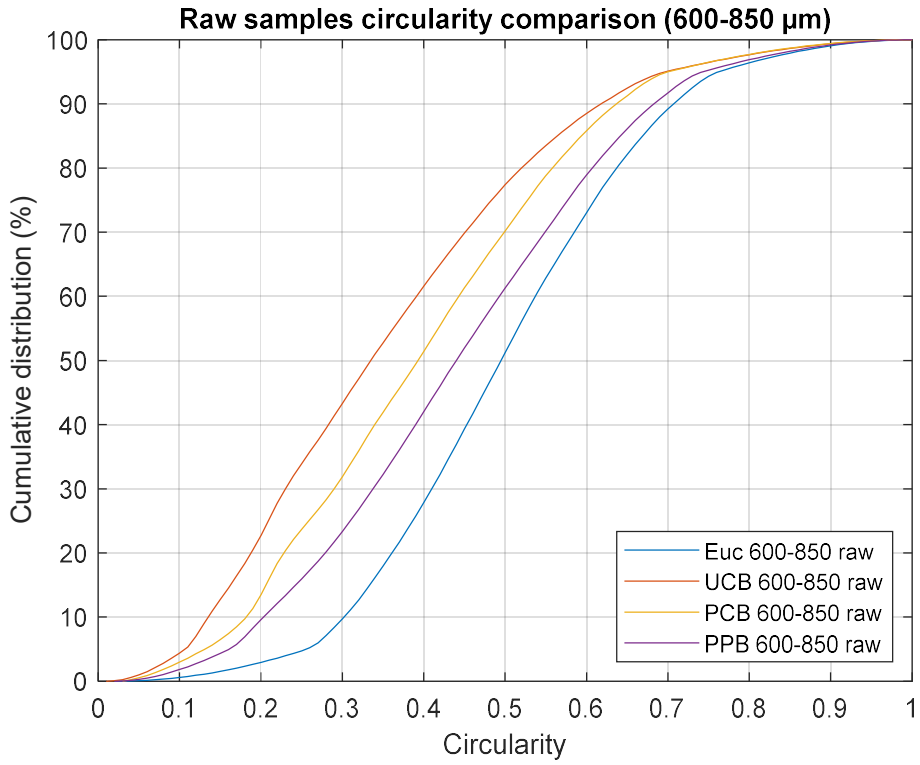

Figure 5-29 Raw samples circularity comparison (600-850 µm)

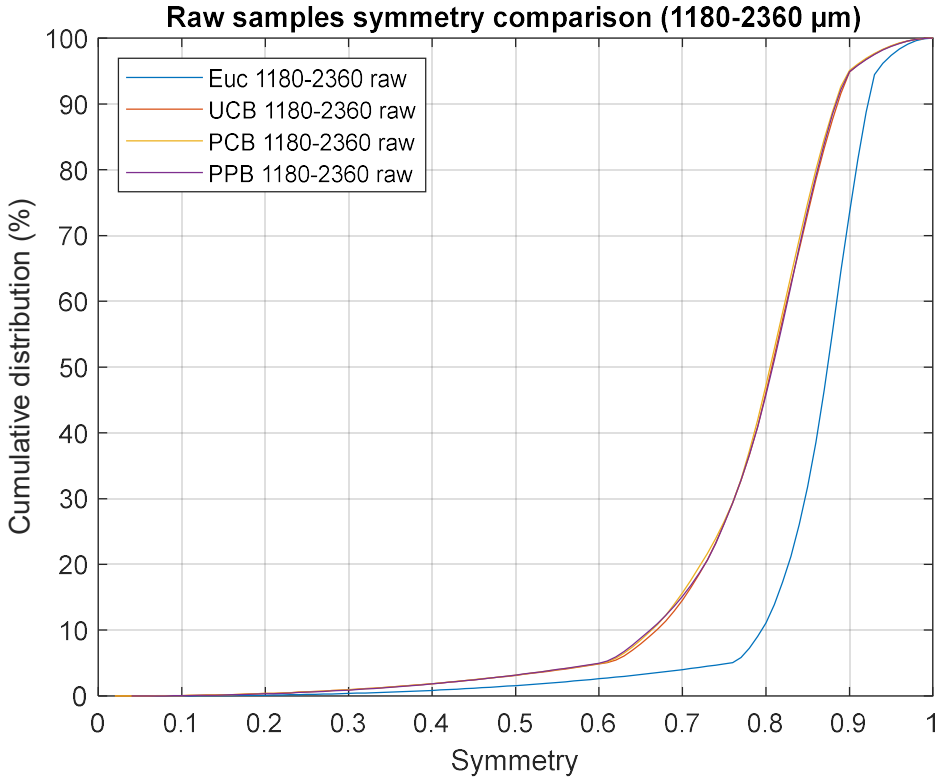

Figure 5-30 Raw samples symmetry comparison (1180-2360µm)

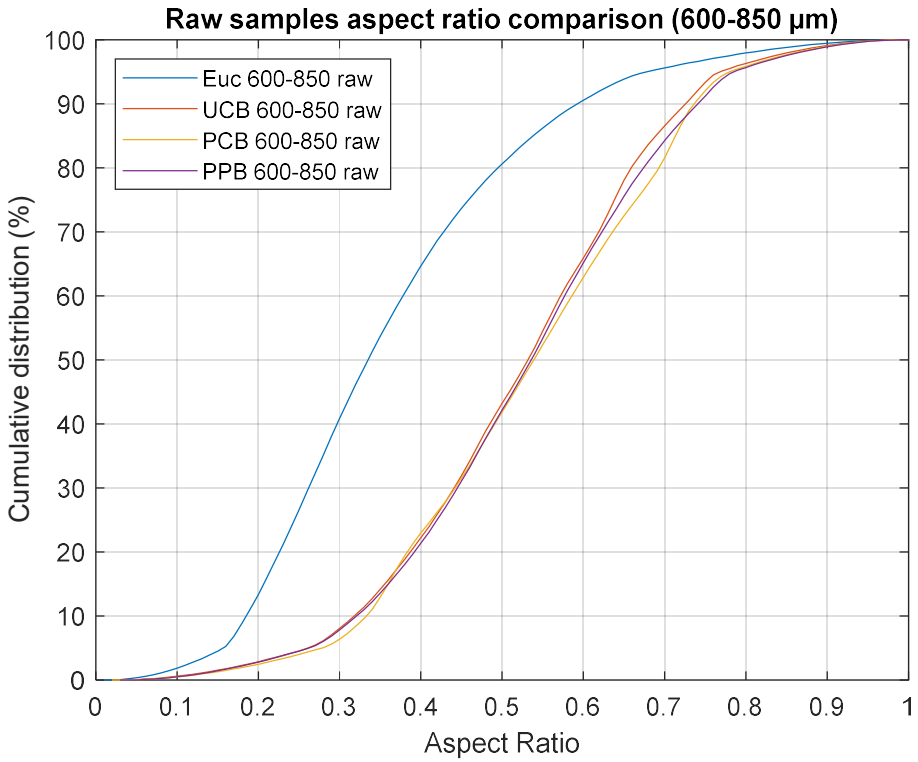

Figure 5-31 Raw samples aspect ratio comparison (600-850 µm)

Sample	Type	Average Sphericity	Average Circularity	Average Symmetry	Average Aspect Ratio
Euc 106-300 µm	Raw	0.329	0.356	0.695	0.397
Euc 106-300 µm	DTF Char	0.504	0.527	0.738	0.578
Euc 600-850 µm	Raw	0.291	0.501	0.842	0.365
Euc 600-850 µm	DTF Char	0.314	0.582	0.867	0.394
Euc 600-850 µm	MF Char	0.285	0.444	0.78	0.348
Euc 1180-2360 µm	Raw	0.355	0.611	0.862	0.445
Euc 1180-2360 µm	MF Char	0.318	0.510	0.830	0.375

UCB 106-300 µm	Raw	0.450	0.282	0.708	0.53
UCB 106-300 µm	DTF Char	0.446	0.493	0.709	0.518
UCB 600-850 µm	Raw	0.447	0.359	0.732	0.524
UCB 600-850 µm	DTF Char	0.482	0.473	0.755	0.564
UCB 600-850 µm	MF Char	0.469	0.389	0.721	0.547
UCB 1180-2360 µm	Raw	0.474	0.524	0.788	0.558
UCB 1180-2360 µm	MF Char	0.480	0.406	0.760	0.560
PCB 106-300 µm	Raw	0.451	0.276	0.702	0.506
PCB 106-300 µm	DTF Char	0.423	0.257	0.644	0.496
PCB 600-850 µm	Raw	0.461	0.400	0.765	0.537
PCB 600-850 µm	DTF Char	0.488	0.598	0.797	0.577
PCB 600-850 µm	MF Char	0.485	0.460	0.741	0.565
PCB 1180-2360 µm	Raw	0.480	0.537	0.785	0.566
PCB 1180-2360 µm	MF Char	0.466	0.446	0.744	0.547
PPB 106-300 µm	Raw	0.429	0.251	0.671	0.506
PPB 106-300 µm	DTF Char	0.512	0.523	0.743	0.586
PPB 600-850 µm	Raw	0.450	0.445	0.768	0.532
PPB 600-850 µm	DTF Char	0.514	0.629	0.799	0.599
PPB 600-850 µm	MF Char	0.475	0.445	0.733	0.554

PPB 1180-2360 µm	Raw	0.479	0.558	0.787	0.561
PPB 1180-2360 µm	MF Char	0.451	0.456	0.745	0.533

Table 5-14 Average shape factors of the raw and char samples for eucalyptus and cardboard materials

5.11.2.2 Particle shape comparison of raw biomass and chars

The particle shape distributions of each raw biomass size fraction and the associated chars for each material were plotted to illustrate the change in shape distribution. Selected graphs are shown in Figure 5-32 to Figure 5-43 and all graphs can be found in Appendix D. The average values of the shape factors are presented in Table 5-14 and the difference in the average values of the shape factors between the raw biomass and chars are presented in Figure 5-44 to Figure 5-47. Only sphericity and aspect ratio are discussed in detail in this Section as these are the most important shape factors for combustion modelling.

Similar trends were observed for the change in sphericity and aspect ratio, and there is a strong correlation between the two shape factors (as shown in Figure 5-48), which is further discussed in Section 7.9.2.2 in conjunction with the particle shape data of the sugarcane straw samples. For both sphericity and aspect ratio, the greatest change (an increase in the average sphericity of 0.18 from 0.329 to 0.504 and an increase in the average aspect ratio of 0.18 from 0.397 to 0.578) was observed for the eucalyptus 106-300 µm DTF char sample. Comparing the effects of the char methods using the 600-850 µm sample, all of the DTF chars saw an increase in average sphericity and aspect ratio, while all MF chars either saw a smaller increase compared to DTF chars or a small decrease. This indicates that the faster heating rate in the DTF caused a greater change in particle sphericity and aspect ratio compared to MF. There are no clear trends between particle size or type of biomass and the change in shape factors.

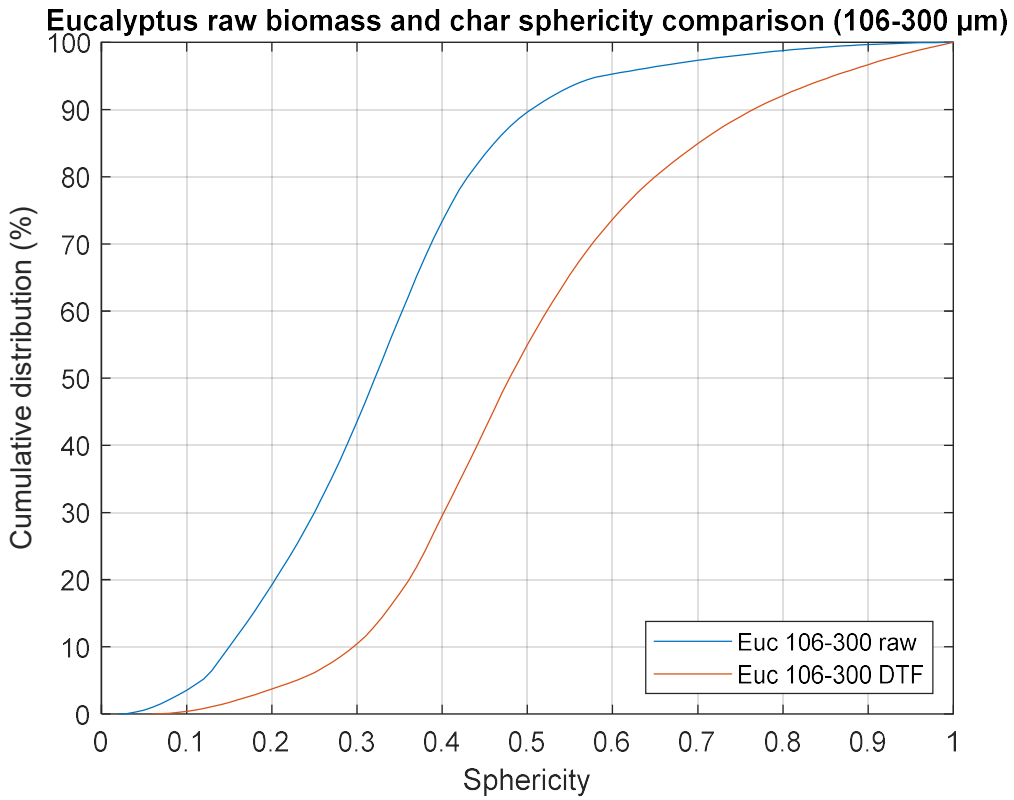

Figure 5-32 Eucalyptus raw biomass and char sphericity comparison (106-300 µm)

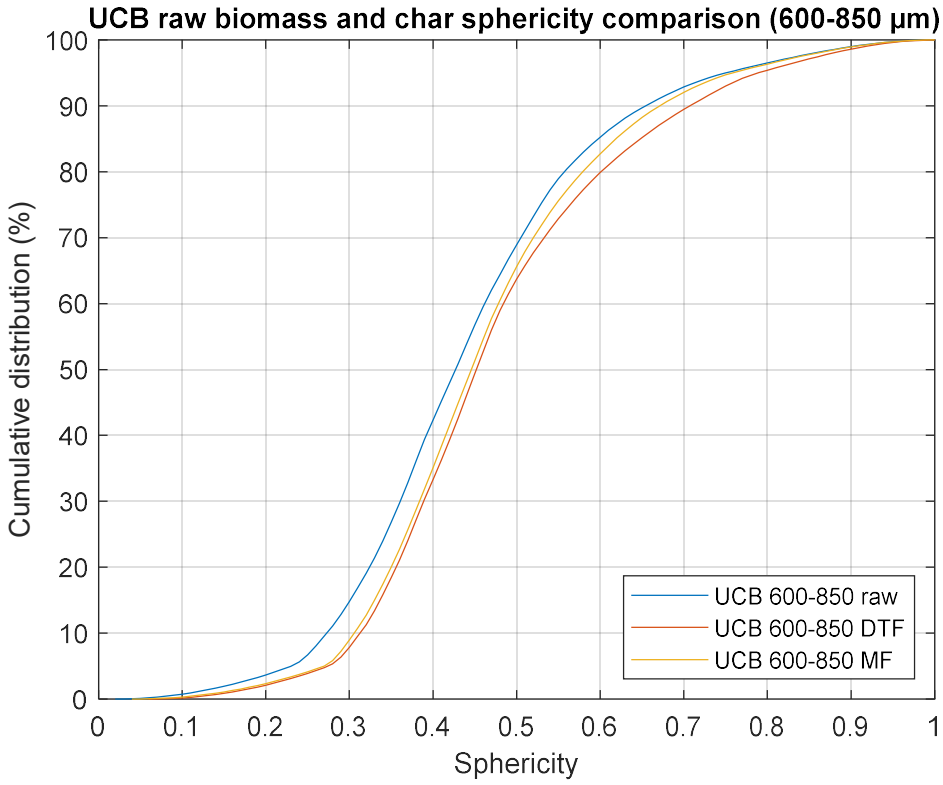

Figure 5-33 UCB raw biomass and char sphericity comparison (600-850 µm)

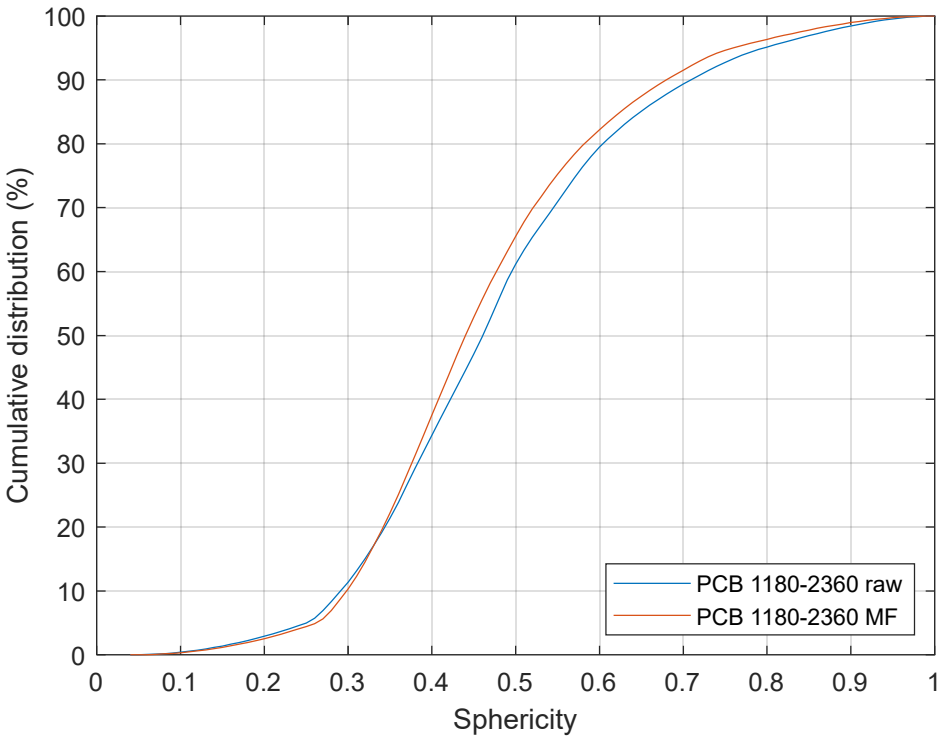

Figure 5-34 PCB raw biomass and char sphericity comparison (1180-2360 µm)

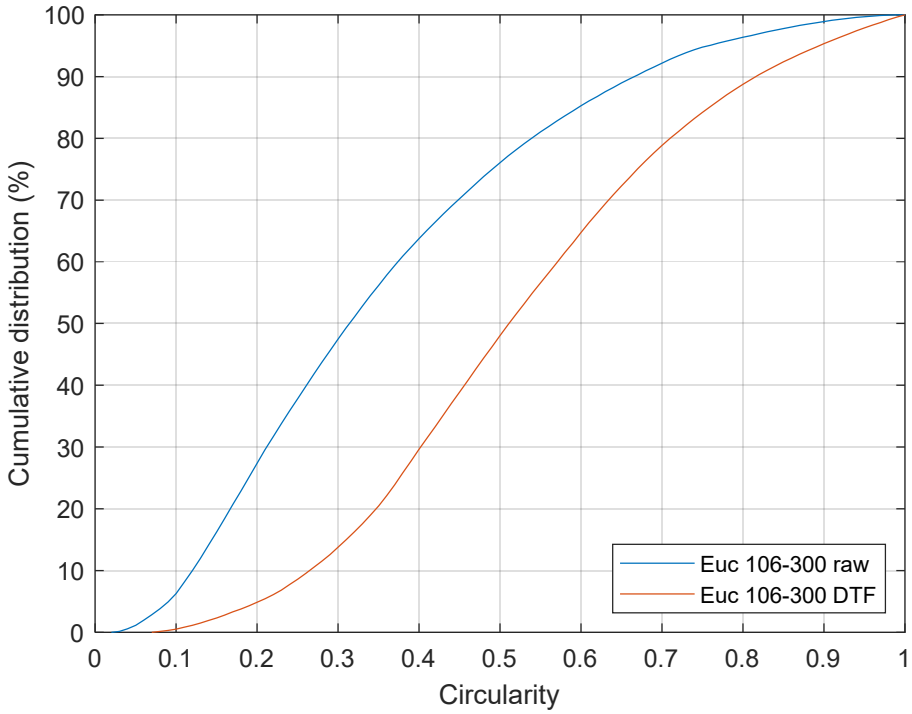

Figure 5-35 Eucalyptus raw biomass and char circularity comparison (106-300 µm)

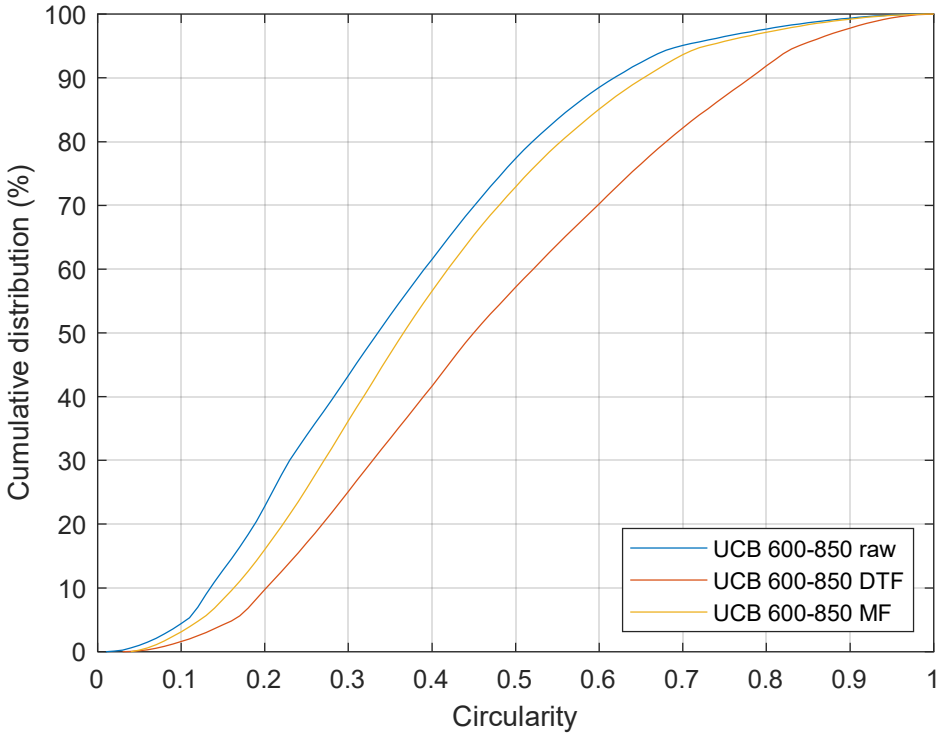

Figure 5-36 UCB raw biomass and char circularity comparison (600-850 µm)

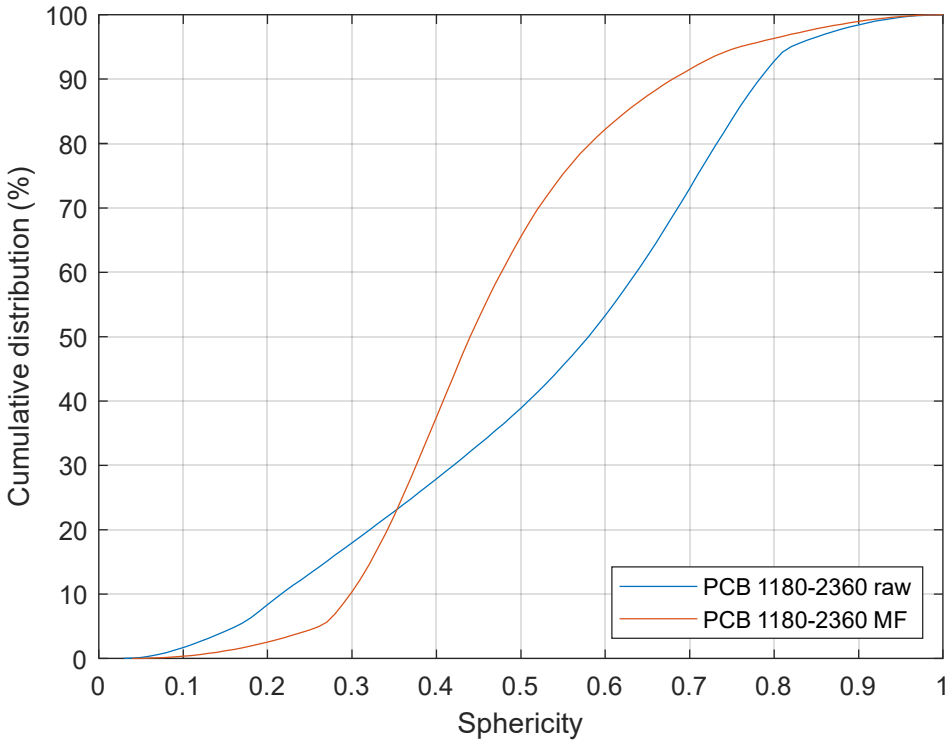

Figure 5-37 PCB raw biomass and char sphericity comparison (1180-2360 µm)

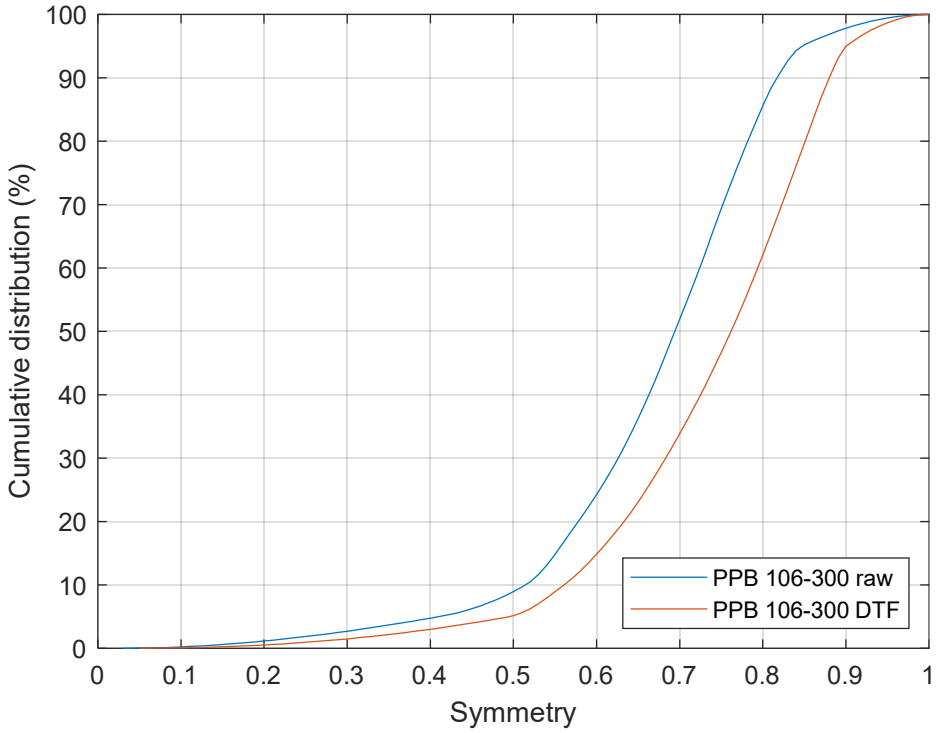

Figure 5-38 PPB raw biomass and char symmetry comparison (106-300 µm)

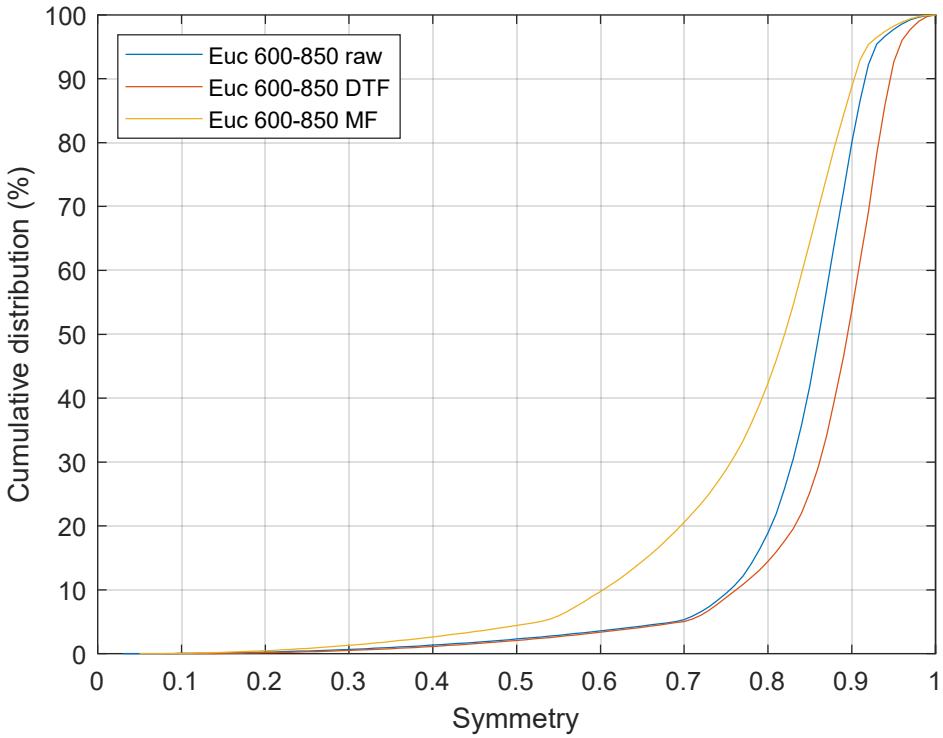

Figure 5-39 Eucalyptus raw biomass and char symmetry comparison (600-850 µm)

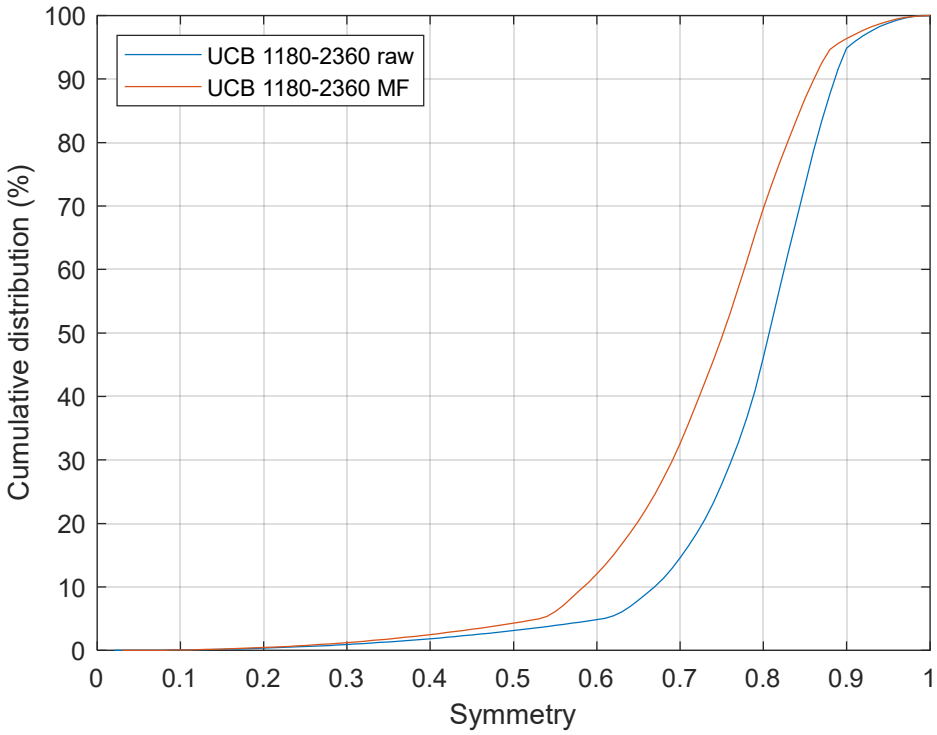

Figure 5-40 UCB raw biomass and char symmetry comparison (1180-2360 µm)

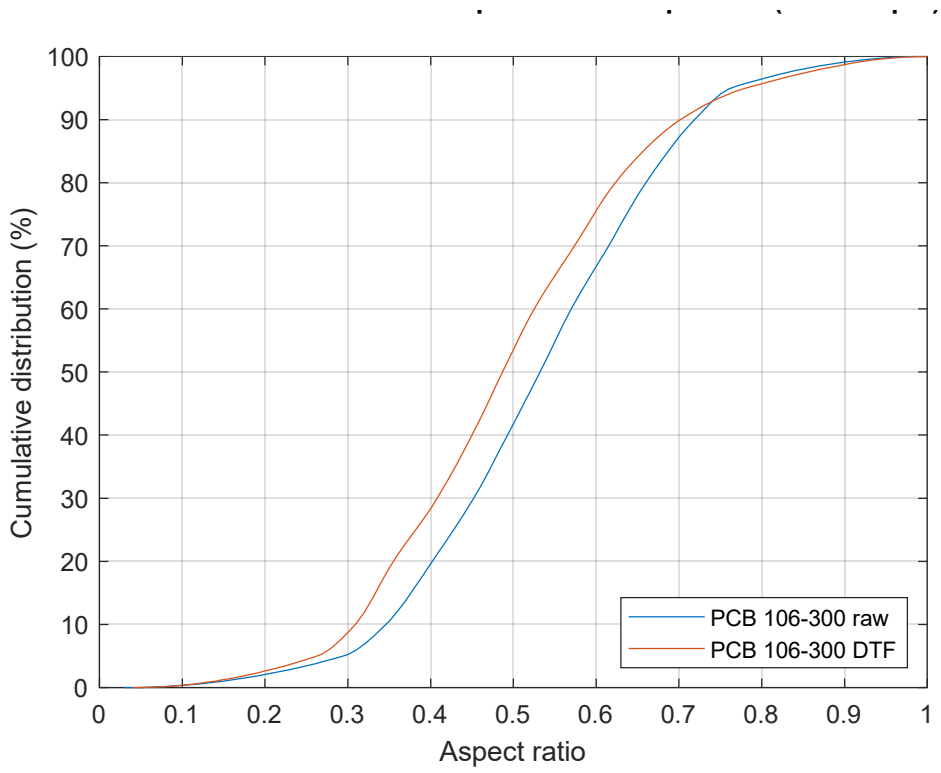

Figure 5-41 PCB raw biomass and char aspect ratio comparison (106-300 µm)

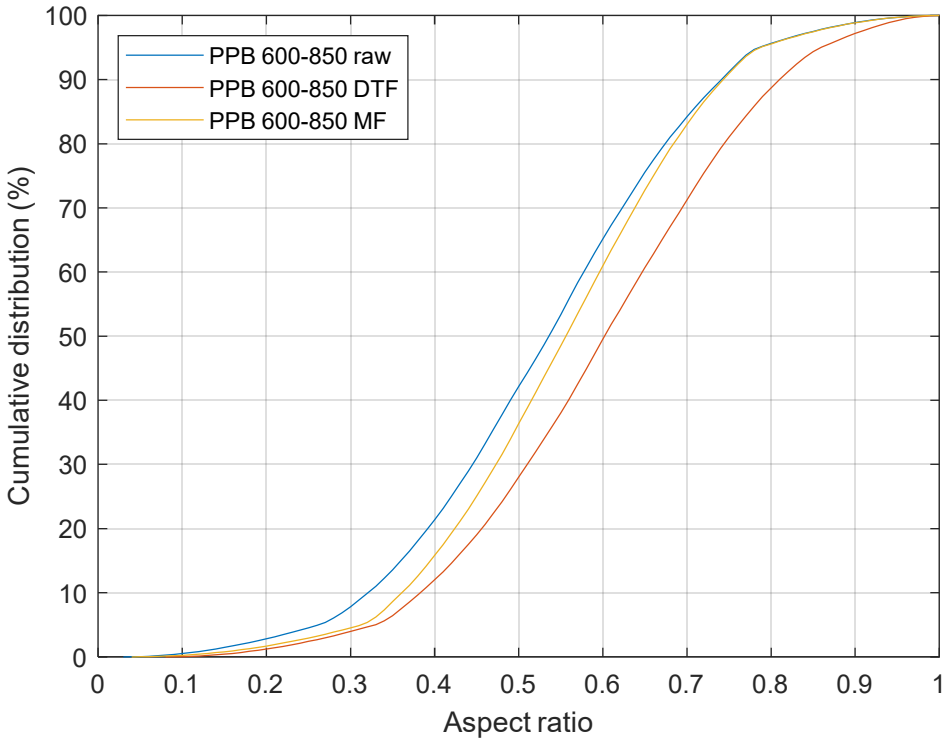

Figure 5-42 PPB raw biomass and char aspect ratio comparison (600-850 µm)

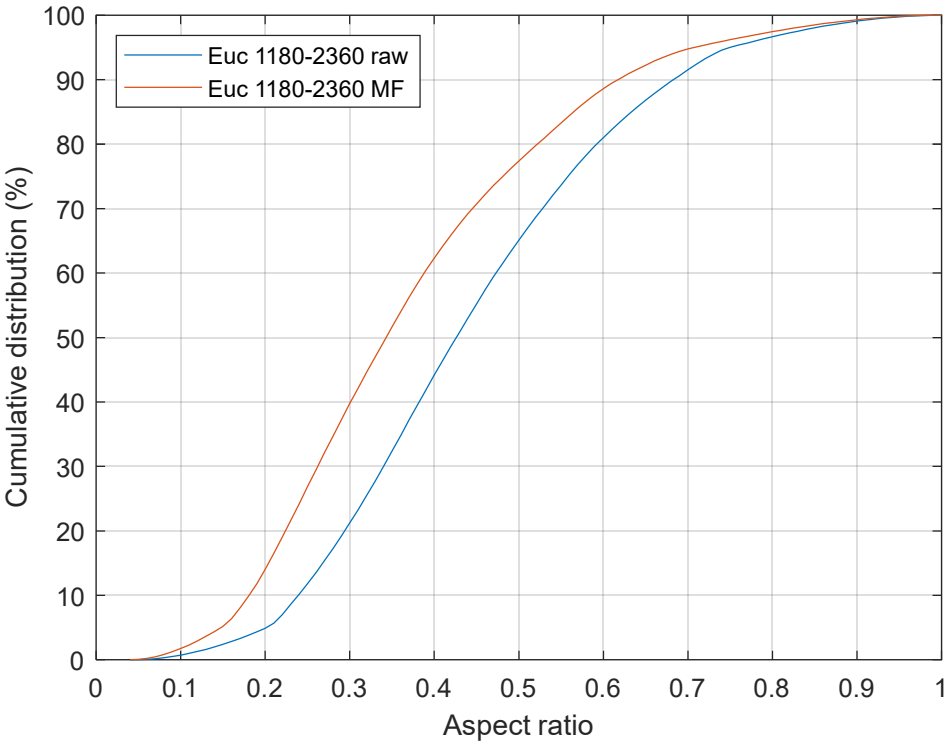

Figure 5-43 Eucalyptus raw biomass and char aspect ratio comparison (1180-2360 µm)

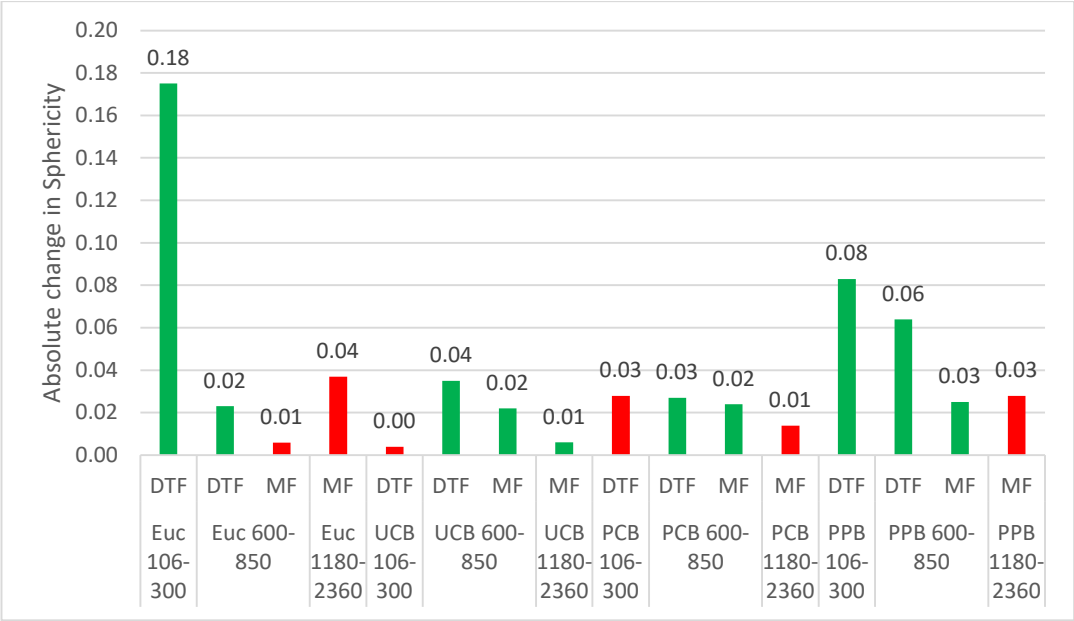

*green bars indicate a positive change and red bars indicate a negative change

Figure 5-44 Change in sphericity of the char samples compared to raw biomass

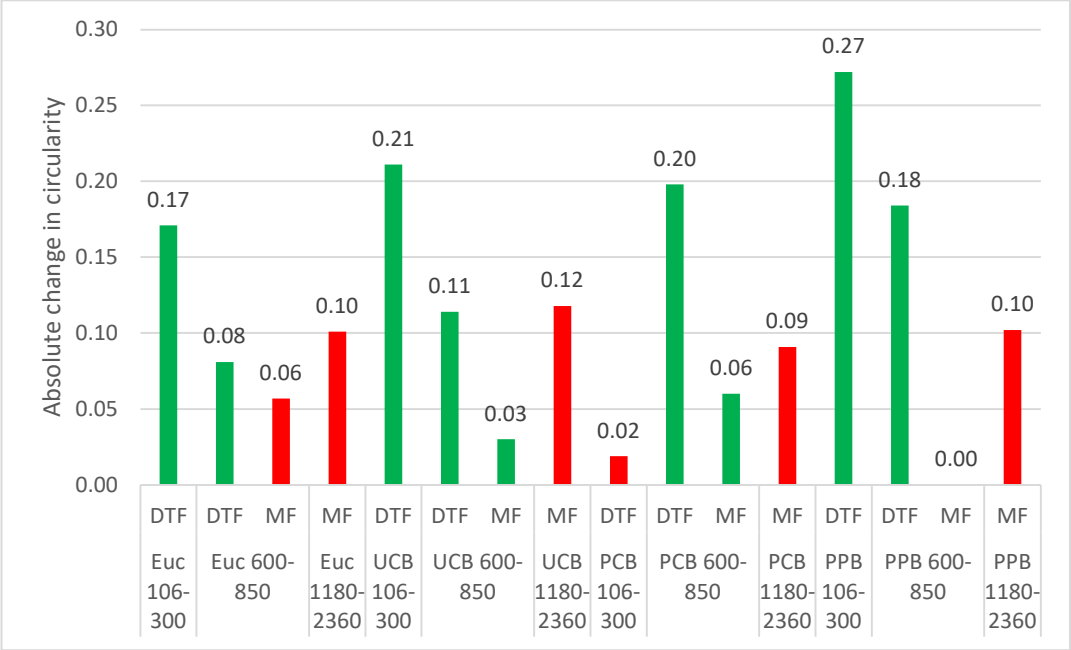

*green bars indicate a positive change and red bars indicate a negative change

Figure 5-45 Change in circularity of the char samples compared to raw biomass

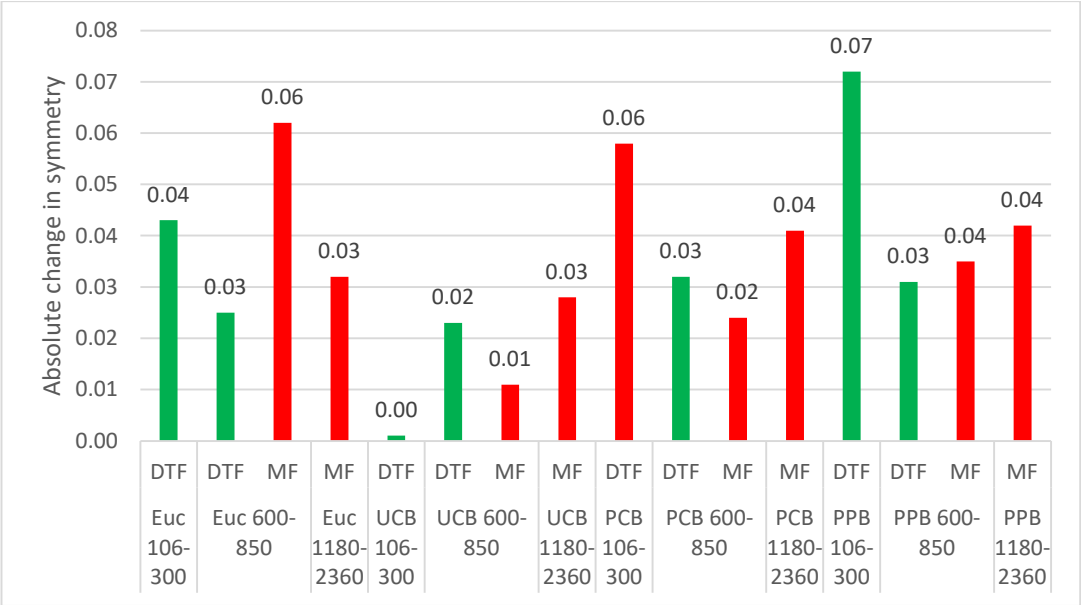

*green bars indicate a positive change and red bars indicate a negative change

Figure 5-46 Change in symmetry of the char samples compared to raw biomass

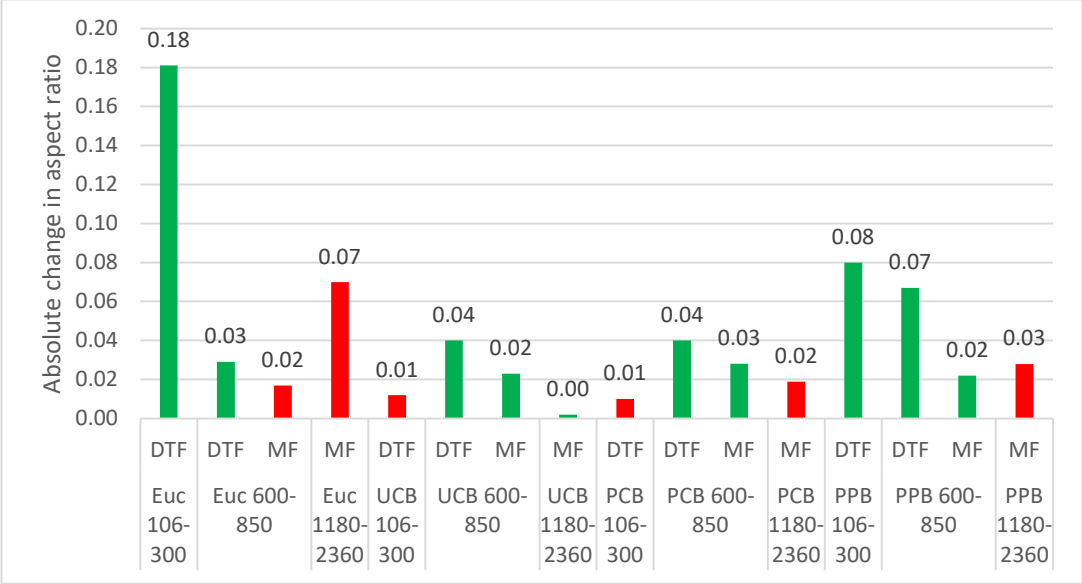

*green bars indicate a positive change and red bars indicate a negative change

Figure 5-47 Change in aspect ratio of the char samples compared to raw biomass

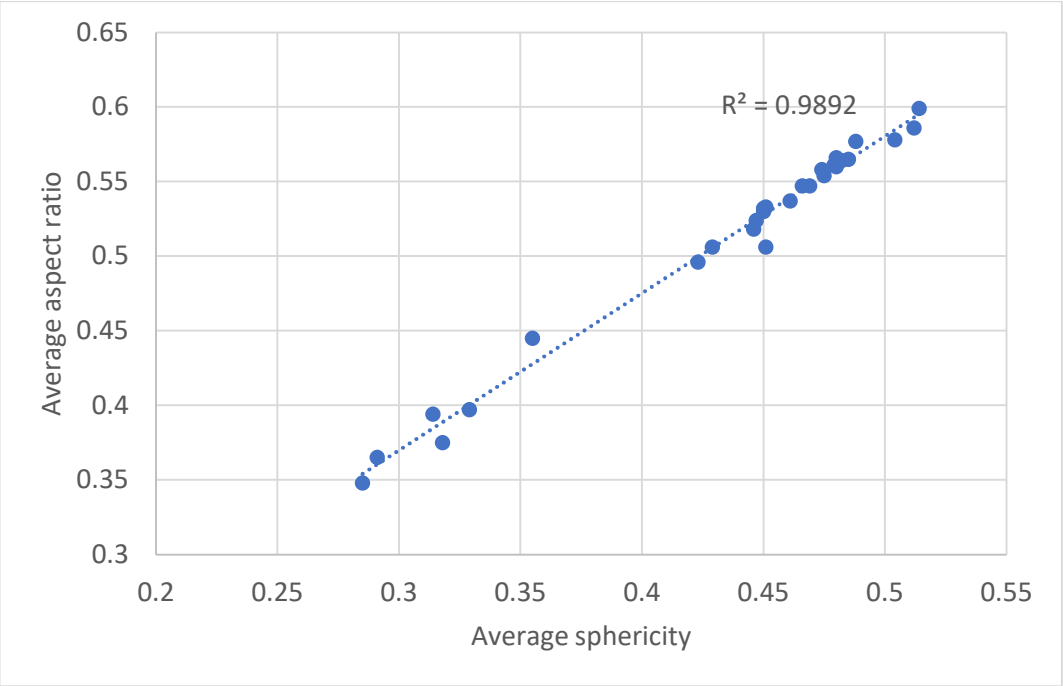

Figure 5-48 Correlation between average sphericity and average aspect ratio of eucalyptus and cardboard materials raw biomass and char samples

5.12 Comparison with Biomass Standards

Commonly used standards exist for woody and non-woody pellets for energy use, namely BS EN ISO 17225-2:2021 (The British Standards Institution, 2021b) and BS EN ISO 17225-6:2021 (The British Standards Institution, 2021c). However, there are currently no similar standards for biowastes or, in particular, cardboard for energy purposes. Yet, the existing standards represent the generally acceptable limits for fuel quality in the industry, and a comparison between the fuel grades specified in these standards would give a useful indication of the challenges and advantages of using cardboard materials for energy applications. The properties that could be compared using the available experimental data include ash content (Section 5.6.1), LHV (Section 5.7), additives content (Section 5.6.1) and nitrogen content (Section 5.7). The comparison between the fuel quality classes specified in the standards and the experimental data for these properties is shown in Table 5-15.

For these properties, the eucalyptus sample is able to meet the most stringent I1 grade for woody pellets in BS EN ISO 17225-2:2021. Although the standards for non-woody pellets (Grade A and B in BS EN ISO 17225-6:2021) are much less stringent

than those for woody pellets, the experimental results indicate that in general, cardboard materials are not able to meet the lower-quality Grade B specifications. UCB and PPB are able to barely meet the ash content requirements for Grade B pellets, while the ash content of PCB exceeds the Grade B specifications. All three cardboard materials are able to meet the LHV specifications for both Grade A and B non-woody pellets.

		BS EN ISO 17225-2:2021			**BS EN ISO 17225-6:2021**		**Experimental**			
Biomass type		**Woody**			**Non-woody**		**Euc**	**UCB**	**PCB**	**PPB**
Grade		**I1**	**I2**	**I3**	**A**	**B**	N/A			
Ash content	% dry basis	≤1.0	≤1.5	≤3.0	≤6	≤10	0.61	8.87	10.6	9.9
LHV	MJ/kg	≥16.5	≥16.5	≥16.5	≥14.5	≥14.5	19.6	15.2	14.7	15.2
Additives[1]	% dry basis	≤3	≤3	≤3	≤5	≤5	0	5.46	10.4	12.2
Nitrogen	% dry basis	≤0.3	≤0.3	≤0.6	≤1.5	≤2.0	0.19	0.25	0.22	0.19

[1]for the cardboard materials, $CaCO_3$ is listed as additives, see discussion

Table 5-15 Comparison between fuel classes in commonly used biomass standards and eucalyptus and cardboard materials samples

Regarding the specifications for additives, it is debatable whether the $CaCO_3$ present in the cardboard materials should be treated as an additive, as its presence is due to the cardboard manufacturing process (Section 2.1.2.1) and it is not intentionally added for energy applications or for the manufacturing of pellets. In addition, $CaCO_3$ may also have the benefit of mitigating slagging issues (Section 2.3). Although there is a case for not regarding $CaCO_3$ as an additive, if it is included, all three cardboard materials would exceed the allowable limits for all of the fuel quality classes. Lastly,

all of the eucalyptus and cardboard samples studied are well within the allowable limits of nitrogen content for all fuel quality classes. Overall, it can be concluded that cardboard materials are not able to fulfil the requirements of any of the commonly used pellet fuel quality classes, and adaptations from the industry would be necessary for their use, with ash content and additives being particular important issues.

5.13 Conclusions

This Chapter studied and analysed the properties of cardboard and its potential use as a biomass feedstock for power generation, filling current knowledge gaps, including the differences in the types of cardboard, the potential impact of fillers, the char morphology of cardboard materials and particle shape change during combustion. Eucalyptus was also used as a baseline material for comparison.

Based on the characterisation tests and analysis, there are likely to be multiple unique challenges and opportunities for the use of cardboard materials. With calcium carbonate being a widely studied additive to tackle slagging issues (see Section 2.3), there is potential for blending cardboard with other fuels to improve combustion performance. Milled cardboard has a strong tendency to form 'fluffy agglomerations', causing severe handling challenges as well as difficulties in traditional particle size analysis. However, useful particle analysis was possible using a vibratory sieve shaker. It was found that there are multiple differences between the PSD of milled eucalyptus and cardboard materials, with cardboard materials demonstrating a narrower and coarser distribution, while there are minimal differences between the types of cardboard. Apart from handling difficulties, other challenges of using cardboard materials for power generation include a relatively low calorific value and high ash content.

To investigate the presence of fillers in cardboard, XRD analysis was carried out, which confirmed the presence of $CaCO_3$. Proximate analysis was carried out, which was also able to identify the presence of $CaCO_3$. In addition, a new technique was developed to estimate the $CaCO_3$ content in cardboard based on the amount of CO_2 released during $CaCO_3$ decomposition, and the differences in $CaCO_3$ content among the types of cardboard were quantified. In terms of lignocellulosic composition,

cardboard materials were found to be hemicellulose-deficient due to its removal during the manufacturing process.

The burnout performance and char morphology of the eucalyptus and cardboard samples were analysed using the production of char from two methods with oil immersion microscopy and burnout simulation. In general, cardboard chars are more porous and thin-walled compared to eucalyptus chars. This indicates that cardboard materials would have a better char burnout performance.

The change in particle size and shape between the raw biomass samples and char (an intermediate combustion product) were studied using a Camsizer. The change in d_{50} (the median particle size) of the samples ranges from 14.6% to 63.7%, and no observable swelling of particles had occurred. Regarding the change in particle shape, the faster heating rate in the DTF caused a greater change in particle sphericity and aspect ratio compared to MF, while there are no clear trends between particle size or type of biomass and the change in shape factors.

Comparing with commonly used standards, it can also be concluded that cardboard materials are not able to fulfil the requirements of any of the commonly used pellet fuel quality classes, and adaptations from the industry would be necessary for their use, with ash content and additives being particular important issues.

Chapter 6 - Pasteurisation and Natural Drying Process

6.1 Introduction

Raw biomass materials often have high moisture content (>50% by weight in some cases) and the energy-intensive nature of biomass drying is a major limitation in bioenergy (Thek & Obernberger, 2012). Various forced drying methods, including rotary drum dryers and belt dryers, which all require heat to be generated and supplied to the material, have been used in industry. Natural drying is a possible technique to reduce drying energy by exposing the biomass to the atmosphere for a substantial period from days to months, using natural evaporation to reduce the moisture content of the material. Natural drying has the disadvantage of incurring a cost as immobilised capital (Labbé et al., 2018), although this is likely outweighed by the benefits in energy savings.

Despite the energy-saving potential of natural drying, preliminary experiments have shown that such long-term storage of biomass, especially if the moisture content is high, is unfeasible due to the rapid fungal growth under these conditions. Thus, pasteurisation is required to limit the growth of fungi during the natural drying stage. Although traditionally used to extend the shelf life of food, pasteurisation can also be adapted to suppress microbial growth in biomass during natural storage. To date, no studies have explored the potential to extend storage periods by using pasteurisation to suppress microbial and fungal growth and allow for natural drying to occur.

This Chapter of the thesis aims to address this major gap in knowledge by exploring the option of using pasteurisation to suppress fungal growth during natural drying, which as a combined process, has the potential of dramatically decreasing the drying energy of biomass while removing the microbial threat.

The development of a new novel combined biomass pasteurisation and natural drying process using microbial and fungal analysis microbial analysis was done as part of an additional grant (£4,436) provided by the University of Nottingham Interdisciplinary Centre for Analytical Science (UNICAS) through the UNICAS at the Researcher Academy scheme. The author was the principal investigator of this grant and was responsible for the project and expenditure management. This grant allowed

for the fungal analysis of the samples, which could not have been done as part of the original EngD. The fungal analysis was conducted with Mr Wade Handley-Hartill and Dr Stephen Lawrence at the School of Biosciences at the University of Nottingham.

6.2 Materials and Methods

Miscanthus (an energy crop) and spent grains from the brewing process were used in this study. The miscanthus samples were obtained from an industrial partner, and the spent grains samples were obtained from the AB INBEV Research Brewery at the University of Nottingham, using the mash filter brewing method.

Figure 6-1 Samples for Pasteurisation and Natural Drying Experiments. Left: Miscanthus; Right: Spent Grains

The methods used in this Chapter are described in Section 3.7, including milling, moisture content measurement and conditioning, briquetting, pasteurisation, heating profile characterisation, storage and storage conditions monitoring, moisture content monitoring, and fungal growth quantification.

6.3 Pasteurisation Conditions

The full list of pasteurisation conditions used is shown in Table 6-1. The experiments were conducted in 2 sets of 4 conditions for each material, i.e. M1-4 and SG1-4 (the first sets) were pasteurised and stored before M5-8 and SG 5-8 (the second sets). The results of the first sets of experiments informed the choice of conditions for the second sets. Briquettes M1, M5, SG1 and SG5 are the baseline briquettes with no pasteurisation. M3 and M4 used the same duration but different pasteurisation

methods to investigate the relative performance of the pasteurisation methods when using identical process times. This also applies to SG3 and SG4.

The pasteurisation conditions chosen were intended to be more severe (higher temperature and longer duration for conventional oven pasteurisation, and equivalent for microwave pasteurisation) than those typically used in industry, as the primary purpose of the current set of experiments is to determine the feasibility of a combined pasteurisation and natural drying process to reduce drying energy for biomass.

To determine the duration of microwave pasteurisation for the first batch of briquettes (M1-4 and SG1-4), multiple test briquettes (which were not used in the main experiment) were made. These test briquettes were processed with the microwave oven at high power (1800 W), and the core temperature was measured immediately afterwards with a mercury thermometer. Using a trial and error process, it was found that approximately 1 min 45 s for miscanthus and 3 min for spent grains was required for the briquettes to reach a core temperature of 90°C. These conditions were chosen for microwave pasteurisation to allow for meaningful comparison with the conventional oven method, which also used a temperature setting of 90°C.

Set 1 was stored for either eight or nine weeks (see Section 6.6) and batch 2 was stored for four or five weeks. The primary purpose of this was to obtain samples from the centre of the briquettes for fungal growth analysis after different storage durations, which can only be done by destroying the briquettes at the end of the storage period.

Following the first batch of experiments for spent grains (SG1-4), it was found that the pasteurisation conditions used for SG2-4 were not sufficient to satisfactorily reduce fungal growth. For SG3 and SG4, visible fungal growth was observed on the top of the briquettes within six days of storage (Figure 6-2 and Figure 6-3). For SG2, the top of the briquette showed no obvious visible fungal growth throughout the storage period (Figure 6-13). However, the bottom of SG2-4 shows severe fungal growth within four weeks of storage (Figure 6-14).

Briquette	Batch	Pasteurisation Condition	Notes
M1	1	Baseline (no pasteurisation)	
M2	1	90°C/45min conventional oven	Same condition as M6
M3	1	105s microwave (1800 W)	Same process time as M4
M4	1	90°C/105s conventional oven	Same process time as M3
SG1	1	Baseline (no pasteurisation)	
SG2	1	90°C/45min conventional oven	
SG3	1	180s microwave (1800 W)	Same process time as SG4
SG4	1	90°C/180s conventional oven	Same process time as SG3
M5	2	Baseline (no pasteurisation)	
M6	2	90°C/45min conventional oven	Same condition as M2
M7	2	105s microwave (1800 W)	'High power, short duration', same overall energy input as M8
M8	2	556s microwave (340 W)	'Low power, long duration', same overall energy input as M7
SG5	2	Baseline (no pasteurisation)	
SG6	2	90°C/90min conventional oven	
SG7	2	360s microwave (1800 W)	
SG8	2	180s microwave, flip briquette over, followed by 180s microwave (1800 W)	

Table 6-1 List of pasteurisation conditions used

Therefore, a higher level of fungal growth suppression was necessary and more severe pasteurisation conditions were chosen for SG6-8. SG6 (90°C/90min conventional oven) used conventional oven pasteurisation at the same temperature (90°C) as SG2 (90°C/45min conventional oven) but for a longer duration. SG7 used microwave pasteurisation with the same power (high power, 1800 W) as SG3 but for a longer duration (360 s). In addition, to investigate whether reducing hot spots and uneven heating would improve the results of microwave pasteurisation, SG8 was pasteurised for the same overall duration as SG7 (360 s) but was flipped upside down halfway through the process.

Figure 6-2 Briquette SG3 on day six of storage, with visible fungal growth

Figure 6-3 Briquette SG4 on day six of storage, with visible fungal growth

In contrast, the first batch of miscanthus briquettes (M1-4) showed no visible fungal growth at the top, bottom and middle of the briquettes (Figure 6-10 and Figure 6-11). This suggests that the miscanthus briquettes could be stored for eight weeks or longer without causing a substantial health & safety hazard due to excessive fungal growth. Therefore, identical pasteurisation were chosen for the following pairs of briquettes are identical: 1) M2 & M6; 2) M3 & M7. This is to investigate the level of fungal growth at the middle of the briquettes after different storage durations. Both M7 and M8 both used microwave pasteurisation with the same overall energy input, but were configured as ‘high power, short duration’ and ‘low power, long duration’

respectively. This was designed to investigate the relative effectiveness of these configurations in suppressing fungal growth.

6.4 Immediate Effects of Pasteurisation

Several immediate effects of pasteurisation were observed, including a decrease in moisture content, decrease in structural integrity, and charring.

6.4.1 Moisture Loss during Pasteurisation

Although the goal of pasteurisation is to suppress fungal growth during the natural drying stage, some moisture is inevitably removed during pasteurisation as it involves treating the briquettes at elevated temperatures. However, the extent of moisture content reduction is small compared to the overall amount of moisture removed during the natural drying stage (Section 6.7).

Briquette	M1	M2	M3	M4	M5	M6	M7	M8
Before (%)	60.1	60.1	60.2	60.4	57.9	58.1	58.0	57.9
After (%)	N/A	56.6	57.1	59.9	N/A	53.8	55.5	55.4
Absolute decrease (%)	N/A	3.6	3.0	0.5	N/A	4.3	2.5	2.6
Percentage decrease (%)	N/A	5.9	5.0	0.8	N/A	7.5	4.3	4.4

Table 6-2 Miscanthus briquettes: moisture content before and after pasteurisation

Table 6-2 and Table 6-3 show the moisture content of each briquette immediately before and after pasteurisation. The pairs M2 & M3, M6 & M7 and SG2 & SG3 each consist of one briquette treated with conventional oven pasteurisation at 90°C for 45 min, and one briquette treated with microwave pasteurisation with durations that would achieve a core temperature of 90°C (see Section 3.8.6). Comparing the amount of moisture removed during pasteurisation within these pairs, it was found that conventional oven pasteurisation at 90°C for 45 min resulted in a significantly higher level of moisture loss compared to microwave pasteurisation that also achieved a core temperature of 90°C.

Comparing the moisture loss during pasteurisation of M7 and M8, it was found that there was no significant differences in the amount of moisture loss for the 'high power, short duration' and 'low power, long duration' of microwave pasteurisation if the overall amount of power delivered is identical. Similarly, comparing the moisture loss during pasteurisation of SG7 and SG8, it was found that there was no significant differences in the amount of moisture loss for the 'normal' and 'flip over halfway through' configurations of microwave pasteurisation.

Briquette	SG1	SG2	SG3	SG4	SG5	SG6	SG7	SG8
Before (%)	63.1	64.1	634.0	63.8	63.8	64.0	64.1	64.0
After (%)	N/A	61.9	63.3	63.1	N/A	61.3	61.3	61.2
Absolute decrease (%)	N/A	2.2	0.7	0.7	N/A	2.7	2.8	2.7
Percentage decrease (%)	N/A	3.5	1.1	1.0	N/A	4.2	4.3	4.3

Table 6-3 Spent grains briquettes: moisture content before and after pasteurisation

6.4.2 Expansion and Structural Integrity

The possible volume expansion of biomass briquettes immediately following densification is a known phenomenon caused by the removal of the applied compacting force, and may occur regardless of whether the briquettes have experienced heat treatment processes (Obi et al., 2022). It has also been reported that the extent of briquette expansion is influenced by factors such as compacting force and compacting speed during densification, material moisture content and particle size (Voicea et al., 2015).

Slight expansion and decrease in density of briquettes were observed immediately after pasteurisation. The appearance of briquettes M2-4 and M6-8 after

pasteurisation, compared to the unpasteurised baseline briquettes M1 and M5, is shown in Figure 6-4 and Figure 6-5. The appearance of briquettes SG2-4 after pasteurisation, compared to the unpasteurised baseline briquette (SG1), is shown in Figure 6-6. The change in appearance of SG6-8 before and after pasteurisation is shown in Figure 6-7. The change in the dimensions of the briquettes is also presented in Table 6-4.

Since this type of mild heat treatment in the form of pasteurisation is not commonly carried out for biomass briquettes, there is no existing research specifically focusing on briquette expansion caused by mild heat treatment. A relevant study was conducted by Tumuluru et al. (2013), who found that pellet durability decreased after being stored at a high temperature and concluded that the likely cause of this was the increase in air-filled cavities in the pellets. Temperature shock may also result in the increase of surface cracks in biomass pellets (Gilvari et al., 2020). It is likely that similar mechanisms were the cause of expansion and loss of structural integrity of briquettes during pasteurisation. Nonetheless, this observed phenomenon caused by pasteurisation represent an area where further work should be conducted to better understand the effects of pasteurisation on biomass briquettes.

It was also found that when a change in dimensions occurs after pasteurisation, the height of a briquette typically increases by a larger percentage (up to 25.0%) than its length (up to 7.1%) or width (up to 11.1%), which suggests that the briquettes have the highest degree of movement in this direction as they are not restrained by the tray in this direction. The pasteurisation conditions for M4, SG2 and SG4 were not sufficiently severe to cause a measurable change in the dimensions of the briquettes. The spent grains briquettes generally showed a smaller extent of overall expansion (up to 14.8%) compared to the miscanthus briquettes (up to 38.2%). However, large cracks can appear in the spent grains briquettes during pasteurisation (see Figure 6-6 and Figure 6-7), which could compromise the structural integrity of the briquettes and introduce handling issues.

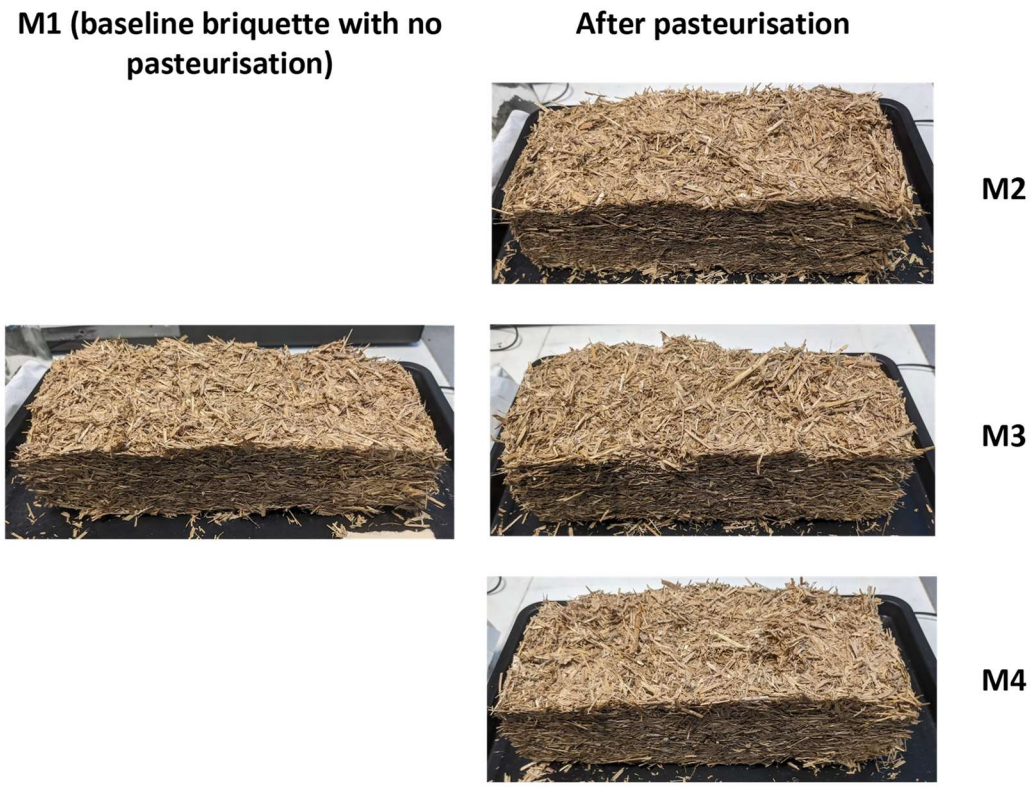

Figure 6-4 The effect of pasteurisation on the appearance of briquettes M2-4, compared to M1

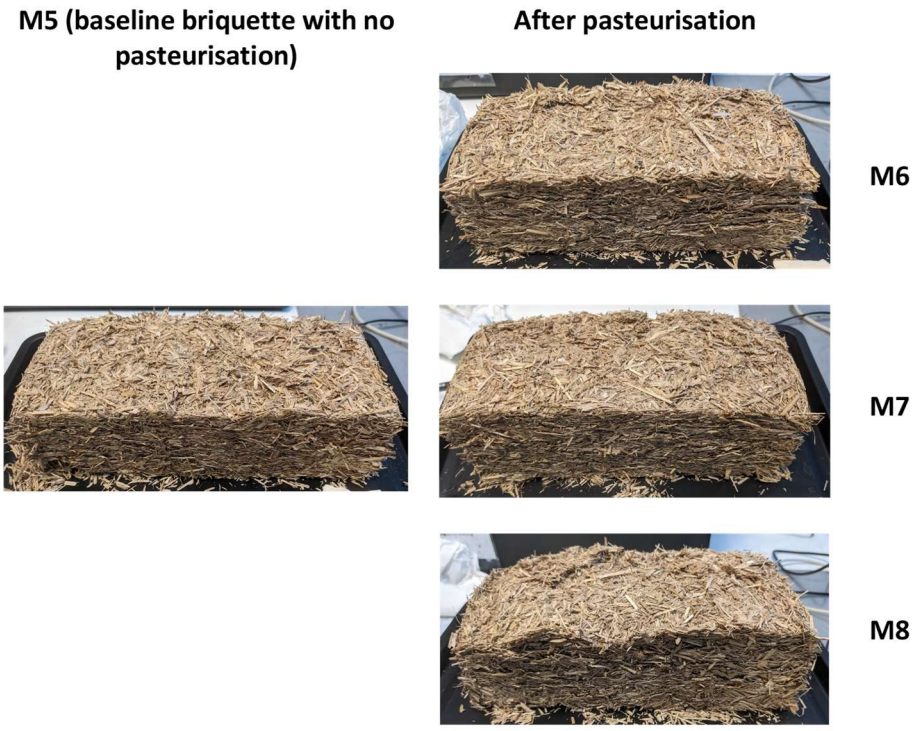

Figure 6-5 The effect of pasteurisation on the appearance of briquettes M6-8, compared to M5

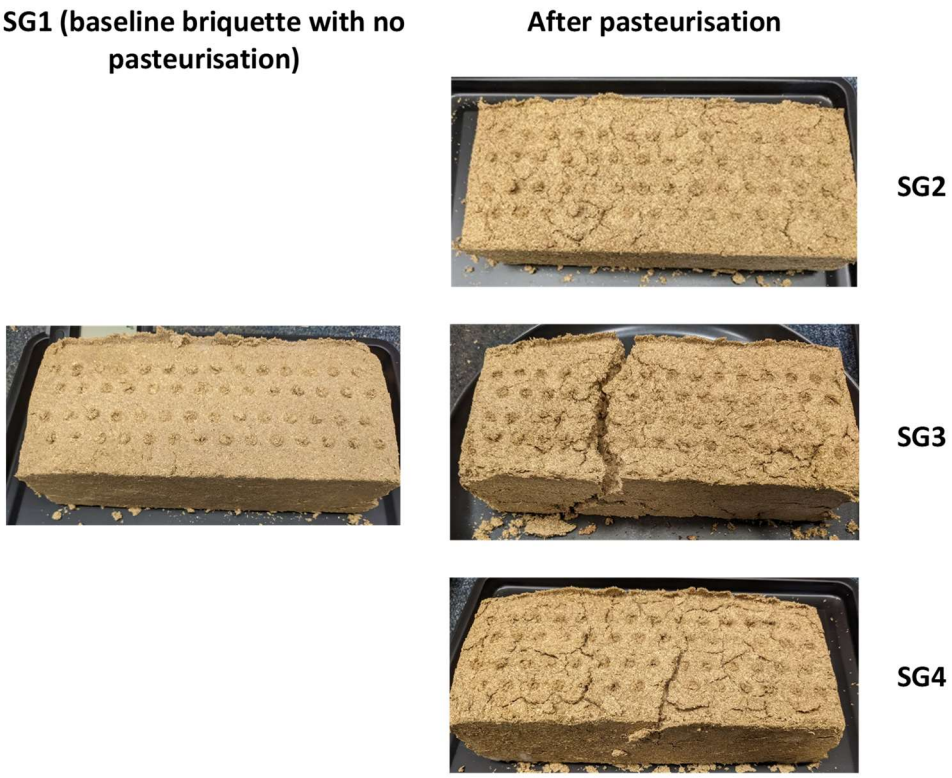

Figure 6-6 The effect of pasteurisation on the appearance of briquettes SG2-4, compared to SG1

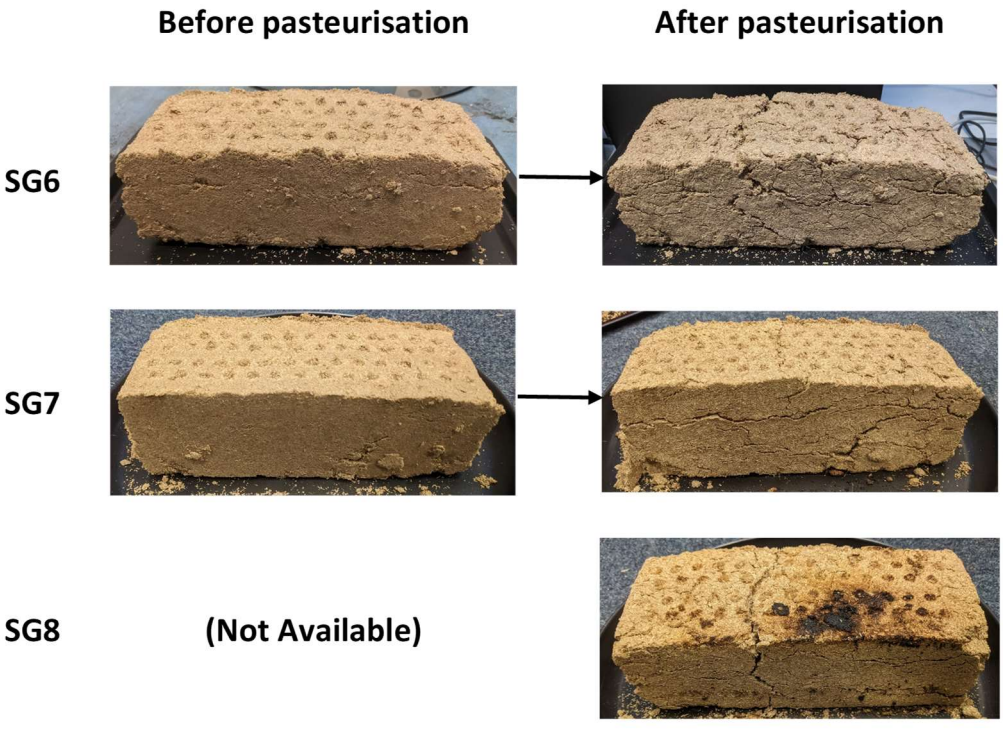

Figure 6-7 Appearance of briquettes SG6-8 before and after pasteurisation

6.4.3 Charring

Charring refers to blackened areas which appear during microwave processing. Charring is due to thermal hotspot and thermal runaway due to concentrations of the electromagnetic field (Luo et al., 2021). Charing was only observed in the spent grains briquettes treated with microwave pasteurisation (SG3, SG7 and SG8). This also only occurs on the side of the briquette which faces downwards during pasteurisation. Therefore, charring was observed on the bottom of the briquettes SG3 and SG7, which were not flipped during pasteurisation, and on both the top and bottom of the briquettes SG8, which was flipped halfway through the duration of pasteurisation. The extent of the charring is shown in Figure 6-7, Figure 6-14, Figure 6-8 and Figure 6-9. The extent of charring was less severe for SG3 compared to SG7, which is consistent with the pasteurisation condition of SG7 being more severe than that of SG3.

Figure 6-8 Charring on the bottom of briquettes SG7 immediately after pasteurisation

Figure 6-9 Charring on the top (left image) and bottom (right image) of briquette SG8 immediately after pasteurisation

	Before pasteurisation				After pasteurisation				Percentage change			
	Length (cm)	**Width (cm)**	**Height (cm)**	**Volume (cm^3)**	**Length (cm)**	**Width (cm)**	**Height (cm)**	**Volume (cm^3)**	**Length**	**Width**	**Height**	**Volume**
M1	21.0	9.0	6.0	1134	N/A	N/A	N/A	N/A	N/A	N/A	N/A	N/A
M2	21.0	9.0	6.0	1134	22.0	9.0	7.0	1386	4.8%	0.0%	16.7%	22.2%
M3	21.0	9.0	6.0	1134	22.0	9.5	7.5	1568	4.8%	5.6%	25.0%	38.2%
M4	21.0	9.0	6.0	1134	21.0	9.0	6.0	1134	0.0%	0.0%	0.0%	0.0%
M5	21.0	9.0	6.0	1134	N/A	N/A	N/A	N/A	N/A	N/A	N/A	N/A
M6	21.0	9.0	6.5	1229	21.0	9.0	7.5	1418	0.0%	0.0%	15.4%	15.4%
M7	21.0	9.0	6.0	1134	21.5	9.0	7.5	1451	2.4%	0.0%	25.0%	28.0%

M8	21.0	9.0	6.0	1134	21.5	10.0	6.5	1398	2.4%	11.1%	8.3%	23.2%
SG1	21.0	9.0	6.5	1229	N/A	N/A	N/A	N/A	N/A	N/A	N/A	N/A
SG2	21.0	9.0	6.5	1229	21.0	9.0	6.5	1229	0.0%	0.0%	0.0%	0.0%
SG3	21.0	9.0	6.5	1229	22.0	9.0	6.5	1287	4.8%	0.0%	0.0%	4.8%
SG4	21.0	9.0	6.5	1229	21.0	9.0	6.5	1229	0.0%	0.0%	0.0%	0.0%
SG5	21.0	9.0	7.0	1323	N/A	N/A	N/A	N/A	N/A	N/A	N/A	N/A
SG6	21.0	9.0	7.0	1323	22.5	9.0	7.5	1519	7.1%	0.0%	7.1%	14.8%
SG7	21.0	9.0	7.0	1323	21.0	9.0	7.5	1418	0.0%	0.0%	7.1%	7.1%
SG8	21.0	9.0	7.0	1323	21.5	9.0	7.5	1451	2.4%	0.0%	7.1%	9.7%

Table 6-4 Change in the dimensions of briquettes due to pasteurisation

Charring indicates that the charred locations of the briquettes experienced higher temperatures compared to the uncharred locations. This was a phenomenon unique to microwave pasteurisation and is due to the presence of hot spots (see Section 2.7.6.1). Another contributing factor could be that heat was not able to dissipate sufficiently quickly at the bottom of the briquette, resulting in the downward-facing side of the briquette experiencing significantly higher temperatures during pasteurisation compared to the rest of the briquette.

Charring was not observed in any of the miscanthus briquettes and any of the briquettes treated with conventional oven pasteurisation. The lack of charring on the miscanthus briquettes could be due to the significantly lower density of the miscanthus briquettes, making them less effective in retaining heat and heat is able to dissipate more efficiently. It is known that significantly higher temperatures are achieved in coal when densified compared to powders (Williams et al., 2019). Conventional oven pasteurisation did not cause any charring, as hot spots were not present. Although differences in the temperatures experienced by different parts of the briquettes exist (Section 6.5), no location in the briquettes would experience sufficiently elevated temperatures to cause charring. Further research is required to optimise the microwave pasteurisation process to avoid charring.

6.5 Briquette Heating Profile

The heating profile of a spent grains briquette during conventional oven pasteurisation at 90°C was characterised using the method described in Section 3.7.7. Seven thermocouples were used and inserted into the briquette at various locations, as shown in Figure 6-10, and a test period of 90 minutes was used, corresponding to the pasteurisation condition used for SG6. The results are presented in Figure 6-11, with T1-7 representing the seven thermocouples. The drops in temperature observed towards the beginning of the test in Figure 6-11 were caused by the opening of the oven door, which was necessary to ensure the thermocouples had stayed in place. However, the overall heating profile should still be largely representative of the heating profile experienced by the briquette if the openings of the oven door did not occur.

It was found that although the set temperature of the conventional oven was 90°C, the temperature experienced by the briquette can be significantly lower than this set temperature, and variations also exist across different locations in the briquette. The highest temperature experienced by the briquette was at the side of the briquette (location 6), which reached up to 75°C towards the end of the 90-minute test period. In addition to the briquettes experiencing lower temperatures than the oven set temperature, the briquettes also require long periods of time to heat up, and most of the briquette locations have not yet reached a stable temperature at the end of the 90-minute test period. This is due to the low thermal conductivity of biomass, which results in a slow transfer of heat through the briquette (Mason et al., 2016; Ogedengbe et al., 2013). Further research is required to explore how the thermal conductivity of biomass briquettes influences the pasteurisation process, as this was beyond the scope of this study. The temperatures at the centre of the briquette (locations 2 and 4) were the lowest, only reaching 45-50°C at the end of the test period. These results demonstrate that conventional oven pasteurisation is limited by heat transfer properties, and different locations of the briquettes could experience drastically different temperatures (see Section 2.7.5.1), which needs to be considered when choosing a pasteurisation condition.

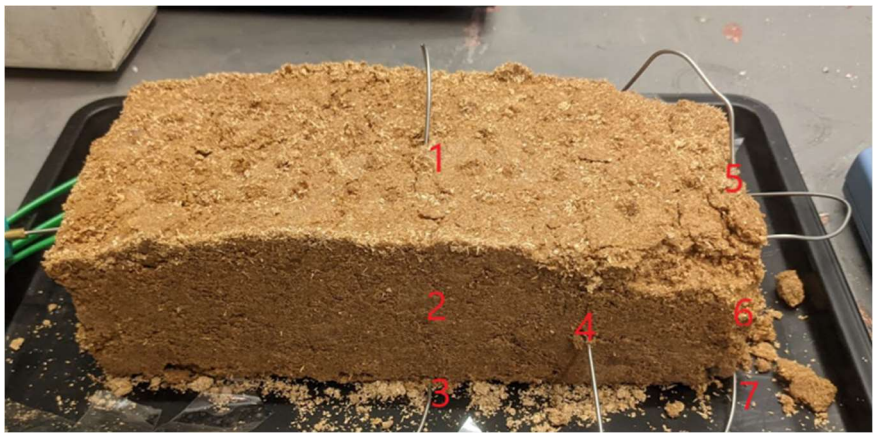

Figure 6-10 The configuration of thermocouples for briquette heating profile characterisation

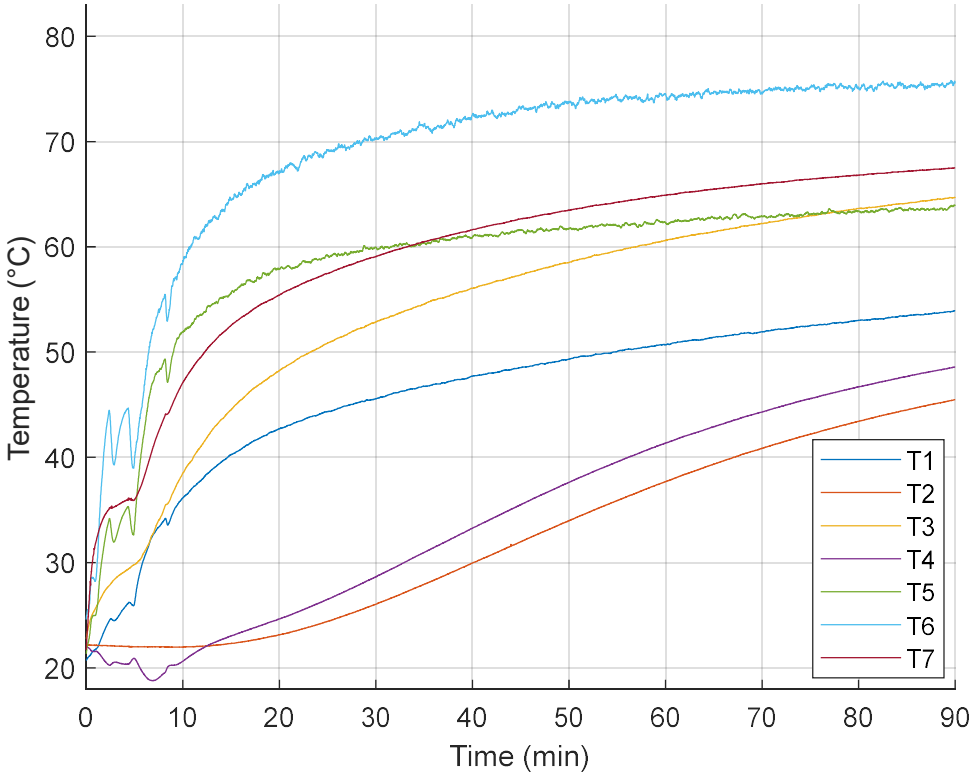

Figure 6-11 Spent grains briquette heating profile

For the microwave-treated briquettes, an in-depth characterisation of heating profiles was not conducted due to technical difficulties in measuring temperature distributions during microwave processing (Section 3.8.7). However, during the preliminary experiments (conducted to determine the pasteurisation conditions for the first set of briquettes, see Section 3.8.6), it was found that microwave pasteurisation resulted in a higher temperature at the centre of the briquettes compared to the surface, due to the volumetric heating effects of microwaves. In contrast, as illustrated above, conventional oven pasteurisation resulted in the opposite trend, where the surface experienced higher temperatures compared to the centre, as heat must be transferred from the air to the surface, and then to the centre of the briquettes. The charring observed on several of the microwaved SG briquettes also demonstrates that significantly higher temperatures were attained in some locations during the microwaving process than in the oven pasteurisation process.

6.6 Storage Conditions

The storage configuration was described in Section 3.7.8 and the method for monitoring the storage temperature and relative humidity was described in Section 3.7.9. Data of the ambient temperature and relative humidity were taken every 15 minutes during storage, and the average values over each 24-hour period for each set of briquettes are presented in Figure 6-12 to Figure 6-15.

It was found that the temperature ranged from 19-25°C and the relative humidity ranged from 45-75%. This reflects the conditions experienced by the briquettes during the storage period in an air-conditioned room. It is likely that a higher temperature and a lower relative humidity would result in a higher drying rates for the briquettes. However, the link between the environmental conditions and drying rate is beyond the scope of the present study.

6.7 Drying Behaviour

The drying rate and the moisture content of the briquettes were monitored during the storage period, as described in Section 3.7.10. The change in moisture content of the briquettes during the storage period is presented in Figure 6-16 to Figure 6-19.

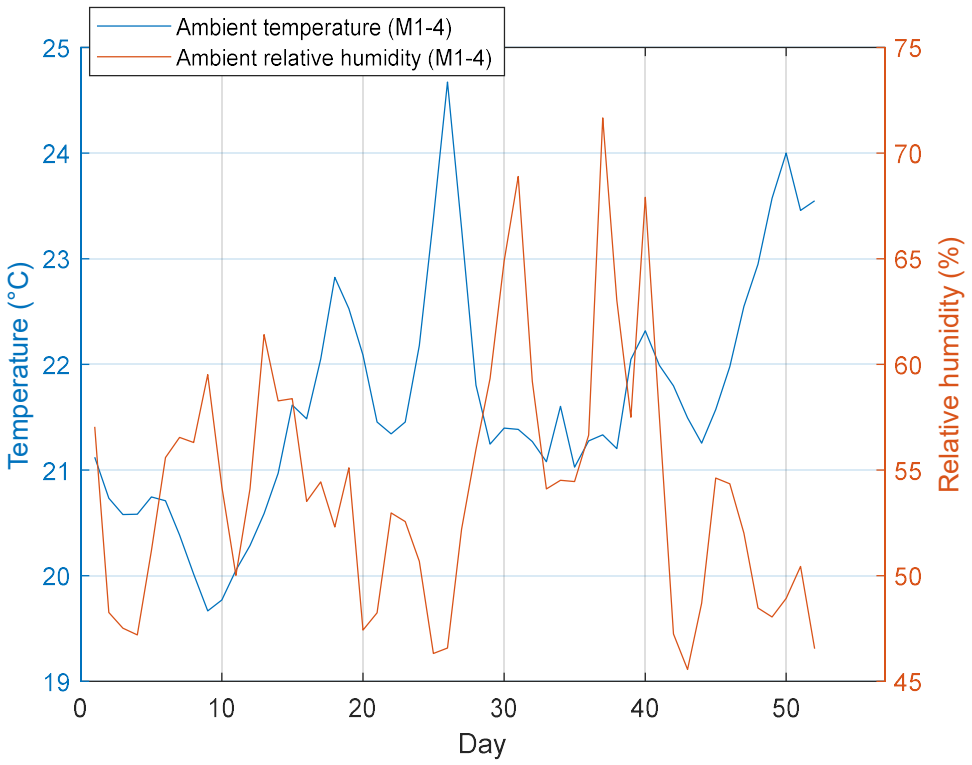

Figure 6-12 Storage conditions for M1-4

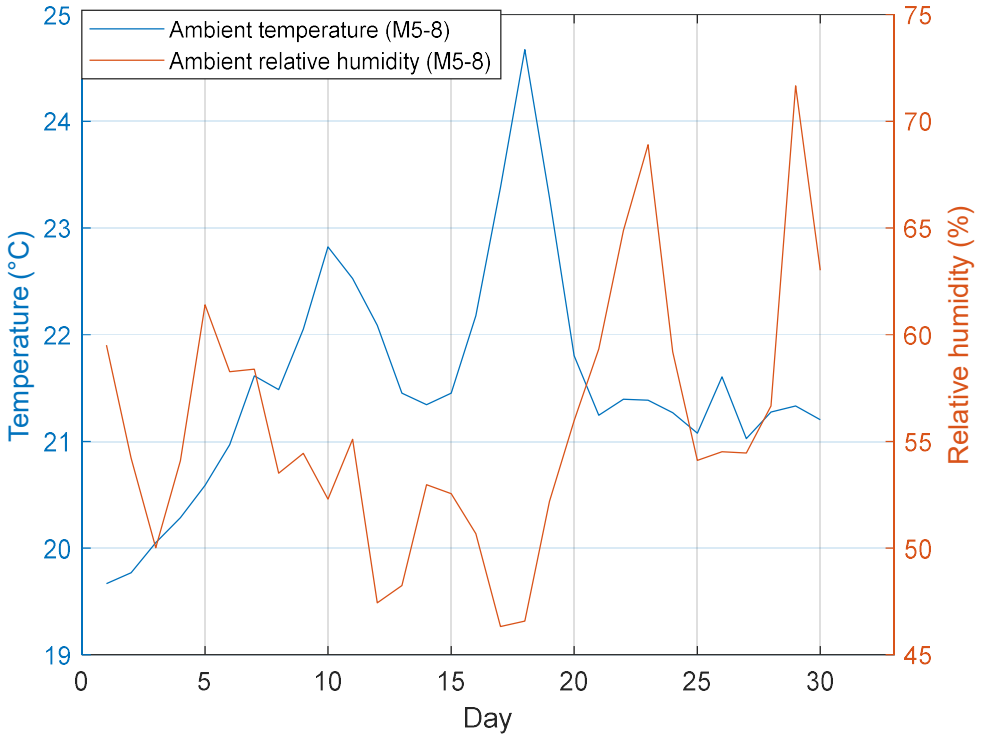

Figure 6-13 Storage conditions for M5-8

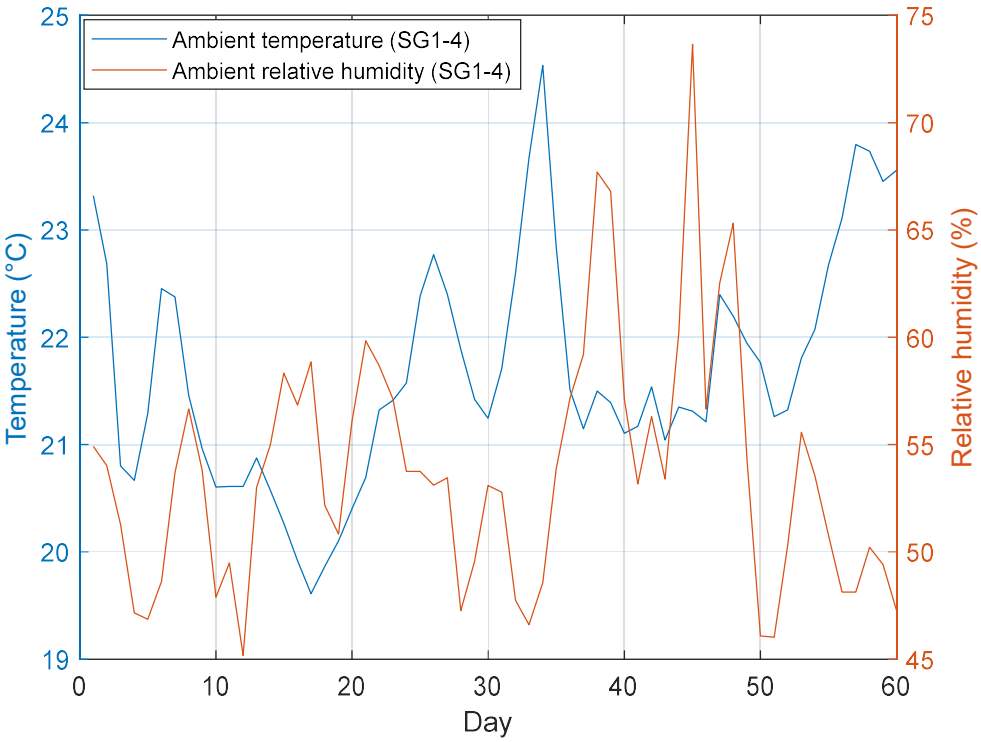

Figure 6-14 Storage conditions for SG1-4

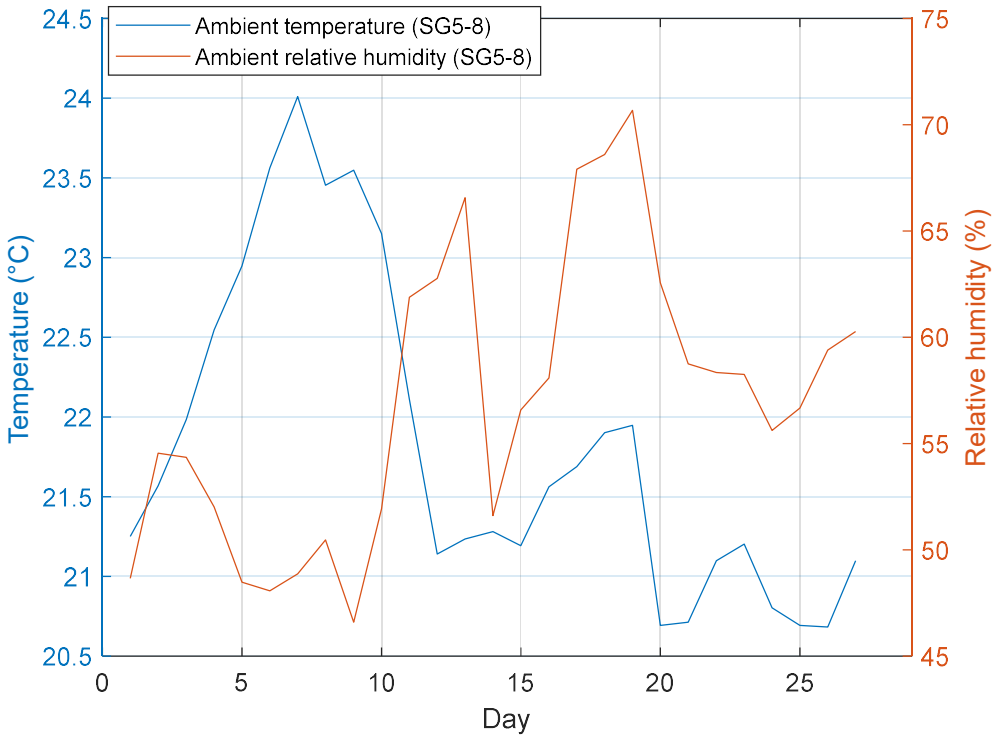

Figure 6-15 Storage conditions for SG5-8

For all of the miscanthus briquettes (M1-8), the moisture content reached a steady value at around week three of storage, fluctuating slightly around values of 10-11%. For the spent grains briquettes, the storage period required to reach a steady moisture content could not be definitively determined, as the data shows that steady state has not been reached at the end of the maximum storage period of nine weeks (Figure 6-18), although the briquettes appear to be approaching steady state at the end of the nine-week storage period. In addition, the data for both miscanthus and spent grains briquettes suggest that pasteurisation does not have a significant effect on the steady-state moisture content. Although the effect of pasteurisation on the steady-state moisture content is minimal, all pasteurised briquettes demonstrated a higher overall drying rate compared to the baseline briquettes.

Under the storage conditions used, the moisture content of miscanthus briquettes could be reduced to 10-11% after three weeks of storage, which is the steady-state value. For spent grains briquettes, the moisture content could be reduced to 12-14% after nine weeks of storage, which also appears to be approaching steady state at the end of this storage period.

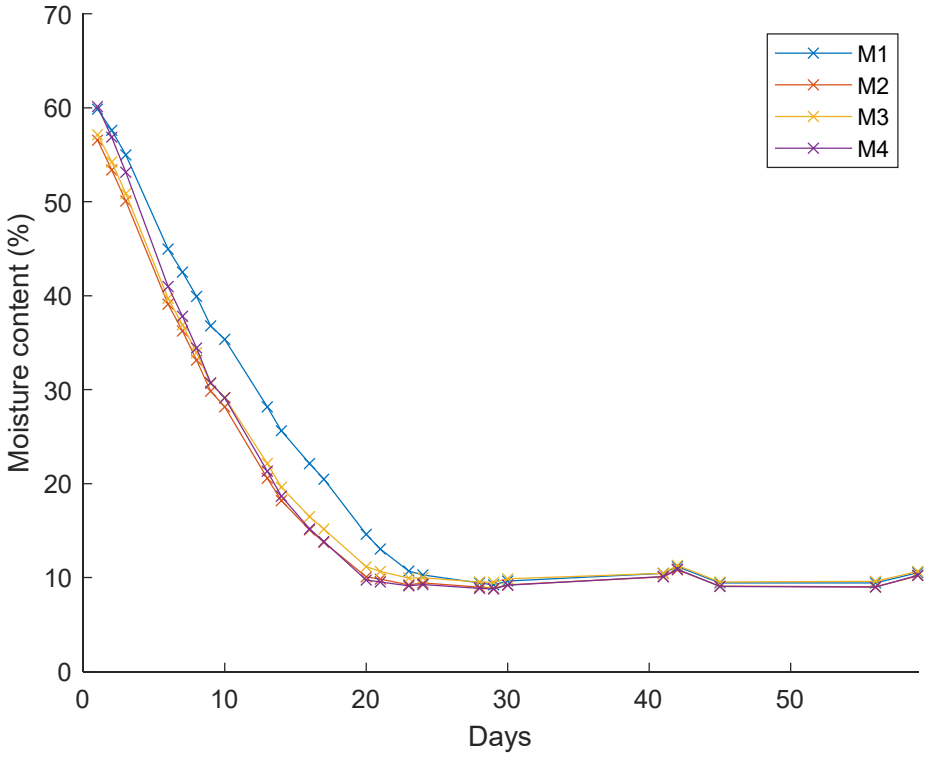

Figure 6-16 Change in moisture content of M1-4 during the storage period

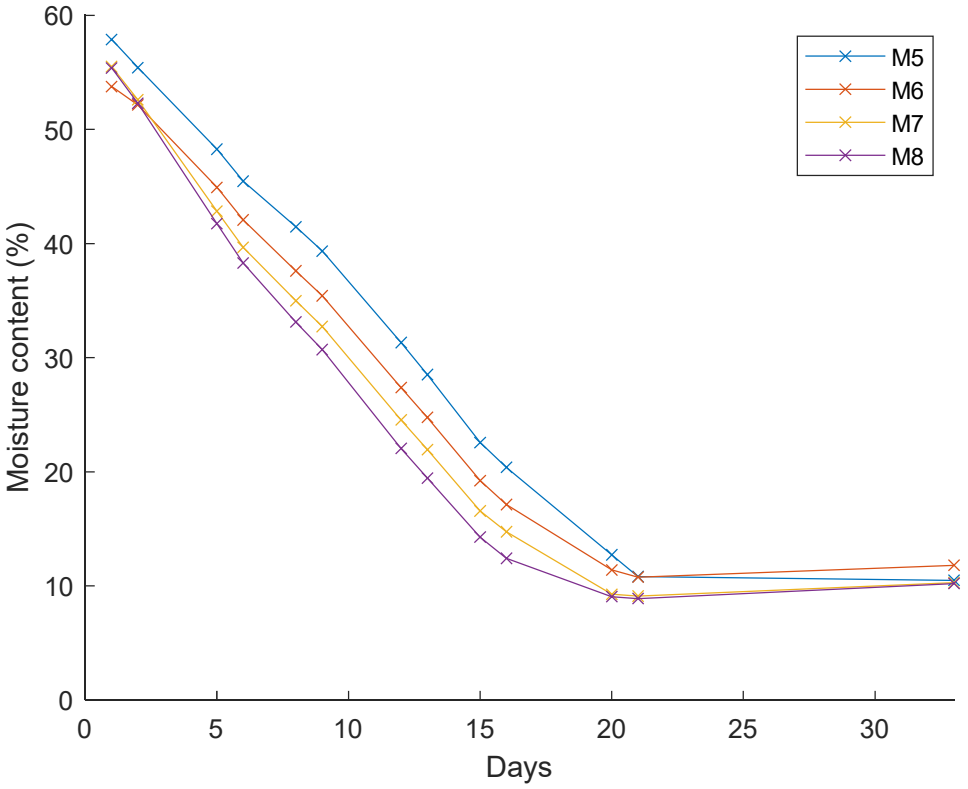

Figure 6-17 Change in moisture content of M5-8 during the storage period

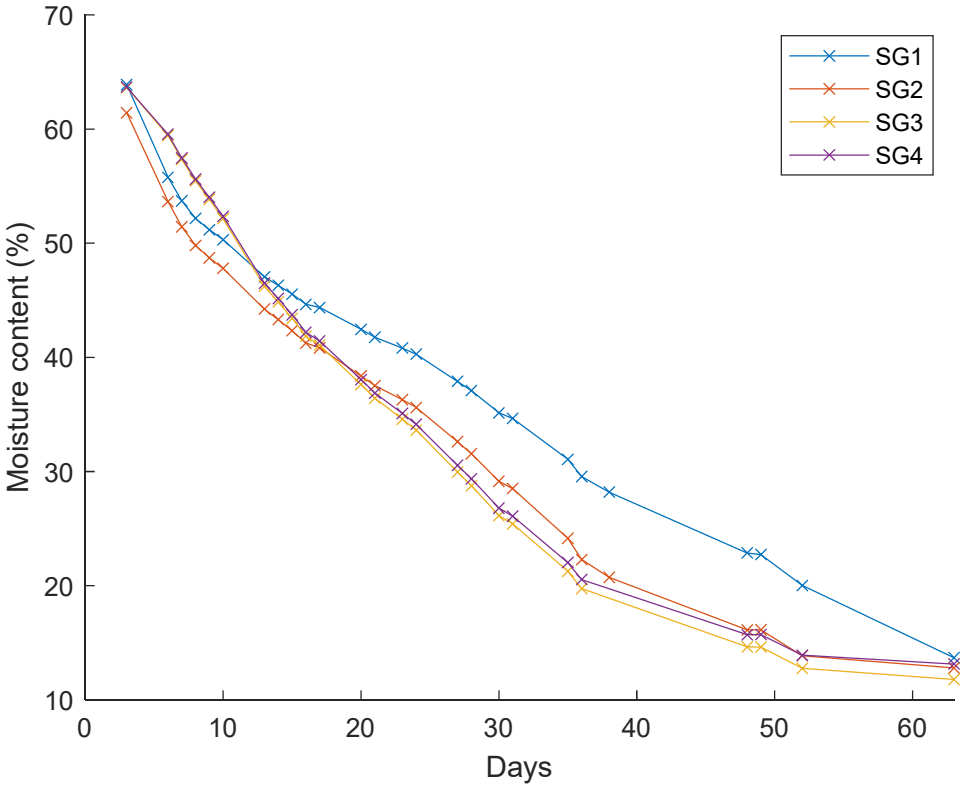

Figure 6-18 Change in moisture content of SG1-4 during the storage period

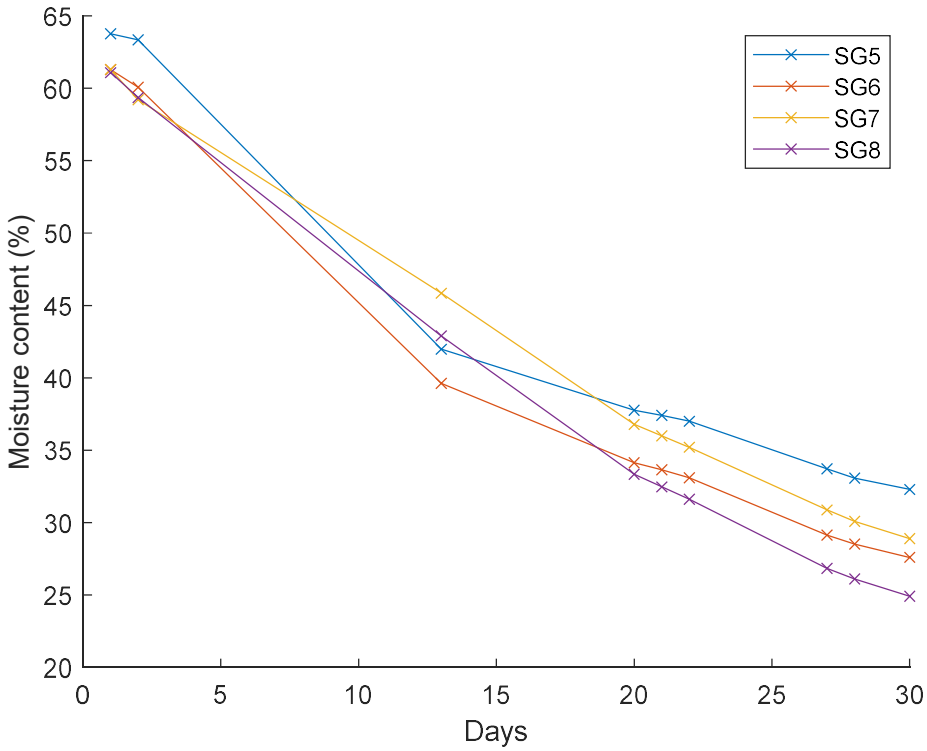

Figure 6-19 Change in moisture content of SG5-8 during the storage period

6.8 General Fungal Growth

6.8.1 Visual Inspection

The briquettes were visually inspected regularly and pictures of the briquettes were taken at multiple points during the storage period. The change in the visual appearance of the briquettes is shown in Figure 6-20 to Figure 6-25. These include both the top and bottom of the briquettes, although the photos for the bottom of the briquettes were taken less frequently than those of the top. At the end of the storage periods, the briquettes were broken apart and selected photos of the middle of the briquettes were also taken. In this Section, 't' stands for 'top', 'b' stands for 'bottom' and 'm' stands for middle (e.g. M1t would be a sample taken from the top of the M1 briquette).

6.8.1.1 Fungal growth variances between miscanthus and spent grains briquettes (for all pasteurisation conditions)

All of the miscanthus briquettes showed no obvious visible changes throughout the storage periods, while most spent grains briquettes have shown substantial fungal growth, which is also typically more severe at the bottom than at the top of the briquettes. This suggests that the miscanthus briquettes could be stored for eight weeks or longer without causing a substantial health hazard due to excessive fungal growth, while effective pasteurisation is necessary for the spent grains briquettes. However, this would need to be confirmed with pathogen testing to ensure that no non-visible hazardous pathogens were forming.

6.8.1.2 Fungal growth variances between the top and bottom of spent grains briquettes (for all pasteurisation conditions)

Compared to the top of the briquettes, the bottom of all spent grains briquettes showed more severe fungal growth. This result shows that the bottom of the briquettes is more susceptible to fungal growth compared to the top.

Visual observations also suggest that using more severe pasteurisation conditions does not necessarily reduce the level of growth at the bottom of briquettes (also see Sections 6.8.1.4 and 6.8.1.5). This is likely due to moisture being trapped on the

bottom of the briquettes as its surface is not exposed to air to allow relatively rapid evaporation to occur. Combined with the poor thermal conductivity of SG, this provides a perfect breeding ground for fungal growth. Therefore, improved storage strategies would be required to satisfactorily suppress fungal growth at the bottom of the briquettes to allow storage of the spent grain briquettes for significant periods of time.

6.8.1.3 Baseline spent grains briquettes (SG1 and SG5)

For SG1 and SG5 (baseline spent grains briquettes without pasteurisation), visible fungal growth was observed within two days of storage on both the top and bottom of the briquettes, demonstrating that pasteurisation is necessary to store the spent grains briquettes for any significant length of time.

6.8.1.4 Conventional oven pasteurised spent grains briquettes (SG2, SG4 and SG6)

For SG2t, no obvious visible fungal growth was observed throughout the storage period of nine weeks (Figure 6-13) while for SG4t, visible fungal growth was observed within six days of storage (Figure 6-3). This suggests '90°C/45min conventional oven' (SG2) is a satisfactory pasteurisation condition with regards to suppressing fungal growth at the top of the briquettes, while '90°C/180s conventional oven' (SG4) does not provide a sufficient level of fungal growth suppression, although the level of visible fungal growth is lower for SG4 compared to the baseline briquette SG1. Both SG2b and SG4b showed substantial fungal growth by week four.

For SG6, the top of the briquette showed no obvious visible fungal growth throughout the storage period of four weeks but the bottom showed severe fungal growth. This is similar to SG2, which showed no visible fungal growth at the top throughout the storage period of nine weeks but the bottom also showed severe fungal growth by week four. In addition, a visual comparison indicates a more severe level of fungal growth for SG6b compared to SG2b. This result suggests that conventional oven pasteurisation for longer than 45 mins may not yield additional benefits and may, counterintuitively, result in a higher level of fungal growth at the bottom of briquettes.

6.8.1.5 Microwave pasteurised spent grains briquettes (SG3, SG7 and SG8)

For SG3t, visible fungal growth was observed within six days of storage (Figure 6-2). In contrast, SG3t only showed visible fungal growth from week three and SG8t showed no obvious visible fungal growth throughout the storage period of four weeks. This shows that regarding the suppression of fungal growth at the top of the briquettes, '180s microwave at 1800 W' (SG3) is not a sufficiently severe pasteurisation condition. The pasteurisation condition '360s microwave at 1800 W' (SG7) provides satisfactory suppression of growth for three weeks, and '180s microwave at 1800 W, flip briquette over, followed by 180s microwave at 1800 W' (SG8) further extend this to at least four weeks. All of SG3b, SG7b and SG8b showed substantial fungal growth by week four.

6.8.1.6 Mould coloration

Variations in the coloration of the fungi present in the briquettes were also found. For SG1, SG2, SG4, SG5 and SG6, only white and grey moulds were observed (Figure 6-23 to Figure 6-25). For SG3, in addition to white and grey moulds, moulds with orange and pale green coloration were also observed (Figure 6-23 and Figure 6-24). For SG7 and SG8, in addition to white and grey moulds, moulds with pale green coloration were observed (Figure 6-25). Although it is not possible to identify the types of fungi present solely based on their colour, these may include species of the genera *Aspergillus* (usually coloured in shades of green, from very light green to brown-green or black) and *Penicillium* (usually white and may change to other colours like green–blue, pink, yellow or grey over time (Mirski et al., 2023). These results suggest that microwave pasteurisation caused significant changes in the relative abundance of the types of fungi growing on the briquette, while conventional oven pasteurisation had limited effects on this relative abundance, although it is also effective in reducing growth generally.

6.8.1.7 Effects of microwave pasteurisation on fungal growth at the middle of spent grains briquettes

Visual inspection of the middle of the spent grain briquettes at the end of the storage periods reveals the following trends:

1. The middle of the briquettes was visibly more moist compared to the edges, as evaporation would mostly occur at the exposed surfaces of the briquettes and moisture at the middle of briquettes would need to diffuse outwards before effective evaporation can occur, thus requiring much longer durations.
2. Very limited visible fungal growth was observed for the middle of the baseline (SG1 and SG5) and conventional oven pasteurised briquettes (SG2, SG4 and SG6), suggesting that the pasteurisation conditions used for these briquettes are sufficient for suppressing fungal growth at the middle of the briquettes.
3. Substantial fungal growth was observed for the middle of the microwave pasteurised briquettes (SG3, SG7 and SG8), suggesting that the pasteurisation conditions used for these briquettes are sufficient for suppressing fungal growth at the middle of the briquettes. A possible explanation for this phenomenon is that due to the presence of hot and cold spots during microwave pasteurisation (Birla & Pitchai, 2017; Gaukel et al., 2017; Wäppling Raaholt & Isaksson, 2017), limited fungal growth suppression is achieved at the cold spots, and rapid growth originating in these cold spots would occur during the storage period.

These observations, together with the discussion of mould coloration in Section 6.8.1.6, support that microwaves have unique effects on the relative abundance of the types of fungi growing in the briquettes. A possible explanation is that microwave pasteurisation is more effective in killing certain species of fungi compared to conventional pasteurisations.

6.8.2 Fungal Growth Quantification

The level of fungal growth was measured using the method described in Section 3.7.11. For the first set of experiments (M1-4 and SG1-4), measurements for the top and bottom of briquettes were conducted immediately after pasteurisation (week 0) and after four (SG1-4) or five (M1-4) weeks and then after either eight (M1-4) or nine (SG1-4) weeks of storage (see Section 6.6). At the end of the eight-week or nine-week storage period, the briquettes were broken apart and measurements for the middle of the briquette were conducted. For the second set of experiments (M5-8 and SG 5-8), measurements for the top and bottom of briquettes were conducted immediately

after pasteurisation (week 0) and after four or five weeks of storage. At the end of the four-week or five-week storage period, the briquettes were also broken apart and measurements for the middle of the briquette were conducted. Examples of the growth of fungi on petri dishes for the fungal incubation tests are shown in Figure 6-26 and Figure 6-27. This Section describes in detail the fungal growth quantification for the different groups of tests: Briquettes M1-4, M5-8, SG1-4 and SG5-8. The data for the fungal growth tests are shown in Table 6-5 to Table 6-8.

6.8.2.1 Miscanthus Briquettes M1-4

The data for the unpasteurised baseline briquette (M1t) shows an initial decrease in the amount of fungi from week 0-4, followed by an increase from week 4-8. The amount of fungi present for M1-4t at week 0 are comparable, showing that the amount of fungi eliminated at the top of the briquettes by the pasteurisation process was small for the conditions used for M1-4 and none of the four conditions was significantly more effective than the others in terms of immediately eliminating fungi.

The amount of fungi present for M1t, M2t and M4t at week four are also comparable, showing that the level of initial growth suppression by conventional oven pasteurisation at 90 °C is small regardless of the pasteurisation duration. However, the effect of the longer duration used for M2 (90°C for 45 mins) compared to M4 (90°C for 1 min 45 s) is apparent after eight weeks, as the conventional oven method with a long duration is able to dramatically decrease the amount of fungi present at the top of the briquette after eight weeks of storage.

The data also shows that the microwave pasteurisation method used for M3 (105s at high power) is highly effective in suppressing fungal growth at the top of the miscanthus briquettes. While only a minimal decrease compared to the baseline was measured immediately after pasteurisation, dramatic decreases were measured after four and eight weeks of storage, and only a minimal level of decrease was measured for M4t (conventional oven method at 90°C for the same duration as M3) throughout the storage period.

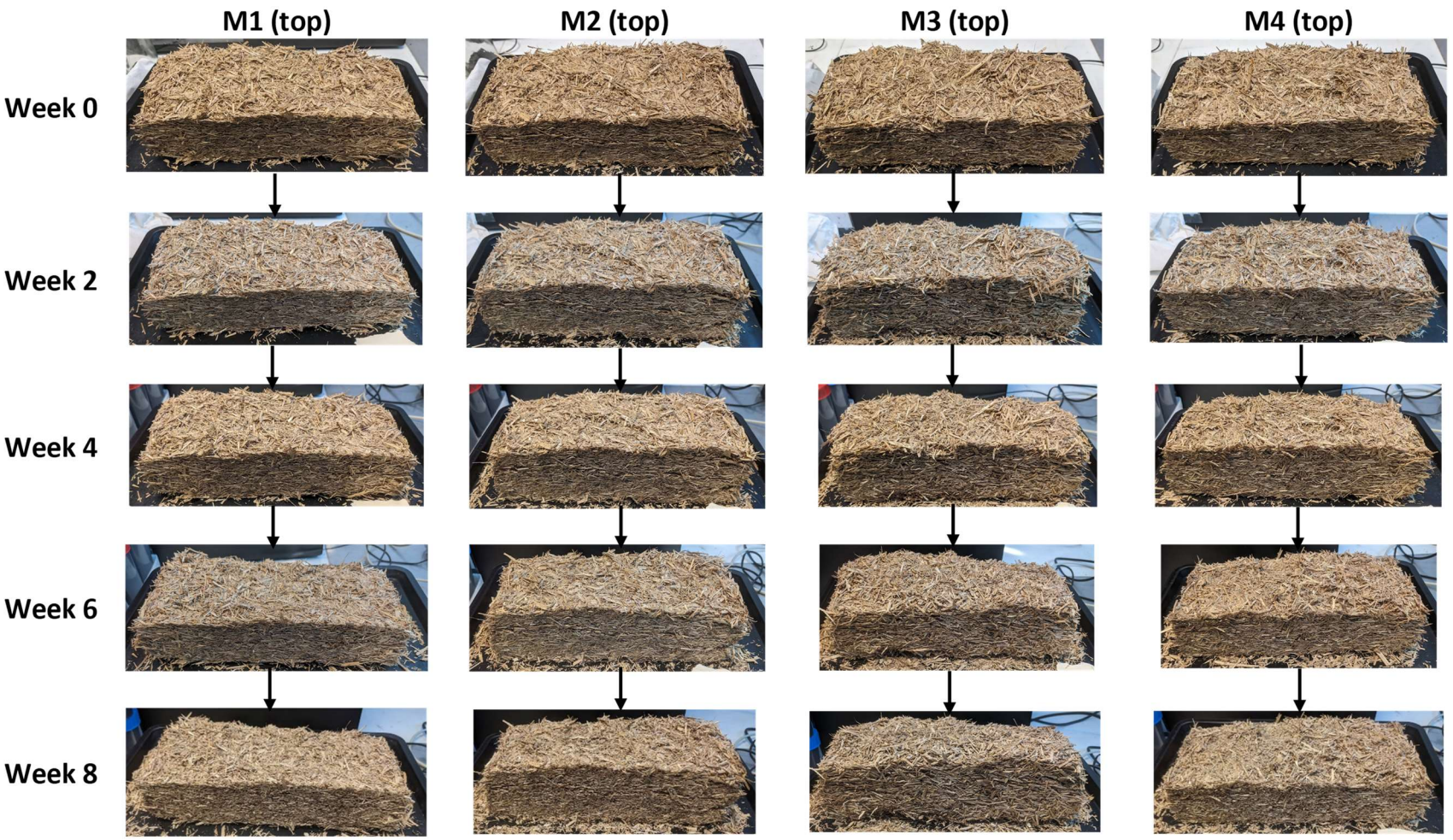

Figure 6-20 Appearance of the top of briquettes M1-4 during the storage period

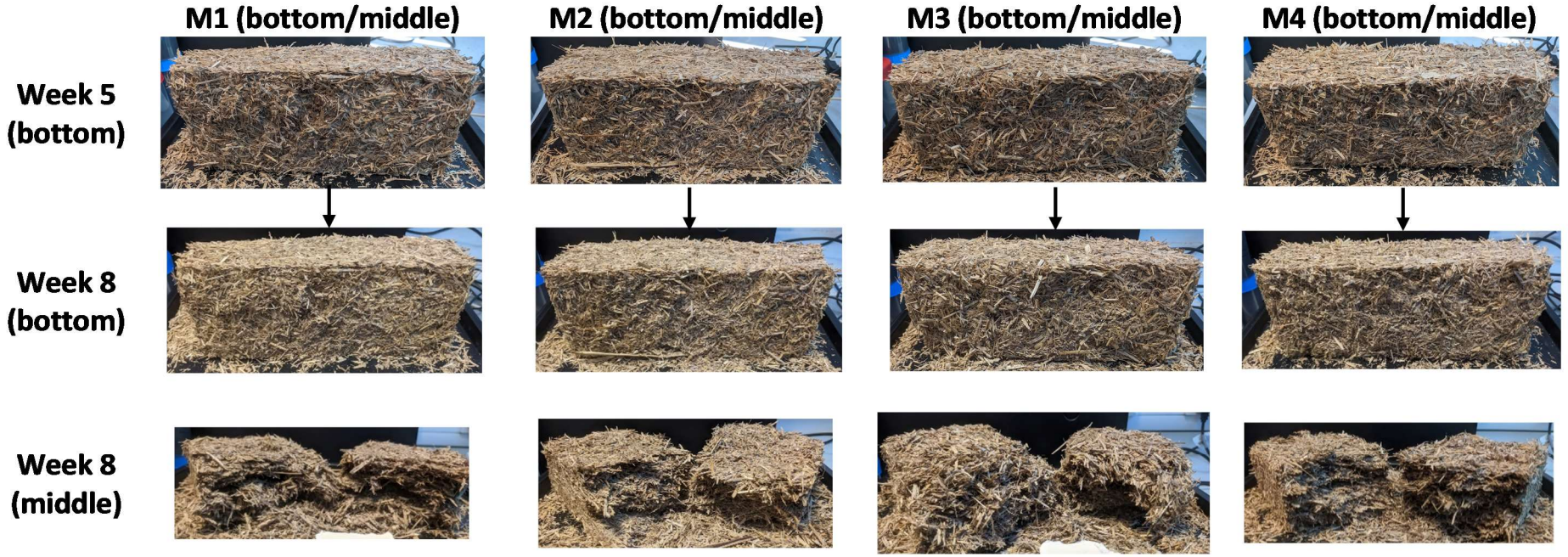

Figure 6-21 Appearance of the bottom and middle of briquettes M1-4 during and at the end of the storage period

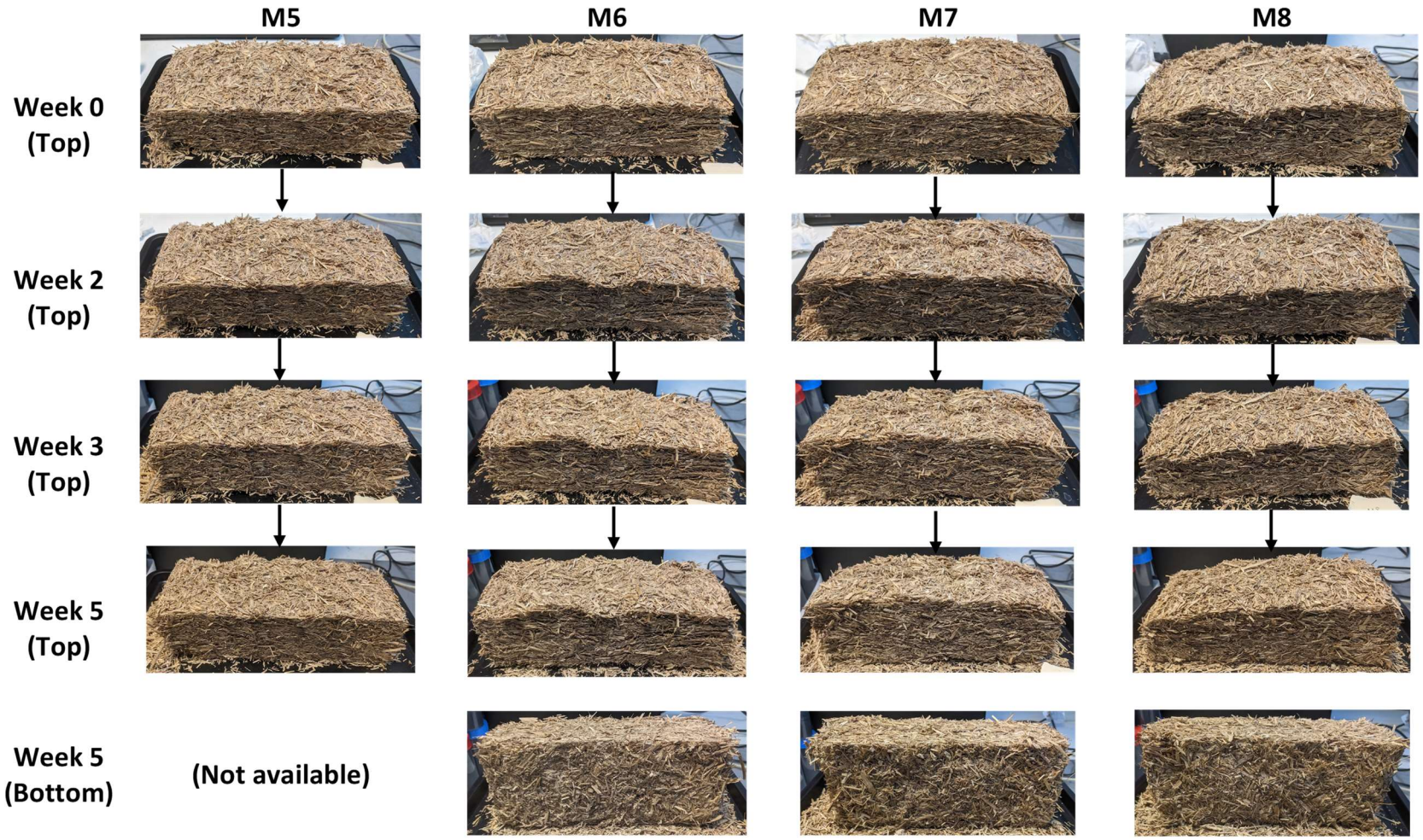

Figure 6-22 Appearance of briquettes M5-8 during the storage period

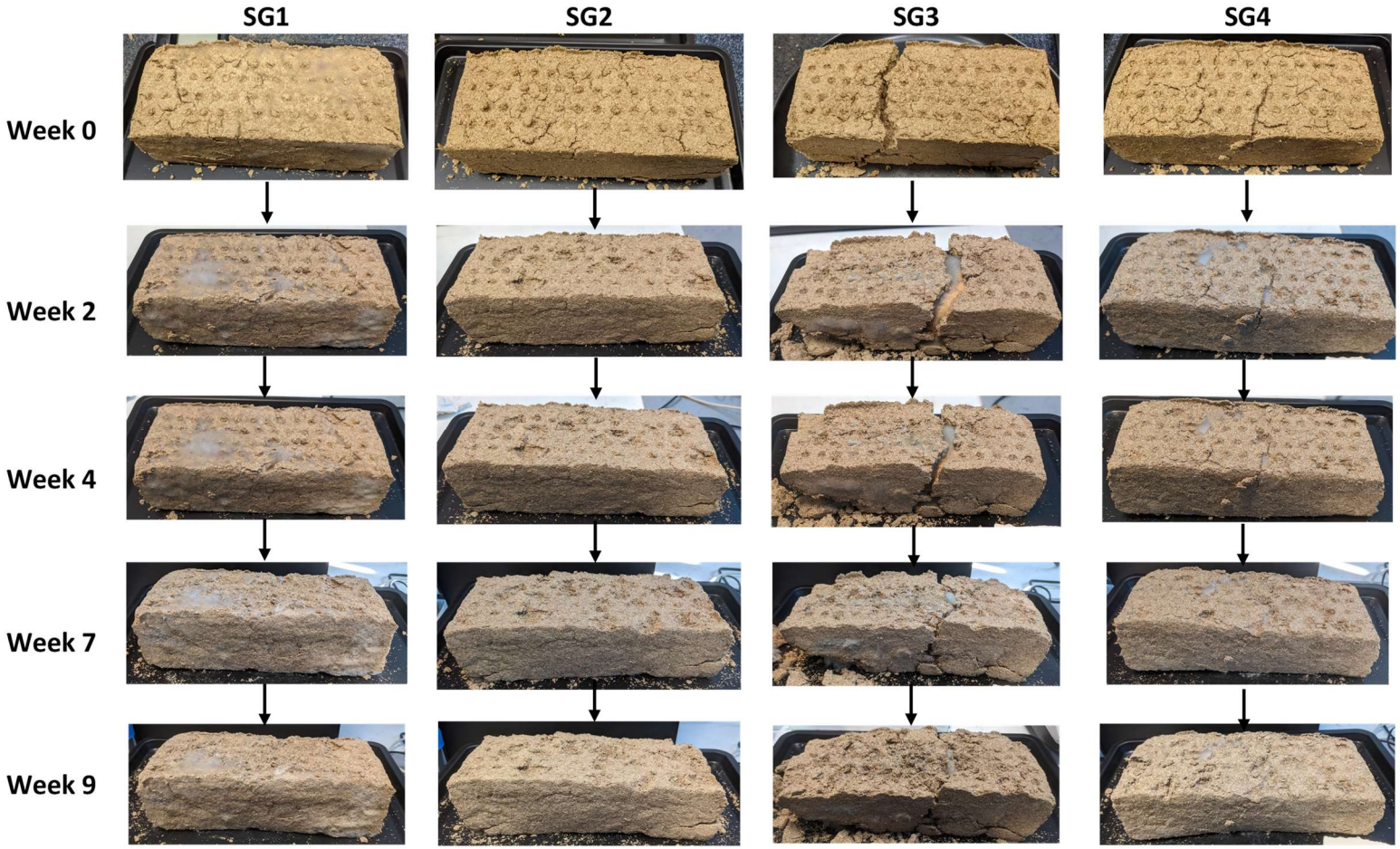

Figure 6-23 Appearance of the top of briquettes SG1-4 during the storage period

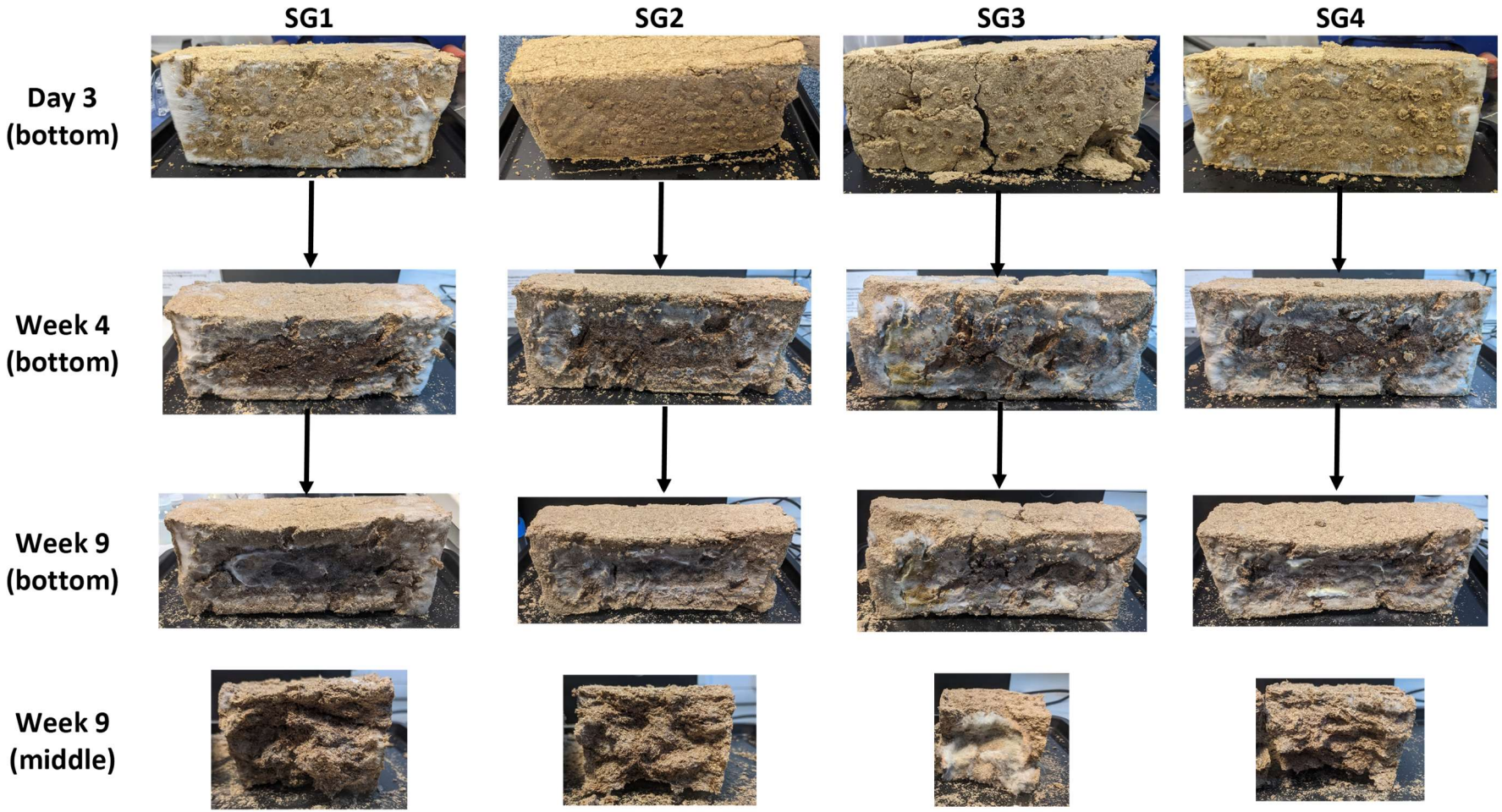

Figure 6-24 Appearance of the bottom and middle of briquettes SG1-4 during and at the end of the storage period

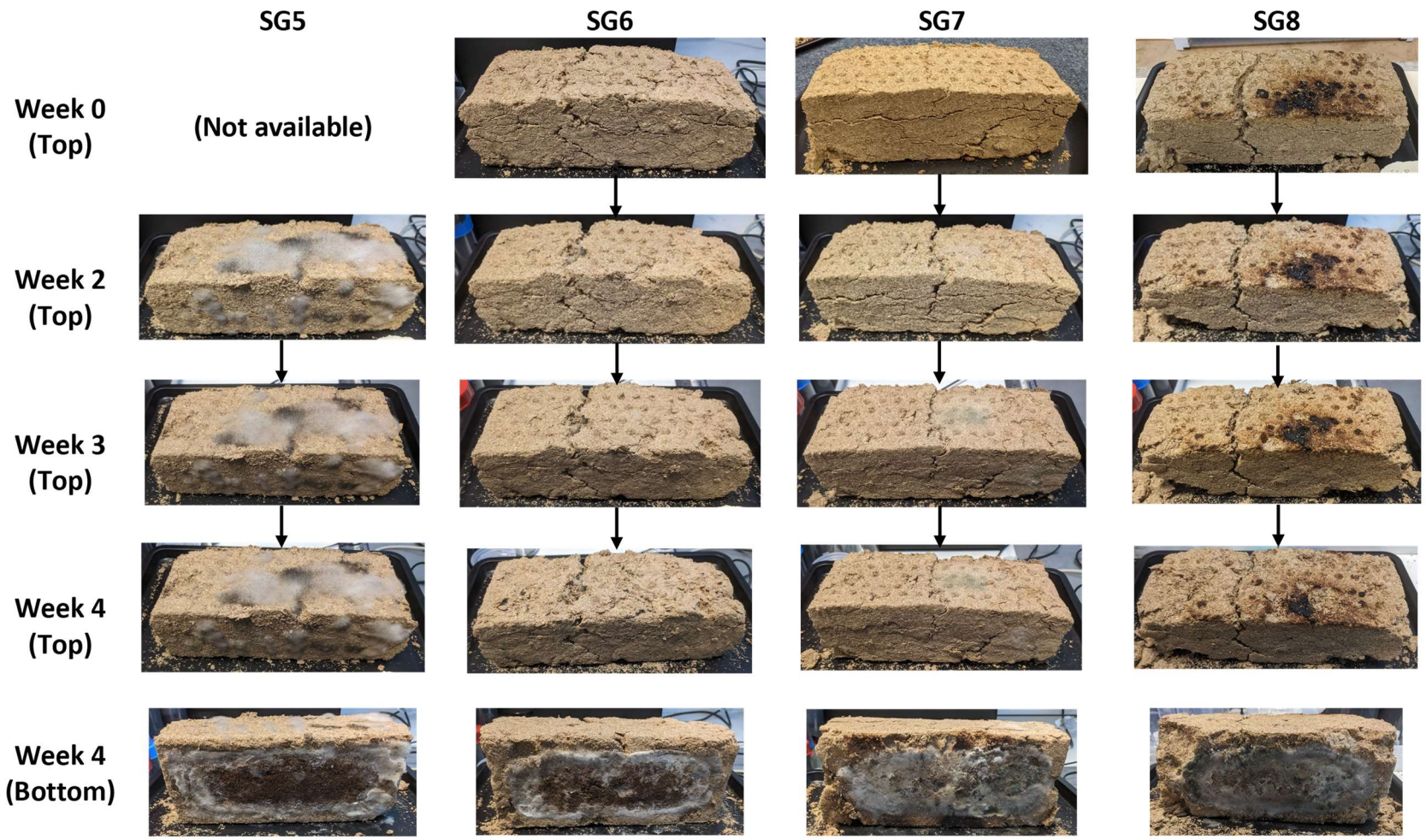

Figure 6-25 Appearance of briquettes SG5-8 during the storage period

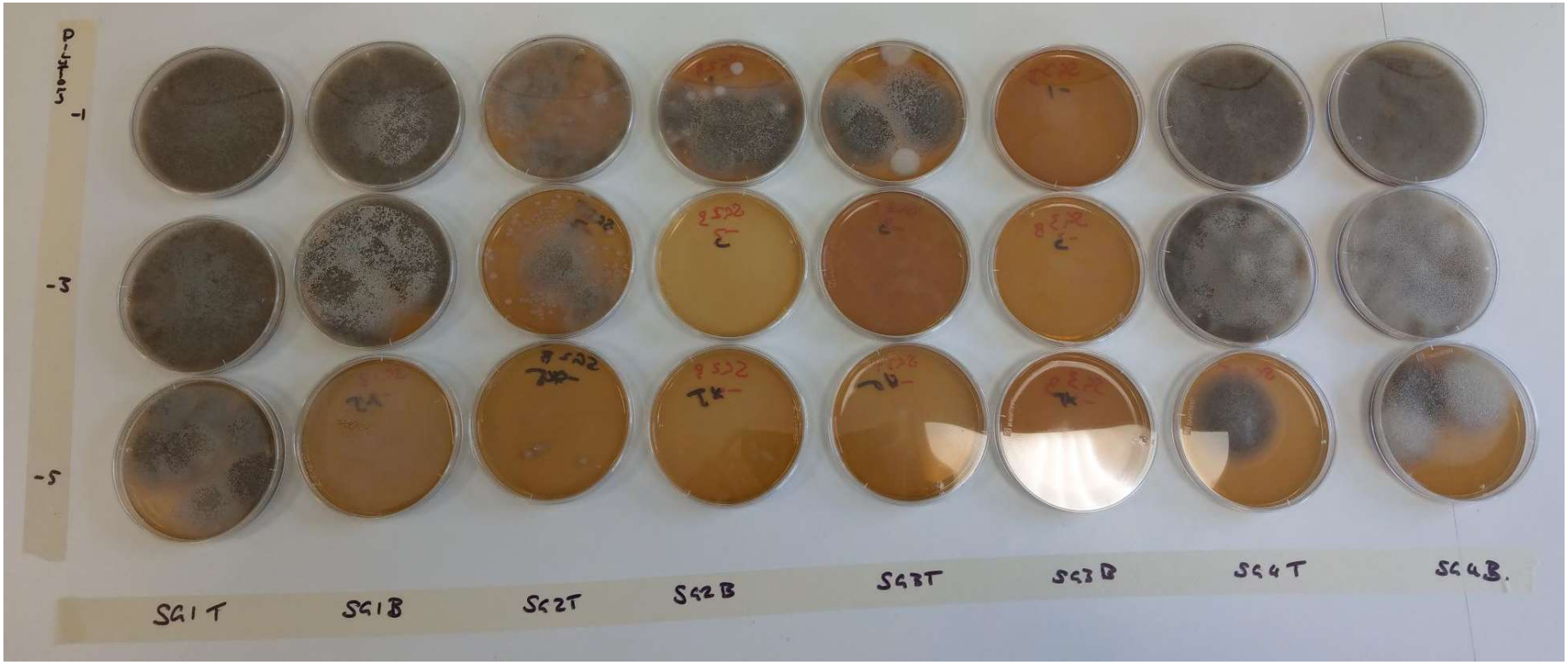

Figure 6-26 Example of fungi incubation tests for briquettes SG1-4

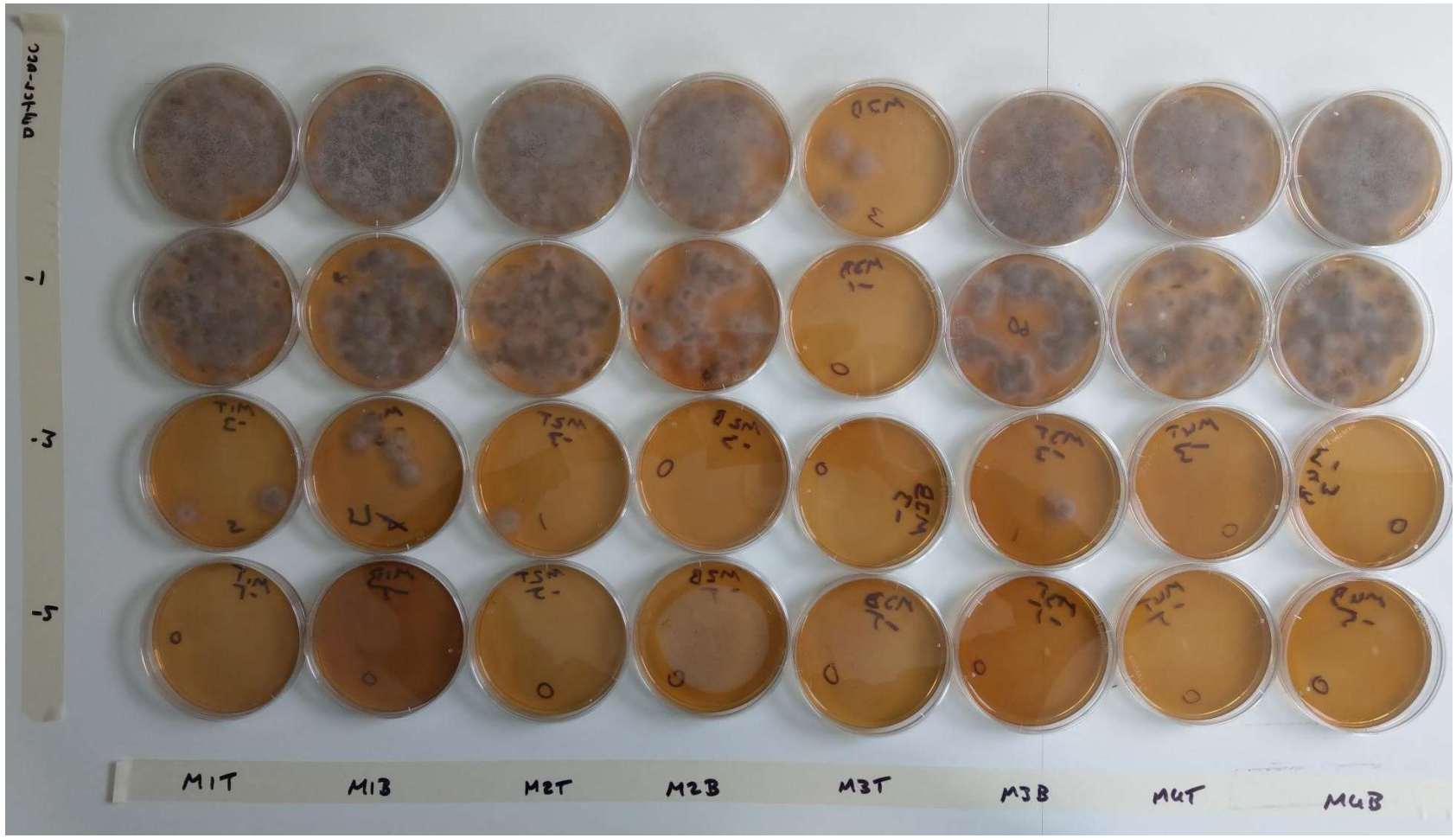

Figure 6-27 Example of fungi incubation tests for briquettes M1-4

	Number of colony forming unit											
Week	**M1t**	**M2t**	**M3t**	**M4t**	**M1b**	**M2b**	**M3b**	**M4b**	**M1m**	**M2m**	**M3m**	**M4m**
0	1.2e5	1.1e5	6.0e4	8.4e4	1.4e5	3.6e4	40	1.1e5	N/A	N/A	N/A	N/A
4	8.0e3	7.5e3	3.0e2	4.8e3	6.3e3	1.7e3	3.2e3	6.7e3	N/A	N/A	N/A	N/A
8	4.0e4	1.2e3	1.0e2	3.0e4	2.0e4	1.6e3	1.7e3	1.0e5	3.0e4	2.0e3	9.0e4	3.0e4

Table 6-5 Fungal growth data for M1-4

	Number of colony forming unit											
Week	**M5t**	**M6t**	**M7t**	**M8t**	**M5b**	**M6b**	**M7b**	**M8b**	**M5m**	**M6m**	**M7m**	**M8m**
0	9.5e3	3.0e3	3.0e2	4.5e3	8.6e3	4.1e3	0	7.6e3	N/A	N/A	N/A	N/A
5	5.1e3	3.4e3	20	2.2e2	1.4e3	7.5e2	7.0e4	3.1e5	1.1e3	8.0e2	3.0e3	3.0e2

Table 6-6 Fungal growth data for M5-8

	Number of colony forming unit											
Week	**SG1t**	**SG2t**	**SG3t**	**SG4t**	**SG1b**	**SG2b**	**SG3b**	**SG4b**	**SG1m**	**SG2m**	**SG3m**	**SG4m**
0	9.0e7	2.0e5	6.0e3	1.0e7	1.1e6	8.0e3	0	3.0e7	N/A	N/A	N/A	N/A
4	5.0e6	7.0e4	6.3e5	9.7e5	4.5e8	8.6e5	8.0e6	2.0e6	N/A	N/A	N/A	N/A
9	9.0e5	2.4e5	6.0e6	7.0e6	6.0e6	4.0e6	6.0e6	5.0e6	1.0e5	6.0e4	6.8e5	3.1e7

Table 6-7 Fungal growth data for SG1-4

	Number of colony forming unit											
Week	**SG5t**	**SG6t**	**SG7t**	**SG8t**	**SG5b**	**SG6b**	**SG7b**	**SG8b**	**SG5m**	**SG6m**	**SG7m**	**SG8m**
0	1.9e5	1.1e2	0	0	2.4e4	2.6e2	0	0	N/A	N/A	N/A	N/A
4	4.0e6	1.0e6	1.0e2	0	6.0e5	7.0e6	5.0e6	1.3e7	1.0e4	2.4e5	1.0e6	1.0e6

Table 6-8 Fungal growth data for SG5-8

Similar to M1t and M4t, M1b and M4b showed an initial decrease in the amount of fungi from week 0-4, followed by an increase from week 4-8. Similar to M2t, M2b showed a significant decrease in the amount of fungi present compared to the baseline throughout the storage period. In contrast to M3t, M3b saw a dramatic decrease in the amount of fungi present immediately after pasteurisation, suggesting that the bottom of the briquette experienced higher temperatures compared to the top during microwave pasteurisation. This is also consistent with the charring observed at the bottom of the spent grains microwave pasteurised briquettes (Section 6.4.3) – although charring was not observed in the miscanthus briquettes, both results support that higher temperatures are reached on the downward-facing side of the briquettes during microwave pasteurisation at 1800 W (high power).

Although a significant decrease in the amount of fungi present compared to the baseline briquette (M1) was observed for both the M3t and M3b, the trends of growth during the storage period were very different. For M3b, a large increase was observed during week 0-4, followed by a small decrease during week 5-8. However, for M3t, a monotonic decrease was observed.

The' 90°C/45 mins conventional oven' pasteurisation condition used for M2 is very effective in reducing the amount of fungi present at the middle of the briquette at the end of the storage period. Meanwhile, M4, which also uses the conventional oven method for a much shorter duration, does not demonstrate any effect on the amount of fungi at the middle of the briquette at the end of the storage period. For M3m, while this microwave pasteurisation method (105s at high power) is highly effective in reducing the amount of fungi present at the top of the briquette, it is ineffective in reducing the amount of fungi in the middle at the end of the storage period, as it was found that more fungi are present compared to the unpasteurised sample. This result is similar to the visual inspection of fungal growth for the middle of spent grains briquettes as discussed in Section 6.8.1.7. Similarly, a possible explanation is that due to the presence of hot and cold spots during microwave pasteurisation (Birla & Pitchai, 2017; Gaukel et al., 2017; Wäppling Raaholt & Isaksson, 2017), limited fungal growth suppression is achieved at the cold spots, and rapid growth originating in these cold spots would occur during the storage period.

6.8.2.2 Miscanthus briquettes M5-8

Miscanthus briquettes M5-8 pasteurisation conditions were set based on the emerging outcomes of M1-4, as discussed in Section 6.3. Since the aim of the experiments is to compare the effectiveness of the pasteurisation conditions, when comparing the results of the two sets of briquettes (M1-4 and M5-8), the main focus is the relative effect of the pasteurisation conditions on fungal growth compared to the unpasteurised baseline briquette (M1 or M5), and not the absolute values of the amount of fungi present on the briquettes.

The pasteurisation conditions used for M6 and M7 were identical to those used for M2 and M3 respectively. Similarly to M1t and M2t, M6t showed a small decrease in the amount of fungi present compared to M5t from week 0-5. M7t showed a larger decrease (relative to M5t) in the amount of fungi present at week 0, compared to the trend observed between M1t and M3t. However, M7t showed effective suppression of growth up to at least week five, which was also observed for M3t. The briquette M8 used the pasteurisation condition '556s microwave at 340 W', which used the same amount of total energy as M3 and M7 but used a 'low power, long duration' configuration instead of the 'high power, short duration' configuration for M3 and M7. The fungal growth data for M8t shows that a significant level of fungal growth suppression was achieved up to at least week five, although it is significantly less effective than the 'high power, short duration' configuration.

Similar to M2b, M6b (same pasteurisation condition as M2b) showed a small decrease in the amount of fungi present throughout week 0-5 compared to M5b. Similar to M3b, M7b showed a large decrease in the amount of fungi present immediately after pasteurisation, followed by a sharp increase during week 0-5. It was also found that the 'low power, long duration' pasteurisation condition used for M8 was ineffective in reducing the amount of fungi present at the bottom of the briquette immediately after pasteurisation, with no significant differences between the fungal growth data of M5b and M8b. This indicates that in contrast to the 'high power, short duration' configuration, the 'low power, long duration' configuration does not result in the bottom of the briquette experiencing significantly higher temperatures. Additionally, unique effects on subsequent fungal growth were

observed, as substantial growth on M8b had occurred by week five, to the extent that a much larger amount of fungi was present than M5b (the baseline briquette).

At week five, the '90°C/45 mins conventional oven' pasteurisation used for M6 was found to result in a small decrease in the amount of fungi present in the middle of the briquette compared to the baseline briquette. M7m shows a substantial increase in the amount of fungi present compared to the baseline briquette at week five. Together with the fungal growth data for M3m at week eight, the results suggest that the pasteurisation condition '105s microwave (1800 W)' would result in a higher amount of fungi present in the middle of the miscanthus briquette at both week five and week eight, compared to the unpasteurised baseline briquette. In contrast, M8m shows a large decrease in the amount of fungi present compared to the baseline briquette, suggesting that the pasteurisation condition ' 556s microwave (340 W)' is very effective at reducing the amount of fungi present in the middle of the miscanthus briquette at week five.

6.8.2.3 Spent grains briquettes SG1-4

The data for the unpasteurised baseline briquette (SG1t) shows a decrease in the amount of fungi during week 0-4 and week 4-9. SG2t showed a good level of fungal growth suppression compared to SG1t throughout the storage period of nine weeks. For SG3t, the pasteurisation condition '180s microwave (1800 W)' eliminated a large amount of fungi during pasteurisation. However, rapid regrowth occurred and after nine weeks of storage, the amount of fungi present at SG3t became higher than that at SG1t. SG4t showed a small level of fungal growth suppression at week 0-4, but the amount of fungi present at SG4t became higher than that at SG1t by week nine.

The results show that for conventional oven pasteurisation at 90°C, the longer duration (45 mins) used for SG2 was more effective at suppressing fungal growth at the top of the briquette compared to the shorter duration (3 mins) used for SG4. Comparing SG3t and SG4t, it is also concluded that microwave pasteurisation at 1800 W for 3 mins is more effective than conventional oven pasteurisation at 90°C for the same duration, especially during week 0-4. It was also observed that over nine weeks of storage, neither the pasteurisation conditions used for SG3 nor SG4 were

sufficient, as the level of fungal growth was more severe at week nine compared to the baseline. However, the '90°C/45min conventional oven' method (SG2) showed a good level of suppression at the top of the briquette throughout the storage period of nine weeks. This is also consistent with the visual observation of SG2 that no visible growth occurred during the storage period (Section 6.8.1.4). Comparing the fungal growth data of M1-4t and SG1-4t at week 0 also reveals differences in the response of the fungi to pasteurisation. While a large amount of fungi was immediately eliminated by pasteurisation in SG2t and SG3t, only a small decrease was observed in M1-4t immediately after pasteurisation. This suggests that the fungi present in the miscanthus briquettes may be more resistant to heat and/or microwave treatment compared to the ones in the spent grains briquettes. In addition, the fungal growth data also reaffirms the visual observations (Section 6.8.1) that the pasteurisation conditions used for SG3 and SG4 were not sufficient to satisfactorily suppress fungal growth for the top of the briquettes.

Similar to SG2t and SG3t, SG2b and SG3b showed a significant reduction in the amount of fungi present immediately after pasteurisation, with the '180s microwave (1800 W)' pasteurisation condition used for SG3 being more effective at the immediate elimination of fungi at the bottom of the briquettes. At week four, the '90°C/45min conventional oven' condition used for SG2 was more effective. Although reductions in the amount of fungi were achieved for SG2-4b at week four, significant regrowth has occurred and all of SG1-4b showed a similar level of fungi present by week nine.

Only SG2m showed a small decrease compared to the baseline, and both SG3m and SG4m showed a significant increase in the amount of fungi present at week nine. This result indicates that sub-optimal pasteurisation conditions could result in rapid regrowth during the storage period to the extent that the amount of fungi could reach similar or higher levels compared to the unpasteurised baseline, even if the pasteurisation condition were effective in immediately removing a large proportion of the fungi present before pasteurisation.

6.8.2.4 Spent grains briquettes SG5-8

All of SG5-8t showed some fungal growth suppression throughout week 0-4. However, the longer duration of conventional oven pasteurisation used for SG6 did not appear to provide substantial benefits in fungal growth suppression at the top of the briquette at week 0-4 compared to SG2. The microwave pasteurisation conditions used for SG7 and SG8 were found to be very effective in suppressing fungal growth at the top of the briquettes throughout week 0-4. For both SG7t and SG8t, the results show that almost all of the fungi present at the top of the briquettes were eliminated by pasteurisation. Some regrowth was observed for SG7t, while no regrowth was observed for SG8t during week 0-4. This suggests that flipping the briquette upside down halfway through the duration of pasteurisation (SG8) yielded additional benefits in fungal growth suppression, confirming that the presence of hot and cold spots is one of the main causes of rapid fungal regrowth and that the procedure of flipping the briquette upside down halfway through the duration of pasteurisation is a useful strategy to combat this issue.

Similar to SG2b, SG6b showed a significant level of fungal growth suppression throughout week 0-4, although the longer duration of conventional oven pasteurisation used for SG6 also did not appear to provide substantial benefits in fungal growth suppression at the bottom of the briquette at week 0-4 compared to SG2. Similar to SG7t and SG8t, the microwave pasteurisation conditions used successfully eliminated almost all of the fungi during pasteurisation. However, very rapid regrowth occurs at the bottom of the pasteurised briquettes, and all of SG6-8b showed more severe fungal growth compared to the baseline.

All of the pasteurised briquettes (SG6-8) showed much higher levels of fungal growth compared to the baseline at the bottom of the briquettes. The pasteurisation condition '90°C/90min conventional oven' (SG7) resulted in a lower level of regrowth at the bottom of the briquette compared to the microwave pasteurisation conditions used for SG7 and SG8. This shows that sub-optimal pasteurisation conditions and/or storage strategies could result in rapid regrowth during the storage period to the extent that the amount of fungi could reach similar or higher levels compared to the unpasteurised baseline, even if the pasteurisation condition was effective in

immediately removing a large proportion of the fungi present before pasteurisation. Meanwhile, SG7m and SG8m showed similar levels of regrowth at week four, which is the expected result considering the pasteurisation conditions used, as the middle of the briquette is expected to receive the same level of pasteurisation when the power and duration used for microwave pasteurisation are identical, even if the briquette was flipped upside down halfway through the pasteurisation process.

6.8.2.5 Overall results of fungal growth quantification

The overall findings of the fungal growth tests are summarised as:

1. Even if a pasteurisation method does not immediately eliminate a large proportion of fungi in the briquette, it could still provide substantial long-term suppression of fungal growth compared to the unpasteurised briquette. Therefore, it is essential to know the acceptable level of fungal growth for a given storage time.
2. For miscanthus, '105s microwave at 1800 W' (M3 and M7) is more effective compared to '90°C/105s conventional oven' (M4) and '90°C/45min conventional oven' (M2), particularly for the top of the briquettes.
3. More severe fungal growth is generally observed at the bottom compared to the top of the briquettes (for both miscanthus and spent grains). This remains the case even if a pasteurisation condition is effective at eliminating a large proportion of fungi present, as rapid regrowth would occur at the bottom of the briquettes.
4. Conducting conventional oven pasteurisation for a longer duration does not necessarily result in a higher level of fungal growth suppression. This is likely due to the temperature within the briquettes not reaching a sufficient level to kill all fungi.
5. For microwave pasteurisation with the same overall energy use, 'high power, short duration' is more effective than 'low power, long duration' in reducing fungal growth at the top and bottom of the briquettes. However, 'low power, long duration' is more effective for the middle of the briquettes as it results

in higher temperatures being reached over the whole briquette, not just in localised hot spots.

6. Microwave pasteurisation was found to have special effects on fungal growth compared to conventional oven pasteurisation, both in terms of the relative abundance of the types of fungi present and the possibility of rapid regrowth if the optimal configuration is not chosen.
7. Flipping the briquette upside down halfway through the duration of microwave pasteurisation provides additional benefits in fungal growth suppression. This should be taken into consideration when designing any microwave pasteurisation system.
8. According to the growth quantification data, the fungi present in the miscanthus briquettes appeared to be more resistant to heat and/or microwave treatment compared to the ones in the spent grains briquettes.
9. Sub-optimal pasteurisation conditions and/or storage strategies could result in rapid regrowth during the storage period to the extent that the amount of fungi could reach similar or higher levels compared to the unpasteurised baseline, even if the pasteurisation condition was effective in immediately removing a large proportion of the fungi present before pasteurisation.

6.9 Conclusions

Combined pasteurisation and natural drying is a novel strategy to reduce the drying energy of biomass and mitigate this major limitation of bioenergy and other industries. The current set of experiments has demonstrated that this is a valid concept for miscanthus and spent grains, although further studies and refinement are required for this new process to be used in industry.

The main experiments were conducted on 16 briquettes, half of which were miscanthus briquettes (M1-8) and the other half were spent grains briquettes (SG1-8). The material was briquetted, pasteurised and stored for a range of storage periods of up to 9 weeks. The pasteurisation experiments were carried out in two sets, with the results of the first set informing the pasteurisation conditions of the second set. Both conventional oven and microwave pasteurisation were used. Apart from comparing the effectiveness of these two pasteurisation methods, the conditions

were chosen to compare conventional oven pasteurisation at different durations and different configurations of microwave pasteurisation. Several immediate effects of pasteurisation were observed, including a slight decrease in moisture content, a loss of structural integrity and charring. It was also found via the heating profile characterisation of a spent grain briquette that during conventional oven pasteurisation, the briquette temperature should not be expected to reach the oven set temperature, and different parts of the briquette would experience substantially different temperatures due to heat transfer limitations. It was also found that natural drying could reduce the moisture content to 10-11% after three weeks of storage for miscanthus briquettes and to 12-14% after nine weeks of storage for spent grains briquettes.

The effectiveness of the pasteurisation conditions in reducing fungal growth was evaluated using both visual inspection and quantitative tests. For the miscanthus briquettes, no visible growth was observed, although the effects of pasteurisation could be seen in the results of the quantitative tests. Visible fungal growth was observed on most spent grains briquettes, with more severe growth typically occurring at the bottom of the briquettes, thus indicating a need for improved storage strategies.

The main differences between conventional oven and microwave pasteurisation were identified to be:

1. Conventional oven pasteurisation is limited by heat transfer properties, whereas microwave pasteurisation can bypass this limitation due to the volumetric heating effect of microwaves, allowing for shorter process times to achieve similar temperatures.
2. Microwave treatment has unique effects on the relative abundance of the types of fungi growing in the briquettes.
3. Microwave pasteurisation has the advantage of being able to achieve similar or better levels of fungal growth suppression with shorter process times compared to conventional oven pasteurisation.

The main differences between the configurations of microwave pasteurisation were identified to be:

1. For microwave pasteurisation with the same overall energy use, 'high power, short duration' is more effective than 'low power, long duration' in reducing fungal growth at the top and bottom of the briquettes. However, 'low power, long duration' is more effective for the middle of the briquettes.
2. Flipping the briquette upside down halfway through the duration of microwave pasteurisation would provide substantial benefits in terms of fungal growth suppression.

Considering the reduction in fungal growth due to pasteurisation and the achievable levels of moisture content reduction by natural drying, it is concluded that a combined pasteurisation and natural drying process is a feasible option to dramatically reduce the specific drying energy of biomass for bioenergy and other applications by eliminating the need to supply the energy needed to overcome the latent heat of evaporation of water by conventional means (such as a rotary drum dryer). In addition, the process has the potential to be tailored to specific storage conditions, thus optimising the temperature and residence time of the pasteurisation process for each biomass. However, several improvements required for successful industrial implementation were identified:

1. The briquetting process should be improved to produce more durable briquettes to limit the deterioration of structural integrity during pasteurisation and to reduce handling issues during storage.
2. Improved storage strategies are needed to reduce fungal growth at the bottom of briquettes. It was found that for the spent grains briquettes, even if a pasteurisation condition is sufficient for suppressing growth at the top of the briquette, it may not be sufficient for the bottom of the briquette, indicating storage strategies that move the briquettes regularly to expose all sides of the briquettes to open air would provide significant improvements both in terms of fungal growth suppression and a higher drying rate.

3. More information is required on the types of fungi that need to be targeted and the pasteurisation conditions that are needed to mitigate the health risks posed by these fungi.

Chapter 7 -Sugarcane Straw Pelleting and Pellet Milling

7.1 Introduction

Pelleting is commonly carried out in the bioenergy industry to increase energy density and reduce transport cost. After being transported to power stations, these pellets would be milled to sizes suitable for pulverised combustion.

The optimisation of pelleting processes can bring multiple benefits for the industry, including reduced energy use, improvement of pellet quality and reduced transport cost, and improvement in combustion performance. The change in particle size and shape during pelleting and pellet milling is also an important topic as it determines the combustion and flow characteristics of the final material fed into boilers (see Section 2.5).

Biomass pelleting and pellet milling are fairly well-studied topics, with studies covering a wide range of feedstocks, including various types of wood, straws, sugarcane bagasse and others (Younis et al., 2018). Despite the potential of sugarcane straw as a bioenergy feedstock, its pelleting behaviour has not been studied in detail before. Therefore, there is significant value in studying the pelleting and pellet milling behaviour of sugarcane straw to provide additional data and evaluate its specific characteristics. Furthermore, the influence of harvesting season on pelleting performance has not been explored in the literature.

Many studies have focused on the effect of various factors on pellet quality, while pelleting process parameters, with the exception of pelleting energy, remain an underexplored area (Section 2.8.4). These parameters are important for industry, as they represent equipment requirements and achievable throughput. This study has addressed this knowledge gap by introducing and analysing new parameters which characterise pelleting processes.

In this study, pelleting and pellet milling experiments were conducted for two Colombian sugarcane straw samples harvested in the dry and wet seasons respectively. A range of tests was conducted to evaluate the quality of the pellets and the influence of various factors on pellet quality, including pelleting feed moisture

content, particle size and harvest season. The pellets were then milled in a laboratory-scale ring-roller mill and their milling performance was evaluated. The particle size and shape of the pre-pellet material, disintegrated pellets and milled pellets were measured to analyse the changes in particle size and shape during pelleting and pellet milling.

7.2 Materials and Methods

Two types of sugarcane straws were used in the experiments for this Chapter, as shown in Figure 7-1. These are sugarcane straws from the Valle del Cauca region of Colombia harvested in the wet and dry season, provided by an industrial partner, Cenicaña, as part of a Royal Academy of Engineering Industrial Academic project entitled *"Exploring Opportunities for Sugarcane (Bagasse) Waste Densification as a Renewable Bioenergy Source in Colombia and the UK"* (grant number IAPP1\100148). Wet and dry season samples were collected from sugarcane plantations in the Cauca Valley and shipped to the UK in 2019. The collection of the samples involved gathering residues left in the field after mechanical sugarcane harvesting. The dry season sample is referred to as SSDS, and the wet season sample is referred to as SSWS.

Figure 7-1 Wet season sugarcane straw (left) and dry season sugarcane straw (right)

In the pelleting experiments, for each harvest season (wet and dry season), two particle sizes ('coarse' and 'fine', as defined in Section 3.8.1) and three moisture contents were used. Prior to pelleting, multiple properties of the samples were

characterised using a range of methods, with the results presented in Chapter 4. The samples for each pelleting condition were created using the methods described in Sections 3.8.1 and 3.8.2. With two harvest seasons, two particle sizes and three moisture contents, a total of 12 conditions were used. The experimental design allows the influence of these factors on the pelleting process and pellet quality to be quantified. The 'fine' (< 2 mm) and 'coarse' (< 3.35 mm) particle sizes were respectively chosen to approximately mimic the disintegrated pellets particle size distributions defined for Grade I1 and I2 pellets in BS EN ISO 17225-2:2021 (The British Standards Institution, 2021b). The aim of the experiments is to produce pellets with a particle size which would be acceptable for bioenergy use.

The milled sugarcane straws were then treated with a moisture conditioning process as described in Section 3.8.2 to achieve three different moisture contents of 10, 15 and 20%. These moisture contents were chosen to be the most beneficial for industry for further investigation. It is commonly known that a minimum moisture content of 10% is required for pelleting most types of biomass (Jackson et al., 2016). The successful production of good-quality pellets with a relatively high feed moisture content would decrease drying requirements, which is one of the major energy consumers in the pellet production process, and would therefore improve the economics of biomass pellets for bioenergy. In this thesis, the notation 'harvest season (particle size, pelleting feed moisture content)' is used to refer to the samples, e.g. 'SSDS (fine, 20%)' refers to the dry season sugarcane straw sample with fine particle size at 20% pelleting feed moisture content.

The pelleting experiments followed the method detailed in Section 3.8.3. After pelleting, the durability and size of the pellets were determined according to the methods detailed in Section 3.8.5. Following pelleting, the pellets were milled in a lab-scale ring-roller mill (Section 3.5.3). To investigate the change in particle size and shape during pelleting and pellet milling, the pre-pellet, disintegrated pellets and milled pellets samples were tested with sieving analysis (Section 3.6.1) and a Camsizer (Section 3.6.4).

Prior to pelleting, the sugarcane samples (dry and wet season) were characterised using a range of tests, including moisture content measurement (Section 3.3),

ultimate analysis (Section 3.2.3), thermogravimetric analysis (Section 3.1.1) and X-ray diffraction (Section 3.2.1). The results from these tests were previously presented in Chapter 4.

Unfortunately, a serious flood occurred in the laboratory where the samples were stored after the completion of the pelleting experiments and before the completion of the pellet characterisation tests. The SSWS (fine, 15%) pellet sample was destroyed in the flood and some subsequent tests could not be conducted.

7.3 Pre-pelleting Material Particle Size Analysis

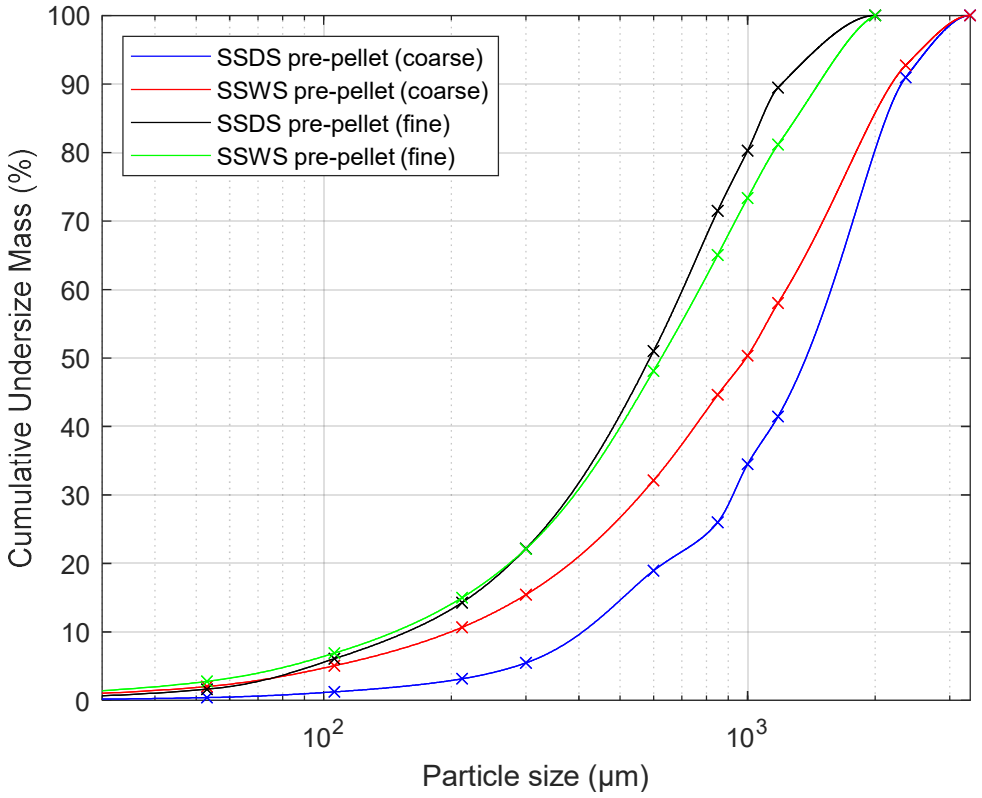

Figure 7-2 Pre-pellet particle size distribution for both particle sizes and harvest season

The first stage of the pelleting experiments was to prepare the samples for pelleting. This was done by milling and sieving of the sample as described in Section 3.8.1. The cumulative particle size distributions for both 'coarse' and 'fine' particle sizes for both dry and wet season sugarcane straw are shown in Figure 7-2. Despite the same milling conditions being used (same size of screen and top size removal, as defined in Section 3.8.1.), SSWS (coarse) has a significantly finer PSD compared to SSDS (coarse), while

the PSDs of the 'fine' samples for both harvest seasons are similar. Rosin-Rammler analysis and calculations of the dispersion and distribution shape parameters were also carried out using the methods described in Section 3.6.2 and 3.6.3. These are shown in Table 7-1 and Table 7-2.

Sample	Rosin-Rammler			Size Parameters (µm) - Cubic interpolation		
	d' (µm)	n	R^2	d_{10}	d_{50}	d_{90}
SSDS (coarse)	1.57	1.89	0.998	408	1373	2305
SSWS (coarse)	1.27	1.30	0.999	199	992	2185
SSDS (fine)	0.73	1.56	0.999	157	589	1203
SSWS (fine)	0.82	1.36	0.999	147	625	1469

Table 7-1 Rosin-Rammler and size parameters of pre-pellet sugarcane straw

Sample	Dispersion Parameters						Distribution Shape Parameters	
	s	hs	ls	MRS	C_u	C_c	Gs_i	K_g
SSDS (coarse)	1.99	1.52	2.60	1.38	3.86	1.33	0.00	0.92
SSWS (coarse)	2.50	1.95	3.20	2.00	6.20	1.28	0.22	0.86
SSDS (fine)	2.14	1.80	2.54	1.78	4.48	1.32	0.21	0.96
SSWS (fine)	2.37	2.03	2.78	2.12	5.24	1.34	0.27	0.93

Table 7-2 Dispersion and distribution shape parameters of pre-pellet sugarcane straw

The Rosin-Rammler analysis gave a good fit for all four samples ($R^2 > 0.997$). For both 'coarse' and 'fine' sizes, the Rosin-Rammler size distribution parameter *n* is smaller for the wet season sample compared to the dry season sample, indicating that the

pre-pellet wet season sugarcane straw has a higher diversity of particle sizes compared to its dry season counterpart.

Clear trends are also observed for the dispersion parameters. All dispersion parameters for the PSDs (*s*, *hs*, *ls*, *MRS* and C_u) apart from C_c are all higher for pre-pellet wet season sugarcane straw compared to its dry season counterpart. The values of *s*, *hs* and *ls* indicate that the geometric standard deviation is higher for wet season sugarcane straw across the whole distribution (both low and high regions). However, the geometric standard deviation of the low region (*ls*) is higher than that of the high region (*hs*) for all four samples, indicating that the variety of particle sizes is more concentrated in the low region. The *MRS* values of all four samples are significantly above one. This indicates a high level of heterogeneity of particle sizes, which is particularly pronounced for the wet season sample. The values of the coefficient of uniformity (C_u) indicate that the wet season samples have large ranges of particle sizes. The coefficient of curvature (C_c) for all four samples are within the narrow range of 1.28-1.44, which is also within the range of between 1 and 3 considered to be a well-graded particle size distribution (Knappett & Craig, 2012).

The inclusive graphical skewness (GS_i) shows that the SSDS (coarse) sample has an almost perfectly symmetrical size distribution graph (Gaussian Distribution), while all three other samples have a larger proportion of finer particles. The values of graphic kurtosis (Kg) indicate that all four samples are platykurtic, meaning that the size distribution graphs are better sorted (closer to a Gaussian distribution) in the tails compared to the central portion.

7.4 Pelleting Process Parameters

Pelleting experiments were conducted to investigate the influence of harvest season, particle size and moisture content on pelleting behaviour. Multiple parameters were measured during the pelleting experiments to quantify pelleting behaviour, including the specific pelleting energy, average pelleting power, pelleting efficiency and pellet production rate. These are presented in Table 7-3. The methods used to measure these parameters were described in Section 3.8.4. The pellet process parameters of average pelleting power, pelleting efficiency and pellet production rate represent new and novel methods of characterising the pelleting process, which have not been

described before and are potentially important for industry as they relate to factors such as equipment requirement and achievable throughput.

For some pelleting conditions, pelleting was found to be impossible with the machine used, as the die and rollers would become jammed and the experiments had to be stopped under these conditions. The failed pelleting runs are indicated in Table 7-3 and are further discussed in Sections 7.5.1 and 7.6.2. The relationship between these parameters and various factors is further discussed in Section 7.6.

Sample	Particle size	Feed moisture content	Pelleting successful?	Specific pelleting energy (kWh/ton)	Average pelleting power (W)	Pelleting efficiency (%)	Pellet production rate (kg/hr)
SSDS	Fine	10%	No	N/A	N/A	N/A	N/A
SSDS	Fine	15%	No	N/A	N/A	N/A	N/A
SSDS	Fine	20%	Yes	33.6	693	93.8	20.6
SSDS	Coarse	10%	No	N/A	N/A	N/A	N/A
SSDS	Coarse	15%	Yes	52.8	636	95.0	12.0
SSDS	Coarse	20%	Yes	27.0	235	93.1	8.7
SSWS	Fine	10%	Yes	38.9	439	87.5	11.3
SSWS	Fine	15%	Yes	50.8	844	89.0	22.1
SSWS	Fine	20%	Yes	18.7	381	89.0	20.4
SSWS	Coarse	10%	Yes	35.7	306	84.0	8.6
SSWS	Coarse	15%	Yes	50.5	862	93.2	17.2
SSWS	Coarse	20%	Yes	21.7	196	93.4	9.0

Table 7-3 Sugarcane Straw Pelleting Process Parameters

7.5 Qualitative Observations (Pelleting)

In addition to the pelleting process parameters presented in Section 7.4, there are several non-quantifiable phenomena observed during the pelleting experiments that are also of significance. These are reported and discussed in this Section.

7.5.1 Failed Runs

During the pelleting process, some of the pelleting runs failed. It was found that pelleting failed for three conditions:

1. SSDS (fine, 10%)
2. SSDS (fine, 15%)
3. SSDS (coarse, 10%)

No pellets could be produced for conditions 1 and 2 above, as the die and rollers became jammed immediately after feeding the sample. A small amount of pellets were produced for condition 3 above, but it was also considered to have failed as the die and rollers became jammed well before a batch 500 g of the sample could be fed through the pellet machine. Although condition 3 is considered a failed run, the pellets produced were also analysed, with the results presented in the relevant Sections. It appeared that pelleting failure is more likely to occur for the dry season sample, at low moisture content and for the fine particle size. When inspecting the die after pelleting failure, it was found that very hard and tough-to-remove material was present inside the die. Further analysis of pelleting failure is provided in Section 7.6.2.

7.5.2 Pelleting Efficiency

When the samples were fed through the pellet machine, some of the material at the pellet machine outlet remained unpelletised. In industrial operations, these would likely be recycled back into the pelletiser feed. The influence of various factors on pelleting efficiency is further discussed in Section 7.6.3.

7.5.3 Pellet Production Rate

Although the manufacturer of the pellet machine specified a pellet production rate of 20-35 kg/hr (Ceccato Olindo srl, n.d.), this range was not achievable for most conditions. When the pellet production rate was observed to be in the manufacturer-specified range, only the lower end of the range could be achieved – experimental pellet production rate in the range of 8.6-22.1 kg/hr were measured (Section 7.4). The 20-35 kg/hr range quoted by the manufacturer (Ceccato Olindo srl, n.d.) is

designated for making wood pellets, and the experimental results suggest that sugarcane straw would generally have a lower pellet production rate than wood. The pellet production rate data is further analysed in Section 7.6.4.

7.5.4 Steam Formation and Pelleting Temperature

Steam formation was observed for all pelleting experiments, although the severity varies between samples. A lower feed moisture content would result in a larger amount of steam during pelleting, indicating a higher pelleting temperature was likely reached compared to the runs with a higher feed moisture content. It was not possible to measure temperature during these pelleting experiments, but future studies should incorporate temperature measurements to ascertain the increase in temperature during milling. This would be valuable as temperature is known to cause glass transitions in some biomasses, which could aid or inhibit the pelleting process (Williams et al., 2017).

7.6 Influence of Feed Conditions on Pelleting

This Section studies the influence of feed moisture content, harvest season and particle size on the pelleting process parameters of pelleting energy, average pelleting power, pelleting efficiency and pellet production rate. Apart from pelleting energy, these are newly introduced parameters and represent novel methods of characterising the pelleting process. In addition, as most available biomass pelleting trails are conducted with single pellet presses (Section 2.8.4) and not continuous machines like in the present study, there is a lack of knowledge of the pelleting process at this scale.

7.6.1 Pelleting Energy

The pelleting energy of each pelleting experiment was measured using the method described in Section 3.8.3, with an example of the measurement data shown in Figure 3-10. The influence of feed moisture content, harvest season and particle size on pelleting energy is shown in Figure 7-3 to Figure 7-5. It was found for SSWS, that a feed moisture content of 15% results in the highest pelleting energy, compared to 10% and 20%. Due to pelleting failure for three conditions (see Section 7.5.1), it is not

possible to draw conclusions on the influence of feed moisture content on pelleting energy for SSDS.

In addition, SSDS was observed to generally have higher pelleting energies compared to their wet season counterparts, and there were no obvious relationships between particle size and pelleting energy. It is known that the harvesting of agricultural residues, including sugarcane straw, often results in soil and mud attachment (Martinez-Mendoza et al., 2023). The soil and mud present likely acted as a binder, resulting in the lower pelleting energies observed for the wet season samples.

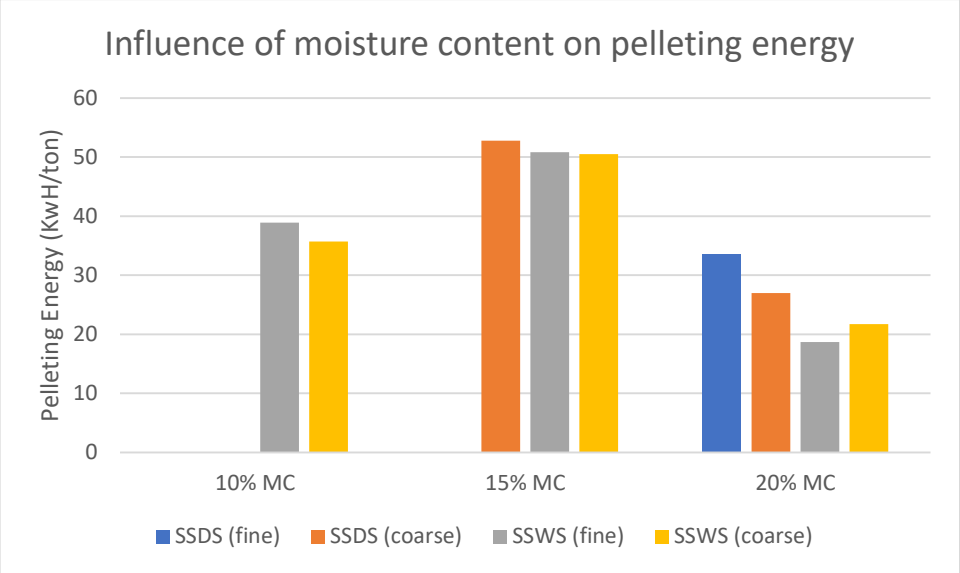

Figure 7-3 Influence of Feed Moisture Content on Pelleting Energy

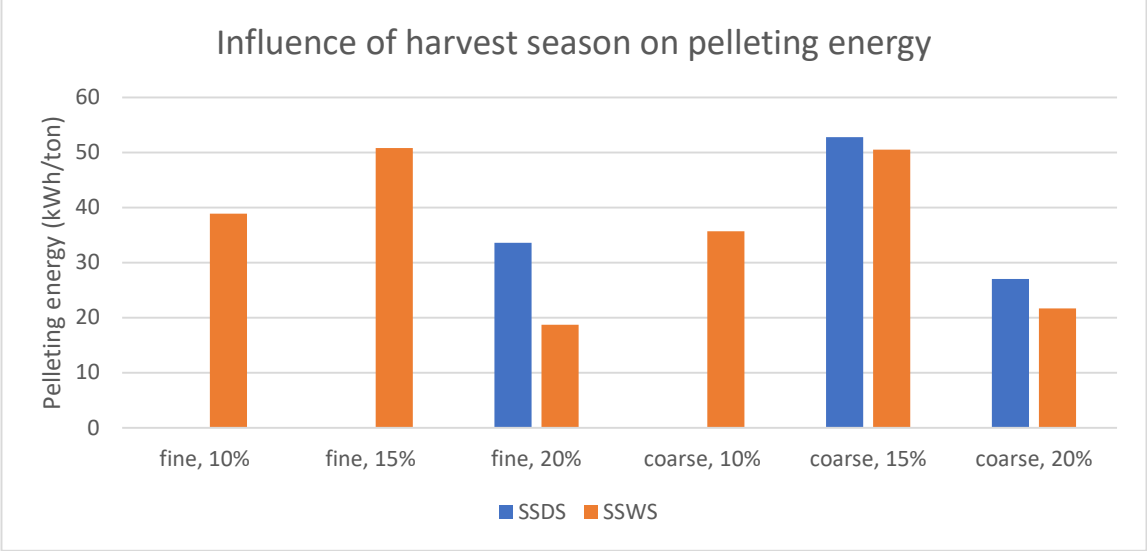

Figure 7-4 Influence of Harvest Season on Pelleting Energy

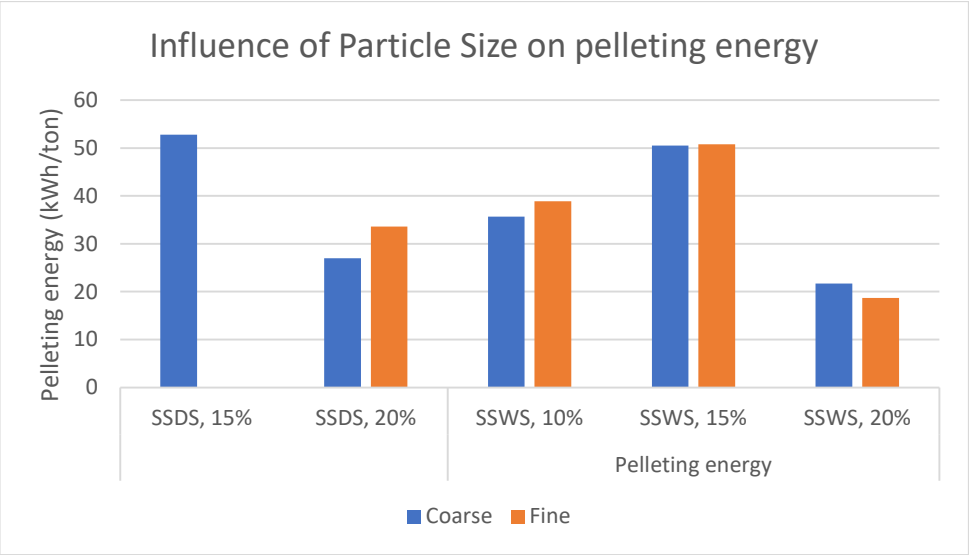

Figure 7-5 Influence of Particle size on pelleting energy

7.6.2 Average Pelleting Power and Pelleting Difficulty

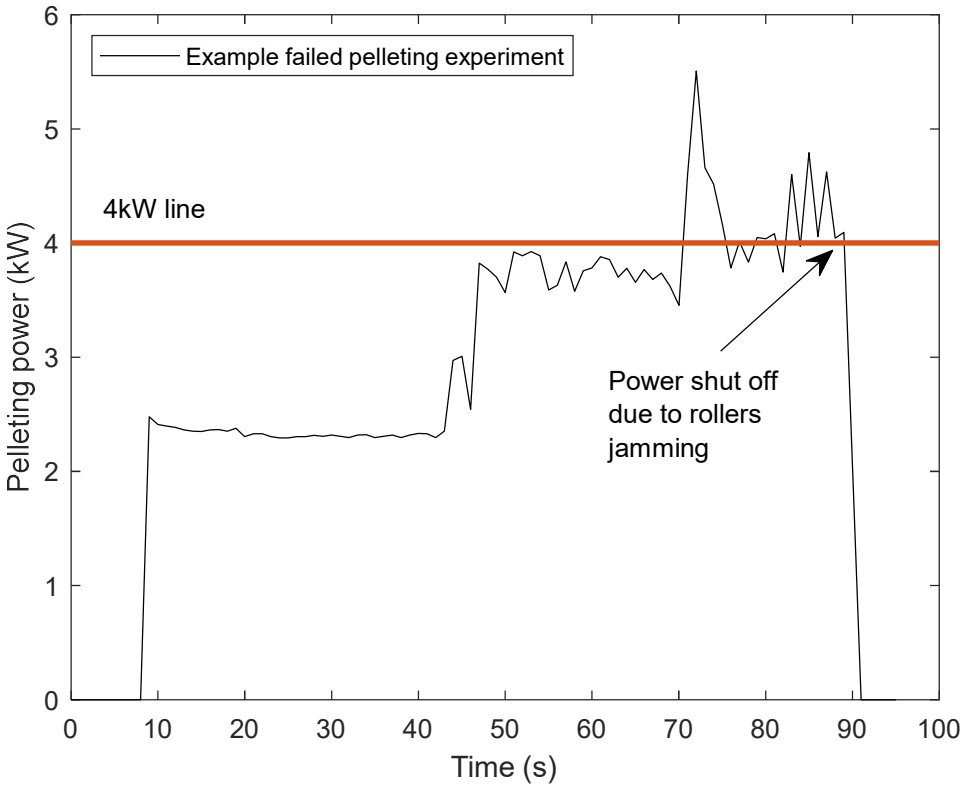

Figure 7-6 Example data of a failed pelleting run

As mentioned in Section 7.5.1, there were three conditions in which pelleting failed. Experimental data (an example pelleting energy measurement data for pelleting

failure is shown in Figure 7-6) for these failed runs show that if the total power delivered by the pellet machine goes above 4 kW for a significant period (several seconds or more), it would result in the rollers being jammed and a failed run. The rated power of the pellet machine is 3 kW (Ceccato Olindo srl, n.d.), although the experimental data demonstrate that it is capable of delivering up to around 4 kW of power before the rollers become jammed. This indicates that for the failed pelleting conditions, the frictional forces are too great for the pellet machine to overcome.

The average idling power of the pellet machine was measured to be 2.41 kW, and as the maximum power that can be supplied is around 4 kW, the maximum theoretical pelleting power is 1.59 kW. However, as the energy use would fluctuate significantly, the average pelleting power would likely need to be significantly below 1.59 kW in order for pelleting to be feasible by the machine used. It is also known that pelleting failure would occur at high-load conditions (Holm et al., 2006), where the capability of the equipment has been exceeded. Thus, the average pelleting power can be used as an indicator of pelleting difficulty, with pelleting becoming more and more difficult and pelleting failure more likely to occur (i.e. demanding more and more power from the machine in order to produce pellets) as it approaches the theoretical maximum value of around 1.59 kW.

The average pelleting power values measured for all samples are shown in Table 7-3. The maximum value measured was 884 W for SSWS (fine) sample at 15% moisture content, and the lowest value measured was 196 W for the SSWS (coarse) sample at 20% moisture content. The influence of feed moisture content, harvest season and particle size on average pelleting power is shown in Figure 7-7 to Figure 7-9. It was found that for SSWS, a feed moisture content of 15% results in the highest average pelleting power, compared to 10% and 20%.

It also appears that for SSWS, 15% feed moisture content generally results in the highest average pelleting power, while the values for 10% and 20% feed moisture content are lower. It is unclear whether this relationship holds true for SSDS due to pelleting failure. There is no apparent relationship between harvest season and average pelleting power. The fine particle size was observed to have higher average pelleting power compared to the coarse particle size.

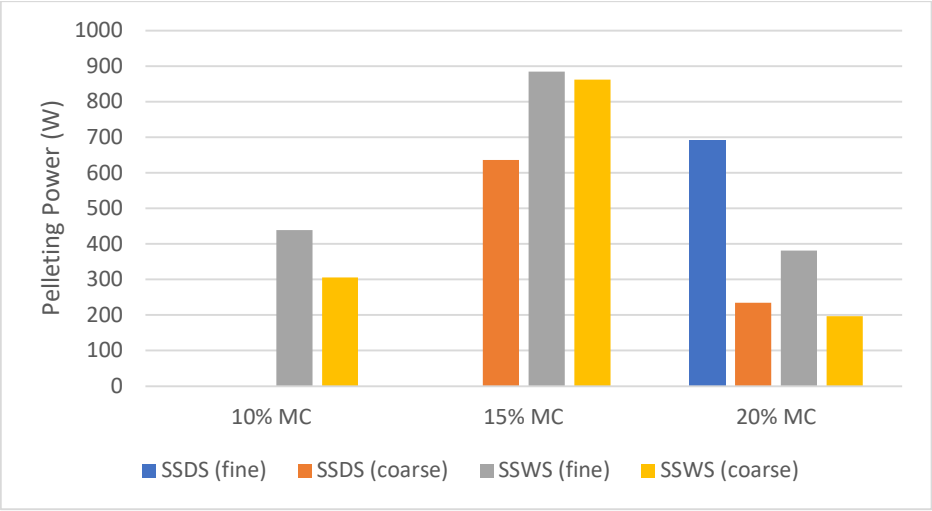

Figure 7-7 Influence of feed moisture content on pelleting power

Figure 7-8 Influence of harvest season on pelleting power

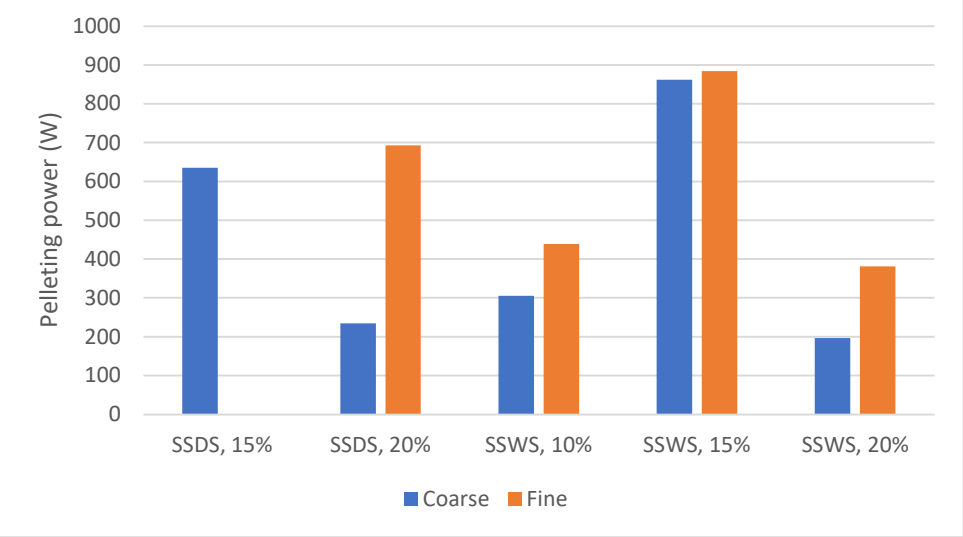

Figure 7-9 Influence of particle size on pelleting power

7.6.3 Pelleting Efficiency

The influence of feed moisture content, harvest season and particle size on pelleting efficiency are shown in Figure 7-10 to Figure 7-12. The highest value of pelleting efficiency was observed for the SSDS (coarse, 15%) sample at 95.0%, and the lowest value was observed for SSWS (coarse, 10%) sample at 84.0%. It was found that for SSWS, a feed moisture content of 15% and 20% results in similar pelleting efficiencies, while a feed moisture content of 10% results in the lowest pelleting efficiencies. Due to pelleting failure for three conditions (see Section 7.5.1), it is not possible to draw conclusions on the influence of feed moisture content on pelleting efficiency for SSDS. In addition, neither the harvest season nor particle size has an obvious effect on pelleting efficiency.

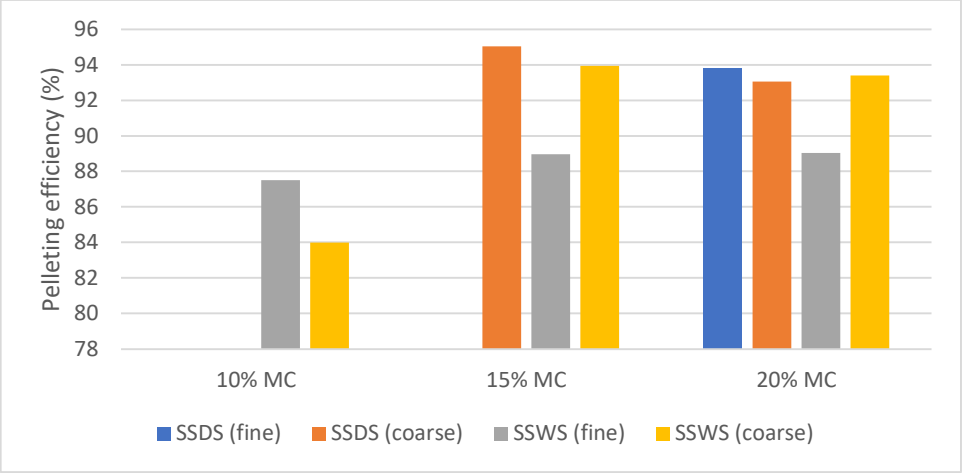

Figure 7-10 Influence of feed moisture content on pelleting efficiency

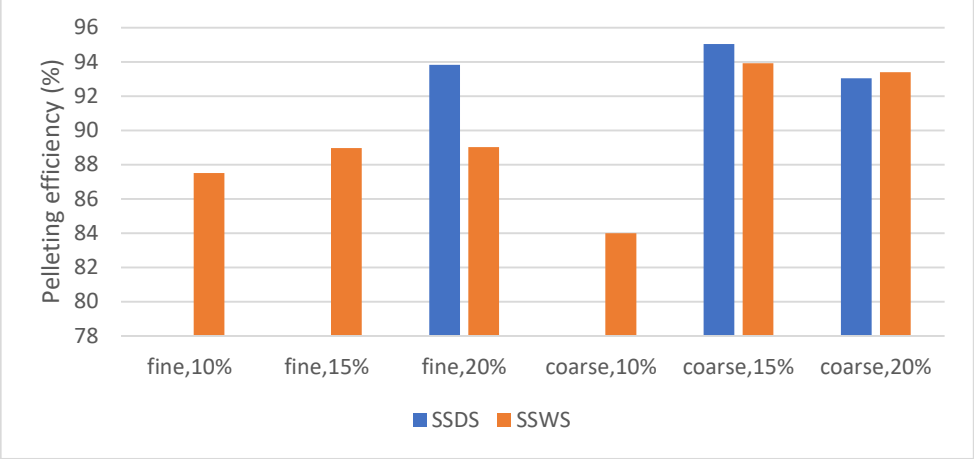

Figure 7-11 Influence of harvest season on pelleting efficiency

Figure 7-12 Influence of particle size on pelleting efficiency

7.6.4 Pellet Production Rate

The influence of feed moisture content, harvest season and particle size on pellet production rate are shown in Figure 7-13 to Figure 7-15. It was found that for SSWS, a feed moisture content of 15% results in the highest pellet production rates, compared to 10% and 20%. Due to pelleting failure for three conditions (see Section 7.5.1), it is not possible to draw conclusions on the influence of feed moisture content on pelleting production rate for SSDS. There were no obvious relationships between harvest season and pellet production rate. The fine particle size results in significantly higher pellet production rates compared to the coarse particle size counterparts, suggesting that higher throughputs could be achieved if a finer particle size is used.

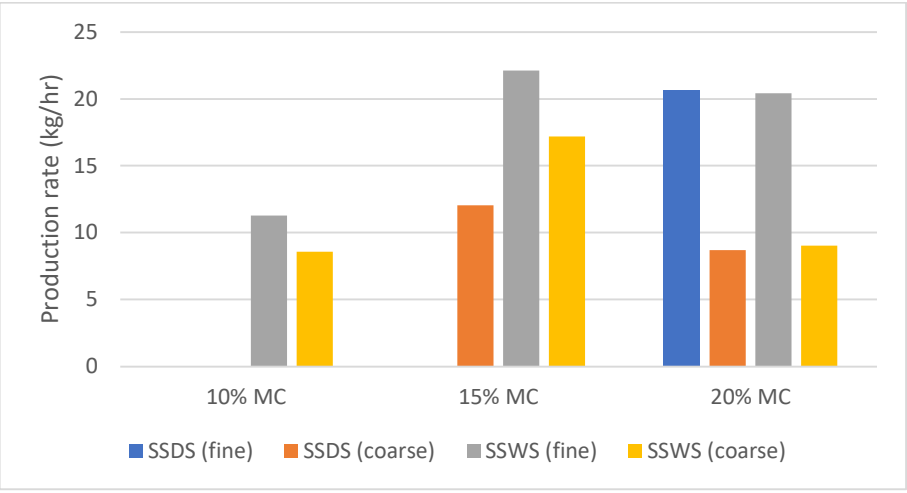

Figure 7-13 Influence of feed moisture content on pellet production rate

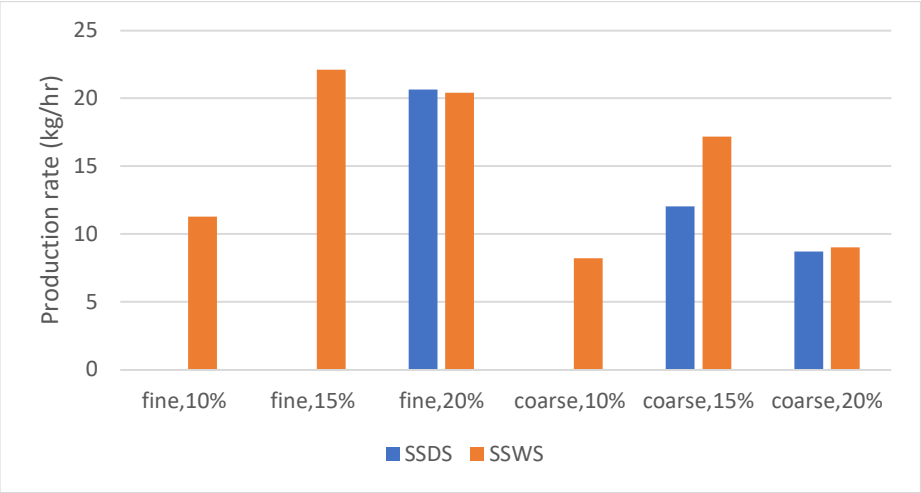

Figure 7-14 Influence of harvest season on pellet production rate

Figure 7-15 Influence of particle size on pellet production rate

7.7 Pellet Properties

In order to assess the quality of pellets, it is essential to measure the pellets' physical properties. Furthermore, in this study, one of the main aims is to ascertain the impact of pelleting on the constituent particle size and shape before and after pelleting. Although the pelleting experiment for SSDS (coarse, 10%) is considered a failed run due to the jamming of rollers (see Section 7.5.1), the pellets produced were also analysed (except for pellet durability, where the amount of pellets available was insufficient for the test) and the results are included in this Section.

7.7.1 Pellet Durability

The influences of feed moisture content, harvest season and particle size on pellet durability are shown in Figure 7-16 to Figure 7-18. The highest pellet durability was measured at 94.1% for the SSWS (coarse, 15%) sample, while the lowest pellet durability was measured at 80.6% for the SSWS (fine, 20%) sample.

It was found that for SSWS, a feed moisture content of 15% results in the highest pellet durability, compared to 10% and 20%. Due to pelleting failure for three conditions (see Section 7.5.1), it is not possible to draw conclusions on the influence of feed moisture content on pellet durability for SSDS. There was no obvious relationship between the harvest season and pellet durability. However, the coarse particle size samples consistently resulted in higher pellet durability compared to their fine particle size counterparts. Additionally, the durability of the pellets produced in this study was not sufficient to meet the requirements in the commonly used non-woody pellet standard BS EN ISO 17225-6:2021 (The British Standards Institution, 2021c), which requires a minimum durability of 96.0%, whereas the highest durability of the pellets produced in this study was 94.1%.

The result that the coarse particle size resulted in higher pellet durability is in contrast to the finding from several authors that using finer particle sizes typically results in pellets with higher durability (Section 2.8.2.2). There are several factors which may have contributed to this result. The positive correlation between particle fineness and pellet durability observed phenomena by several authors could be dependent on the exact type of biomass and may not be valid for sugarcane straw. The ‘fine’ particle size used in this study resulted in disintegrated pellets particle size distributions, which are significantly finer than what is typically expected in industry (further discussed in Section 7.7.4). Therefore, the ‘fine’ particle size could be out of range of the typical particle fineness studied by other authors, which would suggest that reducing size only improves durability up to a limit, and this limit may have been exceeded in the present study.

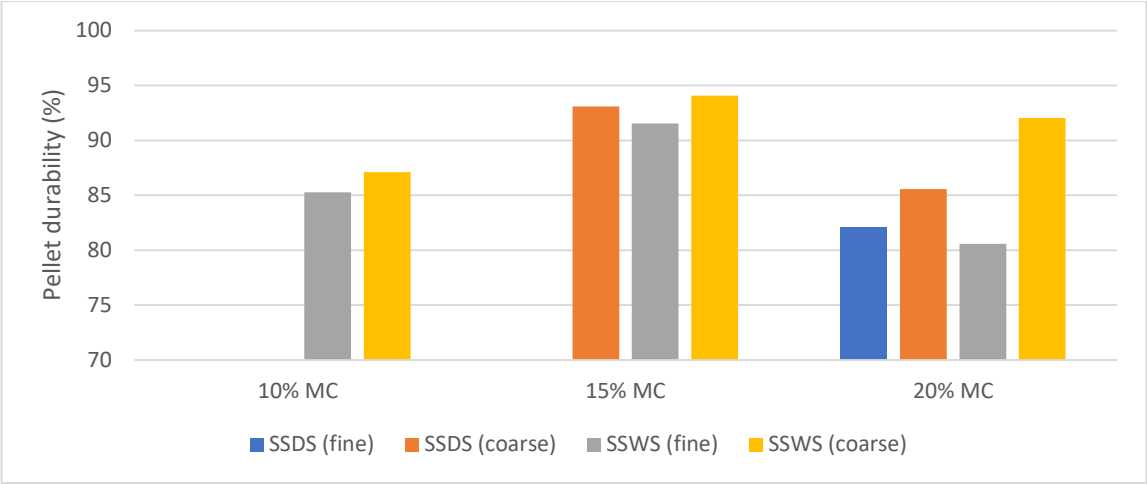

Figure 7-16 Influence of feed moisture content on pellet durability

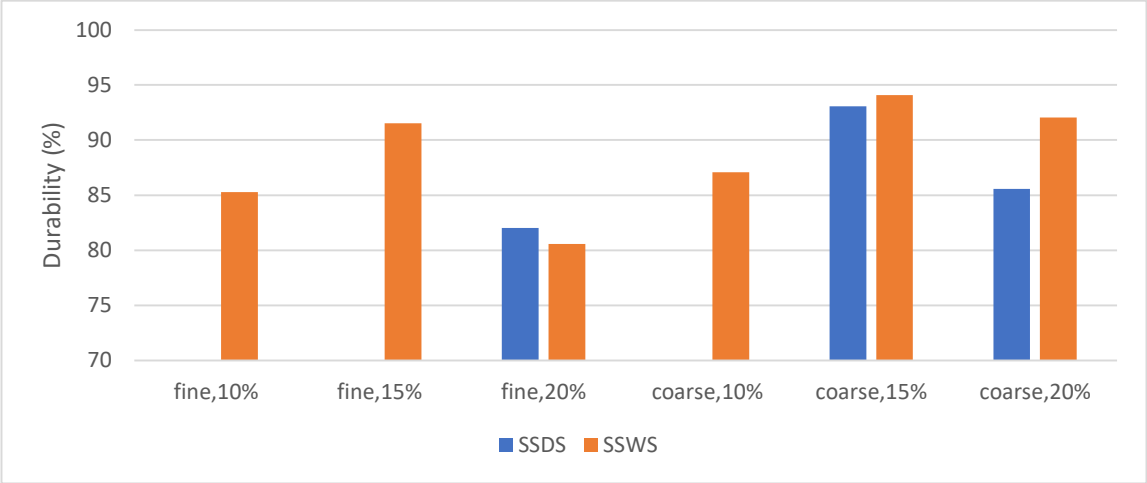

Figure 7-17 Influence of harvest season on pellet durability

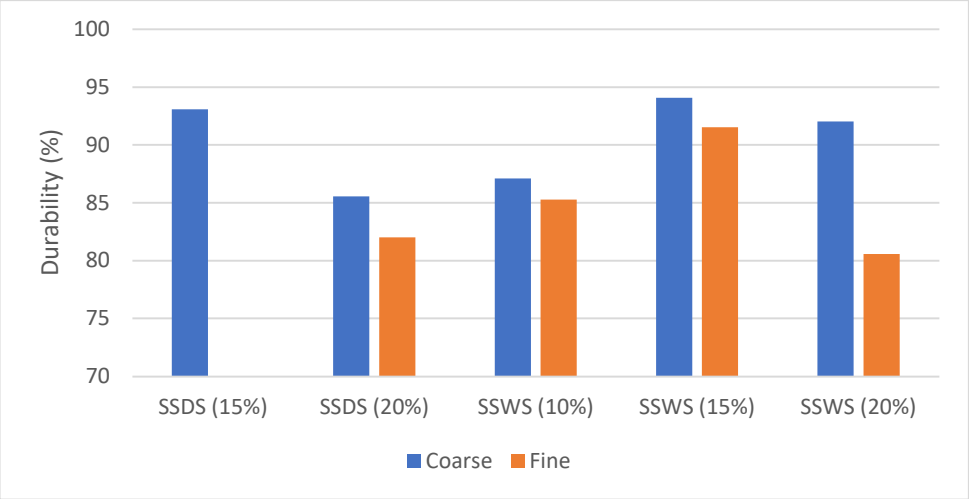

Figure 7-18 Influence of particle size on pellet durability

7.7.2 Pellet Dimensions

The pellet dimensions (diameter, length and aspect ratio) were determined using the method described in Section 3.8.5.2. Box and whisker diagrams (as defined in Section 3.8.5.2) for diameter, length and aspect ratio are shown in Figure 7-19 to Figure 7-21.

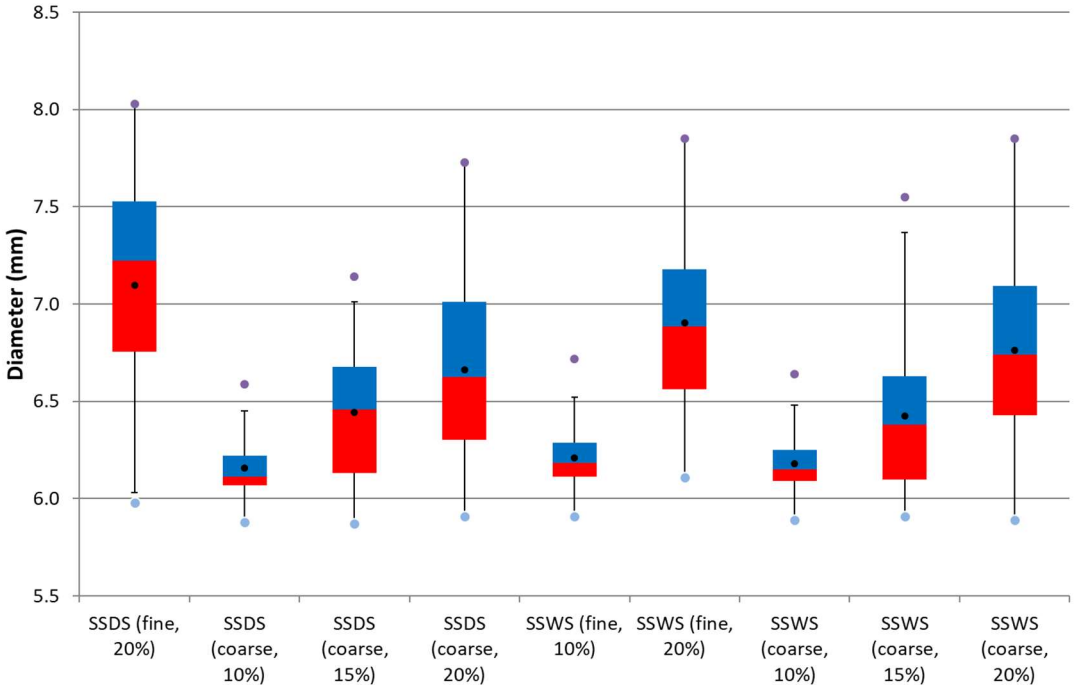

Figure 7-19 Range of pellet diameter

It was observed that feed moisture content has a large impact on pellet diameter, with a higher feed moisture content resulting in a larger value as well as a higher variance in pellet diameter. It was found that for SSWS, particle size has little effect on pellet diameter, which is consistent with the findings of Shaw & Tabil (2007) that particle size has little effect on the expansion of pellets after exiting the die. Due to pelleting failure for three conditions (see Section 7.5.1), it is not possible to draw conclusions on the influence of particle size on pellet diameter for SSDS. For all samples, the large majority of pellets has a diameter above 6 mm, which is expected as the diameter of the pellet die openings is 6 mm. It is known that a degree of swelling typically occurs after material is forced through the pellet die, resulting in pellets with a slightly larger diameter than the pellet die openings (Shaw & Tabil, 2007). The increase in pellet diameter with feed moisture content indicates that a

higher feed moisture content would result in a greater extent of pellet swelling as it exits the pellet die.

The standard for non-woody pellets BS EN ISO 17225-6:2021 states that the pellet diameter should meet the requirement of D_{mean} ± 1 mm, where D_{mean} is the mean pellet diameter. Among the pellets produced in the present study, only those with a feed moisture content of 10% were able to meet this requirement, with the variance of the diameter of all other pellet samples being too large.

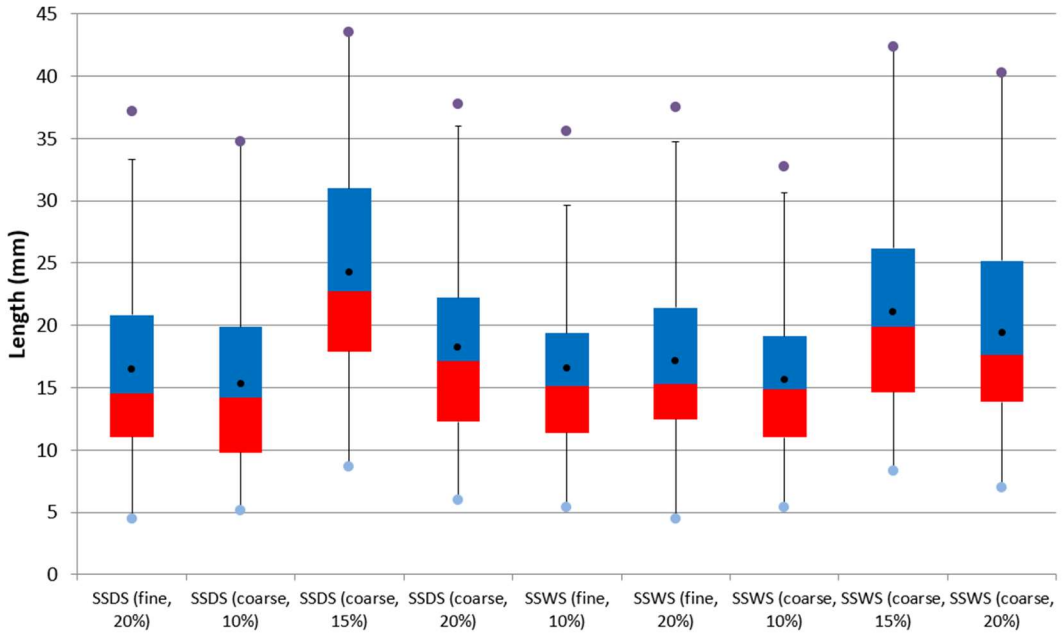

Figure 7-20 Range of pellet length

It can be observed from Figure 7-20 that the pellet length data of the samples demonstrate a large variance. The standard for non-woody pellets, BS EN ISO 17225-6:2021, states that the pellet length should be in the range of 3.15 to 40 mm. While all samples were able to meet the minimum size requirement, the pellet samples for SSDS (coarse, 15%), SSWS (coarse, 15%) and SSWS (coarse, 20%) contain a small percentage of pellets which exceed the maximum size requirement. It is specified by the manufacturer of the pellet machine used that for wood pellets, the expected typical pellet length would be 25-35 mm (Ceccato Olindo srl, n.d.), which indicates that for most pelleting conditions used, the length of sugarcane straw pellets is expected to be shorter than wood pellets.

Some standards have stated requirements for pellet aspect ratio, such as ÖNORM M 7135 (Austrian Standards Institute, 2000), which states a maximum aspect ratio of 5. Pellets with high aspect ratios could cause issues in handling and conveying systems, although there is little information on this topic in the existing literature. Most of the pellet samples produced in the present study were not able to meet the aspect ratio requirement stated in ÖNORM M 7135.

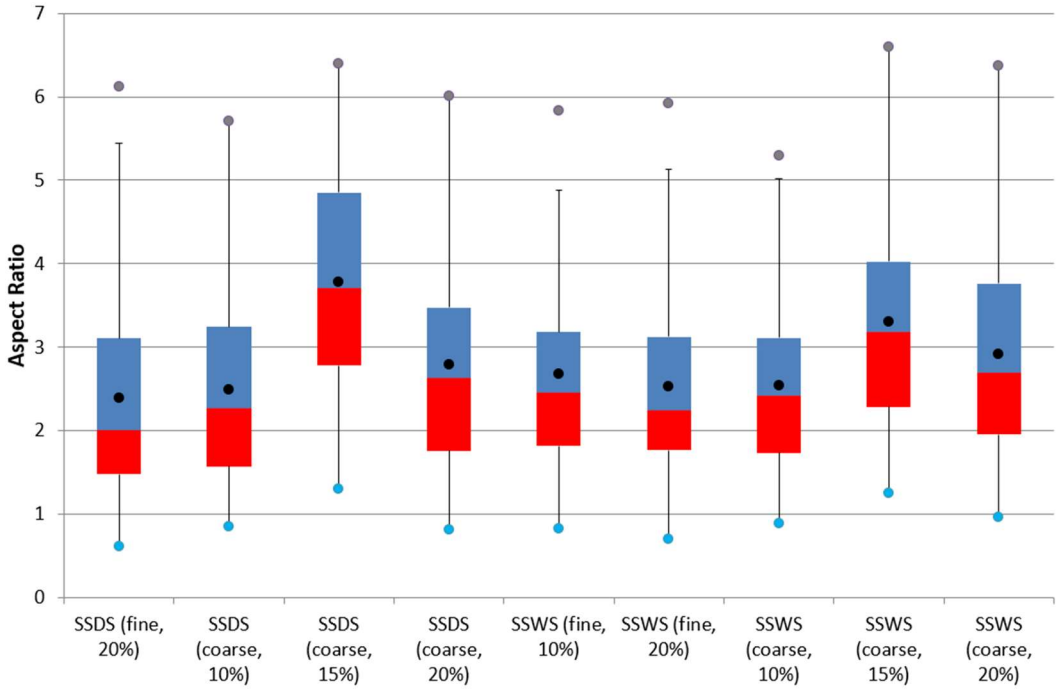

Figure 7-21 Range of pellet aspect ratio

7.7.3 Pellet Bulk Density

A high pellet bulk density is desired by industry as it increases the energy density and can significantly reduce costs associated with storage, transportation and handling (Narra et al., 2012). The pellet bulk density of each sample was measured using the method described in Section 3.8.5.3. The values of pellet bulk density range from 393.0 kg/m^3 for SSDS (fine, 20%) to 710 kg/m^3 for SSDS (coarse, 10%). The influence of feed moisture content on pellet bulk density is shown in Figure 7-22. The pellet bulk density is almost entirely dependent on the feed moisture content, with a higher moisture content resulting in a lower bulk density, while both harvest season and particle size have very little effect. This result is consistent with the findings of Larsson et al. (2008) that pellet bulk density is negatively correlated to moisture content.

The non-woody pellet standard BS EN ISO 17225-6:2021 (The British Standards Institution, 2021c) specifies minimum bulk density requirements of 600 kg/m^3 for Grade A pellets and 550 kg/m^3 for Grade B pellets. Thus, only the samples with 10% feed moisture content are able to meet the bulk density requirement for Grade A pellets. Samples with 15% feed moisture content could only barely meet the requirement for Grade B pellets, and those with 20% feed moisture content could not meet the requirement at all.

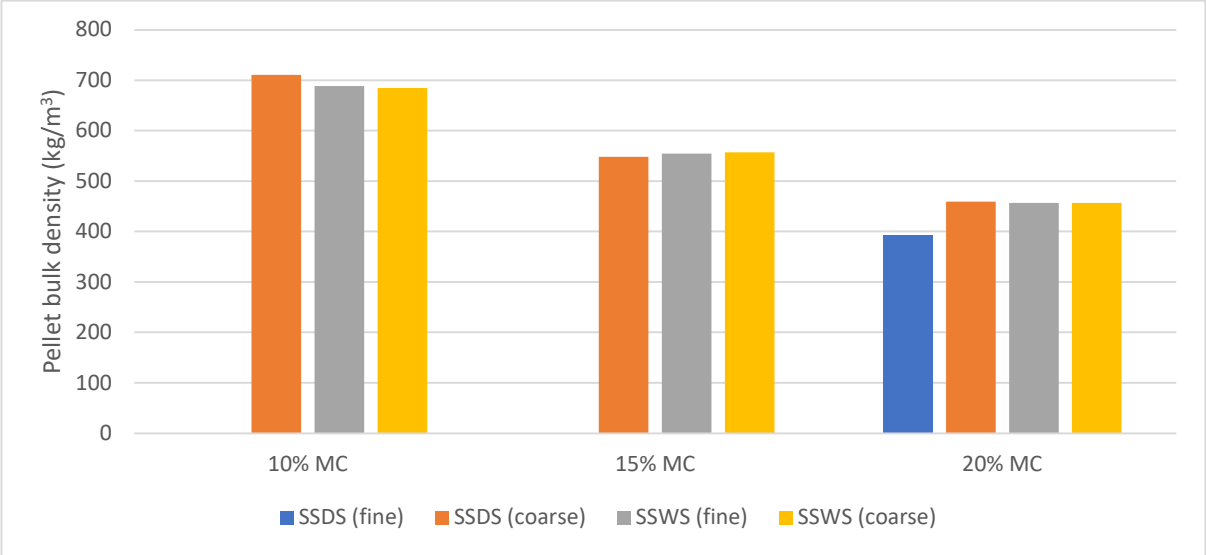

Figure 7-22 Influence of moisture content on pellet bulk density

7.7.4 Disintegrated Pellet Particle Size Distributions

Pellet disintegration tests were carried out in accordance with BS EN ISO 17830:2016 (The British Standards Institution, 2016c) (see Section 3.8.5.4), and the particle size distributions (PSD) of the disintegrated pellets were analysed using the method specified in Section 3.6. The disintegrated pellet PSDs for each sample are shown alongside the pre-pellet PSD in Figure 7-23 to Figure 7-26. For all harvest seasons, feed particle sizes and feed moisture contents, significant reductions in particle size was observed between the pre-pellet and disintegrated pellets samples. This indicates that apart from pressing the material into pellets, there is also a significant 'milling' effect provided by the pelleting process. The reduction in particle size between the pelleting raw material and disintegrated pellets has been described in

literature for wood pellets (Rezaei et al., 2016, 2024), and the results of the present study demonstrates that this phenomenon is also observed for sugarcane straw.

It was also observed that for the coarse feed particle size, the samples with 10% feed moisture content demonstrated the largest decrease in particle size compared to the pre-pellet samples, the samples with 15% feed moisture content demonstrated the smallest decrease in particle size, while the decrease in particle size for the samples with 20% moisture content sits between the two.

There are no requirements specified for the disintegrated pellet particle size in the non-woody pellet standard BS EN ISO 17225-6:2021 (The British Standards Institution, 2021c). However, these requirements are included in the wood pellet standard BS EN ISO 17225-2:2021 (The British Standards Institution, 2021b) and are a good representation of the pellet constituent particle sizes required by industry. The comparison between pre-pellet particle size distributions, disintegrated pellets particle size distributions and the requirements in pellet standard are shown in Table 7-4.

As mentioned in Section 7.2, the feed particle sizes of ‘fine’ and ‘coarse’ were chosen to represent the Grade I1 and I2 pellets respectively. However, due to the significant milling effect observed during the pelleting process, the pellet constituent particles are significantly smaller than the feed sizes, and all but one of the pellet samples exceeded the disintegrated pellet PSD requirement of Grade I1 pellets. The only sample which could not be classed as I1 pellets in terms of disintegrated pellets PSD, SSWS (coarse, 10%), also just marginally missed the requirement. This result indicates that for a desired pellet constituent particle size, biomass materials do not need to be milled to the desired sizes. Instead, for energy optimisation, pelleting processes should be designed so that pre-pelleting milling would produce a PSD significantly coarser than the desired pellet constituent PSD, and the milling effect of the pelleting process would be utilised to produce a pellet product with the desired constituent PSD.

	% wt		
	< 3.15 mm	**< 2.0 mm**	**< 1.0 mm**
Grade I1 pellets	≥99%	≥95%	≥60%
Grade I2 pellets	≥98%	≥90%	≥50%
Grade I3 pellets	≥97%	≥85%	≥40%
SSDS (fine) pre-pellet	100.0%	100.0%	80.3%
SSDS (fine, 20%)	100.0%	100.0%	95.2%
SSDS (coarse) pre-pellet	99.5%	80.4%	34.5%
SSDS (coarse, 10%)	100.0%	99.1%	93.3%
SSDS (coarse, 15%)	99.9%	95.2%	77.0%
SSDS (coarse, 20%)	99.9%	97.6%	87.3%
SSDS (fine) pre-pellet	100.0%	100.0%	73.4%
SSWS (fine, 10%)	100.0%	100.0%	93.2%
SSWS (fine, 20%)	100.0%	100.0%	89.1%
SSWS (coarse) pre-pellet	99.6%	85.8%	50.3%
SSWS (coarse, 10%)	99.7%	94.5%	82.4%
SSWS (coarse, 15%)	99.9%	97.5%	79.8%
SSWS (coarse, 20%)	99.9%	96.1%	82.1%

Table 7-4 Comparison between pre-pellet particle size distribution, disintegrated pellets particle size distributions of sugarcane straw pellets and requirements in pellet standard

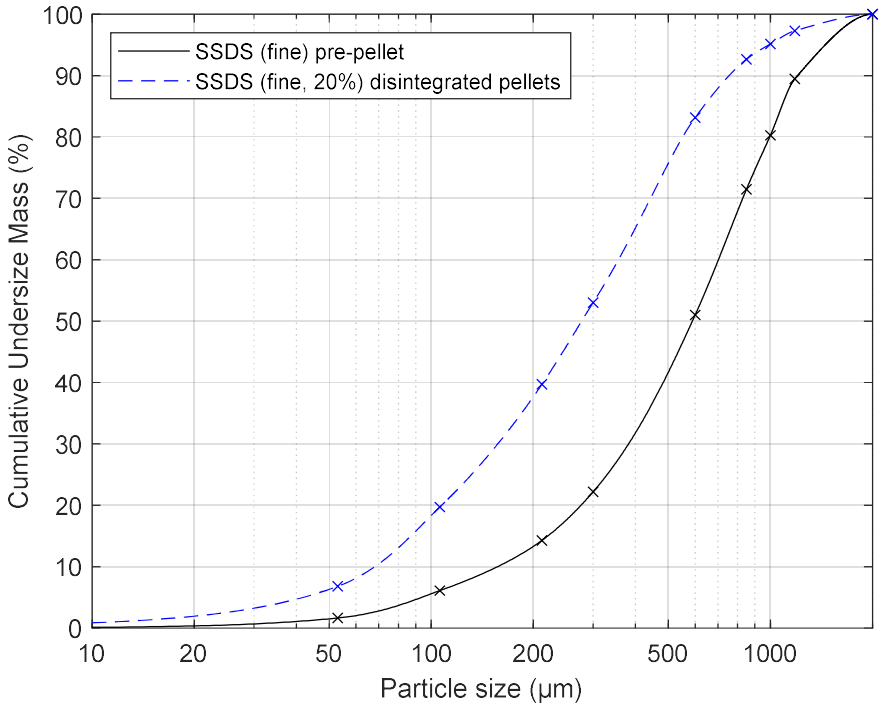

Figure 7-23 Cumulative distribution of particle size for SSDS (fine) - pre-pellet and disintegrated pellets

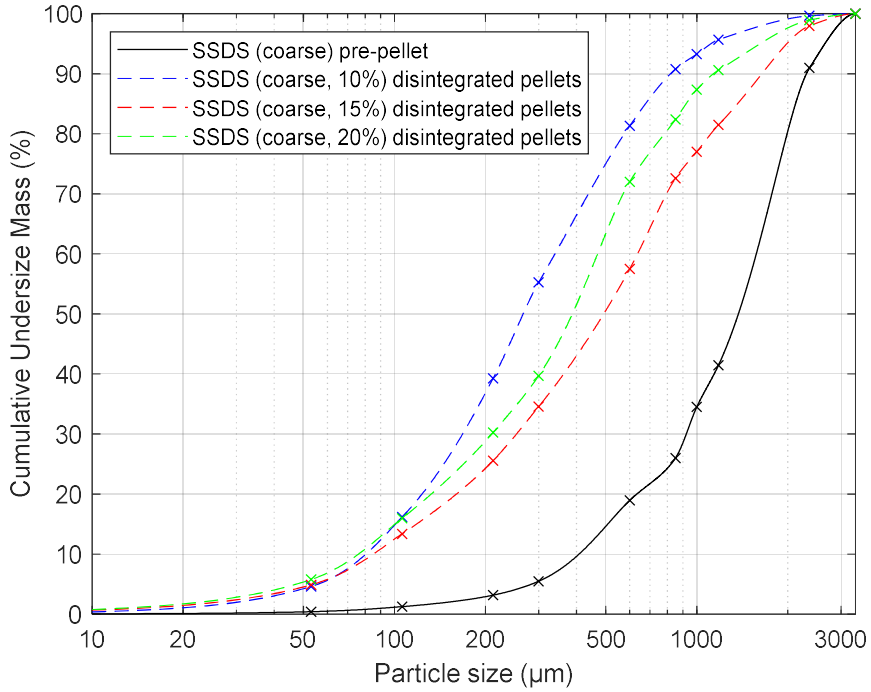

Figure 7-24 Cumulative distribution of particle size for SSDS (coarse) - pre-pellet and disintegrated pellets

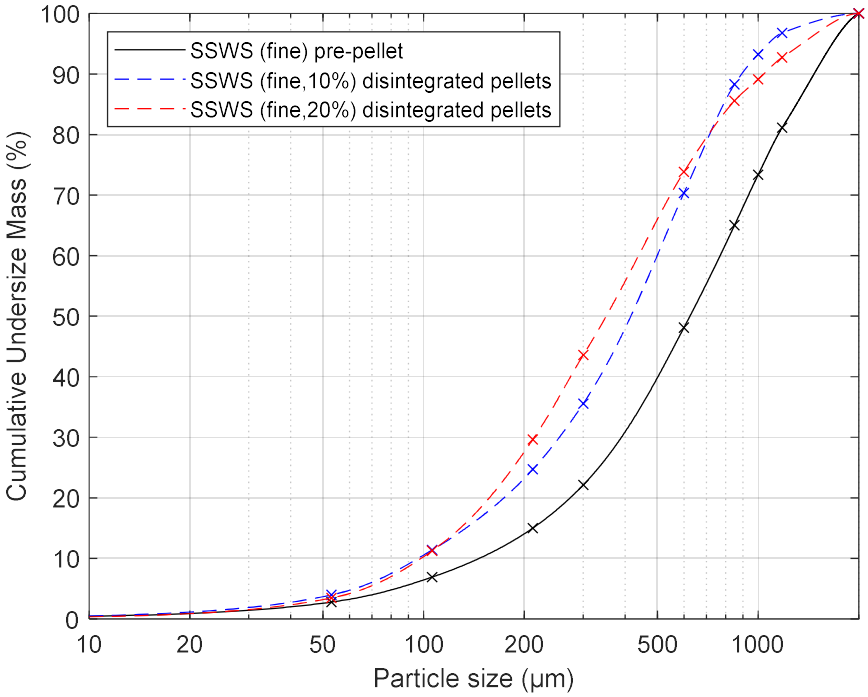

Figure 7-25 Cumulative distribution of particle size for SSWS (fine) - pre-pellet and disintegrated pellets

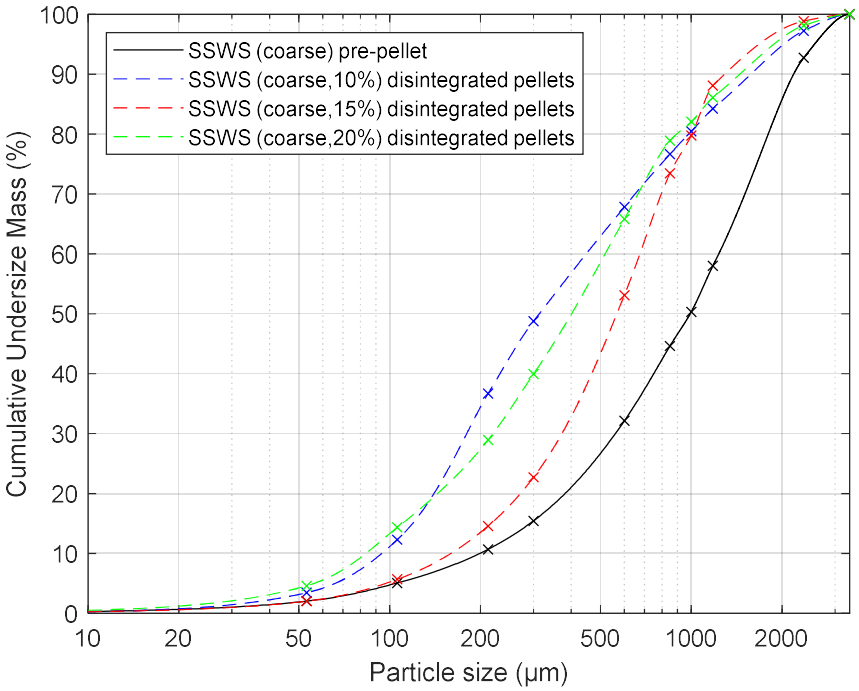

Figure 7-26 Cumulative distribution of particle size for SSWS (coarse) - pre-pellet and disintegrated pellets

7.8 Pellet Milling

7.8.1 Milled Pellets Particle Size Distribution

The particle size distribution (PSD) of the milled pellets were determined by sieving as described in Section 3.6.1. The PSD of disintegrated pellets and milled pellets are shown in Figure 7-27 to Figure 7-30. For all samples, only a small change in PSD was observed between the disintegrated pellets and milled pellets samples. For optimal pellet milling, it is typically desired that only pellet breakdown occurs, i.e. no change in particle size should be observed when comparing the disintegrated pellets and milled pellets (Williams et al., 2016).

7.8.2 Pellet Milling Energy and von Rittinger Analysis

The pellet samples were milled in a Lopulco LM 1.6 laboratory-scale ring-roller mill as described in Sections 3.5.3 and 3.8.6, and the specific effective milling energy was determined using the method described in Section 3.8.3. Specific effective milling energies were measured to be in the range of 8.2-28.9 kWh/ton, with the minimal value observed for the SSDS (coarse, 10%) sample and the maximum value observed for the SSWS (coarse, 15%) sample.

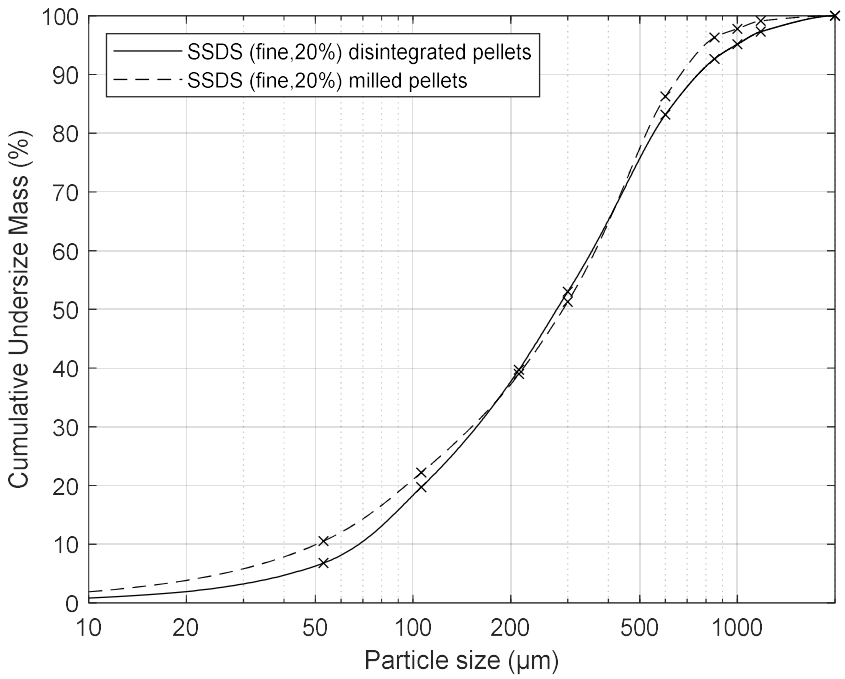

Figure 7-27 Cumulative distribution of particle size for SSDS (fine) – disintegrated pellets and milled pellets

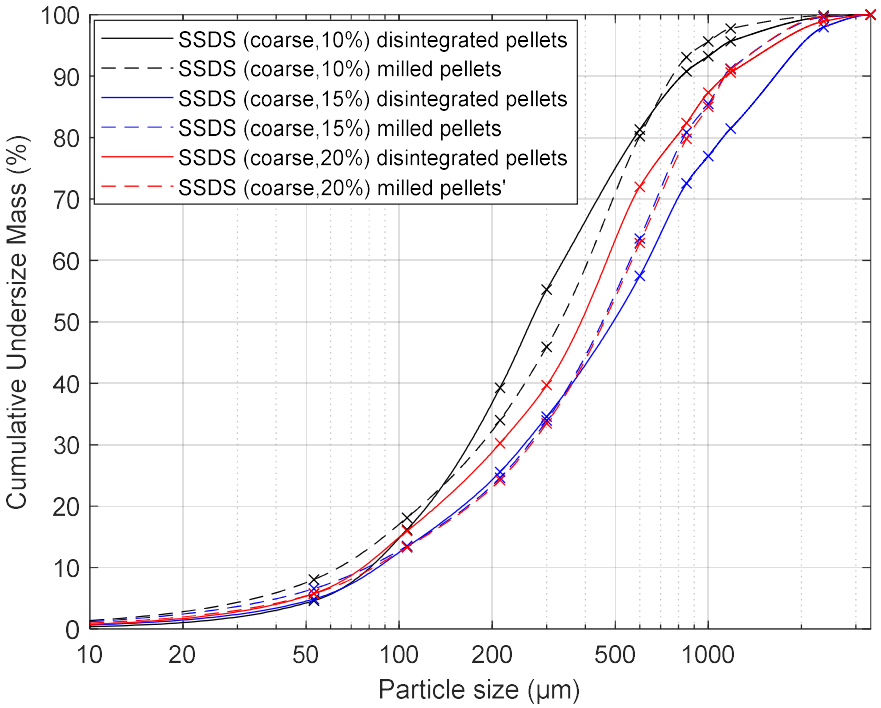

Figure 7-28 Cumulative distribution of particle size for SSDS (coarse) – disintegrated pellets and milled pellets

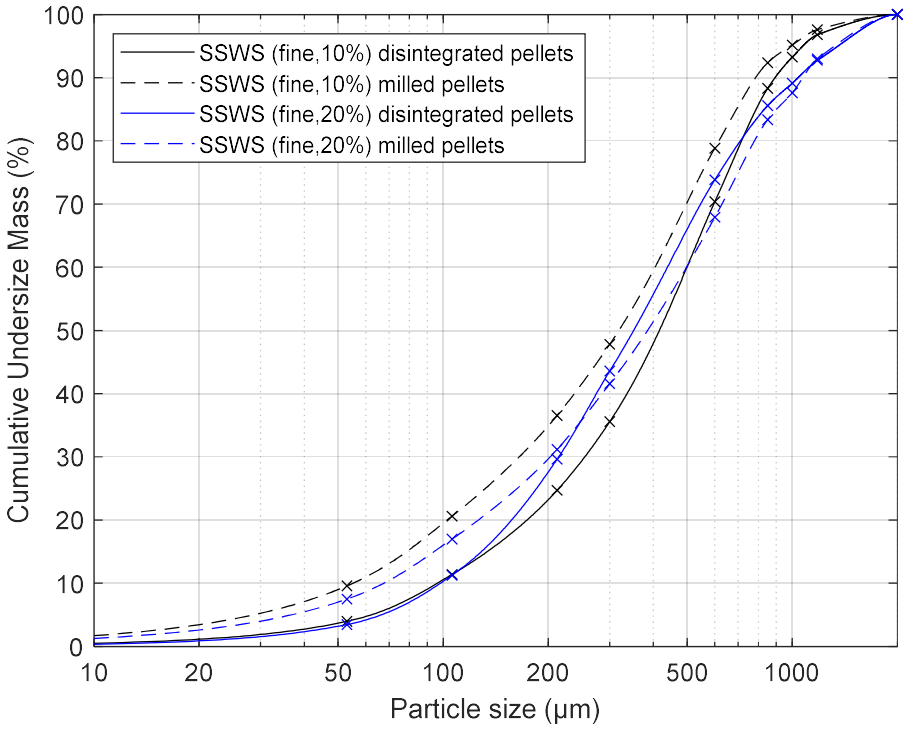

Figure 7-29 Cumulative distribution of particle size for SSWS (fine) – disintegrated pellets and milled pellets

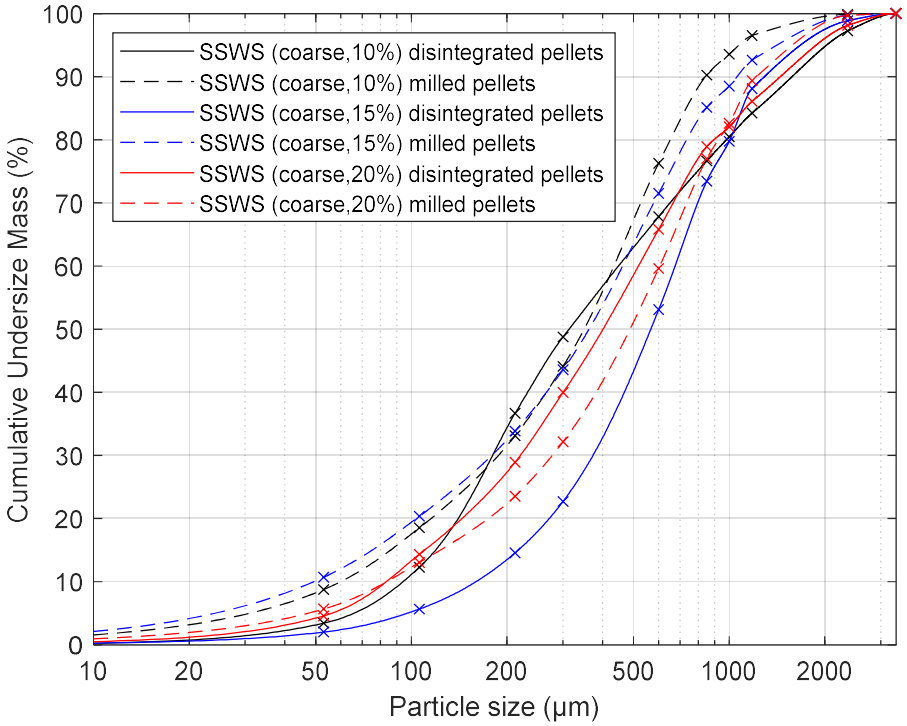

Figure 7-30 Cumulative distribution of particle size for SSWS (coarse) – disintegrated pellets and milled pellets

Von Rittinger analysis is conducted to compare the milling performance of the samples, based on the method described in Section 3.8.6 and the literature review presented in Section 2.9.2. The 80th percentile of the cumulative particle size distribution (d_{80}) was used for von Rittinger analysis since it is closer to the 1 mm size often cited as the maximum size for pulverised combustion than the 50th percentile (d_{50}) (Tamura et al., 2014; Williams, 2016).

According to Temmerman et al. (2013), The specific effective pellet milling energy can be regarded as the sum of energy for breaking down the pellets into their constituent particles and the energy for the further reduction in particle size (if any). Since only a small difference in particle size was observed between the disintegrated pellets and milled pellets (Section 7.8.1), the majority of the milling energy can be attributed to the breaking down of pellets.

The specific effective milling energy, von Rittenger parameter and von Rittenger constant (K_{VR}) are shown in Table 7-5. The samples were also ranked using the K_{VR} values, with a lower K_{VR} value indicating a better milling performance. The von

Rittinger constant (K_{VR}) is a measure of the change in particle size during the milling process relative to the milling energy and therefore can be seen as an indicator of the performance of a pellet sample purely from the pellet milling perspective.

It was observed that pellets with a pelleting feed moisture content of 10% have the highest milling performance. Although pelleting of SSDS failed for three conditions (Section 7.5.1), SSDS pellets were observed to have better milling performance compared to SSWS pellets. There was no clear relationship between particle size and milling performance as measured by the von Rittinger constant.

Sample	Specific effective pellet milling energy (kWh/ton)	von Rittinger parameter $(1/x_2 - 1/x_1)$ (mm^{-1})	von Rittinger constant K_{VR} (kWh·mm/ton)	Ranking
SSDS (coarse, 10%)	8.2	1.51	5.4	1
SSWS (fine, 10%)	11.7	1.46	8.0	2
SSWS (coarse, 10%)	12.5	1.37	9.1	3
SSDS (coarse, 20%)	12.4	1.03	12.0	4
SSDS (coarse, 15%)	12.9	1.06	12.2	6
SSDS (fine, 20%)	22.7	1.78	12.7	5
SSWS (fine, 20%)	16.0	1.15	13.9	7
SSWS (coarse, 20%)	18.5	0.94	19.7	8
SSWS (coarse, 15%)	28.9	1.21	23.8	9

Table 7-5 von Rittinger analysis of pellet milling

7.9 Changes in Particle Size and Shape during Pelleting and Pellet Milling

7.9.1 Particle Size

The change in particle size during pelleting was discussed in Section 7.7.4, and the change during pellet milling was discussed in Section 7.8.1. A brief summary of the particle size change during the complete journey of pelleting and pellet milling is

provided in this Section. The overall changes in d_{80} values of the samples are shown in Table 7-6.

It can be summarised that a large decrease in particle size occurs during pelleting (from pre-pellet material to disintegrated pellets), while only a slight change is typically observed during pellet milling (from disintegrated pellets to milled pellets). Since the mill used in the present study is representative of ring-roller mills used in some biomass power stations (Section 3.5.3), it can be concluded that for these power stations, the disintegrated pellets PSD would be close to the milled pellets PSD which enters the boiler for combustion, and pelleting processes should be optimised so that the disintegrated pellets PSD is close to the desired PSD for combustion.

	d_{80} (µm)			**Percentage change**	
Sample	**Pre-pellet**	**Disintegrated pellets**	**Milled pellets**	**Pre-pellet to disintegrated pellets**	**Disintegrated pellets to milled pellets**
SSDS (fine, 20%)	995	551	524	-44.6%	-4.9%
SSDS (coarse, 10%)	1990	576	597	-71.1%	+3.6%
SSDS (coarse, 15%)	1990	1113	831	-44.1%	-25.3%
SSDS (coarse, 20%)	1990	783	855	-60.7%	+9.2%
SSWS (fine, 10%)	1147	716	616	-37.6%	-14.0%
SSWS (fine, 20%)	1147	710	779	-38.1%	+9.7%
SSWS (coarse, 10%)	1800	981	653	-45.5%	-33.4%
SSWS (coarse, 15%)	1800	1006	734	-44.1%	-27.0%
SSWS (coarse, 20%)	1800	894	925	-50.3%	+3.5%

Table 7-6 Change in d_{80} during the complete journey of pelleting and pellet milling

7.9.2 Particle Shape

As discussed in Section 2.5, particle shape is an important factor in particle flow and combustion. The sphericity, circularity, symmetry and aspect ratio of the sugarcane

straw samples at different stages of the complete pelleting and pellet milling journey (pre-pellet, disintegrated pellets and milled pellets) were measured as described in Section 3.6.4 and presented in this Section. Among these shape factors, sphericity and aspect ratio are discussed in detail, as they are the most important indicators of aerodynamic properties and for combustion modelling.

7.9.2.1 Pre-pellet samples shape distributions

The particle shape distributions of the pre-pellet samples are shown in Figure 7-31 to Figure 7-34. It was found that the values of sphericity, circularity and aspect ratio are higher for the wet season samples compared to the dry season samples, and for the fine samples compared to the coarse samples. Moreover, in general, when comparing the two harvest seasons, the distributions for all shape factors are similar for the fine samples, while the distributions of the coarse samples diverge significantly from each other. This suggests that the harvest season of sugarcane straws significantly affects the particle shape distributions when milled to coarser sizes, while the influence of harvest season on the shape distributions when milled to finer sizes is much smaller.

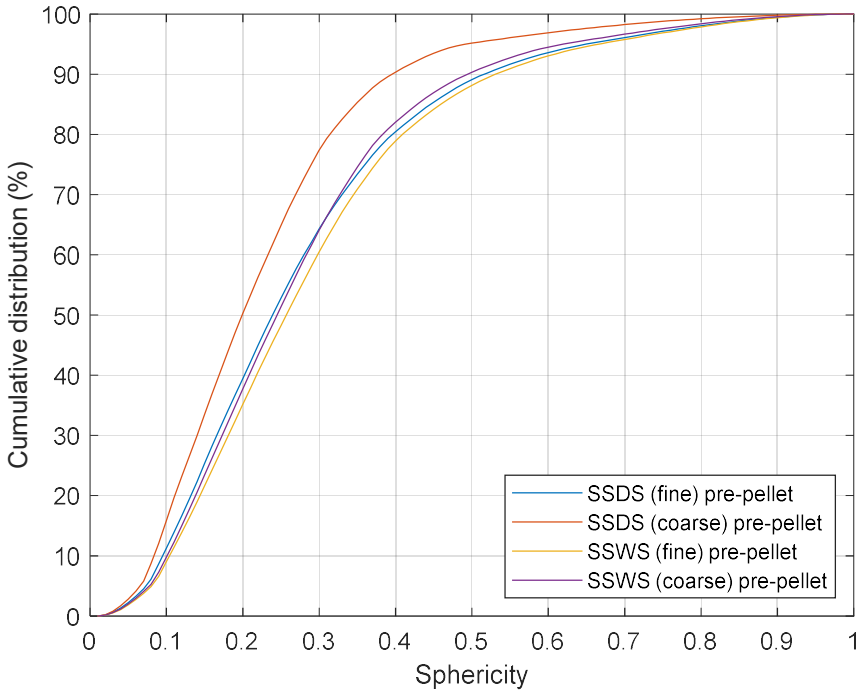

Figure 7-31 Sphericity distribution of pre-pellet samples

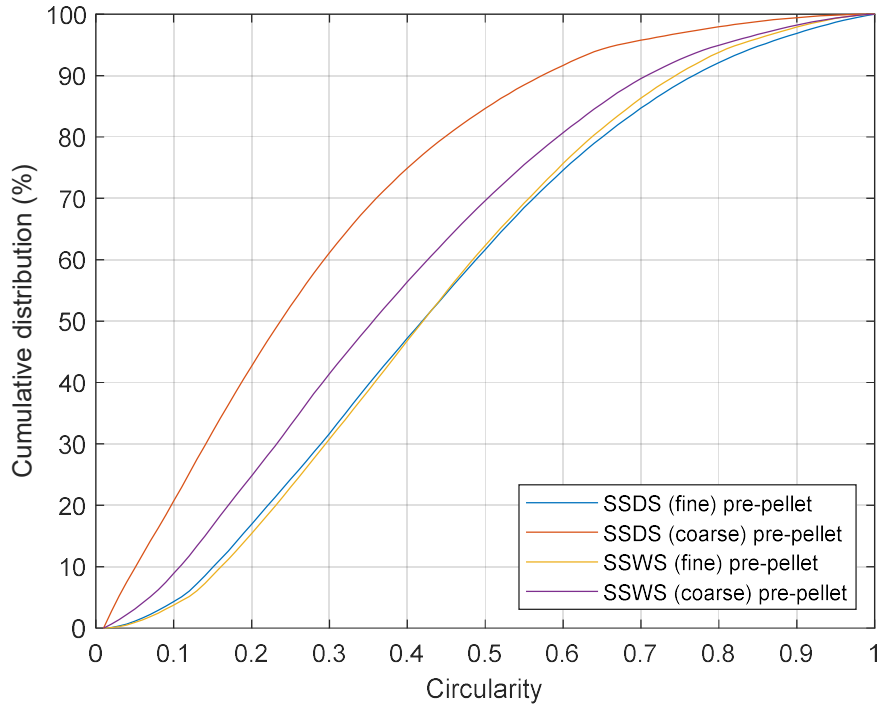

Figure 7-32 Circularity distribution of pre-pellet samples

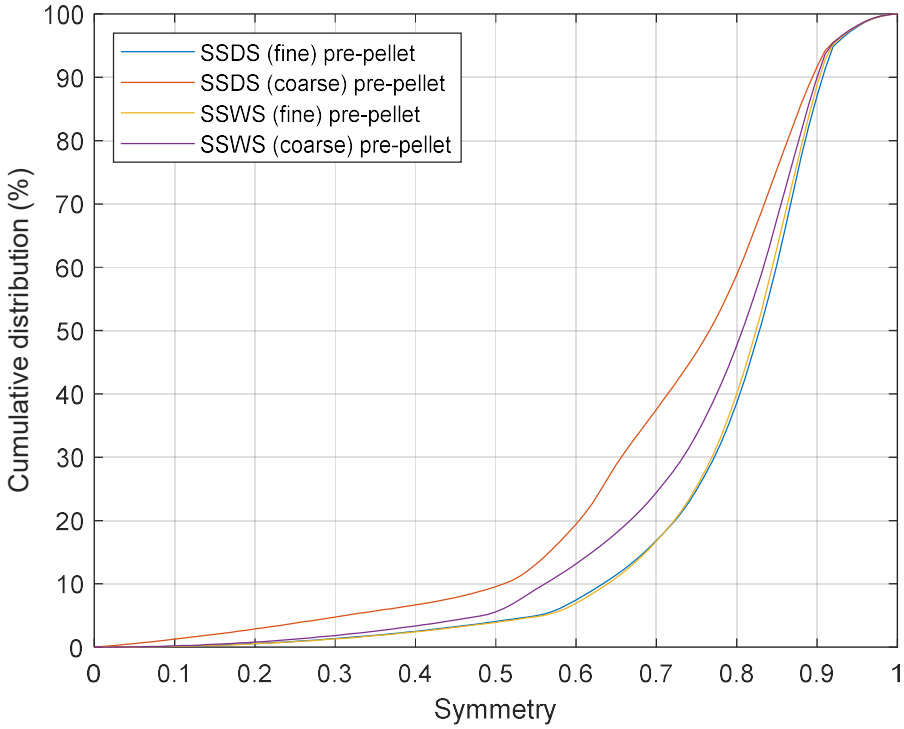

Figure 7-33 Symmetry distribution of pre-pellet samples

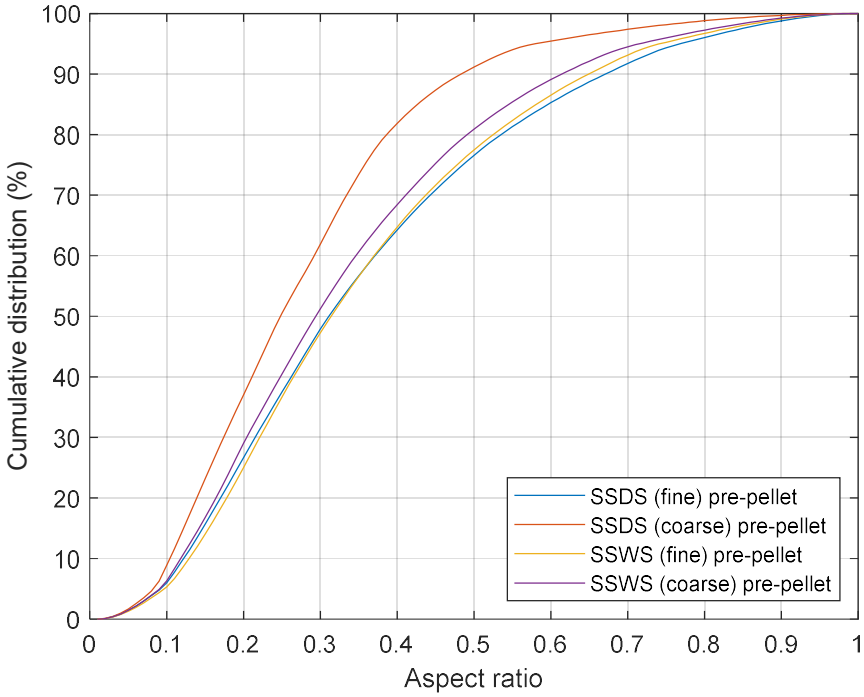

Figure 7-34 Aspect ratio distribution of pre-pellet samples

7.9.2.2 Particle shape change during pelleting and pellet milling

The sphericity and aspect ratio distributions of pre-pellet, disintegrated pellets and milled pellets samples are shown in Figure 7-35 to Figure 7-42 to illustrate the change in shape distributions during the complete journey of pelleting and pellet milling. The circularity and symmetry distributions are shown in Appendix E. The average values of the shape factors are presented in Table 7-7, and the changes in the average values of the shape factors during the complete journey of pelleting and pellet milling are presented in Figure 7-43 to Figure 7-46.

For all samples, a large increase in sphericity and aspect ratio was observed between the pre-pellet and disintegrated samples, while only small changes were observed between the disintegrated pellets and milled pellets samples. Together with the result presented in Section 7.9.1 that similar trends were observed for particle size, it can be concluded that pelleting causes substantial changes in particle size and shape, while the main effect of pellet milling was breaking down the pellets into their constituent particles with limited further changes in particle size and shape. Therefore, pelleting processes should be designed so that the disintegrated pellets

size and shape match the requirements for combustion. In addition, the relatively high sphericity of the disintegrated pellet and milled pellet particles indicate that milled pellets particles would likely have worse aerodynamic performance compared to milled biomass (which has not been pelletised previously) with a similar PSD. This should be taken into account in combustion modelling, process design and when designating fuel specifications.

The result that only small changes were observed between the disintegrated pellets and milled pellets samples is consistent with the previous finding by Williams et al. (2016) that regardless of changes in particle size, the milling of biomass pellets does not result in significant changes in particle shape where comparing disintegrated pellets and milled pellets. However, Williams et al. (2016) did not include agricultural straw residue pellets in their study, and the present study extends the validity of this observation to include sugarcane straw pellets.

In general, it can be expected that longer particles (i.e. particles with lower aspect ratios) are less spherical. Therefore, a positive correlation between sphericity and aspect ratio is expected. The correlation between the average sphericity and average aspect ratio of eucalyptus and cardboard (including both milled and char samples at various size fractions, discussed in detail in Chapter 5) and sugarcane straw samples (including pre-pellet, disintegrated pellets and milled pellets samples) is shown in Figure 7-47. Although a positive correlation between sphericity and aspect ratio is expected, a precise relationship is illustrated in Figure 7-47 and expressed in equation (7.1). In addition, the fact that this relationship holds true across the wide range of samples included in the analysis suggests that this result is valid for multiple types of biomass at different stages of combustion and the pelleting and pellet milling journey. Therefore, equation (7.1) can be used for estimating the average aspect ratio from the average sphericity (or vice versa) for a wide range of materials in cases where data for one of the shape factors are not available.

$$AR_{average} = 1.08\,\phi_{\,average} + 0.04 \qquad (7.1)$$

Where $AR_{average}$ is the average aspect ratio and $\varphi_{average}$ is the average sphericity.

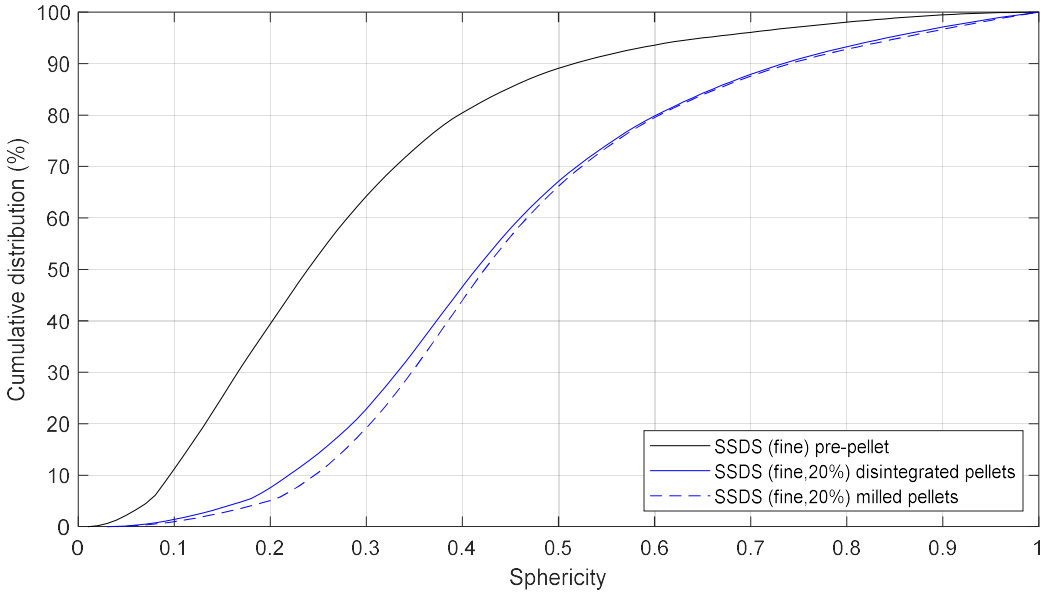

Figure 7-35 Sphericity distributions of pre-pellet, disintegrated pellets and milled pellets - SSDS (fine)

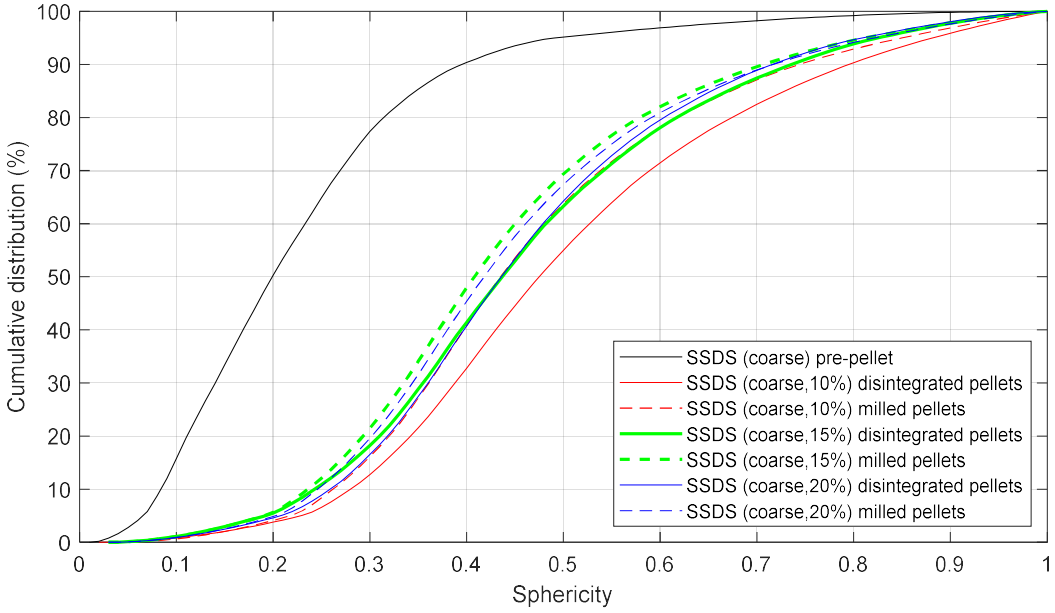

Figure 7-36 Sphericity distributions of pre-pellet, disintegrated pellets and milled pellets - SSDS (coarse)

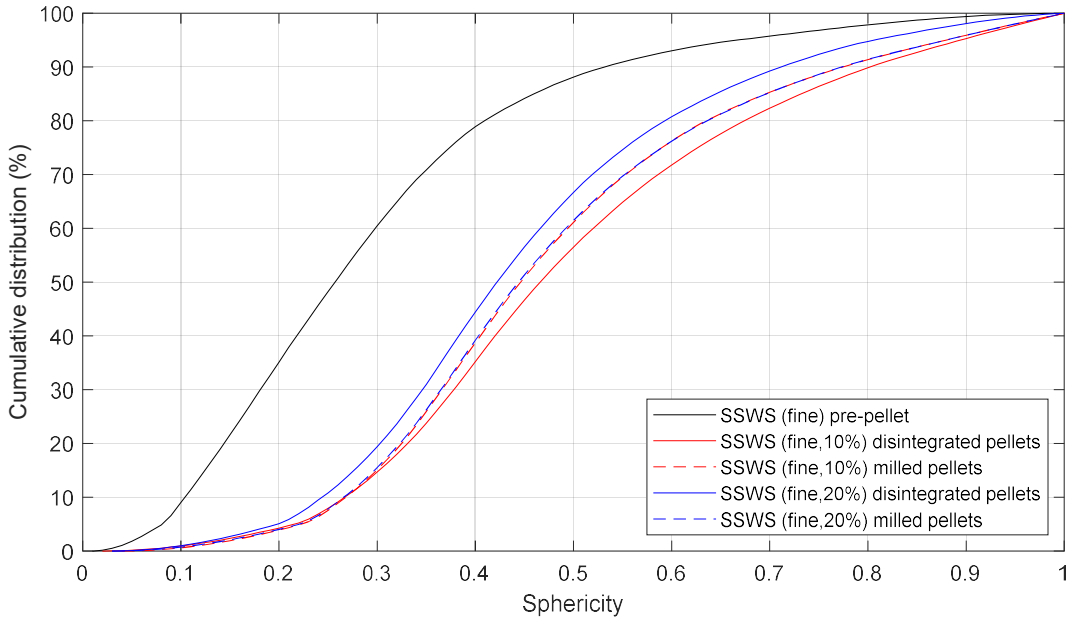

Figure 7-37 Sphericity distributions of pre-pellet, disintegrated pellets and milled pellets – SSWS (fine)

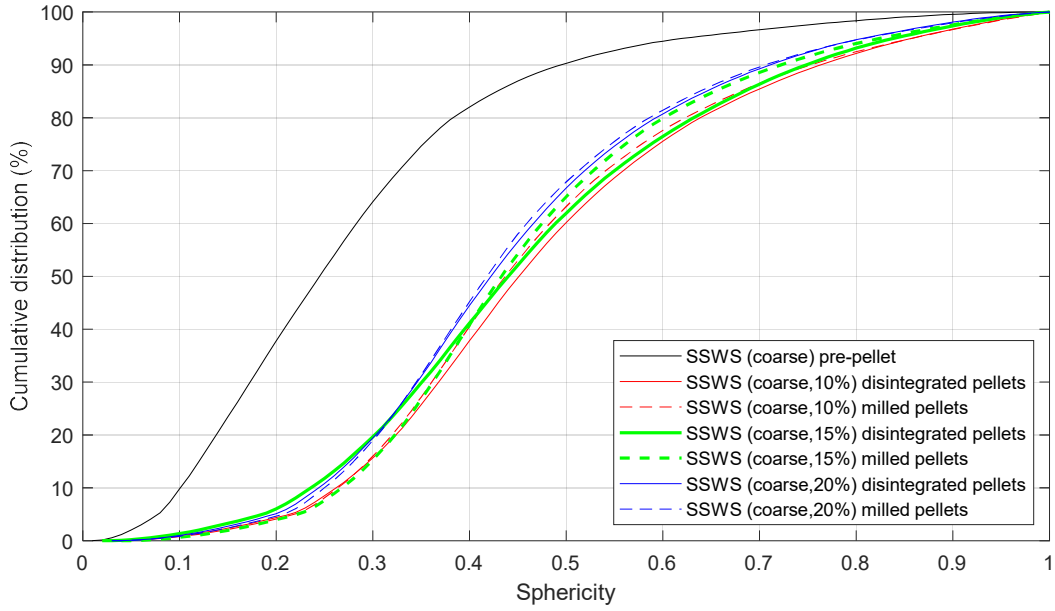

Figure 7-38 Sphericity distributions of pre-pellet, disintegrated pellets and milled pellets – SSWS (coarse)

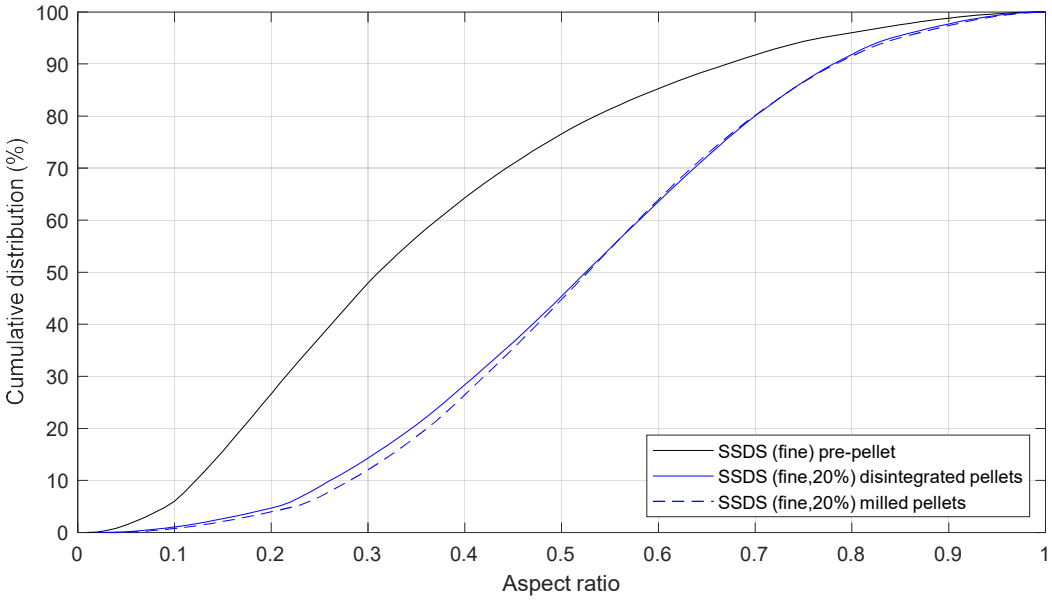

Figure 7-39 Aspect ratio distributions of pre-pellet, disintegrated pellets and milled pellets - SSDS (fine)

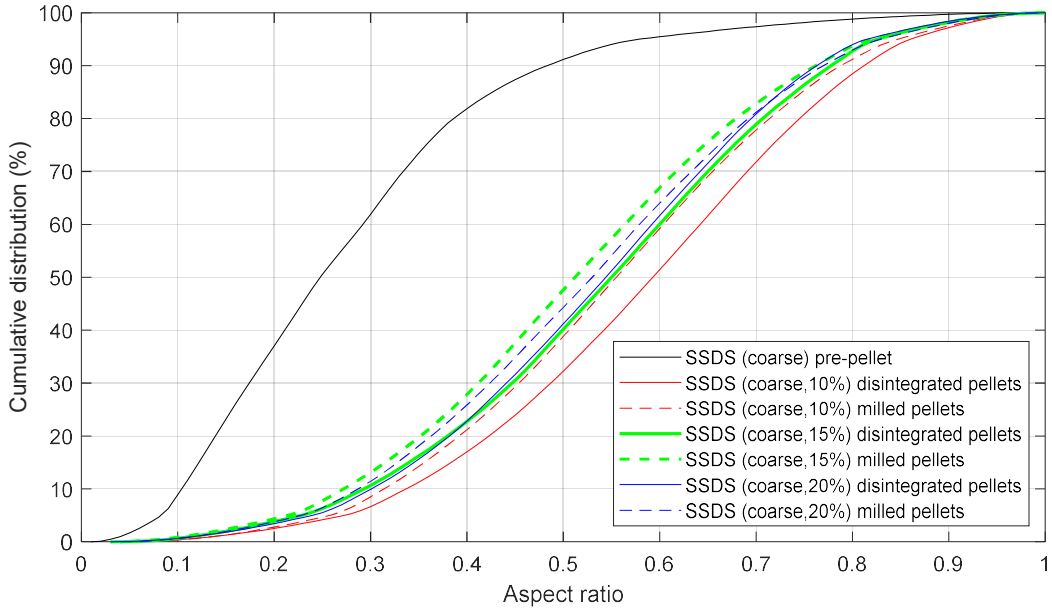

Figure 7-40 Aspect ratio distributions of pre-pellet, disintegrated pellets and milled pellets - SSDS (coarse)

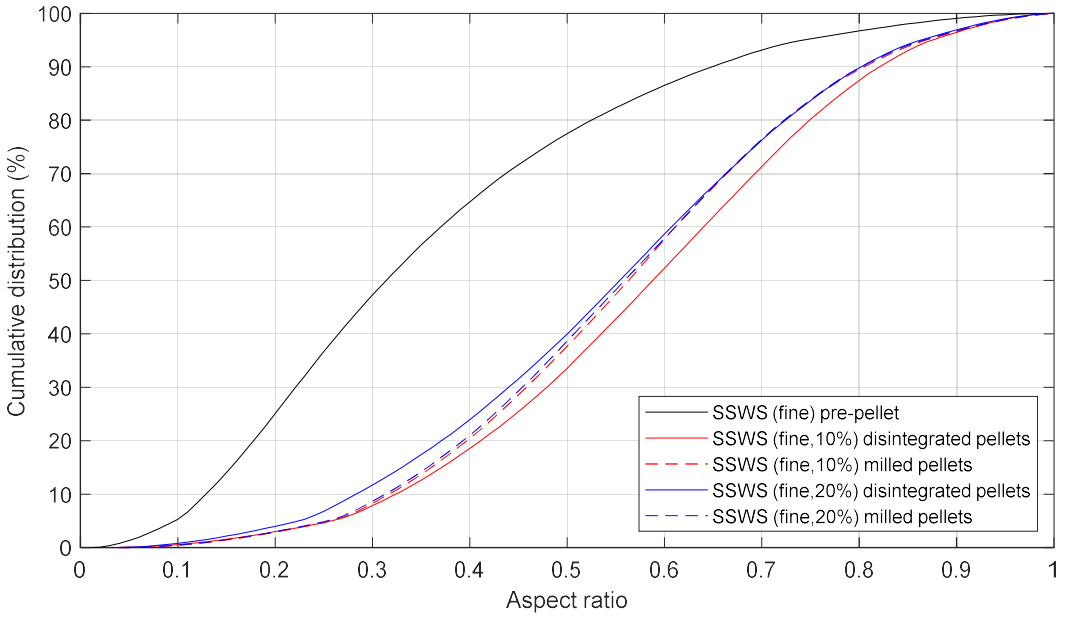

Figure 7-41 Aspect ratio distributions of pre-pellet, disintegrated pellets and milled pellets - SSWS (fine)

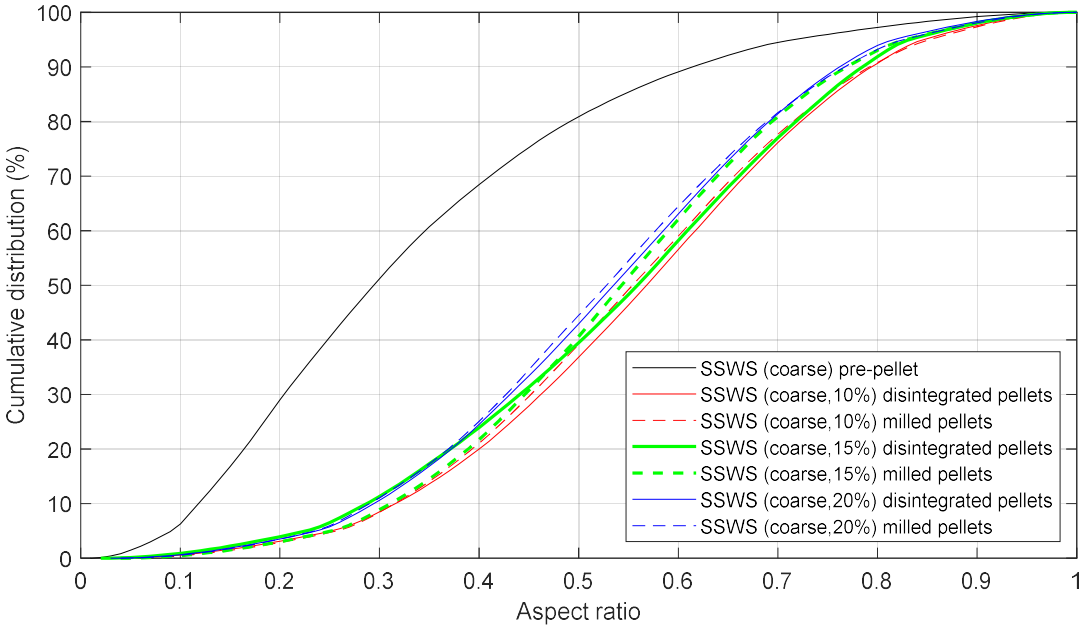

Figure 7-42 Aspect ratio distributions of pre-pellet, disintegrated pellets and milled pellets - SSWS (coarse)

Sample	Average Sphericity	Average Circularity	Average Symmetry	Average Aspect Ratio
SSDS (fine) pre-pellet	0.279	0.429	0.795	0.339
SSDS (coarse) pre-pellet	0.226	0.297	0.727	0.272
SSWS (fine) pre-pellet	0.293	0.439	0.791	0.356
SSWS (coarse) pre-pellet	0.278	0.382	0.758	0.335
SSDS (fine, 20%) disintegrated pellets	0.447	0.555	0.773	0.523
SSDS (coarse, 10%) disintegrated pellets	0.506	0.636	0.801	0.587
SSDS (coarse, 15%) disintegrated pellets	0.464	0.559	0.783	0.543
SSDS (coarse, 20%) disintegrated pellets	0.463	0.517	0.754	0.540
SSWS (fine, 10%) disintegrated pellets	0.501	0.626	0.793	0.580
SSWS (fine, 20%) disintegrated pellets	0.451	0.530	0.768	0.529
SSWS (coarse, 10%) disintegrated pellets	0.482	0.590	0.790	0.563
SSWS (coarse, 15%) disintegrated pellets	0.467	0.577	0.799	0.545
SSWS (coarse, 20%) disintegrated pellets	0.451	0.530	0.768	0.529
SSDS (fine, 20%) milled pellets	0.460	0.535	0.753	0.535
SSDS (coarse, 10%) milled pellets	0.471	0.574	0.776	0.551
SSDS (coarse, 15%) milled pellets	0.442	0.516	0.759	0.517
SSDS (coarse, 20%) milled pellets	0.452	0.525	0.762	0.528
SSWS (fine, 10%) milled pellets	0.483	0.581	0.776	0.562
SSWS (fine, 20%) milled pellets	0.482	0.568	0.775	0.560
SSWS (coarse, 10%) milled pellets	0.474	0.558	0.740	0.552
SSWS (coarse, 15%) milled pellets	0.466	0.498	0.749	0.543
SSWS (coarse, 20%) milled pellets	0.450	0.516	0.759	0.528

Table 7-7 Average shape factors of the sugarcane straw pre-pellet, disintegrated pellets and milled pellets samples

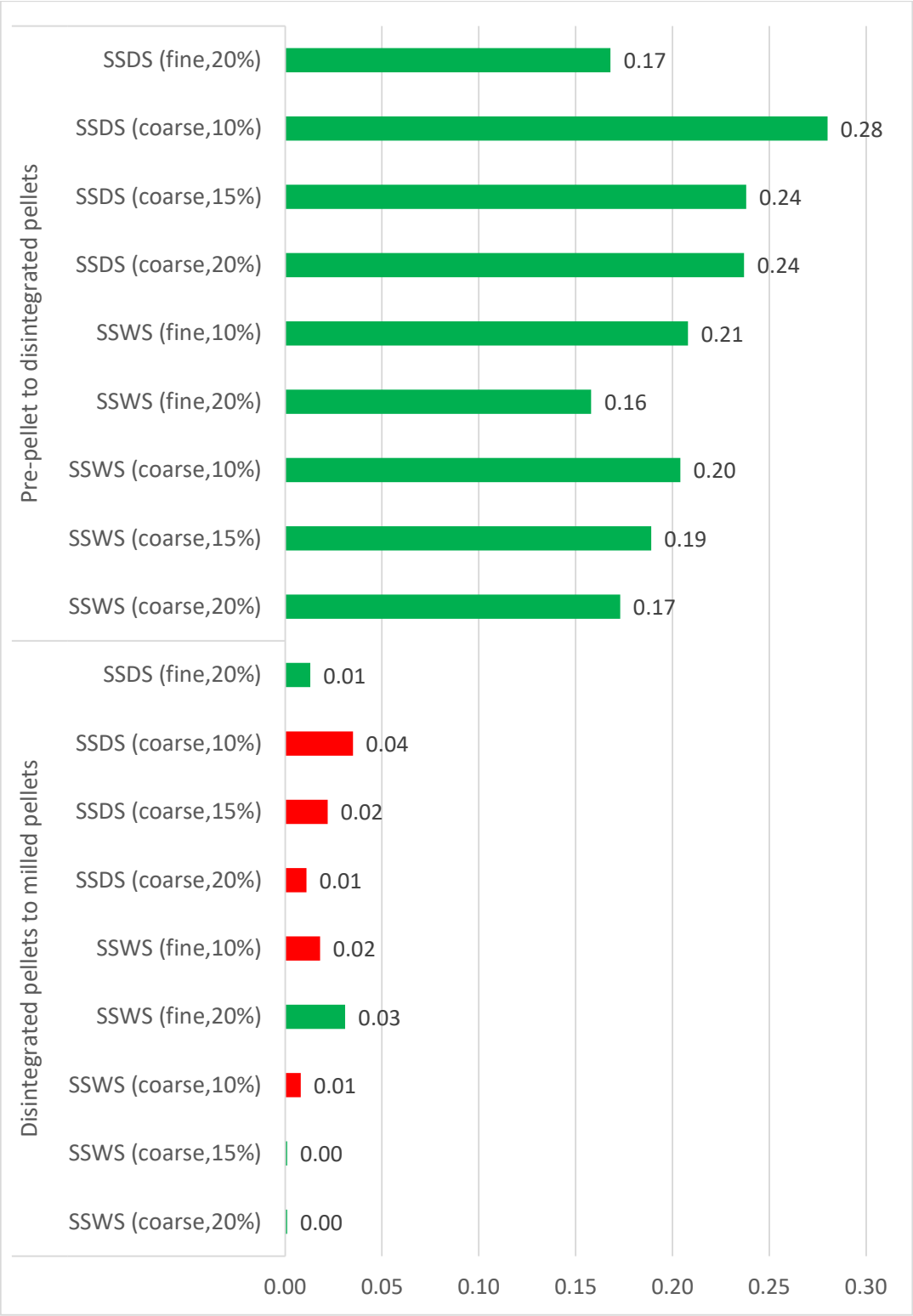

*green bars indicate a positive change and red bars indicate a negative change

Figure 7-43 Change in sphericity of pre-pellet, disintegrated pellets and milled pellets samples

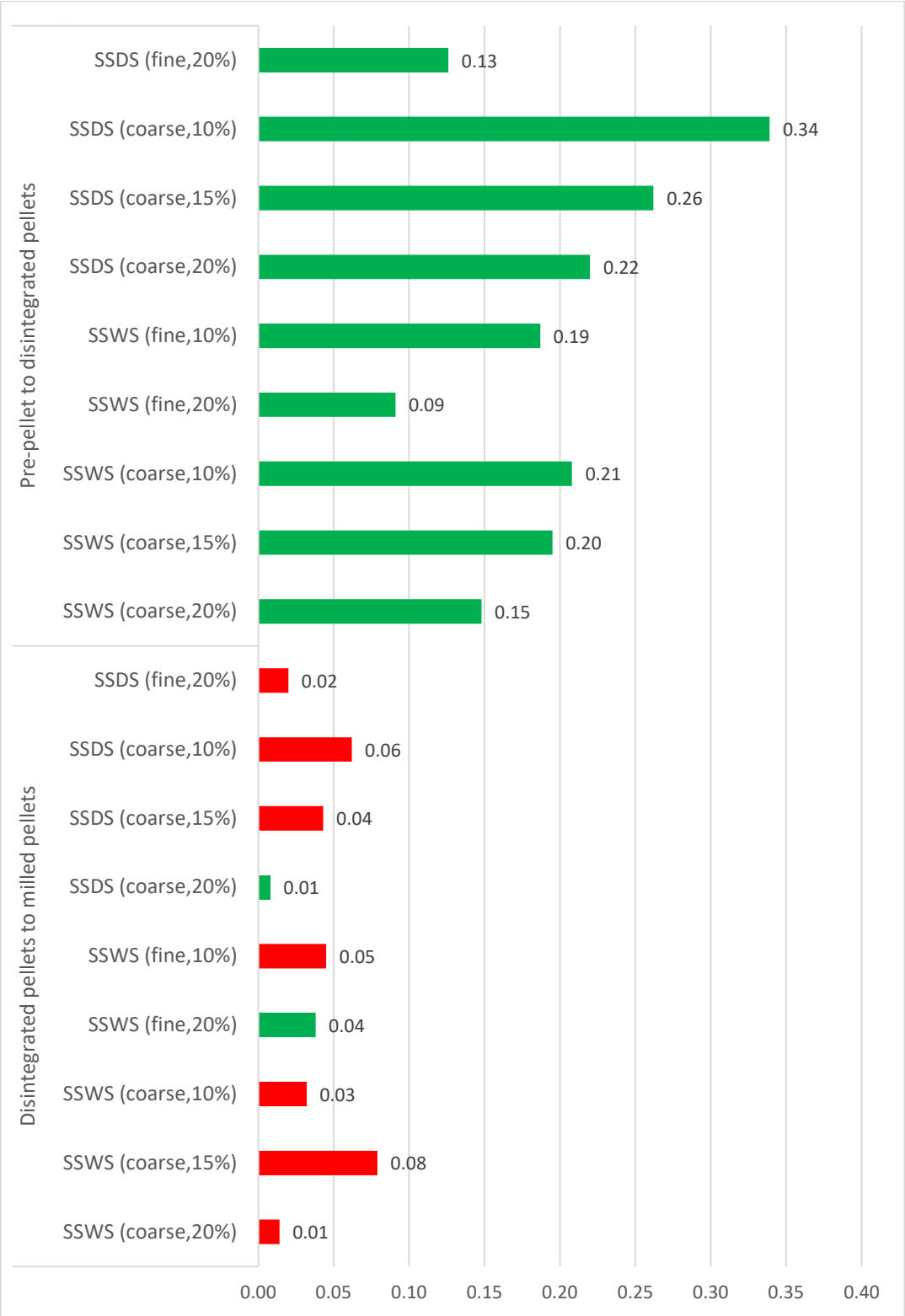

*green bars indicate a positive change and red bars indicate a negative change

Figure 7-44 Change in circularity of pre-pellet, disintegrated pellets and milled pellets samples

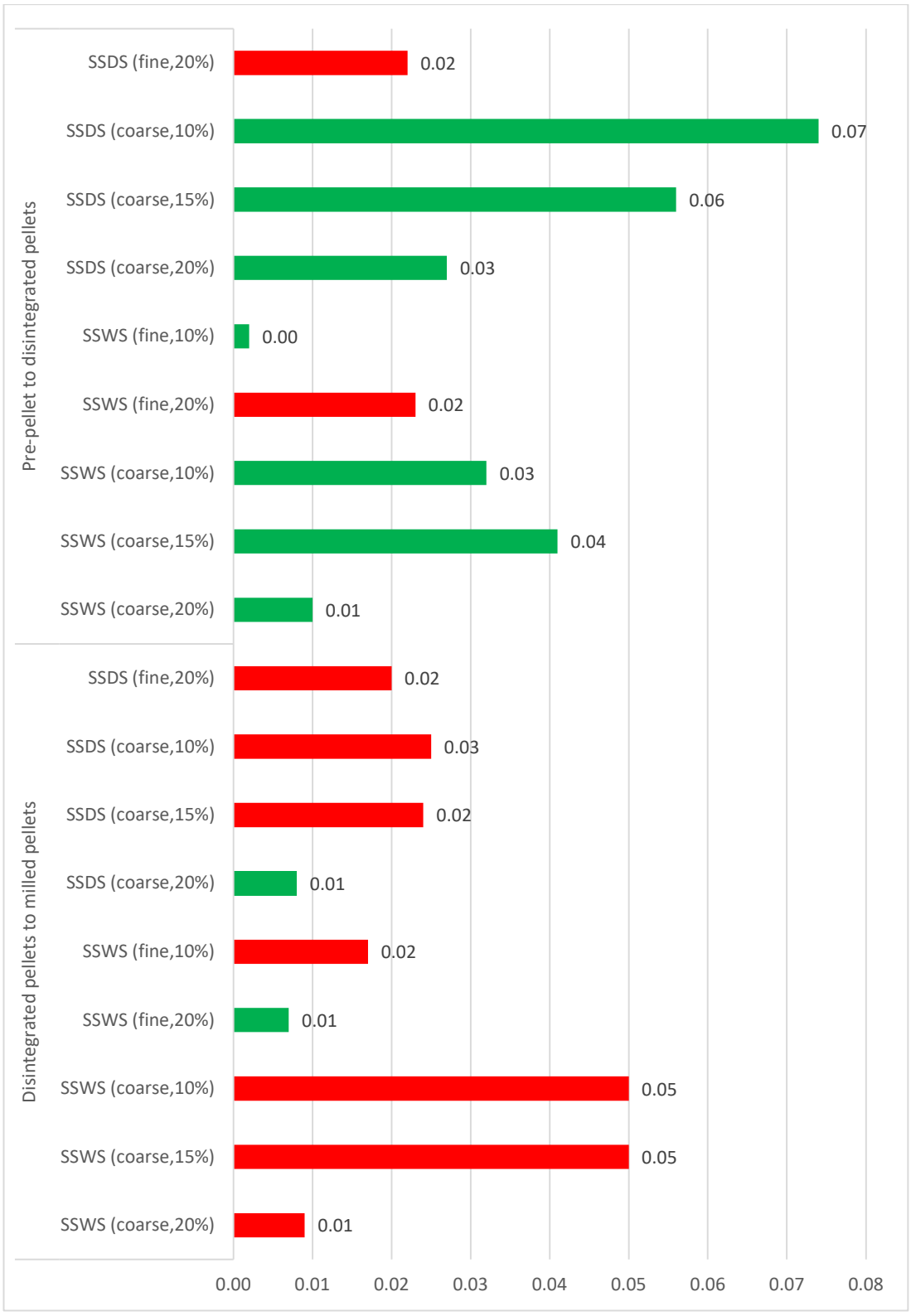

*green bars indicate a positive change and red bars indicate a negative change

Figure 7-45 Change in symmetry of pre-pellet, disintegrated pellets and milled pellets samples

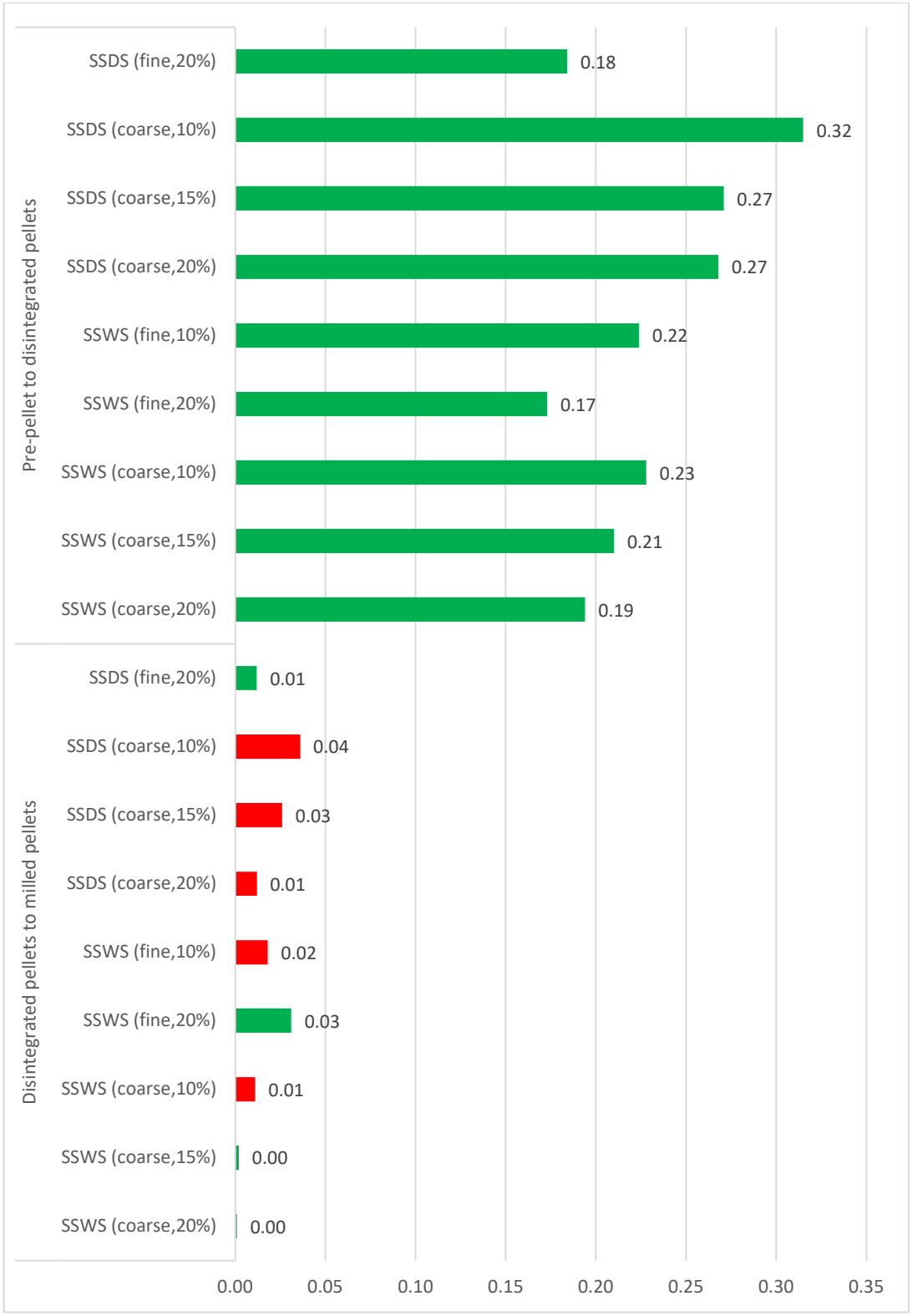

*green bars indicate a positive change and red bars indicate a negative change

Figure 7-46 Change in aspect ratio of pre-pellet, disintegrated pellets and milled pellets samples

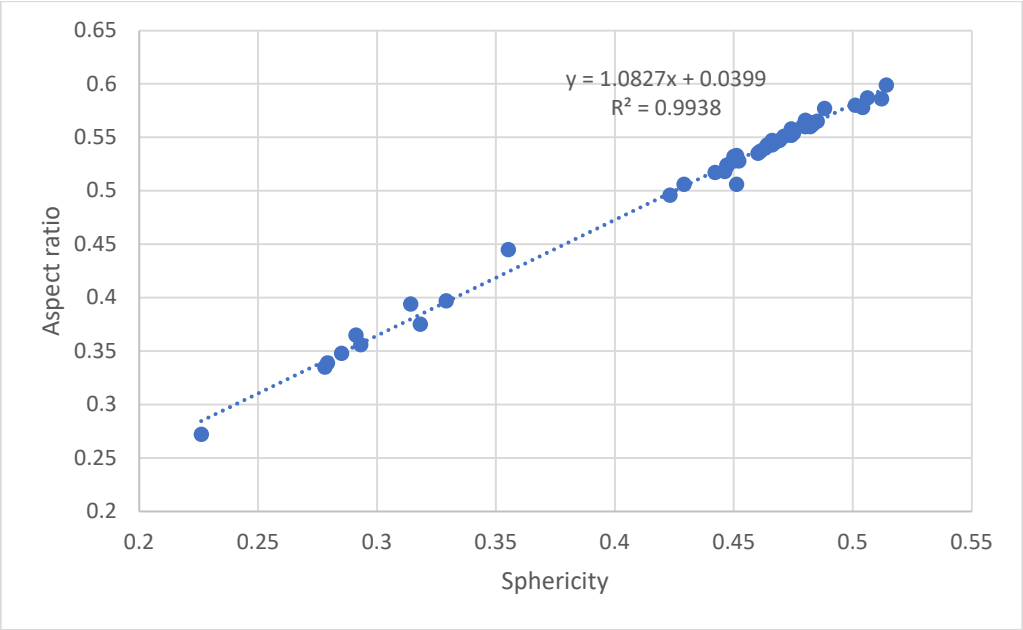

Figure 7-47 Correlation between average sphericity and average aspect ratio of eucalyptus, cardboard and sugarcane straw samples

7.10 Conclusions

This Chapter presented an in-depth study of the pelleting and pellet milling of sugarcane straw. Pelleting and pellet milling experiments were conducted on two Colombian sugarcane straw samples harvested in the dry and wet seasons. The influence of various factors on pelleting process parameters and pellet quality was investigated. The changes in particle size and shape during pelleting and pellet milling were analysed, and energy analysis was conducted for the pelleting and pellet milling processes. The new pellet process parameters of average pelleting power, pelleting efficiency and pellet production rate were introduced and represent novel methods of characterising the pelleting process. These can be valuable for industry as the parameters relate to factors such as equipment requirement and achievable throughput. In addition, the pelleting behaviour of sugarcane straw has not been studied in detail before, and this study has provided considerable value by investigating the pelleting and pellet milling of sugarcane straw.

It was found that pelleting failed for several conditions, and pelleting failure was more likely to occur at low moisture contents, at fine particle sizes, and with the dry season sample. The specific effective milling energies were measured to be in the

range of 18-55 kWh/ton and were lower with the coarse particle size and for the wet season sample. It was proposed that average pelleting power can be used as an indicator of pelleting difficulty and how close a system is to pelleting failure. The fine particle size results in significantly higher pellet production rates compared to the coarse particle size counterparts, suggesting that higher throughputs could be achieved if a finer particle size is used.

The influence of feed moisture content, harvest season and particle size on the indicators of pellet quality, including pellet durability, dimensions and bulk density, was studied. In particular, bulk density, an important pellet property which relates to transport costs, was found to be highly dependent on feed moisture content but not on other factors.

Through milling trials with a laboratory-scale ring-roller mill and von Rittinger analysis, the milling performance of the pellets produced in this study was assessed. It was observed that pellets with a pelleting feed moisture content of 10% have the highest milling performance.

In terms of changes in particle size and shape during pelleting and pellet milling, it is known that for woody biomass, a significant change in particle size and shape occurs during pelleting, while pellet milling typically breaks down the pellets into their constituent particles with limited further change in particle size and shape. The present study has demonstrated that these phenomena are also valid for sugarcane straw.

This Chapter has presented valuable data on the pelleting and pellet milling of sugarcane straw and has introduced new methods for the characterisation of experimental pelleting processes that could be of use to the industry. A degree of variability in pelleting behaviour was observed between the sugarcane samples harvested in the dry season and wet season, which needs to be considered when using sugarcane straw for energy applications. Among the pelleting feed moisture contents used in the present study (10, 15 and 20%), 15% should be used for optimal pellet durability. However, the pelleting energy required for 15% feed moisture content is also the highest. Although it is important to produce pellets that are of

satisfactory quality, pellet quality should not be the only consideration of pelleting operations. In addition to advancing the understanding of the pelleting and pellet milling behaviour of sugarcane straw, the newly introduced parameters, which represent crucial factors like equipment requirement and achievable throughput, can be valuable for the optimisation of industrial pelleting operations.

Chapter 8 - Life Cycle Analysis of Power Generation from Bagasse

8.1 Introduction

Large-scale biomass power generation has been used in the UK and many countries worldwide, although wood-derived fuels remain the predominant biomass source used in power applications. With sustainability (Biofuelwatch, 2024) and economic (Thomas, 2019) concerns regarding the use of woody fuels, there is increasing interest from the industry in alternative biomass sources, with bagasse being one of the options investigated by large-scale biomass power generators such as Drax (Thomas, 2019). Bagasse is a major by-product of the sugar industry and is the fibrous residue left after the extraction of use from sugarcane (Parameswaran, 2009). Sugarcane mills commonly use bagasse to generate heat and electricity to meet the energy requirements of the plant, and some also produce surplus electricity for the grid (Fioranelli & Bizzo, 2023). Multiple LCA studies of sugarcane bagasse electricity generation by direct combustion are available in the existing literature. However, no studies focusing specifically on the densification and international transport and use of bagasse could be found, despite the reported interest from industry (Thomas, 2019). This Chapter uses Life Cycle Analysis (LCA) to evaluate the potential of using the bagasse from the United States for large-scale power generation in the UK, addressing an underexplored area in the existing literature.

The overall process studied in this Chapter consists of the collection of bagasse from sugar mills, processing and pelleting of the raw material, transport to the power station, and combustion. A bespoke model was developed, and the overall carbon footprint was calculated using a combination of the GREET (Wang et al., 2023) and ecoinvent (ecoinvent, n.d.) databases, mass balance calculations, literature sources and data from an industrial partner. For clarity, the complete list of parameters used is provided in Appendix F and the justification for choosing these parameters is provided in Section 8.3.

8.2 Scope and System Boundaries

8.2.1 The Product System

The product system consists of the transport of bagasse from sugar mills to the pellet plant, the drying and pelletisation processes, the transport of pellets to the power station, and the generation of electricity from the pellets. The exact system boundary is defined in Section 8.2.3.

The scenario studied is defined as:

- The pellet plant and sugar mills are located in the US states of Louisiana
- The mean driving distance between the sugar mills and the pellet plant is 20 km
- The driving distance between the pellet plant and the port is 100 km (based on the distance between Drax Amite BioEnergy and the port of Baton Rouge)
- The shipping distance between the origin port and the destination port is 9000 km (based on the approximate distance between Baton Rouge and Immingham)
- The distance between the destination port and the power station is 80 km (based on the distance between Immingham and Drax Power Station)
- The raw material (bagasse) has a moisture content of 50.0% and is used to manufacture bagasse pellets with a moisture content of 6% (see Section 8.3).

8.2.2 Function of the Product System and Functional Unit

The function of the product system is to provide electricity to the grid. The functional unit used in this study is the generation of 1 kWh of electricity (i.e. the carbon footprint was calculated for each kWh of electricity provided to the grid). The carbon footprint is also expressed for each kg and each MJ equivalent of pellets produced at the factory gate in Section 8.9.

8.2.3 The System Boundary

The first life cycle stage of the system is the transport of bagasse from the sugar mills to the pellet plant within the US. The bagasse is then pelletised in the pellet plant. The bagasse is dried in a dryer, ground in a hammermill, densified in a pelletiser and

the pellets are then cooled in a pellet cooler. Part of the dryer outlet stream is used to power a furnace, which supplies heat to the dryer. The finished pellets are then transported to the power station in the UK, passed through a pellet grinder, and combusted. Only the operation of the system was considered in this study, and the commissioning and decommissioning of the facilities are not within the system boundary. The sugar mills and cultivation of the sugarcane crop are not formally inside the system boundary. It is assumed that only excess bagasse not needed for providing the energy needed in the sugar mills and currently treated as wastes are used.

The process flow diagram for the system is shown in Figure 8-1. The system boundary is also clearly marked. The functions of each unit process are shown in Table 8-1. All system streams (both material and energy) are described in Table 8-2.

Process	**Function**
Dryer	Dry the raw material to the required moisture content for subsequent processes
Furnace	Provide heat for the dryer by the combustion of a portion of the dryer outlet
Hammermill	Mill the dried material to the required particle sizes
Pelletiser	Press the material into pellets
Pellet cooler	Cool the pellets to within 5°C of the ambient temperature
Pellet grinder	Grind the pellets to the required particle sizes for combustion
Boiler	Generate electricity by combustion of the material

Table 8-1 The Function of Each Unit Process

Stream	**Type**	**Description**
1	**Material**	Transport of bagasse from the sugar mills to the pellet plant

2	**Material**	Raw bagasse going into the dryer
3	**Material**	Unrecoverable losses from storage at the pellet plant
4	**Material**	Dried material at the dryer outlet
5	**Material**	Dried material going into the hammermill
6	**Material**	Dried material going into the furnace
7	**Energy**	Heat energy from the furnace to the dryer
8	**Material**	Disposal of ash from the furnace
9	**Material**	Emissions to the atmosphere from the furnace at the pellet plant
10	**Energy**	Electricity input to the hammermill
11	**Material**	Hammermill output: dried and milled material
12	**Material**	Pelletiser input: dried and milled material
13	**Material**	Unrecoverable losses from the hammermill
14	**Energy**	Electricity input to the pelletiser
15	**Material**	Pelletiser output: hot pellets
16	**Material**	Pellet cooler input: hot pellets
17	**Material**	Unrecoverable losses from the pelletiser
18	**Energy**	Electricity input to the pellet cooler
19	**Material**	Pellet cooler output: cooled pellets
20	**Material**	Transport of pellets from the pellet plant to the power station; pellet grinder input
21	**Material**	Unrecoverable losses during transport from the pellet plant to the power station and storage

22	**Energy**	Electricity input to the pellet grinder, provided by the boiler
23	**Material**	Pellet grinder output: ground pellets
24	**Material**	Boiler input: ground pellets
25	**Material**	Unrecoverable losses from the pellet grinder
26	**Energy**	Electricity feeding to the grid
27	**Material**	Disposal of ash from the boiler
28	**Material**	Emissions to the atmosphere from the boiler at the power station

Table 8-2 Stream Table with description of all streams in the system

Impact category	Climate change
LCI results	Amount of a greenhouse gas per functional unit
Characterisation model	Baseline model of 100 years of the Intergovernmental Panel on Climate Change
Category indicator	Infrared radiative forcing (W/m2)
Characterisation factor	Global warming potential (GWP100) for each greenhouse gas (kg CO2-equivalents/kg gas)
Category indicator result	Kilograms of CO2-equivalents per functional unit
Category endpoints	Coral reefs, forests, crops
Environmental relevance	Infrared radiative forcing is a proxy for potential effects on the climate, depending on the integrated atmospheric heat adsorption caused by emissions and the distribution over time of the heat absorption

Table 8-3 The LCIA components used in this study, from PD ISO/TR 14047:2012 (The British Standards Institution, 2012)

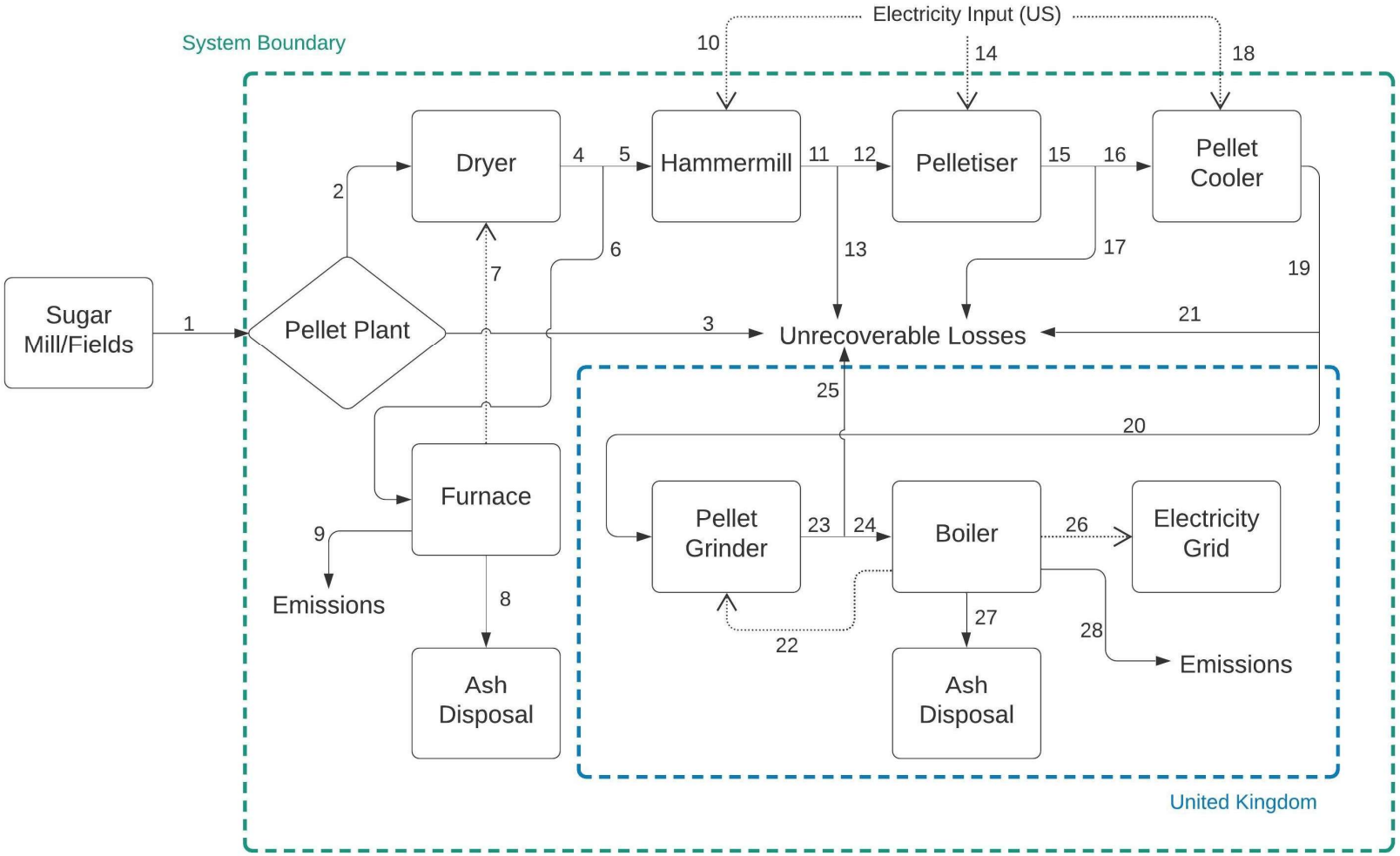

Figure 8-1 Process Flow Diagram of the System

8.2.4 Allocation Procedures

Allocation procedures are a common element of LCA studies to allocate the overall impact of a system to the multiple products produced by the system (The British Standards Institution, 2021a). Since the only function of the product system is to provide electricity and there are no other outputs across the entire value chain, allocation procedures are not relevant in this study.

8.2.5 The Life Cycle Impact Assessment (LCIA) Methodology

The impact category considered in this study is climate change. The LCIA components of this impact category were listed in PD ISO/TR 14047:2012 (The British Standards Institution, 2012) and are shown in Table 8-3.

8.3 Input Parameters

The justification for the input parameters for the LCA model is presented in this Section.

8.3.1 Raw Bagasse Moisture Content

The typical moisture content of bagasse from sugar mills is 45-55% (Celignis Analytical, n.d.; Vijayaraj et al., 2007). In this study, the moisture content of raw bagasse is assumed to be 50.0%.

8.3.2 Electricity Generation Efficiency from Biomass Pellets

The electricity generation efficiency in this study is assumed to be 39.3% (HHV basis), based on the model of a pulverised biomass-fired plant developed by Ali et al. (2017). This value is also consistent with the typical efficiency of pulverised biomass-fired power plants.

8.3.3 Pellet Grinding Energy

The grinding energy of biomass pellets depends on the target particle size for PF combustion. The optimal particle size for pulverised biomass combustion is <1000 µm, as it was demonstrated by Tamura et al. (2014) that unblended pulverised wood smaller than 1 mm shows devolatilisation and char burnout behaviour similar to that of high volatile sub-bituminous coal when 75% by weight is smaller than 75 µm. There are no data on the grinding energy of sugarcane co-product pellets available in

the literature, as the manufacturing and large-scale usage of such pellets is limited. Williams et al. (2016) performed milling experiments on a variety of biomass materials. Their findings suggest that 30 kWh/t (0.108 MJ/kg) is a reasonable estimate for the grinding energy of bagasse pellets for this study.

8.3.4 Higher Heating Value of Bagasse Pellets

The higher heating value of bagasse pellets is around 17-19 MJ/kg (Nhuchhen & Abdul Salam, 2012). The value of 18 MJ/kg is used as the typical HHV of bagasse pellets in this study.

8.3.5 Bagasse Pellets Ash Content

The ash content of the bagasse used by the industrial partner is 6.04%. This value is also similar to the ash content of 8.70% for a Brazilian bagasse pellet obtained by Almeida et al. (2017).

8.3.6 Unrecoverable Losses

The values for unrecoverable losses are either provided by the industrial partner or assumed to be zero. These are clearly stated in Section 8.4 as they are used in mass balance calculations and also in Table 8-10.

8.3.7 Pellet Plant Furnace Requirements

According to the data supplied by the industrial partner, 23.0% of the dryer outlet is diverted as fuel in the furnace to power the dryer, considering factors including the calorific value of the fuel and the efficiency of the dryer.

8.3.8 Use of Databases for the Calculation of Carbon Footprint

Several database sources were used for the calculation of carbon footprint. Ecoinvent is a comprehensive environmental database (ecoinvent, n.d.) which is a widely used data source for conducting LCA. In this Chapter, relevant data from the ecoinvent database were used for the calculation of the carbon footprint of ash disposal and transport (see Sections 8.6 and 8.8). The GREET (Greenhouse gases, Regulated Emissions, and Energy use in Technologies) database, sponsored by the U.S. Department of Energy's Office of Energy Efficiency and Renewable Energy, is an up-to-date database for the comparison of energy use and emissions of conventional

and advanced vehicle technologies with a life-cycle-based approach (M. Wang et al., 2023). In this Chapter, the GREET database was used for the calculation of carbon footprint of transport (see Section 8.8). The Emissions & Generation Resource Integrated Database (eGRID) is a comprehensive database published by the US Environmental Protection Agency (EPA) on electric power in the US, providing environmental data for each subregion in the US (US EPA, 2021). In this Chapter, eGRID was used for the calculation of carbon footprint of pellet plant electricity use (see Section 8.7).

8.4 Mass Balance

The first step in LCI is establishing a mass balance for the overall process based on the system flowsheet in Figure 8-1. The properties of each material stream (listed in Table 8-2) are specified in this Section and summarised in Table 8-5. The energy streams are specified in Section 8.5. The mass balance was calculated by working backwards from the functional unit (f.u.) of 1 kWh of electricity generated at the power plant.

8.4.1 Moisture Content Reductions

The raw bagasse from sugar mills has a moisture content of 50.0% (Section 8.3.1). The processes in the pellet plant would reduce this to 6.0% in the finished pellets. The moisture content at each process stage is shown in Table 8-4. It is also assumed that the pellet cooler and pellet grinder do not change the moisture content of the pellets.

8.4.2 Pellet Grinder and Boiler

Using the electricity generation efficiency (higher heating value basis) and the pellet grinding energy, the relationship between the weight of pellets per f.u. at the pellet grinder inlet (W_{PGin}) and the weight of ground pellets per f.u. at the boiler inlet (W_{Bin}) can be expressed as follows:

$$W_{Bin} \cdot HHV \cdot eff - W_{PGin} \cdot GE = 1\ \text{kWh} \cdot \frac{3.6\ \text{MJ}}{1\ \text{kWh}} \qquad (8.1)$$

Where W_{Bin} is the weight of the pellets per f.u. at the pellet grinder inlet in kg; W_{PGin} is the weight of ground pellets per f.u. at the boiler inlet in kg; HHV is the higher

heating value of the pellets in MJ/kg; GE is the grinding energy of the pellets in MJ/kg; eff is the electricity generation efficiency (HHV basis).

Stage	Stream (s)	Moisture Content (%)	Source
Raw material	1,2,3	50.0	(Celignis Analytical, n.d.; Vijayaraj et al., 2007), see Section 8.3.1
Dryer outlet and feed to the furnace	4,6	12.0	Industrial partner
Hammermill inlet	5	11.5	Industrial partner
Hammermill outlet	11,13	10.5	Industrial partner
Pelletiser inlet	12	10.5	Industrial partner
Pelletiser outlet	15,17	6.0	Industrial partner
Pellet cooler inlet	16	6.0	Assumption
Pellet cooler outlet	19,20,21	6.0	Assumption
Pellet grinder outlet	23,24,25	6.0	Assumption

Table 8-4 Moisture content of the material at each process stage

Using the percentage of unrecoverable losses from the pellet grinder, the relationship between W_{Bin} and W_{PGin} can also be expressed as follows:

$$W_{PGin} - W_{Bin} = W_{Bin} \cdot UL_{PG}$$

$$W_{Bin} = \frac{W_{PGin}}{UL_{PG} + 1} \quad (8.2)$$

where UL_{PG} is the unrecoverable losses from the pellet grinder (%).

Combining Equations (8.1) and (8.2):

$$\frac{W_{PGin}}{UL_{PG}+1}\cdot HHV\cdot eff - W_{PGin}\cdot GE = 1\ \text{kWh}\ \cdot\frac{3.6\ \text{MJ}}{1\ \text{kWh}}$$

$$W_{PGin} = \frac{3.6(UL_{PG}+1)}{HHV\cdot eff - GE\cdot UL_{PG} - GE} \tag{8.3}$$

The unrecoverable losses from the pellet grinder are assumed to be zero in this study, but they are included in the formulae for completeness. When UL_{PG} is assumed to be zero, Equation (8.3) can be simplified to Equation (8.4).

$$W_{PGin} = \frac{3.6}{HHV\cdot eff - GE} \tag{8.4}$$

The electricity generation efficiency is 39.3% (Section 8.3.2) and the pellet grinding energy is 0.108 MJ/kg (Section 8.3.3). The higher heating value (HHV) of bagasse is 18 MJ/kg (Section 8.3.4). Using these values and Equation (8.4), the weight of pellets per f.u. at the pellet grinder inlet (W_{PGin}) is calculated to be 0.517 kg. As it is assumed that UL_{PG} = 0, the weight of ground pellets at the boiler inlet per f.u. is also 0.517 kg.

8.4.3 Boiler Output Streams

8.4.3.1 Ash Disposal from the Power Station

The ash content of the bagasse is 6.04% (Section 8.3.5). Using this value and Equation (8.3), the amount of ash to be disposed from the boiler per f.u. in kg (W_{ash2}) can be calculated by Equation (8.5). With the previous assumption that UL_{PG} = 0, it can be simplified to Equation (8.6).

$$W_{ash2} = W_{Bin}\cdot 6.04\%$$

$$W_{ash2} = \frac{W_{PGin}}{UL_{PG}+1}\cdot 6.04\%$$

$$W_{ash2} = \frac{3.6}{HHV\cdot eff - GE\cdot UL_{PG} - GE}\cdot 6.04\%$$

$$W_{ash2} = \frac{0.217}{HHV\cdot eff - GE\cdot UL_{PG} - GE} \tag{8.5}$$

$$W_{ash2} = \frac{0.217}{HHV\cdot eff - GE} \tag{8.6}$$

Where W_{ash2} is the amount of ash to be disposed from the boiler per f.u. (kg)

Using Equation (8.6), the amount of ash to be disposed from the boiler per f.u. in kg (W_{ash2}) is calculated to be 0.0312 kg.

8.4.3.2 Emissions from the Boiler

The amount of CO_2 released from the combustion of bagasse was calculated through the carbon (C) content of bagasse. To estimate this, six literature sources (Asadullah et al., 2007; Kanwal et al., 2019; Manatura, 2020; Munir et al., 2009; Valix et al., 2017; Varma & Mondal, 2016) of ultimate analysis of bagasse were consulted. In these sources, seven bagasse samples were analysed. The C contents (dry basis) of 5 samples are in the range of 43.79-48.58% and two samples had lower carbon contents of 38.3% and 32.5%. This shows a degree of variability in the carbon content of bagasse from different sources. In the present study, 42.84% (dry basis) is used as the carbon content of bagasse, which is the average value from the six sources consulted. As the bagasse pellets have a moisture content of 6.00% when combusted in the power plant boiler, the wet basis C content is calculated to be 40.42% for the power plant boiler.

As the boiler input was calculated to be 0.517 kg of ground pellets per f.u. (Section 8.3.3), the amount of CO_2 emitted from the boiler per f.u. is calculated to be 0.766 kg, assuming complete carbon burnout.

The amount of CO_2 released during combustion was calculated for completeness, but it is not included in the calculation of the overall carbon footprint of the system, as it is not considered a global warming contributor as it is a part of the carbon cycle and therefore considered to be carbon neutral (Kiatkittipong et al., 2009).

8.4.4 Pellet Cooler and Transport to the UK

8.4.4.1 Pellet Cooler

The relationship between the streams at the pellet cooler inlet, pellet cooler outlet and unrecoverable losses at stream 21 can be represented by Equation (8.7).

$$W_{PGin} = W_{PCout} - W_{PCout} \cdot UL_{21}$$

$$W_{PCout} = \frac{W_{PGin}}{1 - UL_{21}} \tag{8.7}$$

Where W_{PCout} is the weight of the pellets per f.u. at the pellet cooler outlet in kg; UL_{21} is the unrecoverable losses represented by stream 21 in the process flow diagram (%).

8.4.4.2 Unrecoverable losses

The unrecoverable losses from the pellet cooler, transport to the UK and storage at the power station are combined into stream 21 in the process flow diagram (Figure 8-1). The total unrecoverable losses represented by stream 21 (UL_{21}) can be expressed as a function of its components, shown in Equation (8.8).

$$UL_{21} = 1 - (1 - UL_{PC})(1 - UL_T)(1 - UL_{PSS}) \tag{8.8}$$

Where UL_{PC} is the unrecoverable losses from the pellet cooler (%), UL_T is the unrecoverable losses from transport to the UK (%), UL_{PSS} is the unrecoverable losses from the power station storage (%)

All three components of the unrecoverable losses represented by UL_{21} are assumed to be zero, but they are included here for completeness.

With this assumption, the weight of the material at the pellet cooler inlet per f.u. (W_{PCin}) is calculated to be 0.517 kg, using the relationship shown in Equation (8.9).

$$W_{PCin} = W_{PCout} = W_{PGin} = 0.517 \text{ kg} \tag{8.9}$$

Where W_{PCin} is the weight of the pellets per f.u. at the pellet cooler inlet in kg.

8.4.5 Pelletiser

8.4.5.1 Pelletiser Unrecoverable losses

The relationship between the streams at the pellet cooler inlet, pelletiser outlet and unrecoverable losses from the pelletiser can be represented by Equation (8.10).

$$W_{PCin} = W_{Pout} - W_{Pout} \cdot UL_P$$

$$W_{Pout} = \frac{W_{PCin}}{1 - UL_P} \tag{8.10}$$

Where W_{Pout} is the weight of the pellets per f.u. at the pelletiser outlet in kg; UL_P is the unrecoverable losses from the pelletiser (%).

The unrecoverable losses from the pelletiser are 1.00% (Section 8.3.6). Using this figure and Equation (8.10), the weight of the pellets per f.u. at the pelletiser outlet is calculated to be 0.522 kg. The unrecoverable losses at the pelletiser are also calculated to be 0.005 kg per f.u.

8.4.5.2 Moisture Content Reduction in the Pelletiser

The pelletiser processes the dried and mill material into pellets while reducing the moisture content from 10.5% to 6.00%. Thus, the relationship between the weight of the material at the pelletiser inlet and the weight of pellets at the pelletiser outlet can be represented by Equation (8.11).

$$W_{Pin} \times (1 - M_{Pin}) = W_{Pout} \times (1 - M_{Pout})$$

$$W_{Pin} = \frac{W_{Pout} \times (1 - M_{Pout})}{1 - M_{Pin}} \tag{8.11}$$

Where W_{Pin} is the weight of the material per f.u. at the pelletiser inlet in kg; M_{Pin} is the moisture content of the material at the pelletiser inlet (%); M_{Pout} is the moisture content of the pellets at the pelletiser outlet (%).

Using W_{Pout} = 0.522 kg, M_{Pout} = 6.00% and M_{Pin} = 10.5%, the weight of the material per f.u. at the pelletiser inlet (W_{Pin}) is calculated to be 0.548 kg.

8.4.6 Hammermill

8.4.6.1 Hammermill Unrecoverable Losses

The relationship between the streams at the pelletiser inlet, hammermill outlet and unrecoverable losses from the hammermill can be represented by Equation (8.12).

$$W_{Pin} = W_{HMout} - W_{HMout} \cdot UL_{HM}$$

$$W_{HMout} = \frac{W_{Pin}}{1 - UL_{HM}} \tag{8.12}$$

Where W_{HMout} is the weight of the material per f.u. at the hammermill outlet in kg; UL_{HM} is the unrecoverable losses from the hammermill (%).

The unrecoverable losses from the hammermill are 1.00% (Section 8.3.6). Using W_{PMin} = 0.548 kg, UL_{HM} = 1.00% and Equation (8.12), the weight of the material per f.u. at the hammermill outlet (W_{HMout}) is calculated to be 0.554 kg. The unrecoverable losses at the hammermill per f.u. (W_{13}) is also calculated to be 0.006 kg.

8.4.6.2 Moisture Content Reduction in the Hammermill

The hammermill reduces the particle size of the material while also reducing the moisture content from 11.50% to 10.50% (Section 8.4.1). Thus, the relationship between the weight of the material at the hammermill inlet and the weight of the pellets at the pelletiser outlet can be represented by Equation (8.13).

$$W_{HMin} \times (1 - M_{HMin}) = W_{HMout} \times (1 - M_{HMout})$$

$$W_{HMin} = \frac{W_{HMout} \times (1 - M_{HMout})}{1 - M_{HMin}} \quad (8.13)$$

Where W_{HMin} is the weight of the material per f.u. at the hammermill inlet in kg; M_{HMin} is the moisture content of the material at the hammermill inlet (%); M_{HMout} is the moisture content of the material at the hammermill outlet (%).

Using W_{HMout} = 0.554 kg, M_{HMout} = 10.50% and M_{HMin} = 11.50%, the weight of the material per f.u. at the hammermill inlet (W_{HMin}) is calculated to be 0.560 kg.

8.4.7 Dryer and Furnace

8.4.7.1 Dryer Outlet and Furnace Feed

The moisture content at the dryer outlet and furnace feed is 12.00% (Section 8.4.1). Some additional moisture is lost before the material is fed to the hammermill, resulting in a moisture content of 11.50% at the hammermill inlet (Section 8.4.1). The relationship between these streams is represented by Equation (8.14).

$$(W_{Dout} - W_{Dout} \cdot X_F)(1 - M_{Dout}) = W_{HMin} \cdot (1 - M_{HMin})$$

$$W_{Dout} = \frac{W_{HMin} \cdot (1 - M_{HMin})}{(1 - X_F)(1 - M_{Dout})} \quad (8.14)$$

Where W_{Dout} is the weight of the material per f.u. at the dryer outlet in kg; X_F is the fraction of the dryer outlet diverted to fuel the furnace (Section 8.3.7); M_{Dout} is the moisture content of the material at the dryer outlet (%).

Using W_{HMin} = 0.560 kg, M_{HMin} = 11.50%, X_F = 23.0% and M_{Dout} = 12.00%, the weight of the material per f.u. at the dryer outlet (W_{Dout}) is calculated to be 0.731 kg. The weight of the material supplied to the furnace per f.u. is also calculated to be 0.168 kg.

8.4.7.2 Moisture Content Reduction in the Dryer

The dryer reduces the moisture content of the material from 50.00% to 12.00% (Section 8.4.1). Thus, the relationship between the weight of the material at the dryer inlet and outlet can be represented by Equation (8.15).

$$W_{Din} \times (1 - M_{Din}) = W_{Dout} \times (1 - M_{Dout})$$

$$W_{Din} = \frac{W_{Dout} \times (1 - M_{Dout})}{1 - M_{Din}} \quad (8.15)$$

Where W_{Din} is the weight of the material per f.u. at the dryer inlet in kg; M_{Din} is the moisture content of the material at the dryer inlet (%); M_{Dout} is the moisture content of the material at the dryer outlet (%).

Using W_{Dout} = 0.731, MS_{Dout} = 12.00% and MS_{Din} = 50.00%, the weight of the material per f.u. at the dryer inlet (W_{Din}) is calculated to be 1.287 kg.

8.4.7.3 Furnace Output Streams

8.4.7.3.1 Ash Disposal from the Furnace

The ash content of the bagasse is 6.04% and the weight of the material supplied to the furnace per f.u. is 0.168 kg. The amount of ash produced by the furnace is calculated to be 10.1 g per f.u.

8.4.7.3.2 Emissions from the Furnace

Only carbon dioxide (CO_2) emissions are considered in this study. Other emissions, including but not limited to sulphur dioxide, carbon monoxide and particulates, are

of relatively minor importance with regard to climate change impact and thus are not considered.

As in Section 8.4.3.2, 42.84% (dry basis) is used as the carbon content of bagasse. As the bagasse has a moisture content of 12.00% when combusted in the pellet plant furnace (Section 8.4.1), the wet basis C content is calculated to be 38.25% for the pellet plant furnace.

As the furnace input was calculated to be 0.168 kg per f.u., the amount of CO_2 emitted from the boiler per f.u. can be calculated to be 0.236 kg, assuming complete carbon burnout. As in Section 8.4.3.2, the amount of CO_2 released during combustion is calculated for completeness, but it is not included in the calculation of the overall carbon footprint of the system, as it is not considered a global warming contributor as it is a part of the carbon cycle and therefore considered to be carbon neutral (Kiatkittipong et al., 2009).

8.4.8 Pellet Plant Storage and Fuel Supply

The relationship between the streams at the pellet plant feed, storage outlet (equal to dryer inlet) and unrecoverable losses from storage can be represented by Equation (8.16).

$$W_{Din} = W_{feed} - W_{feed} \cdot UL_{PPS}$$

$$W_{feed} = \frac{W_{Din}}{1 - UL_{PPS}} \quad \textbf{(8.16)}$$

Where W_{feed} is the weight of the material per f.u. at the pellet plant feed in kg; UL_{PPS} is the unrecoverable losses from the pellet plant storage (%).

The unrecoverable losses from the pellet plant storage are 1.00% (Section 8.3.6). Using W_{Din} = 1.287 kg, UL_{PPS} = 1.00% and Equation (8.16), the weight of the material per f.u. at the pellet plant feed (W_{feed}) is calculated to be 1.300 kg. The unrecoverable losses at the pellet plant storage per f.u. (W_3) is also calculated to be 0.013 kg.

8.4.9 Stream Table (Material Streams)

The parameters of all material streams, as calculated by mass balance, are shown in Table 8-5.

Stream*	Material	Amount per f.u. (kg)	Moisture content (%)	Notes
1	Raw bagasse	1.300 (W_{feed})	50.0	
2	Raw bagasse	1.287 (W_{Din})	50.0	
3	Pellet plant storage unrecoverable losses (raw bagasse)	0.013 (W_3)	50.0	
4	Dried bagasse	0.731 (W_{Dout})	12.0	
5	Dried bagasse at the hammermill inlet	0.560 (W_{HMin})	11.5	
6	Dried bagasse feeding the furnace	0.168 (W_{Fin})	12.0	
8	Bagasse ash	0.0101		
9	Emissions from the furnace	0.236	N/A	CO_2, assumed complete carbon burnout
11	Milled bagasse	0.554 (W_{HMout})	10.5	
12	Milled bagasse	0.548 (W_{PMin})	10.5	
13	Hammermill unrecoverable losses (milled bagasse)	0.006 (W_{13})	10.5	
15	Hot bagasse pellets	0.522 (W_{PMout})	6.0	
16	Hot bagasse pellets	0.517 (W_{PCin})	6.0	
17	Pelletiser unrecoverable losses	0.005 (W_{17})	6.0	

19	Cooled bagasse pellets	0.517 (W_{PCout})	6.0	
20	Cooled bagasse pellets	0.517 (W_{PGin})	6.0	
21	Unrecoverable losses from the pellet cooler, transport to the UK and storage at the power station	0	6.0	
23	Ground bagasse pellets	0.517 (W_{PGout})	6.0	$W_{PGin} = W_{PGout}$
24	Ground bagasse pellets	0.517 (W_{Bin})	6.0	
25	Pellet grinder unrecoverable losses	0	6.0	
27	Bagasse ash	0.0312 (W_{ash2})		
28	Emissions from the boiler	0.766	N/A	CO_2, assumed complete carbon burnout

*Stream numbers refer to the numbers shown in Figure 8-1

Table 8-5 Stream table with properties of each stream (material streams)

8.5 Energy Streams

The properties of each energy stream are specified in this Section and listed in Table 8-6.

8.5.1 Heat Supplied to the Dryer from the Furnace

According to data supplied by the industrial partner, the heat supplied to the dryer from the furnace per f.u. is 1.93 MJ.

8.5.2 Hammermill Electricity Input

The electricity input requirement for the hammermill depends on multiple factors, including the mill settings, material properties and the degree of particle size

reduction. Therefore, this value cannot be determined precisely without knowledge of the exact mill settings to be used in the plant. Based on literature sources, this is estimated to be 0.163 MJ/kg (45.3 kWh/t), which is the value used by Munagala et al. (2021) in a life cycle analysis study of lactic acid production from bagasse. This value is also consistent with those reported by Bitra, Womac, Chevanan, et al. (2009) for hammermilling of switchgrass, wheat straw and corn stover, which are in the range of 28.8-47.7 kWh/t. As the hammermill input (stream 5) was calculated to be 0.560 kg per f.u. (Table 8-5), the electricity input requirement for the hammermill per f.u. is calculated to be 0.0912 MJ.

8.5.3 Pelletiser Electricity Input

The electricity input requirement for the pelletiser is assumed to be 0.309 MJ/kg, based on the technical specification of a Ceccato Olindo pellet machine (rated power of 3kW with a maximum throughput of 35 kg/hr) (Ceccato Olindo srl, n.d.). This value is also consistent with those used by Kylili et al. (2016) for olive husks (0.225-0.317 MJ/kg) and by Adapa et al. (2013) for agricultural straws (0.297-0.440 MJ/kg). As the pelletiser input (stream 12) was calculated to be 0.548 kg per f.u. (Table 8-5), the electricity input requirement for the pelletiser per f.u. is calculated to be 0.169 MJ.

8.5.4 Pellet Grinder Electricity Input

The pellet grinding energy for bagasse is 0.108 MJ/kg (Section 8.3.3), and the weight of pellets per f.u. at the pellet grinder inlet was calculated to be 0.517 kg (Table 8-5). Therefore, the electricity input to the pellet grinder per f.u. is 0.0560 MJ.

8.5.5 Pellet cooler Electricity Input

The electricity input requirement for the pellet cooler is assumed to be 3.24 kJ/kg, based on the value used by Fantozzi & Buratti (2010) in an LCA study of a wood pellet plant. The usage of this value for bagasse is justified by the similarity in heat capacity of many biomass materials, as demonstrated by Dupont et al. (2014). As the pellet cooler input stream was calculated to be 0.517 kg per f.u. (Table 8-5), the electricity input requirement for the pellet cooler per f.u. was calculated to be 1.68 kJ.

8.5.6 Stream Table (Energy Streams)

The parameters of all energy streams are shown in Table 8-6.

Stream	Process	Type	Amount per f.u. (kJ)	Source	Note
7	Furnace, Dryer	Heat	1930	Industrial partner, Calculation	
10	Hammermill	Electricity	91.2	(Munagala et al., 2021)	
14	Pelletiser	Electricity	169	(Ceccato Olindo srl, n.d.)	
18	Pellet Cooler	Electricity	1.68	(Fantozzi & Buratti, 2010)	
22	Boiler, Pellet grinder	Electricity	56.0	Calculation	
26	Boiler, Electricity grid	Electricity	3600	Functional Unit	Equal to 1 kWh

Table 8-6 Stream table with properties of each stream (energy streams)

8.6 Carbon Footprint of Ash Disposal

In this study, it is assumed that ash from the pellet plant furnace and power plant boiler is disposed of in a landfill. The ecoinvent database was used to estimate the carbon footprint of ash disposal as 1.868×10^{-2} kg CO_2 eq./kg (ecoinvent, n.d.). This value is for wood ash sent to a landfill, as database values specifically for bagasse are not available.

8.7 Carbon Footprint of Pellet Plant Electricity Use

The electricity inputs for the hammermill, pelletiser and pellet cooler were calculated in Section 8.4. The total electricity use per f.u. is 0.262 MJ. As the pellet plant is located in Louisiana, the eGRID data for SRMV (SERC Mississippi Valley subregion) (US

EPA, 2021) was used to estimate the carbon footprint of pellet plant electricity use. This value is 772.7 lbs CO_2 eq./MWh, or 0.215 kg CO_2 eq./MJ.

8.8 Carbon Footprint of Transport

As previously defined (Section 8.2.1), it is assumed that the mean driving distance from the sugar mills to the pellet plant is 20 km, and the driving distance from the pellet plant to the port in the US is 100 km. The material is assumed to be transported by diesel trucks, and the corresponding entry in the GREET database for the carbon footprint is 0.0488 kg CO_2 eq./ton-km, or 4.88 $x10^{-5}$ kg CO_2 eq./kg-km (M. Wang et al., 2023). The shipping distance between the origin and destination ports is 9000 km (Section 8.2.1). The corresponding entry in the ecoinvent database for the carbon footprint of shipping is $4.110x10^{-6}$ kg CO_2 eq./kg-km (ecoinvent, n.d.). The distance between the destination port and the power station is 80 km (Section 8.2.1). The corresponding entry in the ecoinvent database for the carbon footprint of rail transport is $3.694x10^{-5}$ kg CO_2 eq./kg-km (ecoinvent, n.d.).

8.9 Overall Findings and Conclusion

The calculated carbon footprint of the overall system and constituent processes are summarised in Table 8-7. The amount of CO_2 released during combustion is not included in the calculation of the overall carbon footprint of the system, as it is not considered a global warming contributor as it is a part of the carbon cycle and therefore considered to be carbon neutral (Kiatkittipong et al., 2009). It is shown in Figure 8-2 that the main components of the system carbon footprint are pelletiser and pellet cooler electricity use, transport from the pellet plant to the power station, and hammermill electricity use.

It could also be valuable to quantify the carbon footprint with the functional units of each kg and each MJ equivalent of pellets produced at the factory gate (not including transport from the pellet plant to the power station and subsequent downstream processes). For each kWh of electricity generated at the power plant, 0.517 kg of pellets (stream 19, see Table 8-5) is produced at the pellet plant and the total carbon footprint at the factory gate is 57.8 g CO_2 eq/kWh (see Table 8-7). Therefore, the carbon footprint at the factory gate is 111.8 g CO_2 eq/kg of pellets produced. Since the HHV of bagasse pellets is assumed to be 18 MJ/kg (Section 8.3.4), the carbon

footprint at the factory gate can also be expressed in terms of the energy content of the pellets produced as 6.21 g CO_2 eq/MJ.

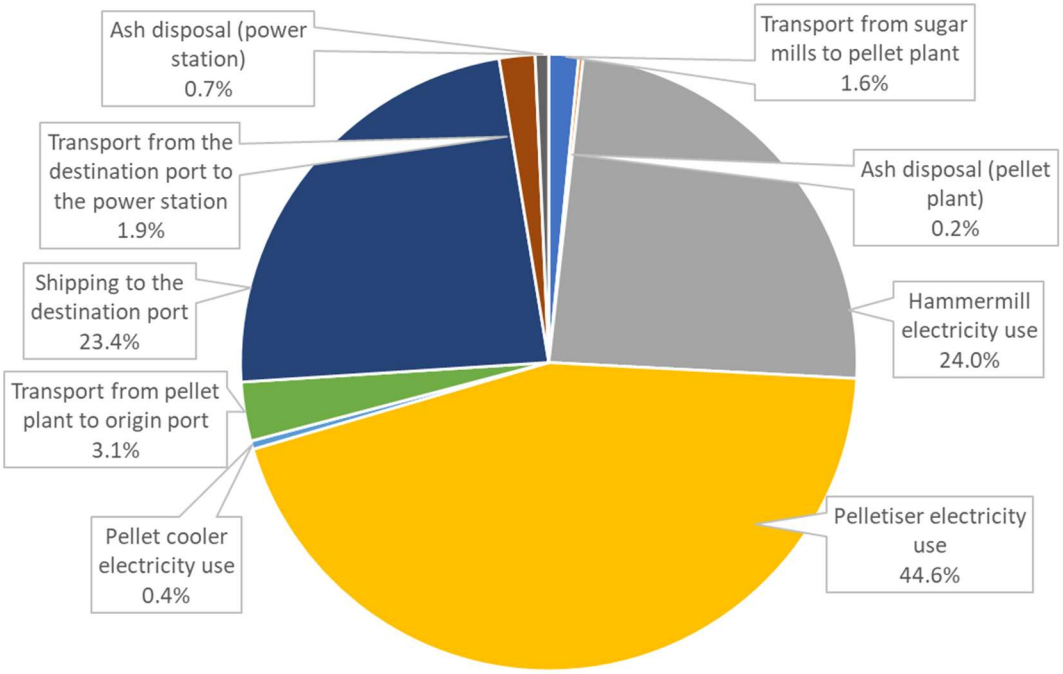

Figure 8-2 Carbon footprint of the system processes

This LCA has filled a knowledge gap in the existing literature by evaluating a system involving the international transport and use of bagasse (see Section 2.10.2). The total carbon footprint of the system was calculated to be 81.6 g CO_2 eq/kWh, compared to 1003 g CO_2 eq./kWh for coal power generation in the UK in 2022 (from GREET database) (M. Wang et al., 2023) and 162 g CO_2 eq./kWh for the UK electricity mix in 2023 (Evans & Viisainen, 2024). The main opportunities of reducing carbon emissions are the electricity use at the pellet plant and shipping between the origin port and the destination port, which together, makes up 92.4% of the overall carbon footprint.

Overall, the results of the model show that substantial benefits in terms of global warming potential could be achieved by transporting and using bagasse from the United States to generate power in the UK, compared to both electricity generation from coal and the current electricity mix. There is the additional potential to integrate carbon capture and storage to capture the majority of the amount of CO_2 emitted from the UK power plant (766 g CO_2 eq/kWh, see Table 8-7) and deliver negative

emissions. Lastly, modifications of the model could be made to compare the performance of different types of type of biomass, pellet plant configuration, and transport options.

Process	Footprint (g CO_2/kWh)	% of total
Transport from sugar mills to pellet plant	1.27	1.6%
Combustion in the pellet plant (not included in the total)	236	N/A
Ash disposal (pellet plant)	0.19	0.2%
Hammermill electricity use	19.6	24.0%
Pelletiser electricity use	36.4	44.6%
Pellet cooler electricity use	0.36	0.4%
Transport from pellet plant to origin port	2.52	3.1%
Shipping to the destination port	19.1	23.4%
Transport from the destination port to the power station	1.53	1.9%
Combustion in the power station (not included in the total)	766	N/A
Ash disposal (power station)	0.58	0.7%
Total	81.6	100.00%
Transport total	24.4	29.9%
Pellet plant electricity use total	56.6	69.4%
Ash disposal total	0.78	1.0%
Total at factory gate	57.8	70.9%
Total biogenic CO_2 released from combustion (not included in the total)	1001	N/A

Table 8-7 Carbon footprint of the overall system and constituent processes

Chapter 9 - Conclusions and Future Work

9.1 Biomass Characterisation

Through the experimental characterisation of several conventional and alternative biomass feedstocks, some of the challenges of using these alternative biomass feedstocks were illustrated, with high ash content and low calorific value being among the main issues. The characterisation data presented in this Chapter can be used as a basis for further research of these biomass feedstocks by future researchers.

9.2 Cardboard Characterisation

The characteristics of cardboard materials relevant for the power industry were analysed in detail, including the differences in the different types of cardboard, the potential impact of fillers, char morphology, burnout performance and particle shape change during combustion. The challenges and opportunities for using cardboard for power generation were identified. For example, milled cardboard materials are likely to have severe handling challenges, while cardboard chars have superior burnout performance and the calcium carbonate present in cardboard materials may be beneficial for tackling slagging issues. In addition, a new method of using thermogravimetric analysis to measure calcium carbonate content, the most important filler in cardboard, was developed. This new method can be used by both academia and industry to identify and quantify calcium carbonate content, which also has the advantage of being integrated into proximate analysis, a routine characterisation technique already commonly carried out for biomass.

9.3 Pasteurisation and Natural Drying Process

The feasibility of a new novel combined pasteurisation and natural drying process was established, which can dramatically decrease the drying energy of biomass by suppressing fungal growth, allowing materials to be stored for set periods, during which natural evaporation would occur. A range of pasteurisation conditions using both conventional oven and microwaves was investigated. It was found that an appropriate pasteurisation process could extend the storage period of biomass by suppressing microbial and fungal growth, during which natural drying would occur

without additional energy input. The results have also provided insights into the optimal pasteurisation conditions and storage strategies.

9.4 Sugarcane Straw Pelleting and Pellet Milling

The pelleting and pellet milling behaviour of sugarcane straws was investigated in detail. New parameters were developed to quantify the pelleting process, including average pelleting power, pelleting efficiency and pellet production rate. The influence of moisture content, harvest season and particle size on pellet quality and pelleting and pellet milling behaviour was studied. Large changes in particle size and shape were observed during pelleting, whereas only small changes were observed during pellet milling. Thus, pelleting processes need to be designed to ensure output particles size is close to the optimal sizes desired for combustion.

9.5 Life Cycle Analysis of Power Generation from Bagasse

An in-depth life cycle analysis (LCA) study of a biomass power generation system using sugarcane bagasse from the US for power generation in the UK was conducted. The processes considered in the LCA model include the collection of bagasse from sugar mills, processing and pelleting of the raw material, transport to the power station and combustion. The overall carbon footprint of the system was calculated. It was found that substantial benefits in terms of global warming potential could be achieved by the system studied, and negative emissions could be achieved by the integration of carbon storage and capture.

9.6 Overall Results

In summary, this thesis has presented valuable studies covering several important aspects of biomass pelleting for biomass power generation, including the characterisation of non-conventional feedstocks, the development of a combined pasteurisation and natural drying process, the pelleting and pellet milling behaviour of sugarcane straw, and the life cycle analysis of a power generation from bagasse.

Chapter 4 and 5 has enhanced the understanding of unconventional biomass feedstocks, in particular cardboard materials. It was found that cardboard materials could cause severe handling challenges but also have superior burnout performance compared to eucalyptus. The high calcium carbonate content of cardboard materials also indicate that there is potential for blending cardboard with other fuels to tackle

slagging issues. Through the study of particle shape change, it was also found that char production methods that uses a faster heating rate (such as a drop-tube furnace) would result in a greater change in particle sphericity and aspect ratio compared to methods that uses a slower heating rate (such as a muffle furnace).

Chapter 6 demonstrated that combined pasteurisation and natural drying is a valid concept to dramatically reduce the drying energy of biomass, with miscanthus and spent grains used for the experiments in this Chapter. Through a process including briquetting, pasteurisation and storage for up to 9 weeks, it was shown that through using optimised pasteurisation conditions, fungal growth can be sufficiently suppressed to allow biomass briquettes to be stored for extended periods for the natural drying of the material to occur without any additional energy input. It was found that natural drying could reduce the moisture content to 10-11% after three weeks of storage for miscanthus briquettes and to 12-14% after nine weeks of storage for spent grains briquettes. In addition, microwave pastuerisation could achieve similar of better levels of fungal growth suppression with shorter process times compared to conventional oven pasteurisation, with 'high power, short duration' being a more effective microwave pasteurisation configuration compared to 'low power, long duration'.

Chapter 7 presented an in-depth study of the pelleting and pellet milling behaviour of sugarcane straw. It was found that pelleting failure is more likely to occur at low moisture contents, at fine particle sizes and with the dry season sample. It was also found that higher throughputs could be achieved for fine particle sizes, although pelleting failure may be more likely to occur. The influence of feed moisture content, harvest season and particle size on pellet quality was studied. In particular, bulk density, an important pellet property which relates to transport costs, was found to be highly dependent on feed moisture content but not on other factors. The experimental design also allowed that changes in particle size and shape to be tracked throughout the entire journey of pelleting and pellet milling. It was found that a significant change in particle size and shape occurs during pelleting, while pellet milling typically breaks down the pellets into their constituent particles with limited further change in particle size and shape.

Chapter 8 presented the life cycle analysis (LCA) of a biomass power generation system using sugarcane bagasse from the US to generate power in the UK.

The total carbon footprint of the system was calculated to be 81.6 g CO_2 eq/kWh. At the factory gate, the carbon footprint was calculated to be 111.8 g CO_2 eq/kg of pellets produced or 6.21 g CO_2 eq/MJ in terms of the energy content of the pellets. The main opportunities of reducing carbon emissions are the electricity use at the pellet plant and shipping between the origin port and the destination port, which together, makes up 92.4% of the overall carbon footprint.

Overall, the findings presented in this thesis have contributed to the understanding of and the development of solutions to several major challenges of the biomass power generation industry. A comprehensive literature review of the existing knowledge of topics relevant to the thesis was conducted. Several new analytical techniques were also developed in the research project, including the introduction of a new method to quantify the calcium carbonate content of materials based on thermogravimetric analysis and the introduction of new pelleting parameters to quantify the pelleting process. The characterisation of several conventional and alternative biomass feedstocks was conducted and the implications for their use for power generation were analysed. A novel low-energy biomass drying solution was developed in the form of a combined pasteurisation and natural drying process, and the pelleting and pellet milling behaviour of sugarcane straw was studied in detail. Lastly, LCA was used to study biomass power generation from bagasse from a system perspective, and the environmental performance of such a system was evaluated.

9.7 Directions for Further Research

This research project has produced multiple results that are of substantial value to academia and industry. Based on these findings, avenues for future work that will provide further value have also been identified.

The accuracy of the new method for measuring calcium carbonate content based on thermogravimetric analysis (presented in Section 5.6.1) should be further established by comparing it with other methods, such as mineral liberation analysis (MLA) as conducted by Gräbner & Lester (2016). It is also proposed that the new method can

be further improved by adding CO_2 cycling at the end of the slow pyrolysis procedure, involving the following steps:

1. Switch gas to CO_2
2. Ramp temperature down from 900°C to 400°C
3. Hold temperature for 20 minutes
4. Switch gas to nitrogen
5. Ramp temperature up from 400°C to 900°C
6. Hold temperature for 20 minutes
7. Repeat the procedure several times

The addition of a CO_2 cycling procedure could potentially improve the accuracy of the calcium carbonate content measurement, as any weight change observed during the cycling procedure would be solely caused by the reactions of interest (the decomposition of calcium carbonate or the absorption of carbon dioxide by calcium oxide) and any inaccuracies caused by the presence of volatiles or fixed carbon in the sample would be eliminated.

Other avenues for further research relevant to the work presented in Chapter 5 (Cardboard Characterisation) include:

- Further study on the possible causes of the phenomenon of severe agglomeration observed in milled cardboard
- Investigate whether alternative size reduction methods such as wet milling can mitigate handling challenges
- Carry out additional analysis such as ash fusion tests to further study the slagging/fouling potential of cardboard materials
- Collaborate with manufacturers of cardboard to investigate how specific manufacturing methods may affect combustion

Avenues for further research relevant to the work presented in Chapter 6 (Pasteurisation and Natural Drying Process) include:

- The present study has used a hand-operated briquette maker due to budgetary constraints. Future studies to further develop the proposed drying

solution can use briquetting machines to make better-quality and more consistent briquettes.

- The present study has mainly focused on the relative effectiveness of pasteurisation conditions. Future studies should also investigate the effect of storage conditions and methods on fungal growth.
- The present study has used indoor storage in a controlled environment, where the opportunities for new spores to land on the samples were limited and the fungal growth observed was likely primarily from spores already present on the sample at the beginning of the storage period. Future studies should consider using outdoor storage during the natural drying stage of the experiment.
- Further research should be conducted on the mechanisms causing briquette expansion during pasteurisation.
- Further research should be conducted on the relationship between storage temperature, relative humidity and drying rate.
- Investigate the potential of enhanced natural drying such as solar drying
- Use image analysis techniques to quantify the coverage of fungi on biomass briquettes as an alternative method to measure fungal growth
- Metagenomic analysis to study the exact species of microorganisms present on the biomass briquettes and identify if these are ones of concern or are benign
- Combining different pasteurisation techniques (e.g. using both conventional oven and microwave pasteurisation series) could have synergistic effects (Raso & Barbosa-Cánovas, 2003) and should be investigated in future studies
- Further research is required to optimise the microwave pasteurisation process to avoid charring.
- Further research is required to explore how the thermal conductivity of biomass briquettes influences the pasteurisation process.

Avenues for further research relevant to the work presented in Chapter 7 (Sugarcane Straw Pelleting and Pellet Milling) include:

- In the present study, pellet shape was characterised by measurement of diameter and length. Although this is a commonly used method, it does not fully describe the shape of pellets as it was observed that some pellets had a curved shape. Future studies should consider the use of automated image analysis (such as Camsizer) to fully characterise pellet shape.
- Future studies should include temperature measurement during pelleting experiments, as temperature is known to cause glass transitions in some biomasses which could aid or inhibit the pelleting process (Williams et al., 2017)

The life cycle analysis (LCA) model presented in Chapter 8 could be further extended to include the following elements:

1. Sensitivity analysis of the model to various input parameters
2. Technoeconomic analysis of part or all of the system
3. Modification of the model for other types of conventional and alternative biomass feedstocks to compare their environmental performance
4. Modification of the model to include torrefaction to quantify its potential benefits
5. Modification of the model to quantify the potential benefits of integrating carbon capture into the system

References

Adapa, P. K., Tabil, L. G., & Schoenau, G. J. (2013). Factors affecting the quality of biomass pellet for biofuel and energy analysis of pelleting process. *International Journal of Agricultural and Biological Engineering*, *6*(2), Article 2. https://doi.org/10.25165/ijabe.v6i2.779

Afilaka, D. T. (2016). *Avoiding the sintering of coal fired shallow fluidized beds* [Thesis (University of Nottingham only), University of Nottingham]. https://eprints.nottingham.ac.uk/33534/

Ali, U., Font-Palma, C., Akram, M., Agbonghae, E. O., Ingham, D. B., & Pourkashanian, M. (2017). Comparative potential of natural gas, coal and biomass fired power plant with post—Combustion CO2 capture and compression. *International Journal of Greenhouse Gas Control*, *63*, 184–193. https://doi.org/10.1016/j.ijggc.2017.05.022

Almeida, L. F. P. de, Sola, A. V. H., & Behainne, J. J. R. (2017). Sugarcane bagasse pellets: Characterization and comparative analysis. *Acta Scientiarum. Technology; Maringa*, *39*(4), 461–468. http://dx.doi.org.ezproxy.nottingham.ac.uk/10.4025/actascitechnol.v39i4.30198

Ambrose, J. (2024, January 18). Fury at plan to extend Drax subsidy to burn trees for electricity. *The Guardian*. https://www.theguardian.com/business/2024/jan/18/ministers-propose-extra-drax-subsidy-burn-trees-electricity-biomass

Andritz. (2022). Andritz to supply biomass handling plant for project in Brazil | Biomass Magazine. *Biomass Magazine*. https://biomassmagazine.com//articles/andritz-to-supply-biomass-handling-plant-for-project-in-brazil-19265

Asadullah, M., Rahman, M. A., Ali, M. M., Rahman, M. S., Motin, M. A., Sultan, M. B., & Alam, M. R. (2007). Production of bio-oil from fixed bed pyrolysis of bagasse. *Fuel*, *86*(16), 2514–2520. https://doi.org/10.1016/j.fuel.2007.02.007

ASTM. (2021). *ASTM D4373-21 Standard Test Method for Rapid Determination of Carbonate Content of Soils*. https://www.astm.org/d4373-21.html

Austrian Standards Institute. (2000). *ÖNORM M 7135—Compressed wood or compressed bark in natural state—Pellets and briquettes—Requirements and test specifications (Austrian Standard)*. https://webstore.ansi.org/standards/on/onorm71352000

Avila, C., Pang, C. H., Wu, T., & Lester, E. (2011). Morphology and reactivity characteristics of char biomass particles. *Bioresource Technology*, *102*(8), 5237–5243. https://doi.org/10.1016/j.biortech.2011.01.071

Azapagic, A. (2010). *CCaLC: Carbon Calculations over the Life Cycle of Industrial Activities* [Computer software]. https://research.manchester.ac.uk/en/projects/ccalc-carbon-calculations-over-the-life-cycle-of-industrial-activ

Barbash, V. A., & Yashchenko, O. V. (2020). Preparation and application of nanocellulose from non-wood plants to improve the quality of paper and cardboard. *Applied Nanoscience*, *10*(8), 2705–2716. https://doi.org/10.1007/s13204-019-01242-8

Barbosa-Cánovas, G., & Bermúdez-Aguirre, D. (2010). Other novel milk preservation technologies: Ultrasound, irradiation, microwave, radio frequency, ohmic heating, ultraviolet light and bacteriocins. In M. W. Griffiths (Ed.), *Improving the Safety and Quality of Milk* (pp. 420–450). Woodhead Publishing. https://doi.org/10.1533/9781845699420.4.420

Beagle, E., & Belmont, E. (2019). Comparative life cycle assessment of biomass utilization for electricity generation in the European Union and the United States. *Energy Policy*, *128*, 267–275. https://doi.org/10.1016/j.enpol.2019.01.006

Bharadwaj, A., Baxter, L. L., & Robinson, A. L. (2004). Effects of Intraparticle Heat and Mass Transfer on Biomass Devolatilization: Experimental Results and Model Predictions. *Energy & Fuels*, *18*(4), 1021–1031. https://doi.org/10.1021/ef0340357

Biermann, C. J. (1996). *Handbook of Pulping and Papermaking*. Elsevier Science & Technology. http://ebookcentral.proquest.com/lib/nottingham/detail.action?docID=305584

Biofuelwatch. (2018, April 11). *Biomass Basics*. https://www.biofuelwatch.org.uk/2018/biomass-basics-2/

Biofuelwatch. (2024, February 28). *Logging what's left: How Drax's pellet mills are sourcing logs from British Columbia's rarest Old Growth forests*. https://www.biofuelwatch.org.uk/2024/drax-bc-pellets-investigation/

Birla, S. L., & Pitchai, K. (2017). Simulation of microwave processes. In M. Regier, K. Knoerzer, & H. Schubert (Eds.), *The Microwave Processing of Foods (Second Edition)* (pp. 407–431). Woodhead Publishing. https://doi.org/10.1016/B978-0-08-100528-6.00018-8

Bitra, V. S. P., Womac, A. R., Chevanan, N., Miu, P. I., Igathinathane, C., Sokhansanj, S., & Smith, D. R. (2009). Direct mechanical energy measures of hammer mill comminution of switchgrass, wheat straw, and corn stover and analysis of their particle size distributions. *Powder Technology*, *193*(1), 32–45. https://doi.org/10.1016/j.powtec.2009.02.010

Bitra, V. S. P., Womac, A. R., Yang, Y. T., Miu, P. I., Igathinathane, C., & Sokhansanj, S. (2009). Mathematical model parameters for describing the particle size spectra of knife-milled corn stover. *Biosystems Engineering*, *104*(3), 369–383. https://doi.org/10.1016/j.biosystemseng.2009.08.007

Boumanchar, I., Chhiti, Y., M'hamdi Alaoui, F. E., El Ouinani, A., Sahibed-Dine, A., Bentiss, F., Jama, C., & Bensitel, M. (2017). Effect of materials mixture on the higher heating value: Case of biomass, biochar and municipal solid waste. *Waste Management*, *61*, 78–86. https://doi.org/10.1016/j.wasman.2016.11.012

Brack, D., Birdsey, R., & Walker, W. (2021, October 14). *Greenhouse gas emissions from burning US-sourced woody biomass in the EU and UK*. https://www.chathamhouse.org/2021/10/greenhouse-gas-emissions-burning-us-sourced-woody-biomass-eu-and-uk

Brezáni, I., & Zeleňák, F. (2010). Improving the effectivity of work with rosin-rammler diagram by using MATLAB® GUI tool. *Acta Montanistica Slovaca*, *15*(2), 152–157. Scopus.

Bridge, C. P. (2018, July 13). *Biomass co-firing to improve the burn-out of unreactive coals in pulverised fuel combustion* [Thesis (University of Nottingham only)]. University of Nottingham. https://eprints.nottingham.ac.uk/50550/

Cabral, R. P., Bui, M., & Mac Dowell, N. (2019). A synergistic approach for the simultaneous decarbonisation of power and industry via bioenergy with carbon capture and storage (BECCS). *International Journal of Greenhouse Gas Control*, *87*, 221–237. https://doi.org/10.1016/j.ijggc.2019.05.020

Carone, M. T., Pantaleo, A., & Pellerano, A. (2011). Influence of process parameters and biomass characteristics on the durability of pellets from the pruning residues of *Olea europaea* L. *Biomass and Bioenergy*, *35*(1), 402–410. https://doi.org/10.1016/j.biombioe.2010.08.052

Ceccato Olindo srl. (n.d.). *Wood Pellet Machine Single-phase 230 V - Instructions and Maintenance Manual*.

Celignis Analytical. (n.d.). *Analysis of Sugarcane Bagasse, Cellulose Content of Sugarcane Bagasse, Lignin Content of Sugarcane Bagasse*. Retrieved 12 March 2020, from https://www.celignis.com/feedstock.php?value=13

Ceylan, İ., & Gürel, A. E. (2016). Solar-assisted fluidized bed dryer integrated with a heat pump for mint leaves. *Applied Thermal Engineering*, *106*, 899–905. https://doi.org/10.1016/j.applthermaleng.2016.06.077

Chandrasekaran, S., Ramanathan, S., & Basak, T. (2013). Microwave food processing—A review. *Food Research International*, *52*(1), 243–261. https://doi.org/10.1016/j.foodres.2013.02.033

Chavan, R. S., Chavan, S. R., Khedkar, C. D., & Jana, A. H. (2011). UHT Milk Processing and Effect of Plasmin Activity on Shelf Life: A Review. *Comprehensive Reviews in Food Science and Food Safety*, *10*(5), 251–268. https://doi.org/10.1111/j.1541-4337.2011.00157.x

Chen, H., Shan, R., Zhao, F., Gu, J., Zhang, Y., Yuan, H., & Chen, Y. (2023). A review on the NOx precursors release during biomass pyrolysis. *Chemical Engineering Journal*, *451*, 138979. https://doi.org/10.1016/j.cej.2022.138979

Chen, W.-H., Lu, K.-M., Lee, W.-J., Liu, S.-H., & Lin, T.-C. (2014). Non-oxidative and oxidative torrefaction characterization and SEM observations of fibrous and ligneous biomass. *Applied Energy*, *114*, 104–113. https://doi.org/10.1016/j.apenergy.2013.09.045

Choi, S.-G., Park, S.-S., Wu, S., & Chu, J. (2017). Methods for Calcium Carbonate Content Measurement of Biocemented Soils. *Journal of Materials in Civil Engineering*, *29*(11), 06017015. https://doi.org/10.1061/(ASCE)MT.1943-5533.0002064

Clare, D. A., Bang, W. S., Cartwright, G., Drake, M. A., Coronel, P., & Simunovic, J. (2005). Comparison of Sensory, Microbiological, and Biochemical Parameters of Microwave Versus Indirect UHT Fluid Skim Milk During Storage. *Journal of Dairy Science*, *88*(12), 4172–4182. https://doi.org/10.3168/jds.S0022-0302(05)73103-9

Cloke, M., Lester, E., & Thompson, A. W. (2002). Combustion characteristics of coals using a drop-tube furnace. *Fuel*, *81*(6), 727–735. https://doi.org/10.1016/S0016-2361(01)00199-5

Cloke, M., Wu, T., Barranco, R., & Lester, E. (2003). Char characterisation and its application in a coal burnout model☆. *Fuel*, *82*(15), 1989–2000. https://doi.org/10.1016/S0016-2361(03)00155-8

Cui, H., & Grace, J. R. (2006). Pneumatic conveying of biomass particles: A review. *China Particuology*, *4*(3), 183–188. https://doi.org/10.1016/S1672-2515(07)60259-0

Cui, X., Yang, J., & Wang, Z. (2021). A multi-parameter optimization of the bio-pellet manufacturing process: Effect of different parameters and different feedstocks on pellet characteristics. *Biomass and Bioenergy*, *155*, 106299. https://doi.org/10.1016/j.biombioe.2021.106299

Darr, M. J., & Shah, A. (2012). Biomass storage: An update on industrial solutions for baled biomass feedstocks. *Biofuels*, *3*(3), 321–332. https://doi.org/10.4155/bfs.12.23

De Feo, G., D'Argenio, F., Ferrara, C., & Grosso, A. (2021). A procedure to assess the environmental, social and economic benefits wasted in the paper and cardboard fraction of the unsorted residual waste. *Journal of Cleaner Production*, *296*, 126566. https://doi.org/10.1016/j.jclepro.2021.126566

De Laporte, A. V., Weersink, A. J., & McKenney, D. W. (2016). Effects of supply chain structure and biomass prices on bioenergy feedstock supply. *Applied Energy*, *183*, 1053–1064. https://doi.org/10.1016/j.apenergy.2016.09.049

de Vries, Y. P. (2006). *Bacillus cereus spore formation, structure and germination*. Wageningen University and Research.

de Wit, M., & Faaij, A. (2010). European biomass resource potential and costs. *Biomass and Bioenergy*, *34*(2), 188–202. https://doi.org/10.1016/j.biombioe.2009.07.011

Deeth, H. (2010). Improving UHT processing and UHT milk products. In M. W. Griffiths (Ed.), *Improving the Safety and Quality of Milk* (pp. 302–329). Woodhead Publishing. https://doi.org/10.1533/9781845699420.4.302

Deeth, H. C. (2021). Heat-induced inactivation of enzymes in milk and dairy products. A review. *International Dairy Journal*, *121*, 105104. https://doi.org/10.1016/j.idairyj.2021.105104

Del Giudice, A., Acampora, A., Santangelo, E., Pari, L., Bergonzoli, S., Guerriero, E., Petracchini, F., Torre, M., Paolini, V., & Gallucci, F. (2019). Wood Chip Drying through the Using of a Mobile Rotary Dryer. *Energies*, *12*(9), Article 9. https://doi.org/10.3390/en12091590

Demirbas, A. (2004). Combustion characteristics of different biomass fuels. *Progress in Energy and Combustion Science*, *30*(2), 219–230. https://doi.org/10.1016/j.pecs.2003.10.004

Deng, T., Garg, V., & Bradley, M. S. A. (2023). Electrostatic Charging of Fine Powders and Assessment of Charge Polarity Using an Inductive Charge Sensor. Nanomanufacturing 2023, 3, 281–292. Htps. *Doi. Org/10.3390/Nanomanufacturing3030018 Academic Editor: Asterios (Stergios) Pispas Received*, *4*. https://www.academia.edu/download/104556300/pdf.pdf

Department for Business, Energy & Industrial Strategy. (2021). *End to coal power brought forward to October 2024*. GOV.UK. https://www.gov.uk/government/news/end-to-coal-power-brought-forward-to-october-2024

Drax Power. (n.d.). *Drax Power Station*. Drax Global. Retrieved 5 March 2024, from https://www.drax.com/about-us/our-sites-and-businesses/drax-power-station/

Dungani, R., Khalil, H. P. S. A., Sumardi, I., Suhaya, Y., Sulistyawati, E., Islam, Md. N., Suraya, N. L. M., & Aprilia, N. A. S. (2014). Non-wood Renewable Materials: Properties Improvement and Its Application. In K. R. Hakeem, M. Jawaid, & U. Rashid (Eds.), *Biomass and Bioenergy: Applications* (pp. 1–29). Springer International Publishing. https://doi.org/10.1007/978-3-319-07578-5_1

Dupont, C., Chiriac, R., Gauthier, G., & Toche, F. (2014). Heat capacity measurements of various biomass types and pyrolysis residues. *Fuel*, *115*, 644–651. https://doi.org/10.1016/j.fuel.2013.07.086

ecoinvent. (n.d.). *ecoinvent—Data with purpose.* Ecoinvent. Retrieved 10 March 2024, from https://ecoinvent.org/

Elliston, A., Collins, S. R. A., Wilson, D. R., Roberts, I. N., & Waldron, K. W. (2013). High concentrations of cellulosic ethanol achieved by fed batch semi simultaneous saccharification and fermentation of waste-paper. *Bioresource Technology*, *134*, 117–126. https://doi.org/10.1016/j.biortech.2013.01.084

Espiner, T. (2022, April 28). Coal plants asked to stay open longer due to energy supply fears. *BBC News*. https://www.bbc.com/news/business-61256615

Evans, S., & Viisainen, V. (2024, January 3). *Analysis: UK electricity from fossil fuels drops to lowest level since 1957*. Carbon Brief. https://www.carbonbrief.org/analysis-uk-electricity-from-fossil-fuels-drops-to-lowest-level-since-1957/

Fagernäs, L., Brammer, J., Wilén, C., Lauer, M., & Verhoeff, F. (2010). Drying of biomass for second generation synfuel production. *Biomass and Bioenergy*, *34*(9), 1267–1277. https://doi.org/10.1016/j.biombioe.2010.04.005

Fantozzi, F., & Buratti, C. (2010). Life cycle assessment of biomass chains: Wood pellet from short rotation coppice using data measured on a real plant. *Biomass and Bioenergy*, *34*(12), 1796–1804. https://doi.org/10.1016/j.biombioe.2010.07.011

Fearon, O., Kuitunen, S., Ruuttunen, K., Alopaeus, V., & Vuorinen, T. (2020). Detailed Modeling of Kraft Pulping Chemistry. Delignification. *Industrial & Engineering Chemistry Research*, *59*(29), 12977–12985. https://doi.org/10.1021/acs.iecr.0c02110

Ferrero, F., Lohrer, C., Schmidt, B. M., Noll, M., & Malow, M. (2009). A mathematical model to predict the heating-up of large-scale wood piles. *Journal of Loss Prevention in the Process Industries*, *22*(4), 439–448. https://doi.org/10.1016/j.jlp.2009.02.009

Fioranelli, A., & Bizzo, W. A. (2023). Generation of surplus electricity in sugarcane mills from sugarcane bagasse and straw: Challenges, failures and opportunities. *Renewable and Sustainable Energy Reviews*, *186*, 113647. https://doi.org/10.1016/j.rser.2023.113647

Flórez-Pardo, L. M., González-Córdoba, A., & López-Galán, J. E. (2018). Evaluation of different methods for efficient extraction of hemicelluloses leaves and tops of sugarcane. *Dyna*, *85*(204), 18–27. http://www.scielo.org.co/scielo.php?pid=S0012-73532018000100018&script=sci_arttext&tlng=en

Folk, R. L. (1980). *Petrology of Sedimentary Rocks*. Hemphill Publishing Company. https://repositories.lib.utexas.edu/handle/2152/22930

Forth, K., Braun, A., & Borrmann, A. (2019). BIM-integrated LCA - model analysis and implementation for practice. *IOP Conference Series: Earth and Environmental Science*, *323*(1), 012100. https://doi.org/10.1088/1755-1315/323/1/012100

Frodeson, S., Berghel, J., & Renström, R. (2013). The Potential of Using Two-Step Drying Techniques for Improving Energy Efficiency and Increasing Drying Capacity in Fuel Pellet Industries. *Drying Technology*, *31*(15), 1863–1870. https://doi.org/10.1080/07373937.2013.833520

Fruit Growers Supply. (2020, February 17). *Cardboard vs Corrugated | Learn the Difference at FGS*. Serving Agriculture Since 1907. https://fruitgrowers.com/the-difference-between-corrugated-fiberboard-and-cardboard/

Gageanu, I., Cujbescu, D., Persu, C., Tudor, P., Cardei, P., Matache, M., Vladut, V., Biris, S., Voicea, I., & Ungureanu, N. (2021). Influence of Input and Control Parameters on the Process of Pelleting Powdered Biomass. *Energies*, *14*(14), Article 14. https://doi.org/10.3390/en14144104

Galan, I., Glasser, F. P., & Andrade, C. (2013). Calcium carbonate decomposition. *Journal of Thermal Analysis and Calorimetry*, *111*(2), 1197–1202. https://doi.org/10.1007/s10973-012-2290-x

Gaukel, V., Siebert, T., & Erle, U. (2017). Microwave-assisted drying. In M. Regier, K. Knoerzer, & H. Schubert (Eds.), *The Microwave Processing of Foods (Second Edition)* (pp. 152–178). Woodhead Publishing. https://doi.org/10.1016/B978-0-08-100528-6.00008-5

Ghorbani, Z., Masoumi, A. A., & Hemmat, A. (2010). Specific energy consumption for reducing the size of alfalfa chops using a hammer mill. *Biosystems Engineering*, *105*(1), 34–40. https://doi.org/10.1016/j.biosystemseng.2009.09.006

Gil, M., Arauzo, I., Teruel, E., & Bartolomé, C. (2012). Milling and handling Cynara Cardunculus L. for use as solid biofuel: Experimental tests. *Biomass and Bioenergy*, *41*, 145–156. https://doi.org/10.1016/j.biombioe.2012.02.023

Gil, M., Teruel, E., & Arauzo, I. (2014). Analysis of standard sieving method for milled biomass through image processing. Effects of particle shape and size for poplar and corn stover. *Fuel*, *116*, 328–340. https://doi.org/10.1016/j.fuel.2013.08.011

Gilvari, H., Cutz, L., Tiringer, U., Mol, A., de Jong, W., & Schott, D. L. (2020). The Effect of Environmental Conditions on the Degradation Behavior of Biomass Pellets. *Polymers*, *12*(4), Article 4. https://doi.org/10.3390/polym12040970

Glushkov, D., Kuznetsov, G., & Paushkina, K. (2020). Switching Coal-Fired Thermal Power Plant to Composite Fuel for Recovering Industrial and Municipal Waste: Combustion Characteristics, Emissions, and Economic Effect. *Energies*, *13*(1), Article 1. https://doi.org/10.3390/en13010259

Glushkov, D., Paushkina, K., Shabardin, D., Strizhak, P., & Gutareva, N. (2019). Municipal solid waste recycling by burning it as part of composite fuel with energy generation. *Journal of Environmental Management*, *231*, 896–904. https://doi.org/10.1016/j.jenvman.2018.10.067

González-Bautista, E., Alarcón-Gutiérrez, E., Dupuy, N., Gaime-Perraud, I., Ziarelli, F., Foli, L., & Farnet-Da-Silva, A.-M. (2020). Preparation of a sugarcane bagasse-based substrate for second-generation ethanol: Effect of pasteurisation conditions on dephenolisation. *Renewable Energy*, *157*, 859–866. https://doi.org/10.1016/j.renene.2020.05.116

Gräbner, M., & Lester, E. (2016). Proximate and ultimate analysis correction for kaolinite-rich Chinese coals using mineral liberation analysis. *Fuel*, *186*, 190–198. https://doi.org/10.1016/j.fuel.2016.08.074

Graham, S. L. (2015). *Degradation of biomass fuels during long term storage in indoor and outdoor environments* [Thesis (University of Nottingham), University of Nottingham]. https://doi.org/10/1/Shalini%20Graham%20EngD%20thesis%20for%20e-thesis.pdf

Gravelsins, R. J., & Trass, O. (2013). Analysis of grinding of pelletized wood waste with the Szego Mill. *Powder Technology*, *245*, 189–198. https://doi.org/10.1016/j.powtec.2013.04.018

Grisoli, P., Rodolfi, M., Villani, S., Grignani, E., Cottica, D., Berri, A., Maria Picco, A., & Dacarro, C. (2009). Assessment of airborne microorganism contamination in an industrial area characterized by an open composting facility and a wastewater treatment plant. *Environmental Research*, *109*(2), 135–142. https://doi.org/10.1016/j.envres.2008.11.001

Grönfors, J. (2010). *Use of fillers in paper and paperboard grades, Tampere University of Applied Sciences, International Pulp and Paper Technology* [PhD Thesis, Tesis]. https://www.theseus.fi/bitstream/handle/10024/16226/gronfors_jarkko.pdf?sequence=1

Gubba, S. R., Ma, L., Pourkashanian, M., & Williams, A. (2011). Influence of particle shape and internal thermal gradients of biomass particles on pulverised coal/biomass co-fired flames. *Fuel Processing Technology*, *92*(11), 2185–2195. https://doi.org/10.1016/j.fuproc.2011.07.003

Guinée, J. B., Heijungs, R., Huppes, G., Zamagni, A., Masoni, P., Buonamici, R., Ekvall, T., & Rydberg, T. (2011). Life Cycle Assessment: Past, Present, and Future. *Environmental Science & Technology*, *45*(1), 90–96. https://doi.org/10.1021/es101316v

Guizani, C., Jeguirim, M., Valin, S., Limousy, L., & Salvador, S. (2017). Biomass Chars: The Effects of Pyrolysis Conditions on Their Morphology, Structure, Chemical Properties and Reactivity. *Energies*, *10*(6), Article 6. https://doi.org/10.3390/en10060796

Güleç, F., Williams, O., Kostas, E. T., Samson, A., & Lester, E. (2022). A comprehensive comparative study on the energy application of chars produced from different biomass feedstocks via hydrothermal conversion, pyrolysis, and torrefaction. *Energy Conversion and Management*, *270*, 116260. https://doi.org/10.1016/j.enconman.2022.116260

Guo, Q., Chen, X., & Liu, H. (2012). Experimental research on shape and size distribution of biomass particle. *Fuel*, *94*, 551–555. https://doi.org/10.1016/j.fuel.2011.11.041

Hayes, M., Mitra, A., Lin, R., & Catgiu, C. (2023, October 19). *Life Cycle Assessment Guide—KPMG Global*. KPMG. https://kpmg.com/xx/en/home/insights/2023/10/life-cycle-assessment-guide.html

Herrmann, I. T., & Moltesen, A. (2015). Does it matter which Life Cycle Assessment (LCA) tool you choose? – A comparative assessment of SimaPro and GaBi. *Journal of Cleaner Production*, *86*, 163–169. https://doi.org/10.1016/j.jclepro.2014.08.004

Holm, J. K., Henriksen, U. B., Hustad, J. E., & Sørensen, L. H. (2006). Toward an Understanding of Controlling Parameters in Softwood and Hardwood Pellets Production. *Energy & Fuels*, *20*(6), 2686–2694. https://doi.org/10.1021/ef0503360

Holsinger, V. H., Rajkowski, K. T., & Stabel, J. R. (1997). Milk pasteurisation and safety: A brief history and update. *Revue Scientifique et Technique-Office International Des Epizooties*, *16*(2), 441–466. https://www.researchgate.net/profile/A-P-L-Martins-2/post/For-how-long-raw-milk-should-be-boiled-for-complete-destruction-of-Mycobacterium-tuberculosis/attachment/5b23a79ab53d2f63c3d15ffa/AS%3A637751951114241%401529063322636/download/d9152.pdf

Hossain, S. S., Mathur, L., & Roy, P. K. (2018). Rice husk/rice husk ash as an alternative source of silica in ceramics: A review. *Journal of Asian Ceramic Societies*, *6*(4), 299–313. https://doi.org/10.1080/21870764.2018.1539210

Hudson, A., Wong, T., & Lake, R. (2003). Pasteurisation of dairy products: Times, temperatures and evidence for control of pathogens. *Institute of Environmental Science and Research, Ltd., Christchurch, New Zealand*, 62. https://innoquamexico.com/wp-content/uploads/2020/10/Pasteurisation_Dairy-Science_Research.pdf

Hurt, R. H., & Calo, J. M. (2001). Semi-global intrinsic kinetics for char combustion modeling†. *Combustion and Flame*, *125*(3), 1138–1149. https://doi.org/10.1016/S0010-2180(01)00234-6

Hurt, R., Sun, J.-K., & Lunden, M. (1998). A Kinetic Model of Carbon Burnout in Pulverized Coal Combustion. *Combustion and Flame*, *113*(1), 181–197. https://doi.org/10.1016/S0010-2180(97)00240-X

Ibitoye, S. E., Jen, T.-C., Mahamood, R. M., & Akinlabi, E. T. (2021). Densification of agro-residues for sustainable energy generation: An overview. *Bioresources and Bioprocessing*, *8*(1), 75. https://doi.org/10.1186/s40643-021-00427-w

Ilic, D., Williams, K., Farnish, R., Webb, E., & Liu, G. (2018). On the challenges facing the handling of solid biomass feedstocks. *Biofuels, Bioproducts and Biorefining*, *12*(2), 187–202. https://doi.org/10.1002/bbb.1851

Jackson, J., Turner, A., Mark, T., & Montross, M. (2016). Densification of biomass using a pilot scale flat ring roller pellet mill. *Fuel Processing Technology*, *148*, 43–49. https://doi.org/10.1016/j.fuproc.2016.02.024

Jeetah, P., Golaup, N., & Buddynauth, K. (2015). Production of cardboard from waste rice husk. *Journal of Environmental Chemical Engineering*, *3*(1), 52–59. https://doi.org/10.1016/j.jece.2014.11.013

Kaaya, A. N., & Kyamuhangire, W. (2010). Drying maize using biomass-heated natural convection dryer improves grain quality during storage. *Journal of Applied Sciences*, *11*, 967–974. https://www.researchgate.net/profile/William-Kyamuhangire-2/publication/49591520_Drying_Maize_Using_Biomass-Heated_Natural_Convection_Dryer_Improves_Grain_Quality_During_Storage/links/00b4951d5652e58575000000/Drying-Maize-Using-Biomass-Heated-Natural-Convection-Dryer-Improves-Grain-Quality-During-Storage.pdf

Kabir, E., Kumar, P., Kumar, S., Adelodun, A. A., & Kim, K.-H. (2018). Solar energy: Potential and future prospects. *Renewable and Sustainable Energy Reviews*, *82*, 894–900. https://doi.org/10.1016/j.rser.2017.09.094

Kalaiselvan, N., & Mathimani, T. (2022). Design and fabrication of box-type passive solar dryer (BTPSD) with thermal insulation material for valorizing biomass and neutral lipids of marine Chlorella vulgaris for biodiesel application. *Scientific Reports*, *12*(1), 6046. https://doi.org/10.1038/s41598-022-09665-0

Kaliyan, N., & Morey, R. V. (2009a). Densification Characteristics of Corn Stover and Switchgrass. *Transactions of the ASABE*, *52*(3), 907–920. https://doi.org/10.13031/2013.27380

Kaliyan, N., & Morey, R. V. (2009b). Factors affecting strength and durability of densified biomass products. *Biomass and Bioenergy*, *33*(3), 337–359. https://doi.org/10.1016/j.biombioe.2008.08.005

Kaliyan, N., & Morey, R. V. (2010). Natural binders and solid bridge type binding mechanisms in briquettes and pellets made from corn stover and switchgrass. *Bioresource Technology*, *101*(3), 1082–1090. https://doi.org/10.1016/j.biortech.2009.08.064

Kanwal, S., Chaudhry, N., Munir, S., & Sana, H. (2019). Effect of torrefaction conditions on the physicochemical characterization of agricultural waste (sugarcane bagasse). *Waste Management*, *88*, 280–290. https://doi.org/10.1016/j.wasman.2019.03.053

Kenney, K. L., Smith, W. A., Gresham, G. L., & Westover, T. L. (2013). Understanding biomass feedstock variability. *Biofuels*, *4*(1), 111–127. https://doi.org/10.4155/bfs.12.83

Kerr, W. L. (2019). Chapter 14—Food Drying and Evaporation Processing Operations. In M. Kutz (Ed.), *Handbook of Farm, Dairy and Food Machinery Engineering (Third Edition)* (pp. 353–387). Academic Press. https://doi.org/10.1016/B978-0-12-814803-7.00014-2

Khouya, A., & Draoui, A. (2019). Computational drying model for solar kiln with latent heat energy storage: Case studies of thermal application. *Renewable Energy*, *130*, 796–813. https://doi.org/10.1016/j.renene.2018.06.090

Kiatkittipong, W., Wongsuchoto, P., & Pavasant, P. (2009). Life cycle assessment of bagasse waste management options. *Waste Management*, *29*(5), 1628–1633. https://doi.org/10.1016/j.wasman.2008.12.006

Kim, M., & Day, D. F. (2011). Composition of sugar cane, energy cane, and sweet sorghum suitable for ethanol production at Louisiana sugar mills. *Journal of*

Industrial Microbiology and Biotechnology, *38*(7), 803–807. https://doi.org/10.1007/s10295-010-0812-8

Kissinger, M., Fix, J., & Rees, W. E. (2007). Wood and non-wood pulp production: Comparative ecological footprinting on the Canadian prairies. *Ecological Economics*, *62*(3), 552–558. https://doi.org/10.1016/j.ecolecon.2006.07.019

Knappett, J., & Craig, R. F. (2012). *Craig's Soil Mechanics*. CRC Press.

Knoerzer, K., Regier, M., & Schubert, H. (2017). Measuring temperature distributions during microwave processing. In M. Regier, K. Knoerzer, & H. Schubert (Eds.), *The Microwave Processing of Foods (Second Edition)* (pp. 327–349). Woodhead Publishing. https://doi.org/10.1016/B978-0-08-100528-6.00015-2

Kpalo, S. Y., Zainuddin, M. F., Manaf, L. A., & Roslan, A. M. (2020). A Review of Technical and Economic Aspects of Biomass Briquetting. *Sustainability*, *12*(11), Article 11. https://doi.org/10.3390/su12114609

Krumbein, W. C., & Sloss, L. L. (1951). Stratigraphy and Sedimentation. *Soil Science*, *71*(5), 401. https://journals.lww.com/soilsci/citation/1951/05000/stratigraphy_and_sedimentation.19.aspx

Kumar, I., Feng, K., Sun, L., & Bandaru, V. (2022). Adoption of biomass for electricity generation in Thailand: Implications for energy security, employment, environment, and land use change. *Renewable Energy*, *195*, 1454–1467. https://doi.org/10.1016/j.renene.2022.05.162

Kylili, A., Christoforou, E., & Fokaides, P. A. (2016). Environmental evaluation of biomass pelleting using life cycle assessment. *Biomass and Bioenergy*, *84*, 107–117. https://doi.org/10.1016/j.biombioe.2015.11.018

Labbé, R., Carey, P., Trincado, G., & Thiers, O. (2018). Natural drying of forest biomass: Effect of stack height and cover in the province of Valdivia, Chile. *BOSQUE*, *39*(3), Article 3. https://doi.org/10.4067/S0717-92002018000300449

Lachman, L., Lieberman, H. A., & Kanig, J. L. (1986). *The theory and practice of industrial pharmacy* (3rd ed.). Lea & Febiger.

Lam, P. S., & Sokhansanj, S. (2014). Engineering Properties of Biomass. In Y. Shastri, A. Hansen, L. Rodríguez, & K. C. Ting (Eds.), *Engineering and Science of Biomass Feedstock Production and Provision* (pp. 17–35). Springer. https://doi.org/10.1007/978-1-4899-8014-4_2

Larsson, S. H., Thyrel, M., Geladi, P., & Lestander, T. A. (2008). High quality biofuel pellet production from pre-compacted low density raw materials. *Bioresource Technology*, *99*(15), 7176–7182. https://doi.org/10.1016/j.biortech.2007.12.065

Leith, D. (1987). Drag on Nonspherical Objects. *Aerosol Science and Technology*, *6*(2), 153–161. https://doi.org/10.1080/02786828708959128

Lela, B., Barišić, M., & Nižetić, S. (2016). Cardboard/sawdust briquettes as biomass fuel: Physical–mechanical and thermal characteristics. *Waste Management*, *47*, 236–245. https://doi.org/10.1016/j.wasman.2015.10.035

Lester, E., Alvarez, D., Borrego, A. G., Valentim, B., Flores, D., Clift, D. A., Rosenberg, P., Kwiecinska, B., Barranco, R., Petersen, H. I., Mastalerz, M., Milenkova, K.

S., Panaitescu, C., Marques, M. M., Thompson, A., Watts, D., Hanson, S., Predeanu, G., Misz, M., & Wu, T. (2010). The procedure used to develop a coal char classification—Commission III Combustion Working Group of the International Committee for Coal and Organic Petrology. *International Journal of Coal Geology*, *81*(4), 333–342. https://doi.org/10.1016/j.coal.2009.10.015

Lester, E., Avila, C., Pang, C. H., Williams, O., Perkins, J., Gaddipatti, S., Tucker, G., Barraza, J. M., Trujillo-Uribe, M. P., & Wu, T. (2018). A proposed biomass char classification system. *Fuel*, *232*, 845–854. https://doi.org/10.1016/j.fuel.2018.05.153

Lester, E., Gong, M., & Thompson, A. (2007). A method for source apportionment in biomass/coal blends using thermogravimetric analysis. *Journal of Analytical and Applied Pyrolysis*, *80*(1), 111–117. https://doi.org/10.1016/j.jaap.2007.01.010

Lester, E., Kingman, S., Dodds, C., & Patrick, J. (2006). The potential for rapid coke making using microwave energy. *Fuel*, *85*(14), 2057–2063. https://doi.org/10.1016/j.fuel.2006.04.012

Lewis, M. (2010). Improving pasteurised and extended shelf-life milk. In M. W. Griffiths (Ed.), *Improving the Safety and Quality of Milk* (pp. 277–301). Woodhead Publishing. https://doi.org/10.1533/9781845699420.4.277

Leyssens, G., Trouvé, G., Caplain, I., Schönnenbeck, C., & Cazier, F. (2014). Energetic performances and environmental impact of the combustion of cardboard/sawdust in a domestic boiler. *Fuel*, *122*, 21–27. https://doi.org/10.1016/j.fuel.2014.01.034

Li, H., Chen, Q., Zhang, X., Finney, K. N., Sharifi, V. N., & Swithenbank, J. (2012). Evaluation of a biomass drying process using waste heat from process industries: A case study. *Applied Thermal Engineering*, *35*, 71–80. https://doi.org/10.1016/j.applthermaleng.2011.10.009

Li, J., & Zhang, J. (2016). A Theoretical Study on Char Combustion of Ellipsoidal Particles. *Combustion Science and Technology*, *188*(1), 40–54. https://doi.org/10.1080/00102202.2015.1079523

Lieskovský, M., & Gejdoš, M. (2023). Monitoring of Respiratory Health Risks Caused by Biomass Storage in Urban-Type Heating Plants. *Forests*, *14*(4), Article 4. https://doi.org/10.3390/f14040707

Lisowski, A., Dąbrowska-Salwin, M., Ostrowska-Ligęza, E., Nawrocka, A., Stasiak, M., Świętochowski, A., Klonowski, J., Sypuła, M., & Lisowska, B. (2017). Effects of the biomass moisture content and pelleting temperature on the pressure-induced agglomeration process. *Biomass and Bioenergy*, *107*, 376–383. https://doi.org/10.1016/j.biombioe.2017.10.029

Liu, X., Liu, X., & Hu, Y. (2014). Investigation of the Thermal Decomposition of Talc. *Clays and Clay Minerals*, *62*(2), 137–144. https://doi.org/10.1346/CCMN.2014.0620206

Liu, Y., Peng, J., Kansha, Y., Ishizuka, M., Tsutsumi, A., Jia, D., Bi, X. T., Lim, C. J., & Sokhansanj, S. (2014). Novel fluidized bed dryer for biomass drying. *Fuel Processing Technology*, *122*, 170–175. https://doi.org/10.1016/j.fuproc.2014.01.036

Llorente, M. J. F., Arocas, P. D., Nebot, L. G., & García, J. E. C. (2008). The effect of the addition of chemical materials on the sintering of biomass ash. *Fuel*, *87*(12), 2651–2658. https://doi.org/10.1016/j.fuel.2008.02.019

Lopes Silva, D. A., Delai, I., Delgado Montes, M. L., & Roberto Ometto, A. (2014). Life cycle assessment of the sugarcane bagasse electricity generation in Brazil. *Renewable and Sustainable Energy Reviews*, *32*, 532–547. https://doi.org/10.1016/j.rser.2013.12.056

Lopes Silva, D. A., Nunes, A. O., Piekarski, C. M., da Silva Moris, V. A., de Souza, L. S. M., & Rodrigues, T. O. (2019). Why using different Life Cycle Assessment software tools can generate different results for the same product system? A cause–effect analysis of the problem. *Sustainable Production and Consumption*, *20*, 304–315. https://doi.org/10.1016/j.spc.2019.07.005

Lorang, E., Lobianco, A., & Delacote, P. (2023). Increasing Paper and Cardboard Recycling: Impacts on the Forest Sector and Carbon Emissions. *Environmental Modeling & Assessment*, *28*(2), 189–200. https://doi.org/10.1007/s10666-022-09850-5

Lu, H., Robert, W., Peirce, G., Ripa, B., & Baxter, L. L. (2008). Comprehensive Study of Biomass Particle Combustion. *Energy & Fuels*, *22*(4), 2826–2839. https://doi.org/10.1021/ef800006z

Lucadamo, L., Gallo, L., & Corapi, A. (2019). Power plants: The need for effective bio-monitoring of the contribution of bio(wood) fuelled stations to atmospheric contamination. *Atmospheric Pollution Research*, *10*(6), 2040–2052. https://doi.org/10.1016/j.apr.2019.09.012

Luo, H., Zhang, Y., Zhu, H., Zhao, X., Zhu, L., Liu, W., Sun, M., Miao, G., Li, S., & Kong, L. (2021). Microwave-assisted low-temperature biomass pyrolysis: From mechanistic insights to pilot scale. *Green Chemistry*, *23*(2), 821–827. https://doi.org/10.1039/D0GC03348K

Lv, Z., Xiong, X., Ruan, R., Wang, Y., & Tan, H. (2023). NO emission and burnout characteristics in co-combustion of coal and sewage sludge following high-temperature preheating. *Fuel*, *331*, 125887. https://doi.org/10.1016/j.fuel.2022.125887

Ma, L., & Mitchell, R. (2009). Modeling char oxidation behavior under Zone II burning conditions at elevated pressures. *Combustion and Flame*, *156*(1), 37–50. https://doi.org/10.1016/j.combustflame.2008.06.015

Madhlopa, A., & Ngwalo, G. (2007). Solar dryer with thermal storage and biomass-backup heater. *Solar Energy*, *81*(4), 449–462. https://doi.org/10.1016/j.solener.2006.08.008

Magaton, A. D. S., Colodette, J. L., Gouvêa, A., Gomide, J. L., Muguet, M. C. S., & Pedrazzi, C. (2009). Eucalyptus wood quality and its impact on kraft pulp production and use. *Tappi J*, *8*(8), 32–39. https://www.eucalyptus.com.br/artigos/outros/2009_Eucalyptus_wood_quality_impact_on_pulping.pdf

Maloney, D. J., Monazam, E. R., Casleton, K. H., & Shaddix, C. R. (2005). Evaluation of char combustion models: Measurement and analysis of variability in char particle size and density. *Proceedings of the Combustion Institute*, *30*(2), 2197–2204. https://doi.org/10.1016/j.proci.2004.08.093

Manatura, K. (2020). Inert torrefaction of sugarcane bagasse to improve its fuel properties. *Case Studies in Thermal Engineering*, *19*, 100623. https://doi.org/10.1016/j.csite.2020.100623

Mandø, M., Rosendahl, L., Yin, C., & Sørensen, H. (2010). Pulverized straw combustion in a low-NO*x* multifuel burner: Modeling the transition from coal to straw. *Fuel*, *89*(10), 3051–3062. https://doi.org/10.1016/j.fuel.2010.05.016

Mani, S., Tabil, L. G., & Sokhansanj, S. (2006). Effects of compressive force, particle size and moisture content on mechanical properties of biomass pellets from grasses. *Biomass and Bioenergy*, *30*(7), 648–654. https://doi.org/10.1016/j.biombioe.2005.01.004

Martinez-Mendoza, K. L., Guerrero-Perez, J., Barraza-Burgos, J., Forero, C. R., Williams, O., Lester, E., & Gil, N. (2023). Thermochemical behavior of agricultural and industrial sugarcane residues for bioenergy applications. *Bioengineered*, *14*(1), 2283264. https://doi.org/10.1080/21655979.2023.2283264

Masche, M., Puig-Arnavat, M., Jensen, P. A., Holm, J. K., Clausen, S., Ahrenfeldt, J., & Henriksen, U. B. (2019). From wood chips to pellets to milled pellets: The mechanical processing pathway of Austrian pine and European beech. *Powder Technology*, *350*, 134–145. https://doi.org/10.1016/j.powtec.2019.03.002

Mason, P. E., Darvell, L. I., Jones, J. M., & Williams, A. (2016). Comparative Study of the Thermal Conductivity of Solid Biomass Fuels. *Energy & Fuels*, *30*(3), 2158–2163. https://doi.org/10.1021/acs.energyfuels.5b02261

MathWorks. (n.d.). *Piecewise Cubic Hermite Interpolating Polynomial (PCHIP)*. Retrieved 1 August 2023, from https://uk.mathworks.com/help/matlab/ref/pchip.html

Megías-Pérez, R., Gamboa-Santos, J., Soria, A. C., Villamiel, M., & Montilla, A. (2014). Survey of quality indicators in commercial dehydrated fruits. *Food Chemistry*, *150*, 41–48. https://doi.org/10.1016/j.foodchem.2013.10.141

Meza, J., Gil, A., Cortés, C., & González, A. (2008). Drying costs of woody biomass in a semi-industrial experimental rotary dryer. *16th European Conference and Exhibition on Biomass for Energy, Biomass Resources*.

Microtrac Retsch GmbH. (2020). *Manual: Evaluation Software CAMSIZER® P4*.

Millard, R. (2024, January 18). *UK prepares to extend subsidy for Drax biomass power station*. https://www.ft.com/content/f0f28bf9-22c7-4a97-8e99-5f1a81ba6713

Miller, B. B., Dugwell, D. R., & Kandiyoti, R. (2002). Partitioning of trace elements during the combustion of coal and biomass in a suspension-firing reactor. *Fuel*, *81*(2), 159–171. https://doi.org/10.1016/S0016-2361(01)00134-X

Mirski, R., Kawalerczyk, J., Dziurka, D., Stuper-Szablewska, K., & Wieruszewski, M. (2023). Mold fungi development during the short-term wood-chips storage depending on the storage method. *Wood Material Science & Engineering*, *18*(4), 1243–1251. https://doi.org/10.1080/17480272.2022.2124124

Mohammadi, F., Roedl, A., Abdoli, M. A., Amidpour, M., & Vahidi, H. (2020). Life cycle assessment (LCA) of the energetic use of bagasse in Iranian sugar industry.

Renewable Energy, *145*, 1870–1882. https://doi.org/10.1016/j.renene.2019.06.023

Momeni, M., Yin, C., Kær, S. K., Hansen, T. B., Jensen, P. A., & Glarborg, P. (2013). Experimental Study on Effects of Particle Shape and Operating Conditions on Combustion Characteristics of Single Biomass Particles. *Energy & Fuels*, *27*(1), 507–514. https://doi.org/10.1021/ef301343q

Montejo, C., Costa, C., Ramos, P., & Márquez, M. del C. (2011). Analysis and comparison of municipal solid waste and reject fraction as fuels for incineration plants. *Applied Thermal Engineering*, *31*(13), 2135–2140. https://doi.org/10.1016/j.applthermaleng.2011.03.041

Morris, J. D., Daood, S. S., & Nimmo, W. (2022). The use of kaolin and dolomite bed additives as an agglomeration mitigation method for wheat straw and miscanthus biomass fuels in a pilot-scale fluidized bed combustor. *Renewable Energy*, *196*, 749–762. https://doi.org/10.1016/j.renene.2022.06.151

Mullerova, J. (2014). Health and safety hazards of biomass storage. *14th International Multidisciplinary Scientific Geoconference (SGEM), Jun*, 17–26. https://www.researchgate.net/profile/Jana-Muellerova-5/publication/273061578_Health_and_Safety_hazards_of_biomass_storage/links/54f60e0f0cf27d8ed71d4cf2/Health-and-Safety-hazards-of-biomass-storage

Munagala, M., Shastri, Y., Nalawade, K., Konde, K., & Patil, S. (2021). Life cycle and economic assessment of sugarcane bagasse valorization to lactic acid. *Waste Management*, *126*, 52–64. https://doi.org/10.1016/j.wasman.2021.02.052

Munir, S., Daood, S. S., Nimmo, W., Cunliffe, A. M., & Gibbs, B. M. (2009). Thermal analysis and devolatilization kinetics of cotton stalk, sugar cane bagasse and shea meal under nitrogen and air atmospheres. *Bioresource Technology*, *100*(3), 1413–1418. https://doi.org/10.1016/j.biortech.2008.07.065

Narra, S., Brinker, M., & Ay, P. (2012). *Particle size distribution of communited and liberated cereal straws measured with different image analysis systems and their characteristic influence on mechanical pellets quality*. XXVI International Mineral Processing Congress - IMPC 2012 : New Delhi, India, September 24 - 28, 2012. https://opus4.kobv.de/opus4-UBICO/frontdoor/index/index/docId/12952

Nhuchhen, D. R., & Abdul Salam, P. (2012). Estimation of higher heating value of biomass from proximate analysis: A new approach. *Fuel*, *99*, 55–63. https://doi.org/10.1016/j.fuel.2012.04.015

Nielsen, S. K., Mandø, M., & Rosenørn, A. B. (2020). Review of die design and process parameters in the biomass pelleting process. *Powder Technology*, *364*, 971–985. https://doi.org/10.1016/j.powtec.2019.10.051

Niu, D., An, W., Yu, C., Zhu, P., Li, C., Yin, D., Zhi, J., Jiang, X., & Ren, J. (2023). Pre-pasteurization enhances the fermentation of wheat straw by *Irpex lacteus*: Chemical composition, enzymatic hydrolysis, and microbial community. *Industrial Crops and Products*, *202*, 116962. https://doi.org/10.1016/j.indcrop.2023.116962

Noll, M., & Jirjis, R. (2012). Microbial communities in large-scale wood piles and their effects on wood quality and the environment. *Applied Microbiology and Biotechnology*, *95*(3), 551–563. https://doi.org/10.1007/s00253-012-4164-3

Norkulova, K., Iskandarov, Z., Safarov, J., & Jumayev, B. (2016). Research dryer for drying agricultural products. *Journal of Food & Industrial Microbiology. USA*, *2*(1), 1–3.

Obi, O. F., Pecenka, R., & Clifford, M. J. (2022). A Review of Biomass Briquette Binders and Quality Parameters. *Energies*, *15*(7), Article 7. https://doi.org/10.3390/en15072426

Office for National Statistics. (2019). *A burning issue: Biomass is the biggest source of renewable energy consumed in the UK*. https://www.ons.gov.uk/economy/environmentalaccounts/articles/aburningissuebiomassisthebiggestsourceofrenewableenergyconsumedintheuk/2019-08-30

Ogedengbe, T. I., Fatomilola, E. O., & Bello, O. R. (2013). Evaluation of thermal conductivity of selected biomass composites. *Research Journal of Engineering and Applied Sciences*, *2*(4), 326–335. https://www.researchgate.net/profile/Tunde-Ogedengbe-2/publication/324820547_Evaluation_of_Thermal_Conductivity_of_Selected_Biomass_Composites/links/5ae45ac1a6fdcc3bea945160/Evaluation-of-Thermal-Conductivity-of-Selected-Biomass-Composites.pdf

Owonikoko, A., Berry, R. J., & Bradley, M. S. A. (2010, September 10). *Characterisation of extreme shape materials: "Biomass and waste materials"* [Conference]. Bulk Solids Europe 2010 Conference and IMechE Symposium in New Frontiers in Bulk Materials Handling, Glasgow. https://gala.gre.ac.uk/id/eprint/7161/

Palzer, St. (2011). Agglomeration of pharmaceutical, detergent, chemical and food powders—Similarities and differences of materials and processes. *Powder Technology*, *206*(1), 2–17. https://doi.org/10.1016/j.powtec.2010.05.006

Panasonic. (n.d.). *Operating Instructions For Commercial Use. Models No. NE-1843/NE-1853 Microwave Ovens*. https://fs.panasonic.com/pdf/user_manual/Pro1/NE-1853/NE-1843_1853BP_OI.pdf

Pang, C. H. (2012). *The characterisation of biomass and biomass/coal blends* [PhD Thesis]. University of Nottingham.

Pang, C. H., Gaddipatti, S., Tucker, G., Lester, E., & Wu, T. (2014). Relationship between thermal behaviour of lignocellulosic components and properties of biomass. *Bioresource Technology*, *172*, 312–320. https://doi.org/10.1016/j.biortech.2014.09.042

Pang, C. H., Lester, E., & Wu, T. (2018). Influence of lignocellulose and plant cell walls on biomass char morphology and combustion reactivity. *Biomass and Bioenergy*, *119*, 480–491. https://doi.org/10.1016/j.biombioe.2018.10.011

Papadakis, S. E., & Bahu, R. E. (1992). The Sticky Issues of Drying. *Drying Technology*, *10*(4), 817–837. https://doi.org/10.1080/07373939208916484

Parameswaran, B. (2009). Sugarcane Bagasse. In P. Singh nee' Nigam & A. Pandey (Eds.), *Biotechnology for Agro-Industrial Residues Utilisation: Utilisation of Agro-Residues* (pp. 239–252). Springer Netherlands. https://doi.org/10.1007/978-1-4020-9942-7_12

Park, Y., Chang, Y.-S., Park, J.-H., Yang, S.-Y., Chung, H., Jang, S.-K., Choi, I.-G., & Yeo, H. (2016). Energy Efficiency of Fluidized Bed Drying for Wood Particles. *Journal of the Korean Wood Science and Technology*, *44*(6), 821–827. https://doi.org/10.5658/WOOD.2016.44.6.821

Pereira, T., Neves, A. S. L., Silva, F. J. G., Godina, R., Morgado, L., & Pinto, G. F. L. (2020). Production Process Analysis and Improvement of Corrugated Cardboard Industry. *Procedia Manufacturing*, *51*, 1395–1402. https://doi.org/10.1016/j.promfg.2020.10.194

Perkins, J. A. (2020, July 24). *Advanced image analysis to characterise coal and predict burnout potential* [Thesis (University of Nottingham only)]. University of Nottingham. https://eprints.nottingham.ac.uk/59786/

Perkins, J., Williams, O., Wu, T., & Lester, E. (2020). Automated image analysis techniques to characterise pulverised coal particles and predict combustion char morphology. *Fuel*, *259*, 116022. https://doi.org/10.1016/j.fuel.2019.116022

Pires, J. C. M. (2019). Negative emissions technologies: A complementary solution for climate change mitigation. *Science of The Total Environment*, *672*, 502–514. https://doi.org/10.1016/j.scitotenv.2019.04.004

Potrč Obrecht, T., Röck, M., Hoxha, E., & Passer, A. (2020). BIM and LCA Integration: A Systematic Literature Review. *Sustainability*, *12*(14), Article 14. https://doi.org/10.3390/su12145534

Ptáček, P., Kubátová, D., Havlica, J., Brandštetr, J., Šoukal, F., & Opravil, T. (2010). Isothermal kinetic analysis of the thermal decomposition of kaolinite: The thermogravimetric study. *Thermochimica Acta*, *501*(1), 24–29. https://doi.org/10.1016/j.tca.2009.12.018

Puig-Arnavat, M., Shang, L., Sárossy, Z., Ahrenfeldt, J., & Henriksen, U. B. (2016). From a single pellet press to a bench scale pellet mill—Pelletizing six different biomass feedstocks. *Fuel Processing Technology*, *142*, 27–33. https://doi.org/10.1016/j.fuproc.2015.09.022

QCR Recycling Equipment. (2022). *How Many Times Can Cardboard Be Recycled?* https://www.qcr.co.uk/news/how-many-times-can-cardboard-be-recycled/

Ramírez-Gómez, Á. (2016). Research needs on biomass characterization to prevent handling problems and hazards in industry. *Particulate Science and Technology*, *34*(4), 432–441. https://doi.org/10.1080/02726351.2016.1138262

Ranieri, M. L., Huck, J. R., Sonnen, M., Barbano, D. M., & Boor, K. J. (2009). High temperature, short time pasteurization temperatures inversely affect bacterial numbers during refrigerated storage of pasteurized fluid milk. *Journal of Dairy Science*, *92*(10), 4823–4832. https://doi.org/10.3168/jds.2009-2144

Raso, J., & Barbosa-Cánovas, G. V. (2003). Nonthermal Preservation of Foods Using Combined Processing Techniques. *Critical Reviews in Food Science and Nutrition*, *43*(3), 265–285. https://doi.org/10.1080/10408690390826527

Regier, M., Rother, M., & Schuchmann, H. P. (2009). Althernative Heating Technologies. In *Processing Effects on Safety and Quality of Foods*. CRC Press.

Rezaei, H., Lim, C. J., Lau, A., & Sokhansanj, S. (2016). Size, shape and flow characterization of ground wood chip and ground wood pellet particles. *Powder Technology*, *301*, 737–746. https://doi.org/10.1016/j.powtec.2016.07.016

Rezaei, H., Tajilrou, M., Lee, J. S., Singaraveloo, K., Lau, A., & Sokhansanj, S. (2024). Evolution of biomass particles during pelletization process. *Particuology*, *86*, 182–187. https://doi.org/10.1016/j.partic.2023.05.007

Riaza, J., Mason, P. E., Jones, J. M., Williams, A., Gibbins, J., & Chalmers, H. (2020). Shape and size transformations of biomass particles during combustion. *Fuel*, *261*, 116334. https://doi.org/10.1016/j.fuel.2019.116334

Roberts, L. J., Mason, P. E., Jones, J. M., Gale, W. F., Williams, A., Hunt, A., & Ashman, J. (2019). The impact of aluminosilicate-based additives upon the sintering and melting behaviour of biomass ash. *Biomass and Bioenergy*, *127*, 105284. https://doi.org/10.1016/j.biombioe.2019.105284

Röser, D., Mola-Yudego, B., Sikanen, L., Prinz, R., Gritten, D., Emer, B., Väätäinen, K., & Erkkilä, A. (2011). Natural drying treatments during seasonal storage of wood for bioenergy in different European locations. *Biomass and Bioenergy*, *35*(10), 4238–4247. https://doi.org/10.1016/j.biombioe.2011.07.011

Ruhul Kabir, M., & Kumar, A. (2012). Comparison of the energy and environmental performances of nine biomass/coal co-firing pathways. *Bioresource Technology*, *124*, 394–405. https://doi.org/10.1016/j.biortech.2012.07.106

Ryu, C., Phan, A. N., Sharifi, V. N., & Swithenbank, J. (2007). Co-combustion of textile residues with cardboard and waste wood in a packed bed. *Experimental Thermal and Fluid Science*, *32*(2), 450–458. https://doi.org/10.1016/j.expthermflusci.2007.05.008

Sahni, E. K., & Chaudhuri, B. (2012). Contact drying: A review of experimental and mechanistic modeling approaches. *International Journal of Pharmaceutics*, *434*(1), 334–348. https://doi.org/10.1016/j.ijpharm.2012.06.010

Santiago-De La Rosa, N., González-Cardoso, G., Figueroa-Lara, J. de J., Gutiérrez-Arzaluz, M., Octaviano-Villasana, C., Ramírez-Hernández, I. F., & Mugica-Álvarez, V. (2018). Emission factors of atmospheric and climatic pollutants from crop residues burning. *Journal of the Air & Waste Management Association*, *68*(8), 849–865. https://doi.org/10.1080/10962247.2018.1459326

Sarkar, S. (2015). Microbiological considerations: Pasteurized milk. *International Journal of Dairy Science*, *10*(5), 206–218. https://www.researchgate.net/profile/Surajit-Sarkar-6/publication/283023438_Microbiological_Considerations_Pasteurized_Milk/links/568b440b08aebccc4e1a3ede/Microbiological-Considerations-Pasteurized-Milk.pdf

Schlünder, E.-U. (2004). Drying of Porous Material During the Constant and the Falling Rate Period: A Critical Review of Existing Hypotheses. *Drying Technology*, *22*(6), 1517–1532. https://doi.org/10.1081/DRT-120038738

Serrano, C., Monedero, E., Lapuerta, M., & Portero, H. (2011). Effect of moisture content, particle size and pine addition on quality parameters of barley straw pellets. *Fuel Processing Technology*, *92*(3), 699–706. https://doi.org/10.1016/j.fuproc.2010.11.031

Shaw, M. D., & Tabil, L. G. (2007). Compression and relaxation characteristics of selected biomassgrinds. *2007 ASAE Annual Meeting*, 1. https://elibrary.asabe.org/abstract.asp?aid=23511

Shirinbakhsh, M., & Amidpour, M. (2017). Design and optimization of solar-assisted conveyer-belt dryer for biomass. *Energy Equipment and Systems*, *5*(2), 85–94. https://doi.org/10.22059/ees.2017.25716

Siddique, I. J., Salema, A. A., Antunes, E., & Vinu, R. (2022). Technical challenges in scaling up the microwave technology for biomass processing. *Renewable and Sustainable Energy Reviews*, *153*, 111767. https://doi.org/10.1016/j.rser.2021.111767

Silva, D., Nunes, A. O., da Silva Moris, A., Moro, C., & Piekarski, T. O. R. (2017). How important is the LCA software tool you choose Comparative results from GaBi, openLCA, SimaPro and Umberto. *Proceedings of the VII Conferencia Internacional de Análisis de Ciclo de Vida En Latinoamérica, Medellin, Colombia*, 10–15. https://www.researchgate.net/profile/Thiago-Rodrigues-20/publication/318217178_How_important_is_the_LCA_software_tool_you_choose_Comparative_results_from_GaBi_openLCA_SimaPro_and_Umberto/links/5fbe51c0299bf104cf75bc02/How-important-is-the-LCA-software-tool-you-choose-Comparative-results-from-GaBi-openLCA-SimaPro-and-Umberto.pdf

Soysal, Y. (2004). Microwave Drying Characteristics of Parsley. *Biosystems Engineering*, *89*(2), 167–173. https://doi.org/10.1016/j.biosystemseng.2004.07.008

Stanley, R. A., & Petersen, K. (2017). Microwave-assisted pasteurization and sterilization—Commercial perspective. In M. Regier, K. Knoerzer, & H. Schubert (Eds.), *The Microwave Processing of Foods (Second Edition)* (pp. 200–219). Woodhead Publishing. https://doi.org/10.1016/B978-0-08-100528-6.00010-3

Statista. (2023). *UK: Packaging waste generated & recycled by material*. https://www.statista.com/statistics/476098/packaging-waste-and-reclycing-uk/

Steenari, B.-M., & Lindqvist, O. (1998). High-temperature reactions of straw ash and the anti-sintering additives kaolin and dolomite. *Biomass and Bioenergy*, *14*(1), 67–76. https://doi.org/10.1016/S0961-9534(97)00035-4

Steenari, B.-M., Lundberg, A., Pettersson, H., Wilewska-Bien, M., & Andersson, D. (2009). Investigation of Ash Sintering during Combustion of Agricultural Residues and the Effect of Additives. *Energy & Fuels*, *23*(11), 5655–5662. https://doi.org/10.1021/ef900471u

Sumner, S. E. (n.d.). *Triboelectric separation of paper and HDPE flake mixture*. California State University, Sacramento.

Šupuk, E., Zarrebini, A., Reddy, J. P., Hughes, H., Leane, M. M., Tobyn, M. J., Timmins, P., & Ghadiri, M. (2012). Tribo-electrification of active pharmaceutical ingredients and excipients. *Powder Technology*, *217*, 427–434. https://doi.org/10.1016/j.powtec.2011.10.059

Tamura, M., Watanabe, S., Kotake, N., & Hasegawa, M. (2014). Grinding and combustion characteristics of woody biomass for co-firing with coal in pulverised coal boilers. *Fuel*, *134*, 544–553. https://doi.org/10.1016/j.fuel.2014.05.083

Tao Wu, Edward Lester, * and, & Cloke, M. (2006, March 16). *A Burnout Prediction Model Based around Char Morphology* (world) [Research-article]. ACS Publications; American Chemical Society. https://doi.org/10.1021/ef050101o

Taylor, H. (2023, January 11). UK coal-burning power facility to stay open two years longer than planned. *The Guardian*. https://www.theguardian.com/environment/2023/jan/11/uk-coal-burning-power-plant-to-stay-open-two-years-longer-than-planned

Temmerman, M., Jensen, P. D., & Hébert, J. (2013). Von Rittinger theory adapted to wood chip and pellet milling, in a laboratory scale hammermill. *Biomass and Bioenergy*, *56*, 70–81. https://doi.org/10.1016/j.biombioe.2013.04.020

The British Standards Institution. (1998). *BS ISO 9276-1:1998—Representation of results of particle size analysis—Part 1: Graphical Representation. BSI*. https://bsol-bsigroup-com.nottingham.idm.oclc.org/Bibliographic/BibliographicInfoData/000000000030149834

The British Standards Institution. (2008). *BS ISO 9276-6:2008 Representation of results of particle size analysis. Descriptive and quantitative representation of particle shape and morphology*. https://bsol.bsigroup.com/Bibliographic/BibliographicInfoData/000000000030153567

The British Standards Institution. (2012). *PD ISO/TR 14047:2012—Environmental management—Life cycle assessment—Illustrative examples on how to apply ISO 14044 to impact assessment situations*.

The British Standards Institution. (2015a). *BS EN ISO 16948:2015 Solid biofuels. Determination of total content of carbon, hydrogen and nitrogen*. https://bsol.bsigroup.com/Bibliographic/BibliographicInfoData/000000000030275856

The British Standards Institution. (2015b). *BS EN ISO 16967:2015 Solid biofuels. Determination of major elements. Al, Ca, Fe, Mg, P, K, Si, Na and Ti*. https://bsol.bsigroup.com/Bibliographic/BibliographicInfoData/000000000030275859

The British Standards Institution. (2015c). *BS EN ISO 17829:2015 Solid biofuels. Determination of length and diameter of pellets*. https://bsol-bsigroup-com.nottingham.idm.oclc.org/Bibliographic/BibliographicInfoData/000000000030275445

The British Standards Institution. (2015d). *BS EN ISO 17831-1:2015 Solid biofuels. Determination of mechanical durability of pellets and briquettes. Pellets*. https://bsol-bsigroup-com.nottingham.idm.oclc.org/Bibliographic/BibliographicInfoData/000000000030275451

The British Standards Institution. (2015e). *PD ISO/TS 16996:2015 Solid biofuels. Determination of elemental composition by X-ray fluorescence*. https://bsol.bsigroup.com/Bibliographic/BibliographicInfoData/000000000030278082

The British Standards Institution. (2016a). *BS EN ISO 16993:2016 Solid biofuels. Conversion of analytical results from one basis to another*. https://bsol.bsigroup.com/Bibliographic/BibliographicInfoData/000000000030333395

The British Standards Institution. (2016b). *BS EN ISO 17827-2:2016 Solid biofuels. Determination of particle size distribution for uncompressed fuels. Vibrating screen method using sieves with aperture of 3,15 mm and below*. https://bsol.bsigroup.com/Bibliographic/BibliographicInfoData/000000000030275873

The British Standards Institution. (2016c). *BS EN ISO 17830:2016—Solid biofuels. Particle size distribution of disintegrated pellets*. https://bsol-bsigroup-com.nottingham.idm.oclc.org/Bibliographic/BibliographicInfoData/000000000030275448

The British Standards Institution. (2017a). *BS EN ISO 18125:2017 Solid biofuels. Determination of calorific value*. https://bsol.bsigroup.com/Bibliographic/BibliographicInfoData/000000000030319065

The British Standards Institution. (2017b). *BS EN ISO 18134-2:2017 Solid biofuels. Determination of moisture content. Oven dry method. Total moisture. Simplified method*. https://bsol-bsigroup-com.nottingham.idm.oclc.org/Bibliographic/BibliographicInfoData/000000000030344291

The British Standards Institution. (2018). *BS EN ISO 14688-2:2018—Geotechnical investigation and testing. Identification and classification of soil. Principles for a classification*. https://bsol-bsigroup-com.nottingham.idm.oclc.org/Bibliographic/BibliographicInfoData/000000000030310841

The British Standards Institution. (2020). *BS EN ISO 14040:2006+A1:2020 Environmental management. Life cycle assessment. Principles and framework*. https://bsol-bsigroup-com.nottingham.idm.oclc.org/Bibliographic/BibliographicInfoData/000000000030379352

The British Standards Institution. (2021a). *BS EN ISO 14044:2006+A2:2020 Environmental management. Life cycle assessment. Requirements and guidelines*. https://bsol-bsigroup-com.nottingham.idm.oclc.org/Bibliographic/BibliographicInfoData/000000000030379355

The British Standards Institution. (2021b). *BS EN ISO 17225-2:2021 Solid biofuels. Fuel specifications and classes. Graded wood pellets*. https://bsol-bsigroup-com.nottingham.idm.oclc.org/Bibliographic/BibliographicInfoData/000000000030399877

The British Standards Institution. (2021c). *BS EN ISO 17225-6:2021 Solid biofuels. Fuel specifications and classes. Graded non-woody pellets*. https://bsol-bsigroup-com.nottingham.idm.oclc.org/Bibliographic/BibliographicInfoData/000000000030399889

The British Standards Institution. (2022a). *BS EN ISO 16559:2022 Solid biofuels. Vocabulary*. https://bsol-bsigroup-com.nottingham.idm.oclc.org/Bibliographic/BibliographicInfoData/000000000030409825

The British Standards Institution. (2022b). *BS EN ISO 18122:2022 Solid biofuels. Determination of ash content*. https://bsol-bsigroup-com.nottingham.idm.oclc.org/Bibliographic/BibliographicInfoData/000000000030439830

The British Standards Institution. (2023). *BS EN ISO 18123:2023 Solid biofuels. Determination of volatile matter*. https://bsol-bsigroup-com.nottingham.idm.oclc.org/Bibliographic/BibliographicInfoData/000000000030439838

The British Standards Institution. (2024). *BS ISO 562:2024 Hard coal and coke. Determination of volatile matter*. https://bsol-bsigroup-com.nottingham.idm.oclc.org/Bibliographic/BibliographicInfoData/000000000030474141

The International Centre for Sustainable Carbon. (2024, January 26). Biomass to Power: Europe with strong capacity growth, market slump in China. *ICSC*. https://www.sustainable-carbon.org/biomass-to-power-europe-with-strong-capacity-growth-market-slump-in-china/

The National Advisory Committee on Microbiological Criteria for Foods. (2006). Requisite Scientific Parameters for Establishing the Equivalence of Alternative Methods of Pasteurization†. *Journal of Food Protection*, *69*(5), 1190–1216. https://doi.org/10.4315/0362-028X-69.5.1190

Thek, G., & Obernberger, I. (2012). *The Pellet Handbook: The Production and Thermal Utilization of Biomass Pellets*. Routledge. https://doi.org/10.4324/9781849775328

Thomas, N. (2019, December 8). *Clock ticks for Drax to find a new financial model*. https://www.ft.com/content/0ea774da-1680-11ea-9ee4-11f260415385

Thrän, D., Dotzauer, M., Lenz, V., Liebetrau, J., & Ortwein, A. (2015). Flexible bioenergy supply for balancing fluctuating renewables in the heat and power sector—A review of technologies and concepts. *Energy, Sustainability and Society*, *5*(1), 35. https://doi.org/10.1186/s13705-015-0062-8

Toneva, P., Wirth, K.-E., & Peukert, W. (2011). Grinding in an air classifier mill — Part II: Characterisation of the two-phase flow. *Powder Technology*, *211*(1), 28–37. https://doi.org/10.1016/j.powtec.2011.03.010

Trubetskaya, A., Beckmann, G., Jensen, P. A., Jensen, A. D., & Glarborg, P. (2014). *A way of a single biomass particle shape characterization in a CFD model: 22nd European Biomass Conference and Exhibition*.

Tumuluru, J. S., Sokhansanj, S., Lim, C. J., Bi, T., Kuang, X. Y., & Melin, S. (2013). Effect of low and high storage temperatures on headspace gas concentrations and physical properties of wood pellets. *International Wood Products Journal*, *4*(4), 207–216. https://doi.org/10.1179/2042645312Y.0000000019

Tumuluru, J. S., Wright, C. T., Hess, J. R., & Kenney, K. L. (2011). A review of biomass densification systems to develop uniform feedstock commodities for bioenergy application. *Biofuels, Bioproducts and Biorefining*, *5*(6), 683–707. https://doi.org/10.1002/bbb.324

Tunde-Akintunde, T. Y., Afolabi, T. J., & Akintunde, B. O. (2005). Influence of drying methods on drying of bell-pepper (Capsicum annuum). *Journal of Food Engineering*, *68*(4), 439–442. https://doi.org/10.1016/j.jfoodeng.2004.06.021

Turconi, R., Tonini, D., Nielsen, C. F. B., Simonsen, C. G., & Astrup, T. (2014). Environmental impacts of future low-carbon electricity systems: Detailed life cycle assessment of a Danish case study. *Applied Energy*, *132*, 66–73. https://doi.org/10.1016/j.apenergy.2014.06.078

Turunen, K. (2017). *Energy efficiency improvement potential in a paper mill by means of heat load balancing* [Master's Thesis]. https://aaltodoc.aalto.fi/handle/123456789/24458

Tymoszuk, M., Mroczek, K., Kalisz, S., & Kubiczek, H. (2019). An investigation of biomass grindability. *Energy*, *183*, 116–126. https://doi.org/10.1016/j.energy.2019.05.167

Ugwu, S. N., Ugwuishiwu, B. O., Ekechukwu, O. V., Njoku, H., & Ani, A. O. (2015). Design, construction, and evaluation of a mixed mode solar kiln with black-painted pebble bed for timber seasoning in a tropical setting. *Renewable and Sustainable Energy Reviews*, *41*, 1404–1412. https://doi.org/10.1016/j.rser.2014.09.033

Ungureanu, N., Vlăduț, V., & Biriș, S.-Ștefan. (2022). Sustainable Valorization of Waste and By-Products from Sugarcane Processing. *Sustainability*, *14*(17), Article 17. https://doi.org/10.3390/su141711089

Unsworth, J., Barratt, D. J., & Roberts, P. T. (1991). *Coal quality and combustion performance*. https://www.osti.gov/etdeweb/biblio/5896922

US EPA, O. (2021, July 23). *Power Profiler* [Data and Tools]. https://www.epa.gov/egrid/power-profiler

Vainikka, P., Nieminen, M., & Sipilä, K. (2013). 7—Waste firing in large combustion plants. In N. B. Klinghoffer & M. J. Castaldi (Eds.), *Waste to Energy Conversion Technology* (pp. 98–119). Woodhead Publishing. https://doi.org/10.1533/9780857096364.2.98

Valentim, B. (2020). Petrography of coal combustion char: A review. *Fuel*, *277*, 118271. https://doi.org/10.1016/j.fuel.2020.118271

Valix, M., Katyal, S., & Cheung, W. H. (2017). Combustion of thermochemically torrefied sugar cane bagasse. *Bioresource Technology*, *223*, 202–209. https://doi.org/10.1016/j.biortech.2016.10.053

Varma, A. K., & Mondal, P. (2016). Physicochemical Characterization and Pyrolysis Kinetic Study of Sugarcane Bagasse Using Thermogravimetric Analysis. *Journal of Energy Resources Technology*, *138*(052205). https://doi.org/10.1115/1.4032729

Vijayaraj, B., Saravanan, R., & Renganarayanan, S. (2007). Studies on thin layer drying of bagasse. *International Journal of Energy Research*, *31*(4), 422–437. https://doi.org/10.1002/er.1237

Voegele, E. (2018). Hekotek to supply pellet plant to customer in Vietnam | Biomass Magazine. *Biomass Magazine*. https://biomassmagazine.com//articles/hekotek-to-supply-pellet-plant-to-customer-in-vietnam-15562

Voegele, E. (2023). Report: UK's biomass electricity generation fell in 2022. *Biomass Magazine*. https://biomassmagazine.com//articles/report-uks-biomass-electricity-generation-fell-in-2022

Voegele, E. (2024). UK considers extending subsidies for large-scale biomass power producers. *Biomass Magazine*. https://biomassmagazine.com//articles/uk-considers-extending-subsidies-for-large-scale-biomass-power-producers

Voicea, I., Vlăduţ, V., Cardei, P., Matache, M., Găgeanu, I., Voicu, G., Popescu, C., Paraschiv, G., & Kabas, O. (2015). Compacting process and mathematical analysis of miscanthus briquettes expansion. *Proceeding of the 43rd International Symposium "Actual Tasks on Agricultural Engineering", Opatija, Croaţia*, 24–27. https://www.academia.edu/download/41540133/

COMPACTING_PROCESS_AND_MATHEMATICAL_ANAL20160124-22097-1d7y8wn.pdf

von Rittinger, P. (1867). *Lehrbuch der Aufbereitungskunde: In ihrer neuesten Entwicklung und Ausbildung systematisch dargestellt*. Ernst & Korn.

Wang, L., Skreiberg, Ø., & Becidan, M. (2014). Investigation of additives for preventing ash fouling and sintering during barley straw combustion. *Applied Thermal Engineering*, *70*(2), 1262–1269. https://doi.org/10.1016/j.applthermaleng.2014.05.075

Wang, M., Elgowainy, A., Lu, Z., Baek, K., Balchandani, S., Benavides, P., Burnham, A., Cai, H., Chen, P., Gan, Y., Gracida-Alvarez, U., Hawkins, T., Huang, T.-Y., Iyer, R., Kar, S., Kelly, J., Kim, T., Kolodziej, C., Lee, K., … Zhang, J. (2023). *Greenhouse gases, Regulated Emissions, and Energy use in Technologies Model ® (2023 .Net)* [Computer software]. [object Object]. https://doi.org/10.11578/GREET-NET-2023/DC.20230907.2

Wäppling Raaholt, B., & Isaksson, S. (2017). Improving the heating uniformity in microwave processing. In M. Regier, K. Knoerzer, & H. Schubert (Eds.), *The Microwave Processing of Foods (Second Edition)* (pp. 381–406). Woodhead Publishing. https://doi.org/10.1016/B978-0-08-100528-6.00017-6

Watts, S. (2016). A mini review on technique of milk pasteurization. *Journal of Pharmacognosy and Phytochemistry*, *5*(5), 99–101. https://www.phytojournal.com/archives/2016.v5.i5.944/a-mini-review-on-technique-of-milk-pasteurization

Wells, W. F., & Smoot, L. D. (1991). Relation between reactivity and structure for coals and chars. *Fuel*, *70*(3), 454–458. https://doi.org/10.1016/0016-2361(91)90138-Z

Williams, O. (2016, July 15). *On biomass milling for power generation* [Thesis (University of Nottingham only)]. University of Nottingham. https://eprints.nottingham.ac.uk/33464/

Williams, O., Eastwick, C., Kingman, S., Giddings, D., Lormor, S., & Lester, E. (2015). Investigation into the applicability of Bond Work Index (BWI) and Hardgrove Grindability Index (HGI) tests for several biomasses compared to Colombian La Loma coal. *Fuel*, *158*, 379–387. https://doi.org/10.1016/j.fuel.2015.05.027

Williams, O., Eastwick, C., Kingman, S., Giddings, D., Lormor, S., & Lester, E. (2017). Overcoming the caking phenomenon in olive mill wastes. *Industrial Crops and Products*, *101*, 92–102. https://doi.org/10.1016/j.indcrop.2017.02.036

Williams, O., Lester, E., Kingman, S., Giddings, D., Lormor, S., & Eastwick, C. (2017). Benefits of dry comminution of biomass pellets in a knife mill. *Biosystems Engineering*, *160*, 42–54. https://doi.org/10.1016/j.biosystemseng.2017.05.011

Williams, O., Newbolt, G., Eastwick, C., Kingman, S., Giddings, D., Lormor, S., & Lester, E. (2016). Influence of mill type on densified biomass comminution. *Applied Energy*, *182*, 219–231. https://doi.org/10.1016/j.apenergy.2016.08.111

Williams, O., Nichols, D., Stevens, L., Güleç, F., Perkins, J., & Lester, E. (2024). Evaluation of a Proposed Milling Performance Metric for a Vertical Spindle Mill and Novel Burnout Prediction Tool for a Drop Tube Furnace. *In Preparation*.

Williams, O., Ure, A., Stevens, L., Binner, E., Dodds, C., Kingman, S., Das, B., Dash, P. S., & Lester, E. (2019). Formation of Metallurgical Coke within Minutes through Coal Densification and Microwave Energy. *Energy & Fuels*, *33*(7), 6817–6828. https://doi.org/10.1021/acs.energyfuels.9b00511

Windsor, Z., & Bate, S. T. (2019). Assessing the safety and suitability of nesting material for singly housed mice with surgically fitted head plates. *Heliyon*, *5*(7). https://www.cell.com/heliyon/pdf/S2405-8440(19)35757-3.pdf

Xie, H.-Y., & Zhang, D.-W. (2001). Stokes shape factor and its application in the measurement of sphericity of non-spherical particles. *Powder Technology*, *114*(1), 102–105. https://doi.org/10.1016/S0032-5910(00)00269-2

Yadav, R., Omrani, A., Link, G., Vauhkonen, M., & Lähivaara, T. (2021). Microwave Tomography Using Neural Networks for Its Application in an Industrial Microwave Drying System. *Sensors*, *21*(20), Article 20. https://doi.org/10.3390/s21206919

Yahya, M., Fudholi, A., & Sopian, K. (2017). Energy and exergy analyses of solar-assisted fluidized bed drying integrated with biomass furnace. *Renewable Energy*, *105*, 22–29. https://doi.org/10.1016/j.renene.2016.12.049

Yi, J., Li, X., He, J., & Duan, X. (2019). Drying efficiency and product quality of biomass drying: A review. *Drying Technology*, *0*(0), 1–16. https://doi.org/10.1080/07373937.2019.1628772

Yin, C., Rosendahl, L., K. Kær, S., & J. Condra, T. (2004). Use of numerical modeling in design for co-firing biomass in wall-fired burners. *Chemical Engineering Science*, *59*(16), 3281–3292. https://doi.org/10.1016/j.ces.2004.04.036

Younis, M., Alnouri, S. Y., Abu Tarboush, B. J., & Ahmad, M. N. (2018). Renewable biofuel production from biomass: A review for biomass pelletization, characterization, and thermal conversion techniques. *International Journal of Green Energy*, *15*(13), 837–863. https://doi.org/10.1080/15435075.2018.1529581

Zahirović, S., Scharler, R., Kilpinen, P., & Obernberger, I. (2010). Validation of flow simulation and gas combustion sub-models for the CFD-based prediction of NOx formation in biomass grate furnaces. *Combustion Theory and Modelling*, *15*(1), 61–87. https://doi.org/10.1080/13647830.2010.524312

Zhan, H., Zhuang, X., Song, Y., Yin, X., & Wu, C. (2018). Insights into the evolution of fuel-N to NO*x* precursors during pyrolysis of N-rich nonlignocellulosic biomass. *Applied Energy*, *219*, 20–33. https://doi.org/10.1016/j.apenergy.2018.03.015

Zhuikov, A. V., Fetisova, O. Yu., & Glushkov, D. O. (2022). Thermal Analysis of the Combustion Processes of Brown Coal, Pine Sawdust, Cardboard, and Their Mixtures. *Solid Fuel Chemistry*, *56*(4), 285–292. https://doi.org/10.3103/S0361521922040115

Appendix A XRD Analysis of Sugarcane Straws

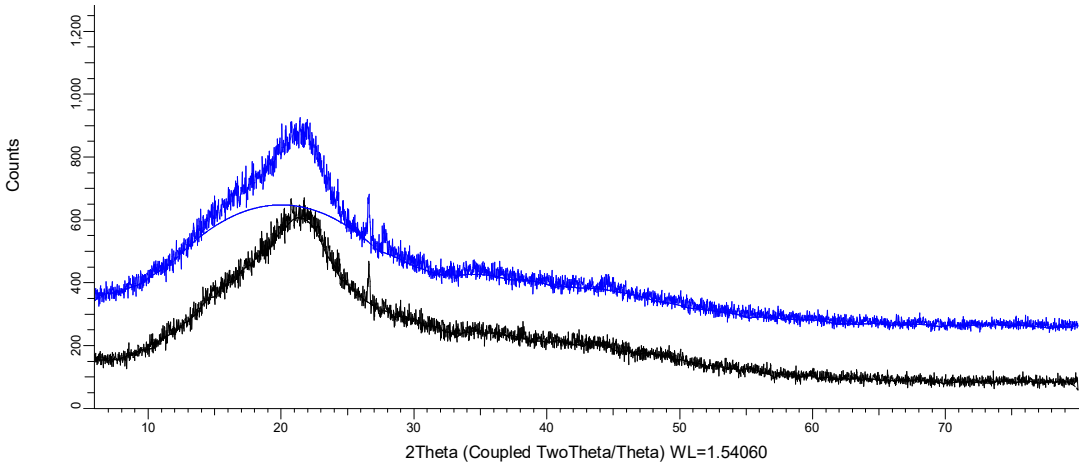

*The black line shows the XRD analysis of dry season sugarcane straw, and the blue line shows the XRD analysis of wet season sugarcane straw; the blue line is shifted upwards by 200 counts to illustrate the similarity in shape of the two lines.

Figure 0-1 XRD analysis of sugarcane straws

Appendix B Particle Size Distribution of Raw Biomass and Chars for the Eucalyptus and Cardboard Samples

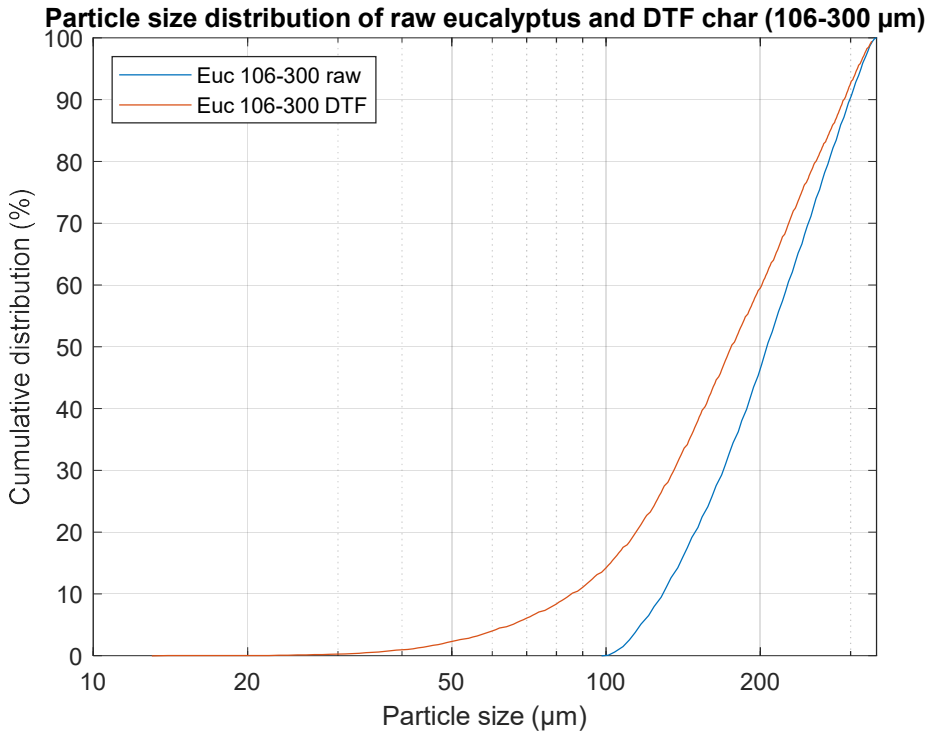

Figure 0-2 Particle size distribution of raw eucalyptus and DTF char (106-300 µm)

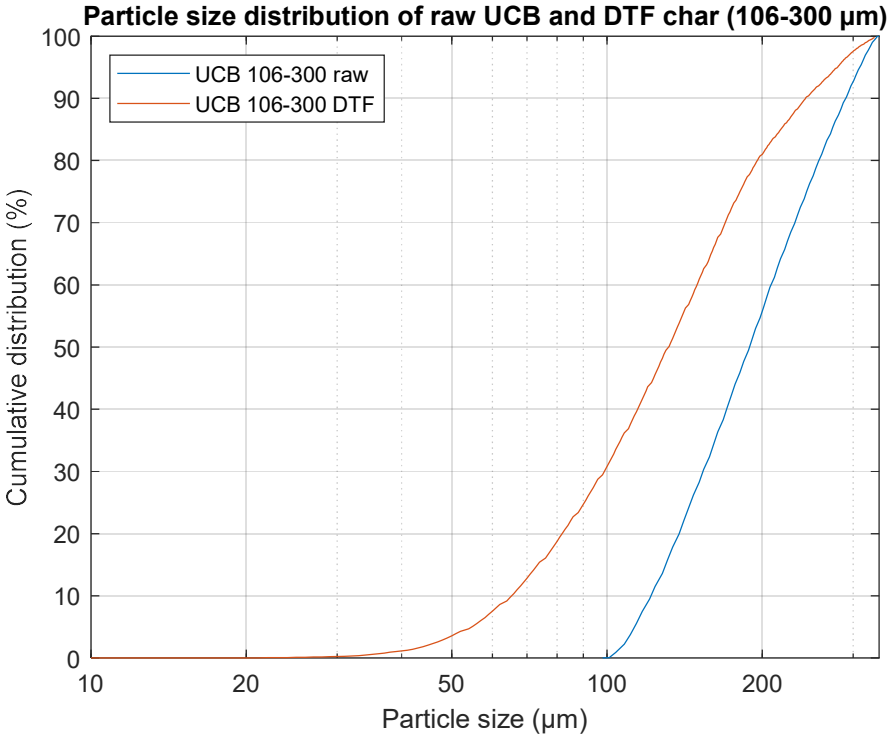

Figure 0-3 Particle size distribution of raw UCB and DTF char (106-300 µm)

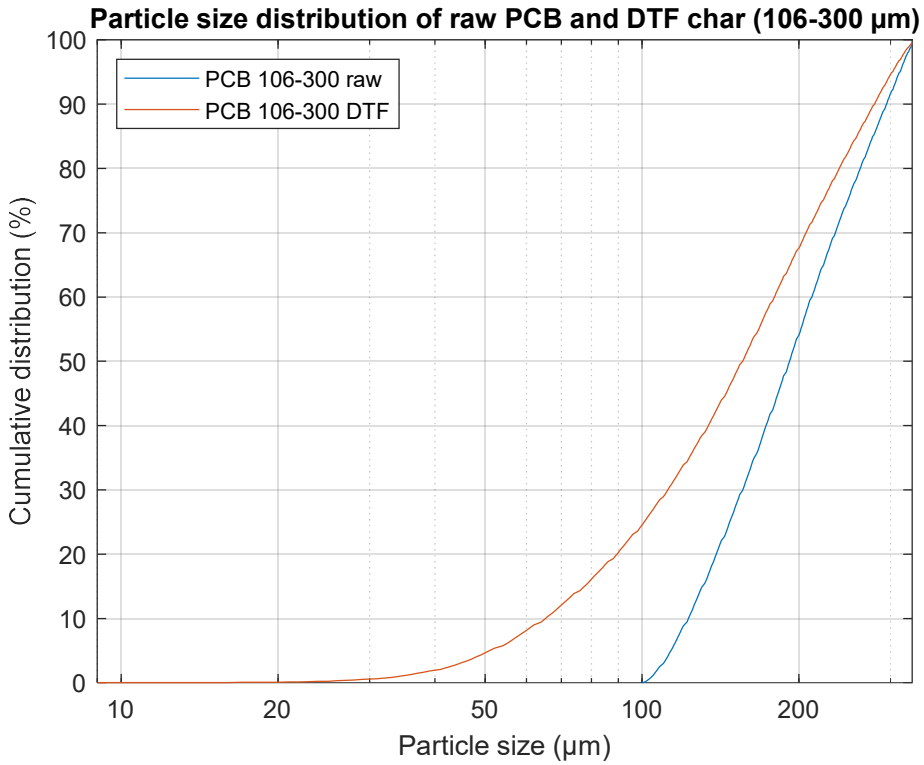

Figure 0-4 Particle size distribution of raw PCB and DTF char (106-300 µm)

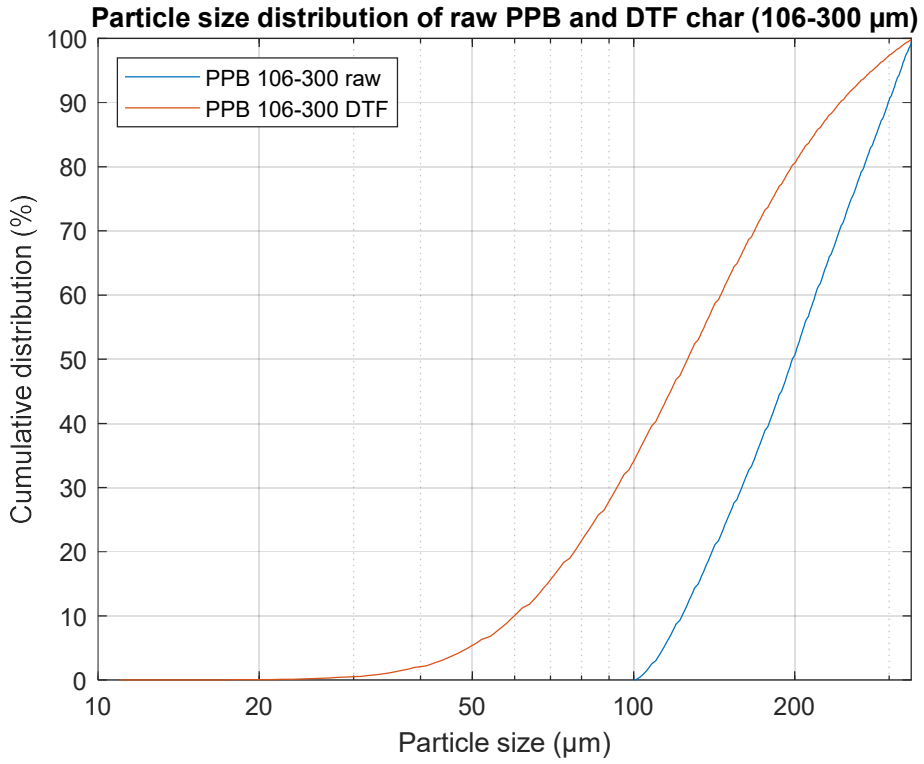

Figure 0-5 Particle size distribution of raw PPB and DTF char (106-300 µm)

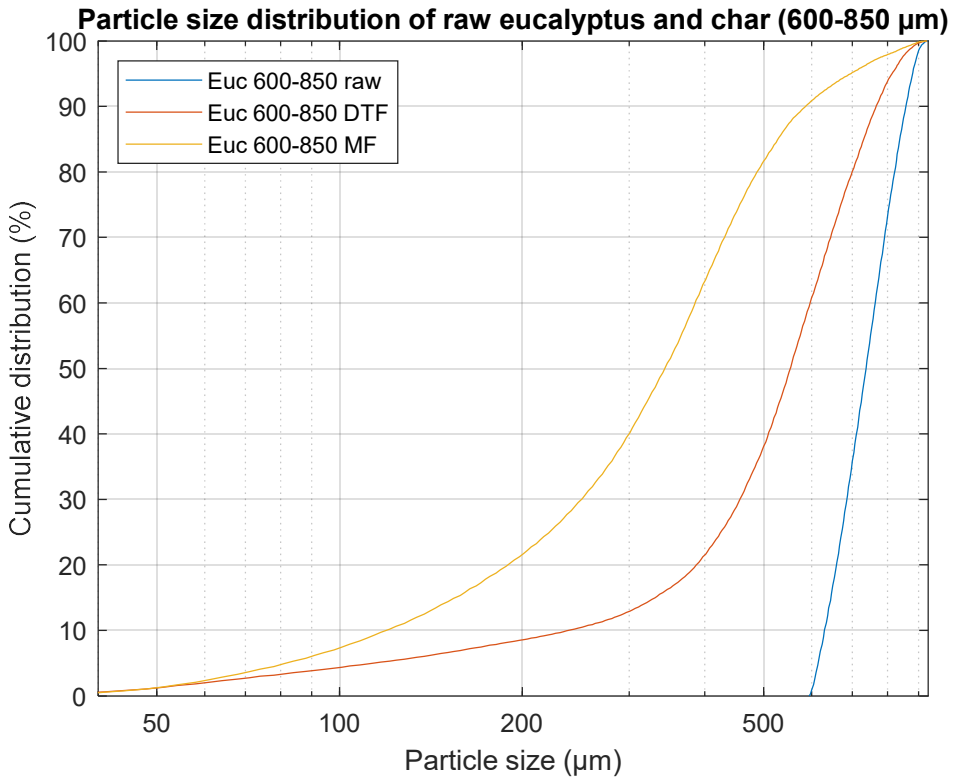

Figure 0-6 Particle size distribution of raw eucalyptus and char (600-850 µm)

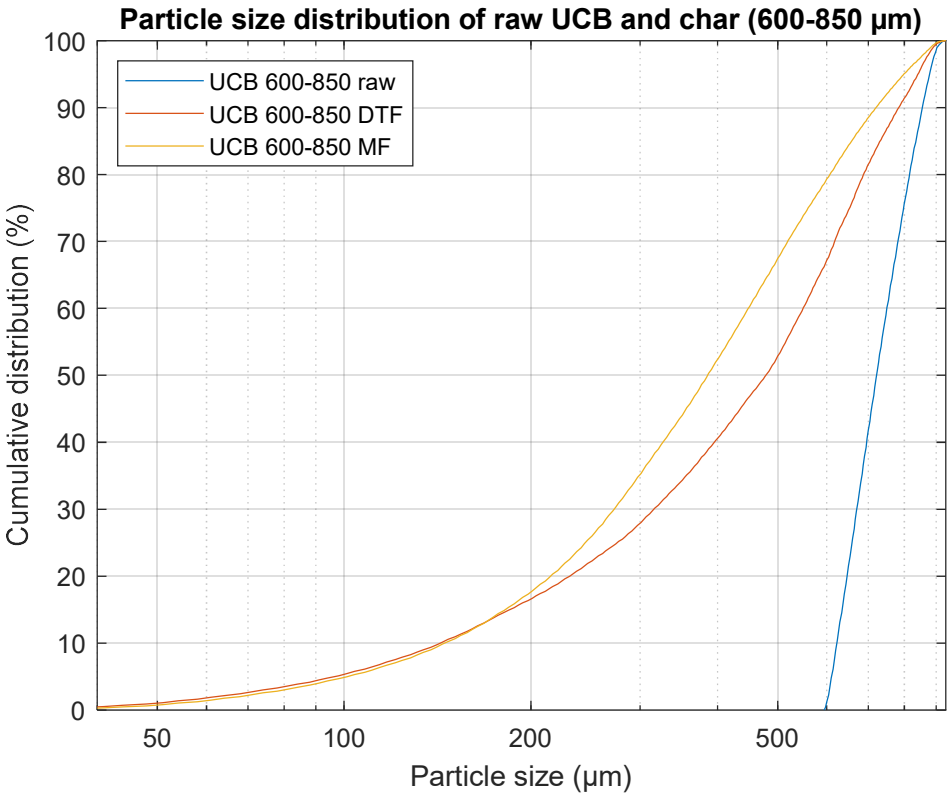

Figure 0-7 Particle size distribution of raw UCB and char (600-850 µm)

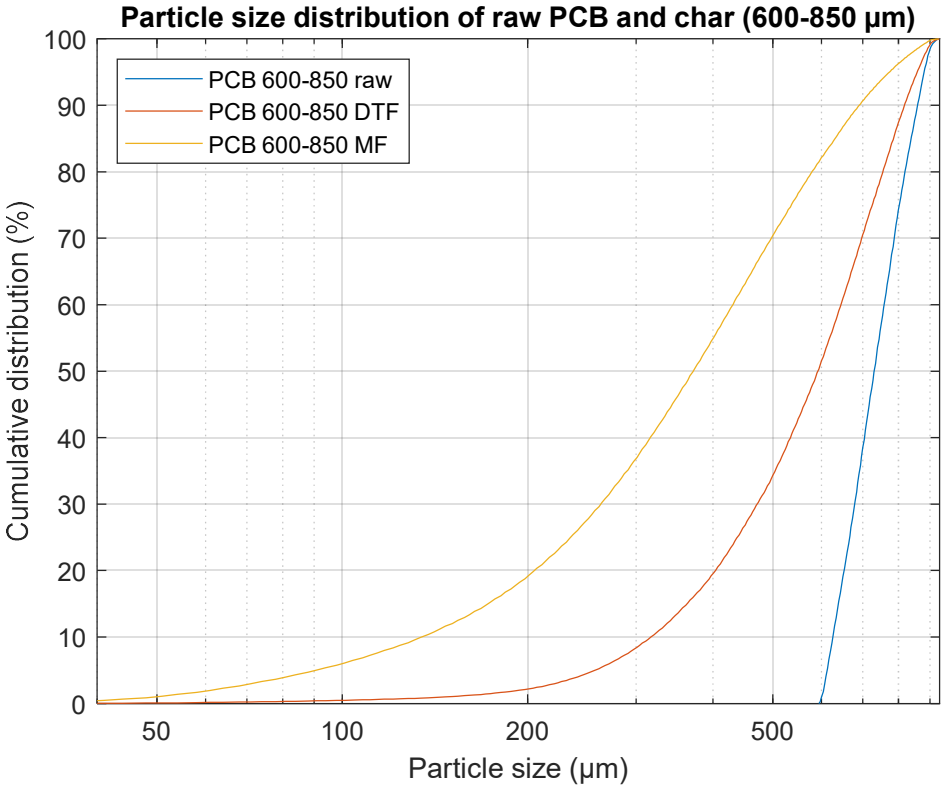

Figure 0-8 Particle size distribution of raw PCB and char (600-850 µm)

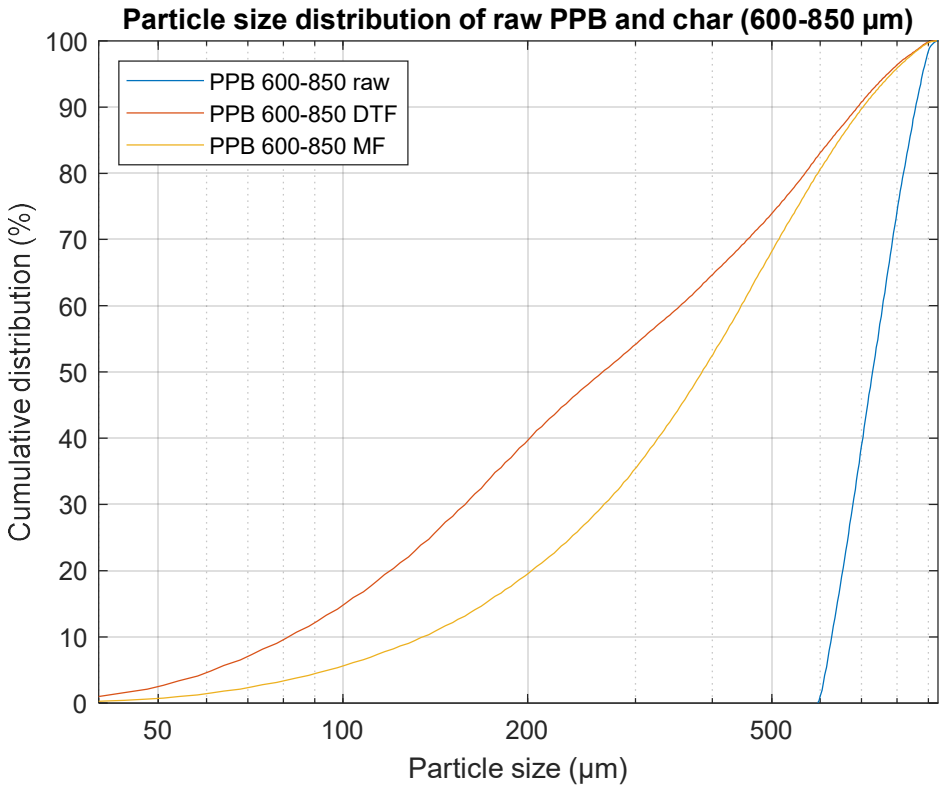

Figure 0-9 Particle size distribution of raw PPB and char (600-850 µm)

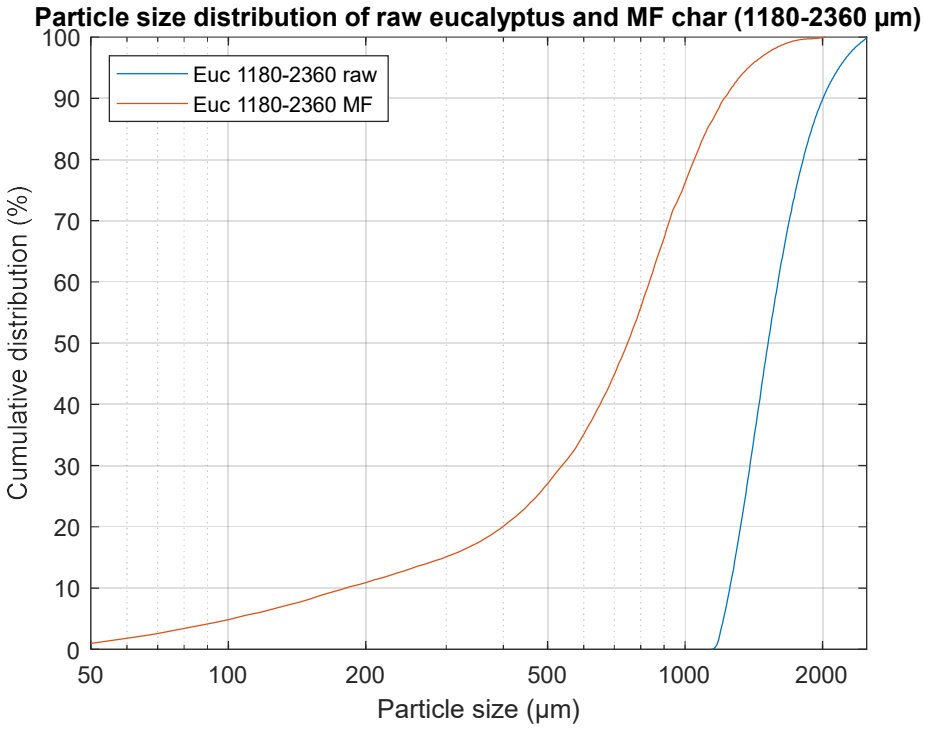

Figure 0-10 Particle size distribution of raw eucalyptus and MF char (1180-2360 µm)

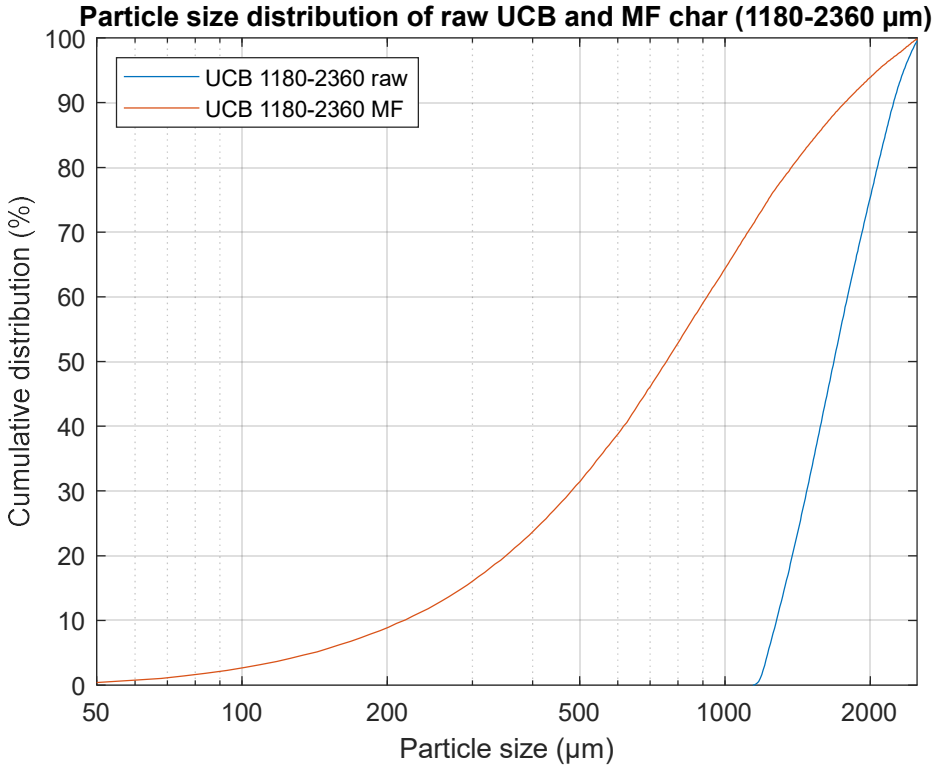

Figure 0-11 Particle size distribution of raw UCB and MF char (1180-2360 µm)

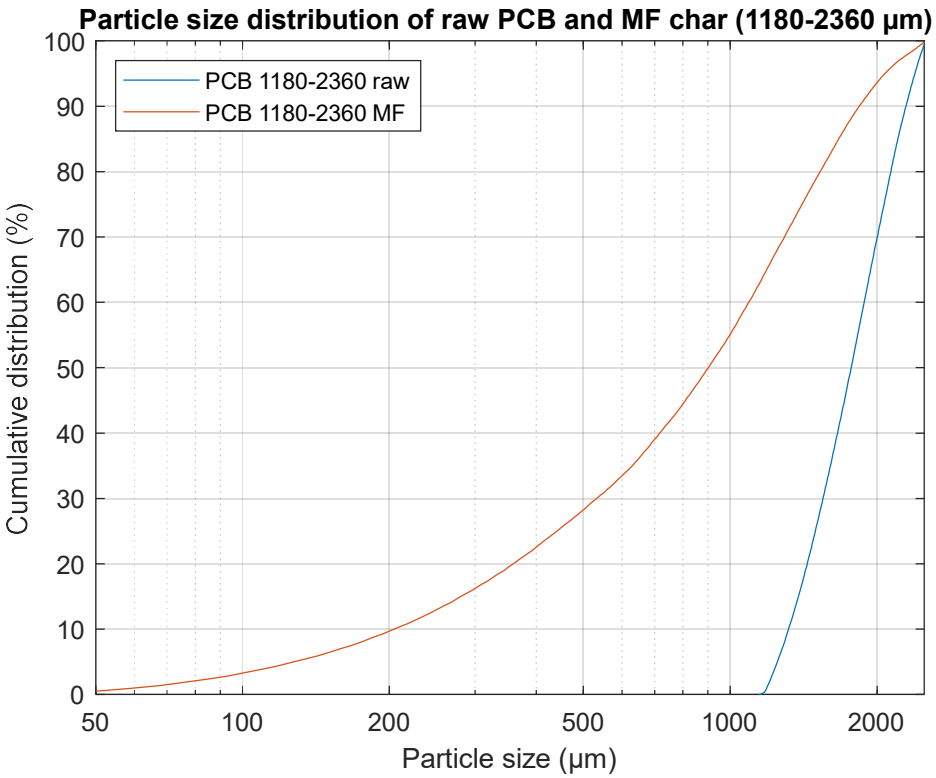

Figure 0-12 Particle size distribution of raw PCB and MF char (1180-2360 µm)

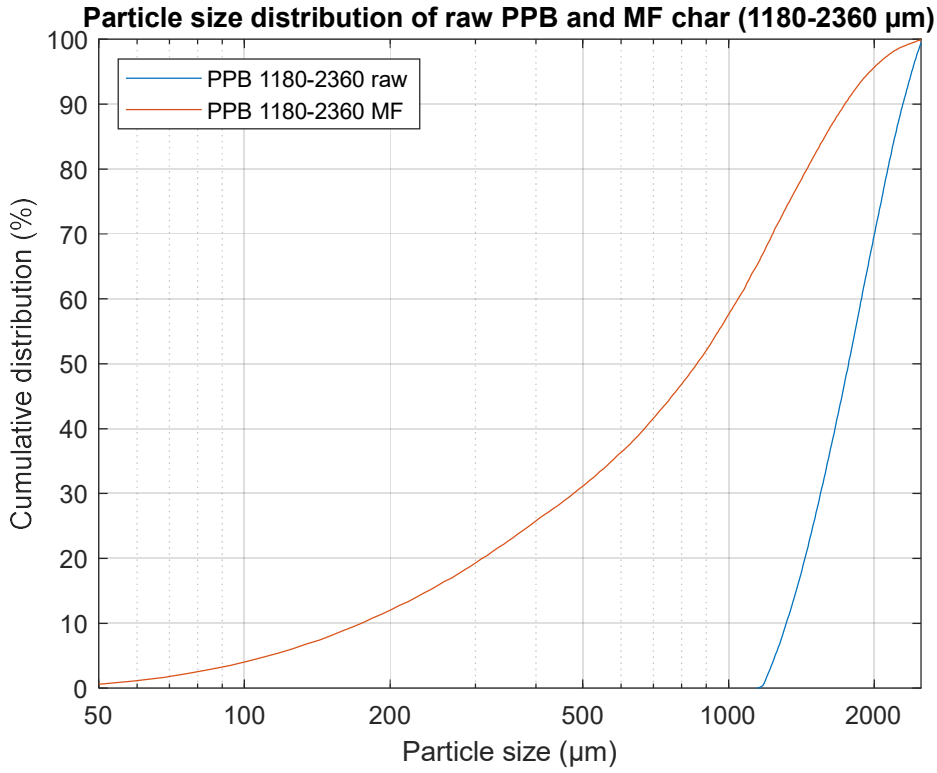

Figure 0-13 Particle size distribution of raw PPB and MF char (1180-2360 µm)

Appendix C Particle Shape Distribution of Raw Eucalyptus and Cardboard Samples

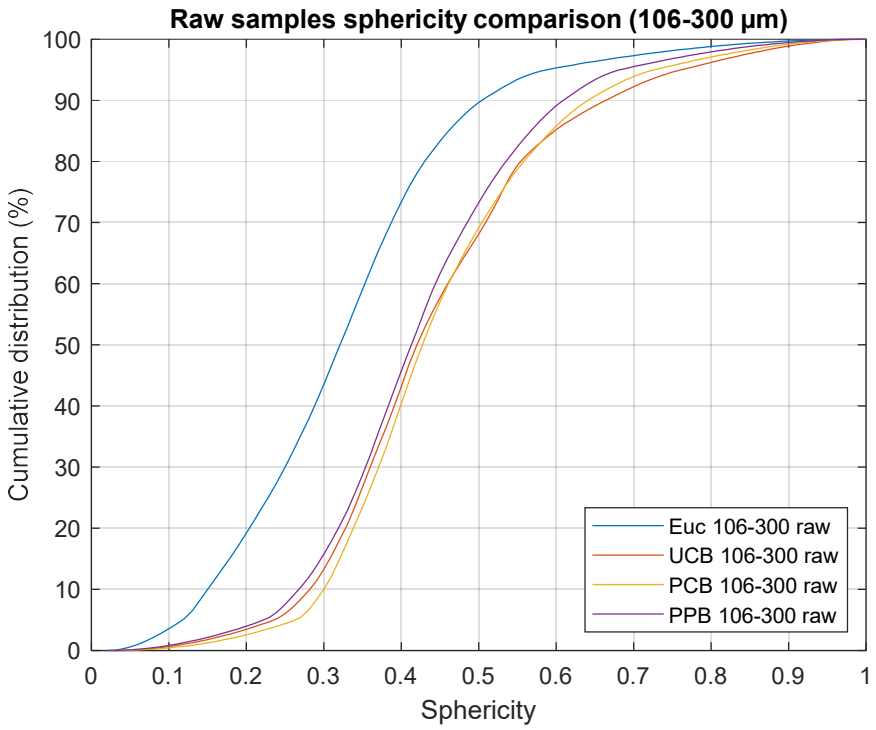

Figure 0-14 Raw samples sphericity comparison (106-300 µm)

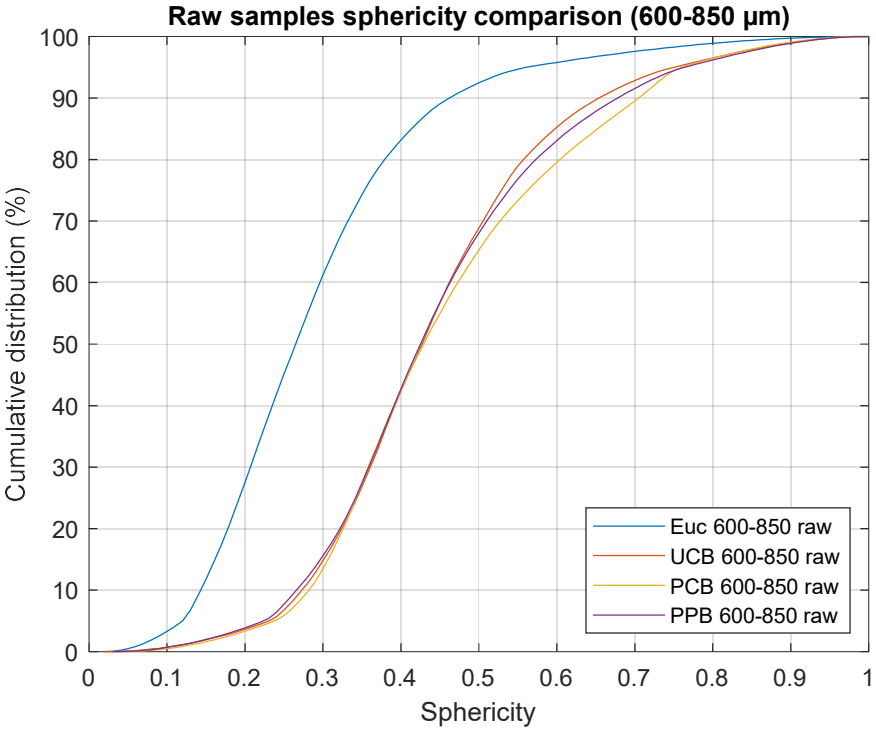

Figure 0-15 Raw samples sphericity comparison (600-850 µm)

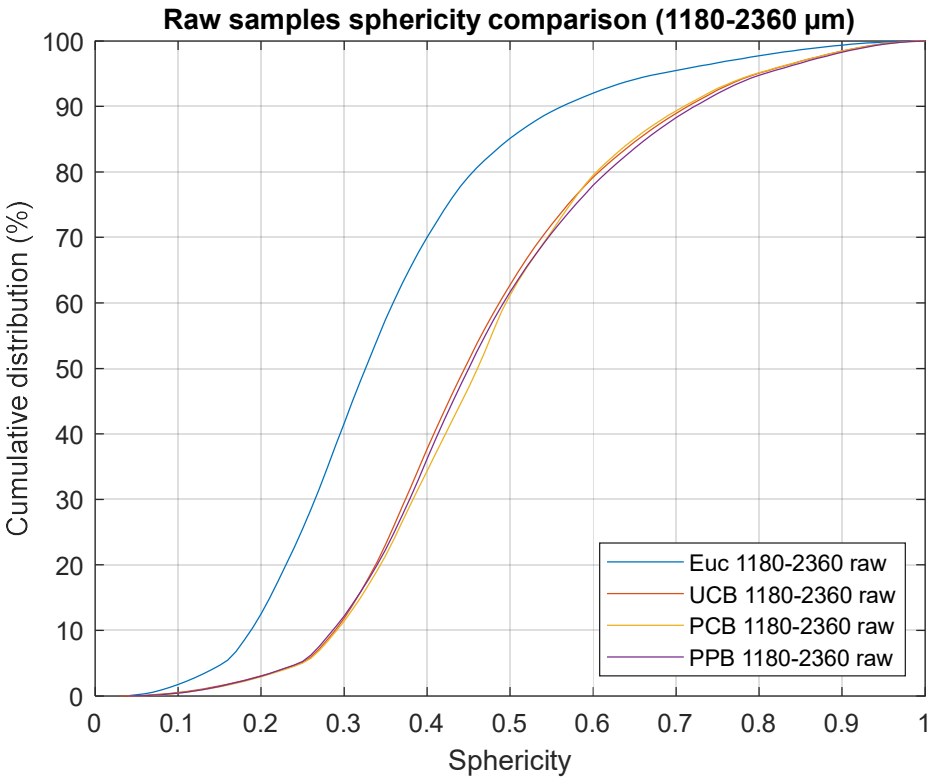

Figure 0-16 Raw samples sphericity comparison (1180-2360 µm)

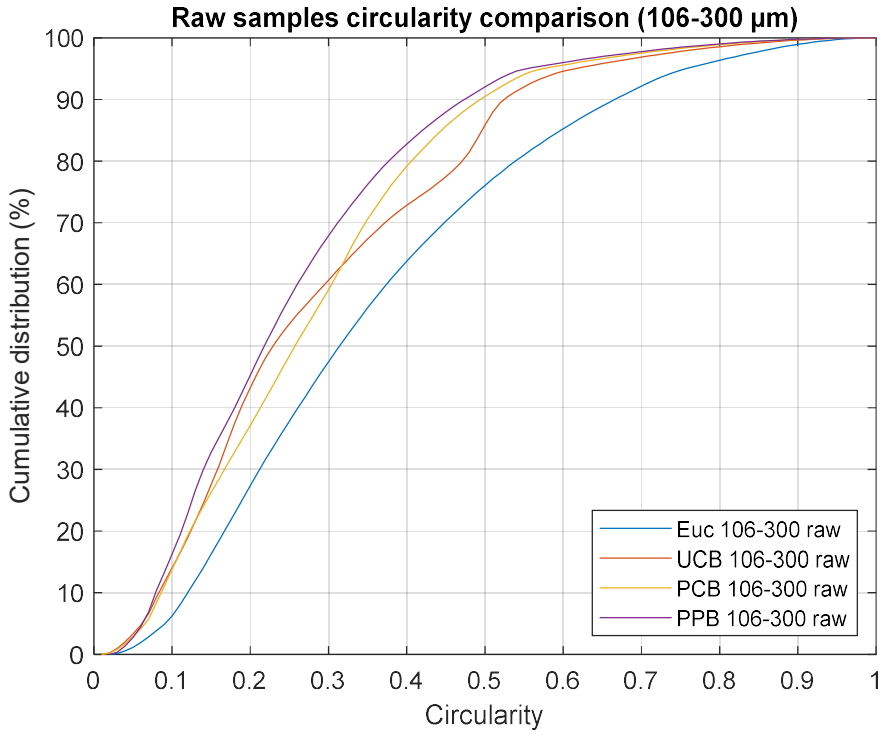

Figure 0-17 Raw samples circularity comparison (106-300 µm)

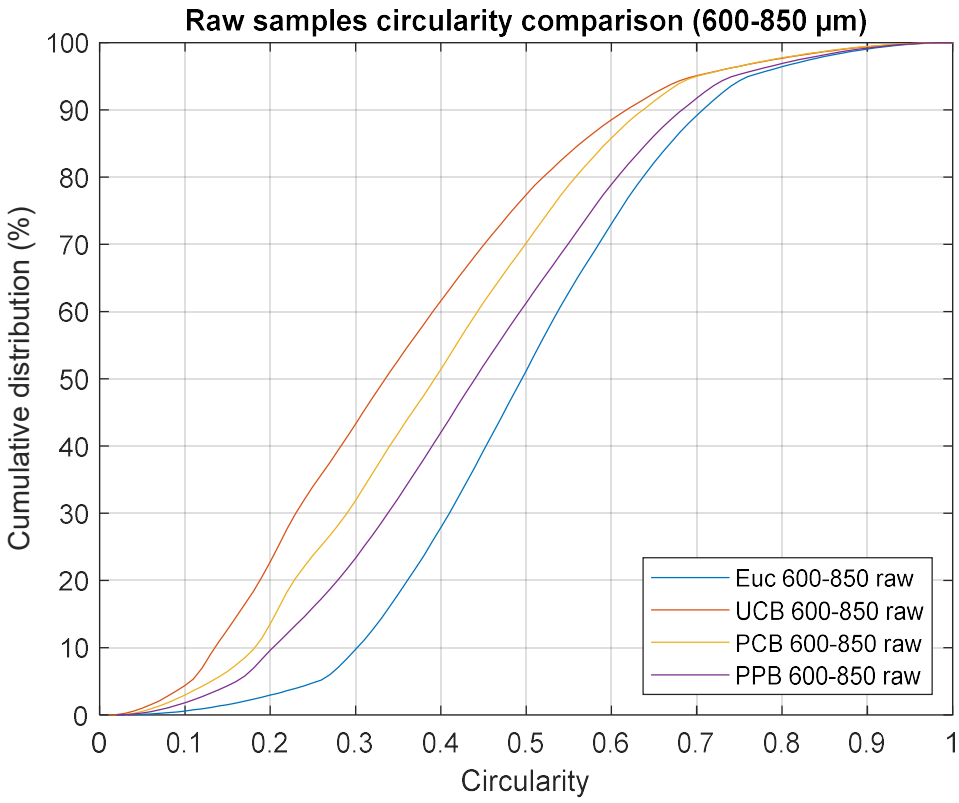

Figure 0-18 Raw samples circularity comparison (600-850 µm)

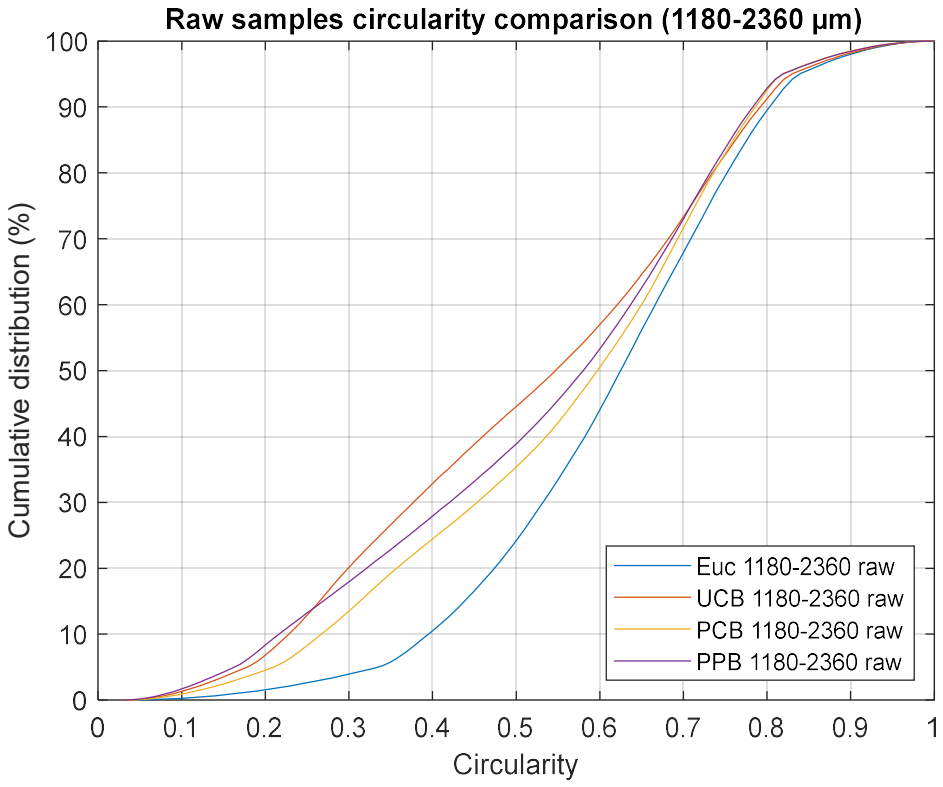

Figure 0-19 Raw samples circularity comparison (1180-2360 µm)

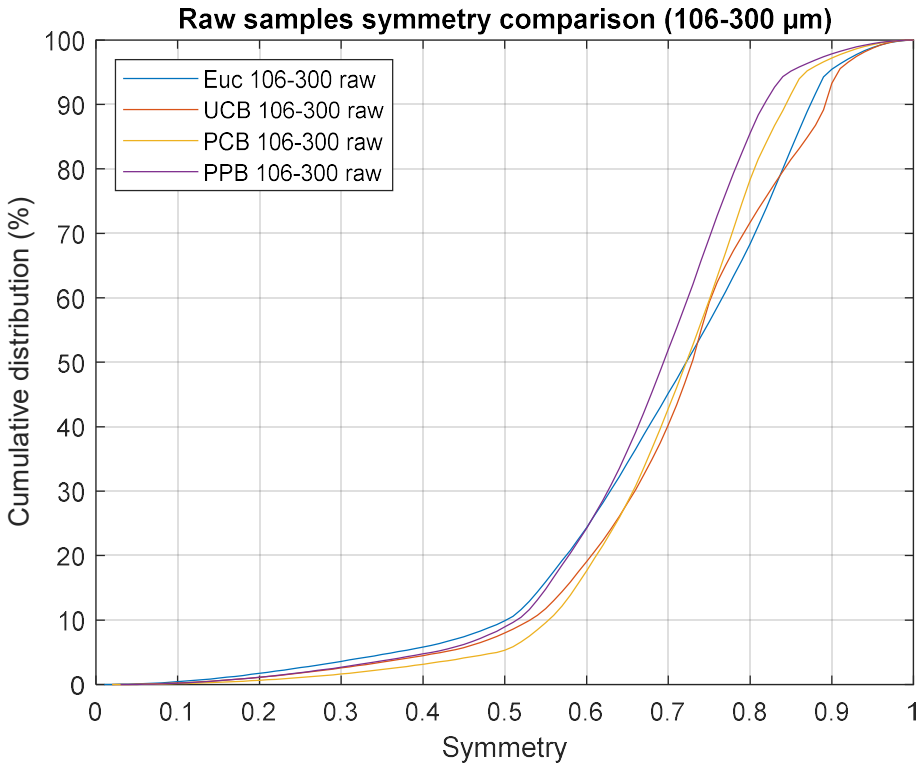

Figure 0-20 Raw samples symmetry comparison (106-300 µm)

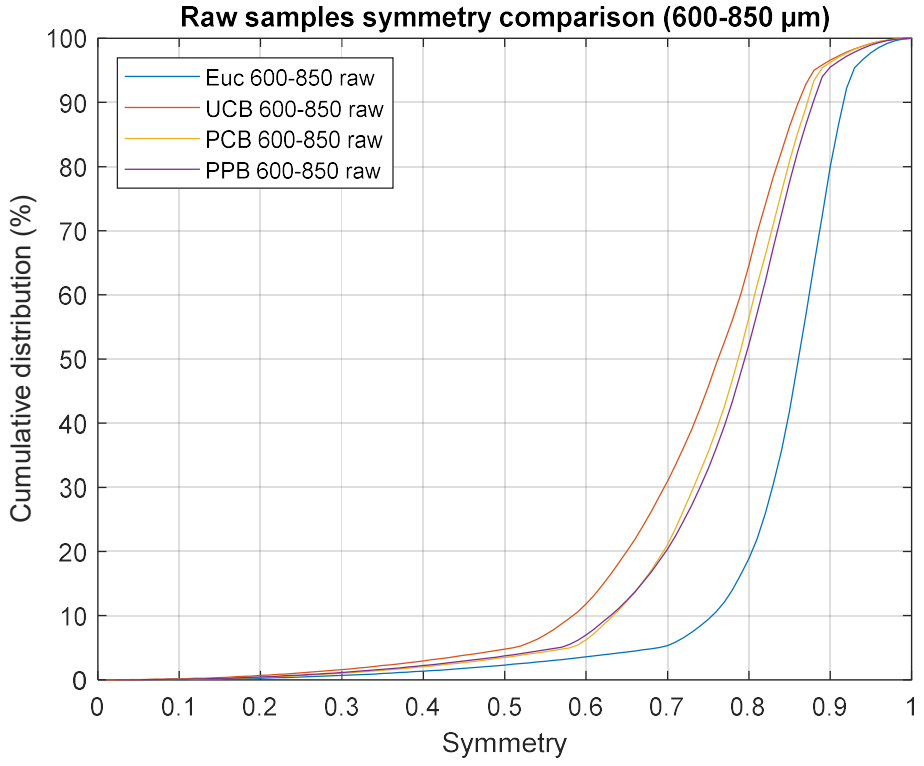

Figure 0-21 Raw samples symmetry comparison (600-850 µm)

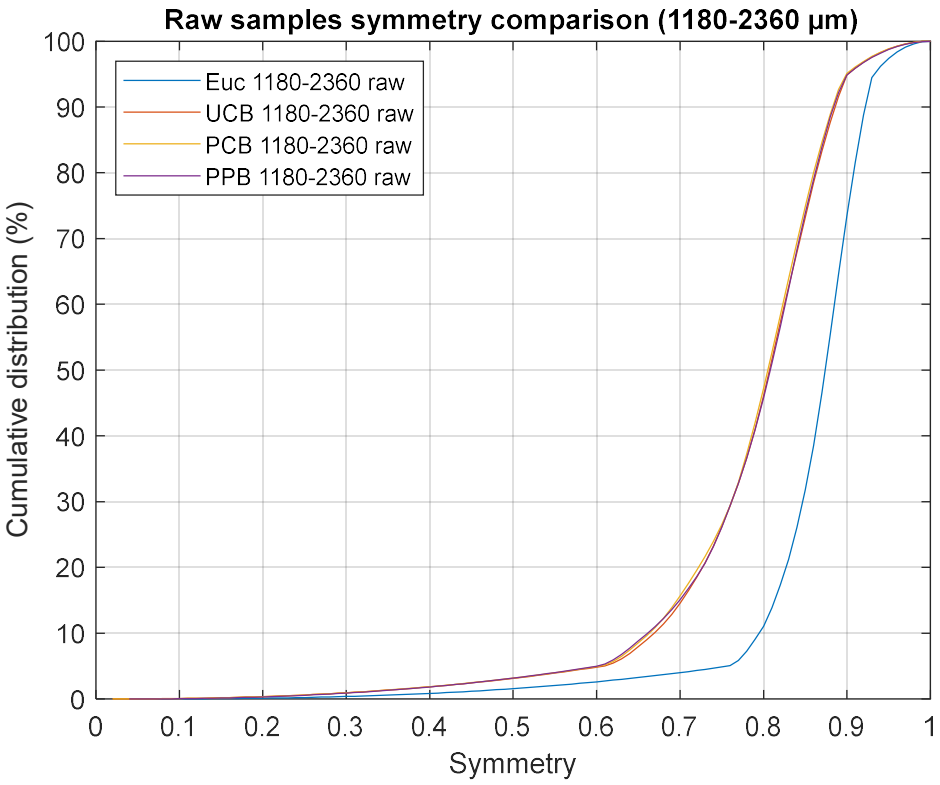

Figure 0-22 Raw samples symmetry comparison (1180-2360µm)

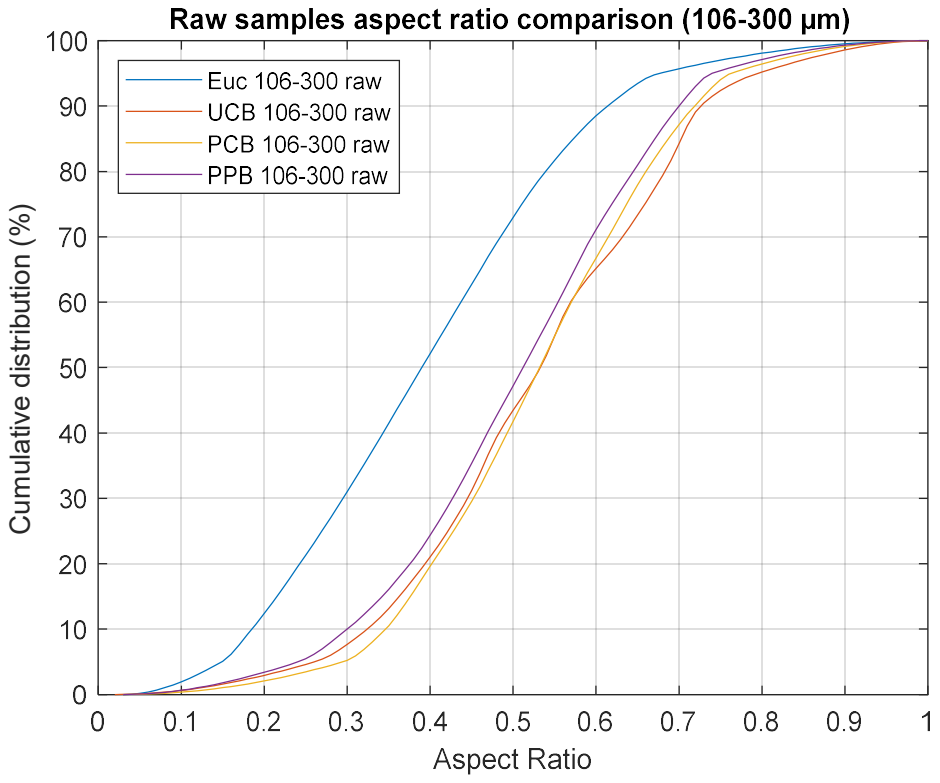

Figure 0-23 Raw samples aspect ratio comparison (106-300 µm)

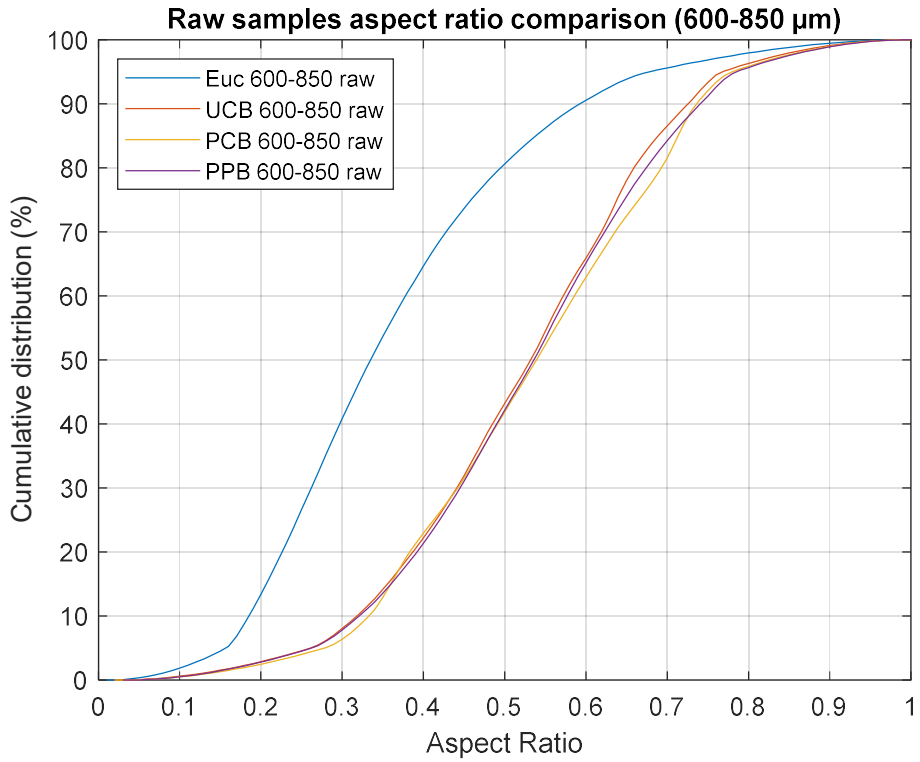

Figure 0-24 Raw samples aspect ratio comparison (600-850 µm)

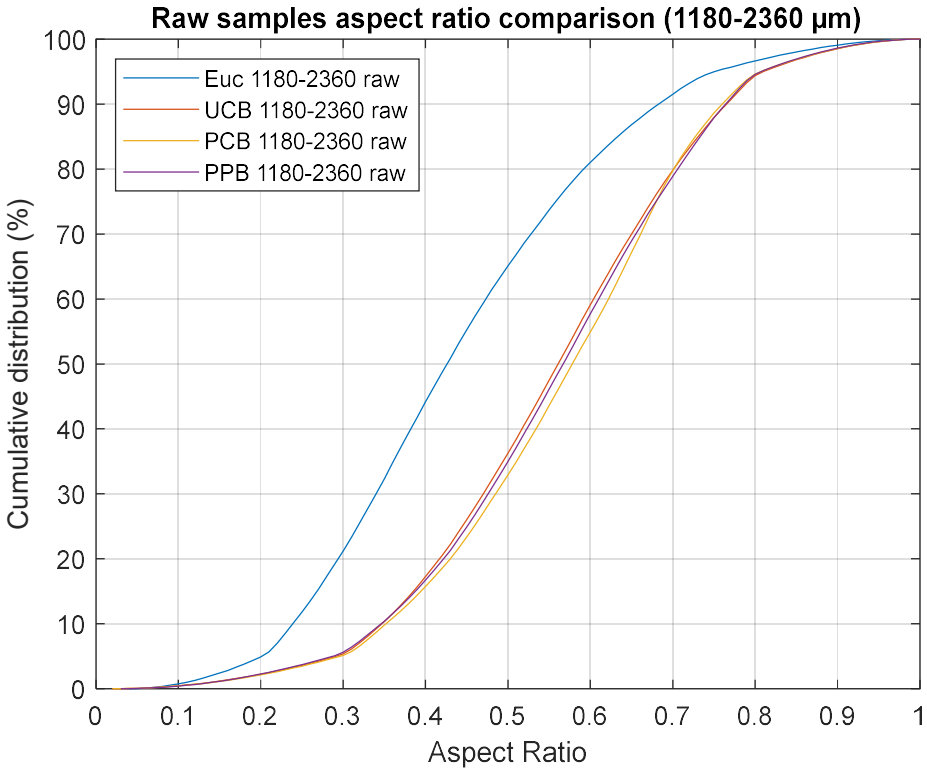

Figure 0-25 Raw samples aspect ratio comparison (1180-2360 µm)

Appendix D Particle Shape Distribution Comparison of Raw Biomass and Char for Eucalyptus and Cardboard Samples

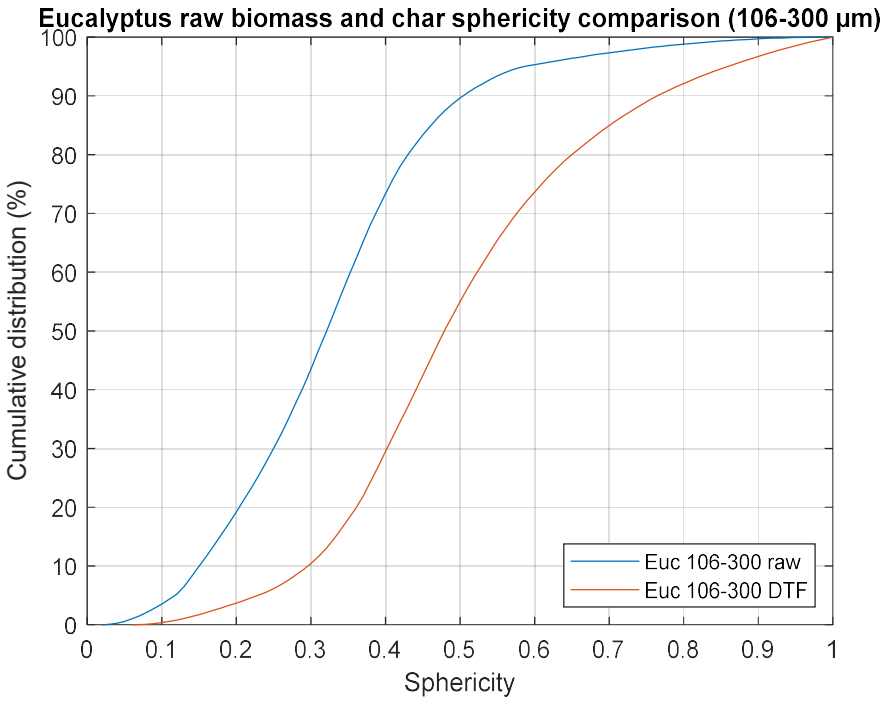

Figure 0-26 Eucalyptus raw biomass and char sphericity comparison (106-300 µm)

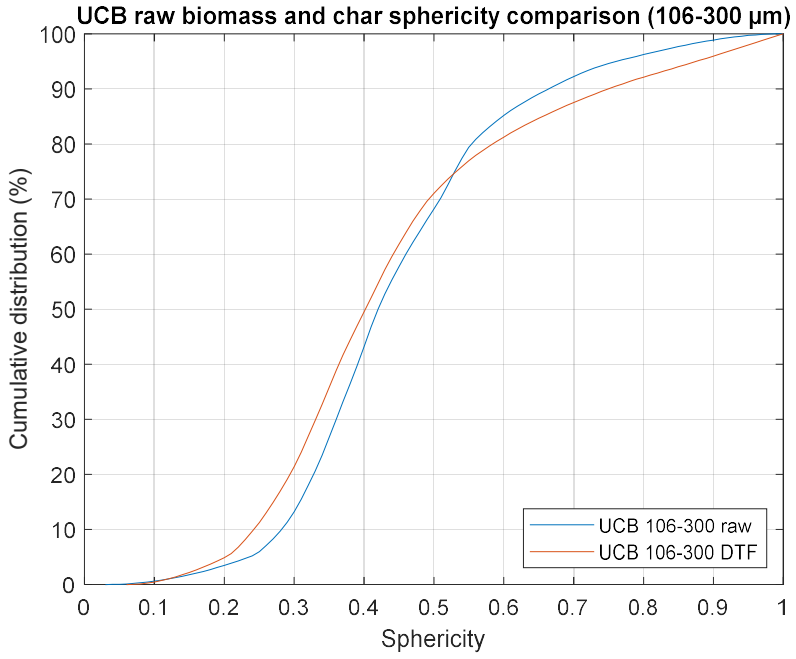

Figure 0-27 UCB raw biomass and char sphericity comparison (106-300 µm)

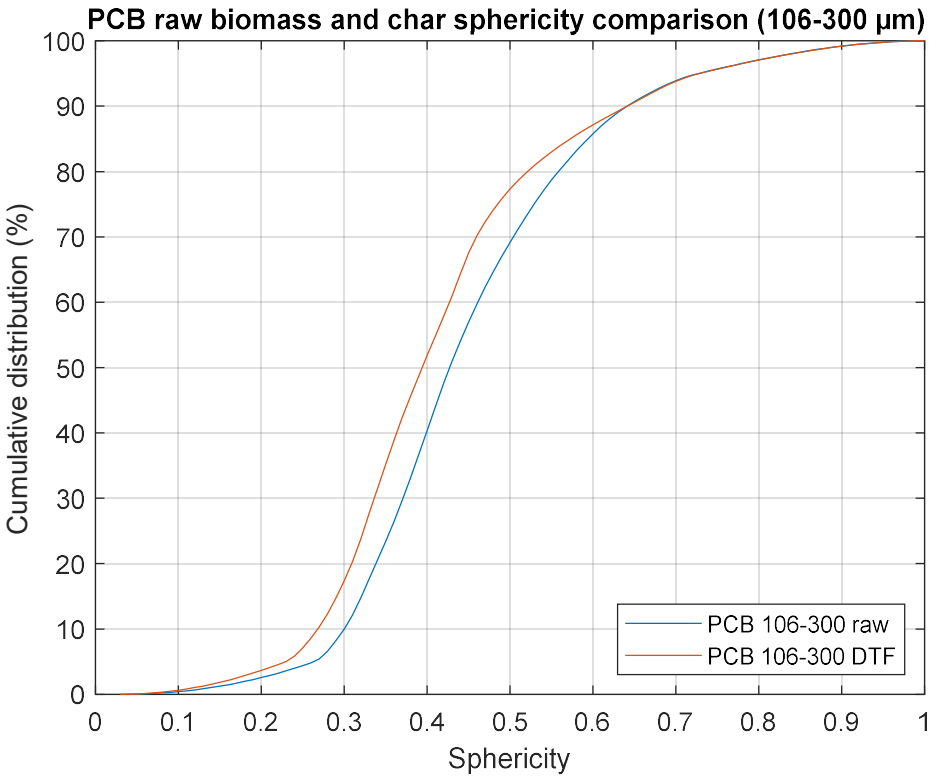

Figure 0-28 PCB raw biomass and char sphericity comparison (106-300 µm)

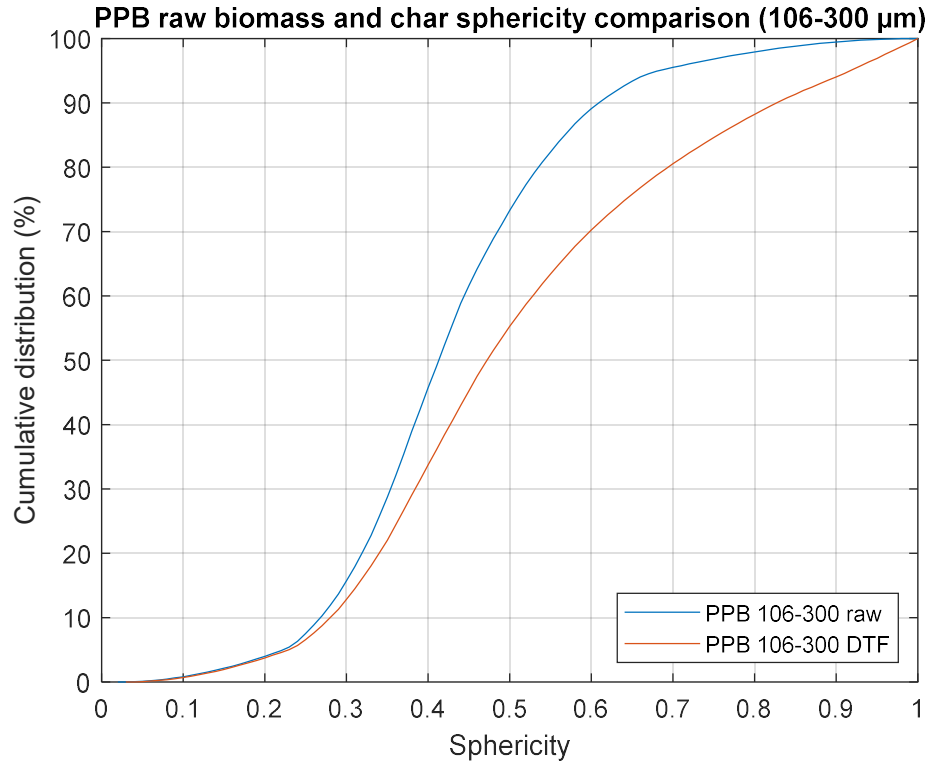

Figure 0-29 PPB raw biomass and char sphericity comparison (106-300 µm)

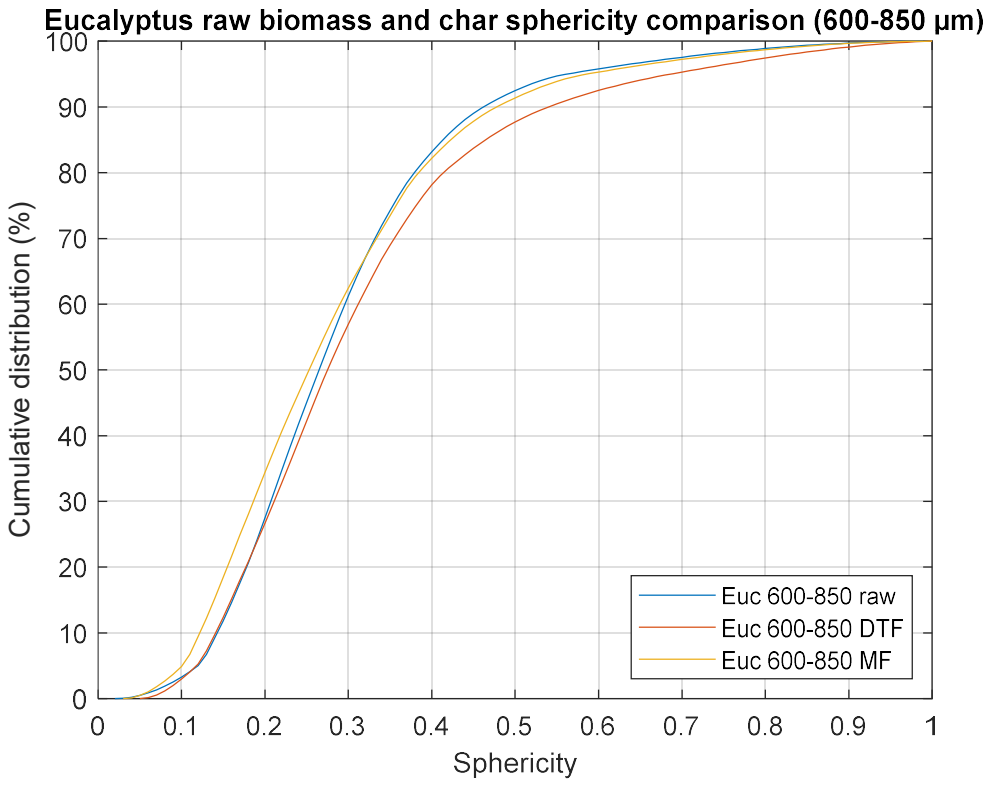

Figure 0-30 Eucalyptus raw biomass and char sphericity comparison (600-850 µm)

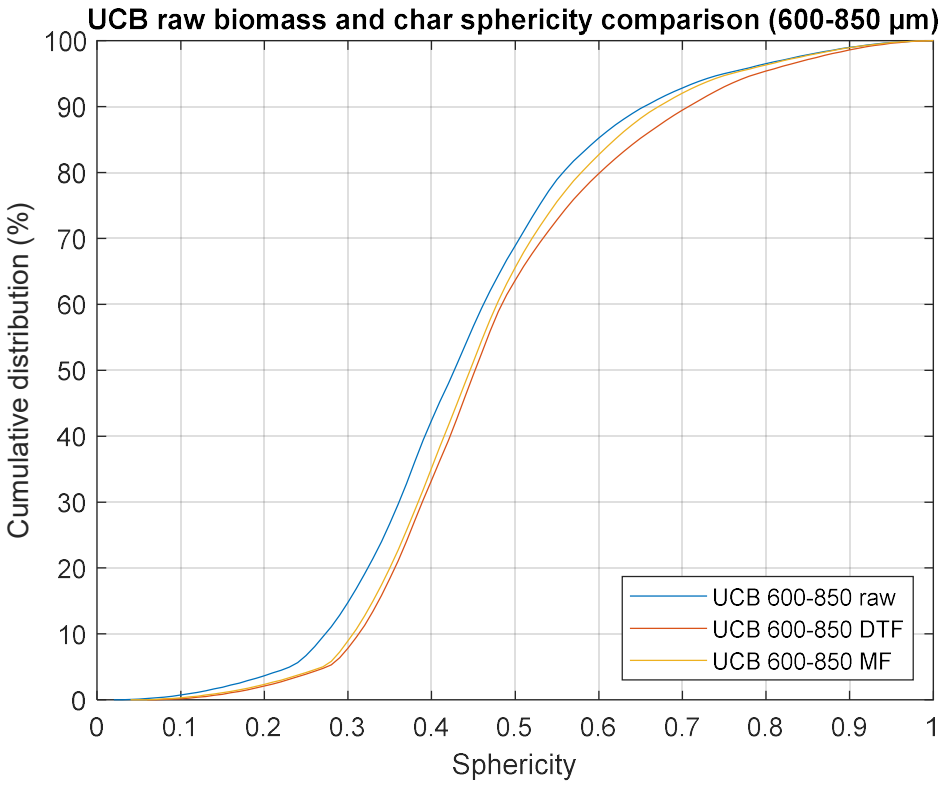

Figure 0-31 UCB raw biomass and char sphericity comparison (600-850 µm)

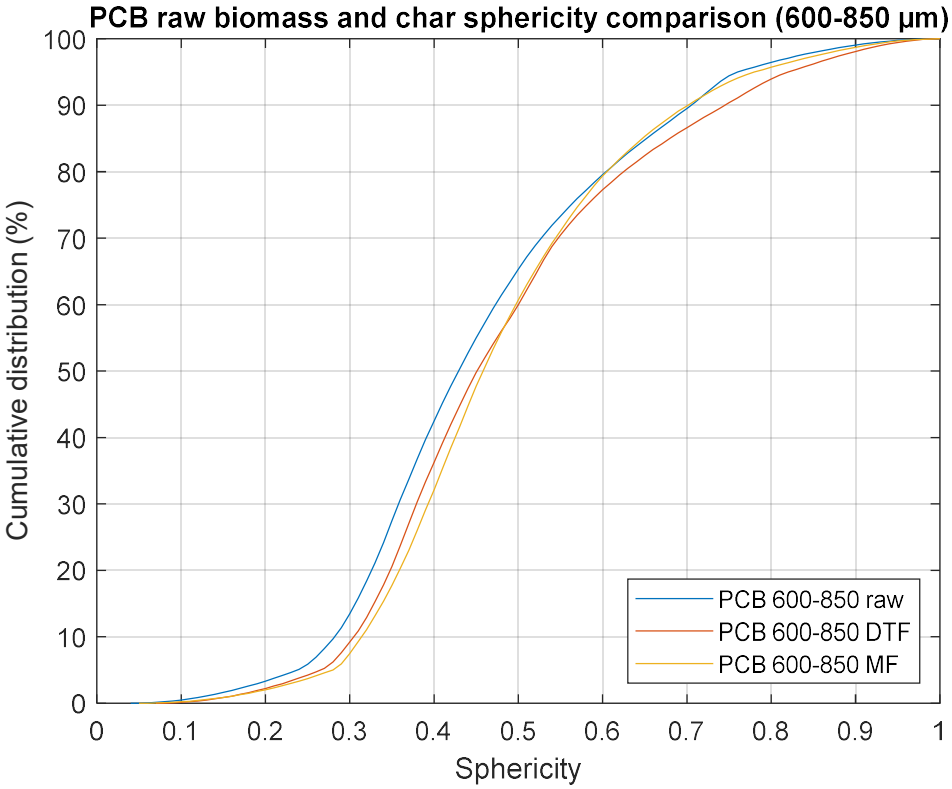

Figure 0-32 PCB raw biomass and char sphericity comparison (600-850 µm)

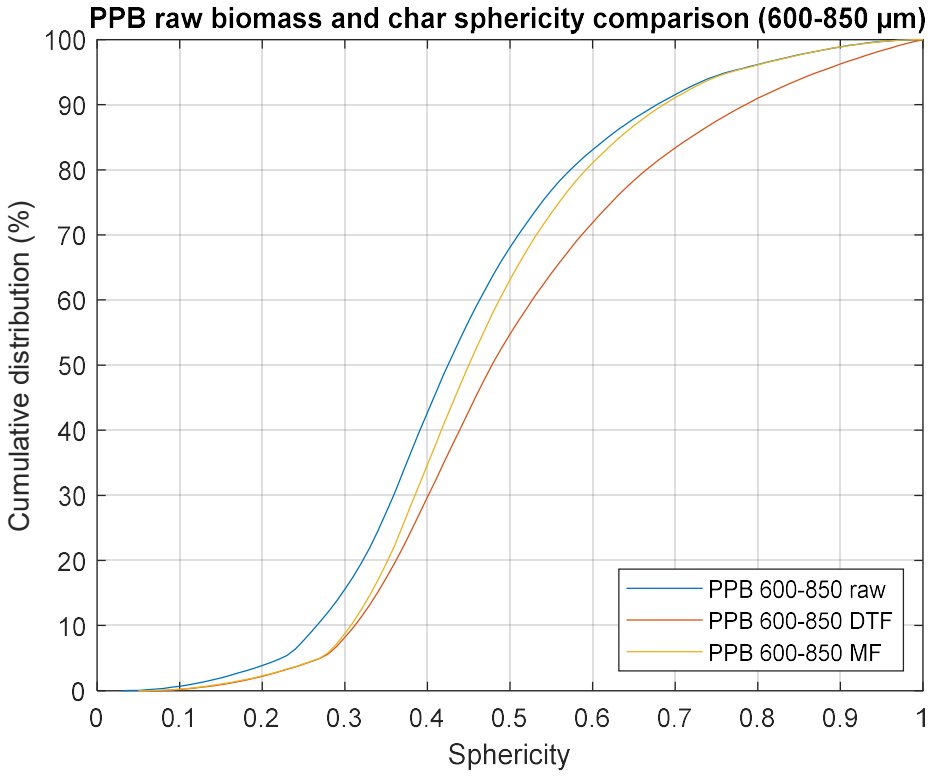

Figure 0-33 PPB raw biomass and char sphericity comparison (600-850 µm)

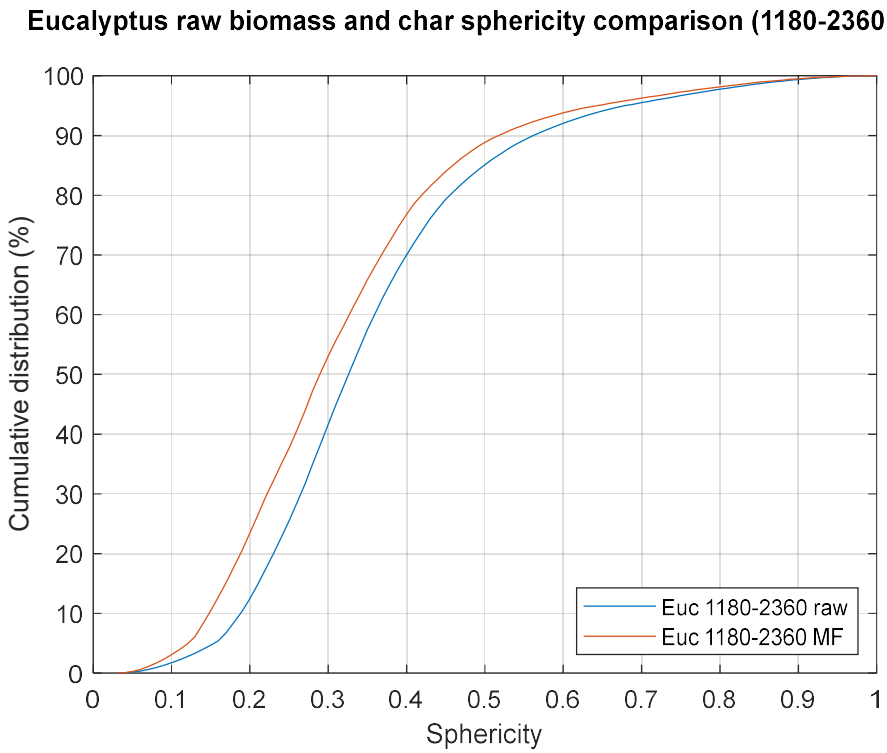

Figure 0-34 Eucalyptus raw biomass and char sphericity comparison (1180-2360 µm)

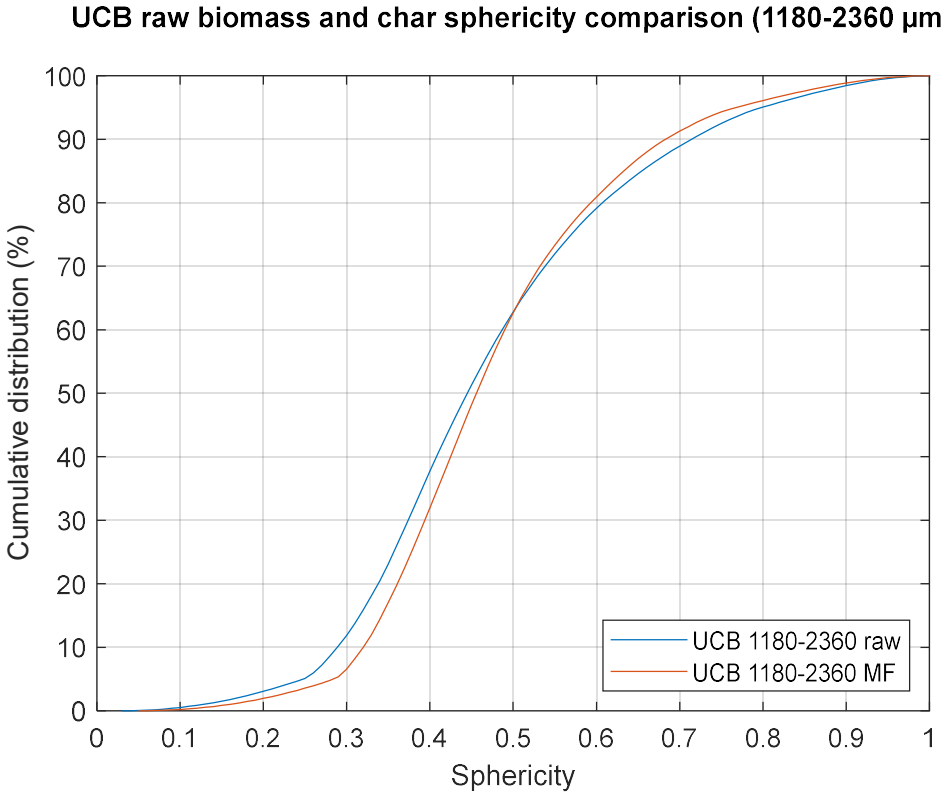

Figure 0-35 UCB raw biomass and char sphericity comparison (1180-2360 µm)

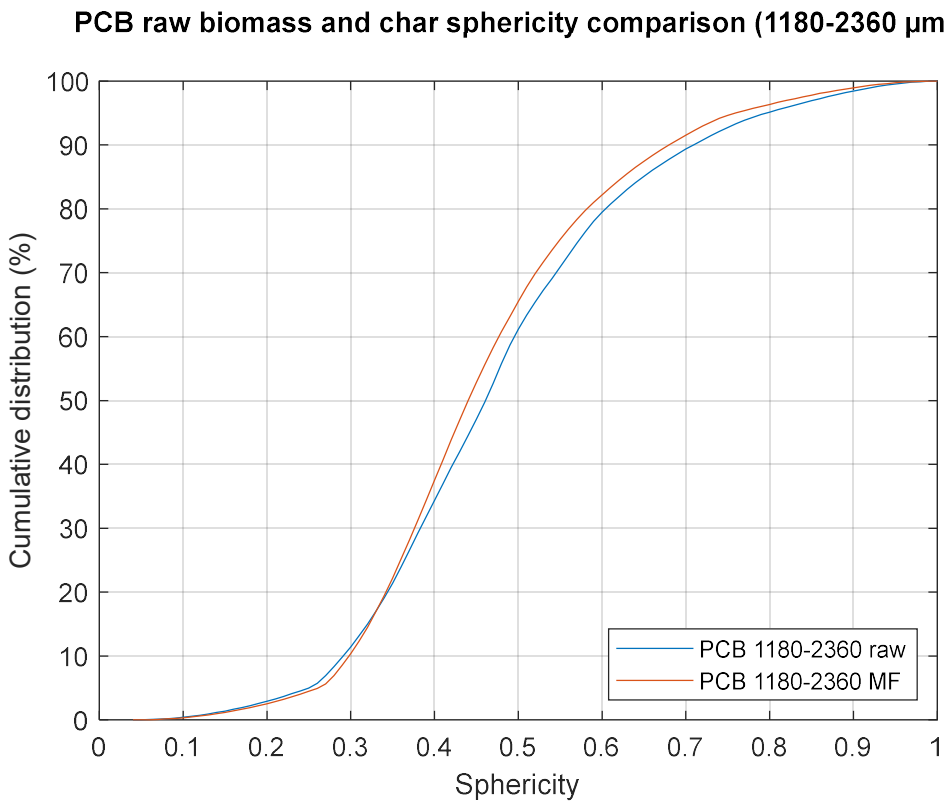

Figure 0-36 PCB raw biomass and char sphericity comparison (1180-2360 µm)

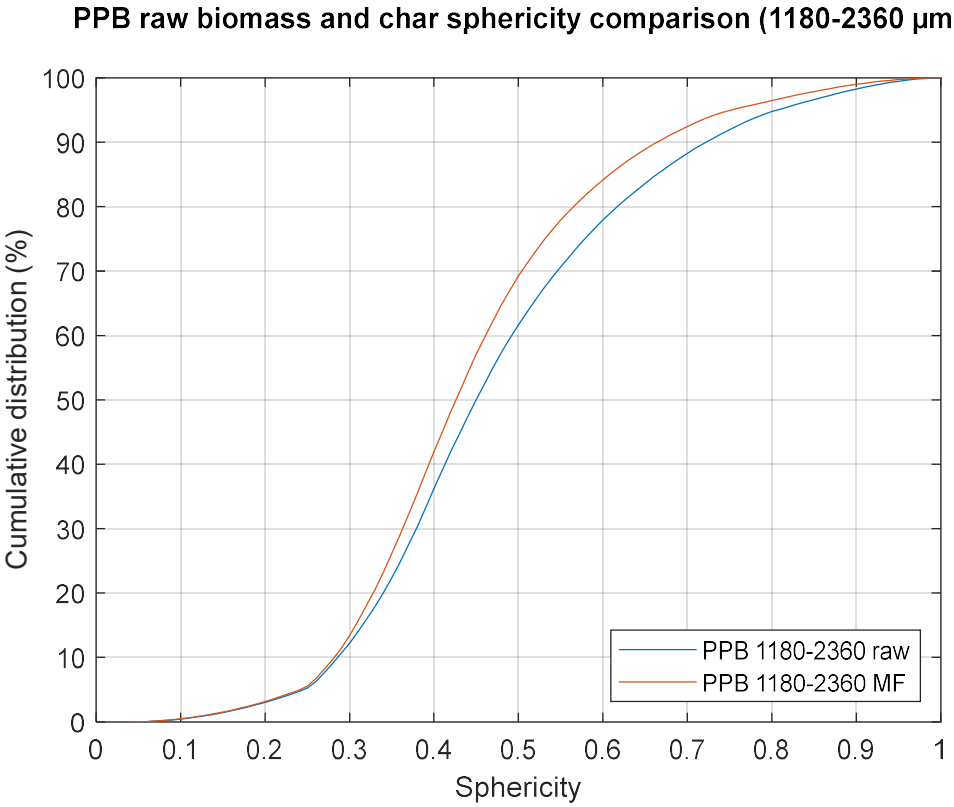

Figure 0-37 PPB raw biomass and char sphericity comparison (1480-2360 µm)

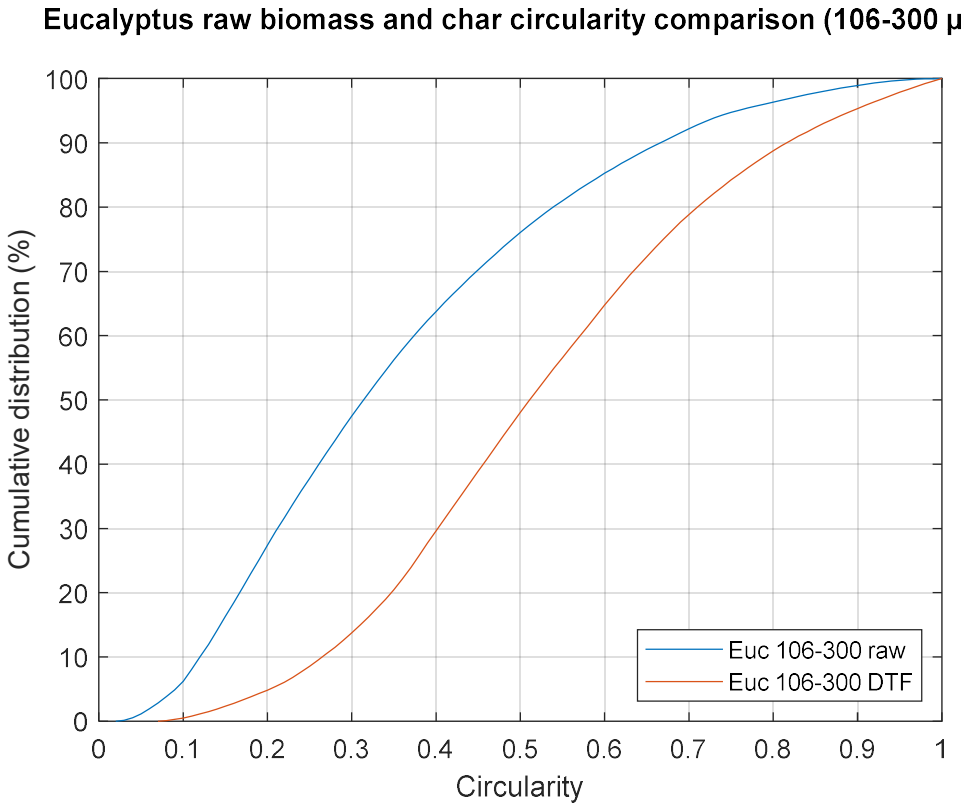

Figure 0-38 Eucalyptus raw biomass and char circularity comparison (106-300 µm)

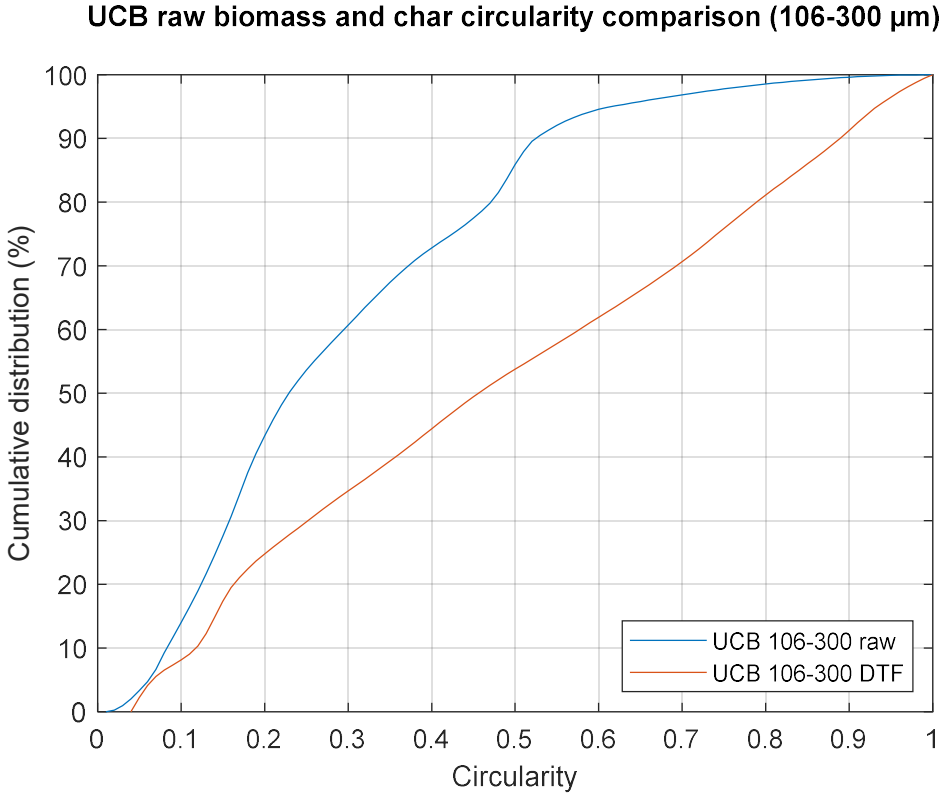

Figure 0-39 UCB raw biomass and char circularity comparison (106-300 µm)

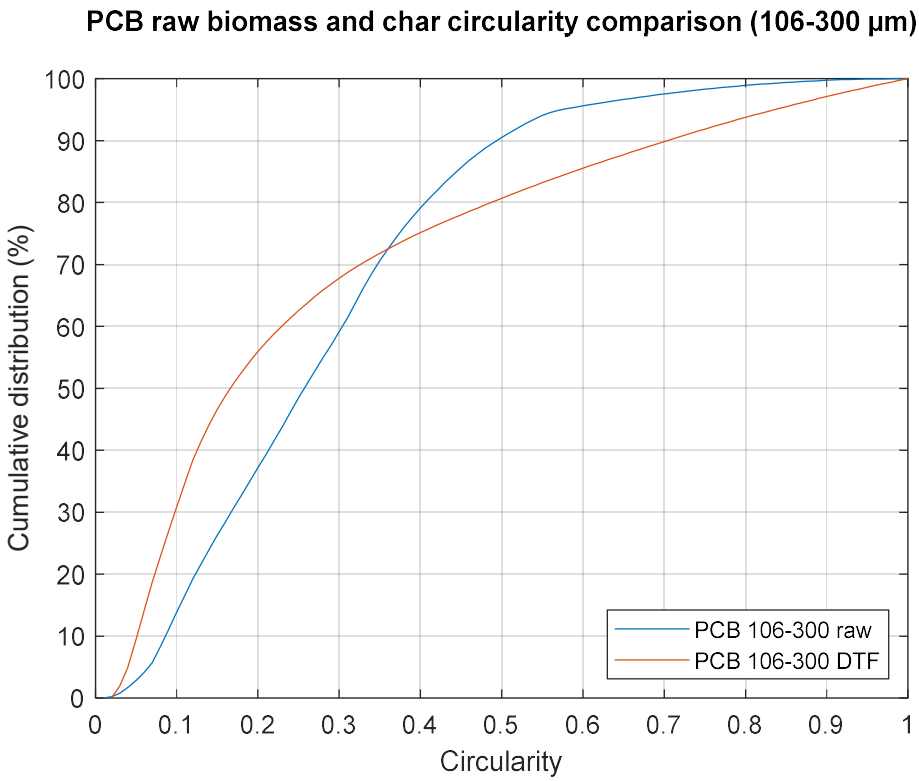

Figure 0-40 PCB raw biomass and char circularity comparison (106-300 µm)

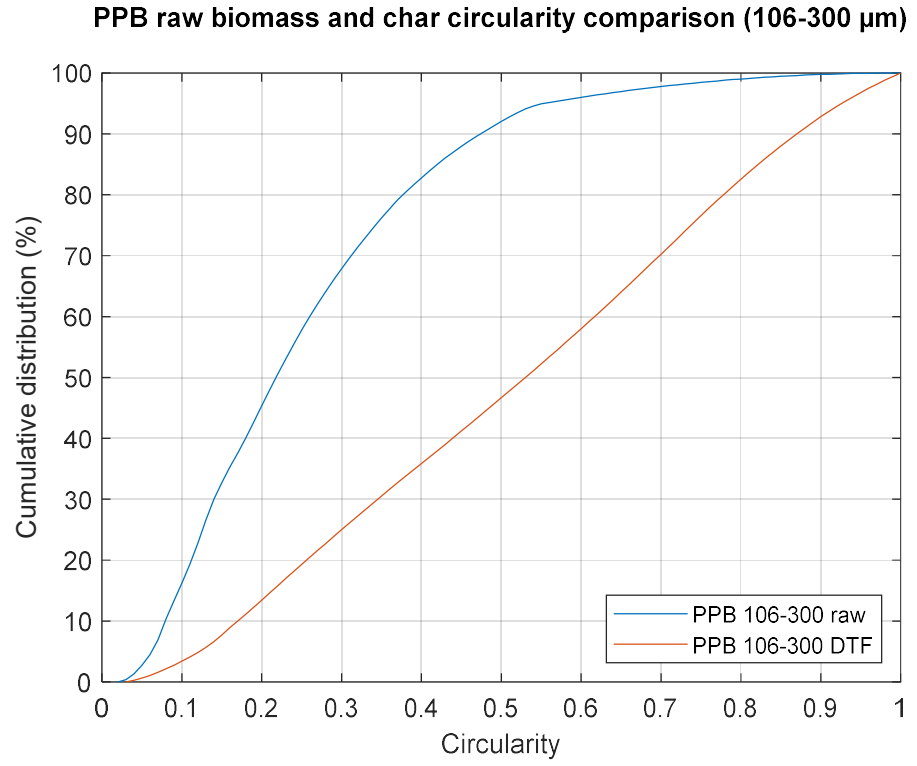

Figure 0-41 PPB raw biomass and char circularity comparison (106-300 µm)

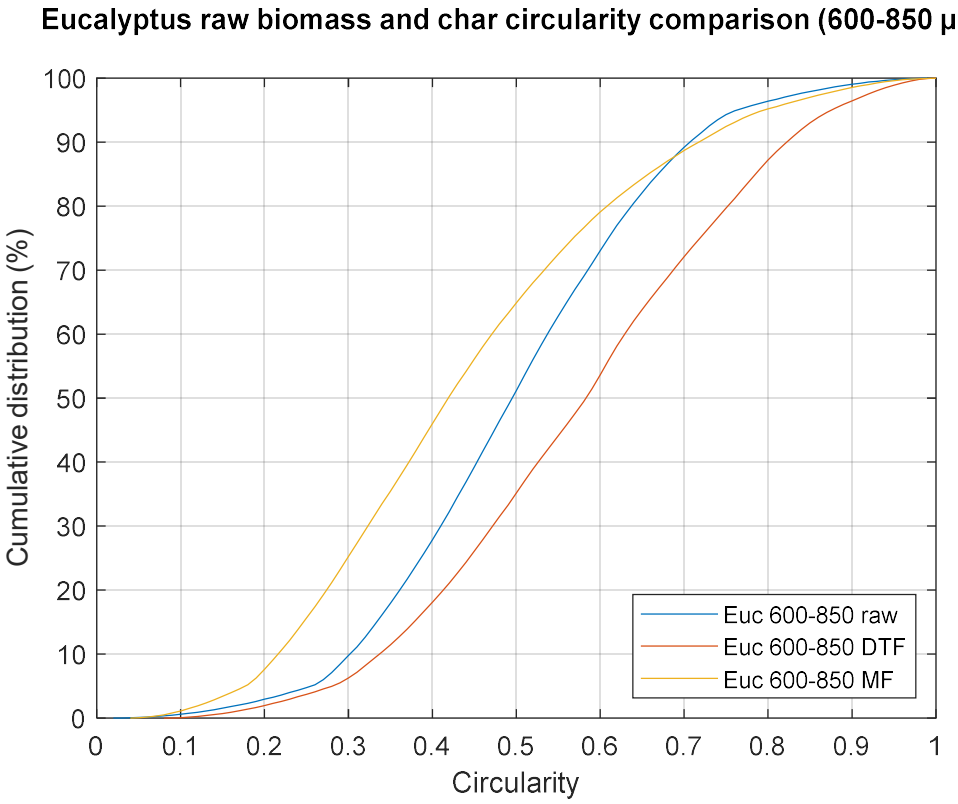

Figure 0-42 Eucalyptus raw biomass and char circularity comparison (600-850 µm)

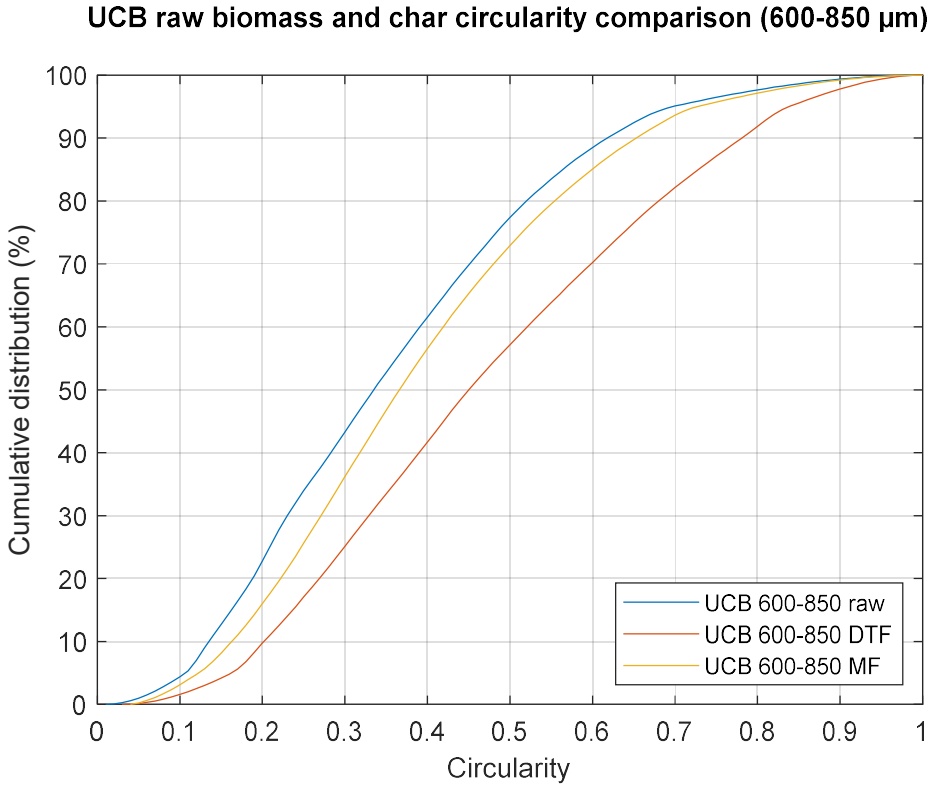

Figure 0-43 UCB raw biomass and char circularity comparison (600-850 µm)

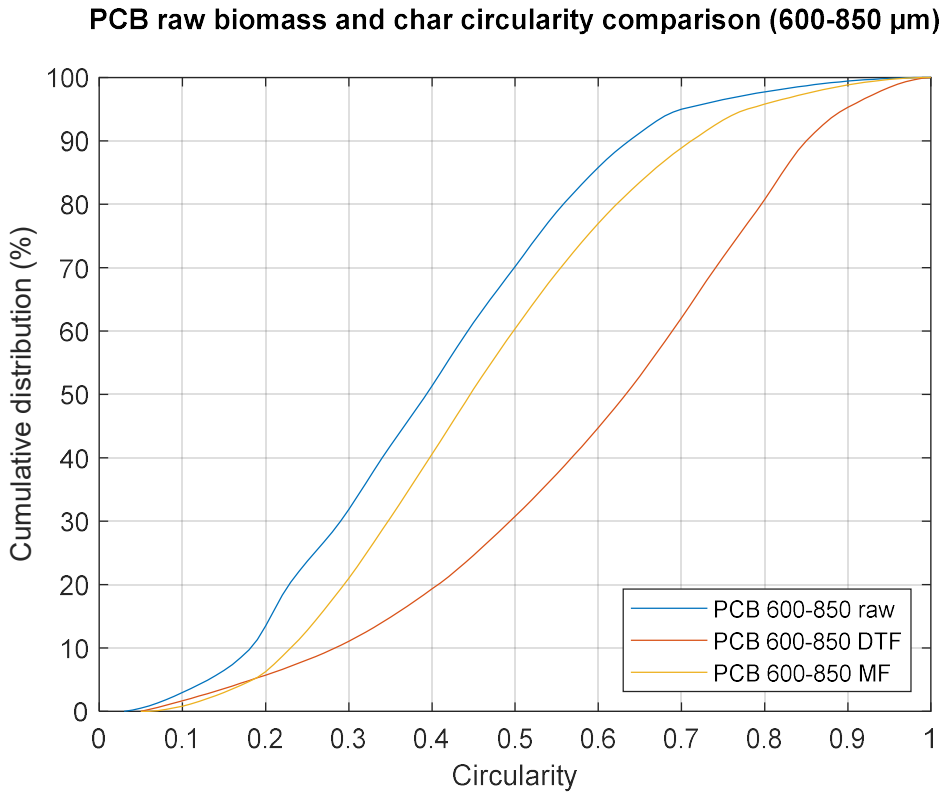

Figure 0-44 PCB raw biomass and char circularity comparison (600-850 µm)

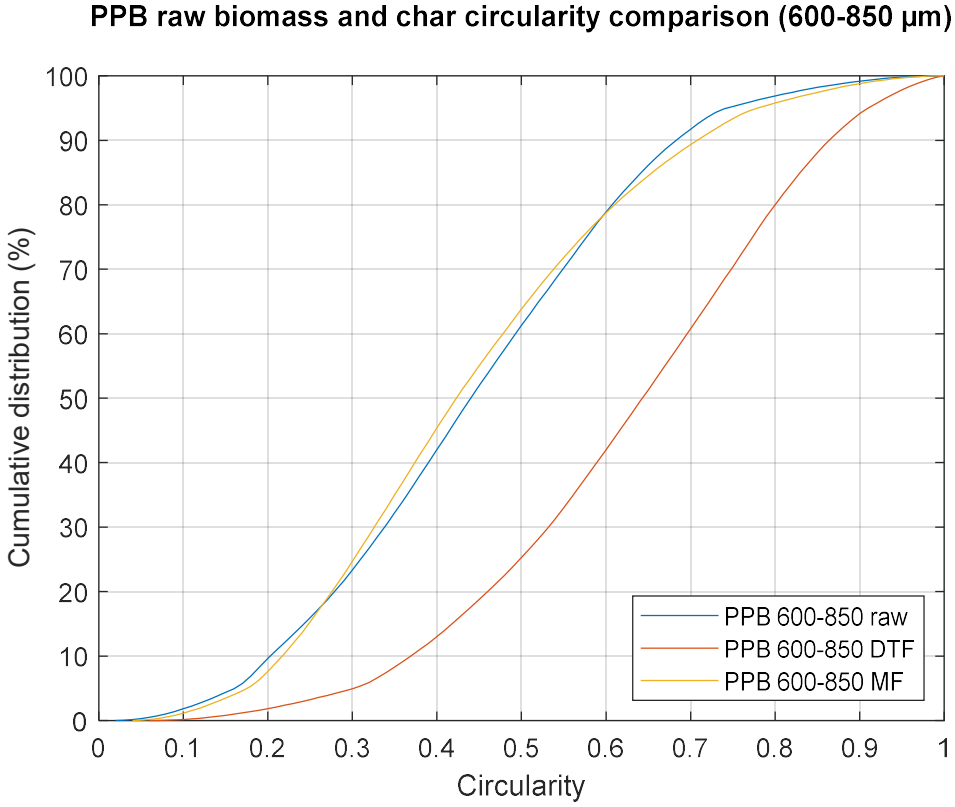

Figure 0-45 PPB raw biomass and char circularity comparison (600-850 µm)

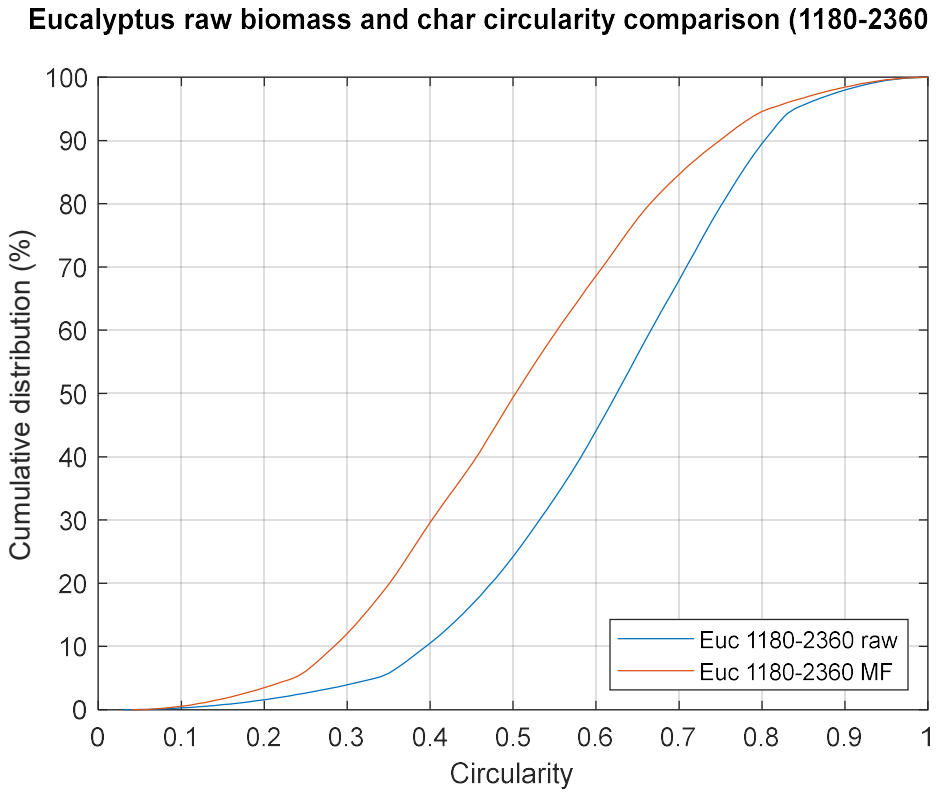

Figure 0-46 Eucalyptus raw biomass and char circularity comparison (1180-2360 µm)

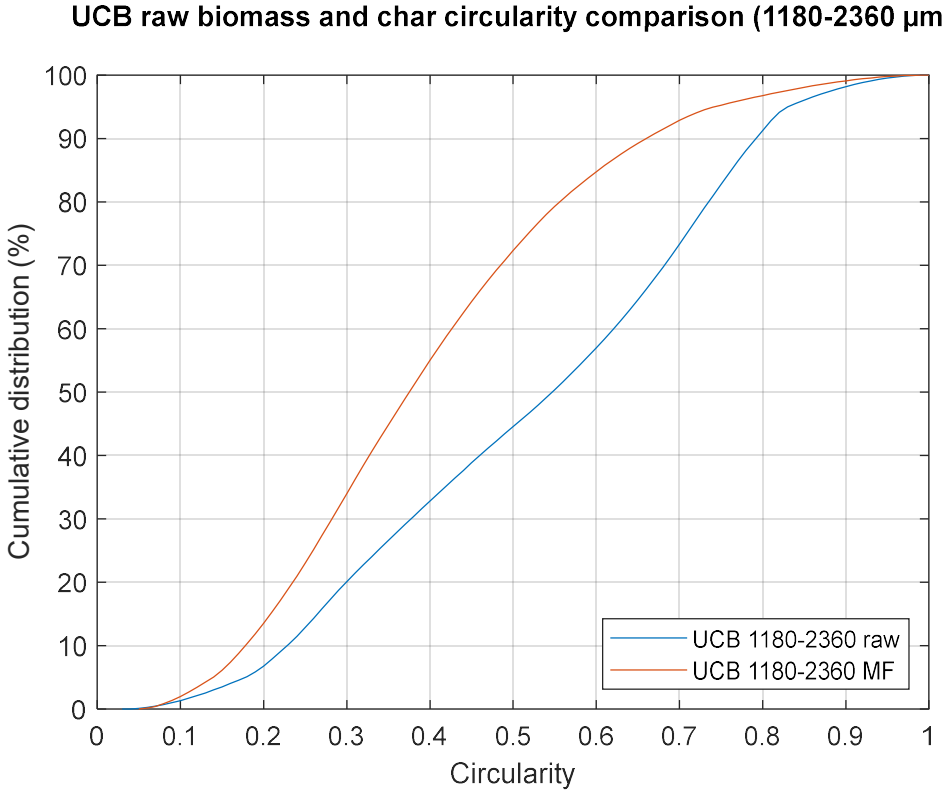

Figure 0-47 UCB raw biomass and char circularity comparison (1180-2360 µm)

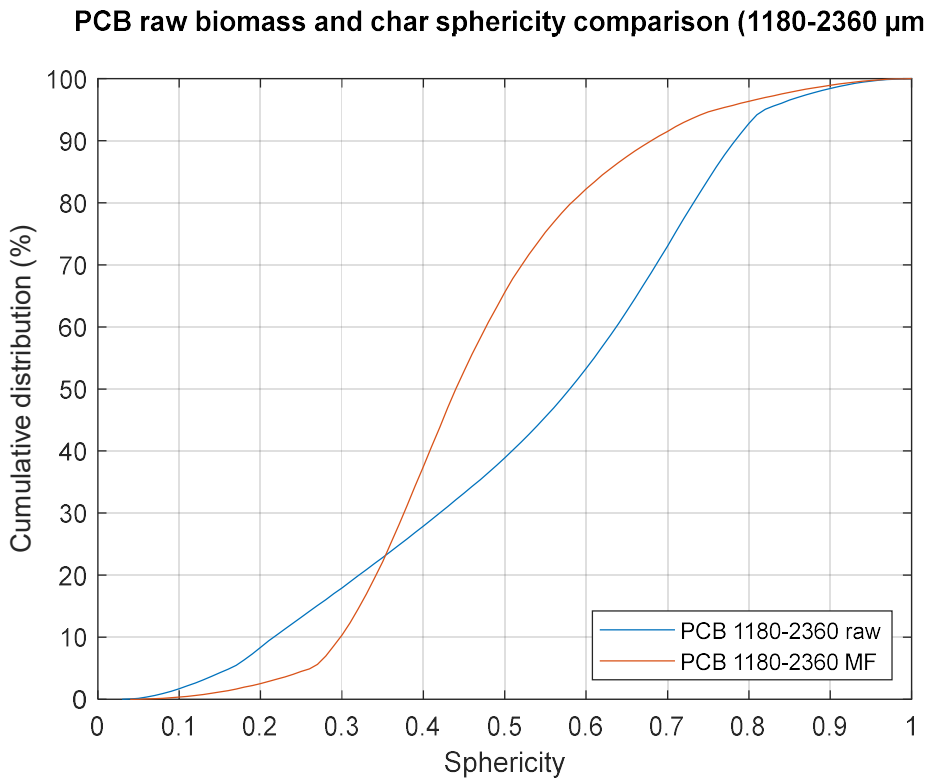

Figure 0-48 PCB raw biomass and char sphericity comparison (1180-2360 µm)

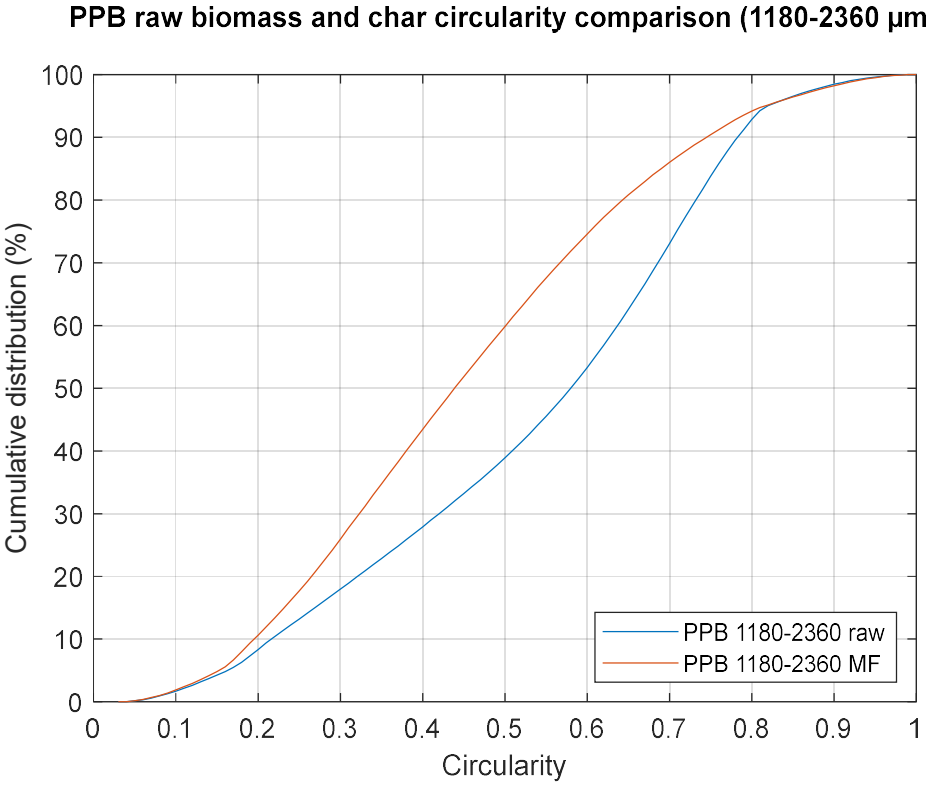

Figure 0-49 PPB raw biomass and char circularity comparison (1180-2360 µm)

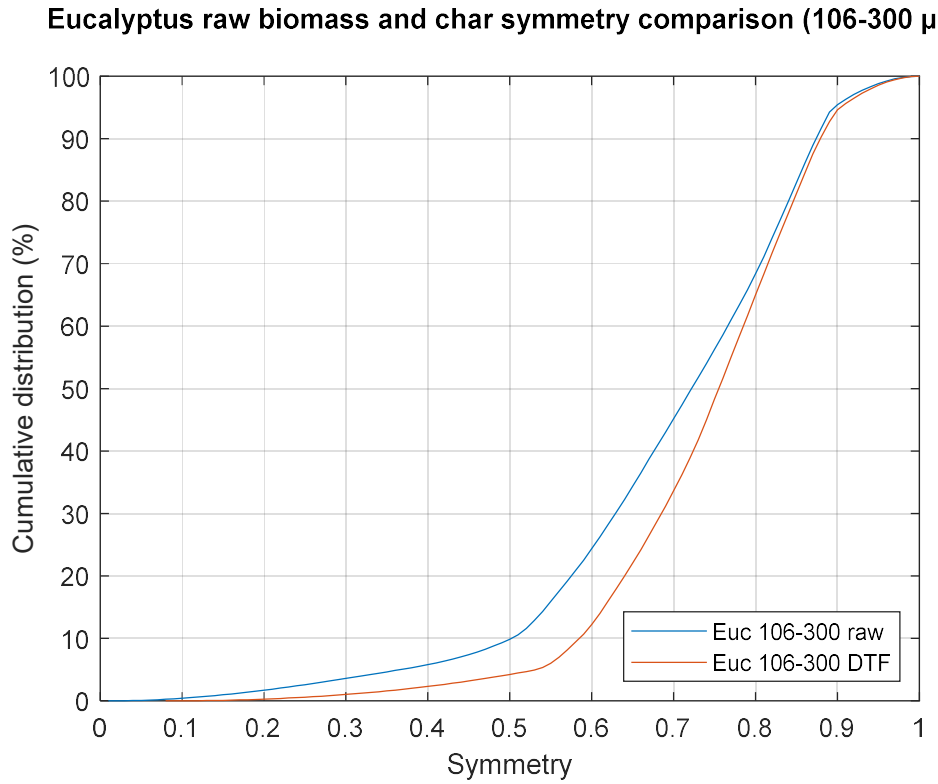

Figure 0-50 Eucalyptus raw biomass and char symmetry comparison (106-300 µm)

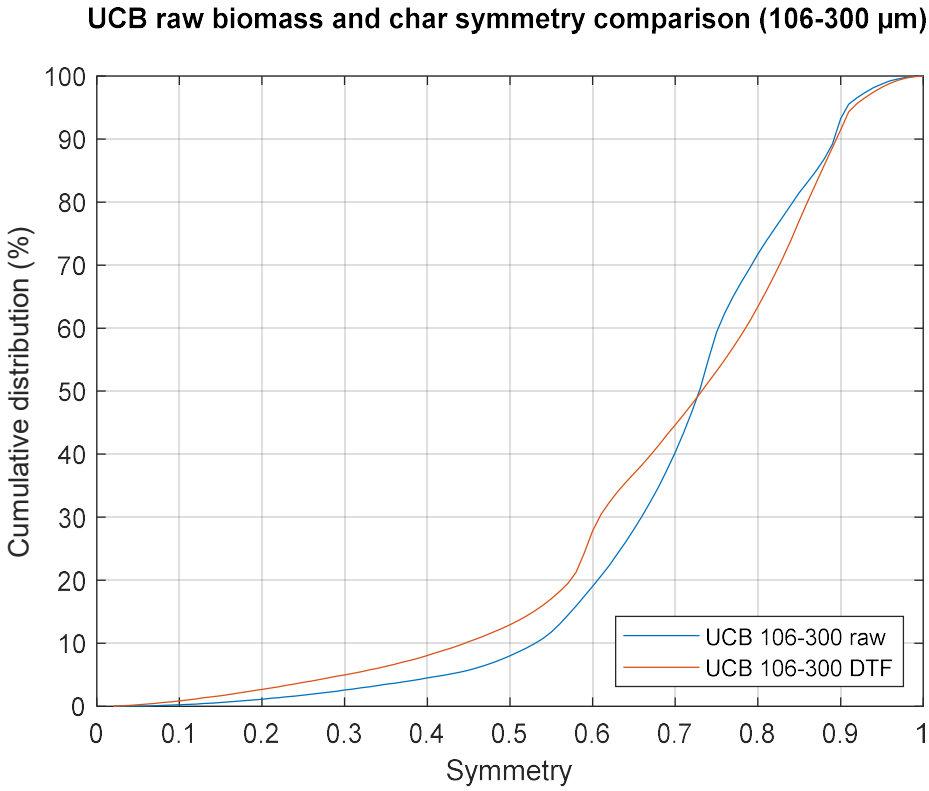

Figure 0-51 UCB raw biomass and char symmetry comparison (106-300 µm)

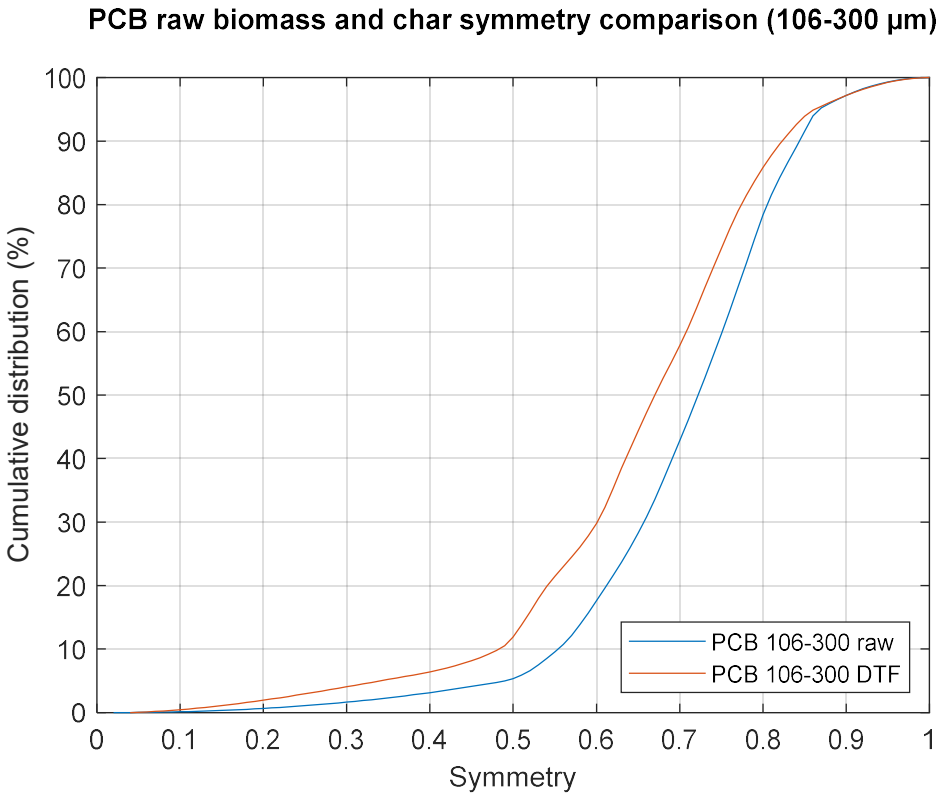

Figure 0-52 PCB raw biomass and char symmetry comparison (106-300 µm)

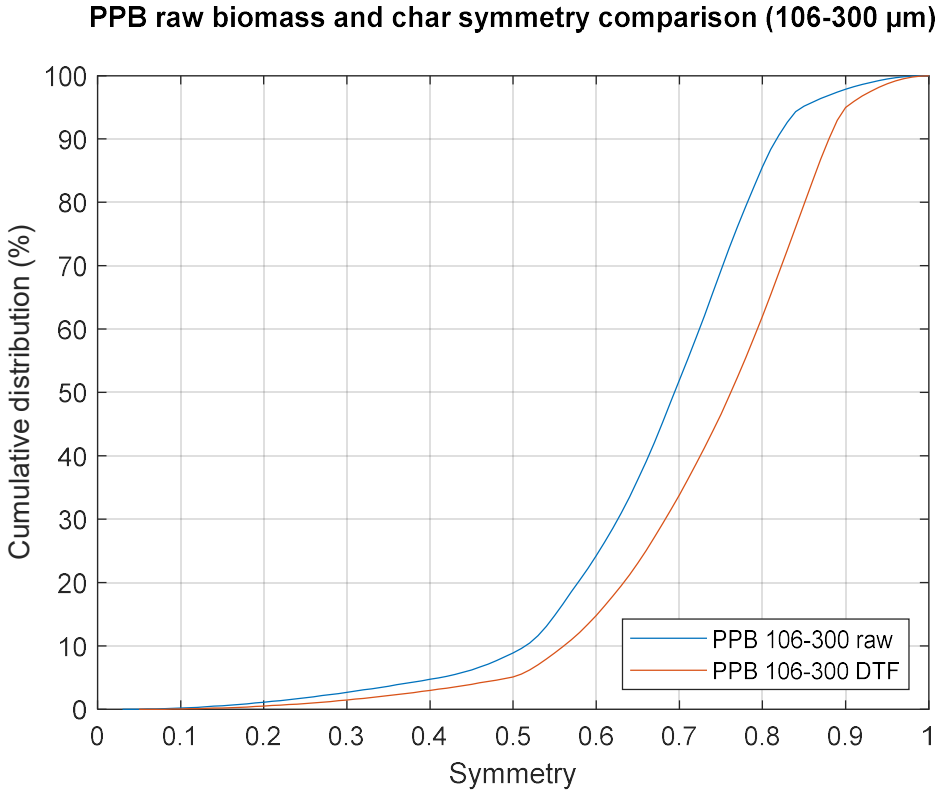

Figure 0-53 PPB raw biomass and char symmetry comparison (106-300 µm)

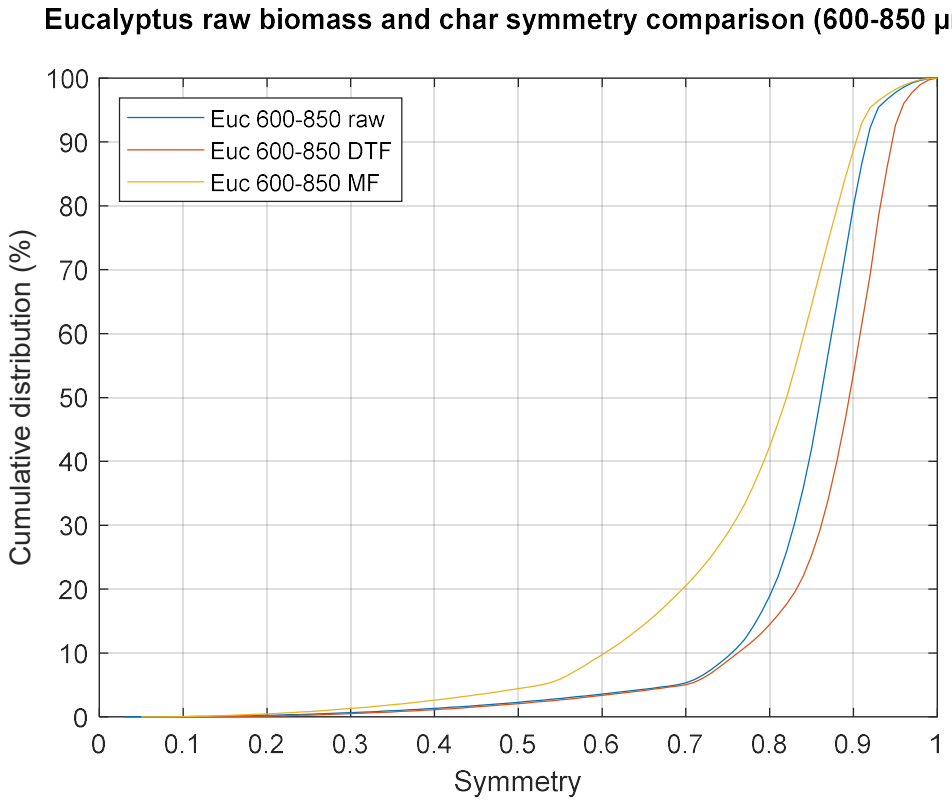

Figure 0-54 Eucalyptus raw biomass and char symmetry comparison (600-850 µm)

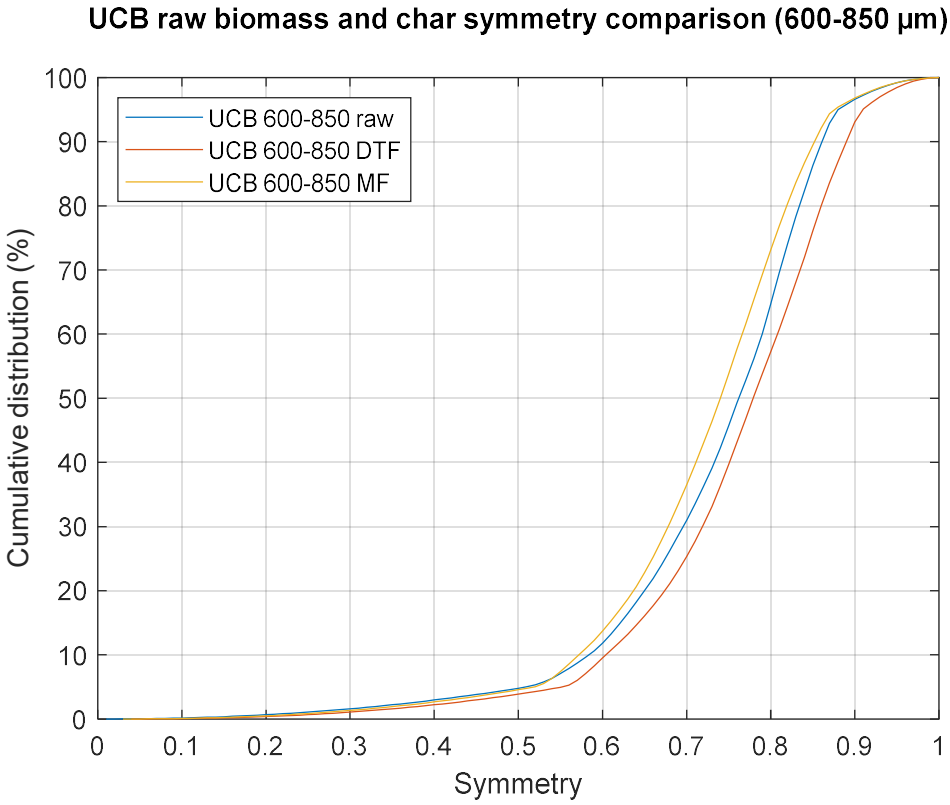

Figure 0-55 UCB raw biomass and char symmetry comparison (600-850 µm)

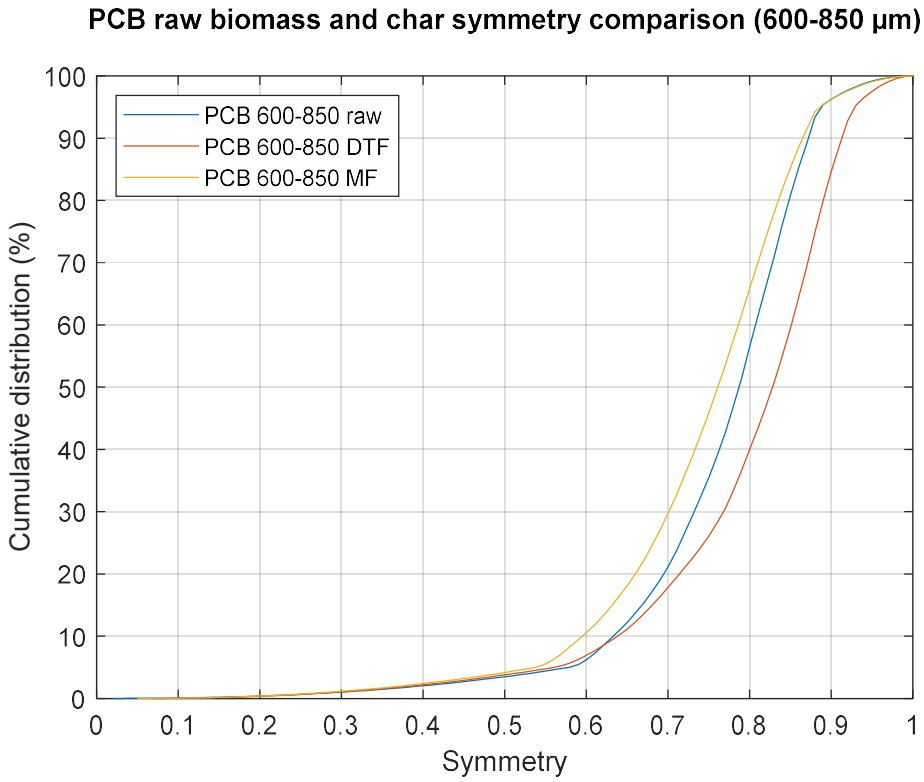

Figure 0-56 PCB raw biomass and char symmetry comparison (600-850 µm)

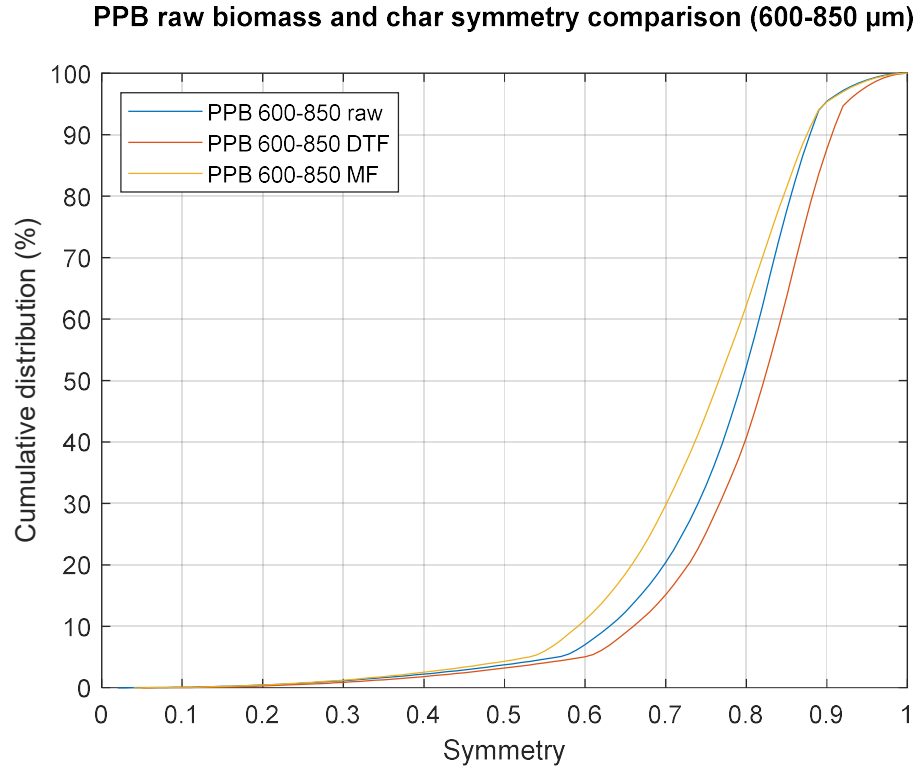

Figure 0-57 PPB raw biomass and char symmetry comparison (600-850 µm)

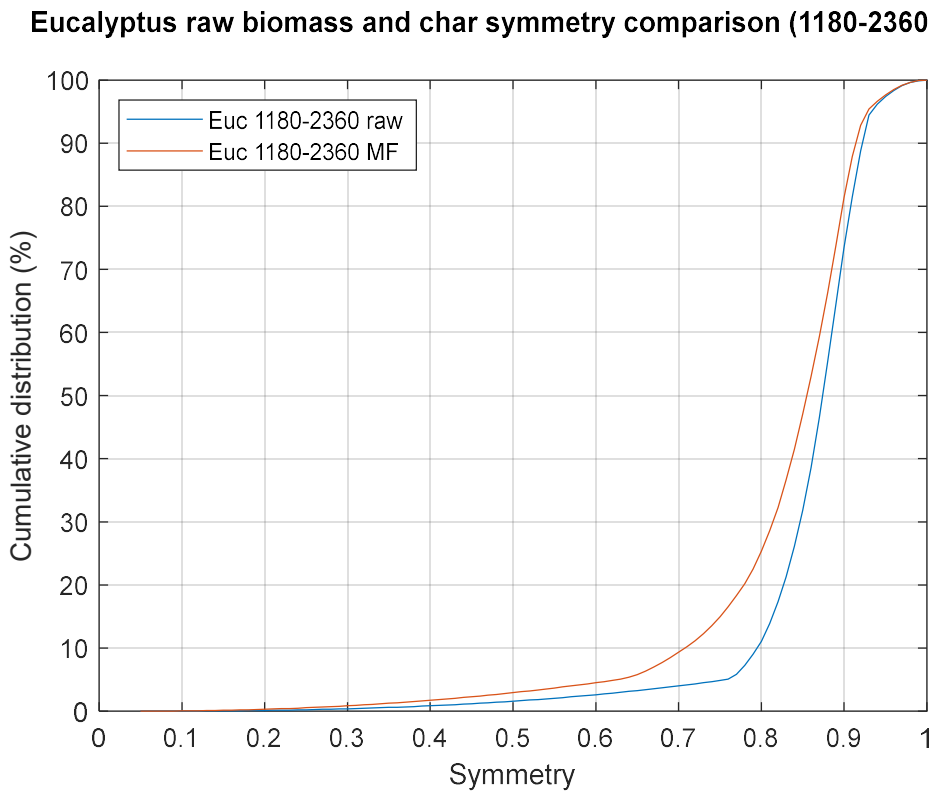

Figure 0-58 Eucalyptus raw biomass and char symmetry comparison (1180*2360 µm)

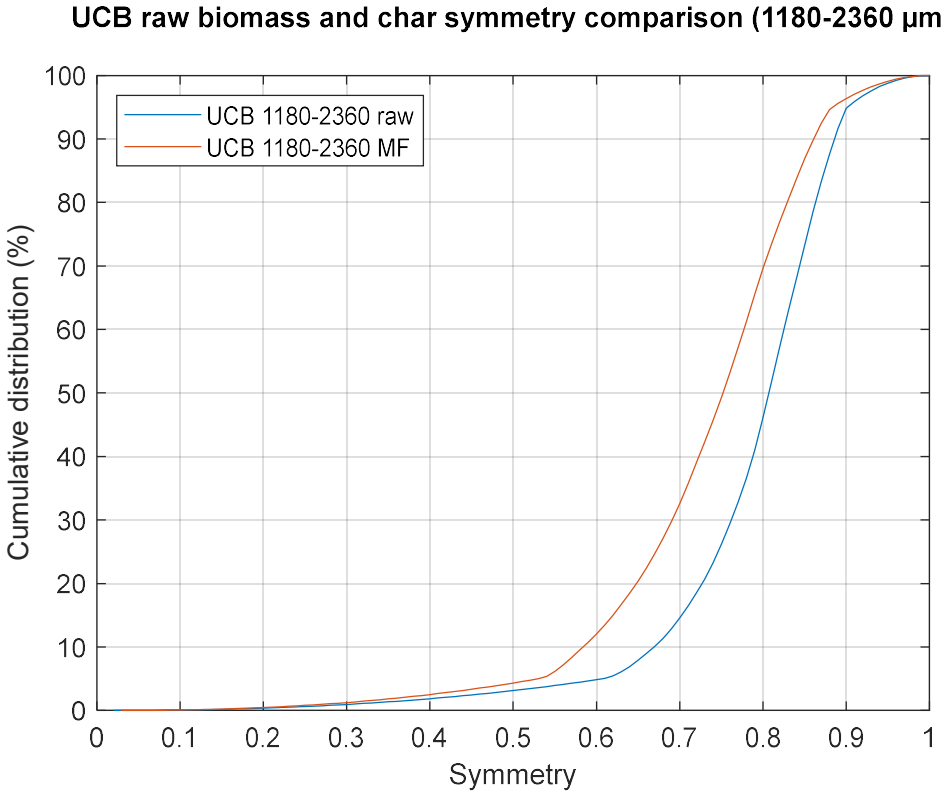

Figure 0-59 UCB raw biomass and char symmetry comparison (1180-2360 µm)

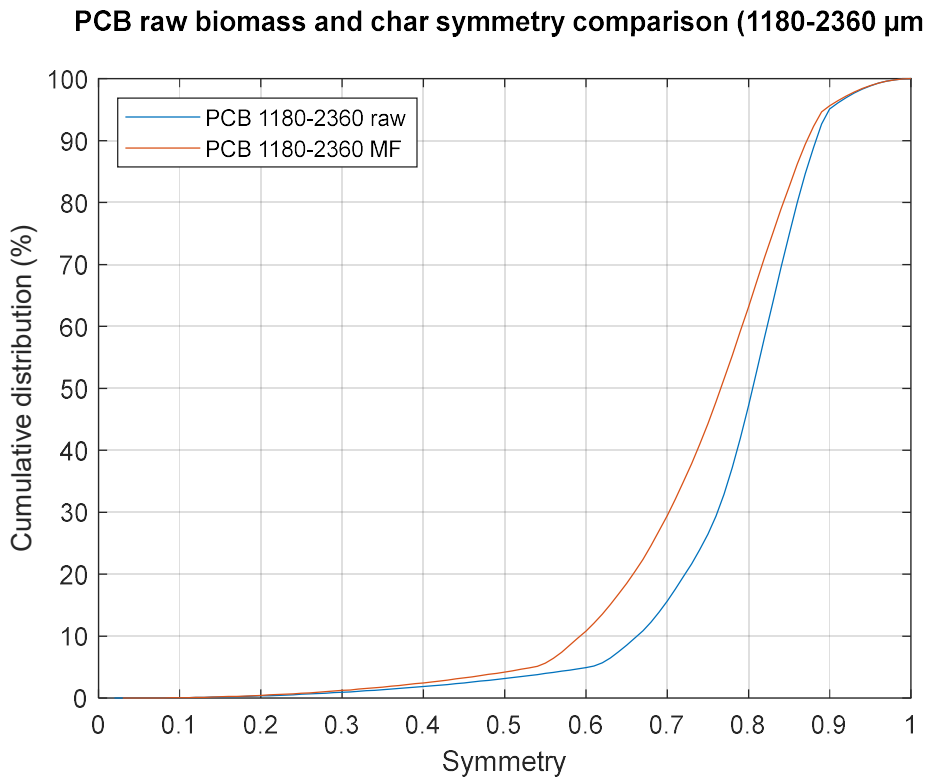

Figure 0-60 PCB raw biomass and char symmetry comparison (1180-2360 µm)

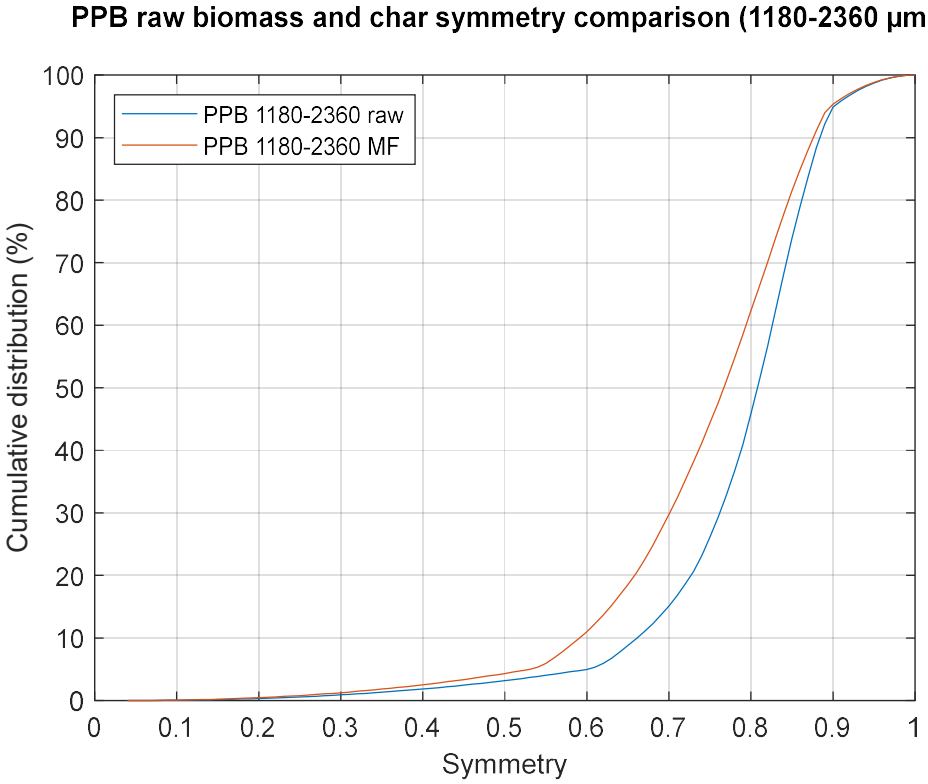

Figure 0-61 PPB raw biomass and char symmetry comparison (1180-2360 µm)

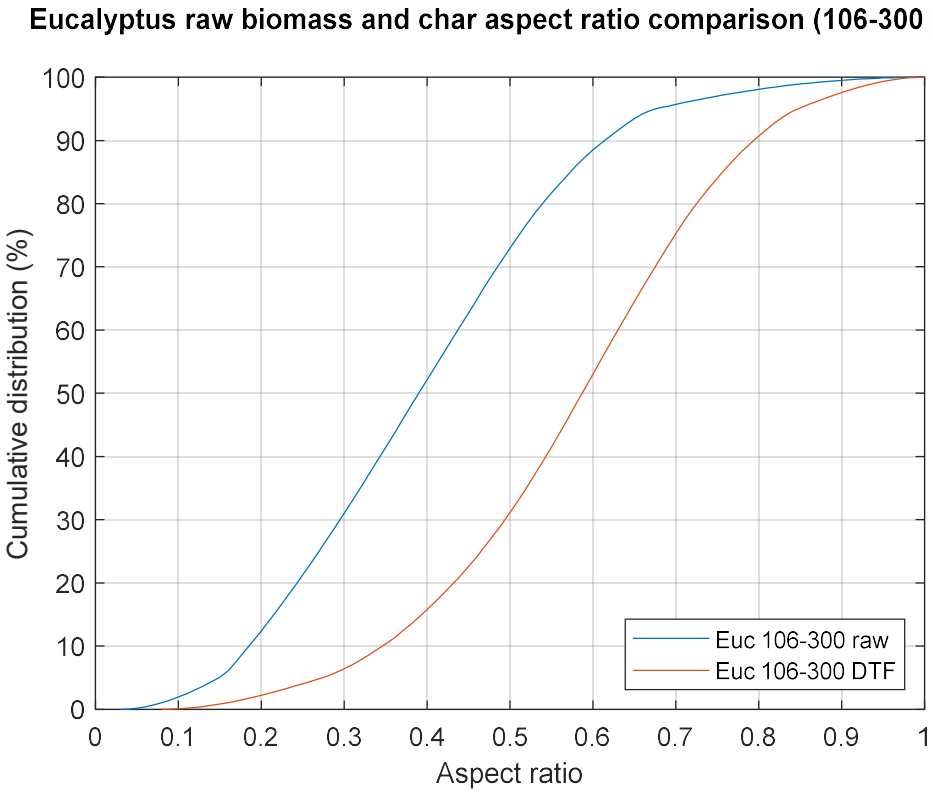

Figure 0-62 Eucalyptus raw biomass and char aspect ratio comparison (106-300 µm)

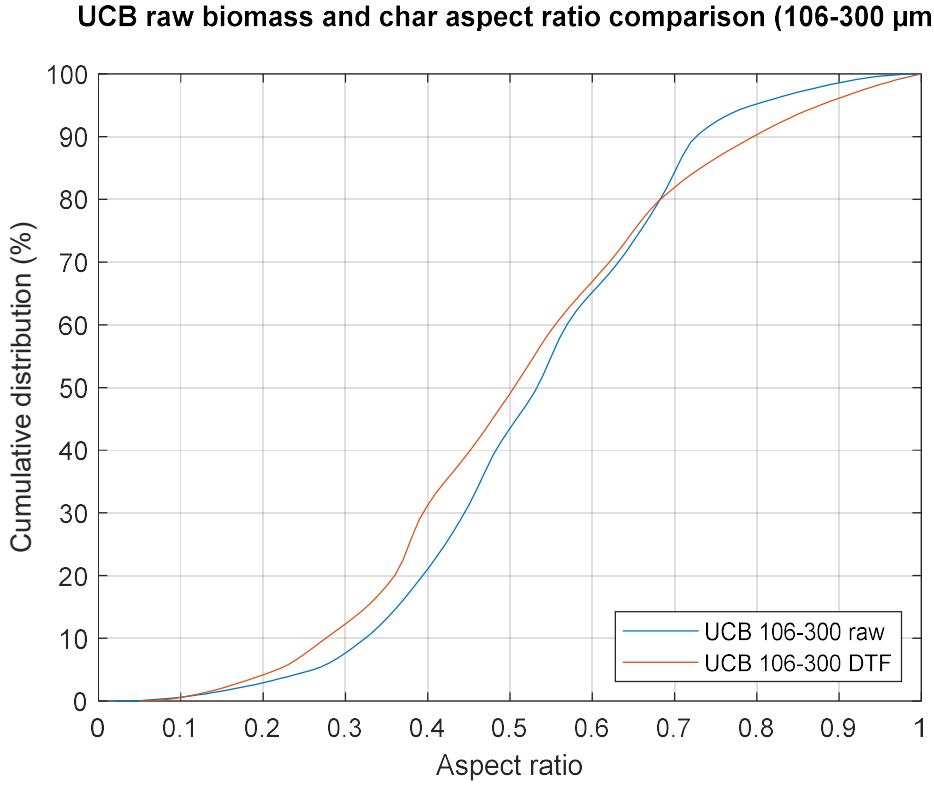

Figure 0-63 UCB raw biomass and char spect ratio comparison (106-300 µm)

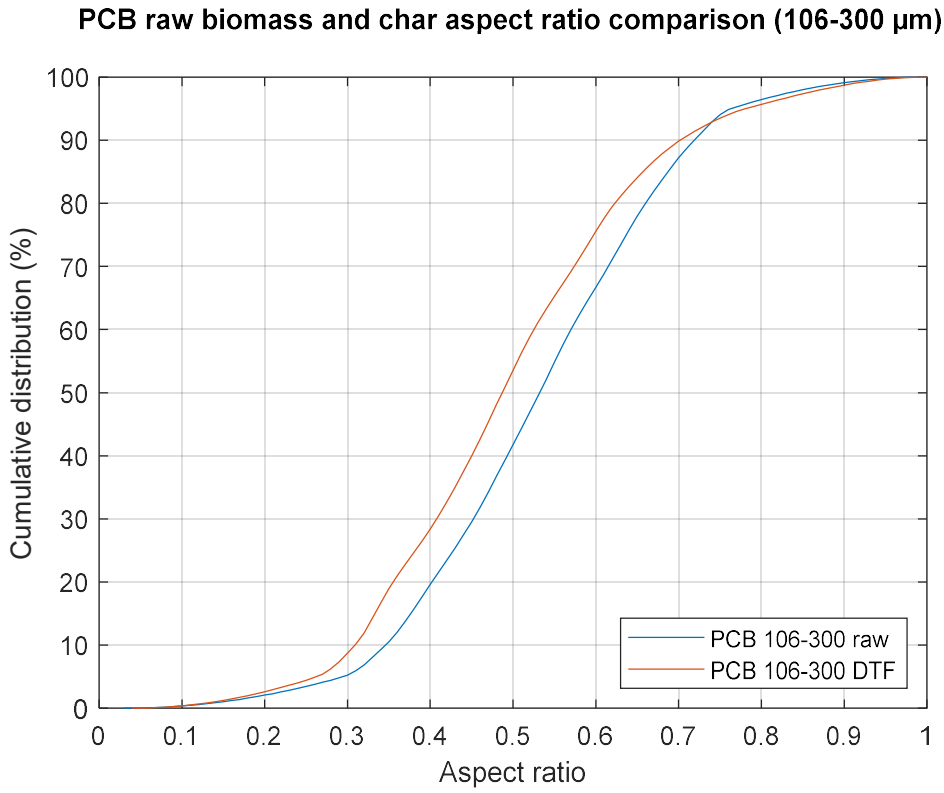

Figure 0-64 PCB raw biomass and char aspect ratio comparison (106-300 µm)

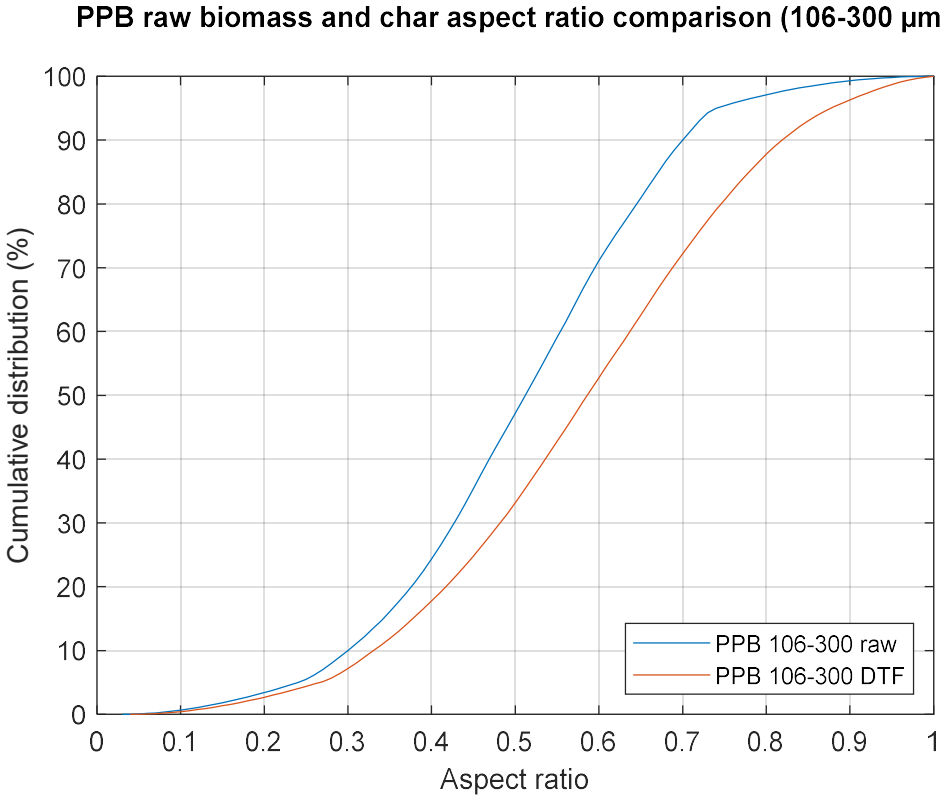

Figure 0-65 PPB raw biomass and char aspect ratio comparison (106-300 µm)

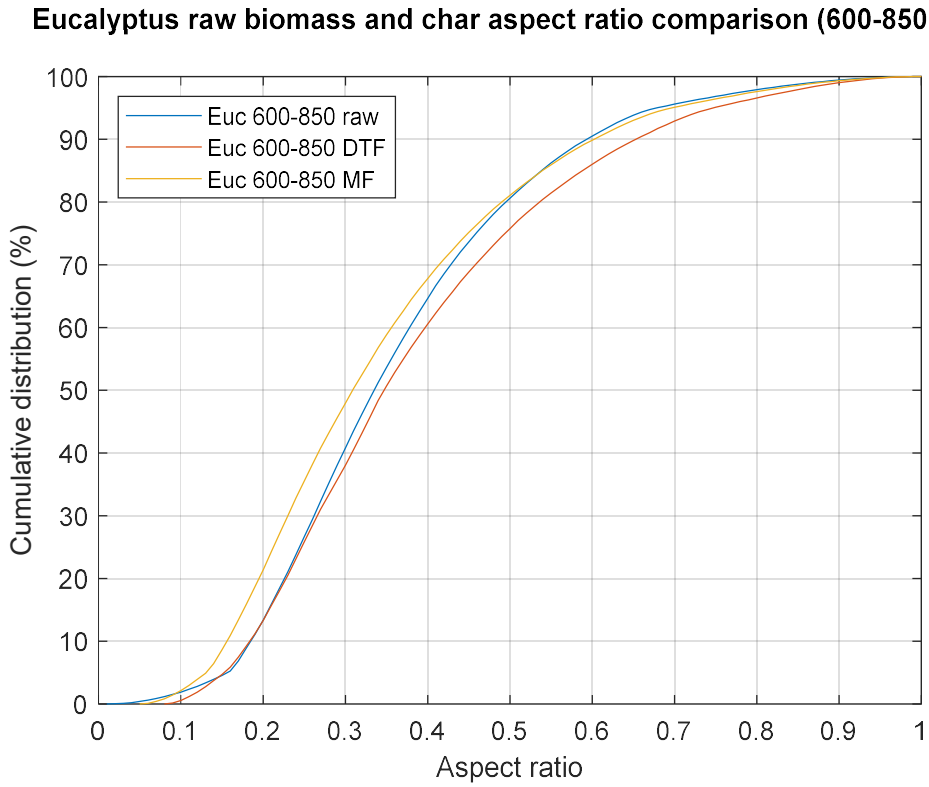

Figure 0-66 Eucalyptus raw biomass and char aspect ratio comparison (600-850 µm)

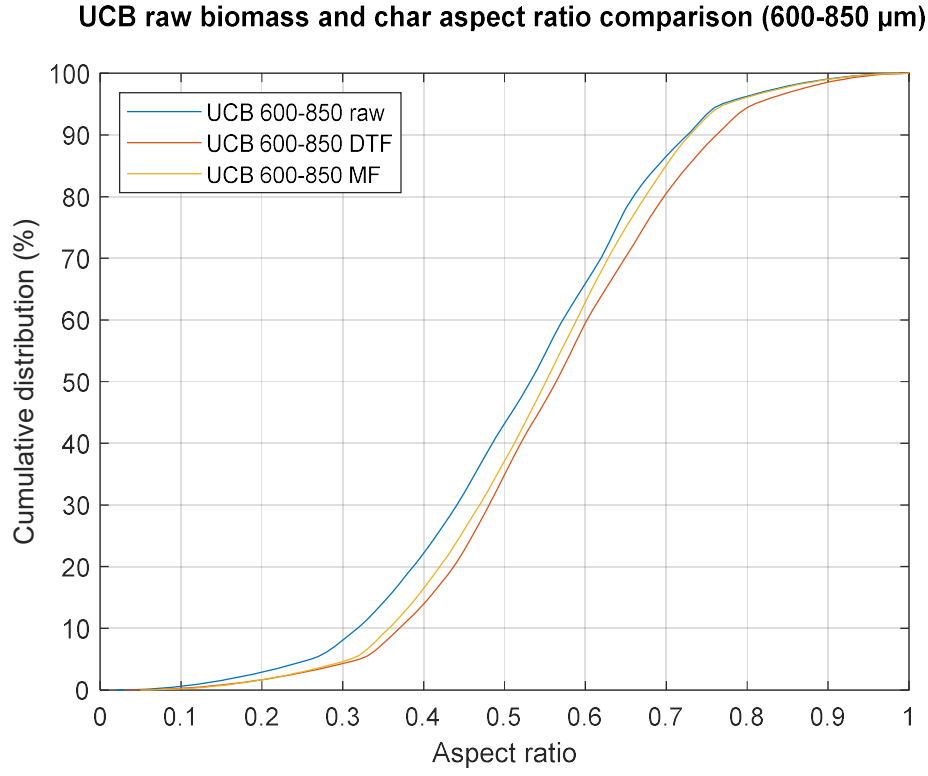

Figure 0-67 UCB raw biomass and char aspect ratio comparison (600-850 µm)

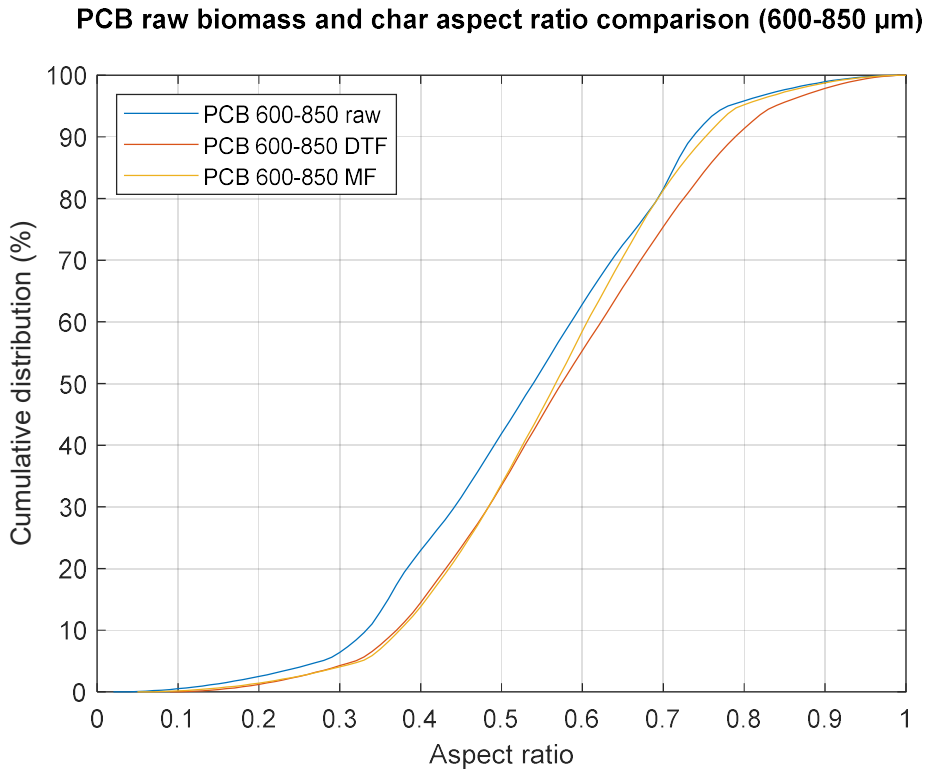

Figure 0-68 PCB raw biomass and char aspect ratio comparison (600-850 µm)

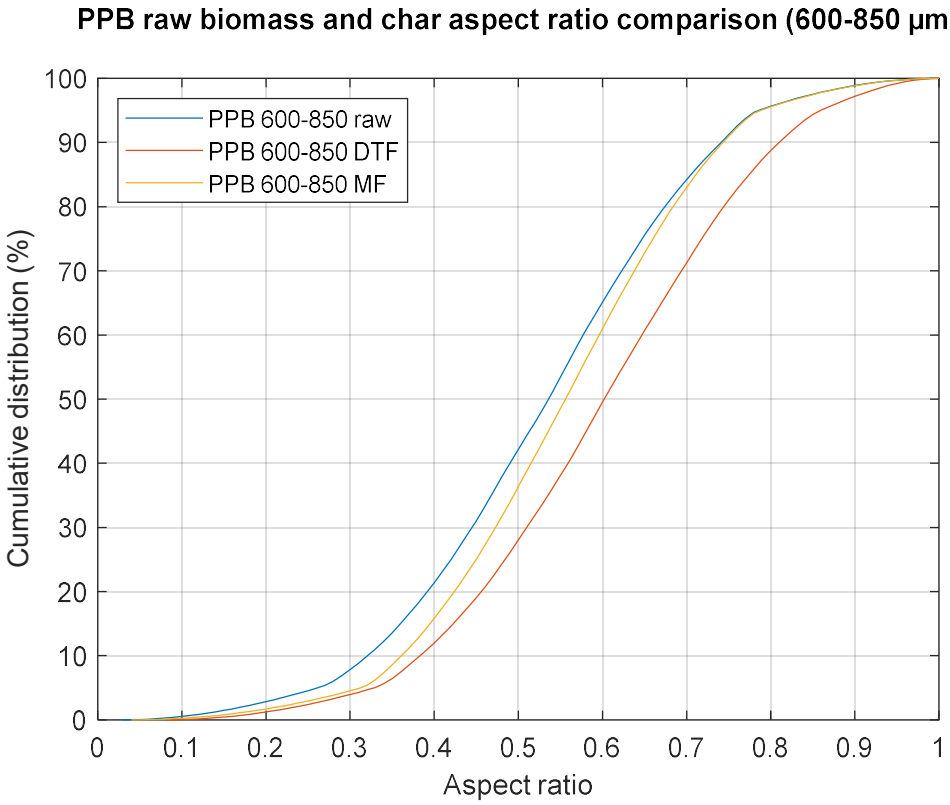

Figure 0-69 PPB raw biomass and char aspect ratio comparison (600-850 µm)

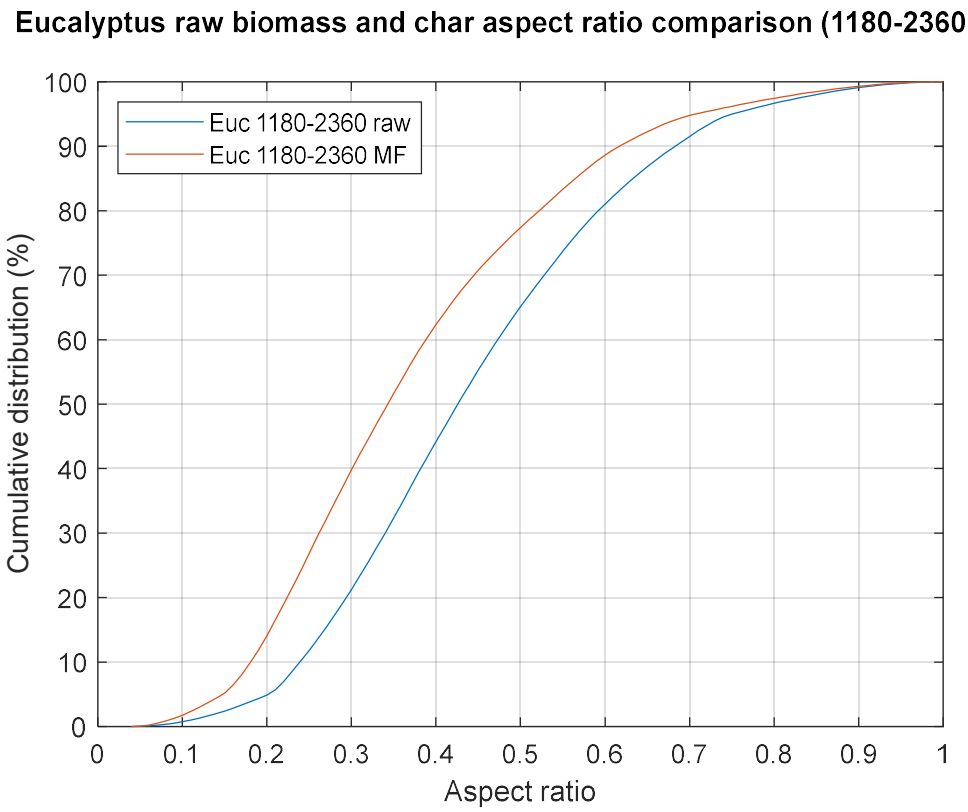

Figure 0-70 Eucalyptus raw biomass and char aspect ratio comparison (1180-2360 µm)

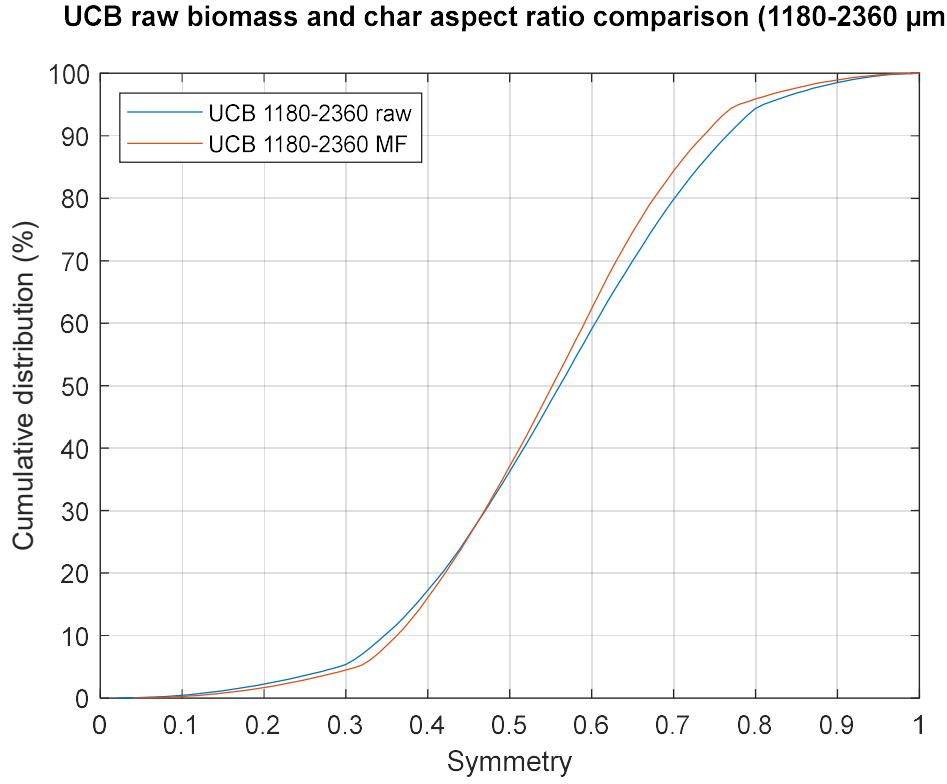

Figure 0-71 UCB raw biomass and char aspect ratio comparison (1180-2360 µm)

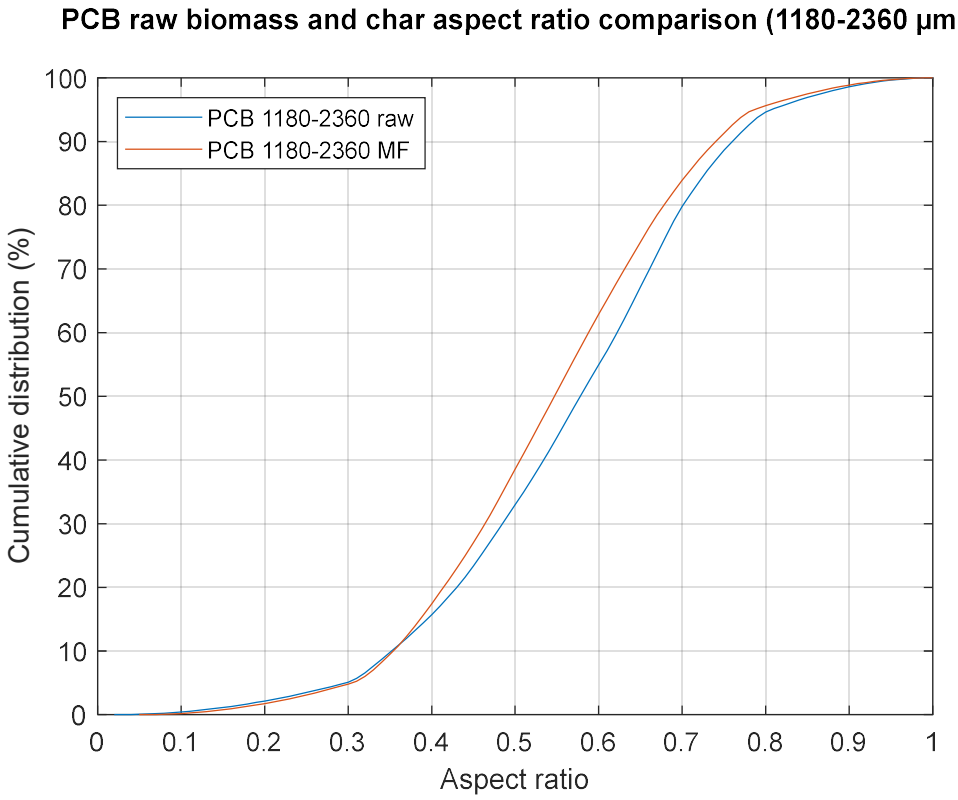

Figure 0-72 PCB raw biomass and char aspect ratio comparison (1180-2360 µm)

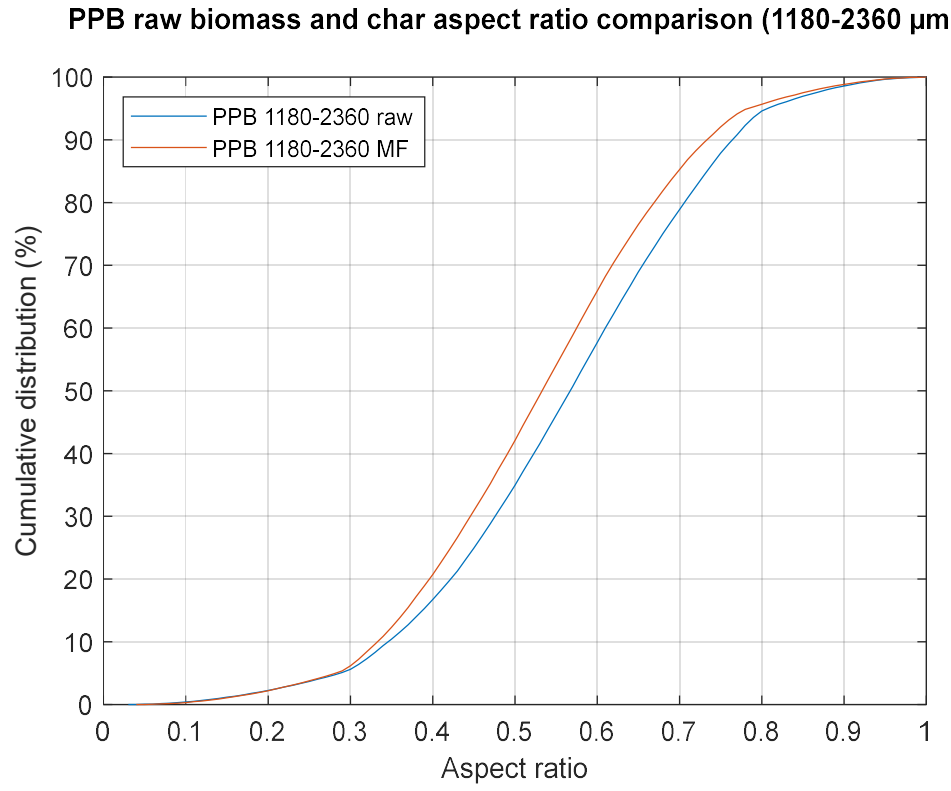

Figure 0-73 PPB raw biomass and char aspect ratio comparison (1180-2360 µm)

Appendix E CIrcularity and Symmetry Distribution of Pre-pellet, Disintegrated Pellets and Milled Pellets Samples

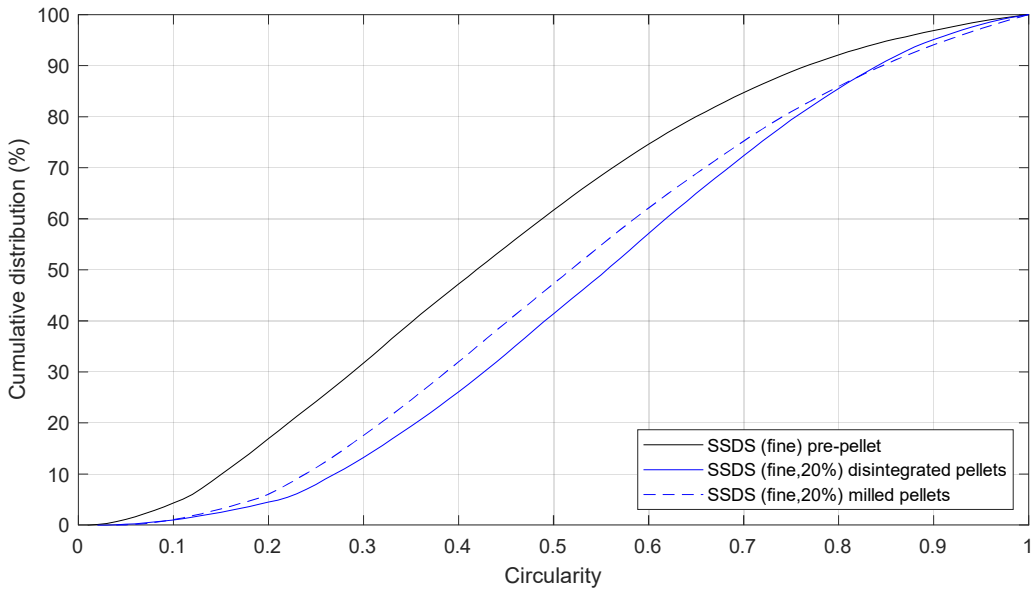

Figure 0-74 Circularity distributions of pre-pellet, disintegrated pellets and milled pellets - SSDS (fine)

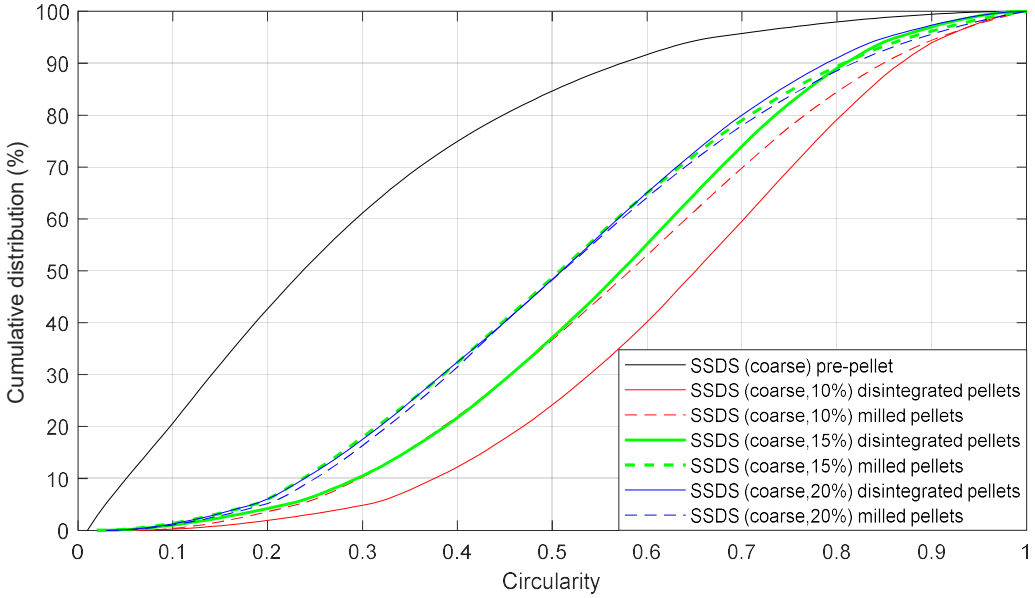

Figure 0-75 Circularity distributions of pre-pellet, disintegrated pellets and milled pellets - SSDS (coarse)

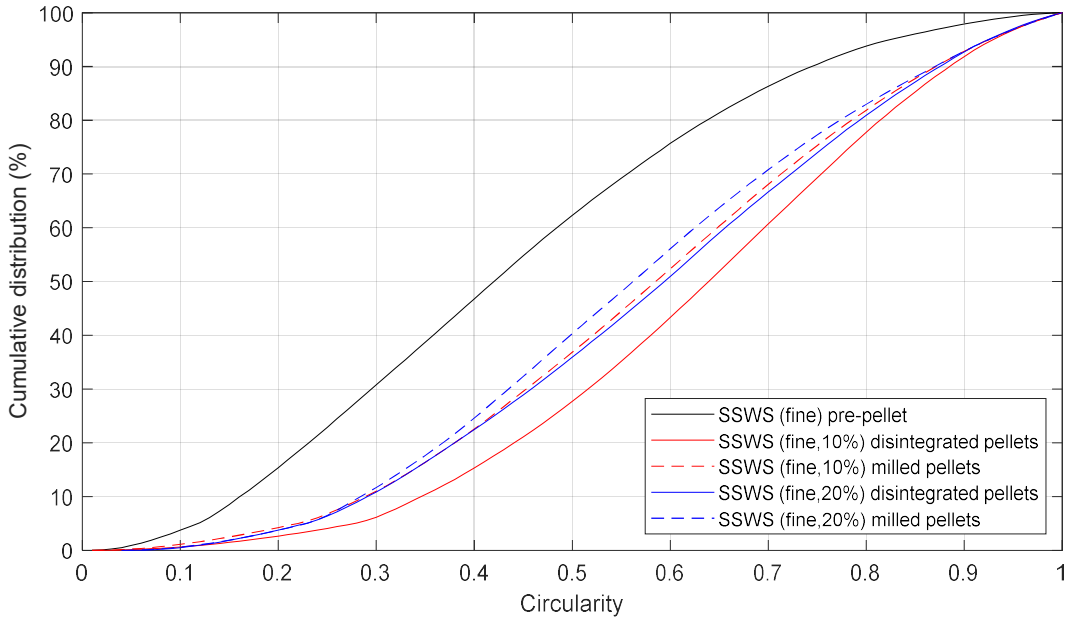

Figure 0-76 Circularity distributions of pre-pellet, disintegrated pellets and milled pellets - SSWS (fine)

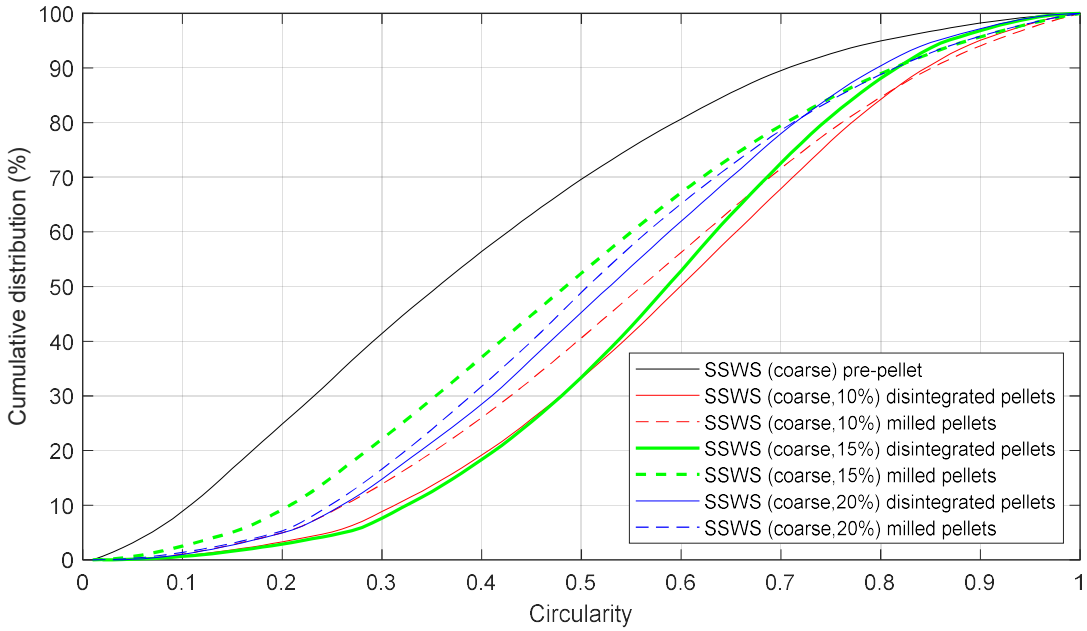

Figure 0-77 Circularity distributions of pre-pellet, disintegrated pellets and milled pellets - SSWS (coarse)

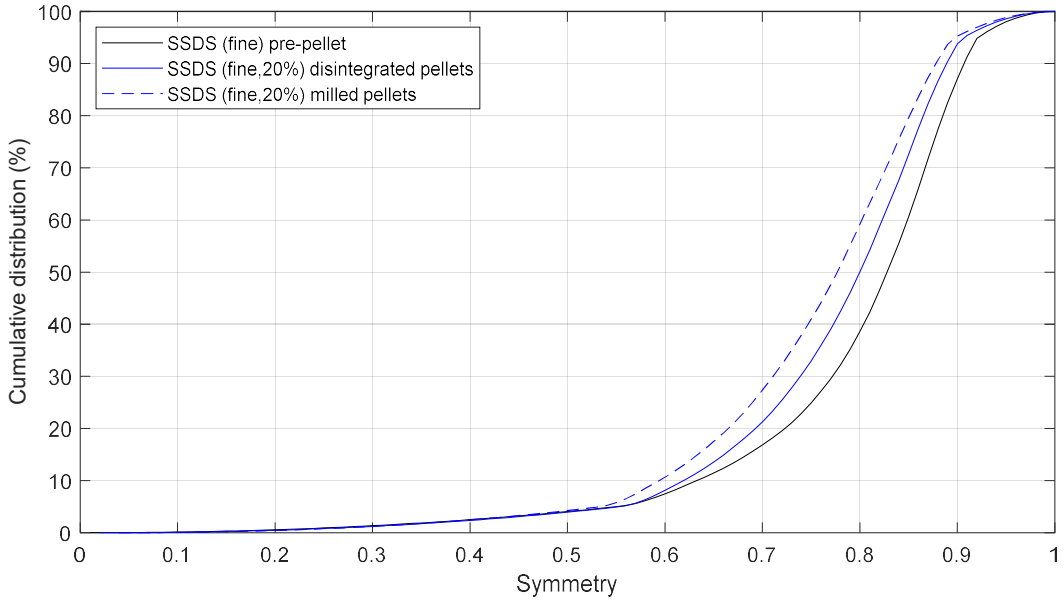

Figure 0-78 Symmetry distributions of pre-pellet, disintegrated pellets and milled pellets - SSDS (fine)

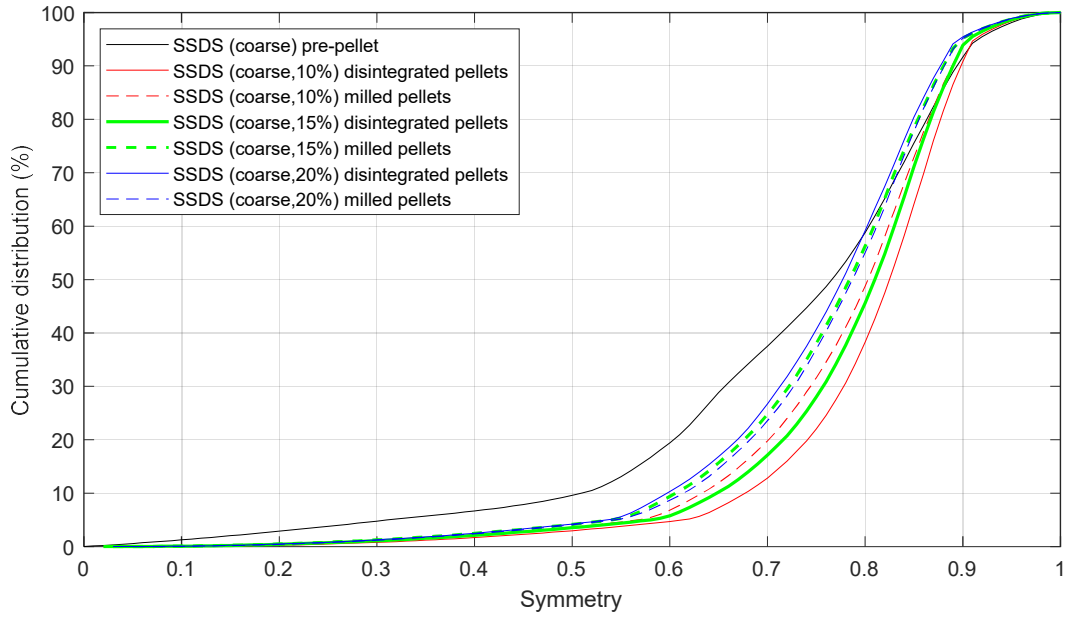

Figure 0-79 Symmetry distributions of pre-pellet, disintegrated pellets and milled pellets - SSDS (coarse)

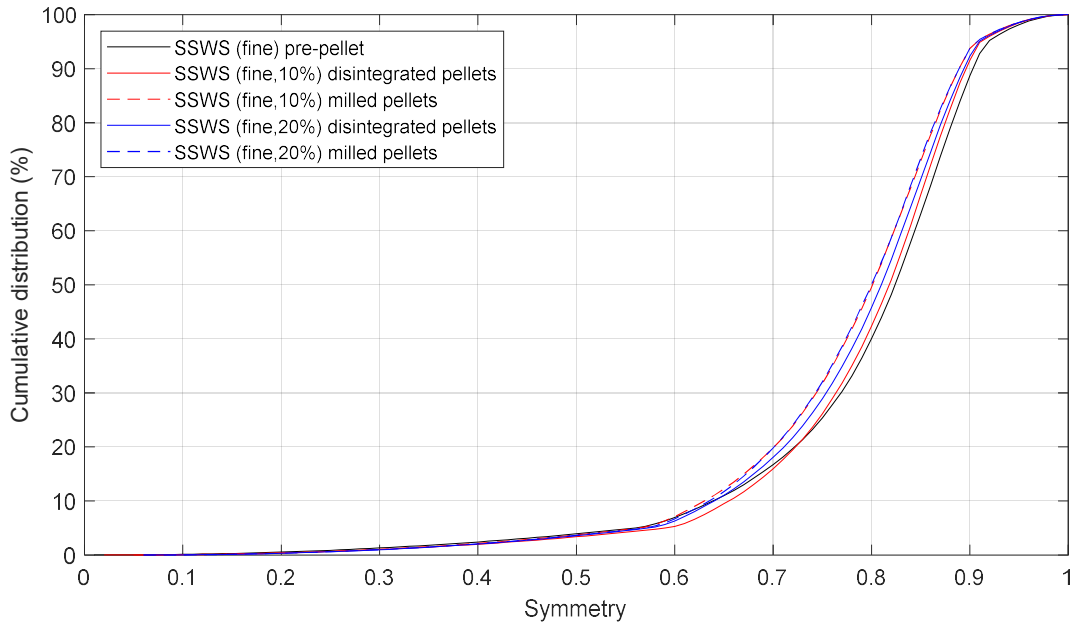

Figure 0-80 Symmetry distributions of pre-pellet, disintegrated pellets and milled pellets - SSWS (fine)

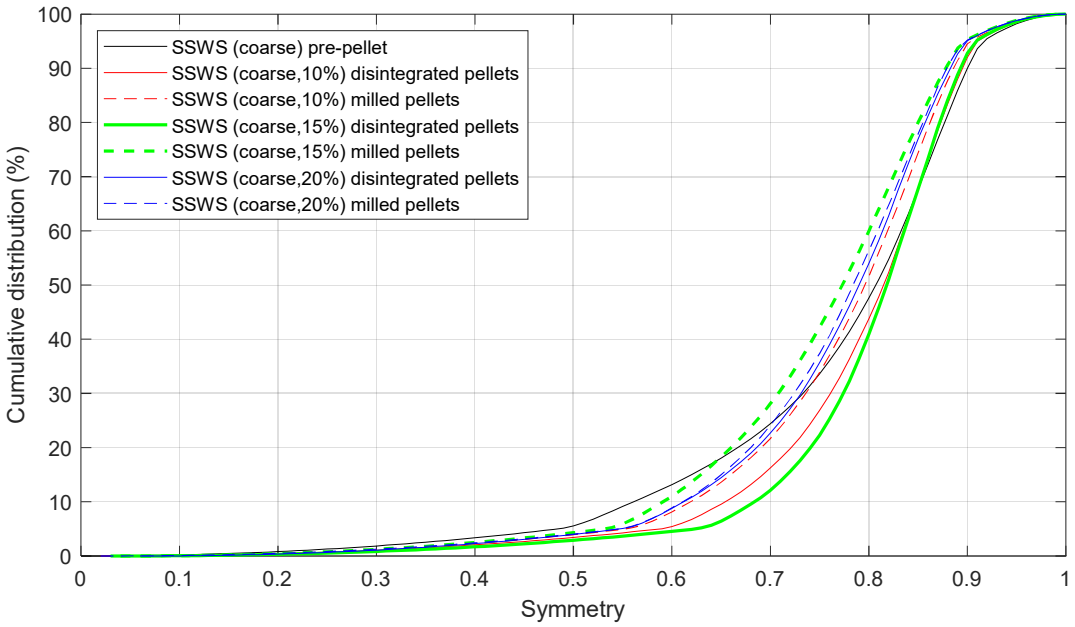

Figure 0-81 Symmetry distributions of pre-pellet, disintegrated pellets and milled pellets - SSWS (coarse)

Appendix F List of Input and Calculated Process Parameters for Life Cycle Analysis

A complete list of all input parameters used in this study, with their sources and associated processes and streams (as specified in the process flow diagram in Figure 8-1), is shown below.

Process	Streams	Data	Value	Unit	Source
Sugar mill, Pellet plant storage	1,2,3	Raw bagasse moisture content	50.0	%	Industrial partner
Dryer	4,6	Moisture content at dryer outlet and feed to furnace	12.0	%	Industrial partner
Hammermill, Furnace	5	Moisture content at hammermill inlet	11.5	%	Industrial partner
Hammermill	11,13	Moisture content at the hammermill outlet	10.5	%	Industrial partner
Pelletiser	12	Moisture content at the pelletiser inlet (M_{Pin})	10.5	%	Industrial partner
Pelletiser	15,17	Moisture content at the pelletiser outlet (M_{Pout})	6.0	%	Industrial partner
Pellet cooler	16	Moisture content at the pellet cooler inlet	6.0	%	Assumption
Pellet cooler	19,20,21	Moisture content at the pellet cooler outlet	6.0	%	Assumption
Pellet ginder	23,24,25	Moisture content at the pellet grinder outlet	6.0	%	Assumption

Pellet plant storage	1,2,3	Unrecoverable losses from the pellet plant storage	1.0	%	Industrial partner
Hammermill	11,12,13	Unrecoverable losses from the hammermill	1.0	%	Industrial partner
Pelletiser	15,16,17	Unrecoverable losses from the pelletiser (UL_P)	1.0	%	Industrial partner
N/A	19,20,21	Unrecoverable losses from the power station storage (UL_{PSS})	0	%	Assumption
N/A	19,20,21	Unrecoverable losses from transport to the UK (UL_T)	0	%	Assumption
Pellet cooler	19,20,21	Unrecoverable losses from the pellet cooler (UL_{PC})	0	%	Assumption
Pellet Grinder	23,24,25	Pellet grinder unrecoverable losses	0	%	Assumption
Pellet Grinder	N/A	Pellet grinding energy	0.108	MJ/kg	(Williams et al., 2016)
Boiler	N/A	Bagasse Higher Heating Value	18	MJ/kg	(Nhuchhen & Abdul Salam, 2012)
Boiler	27	Bagasse pellets ash content	6.04	%	Industrial partner

Boiler	N/A	Electricity generation efficiency from biomass pellets	39.9	%	(Ali et al., 2017)

Table A-1 List of Input and Calculated Process Parameters